STRENGTH AND CONSOLIDATION CHARACTERISTICS OF COMPACTED SOILS

A thesis submitted to the

University of London

(Imperial College of Science and Technology)

for the degree of

Doctor of Philosophy in the Faculty of Engineering

by

G.E. Blight, M.Sc.(Eng.) (Witwatersrand)

February, 1961.

ABSTRACT

Effective stress conditions for shear and volume change of partly saturated compacted soils are investigated by comparing the behaviour of the soil in the partly saturated state with its behaviour when fully saturated.

Techniques and apparatus are described which have been used to measure or control pore air and pore water pressures in partly saturated soils.

An equation is presented which relates the effective stress in a partly saturated soil to measured pore air and water pressures and experiments are described which demonstrate the validity of the equation. The effective stress equation contains a parameter which has been evaluated experimentally for conditions of shear failure in several partly saturated soils at a range of degrees of saturation.

Causes and effects of non-uniformity of pore pressure during triaxial shear have been investigated. A theory is presented which enables the choice of rates of strain which will result in tolerable errors in base pore pressure measurement in triaxial tests at constant overall water content.

A preliminary investigation of consolidation phenomena in partly saturated soils is described and tentative equations are presented which describe the process of consolidation.

TABLE OF CONTENTS

CHAPTER 1 -	INTRODUCTION AND REVIEW OF RECENT RESEARCH.	1
(1.1)	Definitions and units of measurement related to pore pressures and suctions in soils.	2
(1.2)	The measurement of pore pressures in partly saturated soils.	5
(1.3)	The principle of effective stress.	8
(1.4)	The tensile strength of water.	11
(1.5)	The measurement of soil strength and its correlation with measured negative pore water pressures.	13
(1.6)	Non-uniform pore pressures during undrained triaxial shear.	14
(1.7)	Consolidation in partly saturated soils.	15
(1.8)	The range of the present work.	16
CHAPTER 2 -	DESCRIPTION OF APPARATUS.	18
(2.1)	Control of cell pressure and measurement of overall volume change.	18
(2.2)	Apparatus for measurement and control of pore water pressure.	19
(2.3)	Apparatus for measurement and control of pore air pressure.	22
(2.4)	Axial loading.	23
(2.5)	Frictionless loading plates.	23
CHAPTER 3 -	TECHNIQUES OF PORE PRESSURE MEASUREMENT AND CHARACTERISTICS OF POROUS ELEMENTS.	25
(3.1)	Measurement of pore water pressures in partly saturated soils.	26
(3.2)	Response times in reading pore water pressures.	29
(3.3)	De-airing the measuring system and practical hints.	30
(3.4)	Characteristics of porous ceramic materials.	32

(3.5) Production of porous ceramic materials. 36

(3.6) Measurement of pore air pressures. 37

(3.7) Air diffusion through latex rubber membranes. 38

CHAPTER 4 - DESCRIPTIVE SOIL PROPERTIES. 40

(4.1) Mangla shale. 40

(4.2) Talybont clay. 40

(4.3) Selset clay. 41

(4.4) Miscellaneous. 41

CHAPTER 5 - THE PRINCIPLES OF EFFECTIVE STRESS AND PORE PRESSURE MEASUREMENT IN PARTLY SATURATED COMPACTED SOILS. 42

(5.1) A simple derivation of the principle of effective stress for a partly saturated soil. 42

(5.2) Theoretical relations between the χ factor and degree of saturation. 46

(5.3) Characteristics of the effective stress equation. 50

(5.4) Experimental demonstrations of the characteristics of the effective stress equation. 51

(5.5) Anomalies due to incorrect pore pressure measurement or use of the wrong form of the effective stress equation. 55

(5.6) Conclusions. 56

CHAPTER 6 - THE STRENGTH OF SATURATED COMPACTED SOILS. 57

(6.1) Presentation of test results. 57

(6.2) Failure criteria for saturated soils. 58

(6.3) Testing procedure. 61

(6.4) Notes on testing procedure. 63

(6.5) Test Series 1A: Mangla shale compacted at w = 18.6%. 64

(6.6) Test Series 3A: Mangla shale compacted at w = 16.3%. 65

(6.7) Test Series 2A: Selset clay compacted at w = 11.6%. 65

(6.8) Test Series 4A: Saturated drained tests on compacted Talybont clay. 66

(6.9) Discussion of the strength of saturated compacted soils. 67

CHAPTER 7 - THE STRENGTH OF COMPACTED PARTLY SATURATED SOILS AND THE MEASUREMENT OF THE PARAMETER χ IN THE EFFECTIVE STRESS LAW FOR SHEAR. 72

(7.1) Types of strength test used. 72

(7.2) The determination of the χ factor from the results of tests on partly saturated soils. 75

(7.3) Semi-graphical procedures for determining χ. 76

(7.4) The comparison of tests which fail at different strains and a note on failure criteria for partly saturated soils. 79

(7.5) Correction of deviator stress for rate of dilatation at failure in constant water content tests on partly saturated soils. 83

(7.6) Procedure in testing. 85

(7.7) Tests on compacted Talybont clay. 89

(7.8) Tests on compacted Mangla shale. 96

(7.9) Tests on compacted Selset clay. 101

(7.10) Tests on compacted Vaich moraine. 103

(7.11) Discussion of experimental results. 103

(7.12) Conclusions. 110

CHAPTER 8 - NON-UNIFORMITY OF PORE PRESSURE DURING TRIAXIAL SHEAR. 112

(8.1) Causes of non-uniform pore pressures. 112

(8.2) Characteristics of pore pressure non-uniformity. 113

(8.3) Special tests for detailed investigation of characteristics of pore pressure non-uniformity. 116

(8.4) The theoretical relation between testing times and the degree of equalisation of pore pressure in the triaxial test. 124

(8.5) Experimental confirmation of the theory. 129

(8.6) Estimation of the 'instantaneous' pore pressure difference p_o from elastic stress theory. 136

(8.7) The effectiveness of paper drains. 139

(8.8) Summary. 140

CHAPTER 9 - PROPERTIES OF PARTLY SATURATED COMPACTED SOILS AT CONSTANT WATER CONTENT UNDER ISOTROPIC STRESSES. 142

(9.1) The principle of effective stress for volume change in partly saturated soils. 142

(9.2) Semi-graphical method of determining α_v. 143

(9.3) Experimental values of α_v. 143

(9.4) Theoretical relation between volume change and pore air pressure in undrained compression of a partly saturated soil. 145

(9.5) Initial pore air pressures in compacted soils. 148

(9.6) Changes in pore water pressure after compression of freshly compacted soils. 150

(9.7) Changes in pore water pressure in unconfined samples of freshly compacted soils. 151

(9.8) Simulation of the non-equilibrium behaviour of partly saturated soils by a simple model. 152

(9.9) Calculated variation of pore water and pore air pressure in a compacted soil. 157

(9.10) Summary. 158

CHAPTER 10 - THE FLOW OF AIR THROUGH DRY SOILS. 159

(10.1) Summary of factors affecting consolidation in partly saturated soils. 159

(10.2) Nomenclature of this chapter. 162

(10.3) The laws of fluid flow through partly saturated soils. 163

(10.4) Experiments on the steady state flow of air through dry soils. 167

(10.5) Simplified equations for the consolidation of partly saturated soils. 173

(10.6) The sub-division of consolidation and swelling processes in partly saturated soils. 179

(10.7) Experimental data on unsteady flow of air through dry rigid soils. 183

(10.8) Approximate solution of consolidation equations from known shape of isochrones. 185

(10.9) Experimental data on consolidation of dry compressible soils. 189

(10.10) Summary and conclusions. 190

CHAPTER 11 - REVIEW AND CONCLUDING REMARKS. 192

(11.1) Measurement of pore pressures. 192

(11.2) The principle of effective stress in partly saturated soils. 192

(11.3) Non-uniform pore pressures in triaxial testing. 194

(11.4) Consolidation of partly saturated soils. 194

(11.5) Concluding remarks. 195

ACKNOWLEDGEMENTS. 197

LIST OF REFERENCES. 198

APPENDICES.

Appendix to Chapter 6. 205

Appendix to Chapter 7. 208

Appendix to Chapter 8. 215

Appendix to Chapter 10. 218

CHAPTER 1

INTRODUCTION AND REVIEW OF RECENT RESEARCH

The work of this thesis comprises an investigation of some of the strength and consolidation characteristics of compacted soils.

In the past, the investigation of the strength of compacted soils has not been on a completely satisfactory basis. There are a number of reasons for this:

(a) Workers in soil mechanics, although realising that in partly saturated compacted soils there would probably be a considerable difference between the pore pressures of the gaseous and liquid components of the pore fluid, have lacked apparatus to measure this difference. The pore pressure difference is due to the effects of surface tension at the air-water interfaces in the pore fluid and as a result the pore air pressure always exceeds the pore water pressure. Loose, coarse porous discs have usually been used to effect communication between the pore fluid in the soil and the fluid in the pore pressure measuring system. This method of measurement is unable to differentiate between the two pore pressures in the soil.

(b) It has been the practice in the past to use the same form of effective stress equation for partly saturated soils as for saturated soils. Due to the differing pressures in the two components of the pore fluid and the reduced areas of the soil skeleton over which the pressures are effective, a modified form of the effective stress equation must be used for partly saturated soils.

(c) The significance and effects of non-uniform pore pressure conditions in undrained triaxial testing have not been fully appreciated. As a result, even when methods of pore pressure measurement have been reliable, testing times have often been too short to enable representative pore pressure measurements to be made.

It has long been realised that the classical theory of consolidation for saturated soils is not really applicable to partly saturated soils. Even in soils with relatively high degrees of saturation, significant deviations occur from the classical theory. The study of consolidation in partly saturated soils has been handicapped by the lack of reliable methods of measuring pore pressures and of differentiating between pressures in the two phases of the pore fluid.

(1.1) Definitions and units of measurement related to pore pressures and suctions in soils.

The pore water pressure in a saturated soil can be defined as the pressure in the pore fluid measured relative to atmospheric pressure. This definition is true for pressures both above and below atmospheric pressure. Pore pressures below atmospheric pressure are referred to as "negative pore pressures".

In partly saturated soils pore air pressures have to be considered as well as pore water pressures. The definition of pore water pressure given above is equally valid for partly saturated soils. Pore air pressure can be defined in a similar fashion.

In soil physics and road engineering, the pore air pressure is generally atmospheric and the pore water pressure is negative (in

consequence of surface tension effects). Use is generally made of the term "suction". Schofield (1960) defines the suction in the pore water of a soil as the level of its free energy relative to pure water at the same temperature and at atmospheric pressure.

Gardner (1960) points out that the total potential of soil water can be expressed as the sum of three components: the gravitational potential, the osmotic potential and the capillary potential. The gravitational potential depends on the elevation of the soil water with reference to a datum level and the osmotic potential depends on the concentration of dissolved ions in the soil water. Gardner regards the capillary potential as being the suction of the soil. He defines the capillary potential as "the pressure difference required across a permeable membrane to produce hydraulic equilibrium between soil water that is subject to surface force action and free water that is not subject to surface force action". (Gardner, 1959).

Marshall (1959) divides the total suction into two components: the matrix suction and the solute suction. The solute suction corresponds to Gardner's osmotic potential while the matrix suction corresponds to the capillary potential.

Gardner, Marshall and Aitchison (1960) all agree that at low suctions the capillary potential or matrix suction can be represented by a capillary model consisting of a column of water, supported by surface tension in a vertical capillary tube so that the pressure in the water immediately beneath the meniscus is equal to the pressure in the soil water. Aitchison considers that the capillary potential may be the only significant component of suction up to total suctions of the order of 220 atmospheres.

According to the above definitions, in the low suction range, if

u_w = pore water pressure, and

u_a = pore air pressure,

then the capillary potential or matrix suction of the soil water measured relative to free water at pressure u_a is given by $(u_a - u_w)$ with little error. It should be noted that as the reference datum for the suction measurement is u_a, the measured value of the suction is independent of the absolute value of u_a.

Aitchison has suggested the term "pressure deficiency" p" where

$$p'' = (u_a - u_w)$$

In soil physics, suction is commonly measured in terms of the height of the column of water represented by the capillary model. If this height is h:

$$\gamma_w h = \frac{2T}{r} = p'' = (u_a - u_w) \qquad E(1.1)$$

where

r is the radius of the capillary.

T is the surface tension of water.

γ_w is the density of water.

If p", u_a and u_w are expressed in lb/in^2, γ_w must be in lb/in^3, h and r in in. and T in lb/in.

The most commonly used suction scale is the pF scale introduced by Schofield (1935). If h is expressed in centimetres of water:

$$pF = \log_{10} h$$

Some comparative values are as follows:

h cm.H_2O	pF	$p'' = (u_a - u_w)$	
		Atm.	p.s.i.
10	1	0.0097	0.142
10^3	3	0.97	14.2
10^5	5	97	1,420
10^7	7	9,700	142,000

(1.2) The measurement of pore pressures in partly saturated soils.

Soil physicists have been mainly interested in equilibrium states in soils under very low applied stresses. Their studies have resulted in the development of a number of methods of producing controlled moisture contents and hence suctions in unconfined samples of soil. A useful summary of these methods and the range over which they are effective is given by Croney and Coleman (1960). The following table is reproduced from their paper.

Methods of producing controlled moisture contents in unconfined samples of soil

Method	Range of suction $(u_a - u_w)$	
	pF units	p.s.i.
Suction plate	0 - 3.0	0 - 14.2
Pressure plate	0 - 3.0	0 - 14.2
Pressure membrane	0 - 6.0	0 - 14,200
Oedometer	2.0 - 4.0	1.4 - 142
Centrifuge	3.0 - 4.5	14.2 - 450
Freezing point depression	3.0 - 4.0	14.2 - 142
Relative humidity	5.0 - 7.0	1,420 - 142,000
Sorption balance	5.0 - 7.0	1,420 - 142,000
Calibrated electrical resistance gauges	3.0 - 7.0	14.2 - 142,000

Several of these methods can be applied directly to the measurement of pore pressures in partly saturated soils.

Suction plate, pressure plate and pressure membrane methods.

In the suction plate method, the sample of soil rests on a saturated fine pored porous disc. A controlled suction is applied to the water in the soil via the water in the disc and the soil is allowed to drain until its suction equals the applied suction. The difficulty of maintaining controlled suctions in water filled apparatus of greater than about 13 p.s.i. limits the range of the suction plate technique.

The pressure plate and pressure membrane are similar in principle to the suction plate. The sample of soil rests on the surface of a saturated fine porous disc or semi-permeable membrane. The lower side of the disc or membrane communicates with free water at atmospheric pressure. A controlled air pressure is applied to the soil sample and the upper surface of the disc or membrane, and the soil is allowed to drain to the free water until its suction is equal to the pressure difference across the membrane.

By connecting the lower side of the plate or membrane to a null indicator, all of these methods can be used to measure changes in pore water pressure at constant water content.

Croney (Croney et al., 1952) used the suction plate technique to measure the suction in undisturbed samples of soil. The applied suction was adjusted to achieve a no-flow condition.

A modification of the suction plate technique is used in the field tensiometer (Black et al., 1958) in which the suction in the soil is balanced against a mercury manometer.

Hilf (1956) used modifications of both the suction and pressure plate techniques in measuring the initial pore water pressures in samples of compacted soil.

More recently Alpan (1959) used the suction and pressure plate technique in conjunction with a null indicator to measure changes in pore pressure in partly saturated compacted soils during shear. Alpan also performed series of tests to compare the performance in transmitting pore water pressures of unsealed coarse porous discs and sealed fine porous discs. He showed that suction or pressure plate techniques were necessary to distinguish between pore air and pore water pressures in partly saturated soils.

The technique used in this thesis is basically the same as that used by Alpan.

Relative humidity method.

The relative humidity method of measurement depends on the well known Kelvin equation:

$$R\theta \log_e \frac{p'}{p} = \frac{2T}{r} \cdot \frac{w}{\rho} \qquad \text{(Adam, 1941)}$$

where

p' is the equilibrium vapour pressure over a spherical surface of liquid of radius r.

p is the equilibrium vapour pressure over a plane surface of the liquid.

w is the molecular weight of the vapour.

ρ is the density of the liquid.

R and θ are respectively the universal gas constant and the absolute temperature.

According to this equation, the vapour pressure over a curved liquid surface is less than that over a plane surface. By measuring the depression of vapour pressure, the suction can be inferred. The relative humidity H is related to the pF value at 20°C by the equation:

$$pF = 6.5 + \log_{10}(2 - \log_{10}H) \qquad \text{(Croney et al., 1952)}$$

Schofield (1958) has used this method successfully to measure suctions as small as pF3 and in a conversation with the writer suggested the use of miniature dew point hygrometers to measure the suction in soil under load.

It appears to be generally agreed that the relative humidity method gives a measure of the total suction of the soil water, while the suction or pressure plate technique gives a measure of the matrix suction.

(1.3) The principle of effective stress.

(a) Saturated soils.

The principle of effective stress has been defined for saturated soils by Bishop (1960). His definition is as follows:

(a) The change in volume of an element of soil depends not on the change in total normal stress applied but on the difference between the change in total normal stress and the change in pore pressure.

(b) The maximum resistance to shear on any plane in the soil is a function not of the total normal stress acting on the plane, but of the difference between the total normal stress and the pore pressure.

This may be expressed algebraically by

$$\sigma' = \sigma - u \qquad E(1.2)$$

where

σ' is the effeotive stress.

σ is the total stress.

u is the pore pressure.

This equation will be discussed also in Chapter 5.

The origin of this principle lies in the work of Terzaghi on the theory of consolidation (1923) and on shear strength (1932). As far as saturated soils are concerned, the principle of effeotive stress has been confirmed by the experimental work of Rendulio (1937), Hvorslev (1937), Taylor (1944), Bishop and Eldin (1950) and Henkel (1958).

Tests by Frazer (1957) have shown that E(1.2) is also valid for the shear strength of dry cohesionless granular materials.

It should be noted that as the effeotive stress depends on the differenoe between total stress and pore pressure it should be independent of the absolute magnitude of either and should be equally valid for positive or negative pore pressures. This has been demonstrated by Bishop and Eldin (1950) who measured negative pore water pressures in saturated sands down to -13 p.s.i. More recently, it has also been oonfirmed by Donald (1961) who performed drained tests on saturated silt with controlled negative pore water pressures and alsc undrained tests on saturated clay with measured suotions up to 20 p.s.i.

(b) Partly saturated soils.

Although the principle of effective stress should be equally valid for partly saturated soils, equation E(1.2) requires modification to account for the differing pressures in the liquid and vapour phases

of the pore fluid and the reduced areas over which they act.

Bishop (1955) has proposed the following equation:

$$\sigma' = (\sigma - u_a) + \chi (u_a - u_w) \qquad E(1.3)$$

In this equation χ is a parameter which must be determined experimentally. The value of χ will be unity for completely saturated soils and zero for completely dry soils. The properties of this equation will be dealt with in detail in Chapter 5.

Several other forms of effective stress equation have been proposed for use with partly saturated soils:

(i) Croney and Coleman (1960), proposed separate but similar effective stress equations for volume change and shear:

For volume change:

$$\sigma'_v = (p - \pi) - \beta(u - \pi) \qquad E(1.4)a$$

For shear:

$$\sigma' = (p - \pi) - \beta'(u - \pi) \qquad E(1.4)b$$

where

σ' is the effective stress.

p is the total stress.

π is the pore air pressure.

u is the pore water pressure.

Rewriting these equations in the notation of this thesis, we have:

$$\sigma' = (\sigma - u_a) - \beta(u_w - u_a) \qquad E(1.4)$$

E(1.4) is identical in form to E(1.3) and hence $\beta = \chi$.

(ii) Jennings (1960) prefers to modify the Terzaghi effective stress equation E(1.2) by using a reduced value of the pore water pressure.

He defines

$$-u = \beta p''$$

and hence $$\sigma' = \sigma - u = \sigma + \beta p'' \qquad E(1.5)$$

This equation was originally proposed on the assumption that u_a would never vary from zero. In this case $p'' = -u_w$. With the restriction that $u_a = 0$, E(1.3) reduces to:

$$\sigma' = \sigma - \chi u_w = \sigma + \chi p''$$

and in this circumstance $\beta = \chi$.

(iii) Aitchison (1960) has proposed a very similar form of equation to that of Jennings. His equation is:

$$\sigma' = \sigma + \psi . p'' \qquad E(1.6)$$

Provided $u_a = 0$, $\psi = \chi$.

To sum up, there seems to be general agreement among these three authorities that the Bishop form of the effective stress equation is correct.

It has been anticipated by Bishop and Croney and Coleman, that the parameter in the effective stress equation may be different for volume change and shear strength.

(iv) Hilf (1956) put forward the following tentative form of effective stress equation:

$$\sigma' = \sigma - u_a - u_c \qquad E(1.7)$$

Hilf referred to u_c in this equation as the "capillary pressure", by which he apparently meant $u_c = (u_a - u_w)$ but not a value of $(u_a - u_w)$ reduced by a factor similar to χ.

(1.4) The tensile strength of water.

In most field problems the equilibrium pore air pressure after any consolidation is complete, will be atmospheric. In this case

E(1.3) implies that when $(u_a - u_w)$ exceeds 1 atmosphere, the pore water will be in a state of absolute tension. Terzaghi (1934) realised that pore water in clays could sustain absolute tension and gives an excellent commentary on his reasons for believing this. He points out that the intrinsic pressure between molecules of water is about 10,000 kg/cm^2 and that this furnishes the maximum value of isotropic tension possible in water. Aitchison (1960) showed that it is unlikely that soil water is ever subjected to absolute tensions exceeding 200 kg/cm^2. Radii of curvature small enough to give larger tensions than this would bring the water within the influence of the adsorption pressures of the surfaces of the soil grains. These pressures (up to 25,000 atmospheres) would increase the pressure in the water. Tensile strengths of pure water up to 200 atmospheres have been demonstrated experimentally (Dorsey, 1940).

The writer and a colleague have attained absolute tensions in tap water of up to about 40 p.s.i. One end of a length of small bore nylon tubing was dipped into a bowl containing water and mercury. A small quantity of water was sucked into the tube followed by a thread of mercury. When the water reached the other end of the tube, the tube was sealed so that there was a short thread of water between the mercury and the sealed end. Keeping the lower end in the mercury the upper end of tube was raised gently to a height of about 10 feet before the water ruptured.

There therefore seems no reason to doubt the ability of soil water to sustain large absolute tensions.

(1.5) The measurement of soil strength and its correlation with measured negative pore water pressures.

Several investigations of shear strength in the past have included the measurement of negative pore water pressures. It is only recently that results of this sort have been used to obtain parameters in the effective stress equations given in section (1.3). It is recalled from (1.3) that Bishop and Eldin (1950) measured negative pore water pressures in saturated sands.

Lewis and Ross (1955) used a miniature vane to measure the strength of several soils with various initial suctions. Towner (1958) related the unconfined strengths of samples of remoulded kaolin to their initial suctions (achieved using a pressure membrane). He compared this relation to strength envelopes from saturated triaxial tests. More recently (Croney and Coleman, 1960), the unconfined strengths of undisturbed samples of London clay have been related to their initial suctions.

Donald (1956) performed drained shear box and triaxial tests on several sands using controlled negative pore water pressures. Aitchison (1956) related the unconfined strengths of several clay soils to their initial suctions. His samples were prepared at the required suction using a pressure membrane.

Recently Alpan (1959) has measured negative pore water pressures during shear in compacted partly saturated soils.

Although these workers established qualitative relations between negative pore water pressures and shear strengths, the data was usually not complete enough to establish the validity of the principle of effective stress for shear of partly saturated soils.

Alpan's tests were an advance in this direction.

(1.6) Non-uniform pore pressures during undrained triaxial shear.

The validity of measuring the pore pressure at a single point during undrained triaxial shear depends on the pore pressure being the same throughout the sample. Taylor (1951) measured the pore water pressure simultaneously at one end of the triaxial sample and at a probe at mid-height. He noted a large difference between probe and end pore pressures which decreased as the time to failure was increased. This is the only published data (prior to 1960) which quotes measured pore pressure differences. Taylor also found appreciable moisture content gradients up the length of his samples at the end of the test.

At Imperial College, it was recognised that non-uniform stress conditions could lead to non-uniformities of pore pressure. Bishop and Henkel (1957) have described the use of paper drains to accelerate the equalisation of pore water pressures and hence reduce errors due to this source.

Recently Alpan (1959) found that the value of the cohesion intercept for a compacted soil calculated in terms of pore water pressures measured at the base of the sample appeared to vary considerably with the time to failure. It was realised that this was probably a manifestation of non-uniform pore water pressures.

Shockley and Ahlvin (1960) have measured vertical stress distributions in large triaxial samples of dry cohesionless sand. Pressure cells were distributed across the diameter of the sample at mid-height and near the top. Appreciable non-uniformities in vertical stress were recorded.

Very little information has been published so far on this

subject. There is enough data, however, to show that non-uniform conditions can be an important factor in the accuracy of the measurement of shear strength parameters and effective stresses.

(1.7) Consolidation in partly saturated soils.

Little work appears to have been done on the consolidation of partly saturated soils as such. However, a great deal of work has been done on the flow of fluids through saturated and partly saturated porous media including soils.

Excellent summaries of flow phenomena from the points of view of the physicist and mining geologist are given in the works of Carman (1956) and Scheidegger (1957).

In the field of soil physics, much work has been done on infiltration problems and the advance of wetting fronts in soils (Philip, 1957, Low, 1959 and many others).

Road research workers have interested themselves in the movement of moisture through soils due to suction, osmotic and thermal gradients. (Winterkorn, 1947, Rollins and Spangler, 1954).

A great deal of work on closely associated flow phenomena has been produced by physical chemists. Much of their work is extremely valuable in any study of mass transport phenomena. (Denbigh, 1951, Crank, 1956).

The electronic computer has been used by Aronofsky (1954) to solve several problems of the unsteady flow of gases through porous media.

There does, however, appear to be considerable disagreement in the literature on several points, notably on the correct form of flow law for steady state conditions.

(1.8) The range of the present work.

It is hoped that the work which is presented in subsequent chapters will help to advance knowledge of the subjects which have been briefly discussed in the pages of this introductory chapter.

Chapter 3 will deal with techniques which have been used to measure both pore water and pore air pressures and will describe some of the properties of porous elements used for pore pressure measurement.

The principle of effective stress for partly saturated soils will be considered more fully in Chapter 5. A theoretical relation between the degree of saturation and the parameter χ will be derived and its application to compacted soils will be illustrated. A number of experiments showing the properties of the effective stress equation will also be presented.

Chapters 6 and 7 contain experimental work on the shear strength of compacted soils in both the saturated and partly saturated states. Values of the parameter χ are derived from a comparison of stresses in partly saturated soils with corresponding stresses in saturated soils.

The problem of non-uniform pore pressures in triaxial shear forms the subject of Chapter 8. Further experimental data on the subject is presented and an approximate theory is formulated which enables the calculation of a suitable time to failure from a knowledge of the consolidation characteristics of the soil.

In Chapter 9 some of the characteristics of compacted soils under isotropic stress are described and the effective stress equation for volume change of a partly saturated soil is considered.

Chapter 10 deals with a preliminary investigation into the consolidation of partly saturated soils. Tentative equations describing the consolidation process are set up and some aspects of steady and unsteady flow of air through dry soils are considered.

CHAPTER 2

DESCRIPTION OF APPARATUS

Most of the apparatus which was used for the experimental work of this thesis has been described in detail by Bishop and Henkel (1957) in their book on triaxial testing. It is not proposed to describe standard items of apparatus and apparatus layouts in detail. The reader is referred to the above source for more detailed descriptions.

Techniques of measurement will be described in Chapter 3 and experimental procedures immediately before the tests to which they refer.

(2.1) Control of cell pressure and measurement of overall volume change.

(a) Tests on 4" diameter x 8" high samples.

Fig. (2.1) shows the layout of the apparatus. The cell pressure was applied by means of the standard self-compensating mercury pressure control which gives constancy to $\pm$ 0.1 p.s.i. Cell pressures below 20 p.s.i. were measured by means of the manometer while those above 20 p.s.i. were measured using the bourdon pressure gauge.

Overall volume changes of the sample were measured by connecting the self-compensating mercury volume gauge into the circuit between the pressure control system and the triaxial cell.

To reduce leakage past the loading ram of the triaxial cell during shear tests, each cell is fitted with an inverted cup which was filled with castor oil before the start of each test. Overall volume changes were corrected for leakage by periodically soaking up the castor oil on a piece of paper towelling and weighing. Volume

changes were also corrected for the measured movement of the ram into the cell during loading.

(b) Tests on 1½" diameter x 3" high samples.

The layout of apparatus used for these tests was the same as that shown in fig. (2.1) except that a more accurate volume gauge was used. This gauge is shown in fig. (2.2) and plate 1 of Chapter 8. Volume changes are shown by movement of the paraffin-water meniscus in the graduated tube. The paraffin is dyed red so that the meniscus stands out clearly. Provided the glass tube is perfectly clean, a uniform meniscus is obtained.

Since the specific gravity of paraffin (0.8) is close to that of water, a volume change using the full range of the apparatus results in a pressure change of less than 0.1 p.s.i. Thus there is no need for automatic compensation for pressure change as in the mercury filled volume gauge. The graduated tube is not subjected to a pressure difference and provided the base of the graduated tube is connected to the triaxial cell its calibration is independent of pressure.

(2.2) Apparatus for measurement and control of pore water pressure.

The layout of the pore pressure measuring apparatus is shown in fig. (2.1) and is the same as that described by Bishop and Henkel (1957).

(a) Valves, tubing and joints.

The valves and joints used in the apparatus were required to be pressure and vacuum tight. The most satisfactory valves for this purpose proved to be piston type valves with O-ring seals. Wherever possible coned compression type joints with O-ring seals (see fig.

2.3) or 'Ermeto' type couplings were used. Where threaded joints were unavoidable, liberal use was made of hemp and sealing compound.

Negative pressure in water contained by plastic tubing causes the diffusion of air from the atmosphere through the walls of the tubing. This air can cause trouble if it reappears as bubbles in the apparatus. Nylon is fairly impermeable to air, but permeable to water. P.V.C. and polythene are more permeable to air, but impervious to water. Nylon tubing is better for use with controlled suctions, but loss of water through its walls by evaporation can cause a noticeable pressure loss in a sealed system over a period of several weeks.

(b) Null indicators.

The standard glass capillary tube type null indicator with the stainless steel body was used for base measurement of pore pressures in all tests on 4" diameter x 8" high samples.

For base measurement of pore pressure in tests on $1\frac{1}{2}$" diameter x 3" high samples and for use with pore pressure probes in tests on 4" diameter x 8" high samples, the larger of the null indicators, shown in fig. (2.3), (also illustrated in plate 4 of Chapter 8) was used. This design is more compact and the null indicator can be mounted closer to the sample. The null indicator is made from a single block of perspex. During de-airing the mercury is tipped into the reservoir so that water being flushed through the apparatus can by-pass it.

In tests on $1\frac{1}{2}$" diameter samples, the oopper tube was connected to a valve which in turn was oonnected to the base of the triaxial oell.

When the null indicator was used with a single probe, it was reversed, the controlled pressure being applied through the copper tube.

A miniature perspex null indicator with a very fine indicating tube was used in conjunction with the miniature probe for tests on $1\frac{1}{2}$" diameter samples. It is shown in fig. (2.3) and also in Plate 1 of Chapter 8. The base of the null indicator enables it to stand independently and the screw plug in the mercury reservoir may be removed for cleaning purposes.

(c) Mounting of porous elements.

For base measurement of pore water pressure in 4" diameter samples, (tests described in Chapters 7, 8 and 9) a porous ceramic disc $2\frac{1}{2}$" in diameter x $\frac{3}{8}$" thick and with its plane surfaces ground flat and parallel was sealed into a brass mounting. Fig. (2.4) and Plate 4 of Chapter 8 show the mounting which is held in position on the pedestal of the triaxial cell base using six cheese-headed screws, and is sealed by means of two O-rings.

The porous disc was sealed into the mounting using an epoxy resin ("Twinbond"). This material was fairly easy to handle, gave a good bond to both metal and ceramic and when set was quite rigid and impermeable. The recess in the brass mounting had originally been provided with radial drainage grooves (Alpan, 1959). These were later eliminated when it was realised that they acted as bubble traps and did not improve flow through the disc. Instead, a coned central depression was provided which ensured continuity in the water of the system even if a small air bubble were to form immediately beneath the ceramic disc.

In several tests, (described in Chapter 8) ceramic probes were used to measure pore water pressures at various points up the height of the sample. These probes and the method used to seal the

probe into the membrane surrounding the sample are shown in fig.(2.4) and Plate 4 of Chapter 8. The ceramic probes were sealed into their holders using "Twinbond".

Small-bore nylon tubing and 'Ermeto' connectors were used to connect the probes for 4" diameter samples to their null indicators. This tubing was fairly inexpansible and nylon has the advantage of being almost impermeable to the diffusion of air. For the miniature probe, small bore thick walled polythene tubing steamed into a spiral curve was used as the nylon tubing proved too stiff for this purpose.

In certain of the tests under all round pressure, pore water pressures were measured at the top of the sample using a porous disc sealed into a perspex top cap. This method has the advantage that de-airing can be checked visually and also that any bubbles which form on the reverse side of the porous disc float upwards and so do not break the continuity of the water in the system.

In the consolidation stage of consolidated undrained tests (described in Chapter 6) use was made of controlled positive pore water pressures. These were applied by connecting the mercury pressure control system directly to the pore pressure inlet of the triaxial cell.

(2.3) Apparatus for measurement and control of pore air pressure.

Pore air pressure was measured using the perspex null indicator shown in fig. (2.3). Nylon tubing and 'Ermeto' connectors were used to connect the null indicator to the sample through a connection just above the base. The connector which passed through the sample membrane is shown in fig. (2.4) and Plate 4 of Chapter 8. The seal is similar to that used for the ceramic probes.

If pore air pressures were to be controlled, a pressure control-valve system was used to apply the constant air pressure through a polythene tube to the top of the sample.

Air pressures were controlled by two control-valves in series. The pressure drop required to switch in the compressor was 40 p.s.i. This fluctuation was evened out by using a coarse diaphragm control-valve which controlled the supply pressure to $\pm$ 2 p.s.i. For the low pressure ranges (0 - 25 p.s.i.) the next stage was an accurate "constant leak" control-valve which was used in conjunction with a manometer to control the pressure to $\pm$ 0.1 p.s.i. For higher pressures, due to shortage of apparatus, a second coarse diaphragm valve was used with a pressure gauge to control the air pressure to $\pm$ .3 p.s.i. The apparatus layout is shown in fig. (2.5).

(2.4) Axial loading.

All shear tests described in this thesis were carried out at a controlled rate of strain. The testing machines used have been described in detail by Bishop and Henkel (1957).

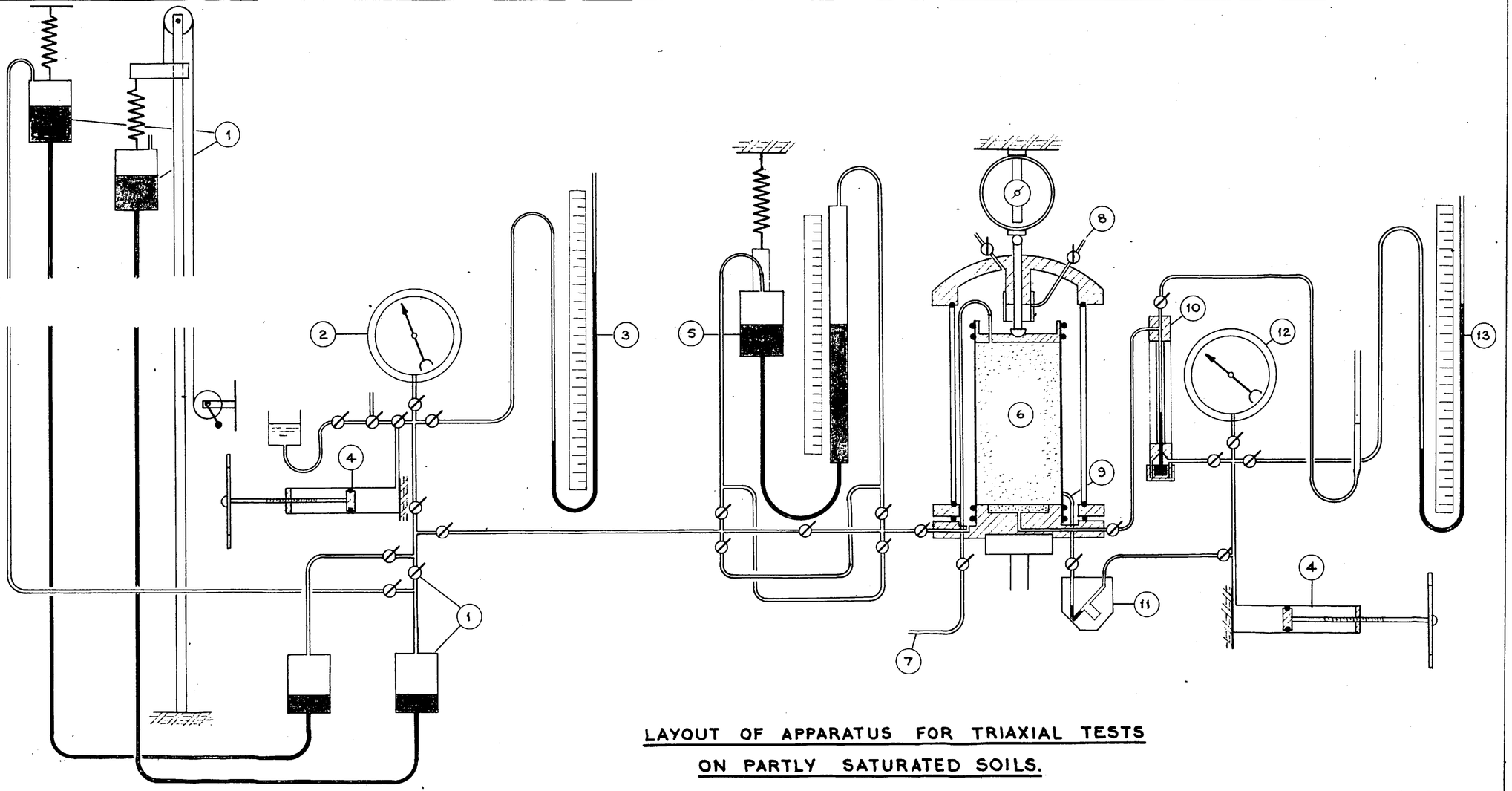
Axial loads were measured by means of proving rings which were calibrated by dead loading up to 500 lb. For higher loads, a manually operated "Buckton" testing machine was used for calibration.

(2.5) Frictionless loading plates.

A special test is described in Chapter 8 in which a sample was loaded between smooth lubricated end plates. Details of these end plates are given in fig. (2.6). The surface of the plates was highly polished by using several grades of water paper and finally jewellers' rouge. In use, the polished surface of each plate was covered by a layer of silicone grease followed by a disc of thin

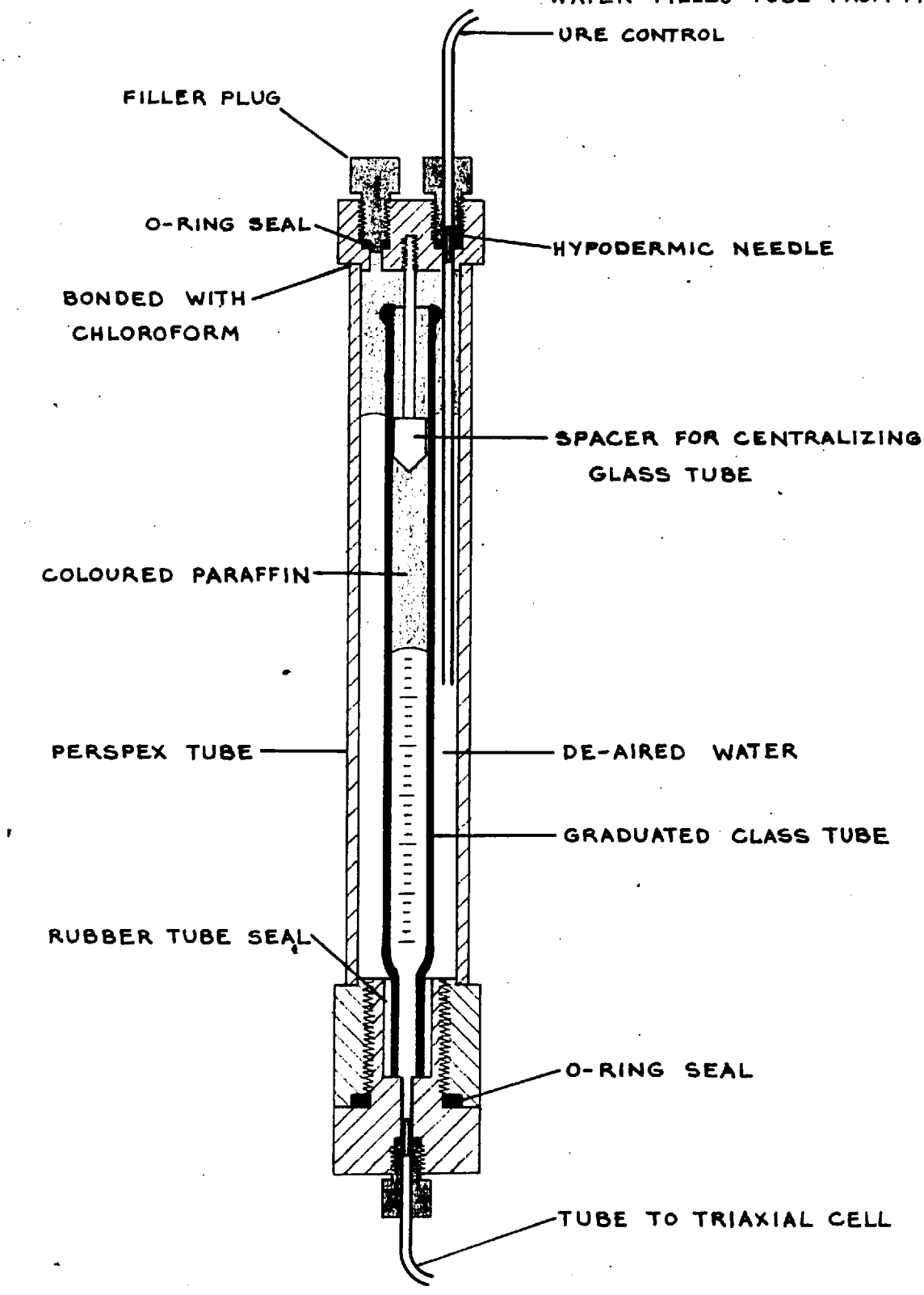
rubber membrane. This resulted in an almost frictionless seating for the sample. The coefficient of friction between rubber lubricated with silicone grease and polished metal was found by Wood (1958) to be only 0.018.

1	SELF COMPENSATING MERCURY PRESSURE CONTROL.
2	CELL PRESSURE GAUGE.
3	CELL PRESSURE MANOMETER.
4	SCREW CONTROL RAMS.
5	SELF COMPENSATING MERCURY VOLUME GAUGE.
6	SAMPLE IN TRIAXIAL CELL.
7	AIR PRESSURE LEAD. (TESTS WITH CONTROLLED U_a ONLY).
8	FILLING LEAD TO OIL RESERVOIR.
9	AIR PRESSURE LEAD. (TESTS WITH MEASURED U_a ONLY).
10	PORE WATER PRESSURE (U_w) NULL INDICATOR.
11	PORE AIR PRESSURE (U_a) NULL INDICATOR.
12	PORE PRESSURE GAUGE.
13	PORE PRESSURE MANOMETER.



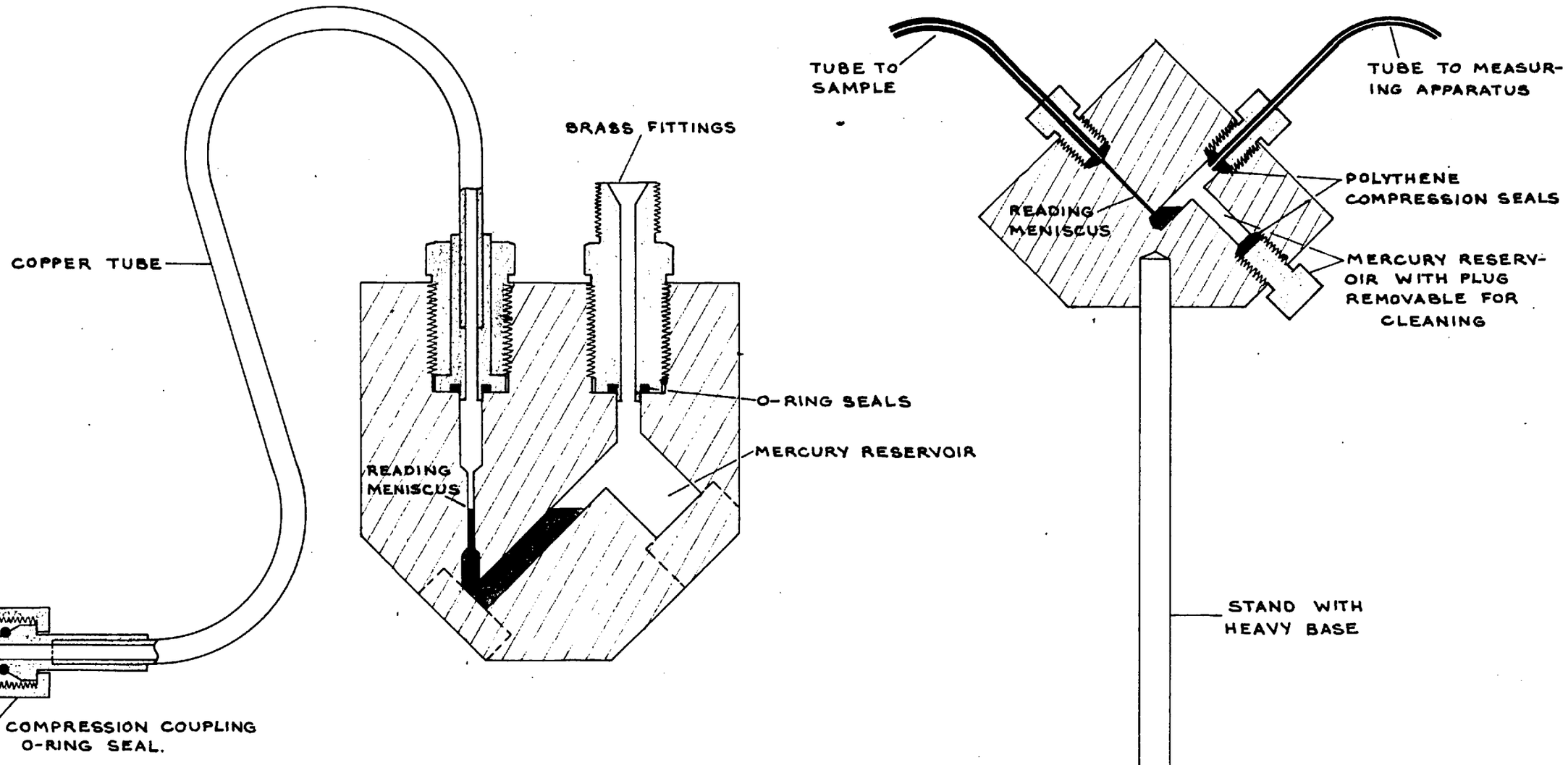
LAYOUT OF APPARATUS FOR TRIAXIAL TESTS ON PARTLY SATURATED SOILS.

FIG. 2.1.



PARAFFIN-TYPE VOLUME GAUGE.

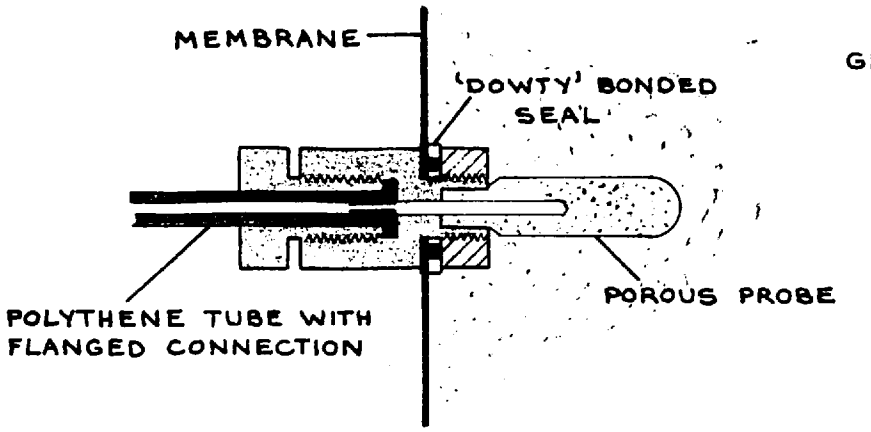
FIG. 2.2.



SECTIONAL VIEWS OF NULL-INDICATORS.

FULL SIZE.

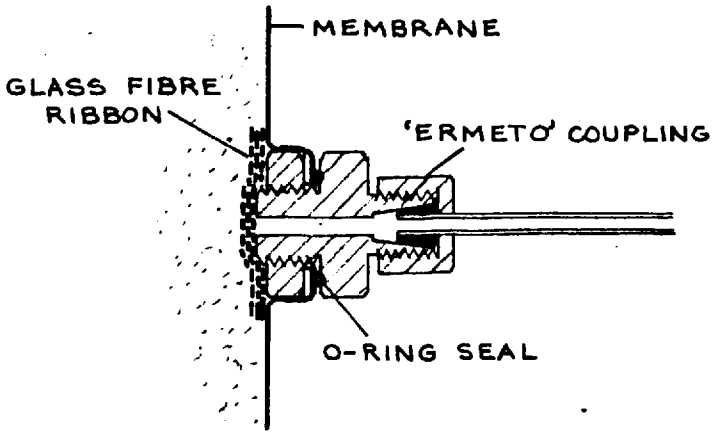
FIG. 2.3.



PORE WATER PRESSURE PROBE

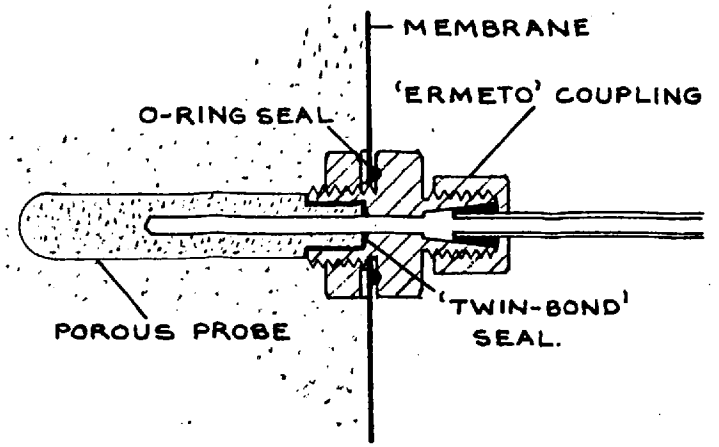
FOR 1½" DIA. SAMPLE

2X FULL SIZE.



PORE AIR PRESSURE CONNECTOR

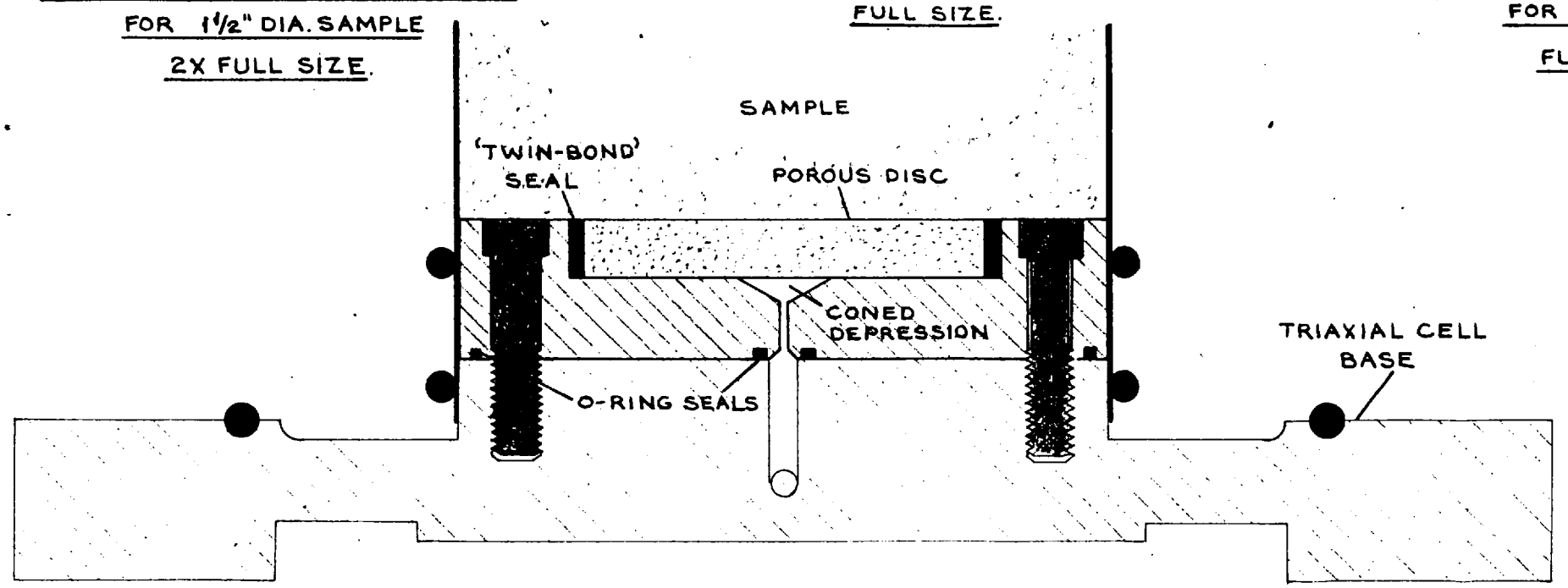
FULL SIZE.



PORE WATER PRESSURE PROBE

FOR 4" DIA. SAMPLE.

FULL SIZE.

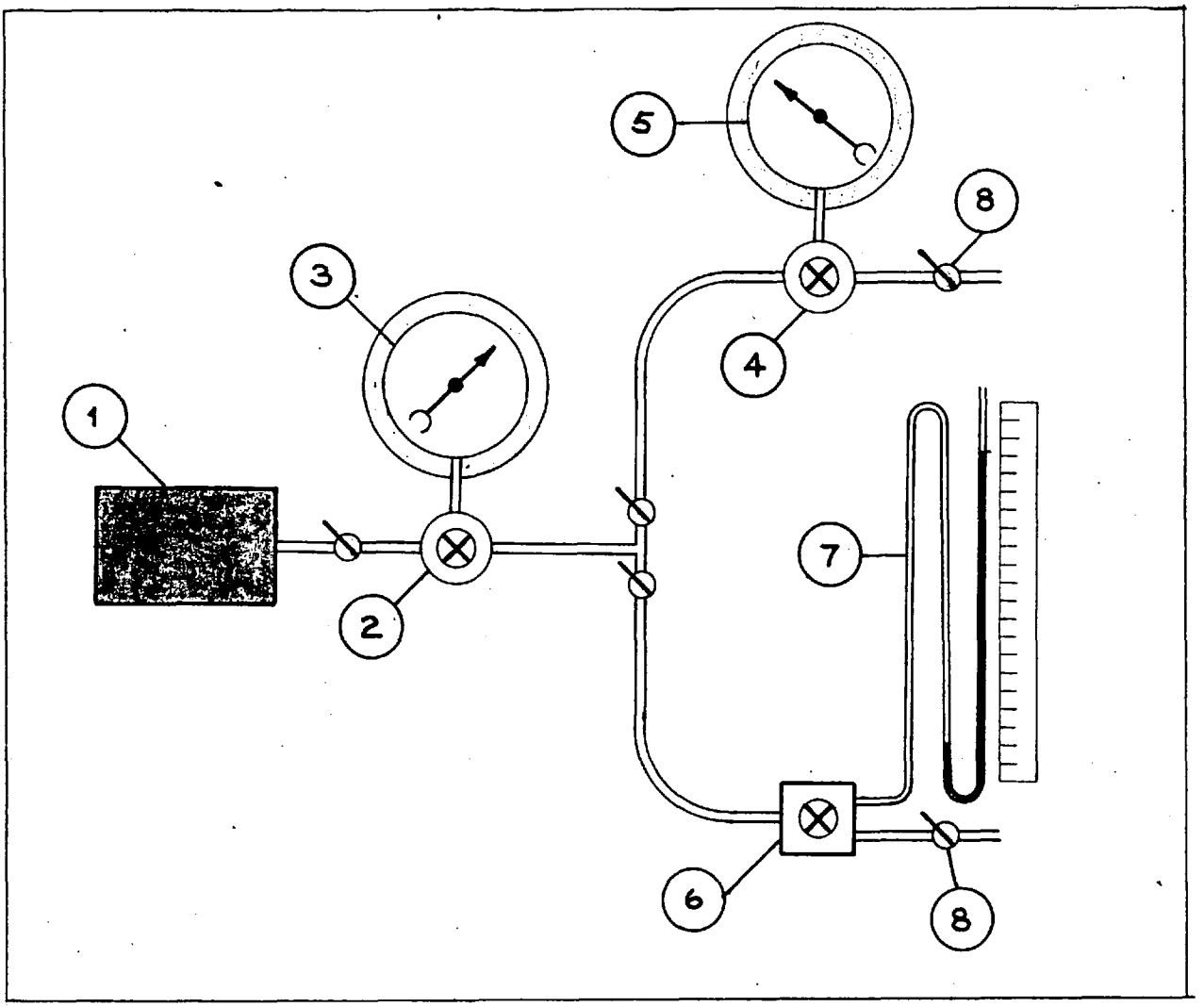


BASE POROUS DISC FOR 4" DIA. SAMPLES.

FULL SIZE.

MOUNTING OF POROUS ELEMENTS.

FIG. 2.4.



1	COMPRESSOR 110 – 140 P.S.I.
2	1ST DIAPHRAGM CONTROL VALVE ±2 P.S.I.
3	PRESSURE GAUGE 0–150 P.S.I.
4	2ND DIAPHRAGM CONTROL VALVE ± ·3 P.S.I.
5	PRESSURE GAUGE 0–100 P.S.I.
6	CONSTANT LEAK CONTROL VALVE ± ·1 P.S.I.
7	MERCURY MANOMETER 0–25 P.S.I.
8	VALVES LEADING TO SAMPLES.

DIAGRAM OF LAYOUT OF PORE AIR PRESSURE CONTROL SYSTEM.

FIG. 2.5.

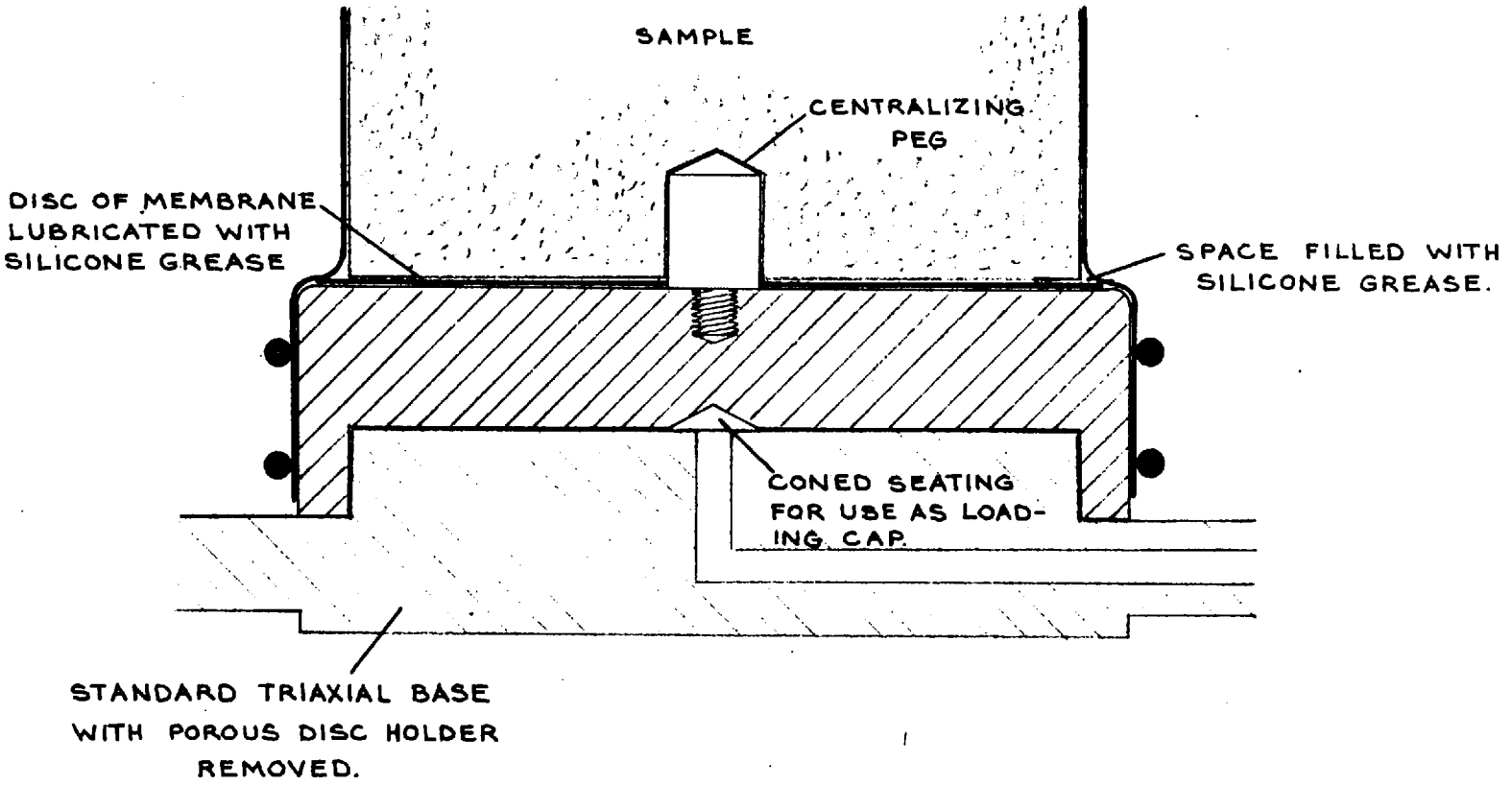


FIG. 2.6.

LUBRICATED END PLATES.

CHAPTER 3

TECHNIQUES OF PORE PRESSURE MEASUREMENT AND CHARACTERISTICS OF POROUS ELEMENTS

This thesis is almost wholly concerned with the estimation of effective stresses in saturated and partly saturated soils. As no method has yet been devised to measure effective stresses directly, they can only be inferred from measurements of total stress and pore pressure and the effects of these stresses on certain properties of the soil which can be shown to be wholly dependent on the effective stress in the soil skeleton.

The main soil property which is purely dependent on effective stress and which will be studied in future chapters is the deviator stress in the triaxial test: $(\sigma_1 - \sigma_3)$. Because the deviator stress is the difference between two total stresses each involving the same pore pressure, it is itself an effective stress.

The other soil property which is purely dependent on effective stress is that of volume change. The relation between volume change and effective stress will also be considered in a later chapter.

The measurement of deviator stress, volume change and total stress is relatively straight forward and well established in Soil Mechanics practice. The measurement of positive pore water pressures in saturated soils is also generally understood and relatively simple. Methods for measuring negative pore water pressures in saturated soils and pore water and pore air pressures in partly saturated soils are relatively new in Soil Mechanics and methods for their measurement are still being developed.

The experimental work which is to be described in later chapters depends entirely for its validity on accurately measured reliable pore air and water pressures. The techniques of measurement which have been used and the properties of the measuring apparatus will now be described in detail.

(3.1) Measurement of pore water pressures in partly saturated soils.

The essential elements of any pore water pressure measuring system are as follows:

(a) A porous element which enables the water in the measuring system to communicate with the pore water in the soil.

(b) An indicator ("null indicator") to show whether water is entering or leaving the soil.

(c) A method of applying controlled pressures (above or below atmospheric pressure) to the water in the measuring system.

(a) The porous element.

In the measurement of pore water pressures in a partly saturated soil, the most important component of the measuring system is the porous element. To maintain communication between the pore water and the water in the measuring system, the porous element must always remain completely saturated. If the measuring system and the porous element are completely saturated and free from large air bubbles, and if no flow is allowed into or out of the system, the water in the system and porous element will come to equilibrium at the pressure of the water in the soil.

In a partly saturated soil the air and water which comprise the pore fluid will exist at pressure differences which can be very large. The air pressure will always exceed the water pressure and

hence will tend to drive the water out of the porous element. This tendency will be resisted by capillary forces at the surface of the porous element.

The maximum resisting pressure which can be mobilised at this surface is:

$$p''_{max} = 2T/r_{max}$$

T is the surface tension of the water. r_{max} is the equivalent radius of the largest continuous channel which passes right through the element. r_{max} will be referred to as the"maximum effective pore size". $2T/r_{max}$ represents the largest value of $(u_a - u_w)$ which can be measured by the porous element. If $(u_a - u_w)$ exceeds $2T/r_{max}$ air enters the porous element, replaces the water which is sucked up by the soil, and the measuring system loses contact with the pore water in the soil. Once this has occurred only pore air pressures will be registered by the measuring system. p''_{max} is commonly known as the "air entry value" of the porous element.

If the measuring system is not completely de-aired, the tubing connecting the null indicator to the porous element may become blocked by an air bubble. This is very likely to happen if the entrapped air bubble expands rapidly because the pressure in the pore water has dropped below atmospheric pressure. If this happens, contact with the soil water is again lost and pore water pressure readings become difficult to obtain and unreliable.

(b) Using the null indicator.

The process of measuring a pore water pressure consists in finding a balance between pressures applied through the measuring

system and the pressure in the pore water. The balance is found as follows:

The pore water pressure is estimated and this value is set in the measuring system. The valve between the measuring system and the porous element is opened and the level of the mercury in the null indicator is observed to see whether water is entering or leaving the soil through the porous element.

If water is leaving the soil, the set pressure is too low and a higher pressure is tried (and vice-versa).

This trial and error procedure is repeated until the direction of flow can be reversed by equal slight alterations of the set pressure about a mean value.

Suppose:

u_{w1} is just too low
and u_{w2} is just too high
} then the estimated pore water pressure is $\frac{1}{2}(u_{w1} + u_{w2})$.

The interval $(u_{w2} - u_{w1})$ can be made as small as accuracy requires. In this thesis $(u_{w2} - u_{w1})$ was taken as 0.2 p.s.i. giving a reading accuracy of $\pm$ 0.1 p.s.i.

The permeability of the porous element is invariably much greater than that of the soil and the flow of water into or out of the measuring system is therefore controlled by the permeability of the soil. Because of this, movement of the mercury meniscus in the null indicator is very, very slow and must be observed through a cathetometer particularly when the pressure difference causing flow is only 0.1 p.s.i.

The pore water pressure in the soil can only be balanced by a pressure applied through the measuring system provided that:

(i) the air entry value of the porous element is not exceeded.

(ii) the pore water pressure does not fall below -1 atmosphere.

If the pore water pressure does fall below -1 atmosphere cavitation will usually occur in the measuring system even if it is well de-aired. The effect of cavitation is the same as that of exceeding the air entry value of the porous element.

It must be emphasized that any sudden movement of the null indicator which is observed on opening the valve between the measuring system and the porous element may be no indication of flow into or out of the soil. Even if the estimated pore pressure is correct, movement may be caused by a slight pumping action of the valve. If the estimate is incorrect a movement may be caused by elasticity in the seating of the porous element or even by the expansion or compression of small bubbles under the porous element. With a completely de-aired measuring system it should be possible to alter the set pressure by 10 p.s.i. either way without any observable instantaneous change of level in the null indicator.

(3.2) Response times in reading pore water pressures.

The response time of a pore water pressure measuring system is inversely proportional to the smallest quantity of flow which can be observed as a change in level of the null indicator. As the rate of flow is governed by the permeability of the soil at a given flow gradient, the only means of improving the response times are:

(i) by the use of increasingly sensitive null indicators, or

(ii) by increasing the collecting area of the porous element.

In the mercury-filled capillary tube type of null indicator the sensitivity can be increased by decreasing the bore of the

capillary. The capillary cannot be made too small or else surface tension effects become too pronounced. Also, unless the bore of a small capillary is perfectly clean and smooth, the mercury clings to the walls and gives an irregular meniscus. One way of increasing the sensitivity is to use a cathetometer to observe changes in level of pin-points of light reflected off the meniscus by suitably placed lights.

The maximum collecting area which can be used is usually dictated by considerations of the overall dimensions of the apparatus and sample.

(3.3) De-airing the measuring system and practical hints.

The most efficient method of de-airing both porous element and measuring system is by solution of the air in de-aired water under pressure.

The method used for de-airing was as follows:

The triaxial cell was filled with de-aired water and put under a high pressure (140 p.s.i.). The mercury in the null-indicator was lowered from the measuring capillary of a glass tube type null indicator or tipped into the bypass reservoir of a perspex null indicator. The bulk of the air was now removed from the porous element and measuring system by flushing through with water from the cell under a high flow gradient, the water passing through the porous element and measuring system and out past the ram to a beaker of free water.

When no more air would emerge using this method, the valve leading to atmosphere was closed and the pressure in the system was allowed to build up to the pressure in the cell. The system

was usually left under pressure over night to dissolve all remaining air.

The system was now flushed through again to remove water containing dissolved air and, shutting off the pressure supply from the oell, the cell pressure was allowed to dissipate to zero by flow through the porous element and out to atmosphere.

The completeness of the de-airing could be checked in two ways:

(i) With the valve leading to the porous element shut and with the mercury level raised in the null indicator, the ram was used to raise the pressure in the measuring system to 100 p.s.i. The system was left for about 15 minutes. If the pressure had not dropped off in this period and if the rise in the meniscus of the null indicator did not exceed $^1/_{10}$", the pressure was lowered to zero. If the rise in mercury meniscus was now reversed, it was known that the measuring system was completely de-aired and that the valves did not leak.

(ii) With the cell removed and excess water wiped from the surface of the porous element, a small suction (about 1 p.s.i.) was applied. When the meniscus of the null indicator came to rest, the suction was suddenly increased to -10 p.s.i. If the meniscus of the null indicator did not move appreciably, the system and porous element were completely de-aired.

It was found necessary to de-air the apparatus after every test. Even though no gaseous air passes through the porous element, there is always a high concentration and pressure gradient between

the pore air and the de-aired water on the other side of the porous element. This causes air to pass through the porous element in solution. If the pore water pressure is subsequently decreased, this air reappears as bubbles which rapidly expand if the pore water pressure drops very much below atmospheric pressure.

For this reason it is a good practice to adjust the pore air pressure to a value high enough to ensure that the pore water pressure never drops below atmospheric pressure, and preferably remains above + 10 p.s.i. In any case, between readings, the measuring system should be isolated from the porous element and kept under a positive pressure (at least +10 p.s.i.). This prevents the formation of air bubbles in the measuring system due to slight leakage under vacuum or inward diffusion of air from the atmosphere through the plastic tubing.

Commercial detergents are commonly used to clean apparatus between tests. One of the properties of detergents is that even a minute concentration will greatly decrease the surface tension of water. (e.g. a 0.01% by weight concentration of "Teepol 500" reduces the surface tension of water from 72.0 to 43 dynes/cm). Hence if water containing traces of detergent is used to de-air a porous element, the value of $p''_{max} = 2T/r_{max}$ may suddenly be reduced by half. Great care must be taken to keep all traces of detergent well away from porous elements.

(3.4) Characteristics of porous ceramic materials.

Materials used as porous elements for pore water pressure measurement should possess the following characteristics:

(i) Adequate mechanical strength both to support direct loading when set into loading plates and to take fairly rough

handling when used as rather slender probes.

(ii) A high air entry value and uniform pore size.

(iii) Reasonably high permeability and porosity.

Four types of ceramic were used in the investigations of this thesis: For fairly low values of $(u_a - u_w)$ two commercial products were used ("Aerox Celloton VI" and "Doulton P6A"). These materials did not have air entry values adequate for the purposes of this thesis and hence it was necessary to produce some more satisfactory materials in the laboratory.

The strength of these ceramic materials seems to be quite adequate and no breakages either under load or during handling were suffered.

(a) Air-entry value and drainage characteristics of porous ceramics.

The air entry value was measured by means of the so-called "blow-through" test.

The porous disc to be tested was sealed into the metal holder described in Chapter 2 and screwed in place to the base pedestal of a triaxial cell. The duct leading from the underside of the disc was connected to an open graduated burette.

After thoroughly de-airing the disc and the duct leading to the burette and removing the triaxial cell, the surplus water was wiped from the surface of the disc, the water in the burette was lowered to a convenient level and the triaxial cell was replaced empty.

A small air pressure was now put into the cell and readings of the water meniscus in the burette were taken until drainage from the disc had ceased. The air pressure was then increased in stages,

allowing ample time at each stage for the disc to drain. The air pressure was increased until a "non-terminating" drainage began and the air forced the water from the pores of the disc and "blew through".

Fig. (3.1) shows the drainage characteristics of four ceramic materials. The large initial drainage is mainly of surplus water left on the surface of the disc before starting the test.

Fig. (3.2) shows some typical drainage-time curves for a ceramic disc - both the terminating drainage before the air-entry value is reached and also the non-terminating drainage when the air entry value is reached.

The maximum effective pore size of the material can be calculated from:

$$r_{max} = \frac{2T}{p''_{max}}$$

A material with a very uniform pore size is more satisfactory for this type of work than one with graded pore sizes. The air entry value is governed by the diameter of the largest channel or void which completely penetrates the disc. Even if the larger voids do not completely penetrate the disc they will drain before the air entry value is reached. This will cause a deterioration in response time due to the decreased area of communication of the water in the porous element with the pore water. Irregularity in pore size will be shown up by the terminal drainage characteristic of the material (see fig. (3.1)). The ideal material should not drain at all until the air entry value is reached.

(b) Permeability and porosity of porous ceramics.

The permeability of these materials is generally rather low and decreases rapidly with increasing air entry value.

Permeability curves for several materials are shown in fig. (3.3). These were measured during the de-airing stage of the "blow through" tests illustrated in fig. (3.1).

The porosity of a porous material can be looked upon as a measure of uniformity of pore size. Aggregates composed of particles of graded size generally have lower porosities than those composed of particles of uniform size. The maximum porosity of an aggregate of open packed single sized spheres is 47.6%. Porosities much greater or less than this in a porous ceramic will probably indicate a non-uniform pore size distribution.

(c) Typical properties of porous ceramics.

The following table summarises the results of the writer's tests on porous ceramics.

Material	Air entry value p.s.i.	Maximum effective pore diameter microns	Permeability cm/sec	Porosity %
Doulton Grade P6A	22	1.7	2.12×10^{-7}	23.2%
Aerox Celloton Grade VI	31	1.4	2.93×10^{-6}	46.4%
Slurried Consolidated Kaolin	46	0.9	6.19×10^{-8}	44.7%
Dust Pressed Kaolin	76	0.54	4.54×10^{-8}	39.0%

(d) Ageing.

The properties of a porous ceramic saturated with water change appreciably with time. The permeability decreases noticeably while the air entry value increases. For example, over a period of about 6 months continual use, the air entry value of the slurried consolidated kaolin disc increased from 46 p.s.i. to above 63 p.s.i. Part of this change is probably because the surface of the disc gradually becomes impregnated with clay. It might also be due to a slow swelling of the china skeleton. In the first few hours after saturating a new disc, the permeability decreases so rapidly that it is not possible to establish a linear relation between hydraulic gradient and permeability.

(3.5) Production of porous ceramic materials.

As materials could not be obtained commercially which had a sufficiently high air entry value, it was decided to attempt to produce the required material from powdered kaolin in the laboratory.

The particle size distribution of the kaolin is shown in fig. (3.4).

As a first attempt, the kaolin was mixed with water to form a slurry, and then consolidated in the oedometer to a pressure of 180 p.s.i. The discs were then removed and air dried very slowly in a closed drawer. When air dry, the discs were fired.

This procedure was unsatisfactory because of the large shrinkage which took place on air drying and firing. Only one sound, crack free disc was produced out of a total of 12. The properties of this disc were very satisfactory and it was used successfully for several months.

Apart from the shrinkage problem this method produced a very

laminated structure due to shear planes which formed in the wet kaolin during consolidation.

Various ways were tried to reduce the shrinkage but without any success. Finally it was decided to try dust pressing under high pressures. A special oedometer was made from mild steel and the powdered kaolin was compressed in a Buckton testing machine to a load of several tons on a 3" diameter area. This procedure reduced shrinkage but still produced a granular, weak structure. This was finally eliminated by sieving the kaolin through a 200 mesh sieve before compressing.

The best compression load appeared to be 7 tons on a 3" diameter disc (2300 p.s.i.). Lower pressures than this produced a weak material while higher pressures caused the development of shear planes.

The most satisfactory method of firing was as follows:

The temperature was raised from 0 to 200°C over a period of 8 hours and maintained at 200°C overnight. The following day it was raised gradually to 1200°C over an 8 hour period. The temperature was then slowly lowered, the cooling occupying about 24 hours.

This procedure produced consistently good discs with very few failures due to cracking. The maximum effective pore size measured for a disc produced by this method was equal to the 46% size of the particle size distribution. (See section (3.4)c).

(3.6) Measurement of pore air pressures.

A porous element used for measuring pore air pressures must have properties which are the opposite of those required for measuring pore water pressures. Air must be able to pass freely through its

pores, and if it does not actually repel water, it should not absorb much water. If, during a test, it does become saturated, it should drain again at a negligible suction.

The material used in this thesis was a coarsely woven ribbon of glass fibre cloth. The air dry moisture content of the ribbon was 0.18% while the saturation moisture content was 55%. The moisture content of the ribbon usually increased during the course of a test to about 2%.

The principles of pore air pressure measurement are very similar to those used to measure pore water pressures. The measuring system is water filled up to the mercury column of the null indicator. From beyond the mercury column an air filled lead communicates with the porous element which is in contact with the soil.

Since air is a compressible fluid and the measuring system has constant volume, before a pressure change can be registered, air must flow into or out of the measuring lead. For this reason, to reduce time lags to a minimum, the measuring lead must be designed with as small a volume as possible.

If pore air pressures are to be controlled, the null indicator is replaced by a pressure control valve and the porous element distributes the air supply to the pores of the soil.

(3.7) Air diffusion through latex rubber membranes.

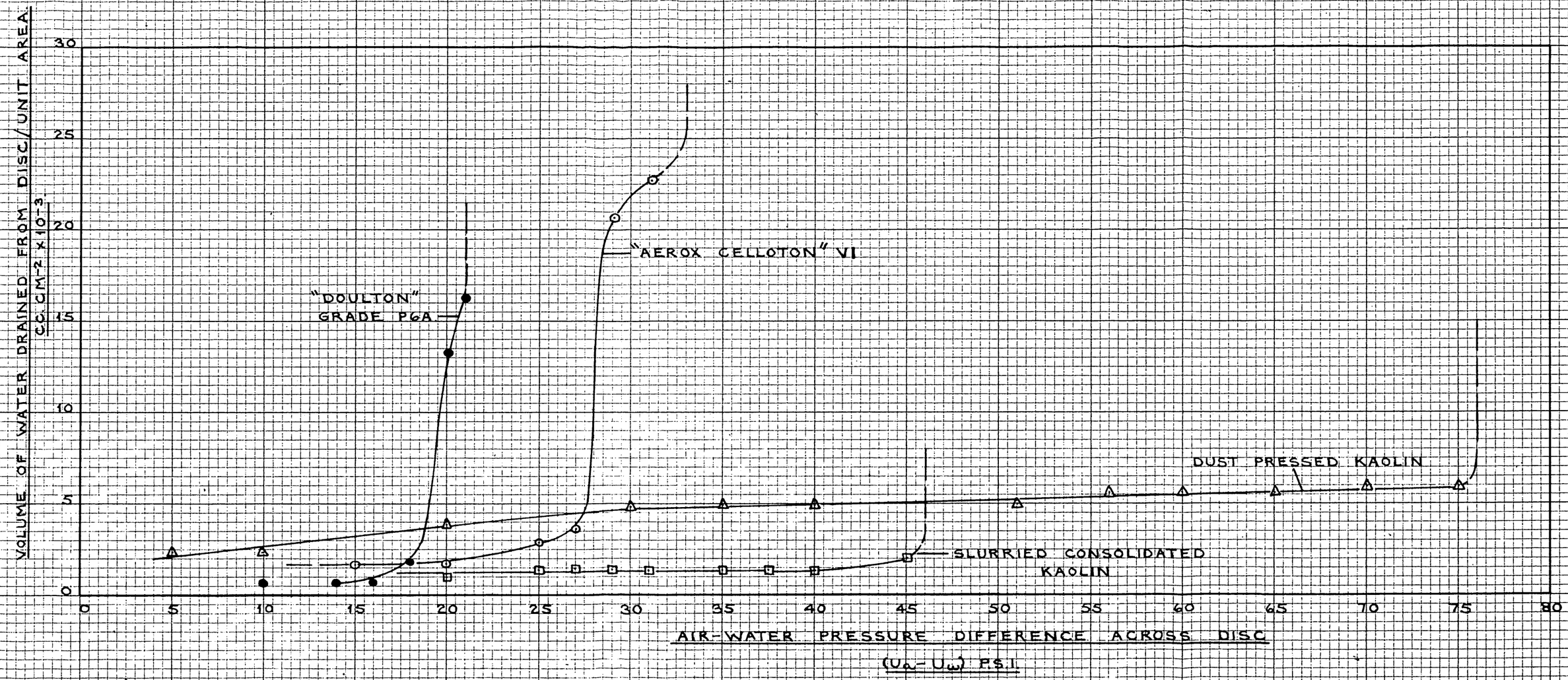
One of the difficulties encountered in measuring pore air pressures in partly saturated soils is that the latex rubber membranes which are commonly used in triaxial testing are permeable to air. As the concentration of dissolved air in the cell water is usually well below that in the soil, there is a progressive loss of air from the

sample to the cell water. Consequently, the pore air pressure is gradually reduced.

Fig. (3.5) gives an illustration of this effect. A $1\frac{1}{2}$" diameter hollow ceramic filter candle was set up as a dummy sample in a triaxial cell. A latex rubber membrane was used to enclose the sample in the usual way. The cell was filled with water at 38 p.s.i. and an air pressure of 28.4 p.s.i. was put into the hollow sample which was then connected to a null indicator. The variation of the internal air pressure with time was studied. Fig. (3.5) shows the percentage changes in air pressure. After 3 weeks the cell pressure was reduced to 20 p.s.i. and the air pressure gradually rose again showing that air was migrating back from the cell water to the sample.

This experiment was repeated except that, before putting on the membrane, the dummy sample was wrapped in a single layer of household aluminium foil which was sealed using P.V.C. insulating tape. The rate of air loss in this second test was much reduced.

These experiments showed that serious losses in pore air pressure can be caused by migration of air through the rubber membrane and showed that completely undrained tests on partly saturated soils cannot be performed unless special precautions are taken to prevent air losses.



DRAINAGE CHARACTERISTICS OF FOUR POROUS CERAMIC MATERIALS

FIG. 3.1.

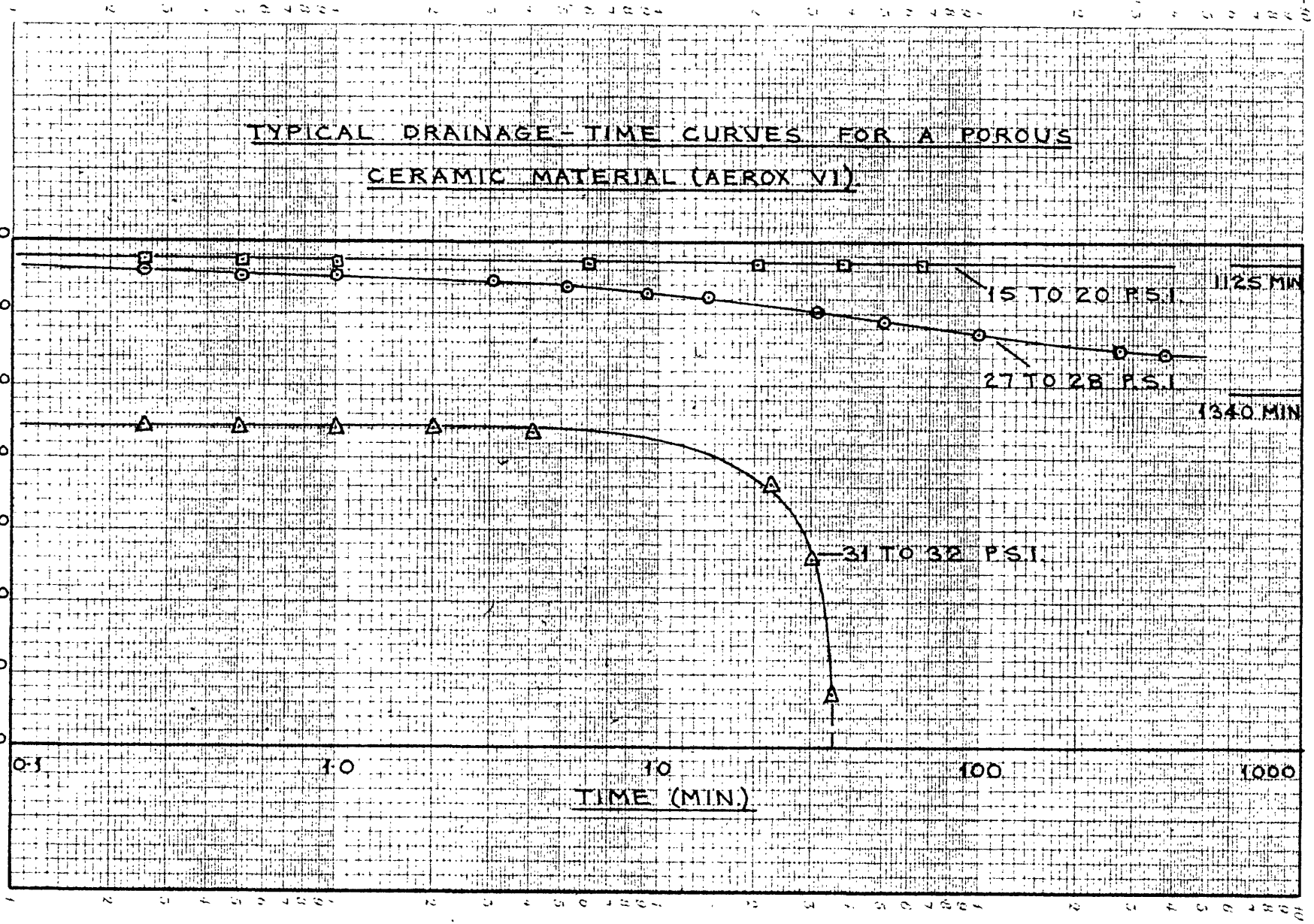
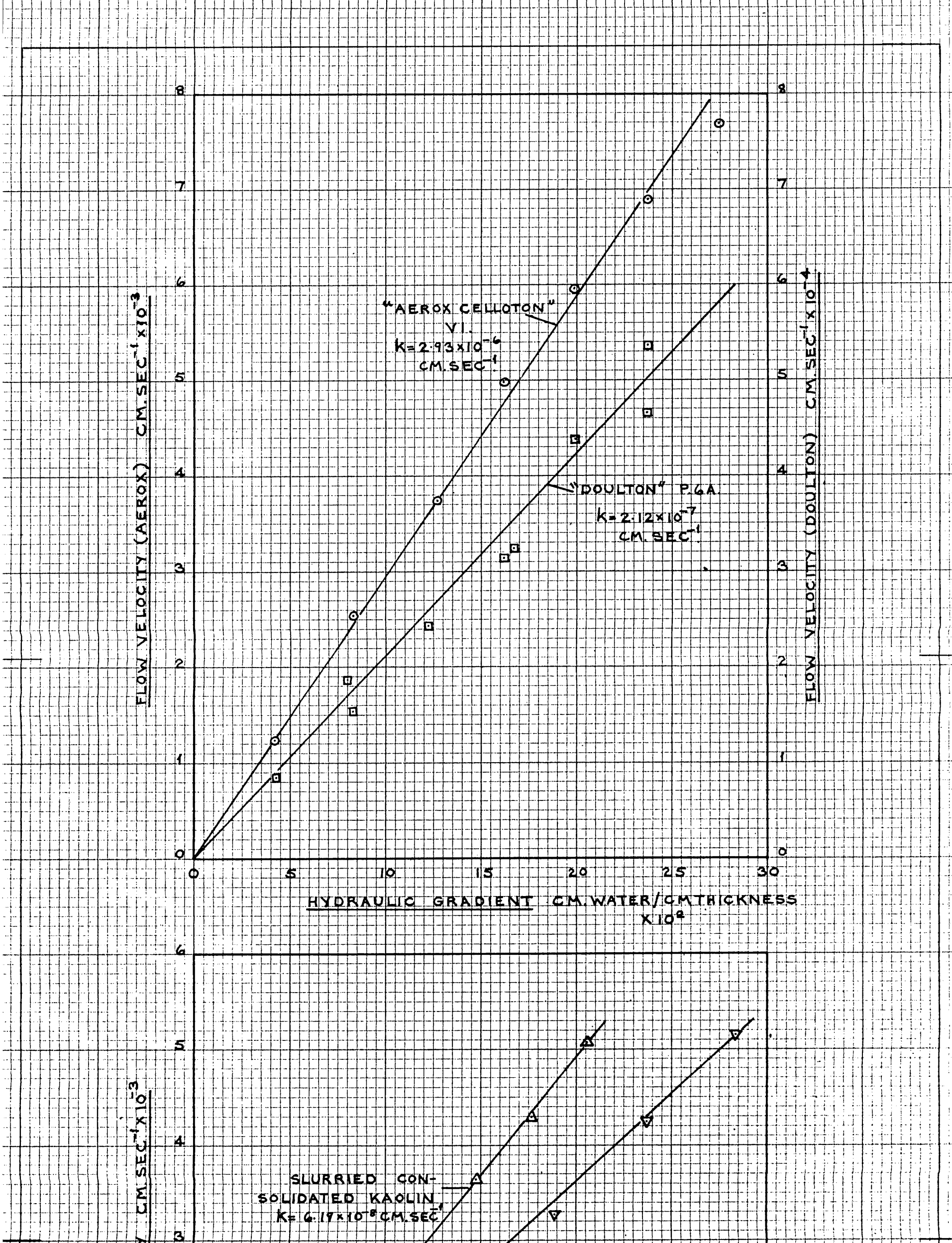
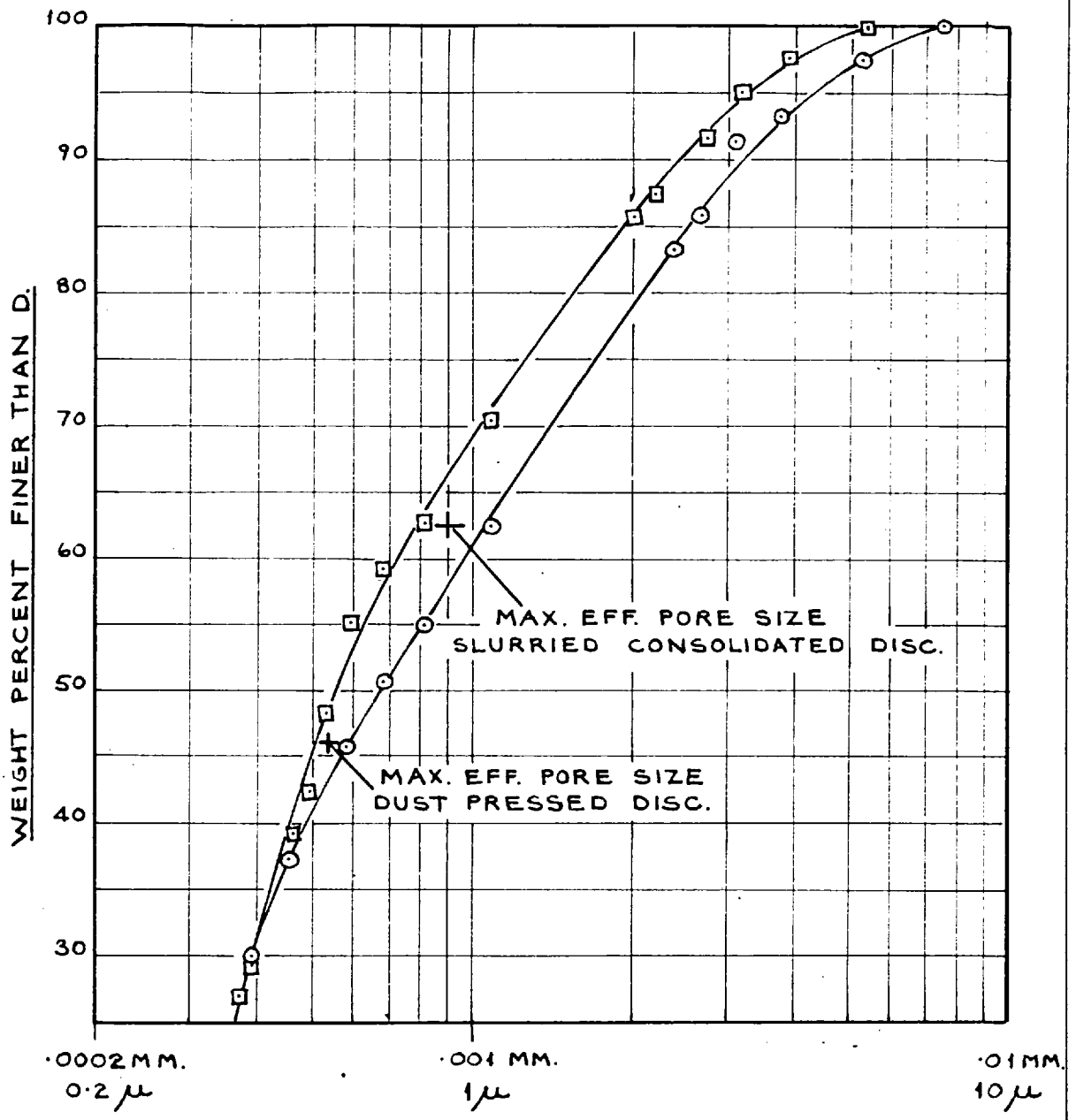

TYPICAL DRAINAGE - TIME CURVES FOR A POROUS CERAMIC MATERIAL (AEROX VI).
VOLUME OF WATER DRAINED/UNIT AREA OF DISC. CC. CM⁻² x 10⁻³
0
10
20
30
40
50
60
70
15 TO 20 P.S.I.
1125 MIN
27 TO 28 P.S.I.
1340 MIN
31 TO 32 P.S.I.
0·1
1·0
10
100
1000
TIME (MIN.)

FIG. 3.2.



WATER PERMEABILITY OF FOUR POROUS CERAMIC MATERIALS.

FIG. 3.3.



PARTICLE SIZE ANALYSIS OF KAOLIN USED FOR POROUS CERAMIC DISCS.

FIG. 3.4.

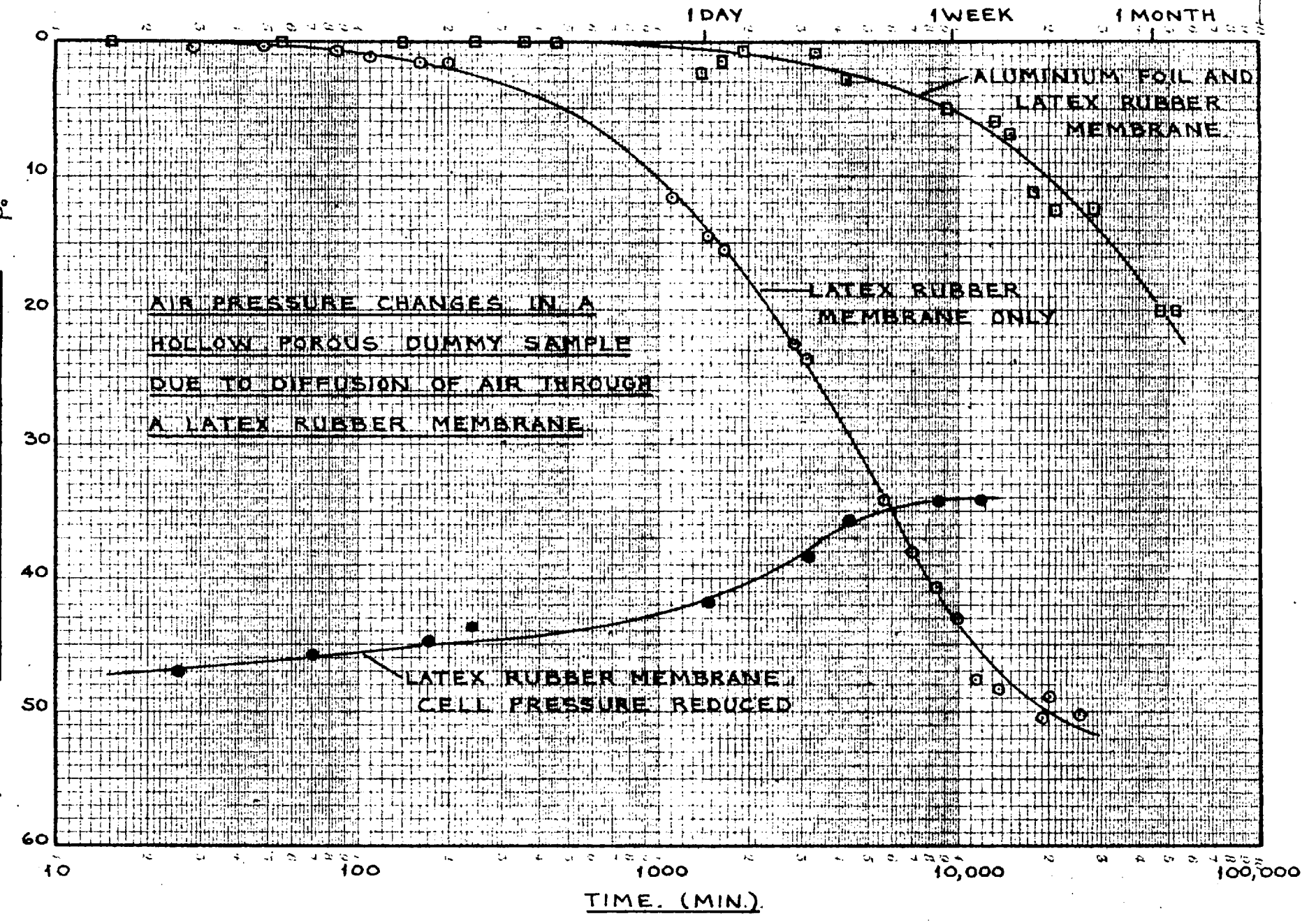

1 DAY
1 WEEK
1 MONTH
0
10
20
30
40
50
60
GAUGE AIR PRESSURE DROP $\frac{P_0-P}{P_0}$ %
ALUMINIUM FOIL AND LATEX RUBBER MEMBRANE
LATEX RUBBER MEMBRANE ONLY
AIR PRESSURE CHANGES IN A HOLLOW POROUS DUMMY SAMPLE DUE TO DIFFUSION OF AIR THROUGH A LATEX RUBBER MEMBRANE
LATEX RUBBER MEMBRANE, CELL PRESSURE REDUCED
10
100
1000
10,000
100,000
TIME. (MIN.)

FIG. 3.5.

CHAPTER 4

DESCRIPTIVE SOIL PROPERTIES

The following are brief descriptions of the various soils used in this investigation.

(4.1) Mangla shale.

The Mangla shale is a material from the site of the Mangla dam in West Pakistan. It consists of a hard sun-dried shale-like material, fawn in colour, which breaks down slowly on wetting to form a silty clay.

The particle size distribution curve is shown in fig. (4.1).

The index properties of the soil are:

Specific Gravity	:	2.79
Liquid Limit	:	38.2%
Plastic Limit	:	21.6%

Standard Proctor compaction curves for the soil are shown in fig. (4.2).

The slabs of dried shale were crushed in a jaw crusher to pass an $\frac{1}{8}$ inch sieve before wetting. The movement of the compaction curve records the slow breakdown of the uncrushed fragments of soil after wetting.

(4.2) Talybont clay.

The Talybont clay is a sandy boulder clay, reddish brown in colour, from the site of the Talybont dam in South Wales.

The grain size distribution is shown in fig. (4.1) while the compaction curve (for compaction in a 4" diameter x 8" high mould) is shown in fig. (4.2).

The specific gravity of the soil is 2.69.

(4.3) Selset clay.

The Selset clay is a dark grey boulder clay from the site of the Selset dam in Yorkshire.

The particle size distribution is shown in fig. (4.1) and the standard Proctor compaction curve is shown in fig. (4.2).

The index properties of the soil are:

Specific gravity	:	2.70
Liquid Limit	:	33.1%
Plastic Limit	:	16.6%

(4.4) Miscellaneous.

Limited use was also made of the following soils:

Vaich moraine : A well graded sandy moraine with negligible clay fraction.

London clay : From the stock of the laboratory at Imperial College.

Some properties of these materials are as follows:

		Vaich moraine	London clay
Specific Gravity	:	2.65	2.75
Liquid Limit	:	-	82%
Plastic Limit	:	-	29%

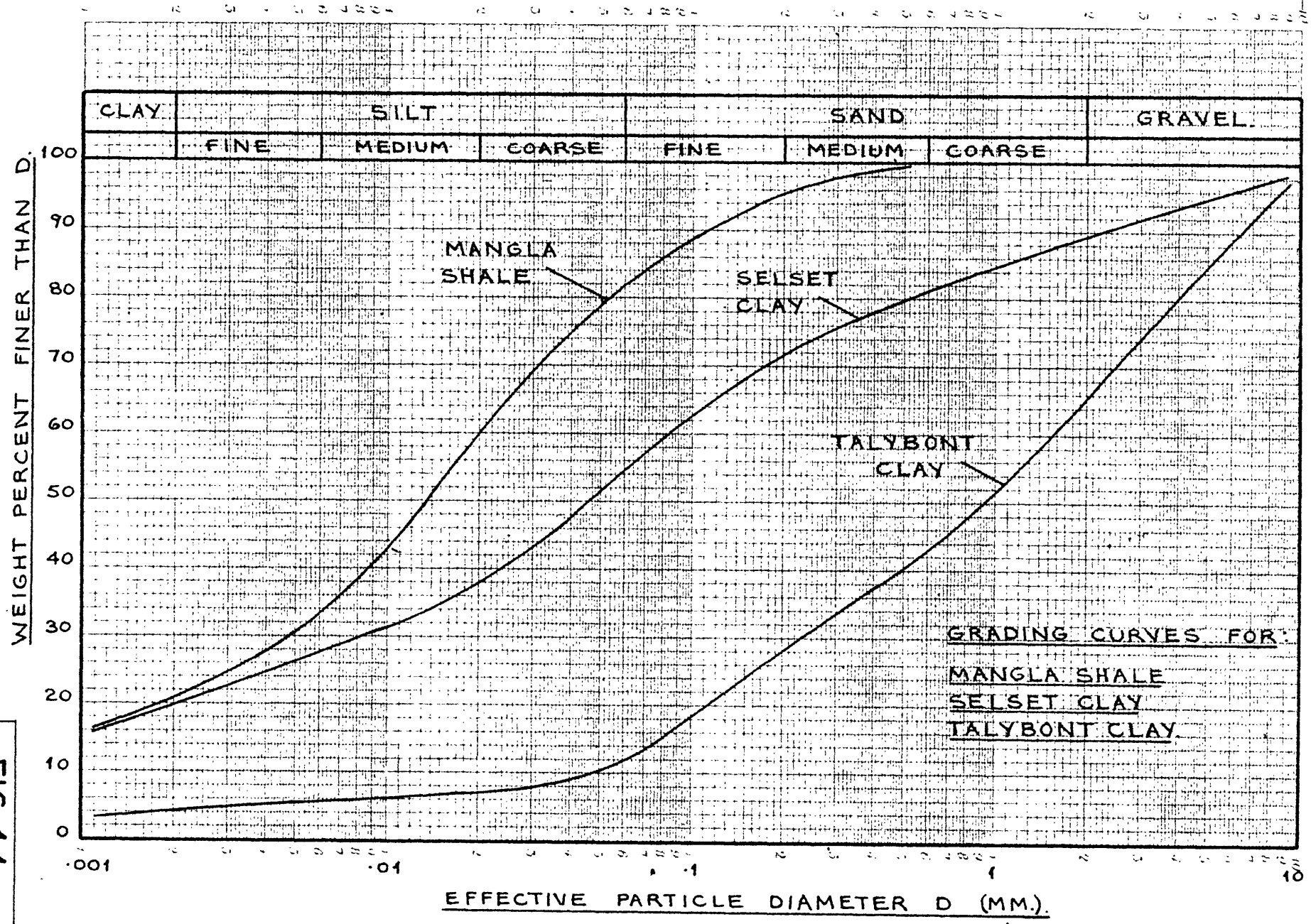
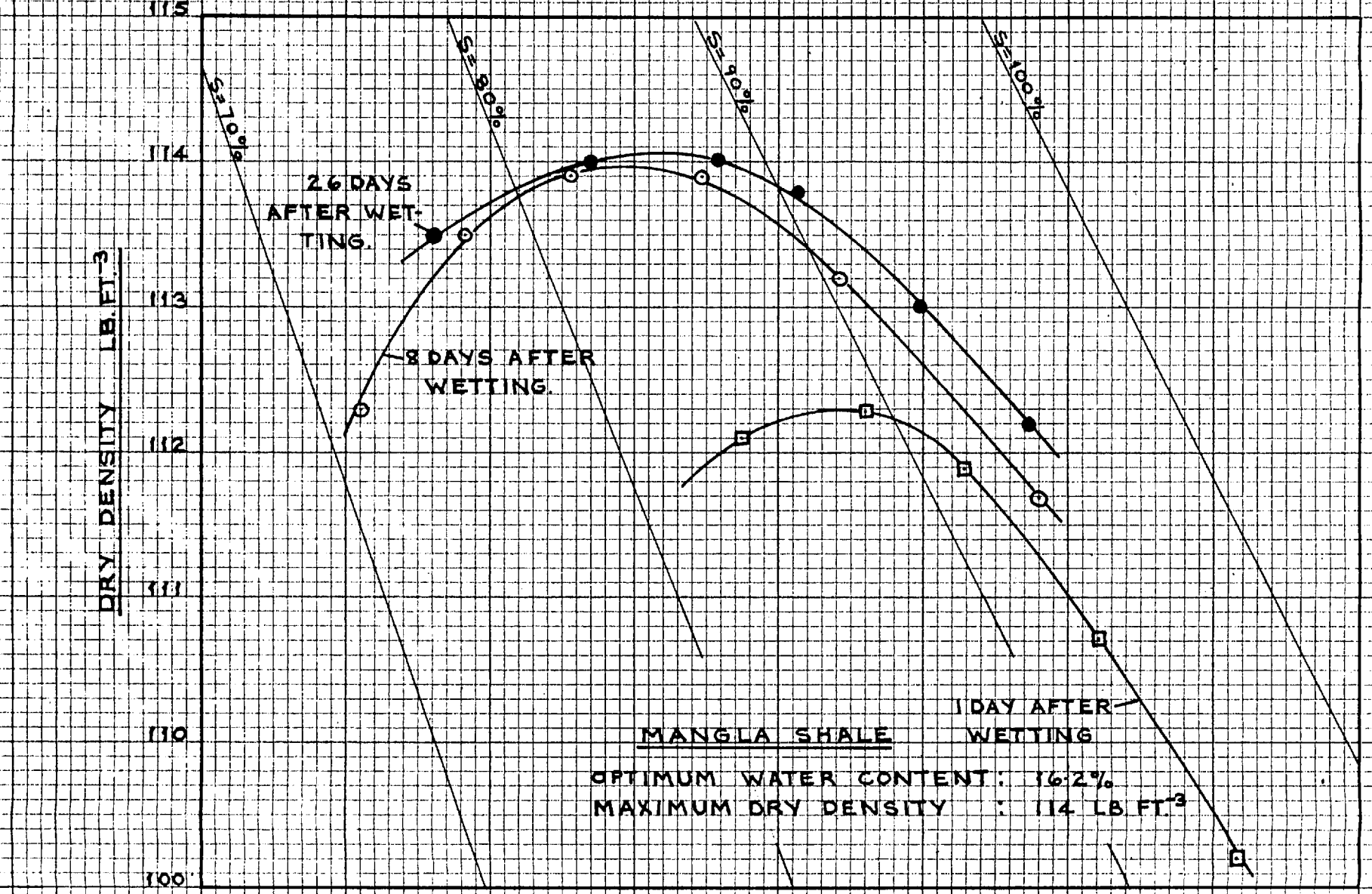
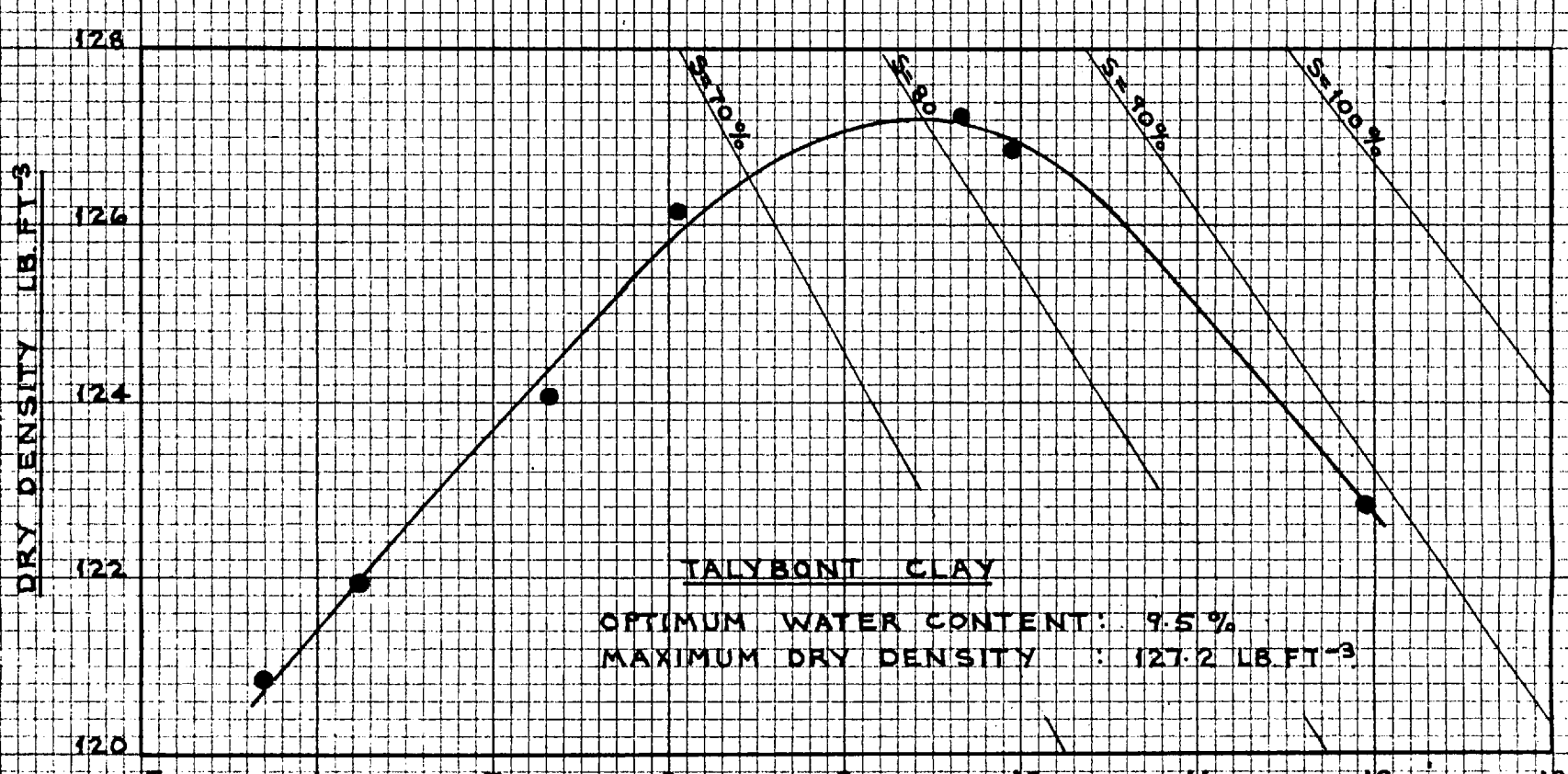
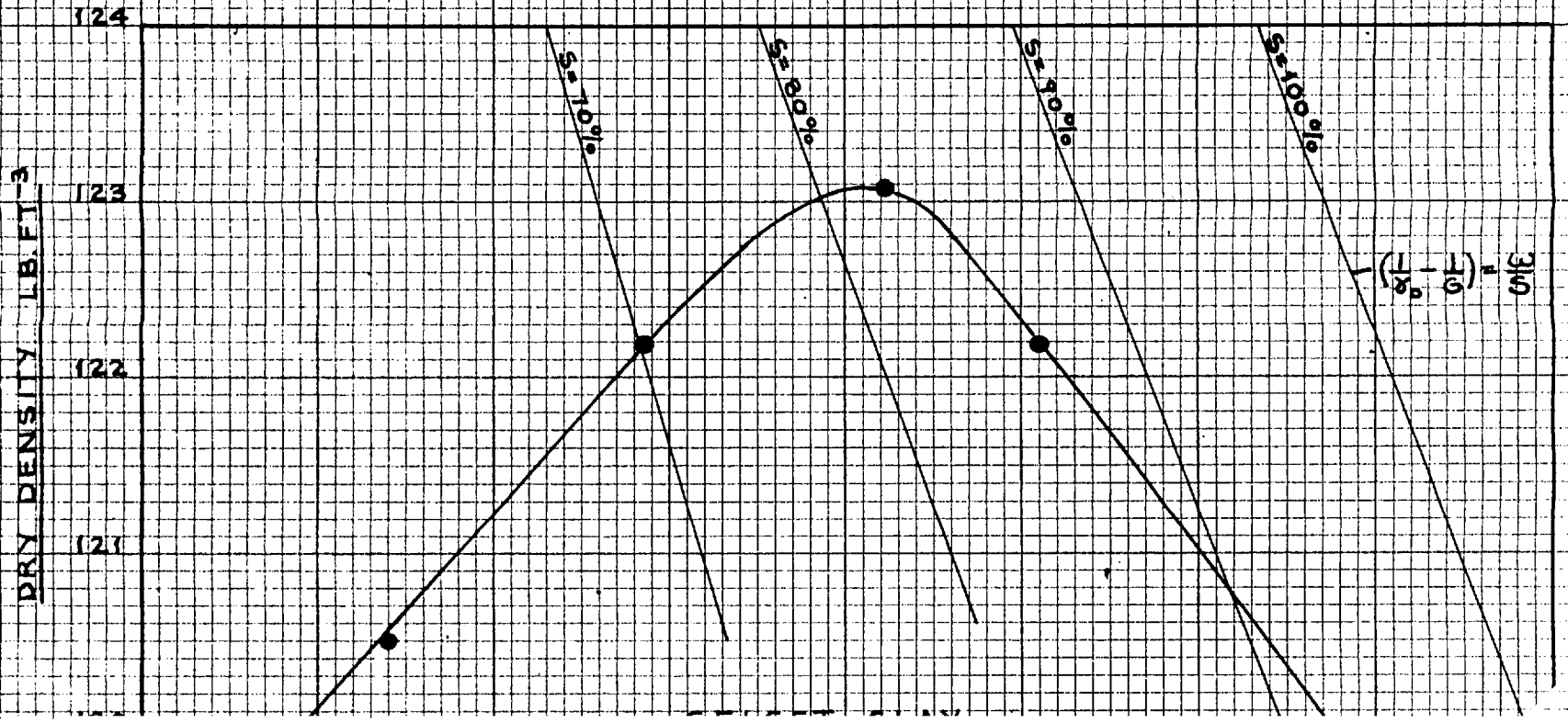

CLAY
SILT
SAND
GRAVEL
FINE
MEDIUM
COARSE
FINE
MEDIUM
COARSE
MANGLA SHALE
SELSET CLAY
TALYBONT CLAY
GRADING CURVES FOR:
MANGLA SHALE
SELSET CLAY
TALYBONT CLAY.
WEIGHT PERCENT FINER THAN D.
100
90
80
70
60
50
40
30
20
10
0
·001
·01
·1
1
10
EFFECTIVE PARTICLE DIAMETER D (MM.)

FIG. 4.1.


DRY DENSITY LB.FT.-3
115
114
113
112
111
110
100
13
14
15
16
17
18
19
20
21
MOISTURE CONTENT %
S=70%
S=80%
S=90%
S=100%
26 DAYS AFTER WETTING.
8 DAYS AFTER WETTING.
1 DAY AFTER WETTING
MANGLA SHALE
OPTIMUM WATER CONTENT: 16·2%
MAXIMUM DRY DENSITY : 114 LB FT.-3


DRY DENSITY LB.FT.-3
128
126
124
122
120
5
6
7
8
9
10
11
12
13
MOISTURE CONTENT %
S=70%
S=80
S=90%
S=100%
TALYBONT CLAY
OPTIMUM WATER CONTENT: 9·5 %
MAXIMUM DRY DENSITY : 127·2 LB FT.-3


DRY DENSITY LB.FT.-3
124
123
122
121
S=70%
S=80%
S=90%
S=100%
$\frac{1}{\gamma_d} - \frac{1}{G} = \frac{w}{S}$

CHAPTER 5

THE PRINCIPLES OF EFFECTIVE STRESS AND PORE PRESSURE MEASUREMENT IN PARTLY SATURATED COMPACTED SOILS

(5.1) A simple derivation of the principle of effeotive stress for a partly saturated soil.

It was noted in Chapter 1 that the form of the effeotive stress equation for a partly saturated soil put forward by Bishop is:

$$\sigma' = (\sigma - u_a) + \chi (u_a - u_w) \qquad E(5.1)$$

where χ is a parameter to be evaluated experimentally. In terms of E(5.1) the modified Coulomb failure criterion becomes:

$$\tau = c' + \left[(\sigma - u_a) + \chi (u_a - u_w)\right] \tan \phi' \qquad E(5.2)$$

where

c' is the apparent cohesion, ϕ' is the angle of shearing resistance — both in terms of effective stress.

χ is a parameter to be evaluated experimentally.

The value of χ will be unity for saturated soils and zero for completely dry soils. At any intermediate degree of saturation, values of χ can be expected to depend primarily on the degree of saturation, on the structure of the soil and possibly on the method of testing. Bishop has pointed out that the values of χ in the relationship between effective stress and shear strength need not necessarily be identical with those in the relationship between effective stress and volume change.

A derivation of E(5.1) will now be given in terms of a simplified geometrical concept of the structure of a partly saturated soil. (Shown in fig. (5.1)a).

The pore space of the soil is partly filled with water at a pressure u_w and partly filled with air at a pressure u_a. The air-water interfaces will be curved in three dimensions and because of the effect of the surface tension forces acting along these surfaces, the air and water will exist in equilibrium with u_a greater than u_w.

(It will be assumed that the soil grains are discreet and of inert mineral matter and that the water is "free" capillary water incapable of sustaining shear stress and able to transmit pressure equally in all directions).

Consider a surface passing through the soil which approximates to a plane, but passes always through the points of contact of the particles and the pore space and never intersects a particle. Two examples of such surfaces (A-A and B-B) are illustrated in fig.(5.1)a. In fig. (5.1)b is shown an enlarged detail of a typical grain to grain contact.

The areas of air, water and grain to grain contact (a, w and g respectively) intersected by surface A-A have been projected onto a plane A'A' which is closely parallel to A-A. There are assumed to be m contacts per unit area of plane A'A'. The normal forces between the grains are P inclined at angle α to the direction of the normal stress on A'A'. The tensile forces along the air-water interfaces are T inclined at θ to the normal to A'A'. The shear forces q are inclined at angle λ to the direction of plane A'A'.

For equilibrium normal to unit area of plane A'A'

$$\sum_1^m P \cos\alpha + \sum_1^m q \sin\lambda + u_a \sum_1^m a + u_w \sum_1^m w - \sum_1^m T \cos\theta = \sigma$$

The average intergranular stress on plane A'A' is:

$$\sigma'_i = \sum P \cos\alpha + \sum q \sin\lambda$$

$$\sigma'_i = \sigma - \left[u_a \sum a + u_w \sum w\right] + \sum T \cos\theta$$

Note that

$$\sum_1^m a + \sum_1^m w + \sum_1^m g = 1$$

hence

$$\sigma'_i = \sigma - \frac{1}{\sum a + \sum w + \sum g}\left[u_a \sum a + u_w \sum w\right] + \sum T \cos\theta \qquad E(5.3)a$$

Also by the principle of Dupuit (1863), the degree of saturation is given by:

$$S = \frac{\sum w}{\sum w + \sum a} \text{ and hence } (1 - S) = \frac{\sum a}{\sum w + \sum a}$$

Bishop (1959) has pointed out that there is no a priori reason why intergranular stress should be identical with effective stress. He has shown for a saturated system that volume changes due to deformation of the soil skeleton are independent of the grain to grain contact area g provided the compressibility of the individual grains is negligible. This has been confirmed experimentally by Laughton (1955). While there is no direct evidence that shear strength is independent of contact area, Bishop believed that this was a reasonable assumption.

Recently, Skempton (1960) has developed the following equation for the effective stress for shear in saturated porous materials:

$$\sigma' = \sigma - \left[1 - g\,\frac{\tan\psi}{\tan\phi'}\right] u$$

In this equation ψ is an intrinsic shear strength parameter for the material composing the grains, and ϕ' is the angle of shearing resistance of the porous material. Hence the effective stress depends on the magnitude of the term $g\,\frac{\tan\psi}{\tan\phi'}$. Skempton quotes typical values

of $\frac{\tan \psi}{\tan \phi'}$ for soils of between 0.3 and 0.15. He concludes that to justify the use of Terzaghi's equation ($\sigma' = \sigma - u$) in shear strength problems, the value of g must be assumed to be small.

Skempton's expression for effective stress changes accompanying volume change is:

$$\Delta\sigma' = \Delta\sigma - (1 - \frac{c_s}{c})\Delta u$$

Where

c_s is the compressibility of the solid particles.

c is the compressibility of the porous material.

Values of c_s/c for soils appear to be very small (0.001 to 0.00003). The conclusion is that, for volume change, the Terzaghi equation should be a close approximation.

Although $\sum g$ is probably very small compared with $(\sum a + \sum w)$, it cannot be zero as this would imply infinite contact stresses between the particles. Nevertheless, since $\sum g$ is small and since the effective stress for volume change is probably independent of $\sum g$ it is reasonable to make the following approximations in equation E(5.3)a:

$$\sum a + \sum w + \sum g = \sum a + \sum w$$

Average intergranular stress = $\sigma'_i = \sigma'$ = effective stress.

Hence:

$$\sigma' = \sigma - (1 - S)u_a - Su_w + \sum T \cos \theta$$

$$\text{or } \sigma' = (\sigma - u_a) + S(u_a - u_w) + \sum T \cos \theta \qquad \text{E(5.3)b}$$

Since the magnitude of both the forces T and of $(u_a - u_w)$ will be a function of S, we may write:

$$S(u_a - u_w) + \sum T \cos \theta = \chi(u_a - u_w)$$

Hence:

$$\sigma' = (\sigma - u_a) + \chi(u_a - u_w) \qquad \text{E(5.1)}$$

and $$\chi = S + \frac{\sum T \cos \theta}{(u_a - u_w)}$$

Hence for the idealised model which has been considered here χ is always greater than S.

(5.2) Theoretical relations between the χ factor and degree of saturation.

(a) Development.

Aitchison (1956, 1960) and Donald (1956, 1960, 1961) have used an idealised model of an unsaturated soil to calculate effective stresses from the geometry of the pore water and grain assembly. The model consists of zones of spherical particles of uniform size. Each zone consists of a particular size of sphere arranged in an ideal open or close packing.

Suppose the model soil is initially saturated. If the suction $(u_a - u_w)$ is gradually increased from zero, then as the air entry or drainage suction of each zone is reached, the zones will drain one by one. Each idealised zone will drain completely to a lenticular state. Depending on whether the spherical particles are in close or open packing, the degree of saturation will decrease from S = 1.00 to S = .058 for close packing or S = .042 for open packing.

If it is assumed for simplicity that both the total stress on the soil and the pore air pressure are zero, then at any degree of saturation S, the effective stress in the soil will be due entirely to $-u_w = p''$ (in Aitchison's terminology).

(a) In the saturated zones of the soil S = 1.0 and $\sigma' = p''$.

(b) In the drained zones of the soil S $\doteq$ .05 and the effective stress can be calculated to be $\sigma' = 0.3\ p''$.

At any stage of the drainage process, the saturated zones will occupy a proportion S of the soil and will contribute a portion S.p" to the average effective stress. (This neglects the small quantity of water retained between the particles in zones which have drained).

Each zone of drained pores will contribute a portion 0.3 p"ΔS to the average effective stress. ΔS is the change in overall saturation of the soil caused by draining of the zone.

The average effective stress in the soil will be

$$\sigma' = Sp'' + \sum_{0}^{p''} 0.3p''\Delta S \qquad E(5.5)$$

(After Aitchison, 1960).

Thus from a knowledge of the relation between degrees of saturation S and suction p" the effective stress can be calculated.

Also note that χ is given by:

$$\chi = \frac{\sigma'}{p''} = S + \frac{1}{p''}\sum_{0}^{p''} 0.3p''\Delta S \qquad E(5.6)$$

(b) Application to a compacted soil.

To simulate the behaviour of a compacted soil at constant water content it must be imagined that the last zone of the soil which will be drained is connected to a closed reservoir through which the suction is applied. It must also be imagined that the saturating and desaturating cycles are reversible.

Each compaction water content will correspond to a certain degree of saturation and suction. As the total stress on the soil or the compaction water content is increased, p" will decrease and water will be drawn from the reservoir to increase the degree of saturation (and vice versa). This will enable changes in suction and saturation to be simulated while preserving the condition of

constant overall water content.

Typical suction-degree of saturation curves for compacted soils are shown in fig. (5.2). These curves can be idealised by the curve shown in fig. (5.3).

p_o'' is the suction at which S = 0.

S_o is degree of saturation corresponding to the 'wet' end of the degree of saturation-water content curve in which S remains almost constant as the suction increases.

p_1'' is the suction at which S starts decreasing below S_o.

Stage 1: $0 < p'' < p_1''$, $S = S_o$

from E(5.6): $\chi = S_o + 0.3\,(1 - S_o)$ E(5.7)

Stage 2: $p_1'' < p'' < p_o''$; $S_o > S > 0$

The shape of the S–p'' curve between $S = S_o$ and $S = 0$ is assumed to be parabolic.

i.e. $p'' = aS^2 + bS + c$

whence, solving for the constants a, b and c

$$(p'' - p_o'') = (p_o'' - p_1'') \left[\left(\frac{S}{S_o}\right)^2 - 2\left(\frac{S}{S_o}\right)\right] \qquad E(5.8)$$

from E(5.6)

$$\chi = S + .3p_1''(1-S_o) - .3\frac{\int_S^{S_o}\left[(p_o''-p_1'')\left[\left(\frac{S}{S_o}\right)^2 - 2\left(\frac{S}{S_o}\right)\right] + p_o''\right]dS}{(p_o''-p_1'')\left[\left(\frac{S}{S_o}\right)^2 - 2\left(\frac{S}{S_o}\right)\right] + p_o''}$$

(Note: Minus before the integral because in increasing p'' from p_1'' S_o is decreased to S).

$$\chi = S + .3\left[\frac{p_1''(1-S_o) - p_o''(S-S_o) - (p_o''-p_1'')\left[\frac{(S^3-S_o^3)}{3S_o^2} - \frac{(S^2-S_o^2)}{S_o}\right]}{(p_o''-p_1'')\left[\left(\frac{S}{S_o}\right)^2 - 2\left(\frac{S}{S_o}\right)\right] + p_o''}\right] \qquad E(5.9)$$

Now consider several limiting cases:

(i) $p_o'' = p_1''$ i.e. portion 2 - 3 of the S - p" curve horizontal.

E(5.9) reduces to:

$$\chi = S + .3(1 - S) \qquad E(5.10)$$

(ii) p_1'' very large i.e. $S = S_o$ and Stage 2 reduces to Stage 1.

$$\chi = S_o + .3(1 - S_o) \qquad E(5.7)$$

(iii) $S_o = 1$, $p_1 = 0$. This reduces the S-p" curve to the type of curve illustrated in fig. (5.2) for changes in saturation at constant water content but varying applied stress σ.

In this case E(5.9) reduces to:

$$\chi = S + .1(1 - S) \qquad E(5.11)$$

Note that case (iii) is perfectly general and is independent of p_o''.

Equations E(5.10) and E(5.11) have been plotted in fig. (5.3).

It is obvious that by changing the origin of the axes the general case of E(5.9) can be reduced to E(5.11).

Hence a curious conclusion is reached: no matter what parabolic relation is chosen between p" and S, the relation between χ and S only varies between

$$\chi = S + .3(1 - S)$$

and $\chi = S + .1(1 - S)$

Donald (1961) has found much the same thing for a series of linear relations between p" and S.

(5.3) Characteristics of the effective stress equation.

According to E(5.1) the effective stress depends on the value of the sum of two pressure differences:

(a) $(\sigma - u_a)$ the difference between total stress and pore air pressure.

(b) $(u_a - u_w)$ the difference between pore air and pore water pressures or the capillary pressure difference.

$(\sigma - u_a)$ is an easily controlled independent variable which is independent of the absolute magnitude of either σ or u_a. $(u_a - u_w)$ in a compacted soil at constant moisture content should depend only on the compaction moisture content and the effective stress in the soil.

Since $(u_a - u_w)$ represents a capillary pressure difference caused purely by surface tension at the curved air-water interface, its magnitude should be independent of the absolute value of u_a. Changes in u_a should be reflected by equal changes in u_w.

It has been pointed out earlier that a column of water such as that in the tubes of the pore pressure measuring apparatus is unable to sustain absolute tension for more than an instant. The capillary water films in soil on the other hand appear capable of sustaining very large absolute tensions.

In order to bring these absolutely negative pore water pressures into the measurable range a value of u_a is chosen which is sufficiently large to raise u_w to above absolute zero and preferably to above atmospheric pressure. Provided the elevated air pressure is applied within the limitation imposed by E(5.1) the effective stress in the soil should remain unchanged.

(5.4) Experimental demonstrations of the characteristics of the effeotive stress equation.

(i) The independence of $(u_a - u_w)$ of the absolute value of u_a:

(a) Under conditions of all round stress.

A sample of oompaoted Mangla shale was set up on a fine ceramic base in a triaxial cell. The sample was surrounded by an unsealed rubber membrane to prevent loss of moisture by evaporation, but was provided with a pair of vertical side drains of glass fibre ribbon which communicated with the air in the triaxial cell. A little water was placed around the base pedestal to keep the air in the cell saturated and thus inhibit evaporation from the sample.

An air pressure was applied directly into the cell and after 24 hours the pore water pressure was measured. The air pressure was then gradually increased over a period of an hour to a new value. After a further 24 hours the pore water pressure was again measured. This was repeated several times. Since σ_3 has been equated to u_a, the effective stress equation in this case reduces to:

$$\sigma' = \chi(u_a - u_w)$$

As the degree of saturation must be virtually constant, any change in effective stress will be shown by a sudden change in $(u_a - u_w)$ as the air pressure is stepped up.

Fig. (5.4) shows the results of this test. It is seen that changes in u_w mirrored the changes in u_a almost exactly and that a smooth variation in $(u_a - u_w)$ was obtained. The value of $(u_a - u_w)$ was found to increase gradually with time. This is a tendency which has been noted in all freshly compacted soils and is found to occur also if u_a is kept constant. (A more detailed discussion of the phenomenon

is given in Chapter 9.) The fact that $(u_a - u_w)$ and hence σ' changed appreciably during the test due to causes independent of changes in u_a rather spoils this test as a demonstration. However, had the effective stress in the sample been suddenly altered by increasing the all round air pressure, $(u_a - u_w)$ would have altered in a series of steps. If the sample had been compressed by the increase in u_a, $(u_a - u_w)$ would have decreased.

The independence of $(u_a - u_w)$ of the absolute value of u_a:

(b) During shear.

A sample of compacted Selset clay was set up exactly as described under (a) above. An all round air pressure was applied and after allowing 36 hours for the sample to come to equilibrium, loading was commenced at a strain rate of .0013% per minute. The value of u_a was varied in a series of steps, each increase in u_a being applied gradually over a period of an hour.

The effective stress equation for this test is obtained by equating $\sigma_3' = u_a$ in E(5.2):

$$\tau = c' + \tan(u_a - u_w) \tan \phi'$$

If the effective stress in the soil is unaffected by varying u_a, the curves of deviator stress and $(u_a - u_w)$ versus strain will be smooth and continuous.

The test observations are shown in fig. (5.5). The measured variation of u_w is discontinuous at the points where u_a is altered. However, there is a smooth continuous variation throughout the test in $(u_a - u_w)$, $(\sigma_1' - \sigma_3')$ and hence in $\frac{(\sigma_1' - \sigma_3')}{(\sigma_3' - u_w)}$. The effective stress was clearly unaffected by variations in u_a.

(ii) The dependence of effective stress on the value of $(\sigma_3 - u_a)$.

(a) Under conditions of all round stress.

A sample of compacted Selset clay was set up on a fine ceramic base in a triaxial cell. The sample was sealed into a rubber membrane and put under a cell pressure. Simultaneously a controlled pore air pressure was applied through the top cap drainage lead of the sample and the same pressure was applied to the free mercury surface of the cell pressure control system. This arrangement enabled simultaneous equal changes to be made in both σ_3 and u_a by merely varying u_a.

Measurements of sample volume change and pore water pressure were commenced immediately and their variation with time was recorded. A series of simultaneous equal reductions in σ_3 and u_a were made from time to time keeping $(\sigma_3 - u_a)$ constant. Finally, u_a was kept constant and σ_3 was increased thus giving an increase in $(\sigma_3 - u_a)$.

The relevant effective stress equation is E(5.1), viz:

$$\sigma' = (\sigma - u_a) + \chi(u_a - u_w)$$

The results of the test are shown in fig. (5.6). Provided the effective stress remains unchanged, the variation of both $(u_a - u_w)$ and $\Delta V/V_o$ should be smooth and continuous. This was obviously true as long as $(\sigma_3 - u_a)$ remained constant. As soon as $(\sigma_3 - u_a)$ was increased, a sudden decrease in both $(u_a - u_w)$ and $\Delta V/V_o$ occurred.

The dependence of effective stress on the value of $(\sigma_3 - u_a)$.

(b) During shear.

To demonstrate this a sample of compacted Talybont clay was chosen. It was set up in exactly the same way as described in (ii)a above with exactly the same provision for simultaneously varying σ_3 and u_a by equal amounts thus keeping $(\sigma_3 - u_a)$ constant. After

allowing 36 hours for the sample to come to equilibrium under $(\sigma_3 - u_a)$, loading was commenced at a strain rate of .0013% per minute.

During the test simultaneous equal increments were given to σ_3 and u_a keeping $(\sigma_3 - u_a)$ constant. Finally, after failure had been reached, $(\sigma_3 - u_a)$ was increased keeping u_a constant.

The effective stress equation for this test is E(5.2), viz:

$$\tau = c' + \left[(\sigma - u_a) + \chi (u_a - u_w)\right] . \tan \phi'$$

The results of the test are shown in fig. (5.7). As in the previous tests, provided $(\sigma_3 - u_a)$ was kept constant, a smooth continuous variation was observed in $(\sigma_3 - u_w)$, $(\sigma_1 - \sigma_3)$ and $\Delta V/V_o$. The effective stress was clearly unaffected by the stepped increases in σ_3, u_a and u_w.

On altering $(\sigma_3 - u_a)$ the change in effective stress is shown by the sharp breaks in the curves of $(\sigma_1 - \sigma_3)$, $(\sigma_3 - u_w)$ and $\Delta V/V_o$.

(iii) <u>The ability of soil water to sustain absolute tension</u>.

Soils engineers often doubt the ability of soil water to support large capillary tensions. The validity of measuring high negative pore pressures using elevated air pressures is questioned on the grounds that the soil water would behave quite differently if its absolute pressure were negative rather than positive. According to this argument, the strength of a given sample of partly saturated soil should be much less when tested with atmospheric air pressure in its voids than when tested using a raised air pressure.

To demonstrate the fallacy of this argument two identical samples of compacted Talybont clay were tested. The first sample

was sheared unconfined using a raised air pressure and measuring pore water pressures. The second sample was also sheared unconfined at the same rate as the first sample, but between solid end plates and with atmospheric air pressure in the voids. The test results are shown in fig. (5.8). The absolute water pressure in sample 1 was about + 23 p.s.i. while the absolute tension in the water of sample 2 was about - 47 p.s.i. The strengths obtained from the two samples were identical. While it is coincidental that the strengths were identical, there was obviously little difference in the behaviour of the samples.

(5.5) Anomalies due to incorrect pore pressure measurement or use of the wrong form of the effective stress equation.

Fig. (5.9)a illustrates a Mohr failure envelope obtained from tests on compacted Selset clay in which pore pressures were measured using a loose coarse porous disc (Hanson, 1955). The results are plotted in terms of "$(\sigma' - u_w)$".

Fig. (5.9)b shows a second envelope obtained by plotting the results of test Series 2 of Chapter 7, also on Selset clay, in terms of $(\sigma' - u_a)$.

The close similarity between the two envelopes suggests that in fig. (5.9)a, what were thought to be pore water pressures were in fact pore air pressures. Note that a large apparent "cohesion intercept" is given in both cases.

In fig. (5.10) are shown two typical tests on compacted Mangla shale plotted in terms of $(\sigma' - u_w)$ with u_w measured on a fine ceramic base. In this case a "negative cohesion intercept" is obtained. The true effective stress failure envelope lies between the two extremes

given by those in terms of $(\sigma - u_a)$ and $(\sigma - u_w)$. It is in fact a function of $\sigma' = \chi (\sigma - u_w) + (1 - \chi) (\sigma - u_a)$. Further examples of "negative cohesion intercepts" are given in Chapter 7. This phenomenon was also noted by Alpan (1959).

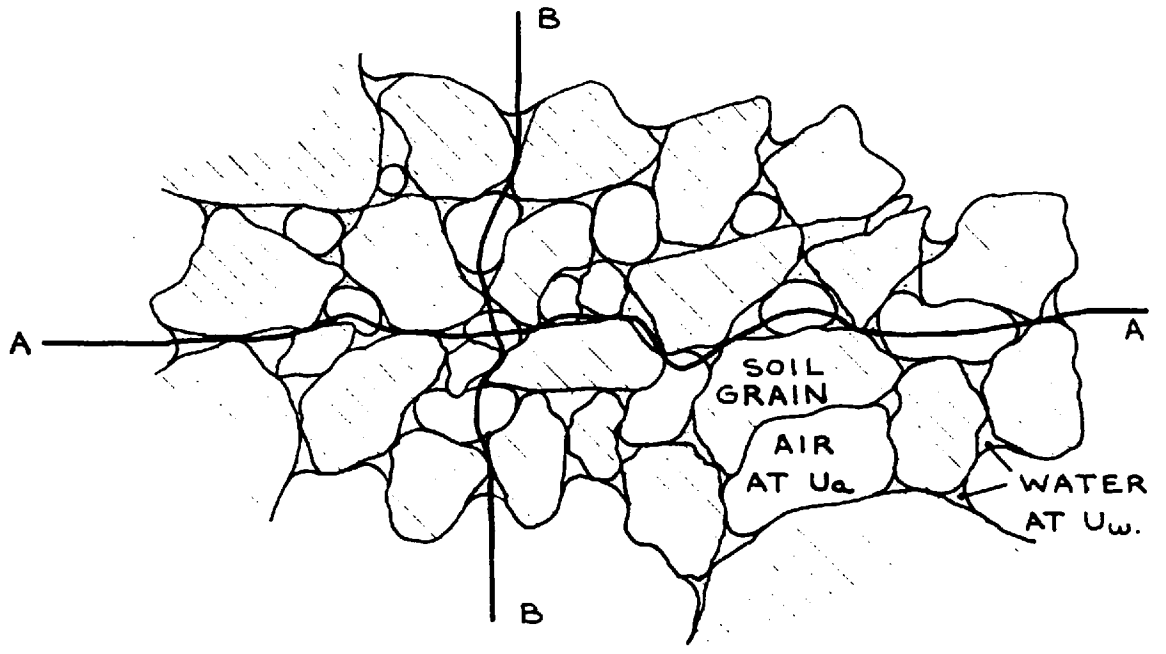
(5.6) Conclusions.

(i) It is possible to calculate simple theoretical relations between the degree of saturation and the χ factor. The calculated relation between χ and S does not depend very much on the relation between S and $(u_a - u_w)$ or p".

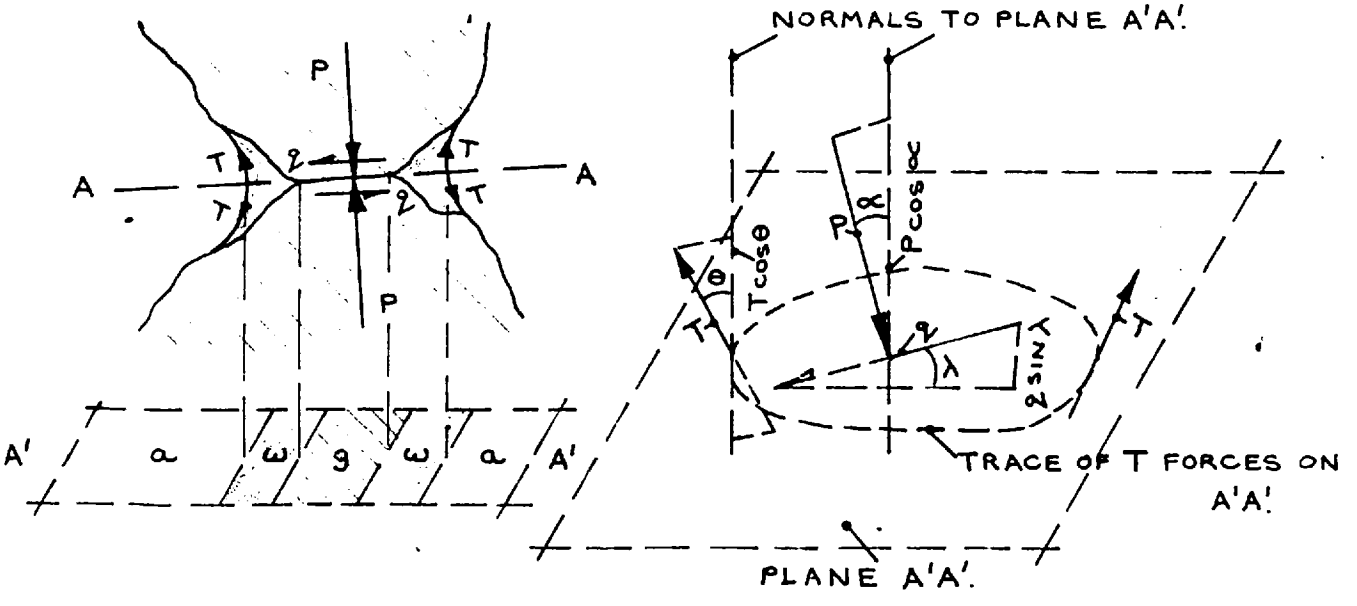
(ii) Experimental evidence shows that the form of the Bishop effective stress equation is correct. The effective stress in a partly saturated soil is controlled by the sum of the two pressure difference terms $(\sigma - u_a)$ and $(u_a - u_w)$. The effective stress is independent of the absolute magnitude of the pressures σ, u_a and u_w.

(iii) Capillary water in the pores of a partly saturated soil is capable of supporting considerable absolute tension.

(iv) Correct pore pressure measurement and the use of a correct form of the effective stress equation are essential in the interpretation of strength tests on partly saturated soils.

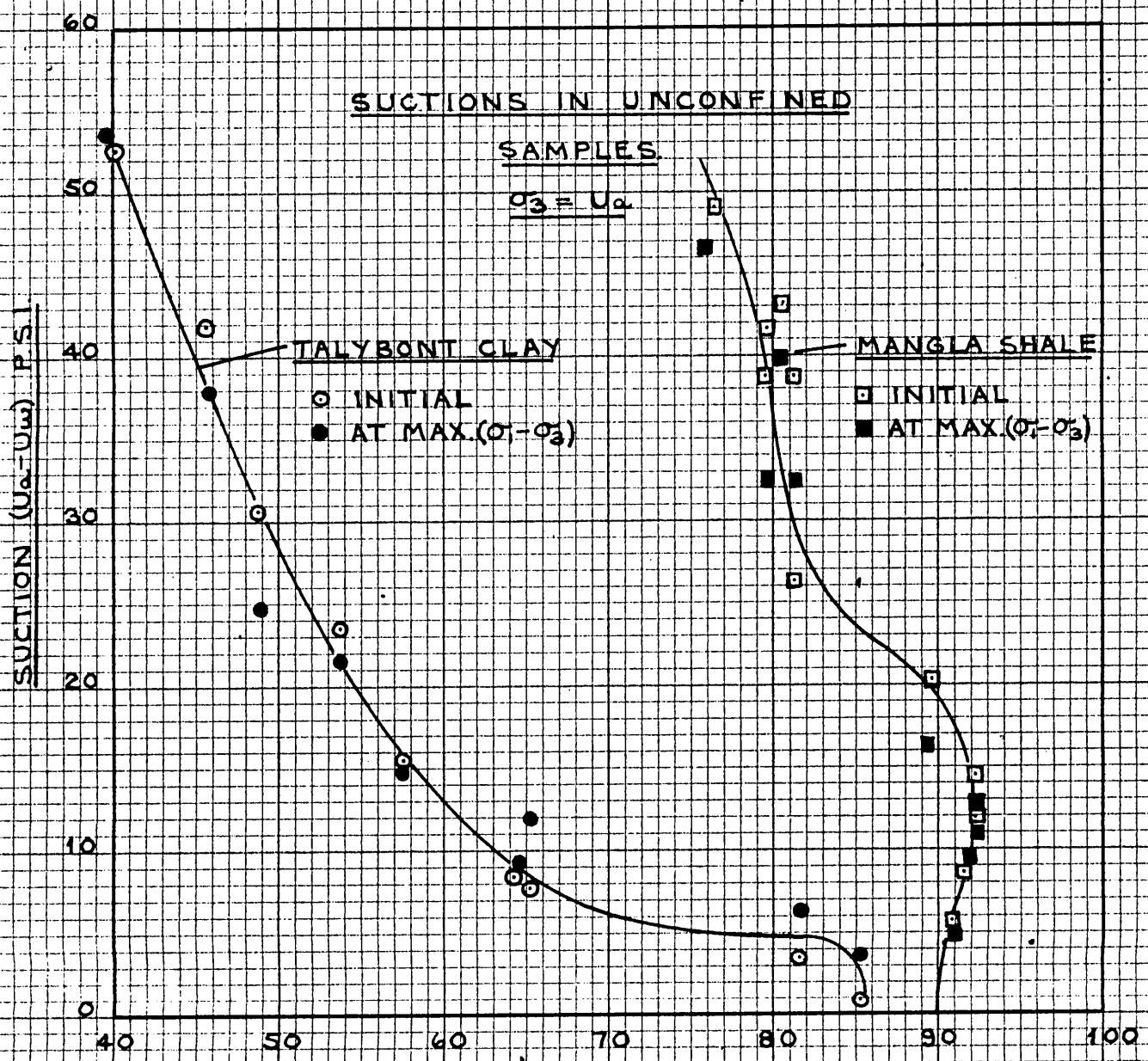


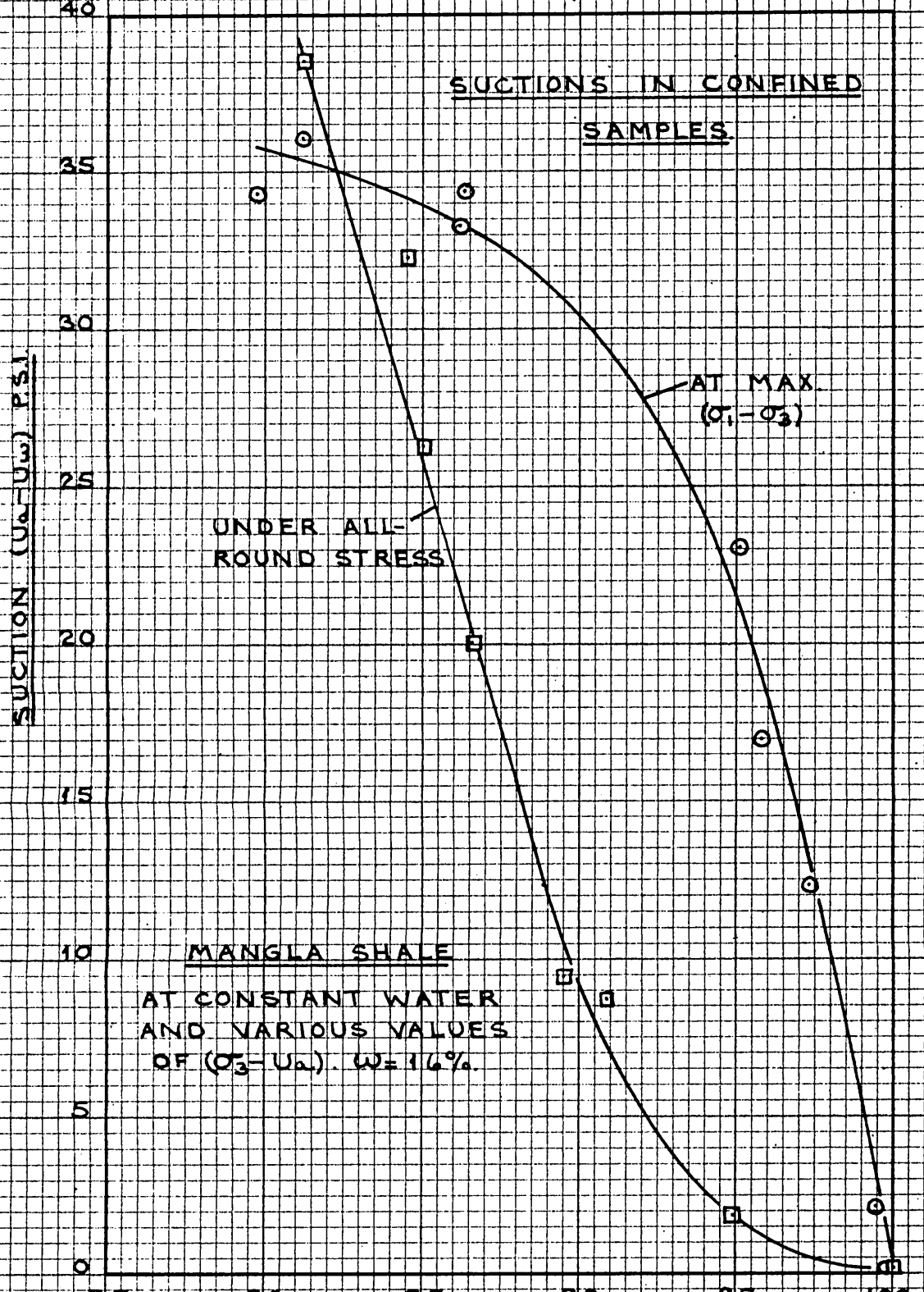
(a) IDEALISED CONCEPT OF THE STRUCTURE OF A PARTLY SATURATED SOIL.



(b) FORCES AT AN INTERGRANULAR CONTACT.

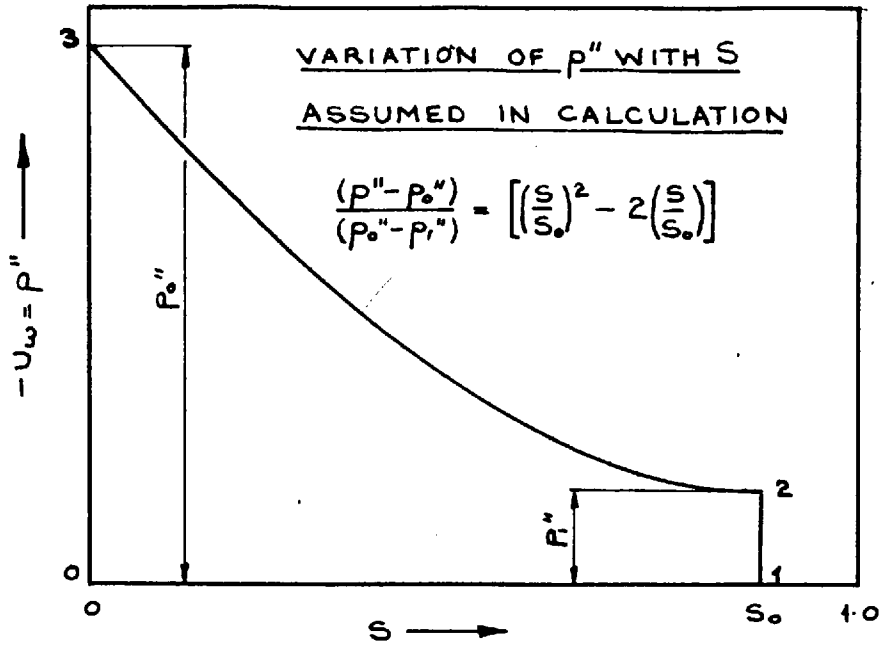
FIG. 5.1.





TYPICAL VARIATION OF $(U_a - U_w)$ WITH S IN PARTLY SATURATED COMPACTED SOILS.

FIG. 5.2.


VARIATION OF p" WITH S
ASSUMED IN CALCULATION
$\frac{(p''-p_0'')}{(p_0''-p_1'')} = \left[\left(\frac{S}{S_0}\right)^2 - 2\left(\frac{S}{S_0}\right)\right]$
3
0
$-U_w = p''$
p_0''
p_1''
2
1
0
S_0
1·0
S

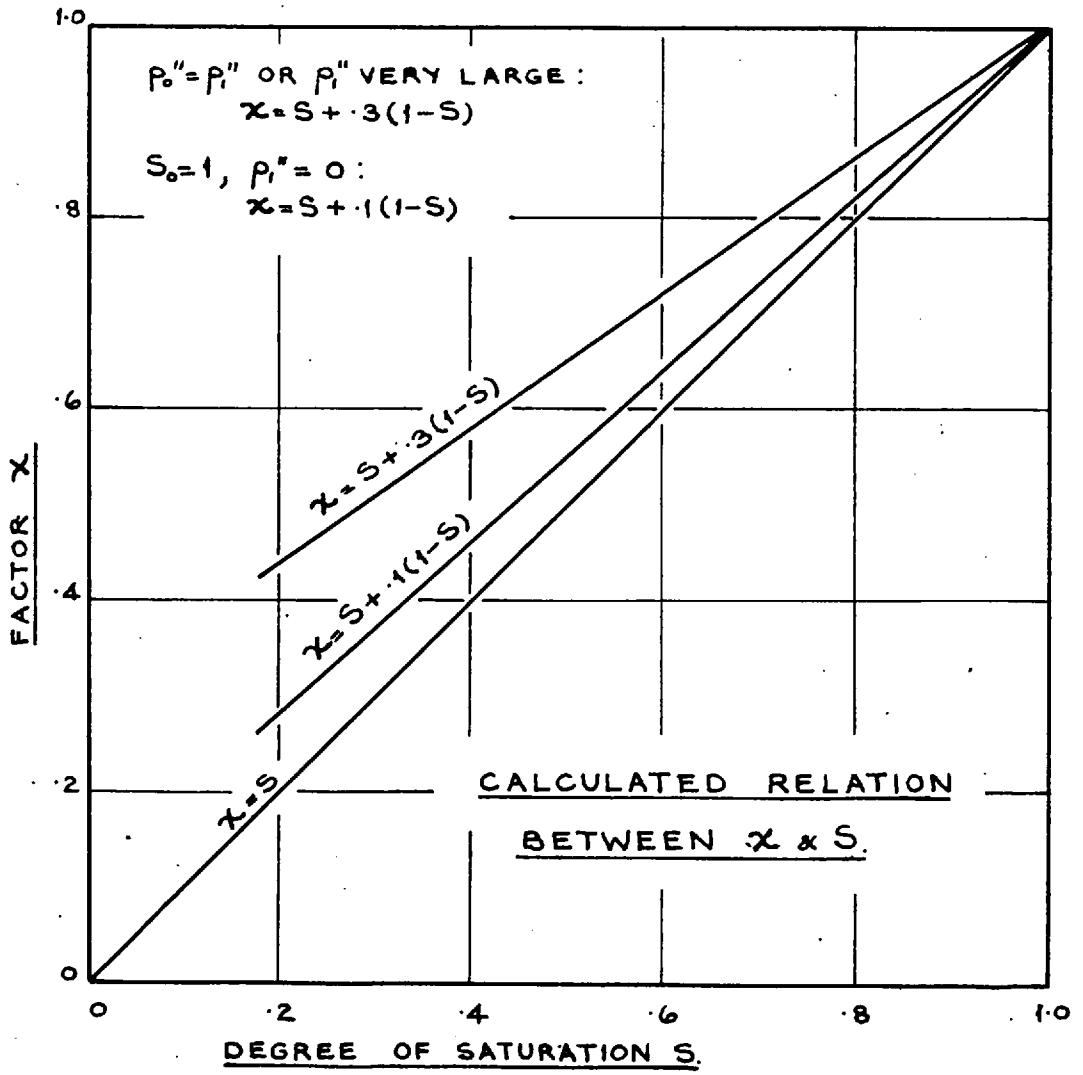
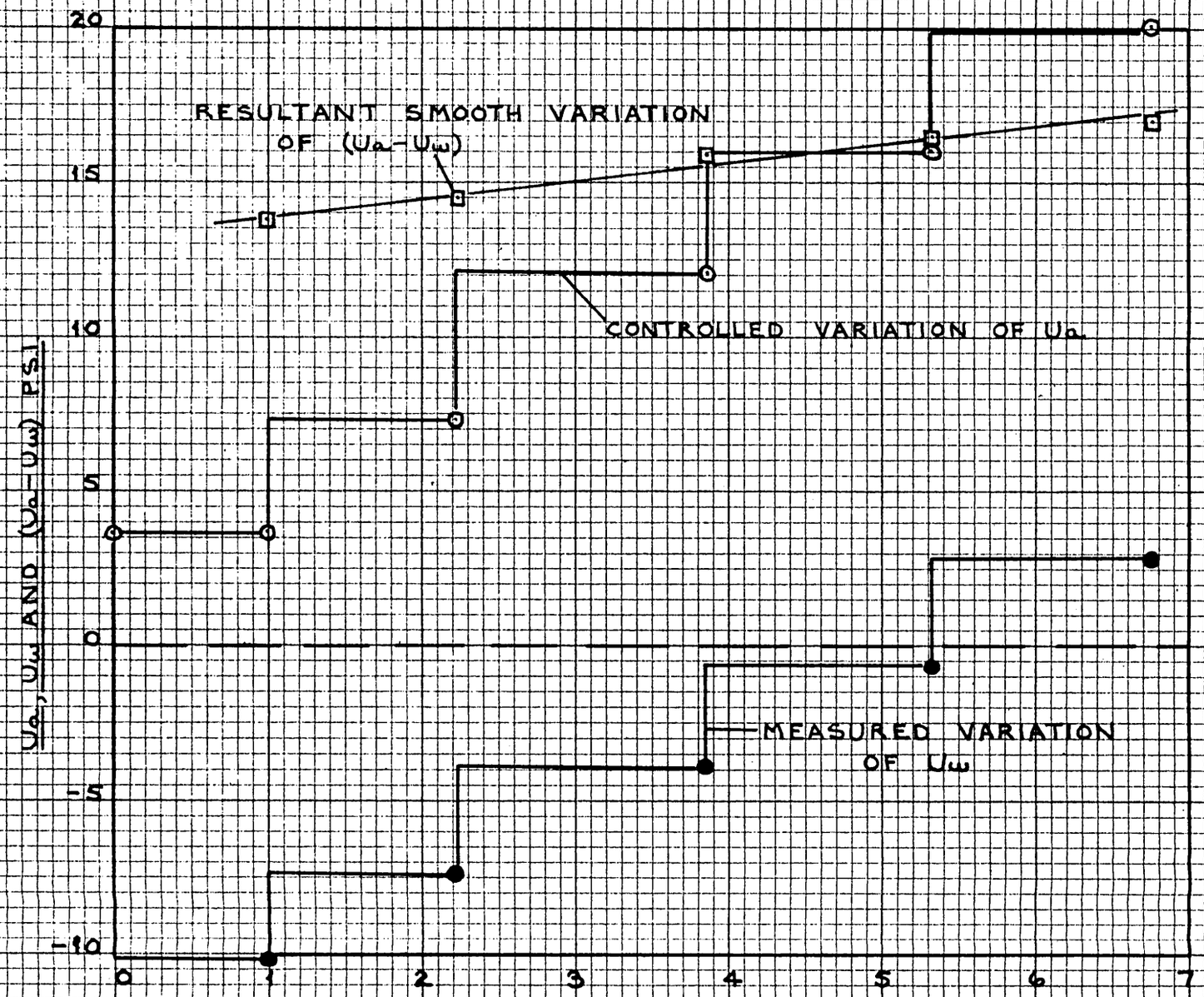

$p_0''=p_1''$ OR p_1'' VERY LARGE :
$\chi = S + \cdot 3(1-S)$
$S_0=1$, $p_1''=0$:
$\chi = S + \cdot 1(1-S)$
$\chi = S + \cdot 3(1-S)$
$\chi = S + \cdot 1(1-S)$
$\chi = S$
CALCULATED RELATION
BETWEEN χ & S.
FACTOR χ
1·0
·8
·6
·4
·2
0
·2
·4
·6
·8
1·0
DEGREE OF SATURATION S.

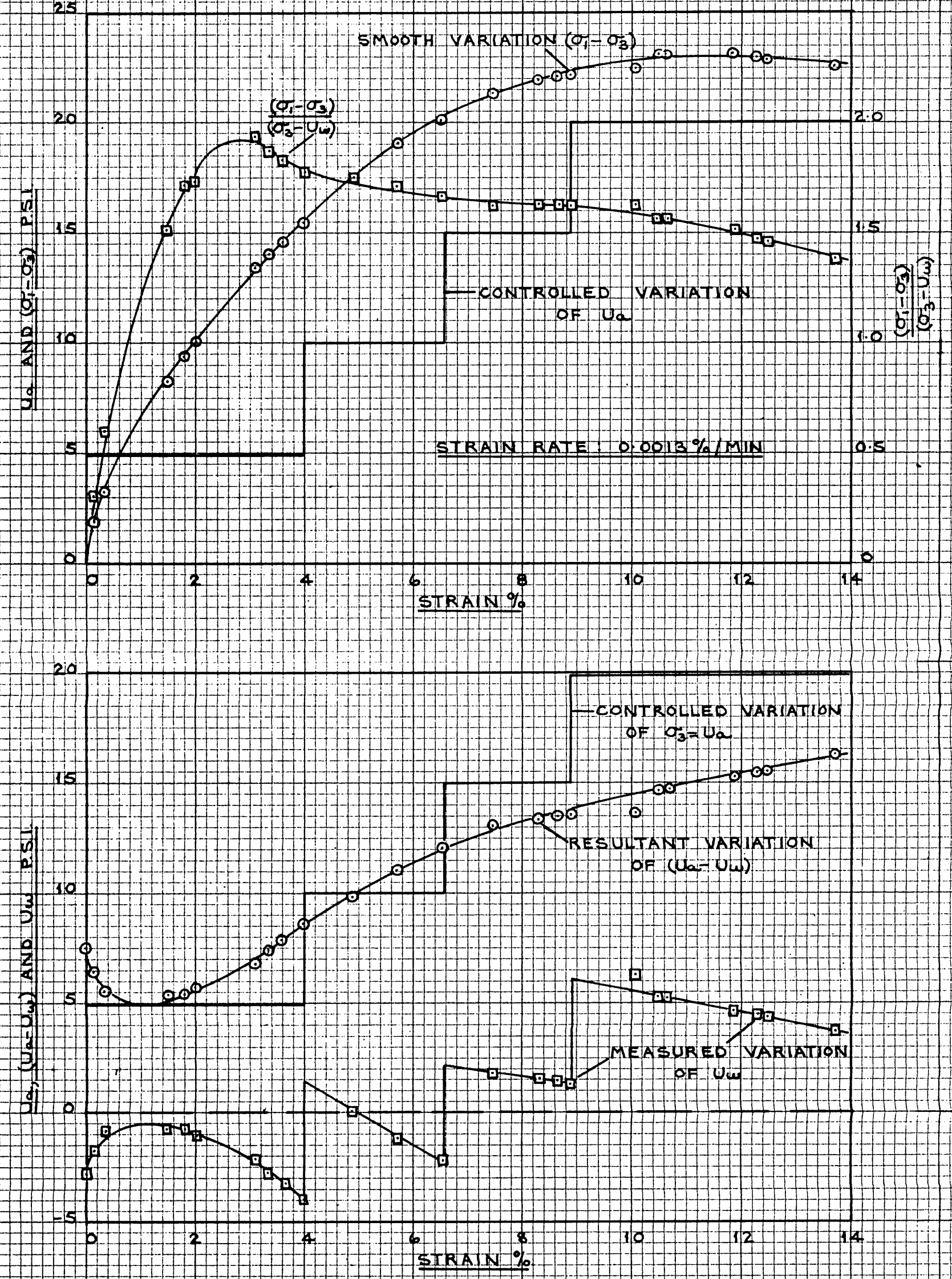
FIG. 5.3.



MEASUREMENTS ON UNCONFINED SAMPLE OF COMPACTED MANGLA SHALE TO ILLUSTRATE PRINCIPLE OF SUCTION MEASUREMENT USING RAISED AIR PRESSURES.

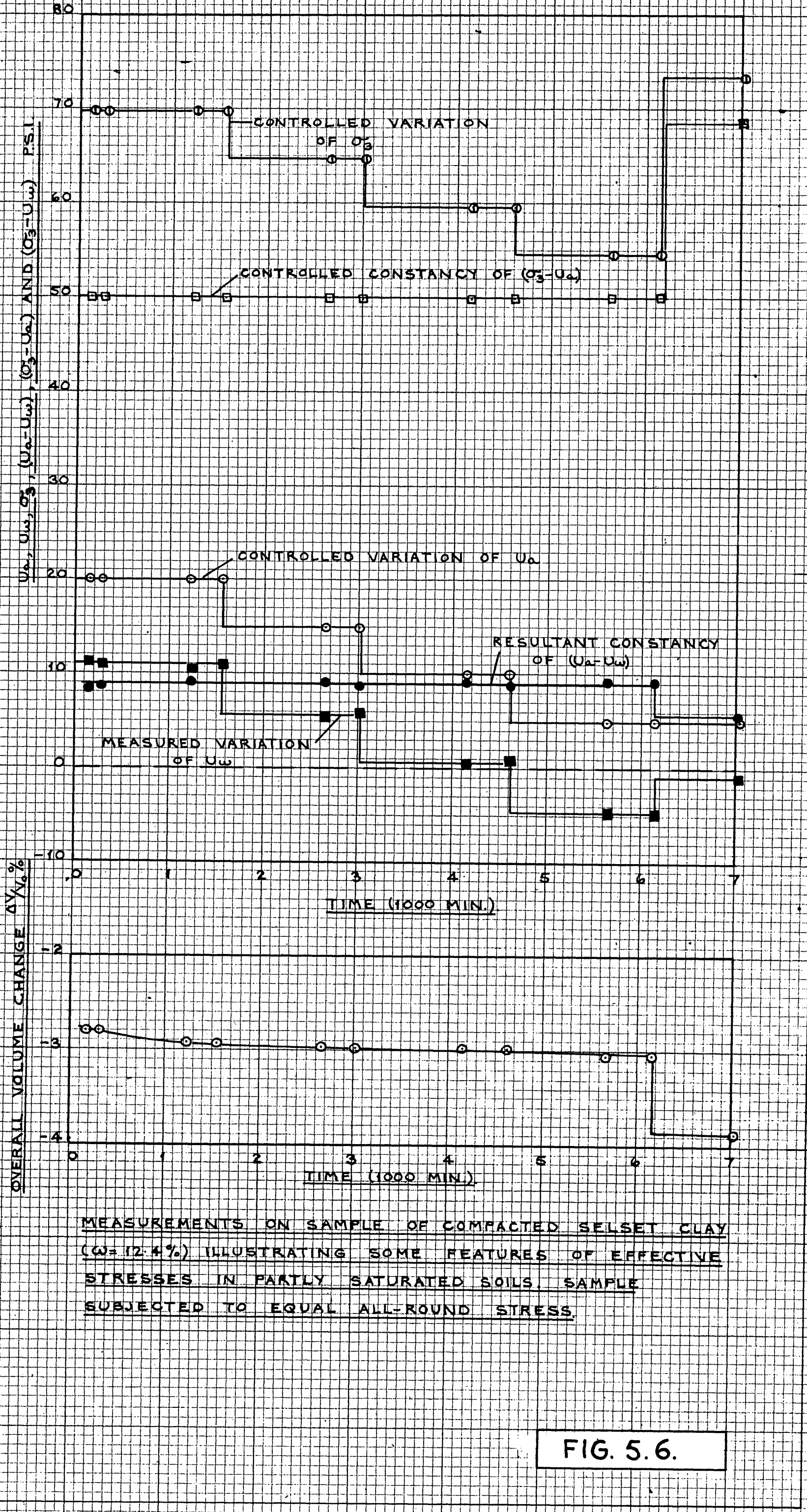
(ω = 18.4 %)

FIG. 5.4.



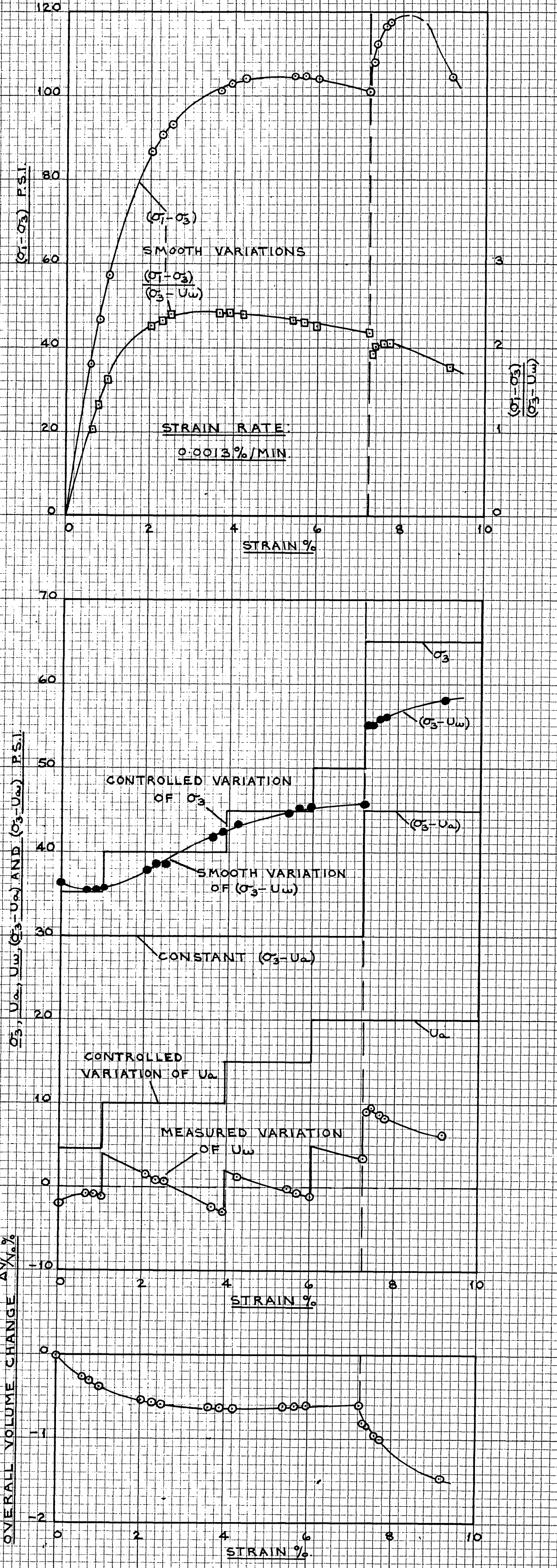
UNCONFINED TEST ON COMPACTED SELSET CLAY (ω=13·7%)
ILLUSTRATING PRINCIPLE OF SUCTION MEASUREMENT
USING RAISED PORE AIR PRESSURES.

FIG. 5.5.



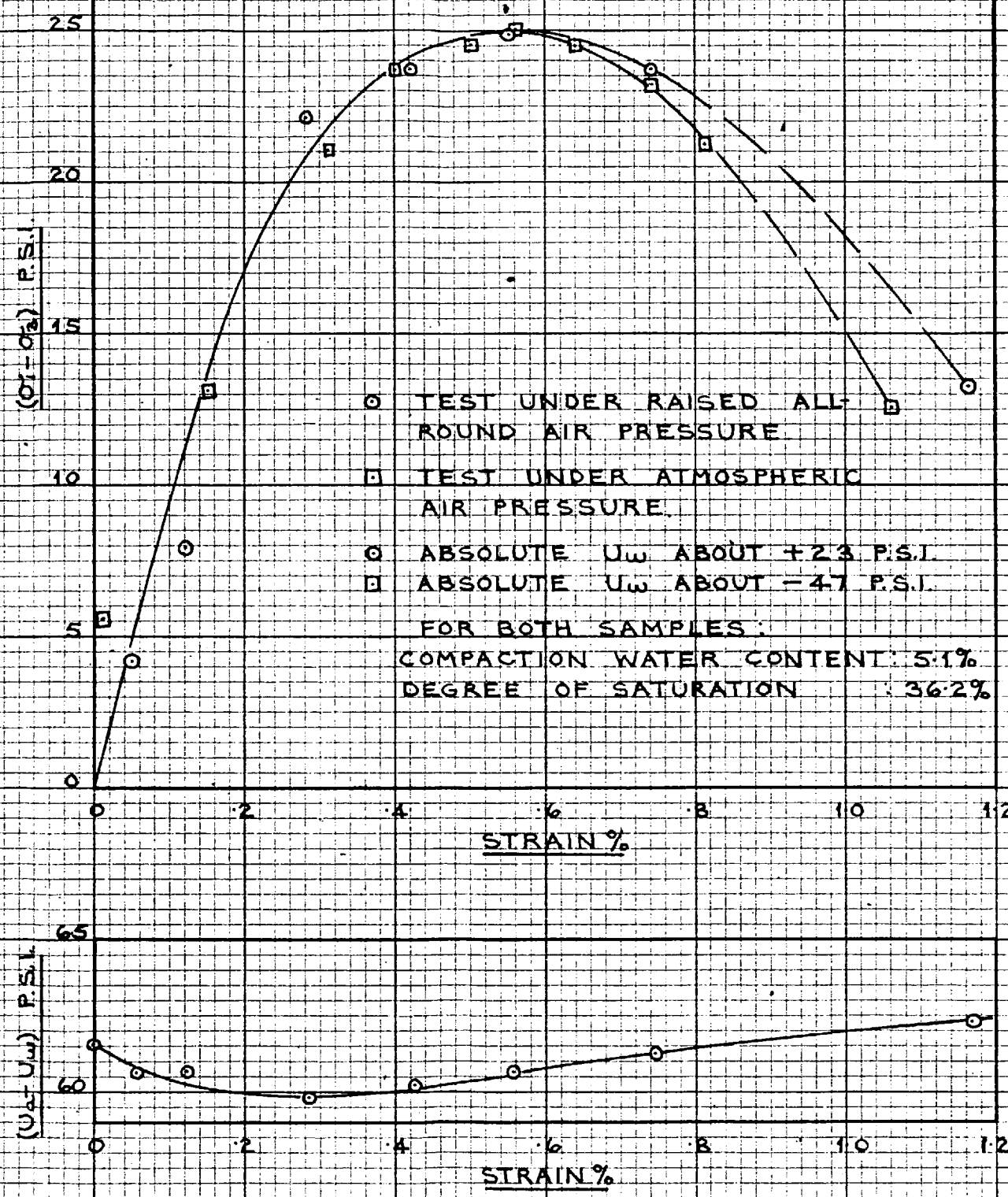
MEASUREMENTS ON SAMPLE OF COMPACTED SELSET CLAY (ω = 12·4%) ILLUSTRATING SOME FEATURES OF EFFECTIVE STRESSES IN PARTLY SATURATED SOILS. SAMPLE SUBJECTED TO EQUAL ALL-ROUND STRESS.

FIG. 5.6.



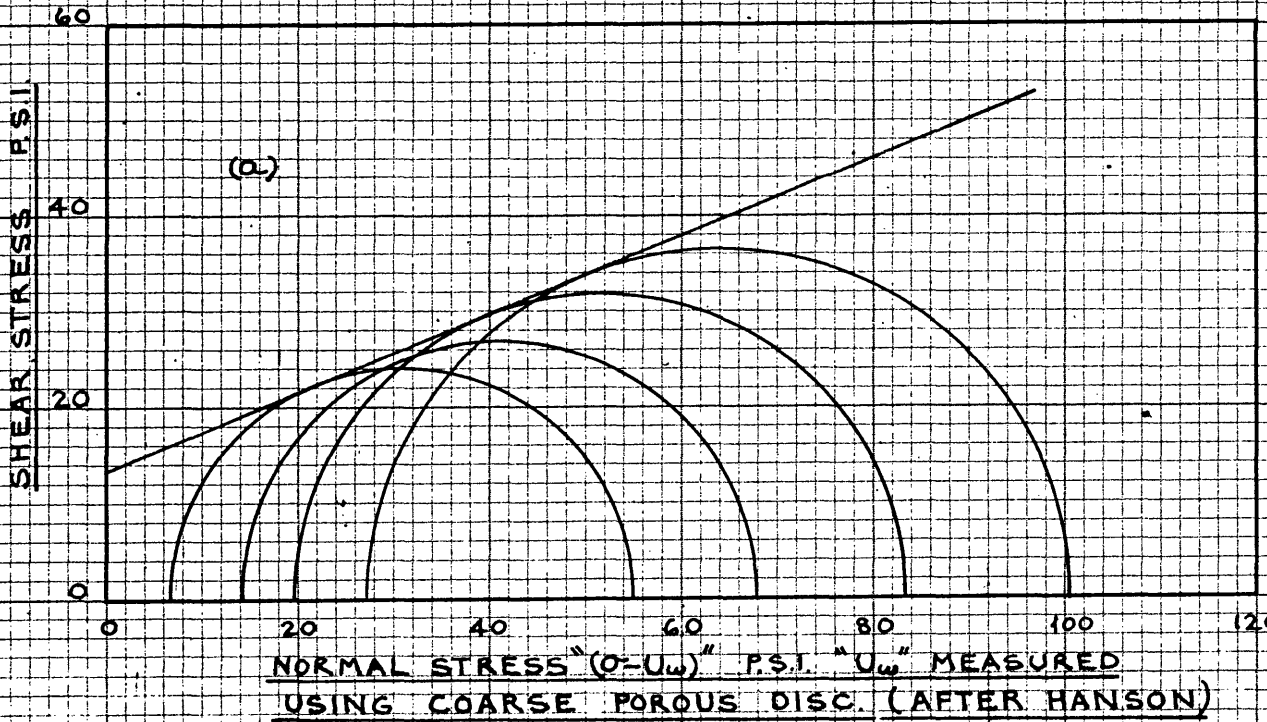
TRIAXIAL TEST ON COMPACTED TALYBONT CLAY (ω=8·04%) ILLUSTRATING SOME FEATURES OF EFFECTIVE STRESSES IN PARTLY SATURATED SOILS.

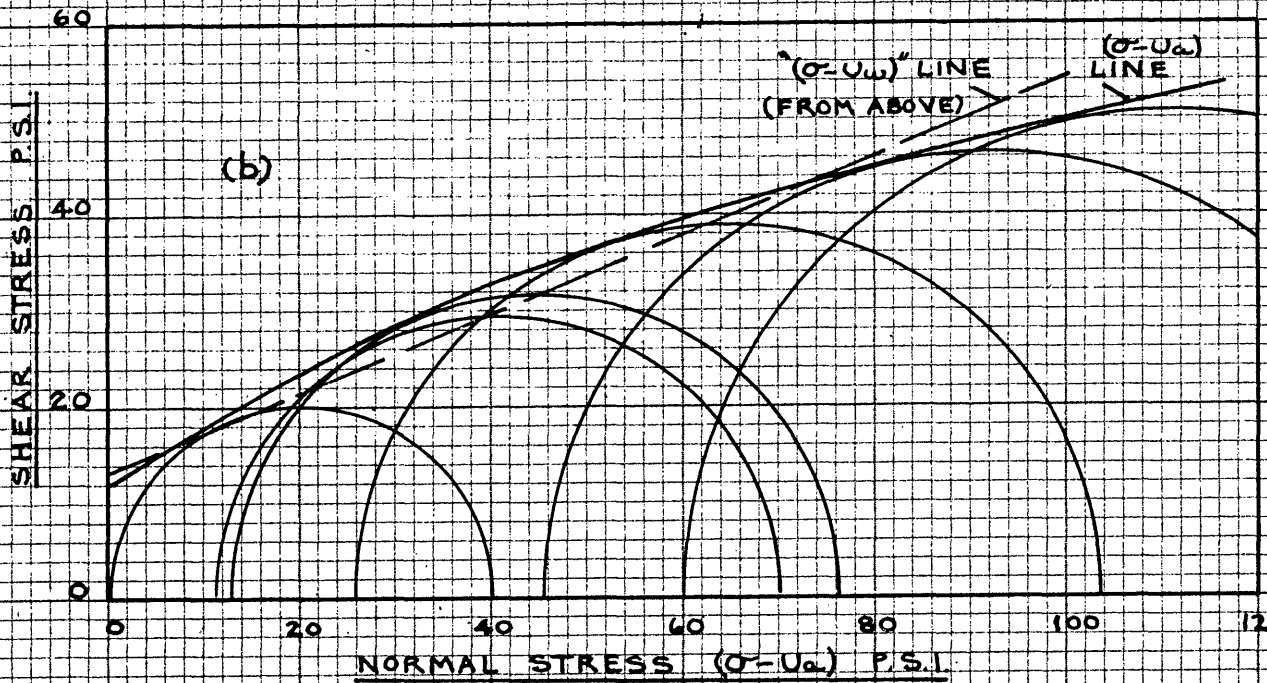
FIG. 5.7.



UNCONFINED TESTS ON COMPACTED TALYBONT CLAY TO SHOW THE ABILITY OF SOIL WATER TO SUSTAIN ABSOLUTE TENSION

FIG. 5.8.

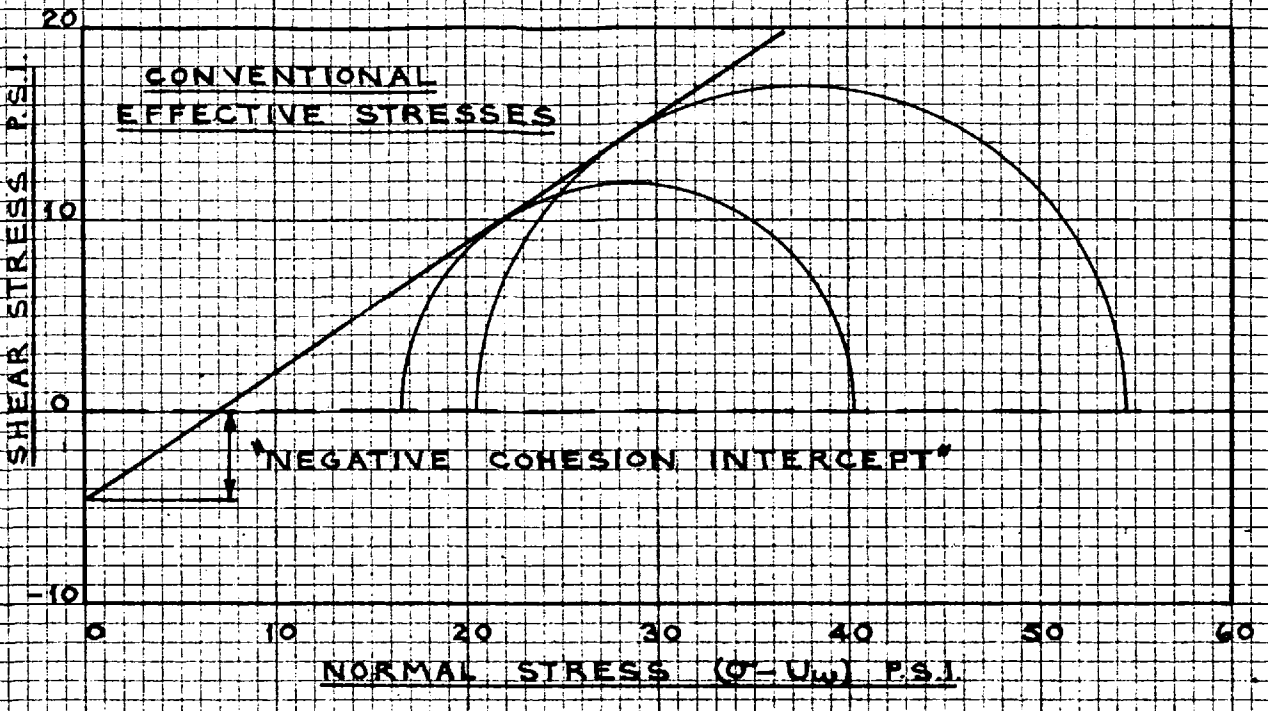


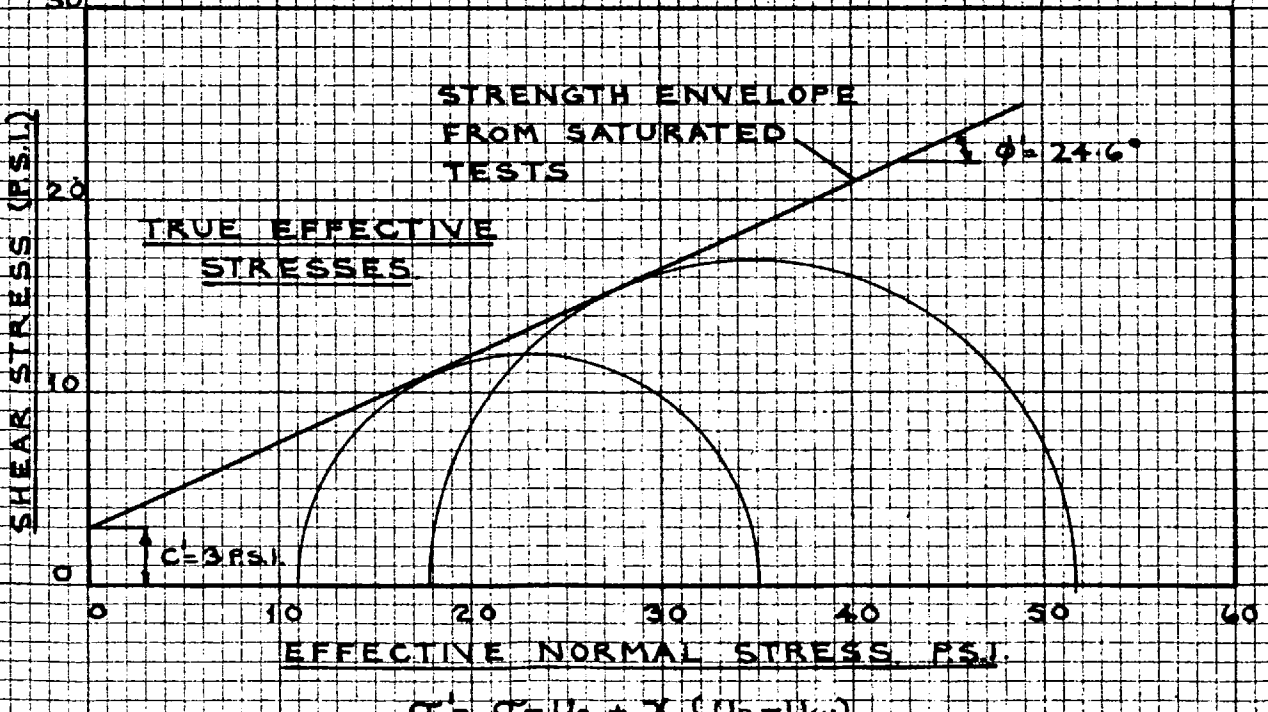


(SERIES 2)

TESTS ON COMPACTED SELSET CLAY (ω = 11%) SHOWING "FALSE COHESION INTERCEPT" DUE TO INCORRECT TECHNIQUE OF MEASURING PORE WATER PRESSURE.

FIG. 5.9.





$$\sigma' = \sigma - U_a + \chi (U_a - U_w)$$

TYPICAL TRIAXIAL TESTS ON PARTLY SATURATED MANGLA SHALE (ω = 13·5%) SHOWING "NEGATIVE COHESION INTERCEPT"

FIG. 5.10.

CHAPTER 6

THE STRENGTH OF SATURATED COMPACTED SOILS

In order to estimate values of the parameter χ in the Bishop effective stress equation, it was necessary to establish strength envelopes in terms of true effective stress which corresponded to each set of strength data in terms of pore air and water pressures.

It seems reasonable to assume that one may obtain the true effective stress-strength envelope for a partly saturated compacted soil by dissolving up all the air in the soil and shearing it in a saturated state.

Aitchison (1960) has calculated that soil grains in a partly saturated soil have a layer of water (of at least 20 Angstrom units in thickness) strongly adsorbed to their surfaces. These adsorbed layers are unlikely to be affected by stress changes due to moderate changes in saturation. If all intergranular contacts are contained within these adsorbed water layers, and if the intrinsic properties of the soil are dependent on the nature of these contacts (Hvorslev 1960), then changes in saturation, apart from altering the effective stress in the soil, should not affect its properties.

(6.1) Presentation of test results.

A method of plotting effective stress-strength results will be adopted in this thesis (see fig. (6.1)) which has several advantages over the conventional Mohr Circle plot. For saturated soils, half the deviator stress at failure, $\frac{1}{2}(\sigma_1 - \sigma_3)$, is plotted against the mean normal effective stress $\frac{1}{2}(\sigma_1' + \sigma_3')$. The resultant point represents the highest point on the corresponding Mohr circle. The slope ψ of

the strength envelope is related to ϕ' by: $\tan\psi = \sin\phi'$, while the intercept of the line on the strength axis is equal to $c' \cdot \frac{\tan\psi}{\tan\phi'}$.

This method avoids the confusion of a large number of superimposed Mohr circles and the natural tendency to unconsciously give greater weight to the larger circles. It is also easily extended for use with results from partly saturated soils.

The method of calculating

$$R = \text{(principal effective stress ratio)} - 1 = \frac{(\sigma_1' - \sigma_3')}{\sigma_3'}$$

is also shown in fig. (6.1).

This ratio is used in Chapter 7 to calculate values of the $\varkappa$ factor

$$R = \frac{2d_o + 2a_1 \tan\psi}{a_1(1-\tan\psi) - d_o}$$

where $a_1 = \frac{1}{2}(\sigma_1' + \sigma_3')$ at the point under consideration. For $d_o = 0$ this reduces to

$$R = \frac{2\tan\psi}{(1 - \tan\psi)} = \frac{2\sin\phi'}{(1 - \sin\phi')}$$

Note from fig. (6.1) that as a line at 45^o through the origin represents the equation $\sigma_3' = 0$, it is impossible to obtain an experimental point to the left of point L without applying effective tensile stresses to the soil.

(6.2) Failure criteria for saturated soils.

The use of the modified Coulomb failure criterion involves a decision on when failure is reached. In drained tests no difficulty arises. Since σ_3' is constant, the only variable is $(\sigma_1' - \sigma_3')$ and a maximum value of $(\sigma_1' - \sigma_3')$ denotes failure. In undrained tests, though, both σ_3' and $(\sigma_1' - \sigma_3')$ vary and the soil can be considered to

have failed when maximum values of either $\frac{(\sigma_1' - \sigma_3')}{\sigma_3'}$ or $(\sigma_1' - \sigma_3')$ are reached.

When maximum deviator stress is reached the shear stress in the soil is at a maximum.

It was seen in section (6.1) that if $c' = 0$

$$\frac{(\sigma_1' - \sigma_3')}{\sigma_3'} = \frac{2 \sin \phi'}{1 - \sin \phi'}$$

From this it follows that a maximum value of $\frac{(\sigma_1' - \sigma_3')}{\sigma_3'}$ will correspond to a maximum value of ϕ'. In tests on some soils, the peak value of $\frac{(\sigma_1' - \sigma_3')}{\sigma_3'}$ is difficult to pick out if values of $\frac{(\sigma_1' - \sigma_3')}{\sigma_3'}$ are plotted against strain. In cases like this an alternative approach in the form of a stress plot is useful.

<u>An alternative criterion for maximum values of the shear strength parameters</u>.

A well known relation between the shear strength parameters and the principal effective stresses at failure is:

$$\sin \phi' = \frac{\frac{1}{2}(\sigma_1' - \sigma_3')}{\frac{1}{2}(\sigma_1' + \sigma_3') + c' \cot \phi'} \qquad E(6.1)$$

(Skempton & Bishop, 1954)

Assume firstly that c' is constant and differentiate E(6.1) with respect to σ_3'. To find the condition for a maximum value of ϕ', equate $\frac{d\phi'}{d\sigma_3'}$ to zero. One finds that the condition for a maximum value of ϕ' for a given value of c' is:

$$\frac{d(\sigma_1' - \sigma_3')}{d\sigma_3'} = \frac{(\sigma_1' - \sigma_3') + c' \cot \phi'}{\sigma_3' + c' \cot \phi'}$$

If this procedure is repeated assuming that ϕ' is constant, and the condition for a maximum value of c' is found, the same equation results. It can thus be concluded that an alternative criterion for maximum shear strength parameters is:

$$\frac{d(\sigma_1' - \sigma_3')}{d\sigma_3'} = \frac{(\sigma_1' - \sigma_3') + c' \cot \phi'}{\sigma_3' + c' \cot \phi'} \qquad E(6.2)$$

The term $c' \cot \phi'$ is always small compared with either $(\sigma_1' - \sigma_3')$ or σ_3' and hence E(6.2) can be written for all practical purposes as:

$$\frac{d(\sigma_1' - \sigma_3')}{d\sigma_3'} = \frac{(\sigma_1' - \sigma_3')}{\sigma_3'} \qquad E(6.3)$$

This criterion can easily be used in practice as shown in fig. (6.2). Firstly, in fig. (6.2)a $(\sigma_1' - \sigma_3')$ is plotted against σ_3'. Then, measuring slopes off this curve, $\frac{d(\sigma_1' - \sigma_3')}{d\sigma_3'}$ is plotted against the ratio $\frac{(\sigma_1' - \sigma_3')}{\sigma_3'}$ in fig. (6.2)b. A line through the origin such that $\frac{(\sigma_1' - \sigma_3')}{\sigma_3'} = \frac{d(\sigma_1' - \sigma_3')}{d\sigma_3'}$ intersects this curve at the point of maximum shear strength parameters.

Finally, in fig. (6.2)c, $(\sigma_1' - \sigma_3')$ and σ_3' have been plotted against the ratio $\frac{d(\sigma_1' - \sigma_3')}{d\sigma_3'}$. It is seen in fig. (6.2)b that the maximum value of the shear strength parameters is reached at the maximum value of $\frac{(\sigma_1' - \sigma_3')}{\sigma_3'}$.

Wherever possible, in this thesis, conditions at both maximum principal stress ratio and at maximum deviator stress have been examined. In a large number of the tests, a maximum deviator stress was never reached. Because of this, conditions at an arbitrary limiting strain of 20% were considered instead. An axial strain of 20% represents the

limit which could be accommodated by the apparatus used.

There are therefore three possible criteria of failure:

(i) A maximum value of $\frac{(\sigma_1' - \sigma_3')}{\sigma_3'}$ giving maximum values of the shear strength parameters.

(ii) A maximum value of $(\sigma_1' - \sigma_3')$ at which the shear stress in the soil is a maximum.

(iii) A limiting value of the axial strain when a maximum deviator stress is not reached.

(6.3) Testing procedure.

(a) Procedure in consolidated undrained tests.

In order to reduce consolidating and shearing times in the consolidated undrained tests on Mangla shale and Selset clay it was decided to use $1\frac{1}{2}$" diameter x 3" long samples.

The soil was compacted in the standard Proctor mould using the standard Proctor compactive effort on each of three layers of soil. The surface of each compacted layer was scarified to key it to the layer above. The $1\frac{1}{2}$" diameter samples were then formed by jacking thin walled brass sampling tubes into the compacted soil in the mould. The samples were then taken from the tubes, trimmed, measured up using vernier calipers and, finally, weighed. The final dry density of samples formed in this way was, at a given water content, about 4% greater than that of the samples used in the partly saturated tests.

Each sample was tested using a coarse porous disc at the bottom covered by a disc of filter paper. A paper radial drain was used together with a disc of filter paper on the top of the sample. The sample was loaded through a solid perspex top cap fitted with a

guiding sleeve. Each cell was provided with valves at the cell pressure and pore water inlets and a paraffin volume gauge was connected between the cell pressure control and the cell pressure inlet. This enabled overall sample volume changes to be measured.

After carefully de-airing all the leads to the cell, the sample was set up and the cell was filled with de-aired water using a funnel. The cell was topped up with a quarter inch layer of castor oil to reduce leakage past the loading ram.

Each sample was saturated by consolidating with a controlled positive pore water pressure. The cell pressure and pore water pressure were applied in stages to avoid over consolidating the sample.

After full consolidation had been reached (a minimum of 48 hours was allowed for this) the final reading of the volume gauge was noted. The cell was now placed in a tray of water and the cell pressure and pore water valves were closed. The volume gauge was replaced by a plain pressure lead and a de-aired perspex null indicator was connected to the pore water valve. The sample was then sheared undrained with measured pore water pressures.

At the end of the test the pore water valve was shut off and the sample was rapidly removed from the cell. After removing the paper drains and drying off any moisture picked up from the porous stone at the base the sample was weighed and then cut up for moisture content measurement.

Moisture content sample slices ($\frac{1}{4}$" thick) were taken from either end and from the central failure zone. The outermost $\frac{1}{8}$" thickness of soil was discarded to avoid moisture picked up from the

drains on releasing the cell pressure.

(b) Procedure in saturated drained tests.

Saturated drained tests were carried out on compacted samples of Talybont clay. As the soil was relatively permeable, 4" diameter x 8" high samples were used. The back pressure was applied through the top cap drainage lead and through the base.

After allowing enough time for consolidation and saturation to be completed the samples were sheared with the back pressure maintained constant. Overall volume changes were measured using the self-compensating mercury volume gauge.

At the end of the test the back pressure was shut off and the cell pressure released. The sample was immediately removed from the cell and moisture content samples were taken from the failure zone.

(6.4) Notes on testing procedure.

(a) For all tests rates of strain were chosen which allowed for virtually complete equalisation of pore pressures during shear. (See Chapter 8).

Consolidated undrained tests.

The usual testing time was 80 hours. The shortest time in which the maximum principal stress ratio was mobilised was about 30 hours. This gives a minimum time factor for the tests on Mangla shale of 2.0 and for those on Selset clay of 4.3. Ignoring the effect of the filter drains, the corresponding degrees of equalisation are 90% and 95% respectively.

Consolidated drained tests.

The samples were sheared at a rate which gave failure in about 100 hours. The time factor for these tests was 6.1 and the

degree of equalisation was 94%.

(b) The back pressure generally used in consolidation was 60 p.s.i. This was found to give virtually complete saturation. The only times that lower back pressures were used were when effective consolidation pressures of 110 p.s.i. were required. In these cases a back pressure of only 34 p.s.i. could be achieved. Fig. (6.3) gives a typical example of the change in pore water pressure with cell pressure under undrained conditions. The initial pore pressure was 60 p.s.i.

(6.5) Test Series 1A : Mangla shale compacted at w = 18.6%.

The summarised test results of this series are shown in fig. (6.4).

The normally consolidated samples were taken directly from the "as compacted" condition to the effective stress at which loading was started.

The "over consolidated" samples on the other hand were first consolidated to an effective stress of 110 p.s.i. before being swelled back to the effective stress at the start of loading.

Although the overconsolidation cycle produced a decrease in water content for the same resultant effective stress, there was no corresponding increase in strength. This will be discussed in a later section.

The soil in this condition shows a very clear cohesion intercept at both maximum $\frac{(\sigma_1 - \sigma_3)}{\sigma_3'}$ and at 20% strain. The shear strength parameters were:

at maximum $\frac{(\sigma_1 - \sigma_3)}{\sigma_3'}$: $c' = 2.6$ p.s.i. $\quad \phi' = 23.6^\circ$.

at 20% strain : $c' = 2.3$ p.s.i. $\quad \phi' = 23.5^\circ$.

The failure zone moisture contents are in all cases higher than the overall moisture contents of the samples. This is a manifestation of the non-uniform stress conditions in the triaxial test. (Considered in greater detail in Chapter 8).

(6.6) Test Series 3A : Mangla shale compacted at w = 16.3%.

This test series was similar to Series 1A except that only "normally consolidated" tests were performed. A similar non-uniformity in water contents at failure was noted.

The values of ϕ' have slightly increased over those found in Series 1A, but the cohesion c' has decreased. Numerical values are:

at maximum $\frac{(\sigma_1' - \sigma_3')}{\sigma_3'}$: c' = 1.4 p.s.i. ϕ' = 24.1°.

at 20% strain : c' = 0.4 p.s.i. ϕ' = 23.8°.

The summarised test results are shown in fig. (6.5).

(6.7) Test Series 2A : Selset clay compacted at w = 11.6%.

This series of tests was again similar to Series 1A. All tests were "normally consolidated". The soil is slightly different to that used for the partly saturated tests in that all stones retained on an $\frac{1}{8}$" sieve have been removed. The summarised test results are shown in fig. (6.6). No cohesion intercept is shown and the shear strength parameters were:

at maximum $\frac{(\sigma_1' - \sigma_3')}{\sigma_3'}$: c' = 0, ϕ' = 26.4°.

at 20% strain : c' = 0. ϕ' = 25.8°.

A series of drained tests on saturated samples of Selset clay by Brown (1961) do show an effective cohesion intercept. Brown's samples were taken undisturbed from the natural clay deposit and were

remoulded at their natural water content of 11.6%. The resulting samples had a dry density of 124.3 lb/ft^3 and a degree of saturation before saturating of 89.3%. The corresponding figures for the compacted samples were: dry density: 124.1 lb/ft^3 and degree of saturation: 87.1%.

The drained shear parameters corrected for rate of dilatation at failure were: $c' = 1.7$ p.s.i. $\phi' = 29.1^\circ$.

It is difficult to see how a difference in testing methods can lead to such a large difference in shear strength parameters. The Selset clay is known to be a fairly variable deposit and the difference may well be due to a genuine difference in soil properties. It is also possible that different stress histories could account for part of the difference. Tests on partly saturated Selset clay also appeared to show a cohesion intercept (see Chapter 7) and a slightly higher angle of friction.

The type of moisture content non-uniformity which is shown by this series of tests is similar to that which was noted in Series 1A and 3A.

(6.8) Test Series 4A : Saturated drained tests on compacted Talybont clay.

This test series had the double object of establishing an effective stress envelope for use in interpreting tests on partly saturated Talybont clay and to compare the results with those obtained by Alpan (1959) from consolidated undrained saturated tests on Talybont clay.

Two compaction moisture contents were used corresponding roughly to optimum and 2% dry of optimum and matching the moisture

contents used by Alpan.

The results of these tests are shown in fig. (6.7) and it is seen that for this soil drained and consolidated undrained saturated tests compare well.

The degree of equalisation for Alpan's tests was 95% which is much the same as that for the drained tests. At both compaction water contents there is good agreement between the consolidated undrained shear strength at maximum $\frac{(\sigma_1' - \sigma_3')}{\sigma_3'}$ and the drained shear strength corrected for the rate of dilatation at failure. Also the water contents of the failure zones in the drained and consolidated undrained tests agree fairly well.

(6.9) Discussion of the strength of saturated compacted soils.

(a) The equivalence of drained and consolidated undrained tests.

The results of test Series 4A shows that shear strengths obtained from drained and consolidated undrained tests on saturated compacted soils can be equivalent. Provided the following conditions are fulfilled, this conclusion will probably be generally true:

(a) Samples must have had the same stress history. This means that compaction water contents, compactive efforts and the method of saturating the soil must be the same in all cases.

(b) The tests must be run slowly enough to ensure that the pore pressure is uniform throughout the sample at failure.

(c) Tests must be compared using equivalent failure criteria.

(a) The effect of differing stress history has already been mentioned as a possible cause of non-equivalence in section (6.6). A difference in compaction water contents will cause differing initial densities and suctions which in turn will cause differences

in soil behaviour. This is shown by the tests of Series 1A, 3A and 4A in which different shear strength parameters were obtained in tests on the same soil compacted at different water contents.

(b) The tests of Series 4A were run at rates which gave about 95% equalisation of pore pressure. Casagrande and Hirschfeld (1960) have reported large differences between drained and consolidated undrained strength envelopes on a compacted clay which appeers to be very similar in its properties to Mangla shale. (L.L. = 34%, P.L. = 15%, 20% clay fraction ($<2_{\mu}$), optimum water content 15.7%, permeability about 10^{-8} cm/sec).

A typical duration for a drained (S) test was 20 days while that for an undrained (Q or R) test was 60 minutes. Assuming that $c_v = 3 \times 10^{-4}$ cm^2/sec., time factors for the 'S' and 'Q'or'R' tests were 10.3 and 0.08 respectively and the corresponding degrees of equalisation were 99% and 42% respectively. It is not surprising that the strength envelopes did not compare. A typical estimate of the error in base pore pressure measurement for one of the wetter Q tests (w = 19%) is 10 p.s.i. in a measured pore pressure change of 15.1 p.s.i.

(c) Fig. (6.7) shows that in order to get correspondence between drained and consolidated undrained tests, the results of the drained tests must be corrected for the rate of dilatation at failure. The consolidated undrained tests must be compared at maximum $\frac{(\sigma_1' - \sigma_3')}{\sigma_3'}$ and not at maximum $(\sigma_1' - \sigma_3')$.

In the drained test the points of maximum $\frac{(\sigma_1' - \sigma_3')}{\sigma_3'}$ and maximum $(\sigma_1' - \sigma_3')$ coincide and the maximum shear strength of the soil is mobilised at this point. In the consolidated undrained

test, however, the maximum shear strength parameters of the soil are developed at maximum $\frac{(\sigma_1' - \sigma_3')}{\sigma_3'}$. By the time maximum $(\sigma_1' - \sigma_3')$ has been reached, the shear strength parameters have usually decreased slightly. The correction of results for the rate of dilatation at failure will be discussed in Chapter 7.

Correlation of failure strains in Series 4A was not so satisfactory. For the tests with a compaction moisture content of 7.16%, the failure strains of the drained tests correlated best with the strains at maximum $\frac{(\sigma_1' - \sigma_3')}{\sigma_3'}$ for the undrained tests. This corresponds with the correlation of the shear strengths. On the other hand, for the tests with a compaction moisture content of 9.04%, the failure strains of the drained tests corresponded best with the strains at maximum $(\sigma_1' - \sigma_3')$ for the undrained tests. Strains at maximum $\frac{(\sigma_1' - \sigma_3')}{\sigma_3'}$ appeared to lie close to the line of correlation for the tests with a compaction water content of 7.16%.

(b) Tests on Mangla shale.

According to Hvorslev (1937, 1960), the shear strength of a soil in a normally consolidated or over consolidated state can be expressed as a function of the effective stress and the void ratio at failure. The measured shear strength τ_f of the soil is written as the sum of four components.

$$\tau_f = \tau_\phi + C_e + C_v + \tau_d$$

where

τ_ϕ is the "friction component" which depends on the effective stress at failure.

C_e is the "cohesion component" which depends on the void ratio (or the water content in saturated soils).

C_v is the "rheological component" which depends on the time to failure and decreases to zero with increasing time.

τ_d is the "dilatation component" due to volume changes at failure.

If C_v and τ_d are accounted for

$$\tau = (\tau_f - C_v - \tau_d) = \tau_\phi + C_e = \sigma'_f . \tan \phi'_e + C_e$$

For saturated soils, Hvorslev has shown that C_e at a given water content w is directly proportional to the equivalent consolidation pressure p_e. In a triaxial test p_e is the all-round consolidation pressure which produces w in a normally consolidated soil.

Bishop and Henkel (1957) have shown a dimensionless plot which can be used to obtain values of the parameters C_e and ϕ'_e. $\frac{(\sigma_1 - \sigma_3)}{2p_e}$ is plotted against σ'_3/p_e. This results in a straight line with a slope of $\frac{\sin \phi'_e}{(1 - \sin \phi'_e)}$ and an intercept on the $\frac{(\sigma_1 - \sigma_3)}{2p_e}$ axis of $\frac{C_e \cos \phi'_e}{p_e(1 - \sin \phi'_e)}$.

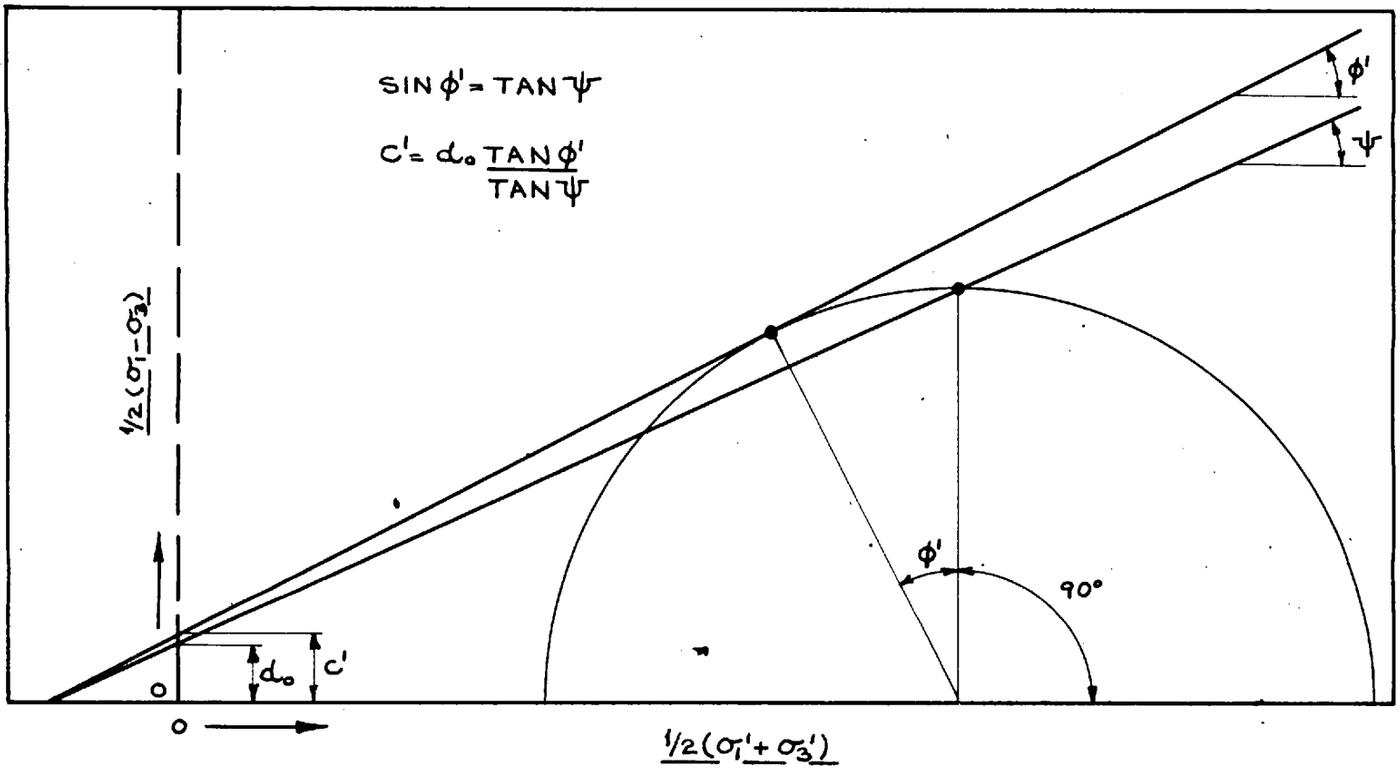
The results of Series 1A and 3A have been plotted on this basis in fig. (6.8). Values of p_e were based on the failure zone water contents. The triaxial consolidation line for Mangla shale normally consolidated from a water content close to the liquid limit is included in the Appendix to Chapter 8. Two distinct lines result, one appropriate to each compaction water content. The "normally" and "over" consolidated tests of Series 1A appear to cluster about a single line. The lines converge and if extended intersect at a point

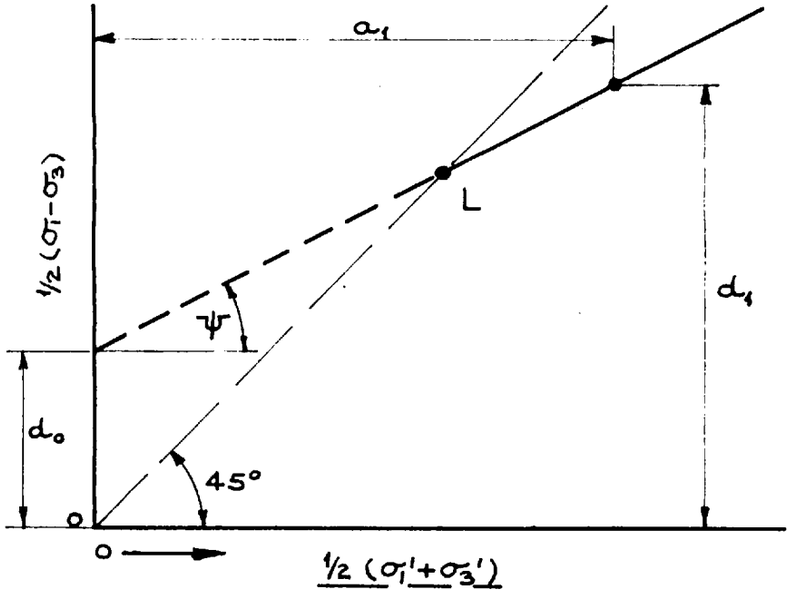
corresponding to $\frac{(\sigma_1' - \sigma_3')}{\sigma_3'} = 1.37$.

Because the strengths do not lie on a single line, it seems that the strength of a saturated compacted soil depends not only on the effective stress and water content at failure, but also on the compaction water content.

In fig. (6.9) maximum values of $\frac{(\sigma_1' - \sigma_3')}{\sigma_3'}$ measured in Series 1A and 3A have been plotted against the corresponding consolidation pressures. If extended, these lines intersect the value of $\frac{(\sigma_1' - \sigma_3')}{\sigma_3'} = 1.37$ at approximately the same consolidation pressure (350 p.s.i.). The result of a test on a moulded consolidated sample (described in Chapter 8) indicates a maximum value of $\frac{(\sigma_1' - \sigma_3')}{\sigma_3'}$ for normally consolidated samples of Mangla shale of 1.3. Allowing for scatter, the true value could easily be 1.37.

The compaction water content seems to have influence on the shear strength of the soil until the consolidation pressure is large enough to exceed the "pre-stress" imparted to the soil by compaction.



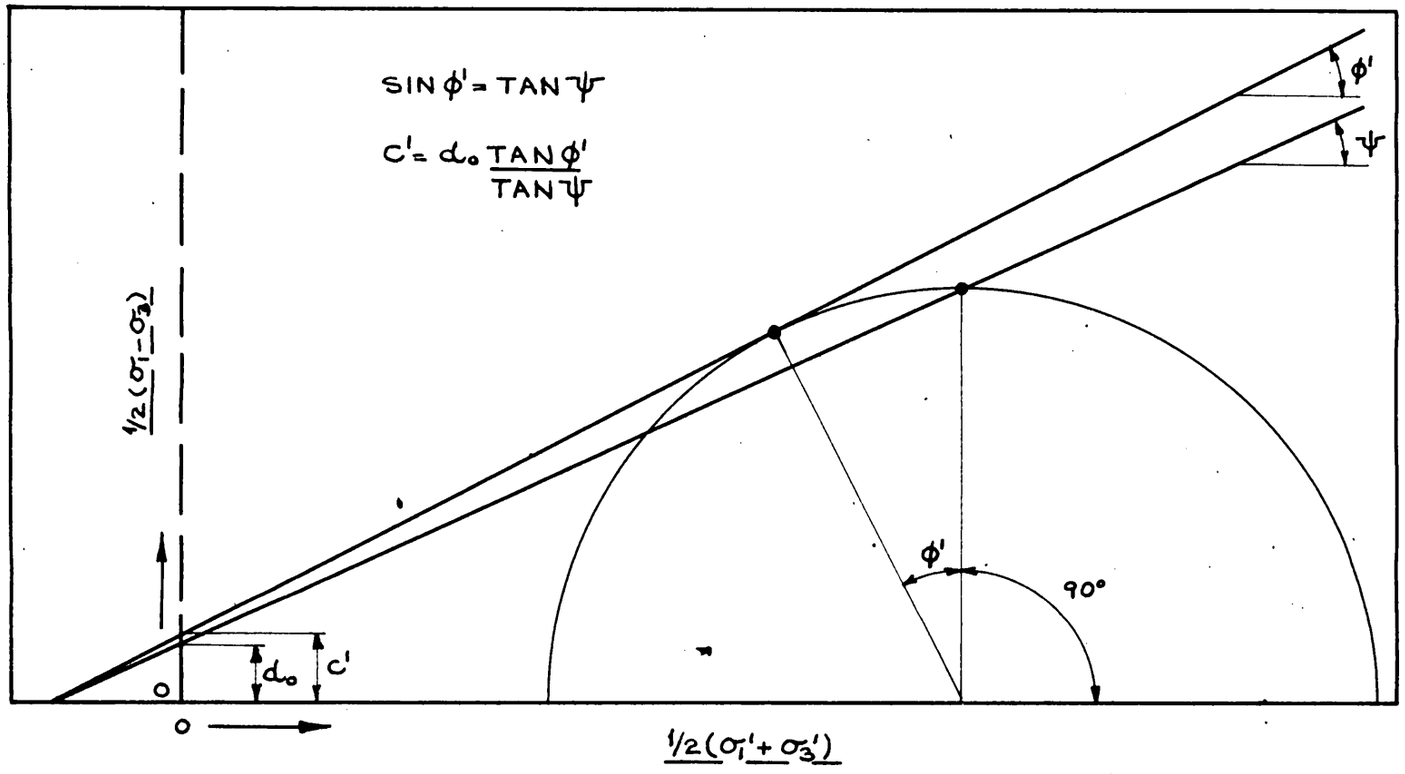


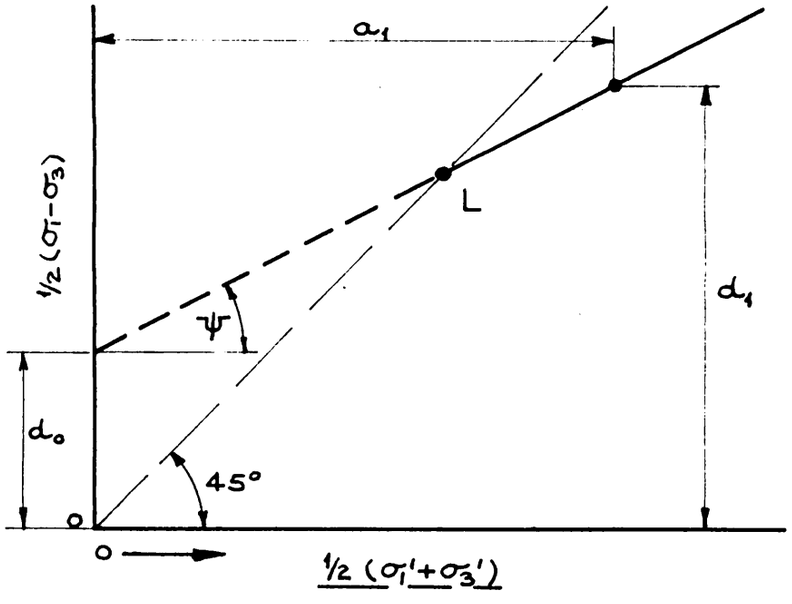
$$R = \frac{\sigma_1 - \sigma_3}{\sigma_3'} = \frac{2d_0 + 2a_1 \tan\psi}{a_1(1-\tan\psi) - d_0}$$

FOR $d_0 = 0$ $\quad R = \frac{2\tan\psi}{(1-\tan\psi)} = \frac{2\sin\phi'}{(1-\sin\phi')}$

METHOD OF PLOTTING TRUE EFFECTIVE STRESS RESULTS.

FIG. 6.1.



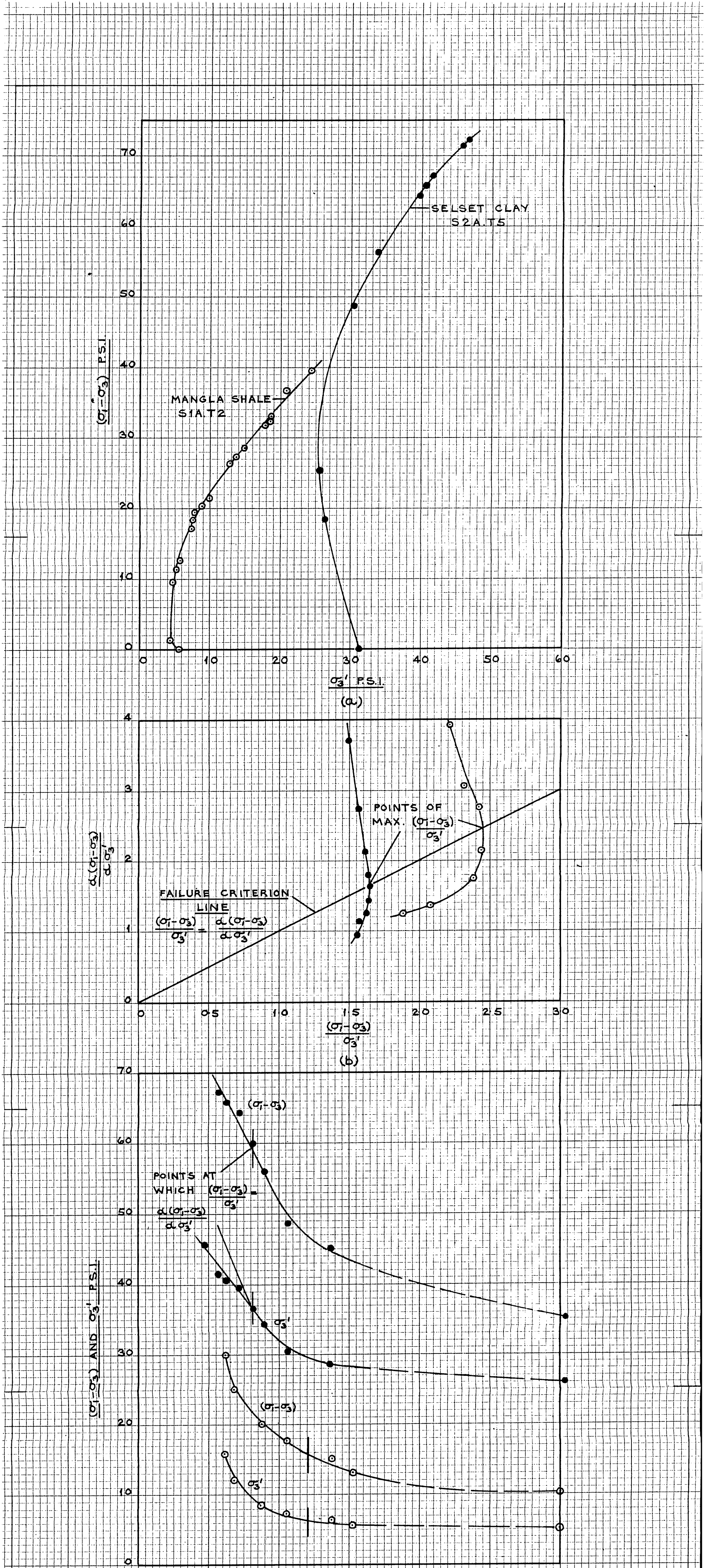


$$R = \frac{\sigma_1 - \sigma_3}{\sigma_3'} = \frac{2d_0 + 2a_1 \tan\psi}{a_1(1-\tan\psi) - d_0}$$

FOR $d_0 = 0$ $\quad R = \frac{2\tan\psi}{(1-\tan\psi)} = \frac{2\sin\phi'}{(1-\sin\phi')}$

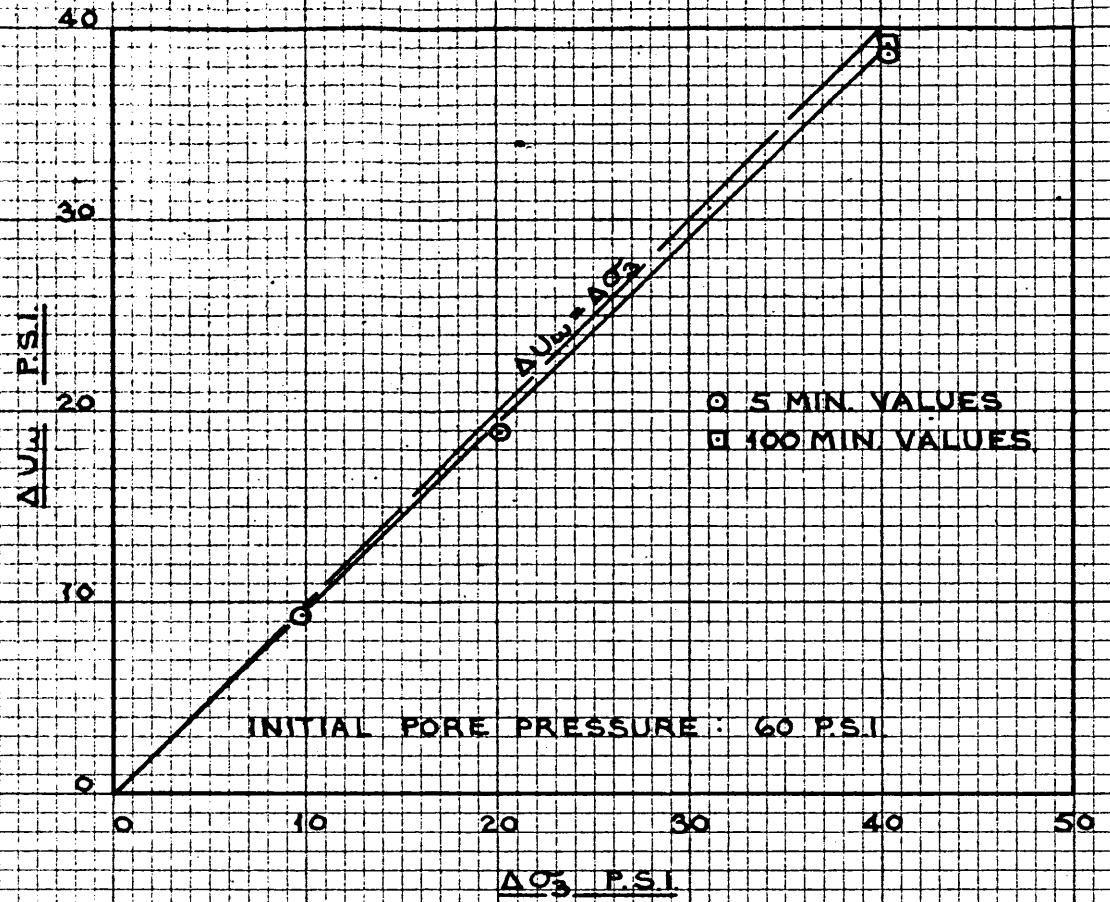
METHOD OF PLOTTING TRUE EFFECTIVE STRESS RESULTS.

FIG. 6.1.



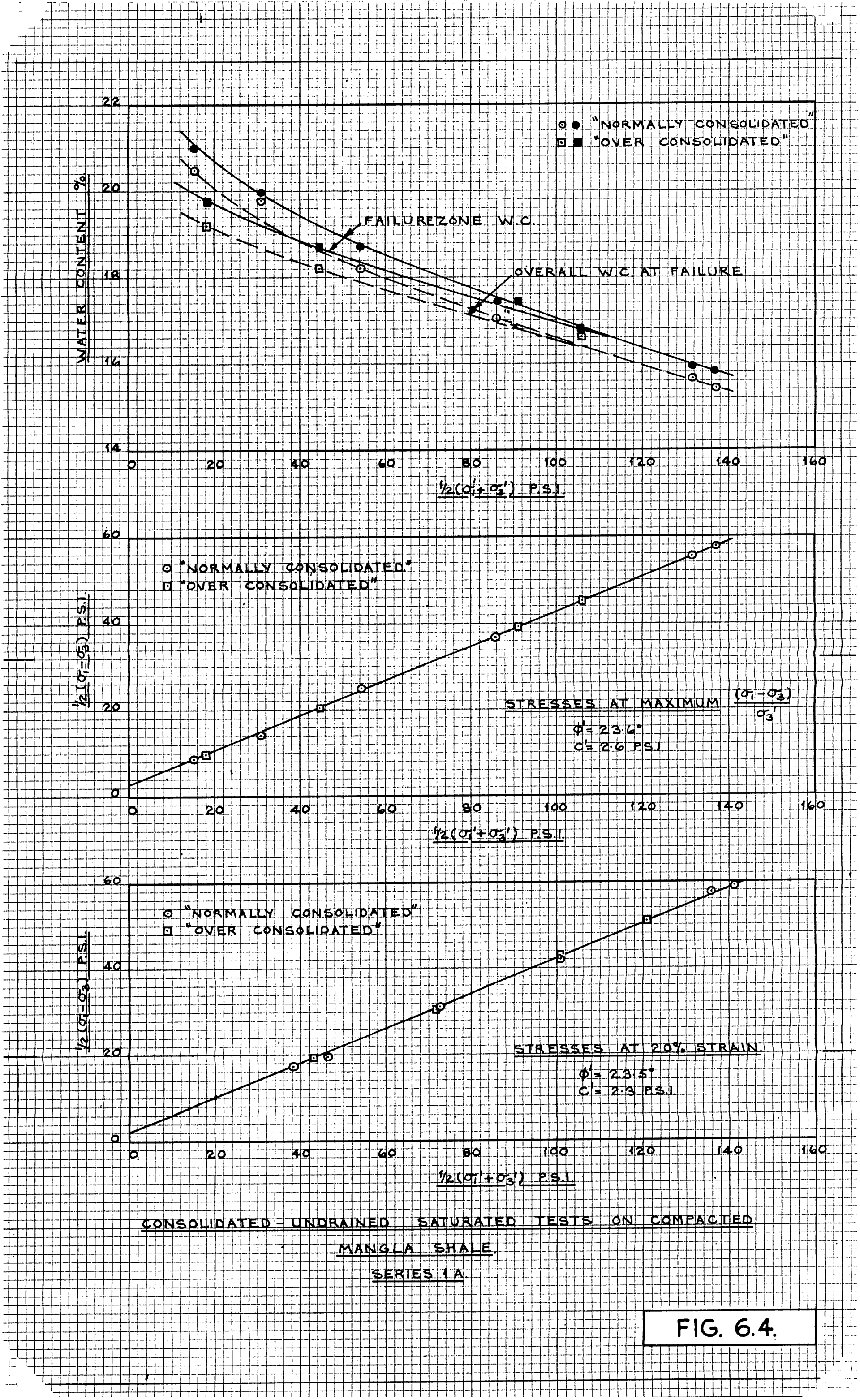
EXAMPLE OF STRESS PLOT USED WITH CRITERION FOR MAXIMUM SHEAR STRENGTH PARAMETERS.

FIG. 6.2.



CHANGES IN PORE WATER PRESSURE WITH ALL-ROUND STRESS IN A SAMPLE OF SELSET CLAY SATURATED BY BACK PRESSURE (= 60 P.S.I.).

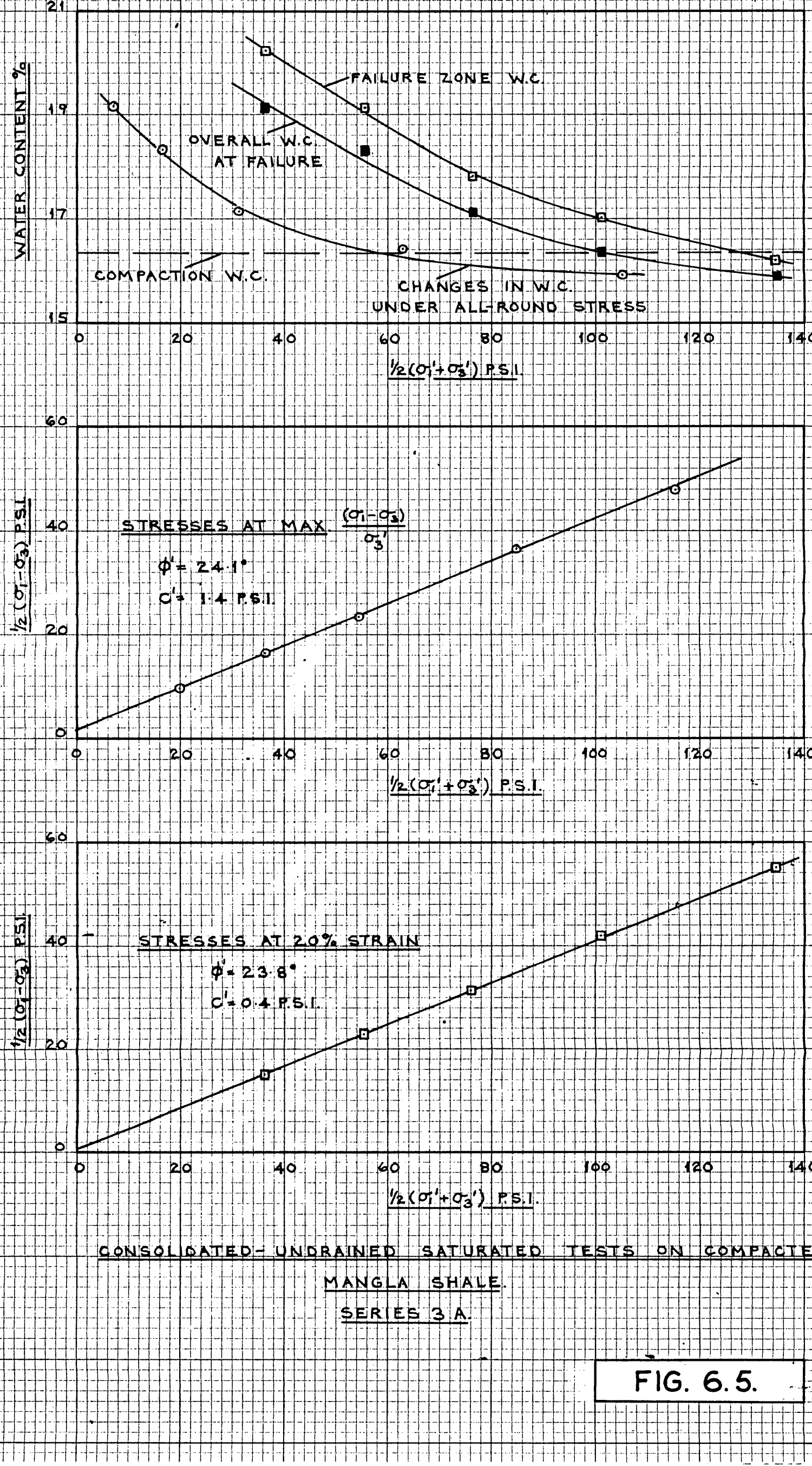
FIG. 6.3.



CONSOLIDATED - UNDRAINED SATURATED TESTS ON COMPACTED MANGLA SHALE.

SERIES 1A.

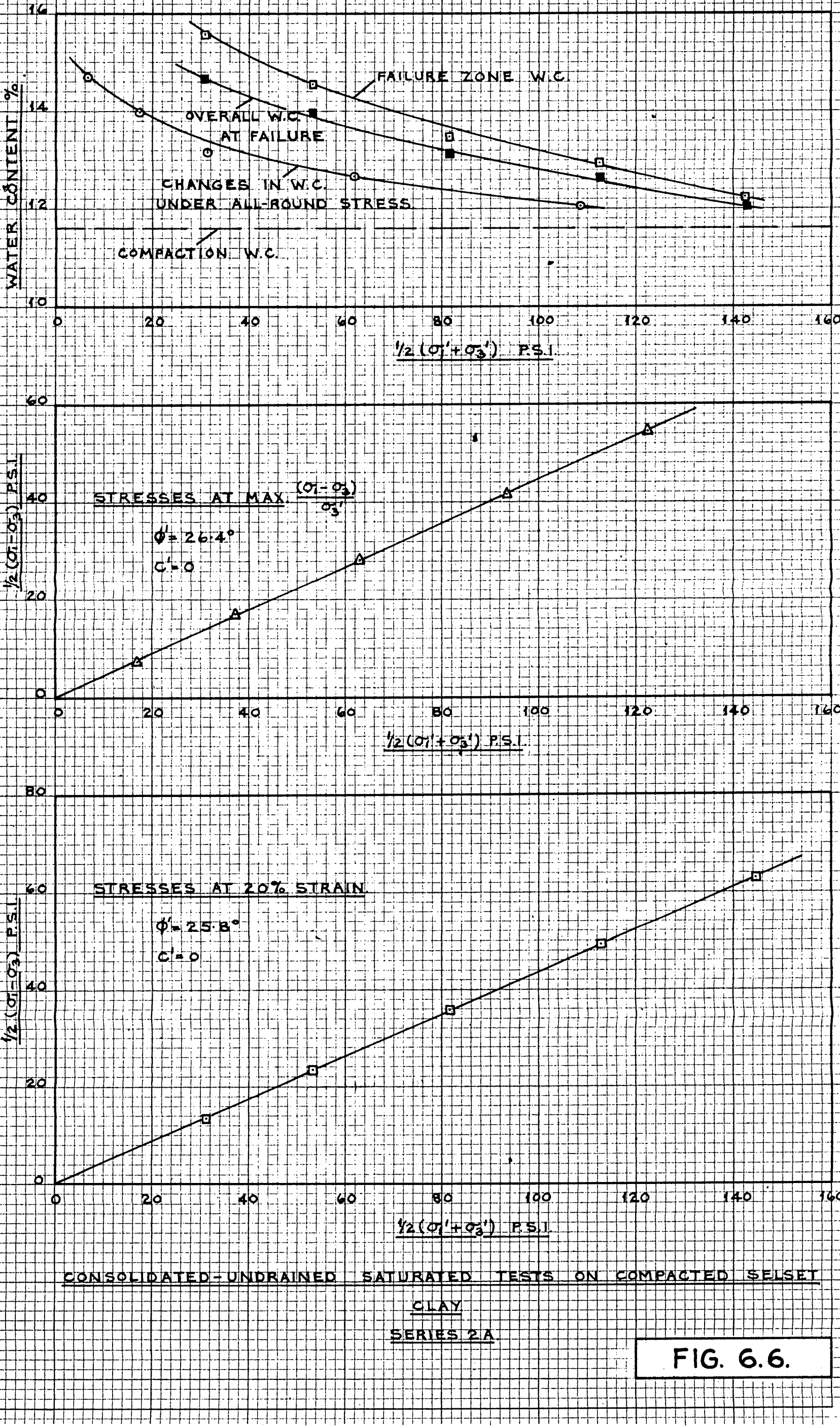
FIG. 6.4.



CONSOLIDATED- UNDRAINED SATURATED TESTS ON COMPACTED MANGLA SHALE.

SERIES 3 A.

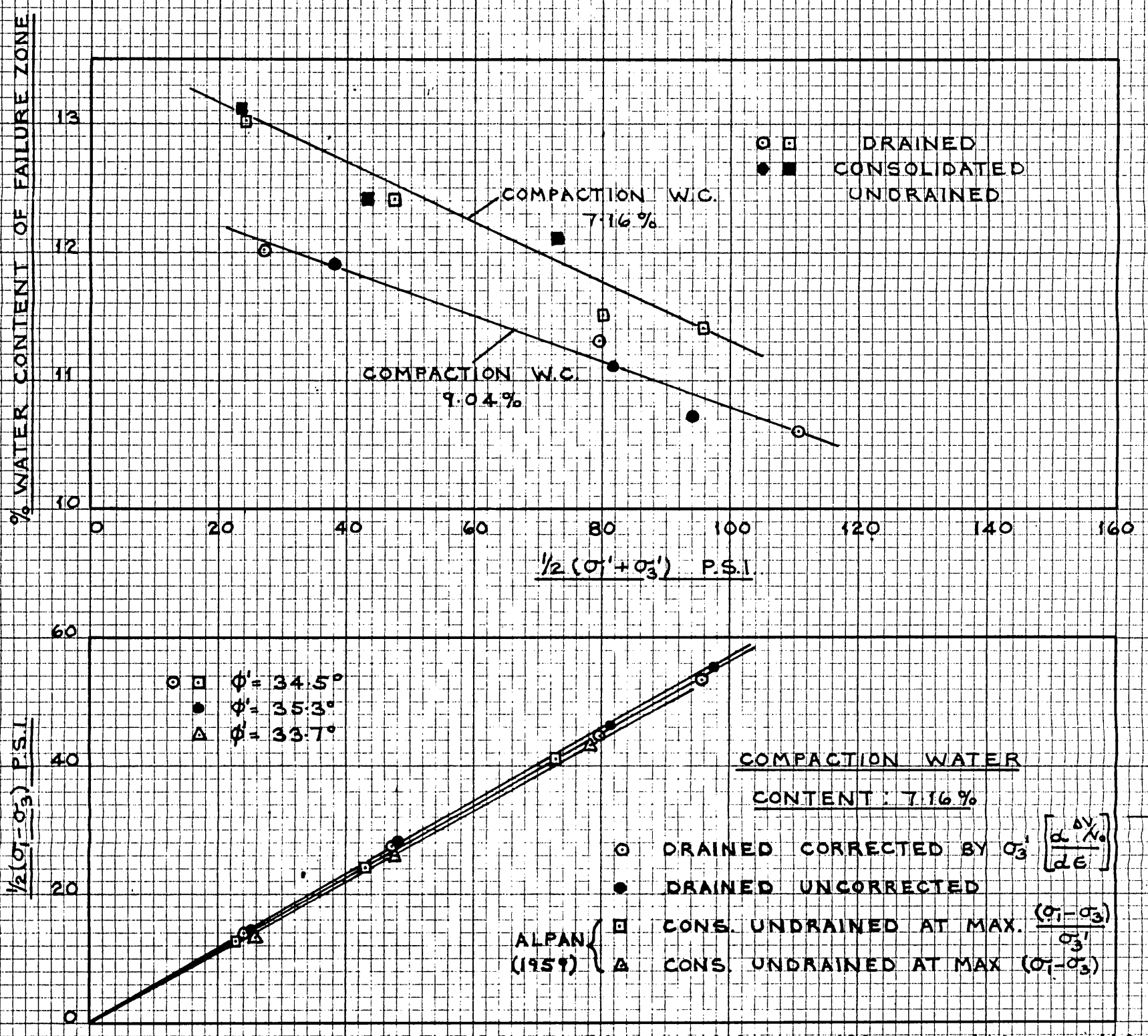
FIG. 6.5.

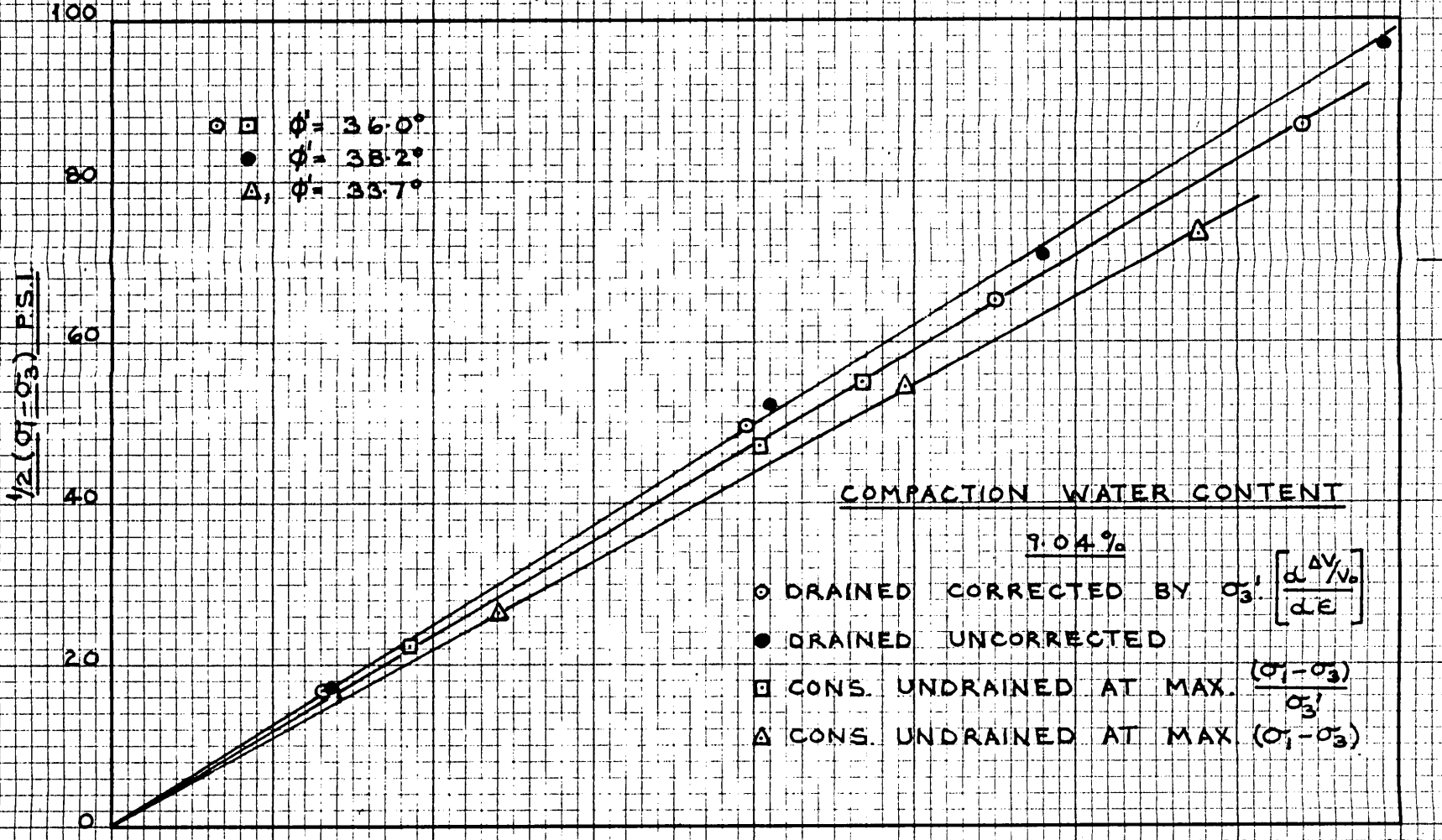


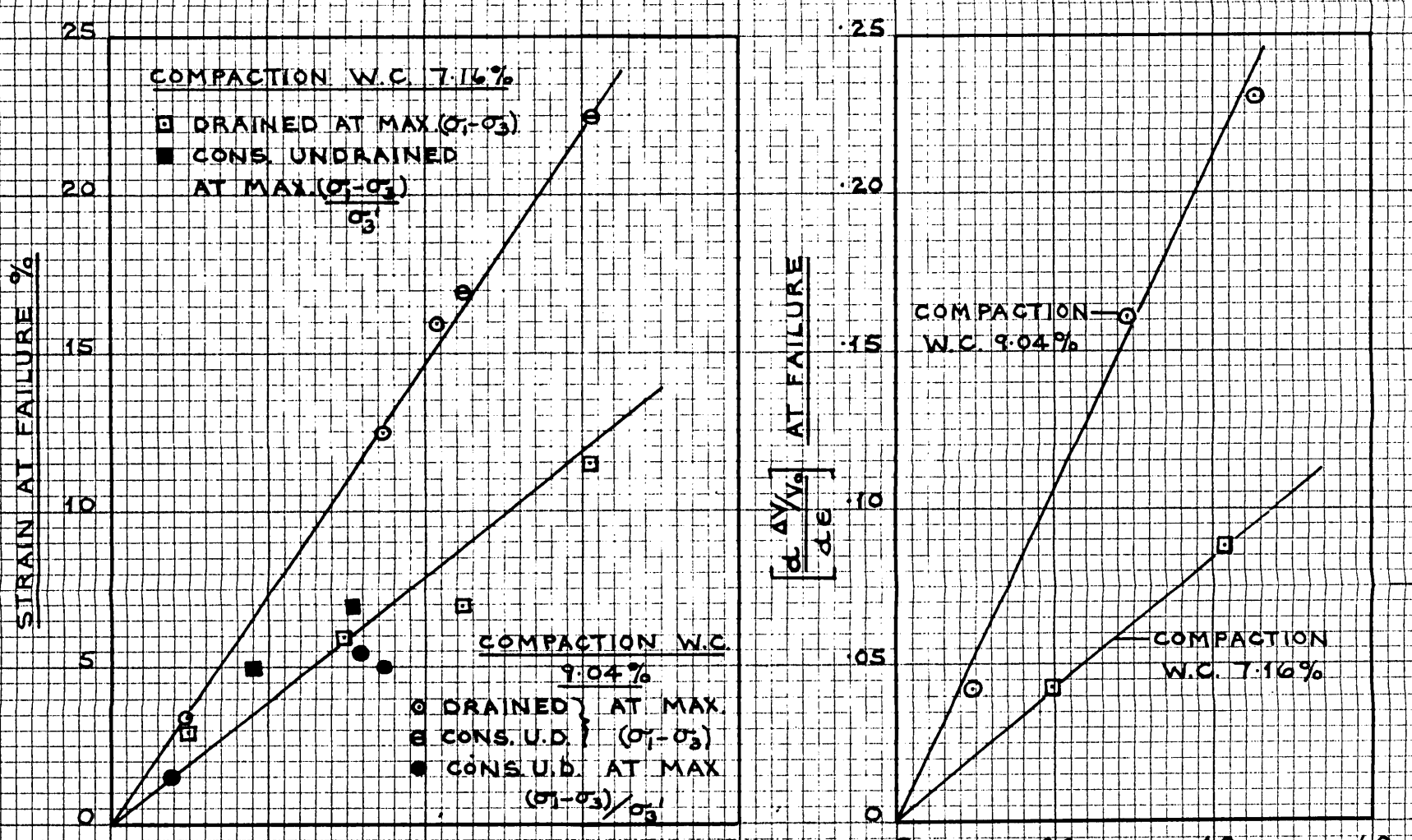
CONSOLIDATED - UNDRAINED SATURATED TESTS ON COMPACTED SELSET CLAY

SERIES 2A

FIG. 6.6.



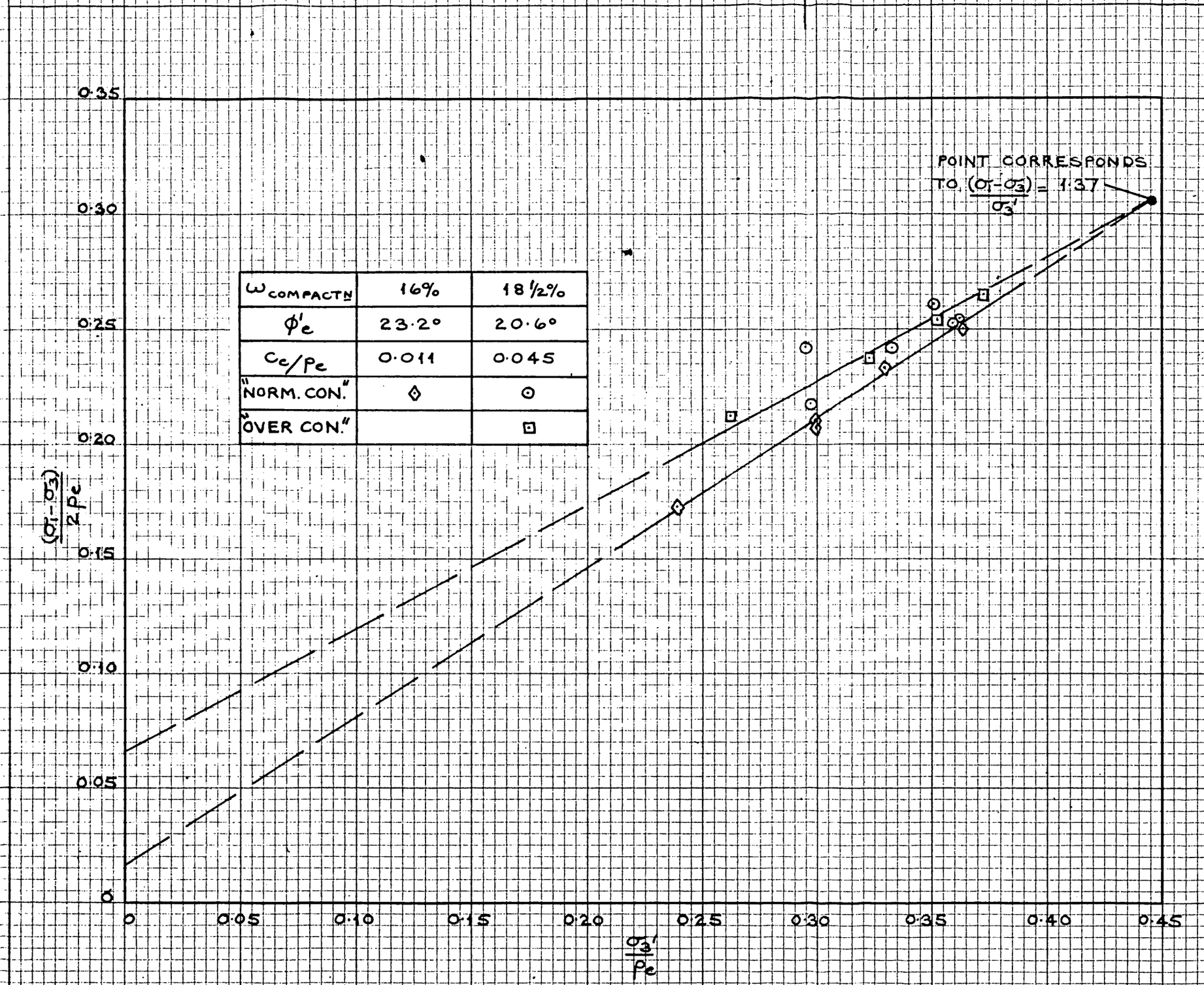




COMPARISON OF DRAINED AND CONSOLIDATED UNDRAINED TESTS ON COMPACTED TALYBONT CLAY SATURATED BY BACK PRESSURE.

SERIES 4A.

FIG. 6.7.



HVORSLEV TYPE PLOT FOR TESTS ON SATURATED COMPACTED MANGLA SHALE.
CONDITIONS AT 20% STRAIN.

FIG. 6.8.

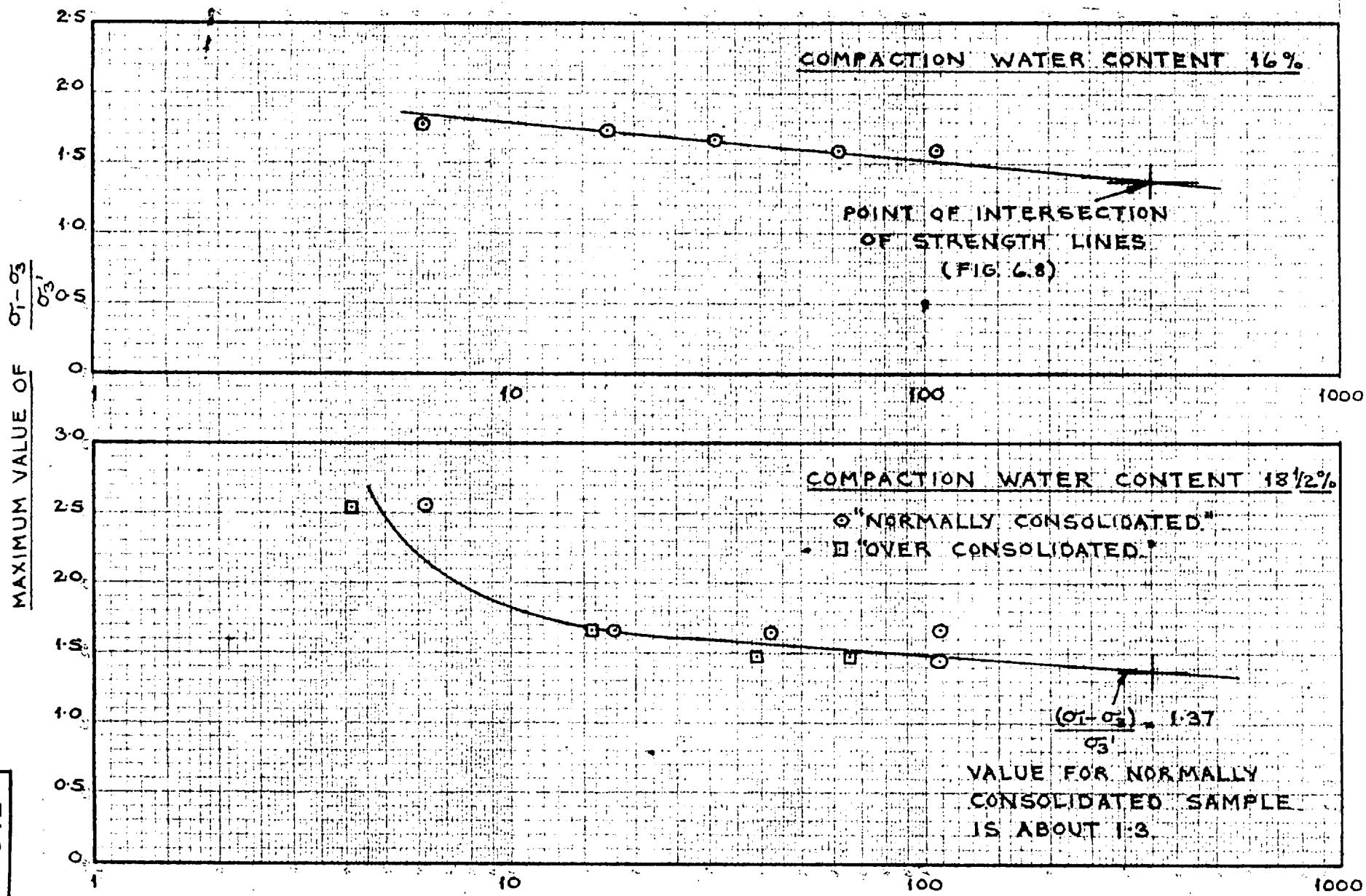


FIG. 6.9.

MANGLA SHALE (TEST SERIES 1A & 3A) – OVERCONSOLIDATION DUE TO COMPACTION.

CHAPTER 7

THE STRENGTH OF COMPACTED PARTLY SATURATED SOILS AND THE MEASUREMENT OF THE PARAMETER χ IN THE EFFECTIVE STRESS LAW FOR SHEAR

(7.1) Types of strength test used.

It was seen in Chapter 5 that the state of effective stress in a compacted soil depends primarily on two factors:

(i) the compaction moisture content, and

(ii) the confining pressure $(\sigma_3 - u_a)$.

The shear strength and effective stress parameters for a partly saturated compacted soil can thus be investigated from two points of view:

(i) Keeping the compaction moisture content constant the effect of varying $(\sigma_3 - u_a)$ can be studied.

(ii) Keeping $(\sigma_3 - u_a)$ constant the effect of a varying compaction moisture content can be investigated.

It is also possible to compare a series of tests with one constant moisture content and varying $(\sigma_3 - u_a)$ with another such series at a second moisture content. The same can be done with two series of tests at differing constant values of $(\sigma_3 - u_a)$ and varying moisture content.

There are basically three types of test which can be performed on partly saturated compacted soils, tested at their compaction water content.

(a) True undrained tests.

(b) Constant water content, varying $(\sigma_3 - u_a)$ tests.

(c) Constant water content, constant $(\sigma_3 - u_a)$ tests.

(a) True undrained tests.

A true undrained test on a partly saturated soil is defined as one in which the masses of air and water contained by the soil remain constant throughout the test. In an undrained test changes occur in both pore air pressure and pore water pressure.

A truly undrained state is difficult to achieve in practice. It was pointed out in Chapter 3 that the normal latex rubber membrane is permeable to air, and most liquids suitable for use as cell fluids have an appreciable capacity for dissolving air.

The only fairly simple and practicable way of ensuring a truly undrained state which has yet been devised is to use mercury as a cell fluid. This type of test has been successfully performed by Donald (1961).

Another limitation of the undrained test is the small range of negative pore pressures which can be measured without using elevated air pressures. The equilibrium pore air pressure in an unstressed sample of compacted soil is generally below atmospheric. Also, in compacted soils, $(u_a - u_w)$ often increases rapidly as the soil approaches failure. (This depends on the compaction water content, the value of $(\sigma_3 - u_a)$ and the soil type). As a result it is rarely possible to successfully complete a true undrained test if the initial value of $(u_a - u_w)$ exceeds about 6 p.s.i.

There are possible ways of extending the range of the true undrained test. One way is to lower the surface tension of the pore water by means of chemical additives. In a soil whose pore water has a lowered surface tension, all values of suction will be lowered

by an amount proportional to the lowering in surface tension.

Another method is to raise the pressure of the water in the measuring system by dissolving in it a substance which at a given concentration and temperature has a known osmotic pressure relative to the pure water in the soil pores. The suction in the soil water will then be registered as a lowering of the pressure in the measuring system. The porous element contacting the soil water would have to be of sufficiently small pore size to act as a semi-permeable membrane.

(b) Constant water content, varying $(\sigma_3 - u_a)$ tests.

This type of test is really a "partially undrained" test. An ordinary latex rubber membrane is used to enclose the sample and the cell fluid is (in this thesis) water. After setting up the sample, the cell pressure is applied and the pore pressures in the sample are allowed to come to equilibrium. The cell fluid dissolves as much of the pore air as it requires. The pore air pressure measuring lead is either left closed and an initial negative air pressure is tolerated or else it is left open and the pore air pressure equalises to atmospheric pressure. Alternatively, an elevated air pressure can be applied to the air lead. In any case, before the axial loading commences, the cell fluid is allowed to take up as much air through the sample membrane as it requires.

Once equilibrium has been reached, the air pressure lead is connected to a null indicator and axial loading is commenced. Changes in both pore air and pore water pressures then take place. As the cell fluid is now saturated at its pressure with dissolved air, little further loss in pore air occurs during the test.

(c) Constant water content, constant $(\sigma_3 - u_a)$ tests.

This type of test is similar to the type of test described under (b). Initial equilibrium is set up with the pore air pressure maintained at atmospheric pressure or at a suitable elevated value. The sample is sheared with the pore air pressure maintained at its constant value. Thus only changes in u_w take place.

This type of test is simpler to perform than types (a) and (b) since only pore water pressures need be measured. The cell fluid is free to take up as much air through the sample membrane as it requires without affecting the pore air pressure.

A limiting form of this type of test is the "unconfined test" in which u_a is controlled to be equal to σ_3.

(d) Testing times.

It must be emphasised that for correct measurement and control of pore air and pore water pressures, not only must sufficient time be allowed for an initial pore pressure equilibrium to be established, but rates of strain must be sufficiently slow to allow for virtually complete equalisation of pore pressures during shear.

The reader is referred to Chapters 8 and 9 for more detailed consideration of equalisation times and rates of strain.

(7.2) The determination of the α factor from the results of tests on partly saturated soils.

In determining values of the parameter α from the results of tests on partly saturated soils, the simplest procedure is to assume that for a given compaction moisture content and hence for a given initial dry density, the values of c' and ϕ' for the soil are independent of the degree of saturation. Values of α can then be

found by a direct comparison of stresses measured on the partly saturated soil with corresponding stresses measured on the saturated soil.

There are, sometimes, certain discrepancies between results which lead one to think that the presence of air in the voids may modify the values of c' and ϕ' of the soil to a slight degree. The structure of a compacted partly saturated soil also leads to rather anomalous values of χ if the simple procedure outlined above is used. Nevertheless, the "apparent" value of χ is still the simplest and most convenient practical way of accounting for the behaviour under stress of a partly saturated soil.

(7.3) Semi-graphical procedures for determining χ.

The comparison between the true effective stress curve and the stress curves obtained from tests on a partly saturated soil is most easily made by semi-graphical means.

(a) Tests at constant moisture content and various values of $(\sigma_3 - u_a)$.

The method of plotting results which was described in Chapter 6 can easily be extended for use with the results of tests on partly saturated soils.

Fig. (7.1)a illustrates the most general form of this type of plot. $\frac{1}{2}(\sigma_1 + \sigma_3) - u_w$ and $\frac{1}{2}(\sigma_1 + \sigma_3) - u_a$ are in turn plotted against $\frac{1}{2}(\sigma_1 - \sigma_3)$. For a series of tests at constant water content and various values of $(\sigma_3 - u_a)$, a pair of lines is obtained which converge as $(\sigma_3 - u_a)$ increases and the degree of saturation of the soil approaches unity. The true effective stress line will be between the lines representing $\frac{1}{2}(\sigma_1 + \sigma_3) - u_w$ and $\frac{1}{2}(\sigma_1 + \sigma_3) - u_a$. These lines will coincide with the true effective stress line once

saturation is reached. i.e. at the point $S = \chi = 1$.

At a given moisture content, the lowest state of stress in the soil is represented by an unconfined test for which $\sigma_3 = u_a$. A line at 45° through the origin represents the equation $(\sigma_3 = u_a)$. No test result can lie to the left of this line.

Referring to fig. (7.1)a:

$$a = \tfrac{1}{2}(\sigma_1 + \sigma_3) - u_w = \tfrac{1}{2}(\sigma_1 - \sigma_3) + (\sigma_3 - u_w)$$

$$b = \tfrac{1}{2}(\sigma_1' + \sigma_3') = \tfrac{1}{2}(\sigma_1 - \sigma_3) + \sigma_3'$$

$$c = \tfrac{1}{2}(\sigma_1 + \sigma_3) - u_a = \tfrac{1}{2}(\sigma_1 - \sigma_3) + (\sigma_3 - u_a)$$

$$d = \tfrac{1}{2}(\sigma_1 - \sigma_3)$$

The effective stress equation is:

$$\sigma_3' = (\sigma_3 - u_a) + \chi(u_a - u_w)$$

or, in terms of a, b, c and d

$$b - d = c - d + \chi(a - c)$$

or $$\chi = \frac{b - c}{a - c}$$

Note that $e = b - c$ and $f = a - c$

hence $$\chi = \frac{e}{f}$$

It is a simple matter to scale off e and f using dividers and hence obtain χ by one setting of a slide rule.

(b) <u>Tests at various moisture contents with $\sigma_3 = u_a$.</u>

In the case of the unconfined test for which $\sigma_3 = u_a$, the pore air pressure stress line degenerates to a line at 45° through the origin. i.e. $\tfrac{1}{2}(\sigma_1 - \sigma_3) = \tfrac{1}{2}(\sigma_1 + \sigma_3) - u_a$

or $$\sigma_3 = u_a$$

Referring to fig. (7.1)b

$$a = \tfrac{1}{2}(\sigma_1' - \sigma_3') + (\sigma_3' - u_w)$$

$$b = \tfrac{1}{2}(\sigma_1' - \sigma_3') + \sigma_3'$$

$$c = \tfrac{1}{2}(\sigma_1' - \sigma_3') = d$$

The effective stress equation becomes:

$$\sigma_3' = \alpha(u_a - u_w)$$

or $$b - c = \alpha(a - c)$$

i.e. $$\alpha = \frac{b - c}{a - c} = \frac{e}{f}$$ as before.

As all compacted unconfined samples are partly saturated the line $\frac{1}{2}(\sigma_1' + \sigma_3') - u_w$ will generally always lie below the true effective stress line.

In a series of tests at a constant confining pressure and at different water contents, the true effective stress line will probably not be straight but a curve. It was found in Chapter 6 that both the cohesion and friction components of the strength of a compacted soil vary with water content. Donald (1961) has found that the strength envelope for a saturated clay remoulded at different water contents is a curve which intersects zero. In the diagrams of fig. (7.1) the true effective stress lines (for convenience) have generally been shown as straight lines although that in fig. (7.1)b has been shown curving round at low stresses as if to intersect the origin.

(c) Tests at various water contents with $(\sigma_3' - u_a)$ constant.

Referring to fig. (7.1)c: A line which represents a constant value of $(\sigma_3' - u_a)$ can be constructed by setting off the value of $(\sigma_3' - u_a)$ along the $\frac{1}{2}(\sigma_1' + \sigma_3') - u_a$ axis. A line at 45° through this point then represents the equation

$$(\sigma_3' - u_a) = Y \text{ (say) where Y is a constant.}$$

This can be seen by extending the 45° line back to cut the $\frac{1}{2}(\sigma_1 - \sigma_3)$ axis. Then:

$$\tfrac{1}{2}(\sigma_1 - \sigma_3) + Y = \tfrac{1}{2}(\sigma_1 + \sigma_3) - u_a$$

or $$(\sigma_3 - u_a) = Y$$

As in cases (a) and (b)

$$\chi = \frac{b - c}{a - c} = \frac{e}{f}$$

The lines $\frac{1}{2}(\sigma_1 + \sigma_3) - u_a$ and $\frac{1}{2}(\sigma_1 + \sigma_3) - u_w$ will in this case start off from a point on the true effective stress line at which $S = \chi = 1$ and diverge as the moisture content and degree of saturation of the samples decrease.

(d) Determination of χ from maximum values of $\frac{(\sigma_1 - \sigma_3)}{(\sigma_3 - u_w)}$ in unconfined tests.

The ratio $\frac{(\sigma_1 - \sigma_3)}{(\sigma_3 - u_w)}$ which in a saturated soil is equal to (principal effective stress ratio) - 1 becomes, in a test on a partly saturated unconfined sample, a direct measure of χ.

Define $R = \frac{(\sigma_1 - \sigma_3)}{\sigma_3'}$ $\qquad R_\chi = \frac{(\sigma_1 - \sigma_3)}{(\sigma_3 - u_w)}$

Referring to fig. (7.1)b

$$R = \frac{2c}{b - c} \qquad R_\chi = \frac{2c}{a - c}$$

$$\frac{R_\chi}{R} = \frac{b - c}{a - c} = \chi$$

The value of R is given by

$$R = \frac{2d_o + 2a_1 \tan\psi}{a_1(1 - \tan\psi) - d_o}$$ (See Chapter 6).

(7.4) The comparison of tests which fail at different strains and a note on failure criteria for partly saturated soils.

In comparing the results of tests on partly saturated soils

with those obtained from saturated soils, the question arises of what to use as a basis of comparison. Tests can be compared at the same strain, at peak principal stress ratio, at peak deviator stress, or at strains proportional to the respective strains at which either peak principal stress ratio or peak deviator stress occur. It is very seldom that a pair of comparable tests fail at the same strain. Even in comparing the results of a series of similar tests at differing effective stresses (e.g. to construct a failure envelope) it is usually found that the failure strain is different at each effective stress (see results of test Series 1A, 2A, 3A).

In fig. (7.2) a test on a partly saturated sample of compacted Mangla shale is compared with a pair of tests on saturated compacted Mangla shale. The strain at which maximum $\frac{(\sigma_1 - \sigma_3)}{(\sigma_3 - u_w)}$ occurred has been taken as the basic unit of strain. The fractions $\frac{3}{4}$, 1, $1\frac{1}{4}$, etc. refer to proportions for each test of the unit strain. In fig. (7.3) the tests have been compared to obtain stress paths (a) and (b) at strains proportional to the unit strain and (c) at the same strain.

Consider, firstly, the comparison of the two saturated tests. In fig. (7.4) is shown the development of the two shear parameters c' and ϕ' with strain. These diagrams were constructed from fig. (7.3). When compared at the same strain, c' increases rapidly to a maximum at a strain proportion of $\frac{3}{4}$ and thereafter declines steadily. ϕ' increases throughout the test. The behaviour of both c' and ϕ' therefore violate the condition discussed in Chapter 6 that both c' and ϕ' must be a maximum at maximum principal stress ratio.

When the tests are compared at proportional strains, c'

increases more slowly and reaches its maximum value at unit strain. Thereafter it remains almost constant. ϕ' reaches its maximum value at about $\frac{1}{2}$ the unit strain, remains constant until unit strain has been reached and then declines gradually. This does not violate the maximum principal stress ratio criterion.

Fig. (7.4) records the development of α with strain. When compared at the same strain, α starts at the unlikely value of 1.21 and then decreases to a more reasonable value of .92 at unit strain. When compared at proportional strains, values of α lie between 0 and 1 throughout.

In fig. (7.5) an unconfined test on Talybont clay at a water content of 7.3% is compared with a saturated drained test on the same soil compacted at 7.3%. (The method used is that of section (7.3)d). It is obviously absurd in this case to compare the tests at the same strain. (At maximum $\frac{(\sigma_1' - \sigma_3')}{(\sigma_3' - u_w)}$, $\alpha = 2.8$). Comparison at proportional strains, however, leads to a variation of α with strain which lies between 0 and 1.

It appears, therefore, that comparison of tests on a basis of strains which are proportional to those at which either maximum principal stress ratio or maximum deviator stress occur, is more reasonable than comparison at the same strain. Certain soils reach a maximum principal stress ratio but do not reach a maximum deviator stress even at very large strains. When all tests which are being compared have long passed the maximum principal stress ratio, i.e. are in a state of progressive failure, it does not appear to matter if the comparison is made at the same strain. It cannot be valid to compare (at the same strain) one test which has failed with another

which has not yet reached failure.

Note on failure criteria for partly saturated soils.

It was noted in Chapter 6 that in general there are three possible criteria of failure:

(1) Maximum $\frac{(\sigma_1' - \sigma_3')}{\sigma_3'}$ giving maximum values of the shear strength parameters.

(2) Maximum $(\sigma_1' - \sigma_3')$ at which the shear stress in the soil is a maximum.

(3) A limiting axial strain in cases where a maximum deviator stress is not reached.

All three criteria must be equally valid for both saturated and partly saturated soils.

The application of criterion (2) to a partly saturated soil presents no difficulty since $(\sigma_1' - \sigma_3')$ is a direct measure of true effective stress.

For a partly saturated soil criterion (1) becomes $\frac{(\sigma_1' - \sigma_3')}{\sigma_3'} = \frac{(\sigma_1' - \sigma_3')}{(\sigma_3 - u_a) + \chi(u_a - u_w)}$ which cannot be calculated without a knowledge of values of χ. The expression can be rewritten as: $\frac{(\sigma_1' - \sigma_3')}{\sigma_3'} = \frac{(\sigma_1' - \sigma_3')}{(\sigma_3 - \chi u_w) - u_a(1 - \chi)}$. As u_a usually does not vary as much as u_w, the obvious choice as an approximate substitute for the correct expression is: $\frac{(\sigma_1' - \sigma_3')}{(\sigma_3 - u_w)}$. This is analogous to the expression for a saturated soil and can be easily calculated.

For an unconfined test we have from section (7.3)d:

$$R_\chi = \chi . R$$

i.e. $$\frac{(\sigma_1' - \sigma_3')}{(\sigma_3 - u_w)} = \frac{\chi(\sigma_1' - \sigma_3')}{\sigma_3'}$$

In figs. (7.4) and (7.5) comparisons are shown between curves of $\frac{(\sigma_1 - \sigma_3)}{\sigma_3'}$ and $\frac{(\sigma_1 - \sigma_3)}{(\sigma_3 - u_w)}$ for the confined and unconfined tests considered earlier. In both cases the maximum values coincide, and hence it is thought that for tests on partly saturated soils a criterion of maximum $\frac{(\sigma_1 - \sigma_3)}{(\sigma_3 - u_w)}$ may be substituted for the correct one of maximum $\frac{(\sigma_1 - \sigma_3)}{\sigma_3'}$ without serious error.

(7.5) Correction of deviator stress for rate of dilatation at failure in constant water content tests on partly saturated soils.

The principle of correcting the results of drained tests on saturated soils for the work done in causing the sample to dilate at failure is well established (Bishop, 1950, Skempton and Bishop, 1954). Undrained tests on saturated soils fail at constant overall volume and hence no external work is consumed in volume change.

In constant water content tests on partly saturated soils, the presence of air in the voids allows the soil skeleton to change volume during shearing. If dilatation occurs at failure a correction should be made for the work expended in causing the dilatation, especially if the strength is to be compared with strengths measured at constant overall volume.

Following the notation of Skempton and Bishop:

let $(\sigma_1 - \sigma_3)_f$ be the measured deviator stress at failure.

$(\sigma_1 - \sigma_3)_{rf}$ be that part of the deviator stress required solely to overcome the cohesive and frictional components of the strength of the sample.

dW be the external work done during an increment of axial strain $d\epsilon$.

The work balance is:

$$(\sigma_1 - \sigma_3)_f \cdot d\epsilon = (\sigma_1 - \sigma_3)_{rf} \cdot d\epsilon + dW$$

i.e. $$(\sigma_1 - \sigma_3)_{rf} = (\sigma_1 - \sigma_3)_f - \frac{dW}{d\epsilon} \qquad E(7.1)$$

In a constant water content test on a partly saturated soil, the term $\frac{dW}{d\epsilon}$ is made up of the following components:

(i) Work done in expanding against the effective confining pressure $= \frac{d(\Delta V/V_o)}{d\epsilon} \cdot \left[(\sigma_3 - u_a) + \chi(u_a - u_w)\right]$.

(ii) Work done in increasing the surface area of the air-water menisci. [Manifested by the rate of increase of $(u_a - u_w)$].

(iii) Work done in causing migration of pore water towards the failure zone.

It is a moot point whether (ii) and (iii) are motivated by the consumption of external work or should be considered as components of a balanced internal redistribution of energy. In any case they are difficult to allow for by simple algebraic terms.

For a constant water content test on a partly saturated soil (neglecting terms due to (ii) and (iii) above):

$$(\sigma_1 - \sigma_3)_{rf} = (\sigma_1 - \sigma_3)_f - \frac{d(\Delta V/V_o)}{d\epsilon}\left[(\sigma_3 - u_a) + \chi(u_a - u_w)\right] \qquad E(7.2)$$

E(7.2) assumes that the parameters χ for volume change and shear are identical. This has not been definitely established, but it will be shown in Chapter 9 that this is not an unreasonable assumption.

Note that there is a dilatation correction even for an unconfined test, viz:

$$\frac{d(\Delta V/V_o)}{d\epsilon} \cdot \chi(u_a - u_w) \qquad E(7.3)$$

The correction for rate of dilatation, in the form of E(7.2) assumes a uniform volume change throughout the mass of the triaxial sample. In actual fact, frictional restraint applied by the rigid loading plates will prevent the ends of the sample from expanding and may even cause the end zones to contract while the central failure zone is expanding. In most cases, end restraint will cause an underestimation of the magnitude of the correction for the rate of dilatation of the failure zone.

(7.6) Procedure in testing.

(a) Procedure in constant water content, varying $(\sigma_3 - u_a)$ tests.

This type of test was used for test Series 1 on Mangla shale and Series 2 on Selset clay. After thoroughly de-airing the pore water pressure measuring system and reducing the de-airing pressure in the manner described in Chapter 3, the cell was emptied of water and removed. A pool of water was left lying on the surface of the ceramic disc to prevent it from drying out. All other water was mopped up and the water was cleared from the air pressure measuring lead.

In tests in which the pore air pressure was measured during the shear stage, the air pressure measuring lead was taken through the base of the cell and connected through the sample membrane about $\frac{1}{2}$" above the base. This reduced the volume of air lead between the sample and the null-indicator to a minimum.

The membrane which was to be used in the test was fitted with the through connector to take the pore air pressure lead and placed ready on the membrane stretcher.

The sample was prepared using the compacting machine and the

4" diameter x 8" high segmental mould described by Bishop and Henkel (1957). A thin film of silicone grease (which does not attack latex rubber) was spread over the surface of the mould to prevent the soil from sticking to it. The soil was compacted in 5 layers with 25 blows per layer. In order to key successive layers of compacted soil together, the surface of each layer was scarified lightly before placing the next layer. Moisture content samples were taken from the soil in the bin as the sample was being compacted.

It was assumed that the water content of the sample was the same as that of the soil in the bin. This assumption was checked on several occasions. A number of water content specimens were taken from various positions in the failed sample and the water contents were graphically integrated over the volume of the sample to obtain an average overall water content. This average was found to check with the water content of the soil at compaction.

After completing the compaction, the collar was removed from the mould and the surface of the soil was trimmed. Particular care was taken to achieve a smooth flat surface for this surface was to make contact with the porous ceramic disc. The response of the pore water pressure measuring system is greatly impaired if its contact area with the sample is small.

Samples which had been tested were broken up using a domestic cheese grater. This procedure produced a uniformly fine crumbled soil for recompaction and helped to standardise the structure of the compacted soil.

The sample was next removed from the mould, its height and diameter were carefully measured and it was weighed. A strip of 1"

wide coarsely woven glass fibre ribbon was next wrapped two or three times around the sample just above the carefully trimmed end and held in place by a narrow elastic band.

After wiping off the excess water from the surface of the ceramic disc using a clean piece of paper towelling, the sample was lightly placed in position with the trimmed end towards the ceramic disc. At this stage, with samples having a high suction, care was taken not to press or rub the sample against the surface of the ceramic disc and thus establish good contact with it. This would have lead to the application of a large suction to the water in the ceramic disc which might have cavitated the water below the disc.

The membrane was now placed over the sample taking care that the hole in the air pressure connector was clear of the elastic band and in contact with the glass fibre ribbon. After fitting the rubber O-rings to seal the membrane to the sample cap and the base pedestal, the air pressure lead was connected into the sample.

The cell was next placed in position, bolted down and filled, taking care not to entrap any bubbles of air. When the cell was full, the air entrapped in the oil cup was sucked out and the oil cup was filled with castor oil. The cell was now sealed with the ram raised and the volume gauge was brought into the circuit.

If the initial pore air pressure was to be atmospheric, the valve at the end of the air pressure lead was left open to atmosphere. If the pore air pressure was to be elevated, the valve was closed and connected to the air pressure control valve. The required pore air pressure was set on the control valve.

The cell pressure was now applied, and as soon as it had

increased above the value of the applied air pressure, the air pressure valve was opened. After allowing the sample to come to equilibrium under the cell pressure and the applied pore air pressure (see Chapter 9 for details of equilibrium times), an initial reading of the pore water pressure was taken. The air pressure valve was then shut, disconnected from the pressure supply and reconnected to the pore air pressure null indicator.

After reading the volume gauge, the strain dial gauge and proving rings were fitted, and the ram was brought into contact with the loading cap. Zero readings for axial strain, load and volume change were now taken and the loading was started.

Readings of pore air and water pressures, axial strain, load and volume change were taken at intervals throughout the test. At the slow rates of strain which were used, it was only necessary to take three sets of readings each day.

At the end of the test, the sample was removed from the cell and check weighed as a precaution against small, unnoticed leaks.

(b) Procedure in constant water content, constant $(\sigma_3' - u_a)$ tests. $(\sigma_3'$ greater than $u_a)$.

The procedure in these tests was very similar to that described in (a) above. When air pressures were being controlled during the shear stage it proved more convenient to connect the air pressure lead through the top cap. This simplified setting up the sample by eliminating the side connection through the membrane. A cross formed of two double pieces of glass fibre tape was laid on the top of the sample to help distribute the application of the air pressure.

The samples were sheared with the pore air pressure maintained

constant. When dismantling the test the air pressure valve was closed before releasing the cell pressure to prevent the membrane from bursting.

(c) Procedure in unconfined tests ($\sigma_3 = u_a$).

In unconfined tests with atmospheric or low pore air pressures (up to about 30 p.s.i.) the procedure was that described in Chapter 5 (Section (5.4)(i)). The air pressure was applied directly into the cell.

When higher air pressures were used (up to 75 p.s.i.), the danger of an accidental explosion of the air filled cell was lessened as follows: The sample was set up as described in (b) above. The ram was brought into contact with the loading cap and clamped in position. The condition that $\sigma_3 = u_a$ was satisfied by applying the internal air pressure and allowing the membrane to balloon away from the sample for a short distance. This ensured that the sample was unconfined and reduced the volume of air under high pressure.

No volume change measurements could be made in the unconfined tests.

(7.7) Tests on compacted Talybont clay.

As the Talybont clay appears to be cohesionless, the results of tests on this soil were easiest to interpret and will be discussed first.

Three series of tests were performed on the partly saturated soil:

Series 4 : Constant water content, constant $(\sigma_3 - u_a)$ tests at various values of $(\sigma_3 - u_a)$ and the same water content.

Series 4B : Constant water content tests with $\sigma_3 = u_a$ (unconfined) at various water contents.

Series 4C : Constant water content tests with $(\sigma_3 - u_a) = 30$ p.s.i. at various water contents.

(a) Series 4.

The average compaction water content for these tests was 6.84% and degrees of saturation at failure ranged from 47.0% to 60.1%, for a range of values of $(\sigma_3 - u_a)$ from 0 to 105.2 p.s.i. Details of the variation of deviator stress, $(\sigma_3 - u_w)$, $\frac{(\sigma_1 - \sigma_3)}{(\sigma_3 - u_w)}$ and volume change with strain are shown in the appendix to this chapter.

Fig. (7.6) shows the stresses at maximum $\frac{(\sigma_1 - \sigma_3)}{(\sigma_3 - u_w)}$ and fig.(7.7) the stresses at maximum $(\sigma_1 - \sigma_3)$. These figures illustrate the pair of 'false' effective stress lines obtained from partly saturated soils. One line (in terms of $(\sigma_3 - u_a)$) gives a false cohesion intercept of about + 8 p.s.i. while the other (in terms of $(\sigma_3 - u_w)$) gives a false cohesion intercept of - 5 p.s.i.

The tests of Series 4A showed a value of ϕ' of 34.5° for saturated Talybont clay compacted at a water content of 7.16%. This value of ϕ' was used to give the true effective stress line for the condition of maximum $\frac{(\sigma_1 - \sigma_3)}{(\sigma_3 - u_w)}$. A slightly lower value of 34° was used for the condition of maximum $(\sigma_1 - \sigma_3)$.

The variation of the rate of dilatation at failure $\frac{(d\Delta V/V_o)}{d\epsilon}$ with $(\sigma_3 - u_a)$ for this series of tests is shown in fig. (7.8). It appeared that for values of $(\sigma_3 - u_a)$ from 60 p.s.i. upwards no dilatation correction was necessary, but for values of $(\sigma_3 - u_a)$ below 60 p.s.i. some correction for rate of dilatation should be made.

If the object of a series of tests is purely to obtain a comparison between stress conditions in a soil in the partly saturated and fully saturated states, the dilatation correction can be accounted for in two different ways. Either the stresses in the partly saturated soil can be corrected to correspond to a condition of no rate of volume change at failure, or the true effective stress line can be adjusted to correspond to the rate of volume change observed in the partly saturated soil. In order to correct stresses in the partly saturated soil, the relevant values of χ must be known. As they were unknown in this case, the correction had to be applied to the true effective stress line.

Extrapolating the curve of $\frac{d(\Delta V/V_o)}{d\epsilon}$ versus $(\sigma_3 - u_a)$ back to $(\sigma_3 - u_a) = 0$ a value of $\frac{d(\Delta V/V_o)}{d\epsilon}$ of 0.8 was obtained. When applied to the results of Series 4A, this correction gave values of ϕ' of 44.0° and 42.0° for the unconfined tests at maximum $\frac{(\sigma_1 - \sigma_3)}{(\sigma_3 - u_w)}$ and maximum $(\sigma_1 - \sigma_3)$ respectively. These angles were taken as the true effective stress lines for the unconfined tests. For the tests between $(\sigma_3 - u_a) = 0$ and $(\sigma_3 - u_a) = 60$ p.s.i. the true effective stress line was assumed to lie between the lines for zero volume change and the line for the unconfined tests. This is shown in figs. (7.6) and (7.7).

Two rather interesting phenomena are shown in fig. (7.8) which also shows the variations of $(u_a - u_w)$ and S with $(\sigma_3 - u_a)$ both before shearing and at failure. While values of $(u_a - u_w)$ decrease with increasing $(\sigma_3 - u_a)$ before shearing (which is to be expected), the values at failure actually increase. This is explained by the variations in $(\sigma_3 - u_w)$ with strain which are shown in the

appendix. While $(\sigma_3 - u_a)$ has no effect on the shape of the $(\sigma_3 - u_w)$ curves, the strain at failure increases with increasing $(\sigma_3 - u_a)$. The increase in failure strain allows a much greater increase in $(u_a - u_w)$ during shear than the initial decrease in $(u_a - u_w)$ under $(\sigma_3 - u_a)$ alone.

The variation in S with $(\sigma_3 - u_a)$ shows an opposite trend. At low values of $(\sigma_3 - u_a)$, S decreases during shear, while at high values, S increases.

(b) Series 4B.

In this series of tests compaction water contents ranged from 5.10% to 11.93% (optimum water content is 9.5%) with a corresponding range in degrees of saturation of 36.2% to 85.4%. Fig. (7.9) shows the variation of compaction dry density and initial degree of saturation with compaction water content. Fig. (7.10) shows the variation with water content of $(u_a - u_w)$ before shearing.

In figs. (7.11) and (7.12) the stresses at failure are shown for the two conditions of maximum $\frac{(\sigma_1 - \sigma_3)}{(\sigma_3 - u_w)}$ and maximum $(\sigma_1 - \sigma_3)$. Also shown on these figures are the results of Series 4C. The detailed results showing the variation of $(\sigma_1 - \sigma_3)$, $(u_a - u_w)$ and $\frac{(\sigma_1 - \sigma_3)}{(\sigma_3 - u_w)}$ are contained in the appendix to this chapter.

The effect of a decreasing degree of saturation is shown up very well by the variation in deviator stress of the unconfined samples. The deviator stress increases to a maximum, decreases slightly and finally levels off at very low degrees of saturation.

The true effective stress lines chosen for this series of tests were: $\phi' = 44.5^\circ$ for the condition of maximum $\frac{(\sigma_1 - \sigma_3)}{(\sigma_3 - u_w)}$ and $\phi' = 42.2^\circ$ for maximum $(\sigma_1 - \sigma_3)$. These values were

arrived at in the manner described in (7.7)a above and are the average values obtained for the two compaction water contents of Series 4A. It was not considered necessary to take into account further variations of ϕ' with compaction density. Information on this point was limited to two densities and in any case most of the experimental points lay so far away from the true effective stress line that small variations in ϕ' would have had a negligible effect on values of χ calculated for the points.

In fig. (7.13) is shown an example of the correction of the strength of unconfined samples for their rate of dilatation at failure. It was found in Series 4C that the rate of dilatation at failure was almost independent of compaction water content and hence the same value of $\frac{d(\Delta V/V_o)}{d\epsilon}$ was used in each case. The failure deviator stress in each case was corrected by:

$$\chi(u_a - u_w)\frac{d(\Delta V/V_o)}{d\epsilon} \qquad \text{(see E.(7.3))}$$

The resultant agreement with the line representing the true effective stress at zero rate of dilatation was satisfactory.

In section (7.3)d it was pointed out that the value of $\frac{(\sigma_1' - \sigma_3')}{(\sigma_3 - u_w)}$ in an unconfined test on a partly saturated soil was a direct measure of the parameter χ. In fig. (7.14) is shown the variation of the maximum value of $R_\chi = \frac{(\sigma_1' - \sigma_3')}{(\sigma_3 - u_w)}$ with initial degree of saturation. One would expect this curve to rise continuously with rising degree of saturation instead of curving over in the way it does. The fall off of R_χ for wetter samples may be due to two things:

(i) a large decrease in S during shear (although fig. (7.8) contradicts this), or

(ii) a large decrease in ϕ' for the wetter samples.

From fig. (7.8) it appears that the rate of volume change at failure is not greatly affected by increasing water content. The decrease in ϕ' is therefore probably due to the decreasing soil densities.

(c) Series 4C.

In this series of tests at a standard value of $(\sigma_3 - u_a) = 30$ p.s.i., compaction water contents ranged from 5.30% to 9.69%. Degrees of saturation at failure varied from 38.0% to 100%.

Fig. (7.10) shows the variation of $(u_a - u_w)$ before shearing with compaction water content.

Figs. (7.11) and (7.12) show the stresses at failure for the conditions of maximum $\frac{(\sigma_1 - \sigma_3)}{(\sigma_3 - u_w)}$ and maximum $(\sigma_1 - \sigma_3)$. Detailed stress-strain curves are shown in the appendix.

Fig. (7.8) shows the variation of $\frac{d(\Delta V/V_o)}{d\epsilon}$ with compaction water content for this series of tests. As the variation with water content was very small, a mean value $\frac{d(\Delta V/V_o)}{d\epsilon}$ of 0.14 was used to obtain a corrected true effective stress envelope from the results of Series 4A. The values of ϕ' were:

at maximum $\frac{(\sigma_1 - \sigma_3)}{(\sigma_3 - u_w)}$: 37.5° and at maximum $(\sigma_1 - \sigma_3)$: 36°.

These angles were the average given by the two compaction water contents considered in Series 4A.

The effect of unsaturation in the series of tests was once again shown by an increasing departure of the partly saturated strength lines from the true effective stress line although in this series a peak strength was not reached.

In order to get some idea of the effect of stress history on the behaviour of partly saturated soils, a special test was performed on the driest sample of this series. After failing the sample in the usual way, the deviator stress was removed and $(\sigma_3 - u_a)$ was increased from 30 p.s.i. to 84 p.s.i. As the pore air pressure was 60 p.s.i., this was the largest increase which could be made. After leaving the sample overnight in this condition, it was removed from the cell, the pore water pressure measuring system was de-aired, the sample was weighed and remeasured and finally set up anew with $(\sigma_3 - u_a) = 30$ p.s.i. as before. The sample was failed again. It was intended to repeat this procedure, but unfortunately the test was ruined at this stage by a leak. This second stage has been shown in figs. (7.11) and (7.12) by shaded symbols.

(d) Variation of parameter α with degree of saturation S for Talybont clay.

The variation of α with S for all three series of tests is shown in fig. (7.15).

In (a) the condition of maximum $\frac{(\sigma_1 - \sigma_3)}{(\sigma_3 - u_w)}$ is considered and values of α are plotted against the corresponding degrees of saturation before shearing. (As no volume measurements could be made in the unconfined tests, only the initial degrees of saturation are known. The use of the degrees of saturation before shearing enables all the tests to be compared).

In (b) values of α at maximum $(\sigma_1 - \sigma_3)$ are again plotted against the degree of saturation before shearing for all tests.

In (c) values of α at maximum $(\sigma_1 - \sigma_3)$ are plotted against the degree of saturation at failure for the tests of Series 4 and 4C.

In each case the average theoretical line (see Chapter 5, section (5.2))

$$\alpha = S + 0.2(1 - S)$$

has been shown by a broken line.

The results for all tests are grouped about a common line. This shows that values of α are unaffected by the method of testing. Also, the point corresponding with the test on the "pre-stressed" sample of Series 4C fits in quite well with the rest of the tests. Thus, in this single test, stress history at a constant water content does not appear to have affected the relation between α and S.

The relation between α and degree of saturation before shearing seems to agree with that between α and S at failure so that the comparison of unconfined tests with confined tests on a basis of initial degree of saturation seems to be justified.

A feature of fig. (7.15) is that the α - S line drops well below the line $\alpha = S$. This is contrary to the ideas put forward in Chapter 5, but can be explained if the structure of a compacted soil is considered.

A more general discussion of the relation between α and S will be given at the end of this chapter.

(7.8) Tests on compacted Mangla shale.

Three series of tests were performed on compacted partly saturated Mangla shale:

Series 1 : Constant water content, varying $(\sigma_3 - u_a)$ tests at various initial values of $(\sigma_3 - u_a)$ and the same water content (w = 18.3%).

Series 3 : Constant water content, constant $(\sigma_3 - u_a)$ tests at various values of $(\sigma_3 - u_a)$ and the same water content (w = 16%).

Series 1B : Constant water content tests with $\sigma_3 = u_a$ (unconfined) at various water contents.

(a) Series 1.

The average compaction water content for this series was 18.34% and degrees of saturation at failure ranged from 93.5% to 100%.

The stress plots at failure are shown:

at maximum $\frac{(\sigma_1 - \sigma_3)}{(\sigma_3 - u_w)}$ in fig. (7.16) and

at maximum $(\sigma_1 - \sigma_3)$ in fig. (7.17).

Details of the variation of $(\sigma_1 - \sigma_3)$, $(\sigma_3 - u_w)$, $\frac{(\sigma_1 - \sigma_3)}{(\sigma_3 - u_w)}$ and $(\sigma_3 - u_a)$ during shear are included in the appendix to this chapter.

Fig. (7.18) shows typical variations of pore air and pore water pressures during shear:

(a) Shows the variation obtained at an initial value of $(\sigma_3 - u_a)$ of 11.7 p.s.i.,

(b) shows the variation at an initial $(\sigma_3 - u_a)$ of 24.5 p.s.i. while in

(c) the initial value of $(\sigma_3 - u_a)$ was 29.1 p.s.i.

It is seen that in each case the pore air and water pressures converge at first and then diverge again. In each case the variation in u_w is larger than the variation in u_a. It is also possible to have a test which first of all becomes saturated as the pore pressures increase and then desaturates as the pore pressures drop off again.

These phenomena will be discussed more generally at the end of this chapter.

The true effective stress lines, given by Series 1A, did not fit the data of this series very well. As all the partly saturated samples failed at approximately constant overall volume, the true effective stress lines could not be corrected for rate of volume change. Nevertheless, in order to fit the stress line from Series 1A to the data from the tests saturated at constant water content by compression, either a higher c' or ϕ' seemed to be required. The true effective stress line for the case of maximum $\frac{(\sigma_1' - \sigma_3')}{(\sigma_3 - u_w)}$ was finally chosen as follows.

A value of stress corresponding to a cohesion intercept of 2.6 p.s.i. (Series 1A) was set off on the $\frac{1}{2}(\sigma_1' - \sigma_3')$ axis. A line was drawn joining this point to the point of convergence of the $\frac{1}{2}(\sigma_1' + \sigma_3') - u_w$ and $\frac{1}{2}(\sigma_1' + \sigma_3') - u_a$ lines (at which $u_a = u_w$ and $S = 100\%$). From this point an angle representing $\phi' = 23.6^\circ$ (Series 1A) was set off and drawn back to cut the $\frac{1}{2}(\sigma_1' - \sigma_3')$ axis. The final true effective stress line was then taken as the line joining the mean intercept on the strength axis to the point at which $u_a = u_w$ and $S = 100\%$.

This gave a line representing $c' = 3.0$ p.s.i., $\phi' = 24.6^\circ$. The same procedure for the case of maximum $(\sigma_1' - \sigma_3')$ gave a line representing $c' = 2.9$ p.s.i., $\phi' = 23.7^\circ$.

This seems to show that in the partly saturated soil either c' or ϕ' or both c' and ϕ' are slightly higher than is shown by tests on the saturated soil, viz:

at maximum $\frac{(\sigma_1 - \sigma_3)}{\sigma_3'}$: $c' = 2.6$ p.s.i. $\phi' = 23.6^\circ$

at maximum $(\sigma_1 - \sigma_3)$: $c' = 2.3$ p.s.i. $\phi' = 23.5^\circ$

(b) Series 3.

In these tests the average compaction water content was 16.24%. Degrees of saturation at failure varied from 79.6% to 100%.

The failure stress plots at maximum $\frac{(\sigma_1 - \sigma_3)}{(\sigma_3 - u_w)}$ and maximum $(\sigma_1 - \sigma_3)$ are shown in figs. (7.19) and (7.20) respectively.

The true effective stress envelopes were fitted in the same way that was used for Series 1. The resultant true effective stress shear parameters were:

at maximum $\frac{(\sigma_1 - \sigma_3)}{(\sigma_3 - u_w)}$: $c' = 1.9$ p.s.i. $\phi' = 24.3^\circ$

at maximum $(\sigma_1 - \sigma_3)$: $c' = 1.9$ p.s.i. $\phi' = 24.1^\circ$

The respective parameters given by the tests of Series 3A were:

at maximum $\frac{(\sigma_1 - \sigma_3)}{\sigma_3'}$: $c' = 1.5$ p.s.i. $\phi' = 24.1^\circ$

at maximum $(\sigma_1 - \sigma_3)$: $c' = 0.5$ p.s.i. $\phi' = 23.8^\circ$

(c) Series 1B.

This series includes the unconfined tests which formed part of Series 1 and 3. The water contents ranged from 15.25% to 23.33% (Proctor optimum water content is 16.2%) while the range of initial degrees of saturation was from 76.6% to 92.1%.

Fig. (7.21) shows the variation of initial degree of saturation and dry density with compaction water content, while fig.(7.22) shows the variation with water content of $(u_a - u_w)$ before shearing.

The stresses at failure are shown in figs. (7.23) and (7.24).

As with the Talybont clay the unconfined strength increases to a maximum and then declines to a lower value.

Considering firstly the case of maximum $\frac{(\sigma_1' - \sigma_3')}{(\sigma_3 - u_w)}$, the true effective stress line was chosen as follows:

For the tests of Series 1 and all tests with lower water contents a line corresponding to

$$c' = 2.4 \text{ p.s.i.} \quad \text{and} \quad \phi' = 24.4^\circ$$

was used. This represented the average of Series 1A and 3A.

It was pointed out in section (7.3)b that the true effective stress line for very wet tests will pass through the zero of the stress plot. To account for this the effective stress line for tests with water contents greater than Series 1 was assumed to be a line passing through the origin and joining the other effective stress line at a point corresponding to the water content of Series 1.

The same assumptions were made for the case of maximum $(\sigma_1' - \sigma_3')$ where the main effective stress line had the parameters:

$$c' = 2.4 \text{ p.s.i.} \quad \text{and} \quad \phi' = 23.6^\circ$$

(d) Variation of parameter α with degree of saturation for compacted Mangla shale.

The variation of α with S for all three series of tests is shown in fig. (7.25).

(a) At maximum $\frac{(\sigma_1' - \sigma_3')}{(\sigma_3 - u_w)}$ values of α are plotted against corresponding values of S before shearing.

(b) At maximum $(\sigma_1' - \sigma_3')$ a similar plot is given.

(c) At maximum $(\sigma_1' - \sigma_3')$ the variation of α with S at failure is shown for the tests of Series 1 and 3.

In (a), (b) and (c) the theoretical line

$$\alpha_c = S + 0.2(1 - S)$$

has been included.

As in the tests on Talybont clay, the points are grouped about a single line regardless of the method of test employed. Once again the experimental line falls steeply below the theoretical line.

(7.9) Tests on compacted Selset clay.

The tests on compacted partly saturated Selset clay consisted of the following series:

Series 2 : Constant water content, varying $(\sigma_3' - u_a)$ tests at various initial values of $(\sigma_3' - u_a)$.

Series 2B : Constant water content tests with $\sigma_3' = u_a$ (unconfined) at various water contents.

(a) Series 2.

The average compaction water content for this series was 11.56% and the range of degrees of saturation at failure was from 79.8% to 100%.

The stress conditions at failure are shown in figs. (7.26), (maximum $\frac{(\sigma_1' - \sigma_3')}{(\sigma_3' - u_w)}$) and (7.27) (maximum $(\sigma_1' - \sigma_3')$). Once again in this series of tests, the true effective stress lines given by tests on the saturated soil (Series 2A) did not completely agree with the tests of this series which were saturated by compression at constant water content.

Accordingly, the method of fitting which was described in Section (7.8)a was applied. This gave effective stress strength parameters as follows:

at maximum $\frac{(\sigma_1 - \sigma_3)}{(\sigma_3 - u_w)}$: c' = 1.1 p.s.i. ϕ' = 26.4°

at maximum $(\sigma_1 - \sigma_3)$: c' = 1.0 p.s.i. ϕ' = 26.1°

The values of c' and ϕ' given by Series 2A were:

at maximum $\frac{(\sigma_1 - \sigma_3)}{\sigma_3'}$: c' = 0 ϕ' = 26.4°

at maximum $(\sigma_1 - \sigma_3)$: c' = 0 ϕ' = 25.8°

Fig. (7.28) shows typical variations of u_a and u_w for three tests of this series at successively higher values of $(\sigma_3 - u_a)$. The general form of these is similar to those shown for Series 1 (tests on Mangla shale) which were described in section (7.8)a.

(b) Series 2B.

This was a very limited series of 6 tests at compaction water contents varying between 11.92% to 16.26%. (Proctor optimum water content for Selset clay is 11.2%).

Fig. (7.29) shows the variation with compaction water content of initial $(u_a - u_w)$, initial degree of saturation and dry density. The failure stresses at both maximum $\frac{(\sigma_1 - \sigma_3)}{(\sigma_3 - u_w)}$ and maximum $(\sigma_1 - \sigma_3)$ are shown in fig. (7.30).

The effective stress lines are the same as those used in Series 2.

(c) Variation of parameter α with degree of saturation for compacted Selset clay.

Values of α are plotted against corresponding values of the degree of saturation before shearing for tests of both series in fig. (7.31).

The trend for these tests is very similar to that shown by the compacted Mangla shale. Unfortunately only a small range of

values of S is represented. Once again results from unconfined and confined tests lie about a common line.

(7.10) Tests on compacted Vaich moraine.

A short series of unconfined tests was carried out on compacted Vaich moraine. The suction-compaction water content curve for the soil is shown in fig. (7.32) which also shows the variation in degree of saturation and dry density.

No pore water pressures were measured during shear, but the suction at failure was estimated from the initial suction-water content curve by assuming that the behaviour of the soil during shear was similar to that of Talybont clay. The assumed variation of failure suction with water content is shown by the dotted line in fig. (7.32).

The failure stress plot is shown in fig. (7.33). In contrast to the Talybont clay and Mangla shale, the unconfined strength did not decrease after reaching a maximum, but remained almost constant. The true effective stress line was taken from tests by Hanson (1955) on the Vaich moraine.

The variation with S of values of α calculated from this stress plot are shown in fig. (7.34).

(7.11) Discussion of experimental results.

(a) Rates of loading.

(A detailed discussion of the effect of rate of loading on non-uniformity of pore pressure during triaxial shear is given in Chapter 8. The reader is referred to Chapter 8 for an explanation of the terms to be used below).

The degree of equalisation in most of the tests described in

this chapter was known or could be estimated. The minimum time factors, degrees of equalisation and corresponding maximum pore pressure differences are summarised in the following table.

Soil	Test Series	Time Factor $T_v = \frac{c_t.t}{H2}$	Degree of Equalisation $\Upsilon\% = (1-p/p_o)$	Estimated value of p_o p.s.i.	Estimated Maximum pore pressure difference $p = u_E - u_c$ p.s.i.
Mangla Shale	1	0.76	89	17.5	1.9
	3	0.76	89	30	3.3
	1B	0.57	85	13.6	2.0
Selset Clay	2 2B	1.61	94	36	2.2
Talybont Clay	4	3.7	97	42	1.2
	4B	0.28	72	4.3	1.2
	4C	3.7	97	15	0.5

Rates of strain were varied as far as possible to take into account differences in failure strain at different values of $(\sigma_3 - u_a)$ and different water contents. In this way, the time to failure for all tests of a particular series was kept as closely as possible to the same value.

The maximum pore pressure differences quoted in the table were estimated for the greatest deviator stress occurring in the test series under consideration. As the pore pressure difference at a given time factor is proportional to the deviator stress (see

Chapter 8, section (8.5)), the figure quoted represents an absolute maximum for the series.

In the unconfined tests of Series 4B, the failure strains of the drier samples were so small that it was found impossible in most tests to extend the time to failure beyond about 20 hours. As this would have meant an all night vigil for each test, it was decided to fail the brittle samples in 8 hours. These samples always failed by a series of almost vertical radial failure cracks which intersected the porous disc of the pore water pressure measuring apparatus. For this reason, the degree of equalisation quoted in the table is probably an underestimate.

As no pore pressures were measured during shear in the unconfined tests on Vaich moraine, the samples were failed rapidly in about an hour. Here again failure took place by a series of near vertical radial cracks.

(b) <u>True effective stress shear parameters in partly saturated compacted soils</u>.

If the shear strength parameters (in terms of true effective stress) of a compacted soil were unaffected by saturating the soil, the data from the tests described in Chapter 6 should have perfectly fitted the data from tests on the partly saturated soil. However, in every case, to obtain a fit, either a greater c' or a greater ϕ' or both were required. In the tests on Talybont clay this could be explained and accounted for by consideration of the different rates of dilatation at failure of the samples. Samples of Mangla shale and Selset clay on the other hand all appeared to fail at almost constant overall volume.

The following table summarises the differences in c' and ϕ' between tests on saturated and partly saturated soil.

Soil	Compaction water content	Failure Criterion	Comparison of c' p.s.i.		Comparison of ϕ'	
			Saturated	Partly Saturated	Saturated	Partly Saturated
Mangla Shale	16%	Maximum $\frac{(\sigma_1'-\sigma_3')}{(\sigma_3'-u_w)}$	1.5	1.9	24.1°	24.3°
	18½%		2.6	3.0	23.6°	24.6°
Selset Clay	11½%		0	1.1	26.4°	26.4°
Mangla Shale	16%	Maximum $(\sigma_1'-\sigma_3')$	0.5	1.9	23.8°	24.1°
	18½%		2.3	2.9	23.5°	23.7°
Selset Clay	11½%		0	1.0	25.8°	26.1°

There are two possible explanations for these discrepancies:

(i) The process of saturating a compacted soil by dissolving out the air causes a slight alteration in its properties.

(ii) Volume changes localised in the zone of failure are not shown up by measurements of total volume change. Although samples of Mangla shale and Selset clay underwent an overall volume decrease during shear and failed at constant overall volume, the failure zones were obviously dilating at failure. This was shown by the decreasing values of u_a and u_w and also by the moisture content profiles after shearing.

(c) Variations in u_a and u_w during shear.

The variations of u_a and u_w found during shear in Series 1 and

2 have the following characteristics:

(i) u_w changes more than u_a.

(ii) The variation in u_a usually approximately mirrors the variations in volume change.

Variations in the pore air pressure u_a could be expected to be controlled by a combination of Boyle's and Henry's laws and hence should be controlled solely by the variation in overall volume change. This was not quite the case. While the volume change curves drop rapidly at first and then level off, the air pressure increases and then decreases again slightly. This may mean that more air has been lost to the cell water, or that Henry's law is not completely reversible. It may also be due to time lags in the air pressure measuring apparatus.

In tests using a mercury-surrounded sample, Donald (1961) has noted the same phenomenon of non-reversibility of air pressure changes. It is shown up particularly well by the test of Series 1 which became saturated during shear and later again became unsaturated. In this case the point of desaturation was at a lower pressure than the point of saturation.

The term $(u_a - u_w)$, which for a given variation in u_a controls variations in u_w, represents the surface energy of the air-water interfaces in the pore fluid. As a fairly small change in soil volume would correspond to a much larger change in specific surface of the air-water interfaces, a larger variation in u_w than in u_a must be expected. The rapid increase in $(u_a - u_w)$ as shearing proceeds shows that although the overall volume of the sample is decreasing, the failure zone, which controls $(u_a - u_w)$, is dilating

fairly rapidly.

(d) The shape of χ - S curves for compacted soils.

In the preceding pages it was found that each soil produced its own characteristic χ - S plot. These curves are summarised in fig. (7.35) which also shows the limits of the theoretical variation of χ with S.

All the experimental curves are of the same general shape. All lie close to the theoretical limits at higher degrees of saturation. All turn over and plunge steeply downwards. Also in fig. (7.35) are shown the values of $(u_a - u_w)$ at which the value of $\chi = S$ and the clay fractions of the various soils. It is clear that less clayey soils conform to the ideal behaviour far better than those with a high clay fraction. Also, considering the range of $(u_a - u_w)$ involved (0 - 60 p.s.i.) the cross-over point always occurs at about the same suction of 20 p.s.i.

The characteristic shape of the χ - S plots is thought to be due to two factors, both of which cause overestimation of the effective degree of saturation of the soil.

(i) Reasons have already been given for the conclusion that overall volume changes are not a true measure of volume changes occurring in the failure zone of the soil. In most of the tests described in this chapter, it is thought that the degrees of saturation of the failure zones were, due to local dilatation, rather lower than those shown by the overall volume changes. In long term tests in which complete equalisation of pore pressures is allowed, migration of moisture might lead to a uniform degree of

saturation throughout a sample (regardless of non-uniformities in volume change). This has not as yet been shown experimentally.

(ii) Fig. (7.36) shows a more realistic concept of the structure of a partly saturated compacted soil than was shown by fig. (5.1). The "single grained" type structure is thought to be built up of a large number of "crumbs" composed of saturated aggregations of small particles and including the odd single larger particle.

For each saturated crumb $S = \chi = 1$. On the other hand, the degree of saturation for the crumb structure, regarding each crumb as a single grain will be very much lower than the degree of saturation given by measurements of overall volume and water content. The value of $(u_a - u_w)$ will be the same throughout the soil, but since $\chi = 1$ in the crumbs, the effective stress within the crumbs will be much higher than between the crumbs. Hence any shear plane will tend to pass between rather than through crumbs, and the χ value of the soil will probably correspond to the low S of the crumb structure. The lower the clay fraction of the soil, the closer the structure will approach to the ideal single grained structure. A combination of these two factors probably accounts for the deviation of the experimental χ - S plots from the ideal shape.

(e) Scatter in χ - S results.

The parameter χ is most difficult to measure accurately as it involves a ratio of the small difference between two pairs of large quantities. An example will illustrate this:

Referring to section (7.3)a:

Suppose the error in $\frac{1}{2}(\sigma_1' - \sigma_3')$, σ_3', σ_3', u_w and u_a is in each case $\pm$ 0.1 p.s.i. It is not likely to be less than this.

$$\text{If } a = \tfrac{1}{2}(\sigma_1' - \sigma_3') \pm .1 + (\sigma_3' \pm .1 - u_w \pm .1)$$

$$b = \tfrac{1}{2}(\sigma_1' - \sigma_3') \pm .1 + \sigma_3' \pm .1$$

$$c = \tfrac{1}{2}(\sigma_1' - \sigma_3') \pm .1 + (\sigma_3' \pm .1 - u_a \pm .1)$$

$$\text{Then } \alpha = \frac{b - c}{a - c} = \frac{b \pm .1 - c \pm .1 \pm .1}{a \pm .1 - c \pm .1} = \frac{b - c \pm .3}{a - c \pm .2}$$

(Possible errors in $\frac{1}{2}(\sigma_1' - \sigma_3')$ cancel out in both $(b - c)$ and $(a - c)$ and errors in σ_3' cancel out in the term $(a - c)$). In the worst combination of circumstances, as α approaches 1, the measured value will be any value between 0 and $\pm\infty$.

Suppose $\alpha = 4$ p.s.i./5 p.s.i., then the measured value will be any value given by $\frac{4 \pm .3}{5 \pm .2}$ = 0.71, .83, .77 or 0.90 as a few examples. Thus it seems that a band of scatter about 10% wide is about the best that can be hoped for in this type of test.

(7.12) Conclusions.

(i) Semi-graphical methods have been presented for determining apparent values of α from the results of triaxial tests on partly saturated soils.

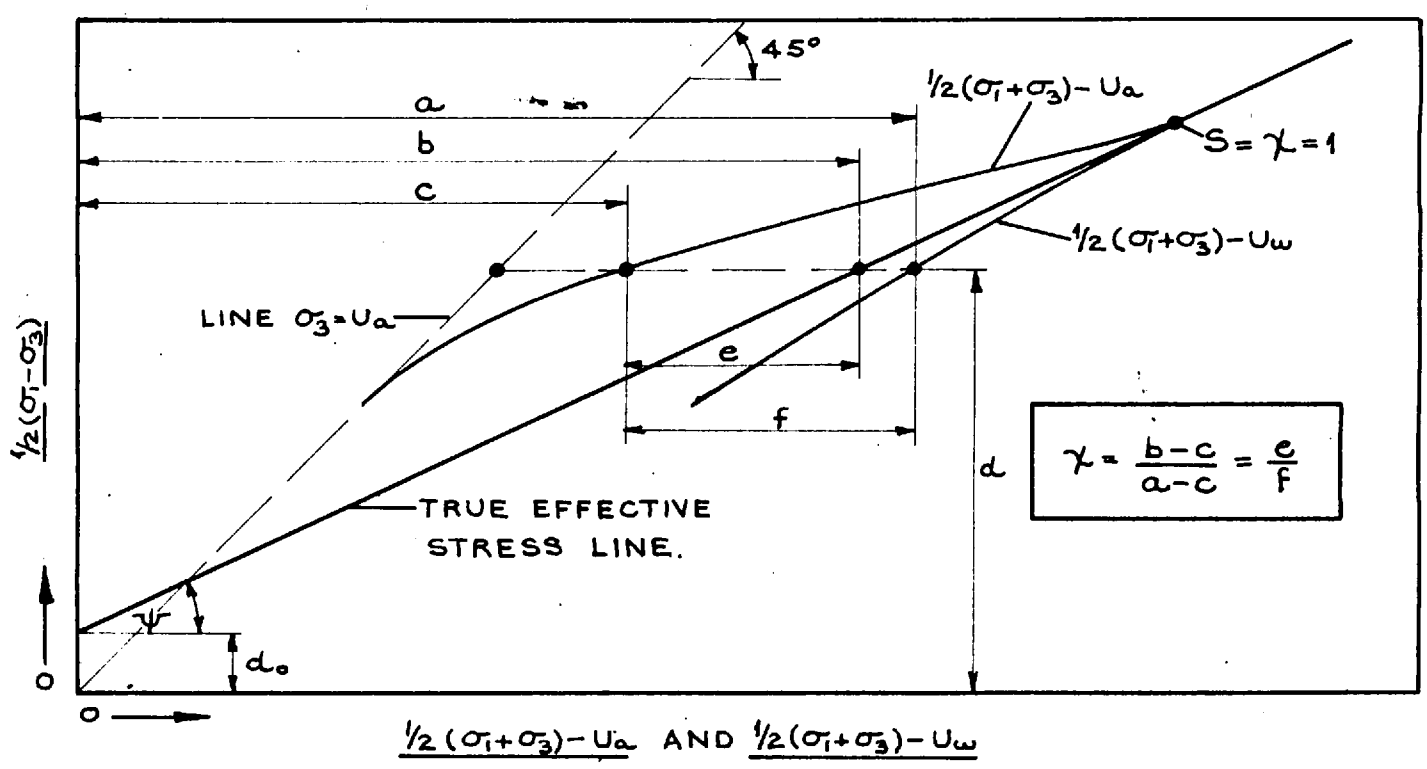
(ii) In comparing tests which reach failure at different strains, it appears more reasonable to use as a basis of comparison strains which are proportional to peak values of $\frac{(\sigma_1' - \sigma_3')}{\sigma_3'}$ or $(\sigma_1' - \sigma_3')$ rather than to compare at equal strains. A failure criterion of maximum $\frac{(\sigma_1' - \sigma_3')}{(\sigma_3' - u_w)}$ appears to be a reasonable approximation for partly saturated soils to the true criterion of maximum $\frac{(\sigma_1' - \sigma_3')}{\sigma_3'}$.

(iii) The correction for the rate of dilatation at failure in partly saturated soils can be taken into account either by correcting measurements on the partly saturated soil, or by

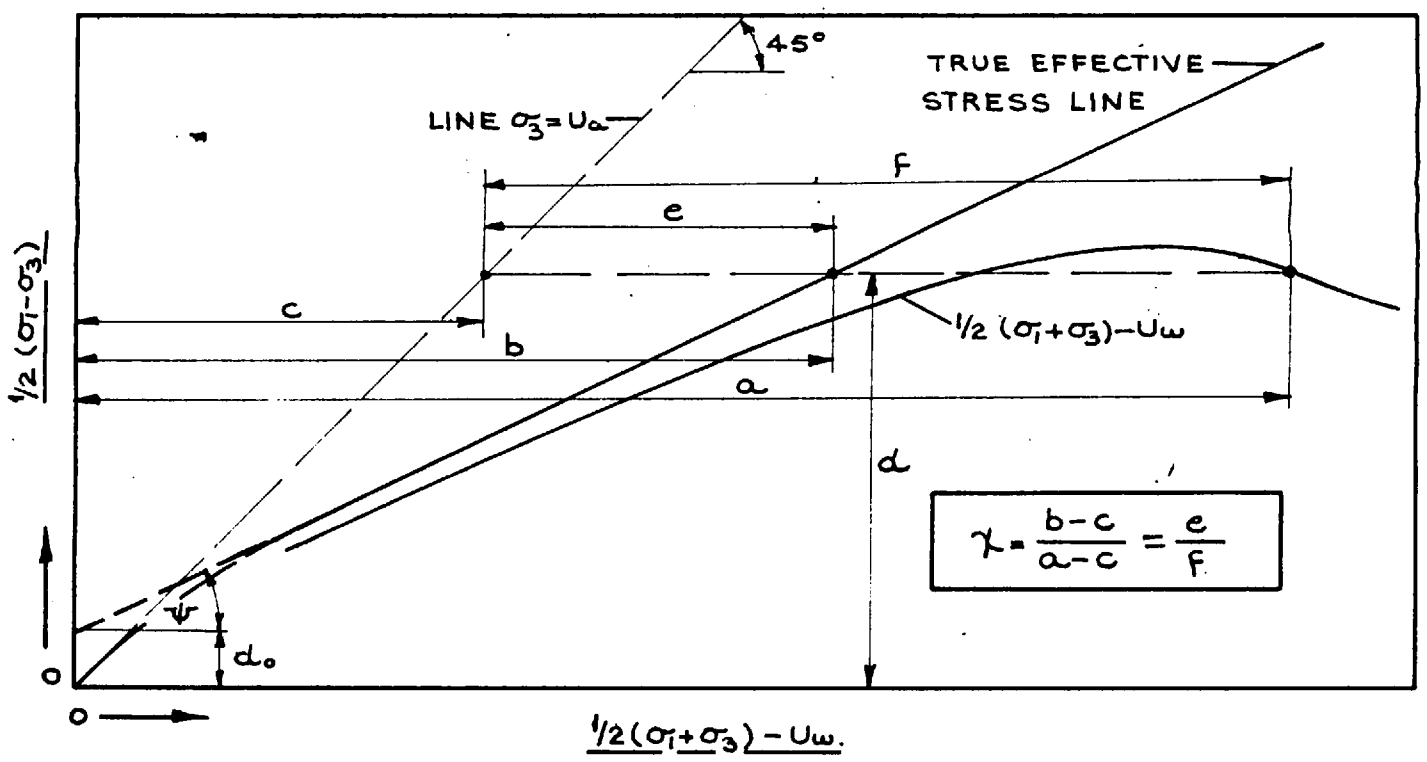
applying a correction in the opposite sense to the shear strength in terms of true effective stress.

(iv) The true effective stress strength parameters for a partly saturated soil appear to be slightly different to those inferred from tests on the saturated soil.

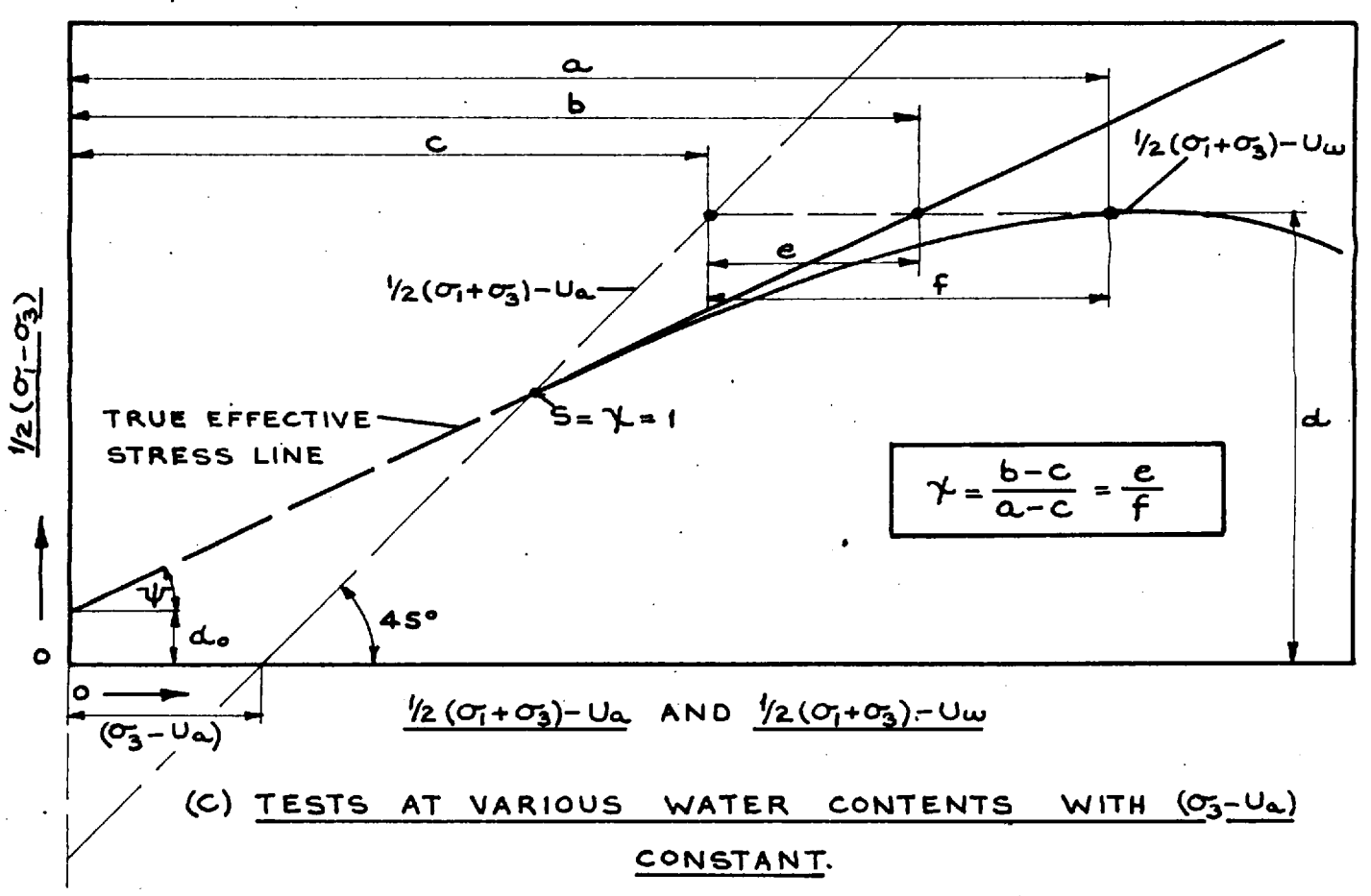
(v) The degree of saturation calculated from measurements of water content and overall volume change does not represent an effective degree of saturation for the soil at failure.



(a) TESTS AT CONSTANT WATER CONTENT & VARIOUS VALUES OF $(\sigma_3 - U_a)$



(b) TESTS AT VARIOUS WATER CONTENTS WITH $\sigma_3 = U_a$.



(C) TESTS AT VARIOUS WATER CONTENTS WITH $(\sigma_3 - U_a)$ CONSTANT.

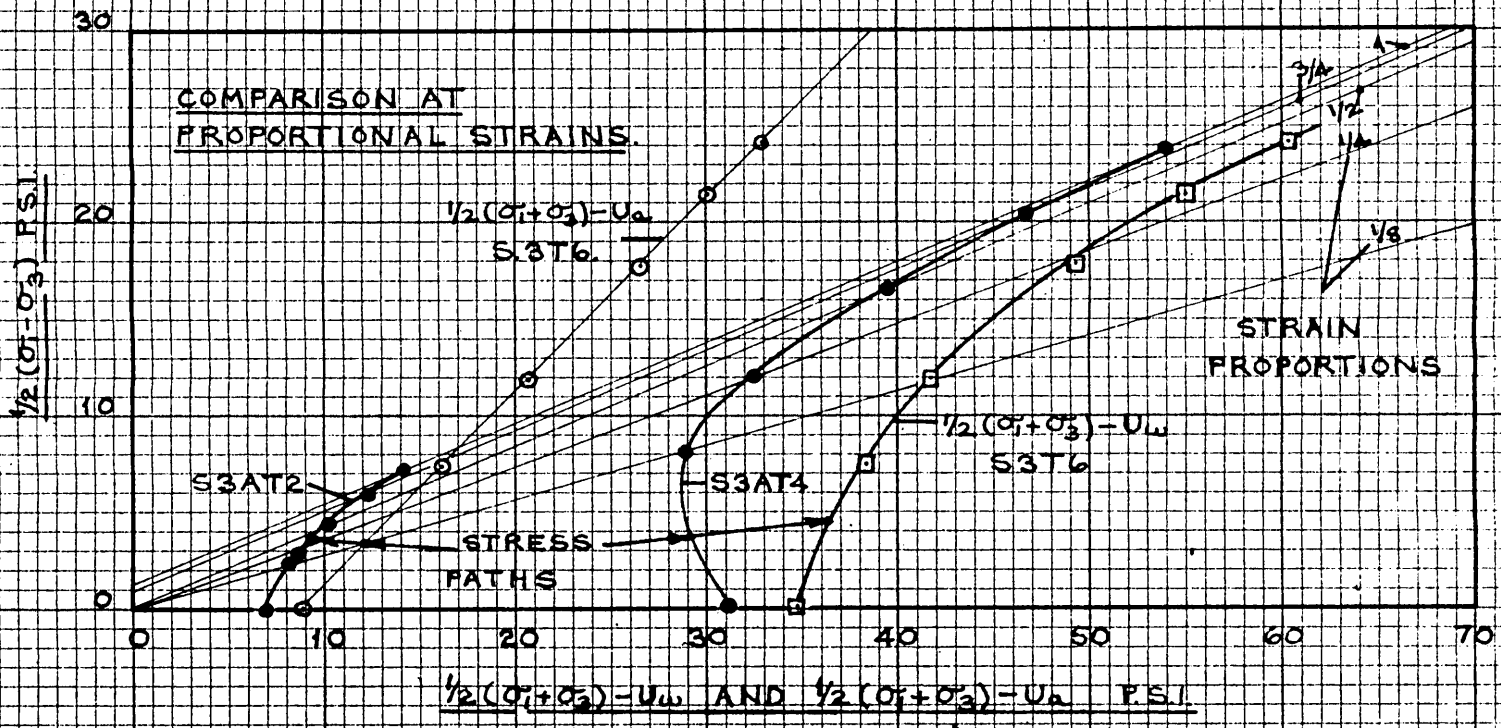
SEMI-GRAPHICAL PROCEDURES FOR DETERMINING χ FROM CURVES OF FAILURE STRESSES.

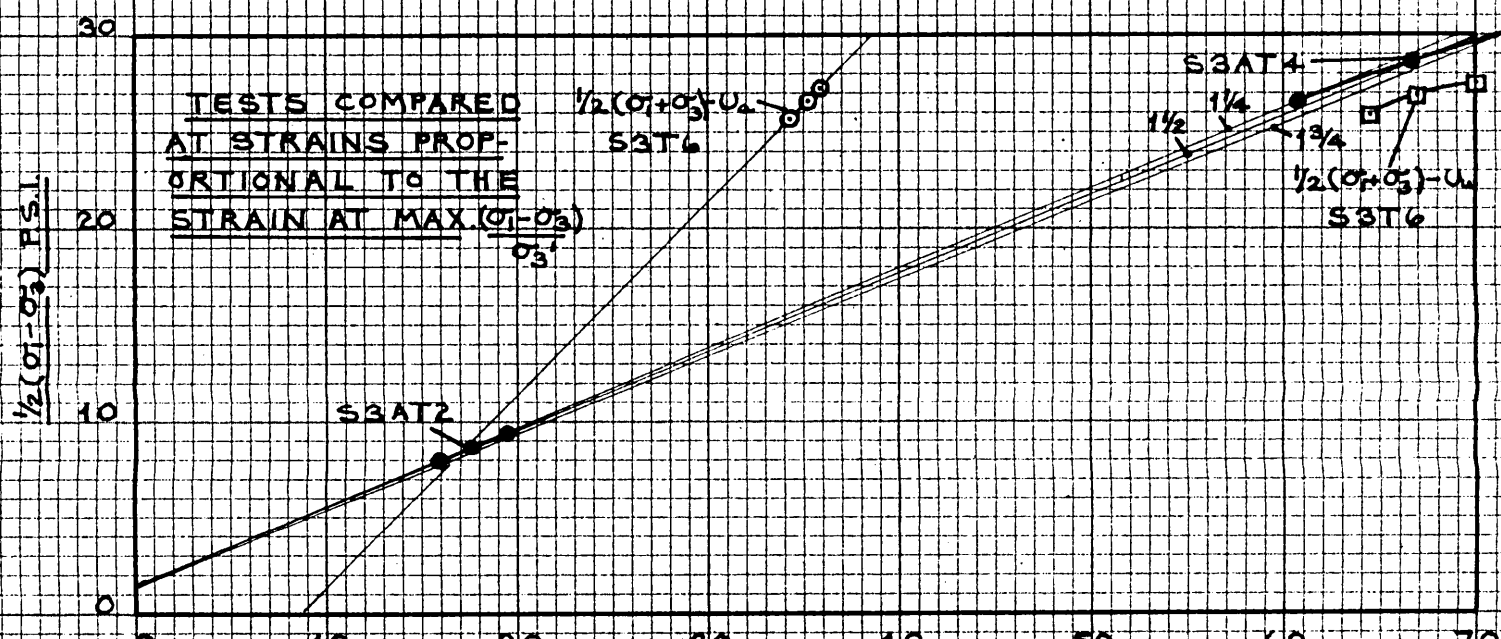
FIG. 7.1.

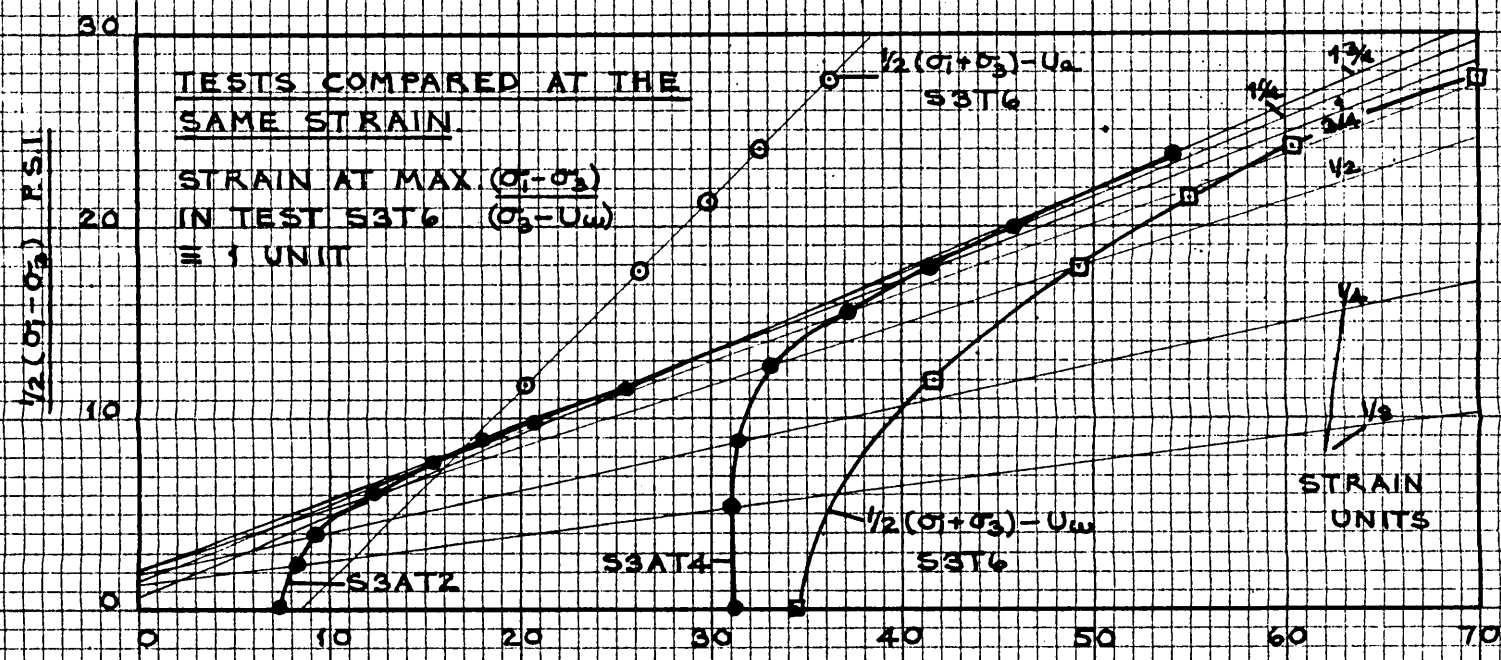
COMPARISON OF TESTS WHICH FAIL AT DIFFERENT STRAINS

SEE ALSO FIGS. 7.3, 7.4 & 7.5.

FIG. 7.2.







COMPARISON OF TESTS WHICH FAIL AT DIFFERENT STRAINS

(SEE ALSO FIGS. 7.2, 7.4 & 7.5).

TESTS ON SATURATED MANGLA SHALE: S3AT2
S3AT4

TEST ON PARTLY SATURATED MANGLA SHALE: S3T6.

FIG. 7.3.

COMPARISON AT THE SAME STRAIN.

SATURATED MANGLA SHALE — TESTS S3A. T2 & T4.

COMPARISON AT PROPORTIONAL STRAINS.

COHESION INTERCEPT C' P.S.I.

3
2
1
0

0 1/4 1/2 3/4 1 1 1/4 1 1/2 1 3/4

STRAIN PROPORTION.

(a) DEVELOPMENT OF COHESION INTERCEPT WITH STRAIN.

30
20
10
0

ANGLE OF SHEARING RESISTANCE ϕ'°

COMPARISON AT THE SAME STRAIN.

COMPARISON AT PROPORTIONAL STRAINS.

UNIT STRAIN PROPORTION = STRAIN AT MAXIMUM $\frac{(\sigma_1-\sigma_3)}{\sigma_3'}$

SATURATED MANGLA SHALE. TESTS S3A. T2 & T4.

0 1/4 1/2 3/4 1 1 1/4 1 1/2 1 3/4

STRAIN PROPORTION

(b) DEVELOPMENT OF ANGLE OF SHEARING RESISTANCE WITH STRAIN

1.4
1.2
1.0
0.8
0.6
0.4

PARAMETER χ

PARTLY SATURATED MANGLA SHALE TEST S3T6.

COMPARISON AT THE SAME STRAIN.

COMPARISON AT PROPORTIONAL STRAINS

0 1/4 1/2 3/4 1 1 1/4 1 1/2 1 3/4

STRAIN PROPORTION.

(c) DEVELOPMENT OF PARAMETER χ WITH STRAIN.

2.0
1.5
1.0
0.5
0

STRESS RATIO

$\frac{(\sigma_1-\sigma_3)}{(\sigma_3-U_a)+\chi(U_a-U_w)}$

$\frac{(\sigma_1-\sigma_3)}{(\sigma_3-U_w)}$

PARTLY SATURATED MANGLA SHALE. TEST S3T6

0 2 4 6 8 10 12 14.

STRAIN %

(d) APPLICATION OF MAXIMUM PRINCIPAL STRESS RATIO CRITERION TO A PARTLY SATURATED SOIL.

TWO METHODS OF COMPARING TESTS WITH DIFFERENT FAILURE STRAINS:

(i) AT THE SAME STRAIN.
(ii) AT STRAINS PROPORTIONAL TO THE STRAIN AT MAXIMUM $\frac{(\sigma_1-\sigma_3)}{\sigma_3'}$

SEE ALSO FIGS. 7.2, 7.3 & 7.5.

FIG. 7.4.

STRAIN IN TEST ON SATURATED SOIL. %

STRESS RATIO

DRAINED TEST ON SATURATED SOIL $\frac{(\sigma_1-\sigma_3)}{\sigma_3'}$

UNCONFINED $\frac{(\sigma_1-\sigma_3)}{\chi(U_a-U_w)}$

UNCONFINED TEST ON PARTLY SATURATED SOIL. $\frac{(\sigma_1-\sigma_3)}{(\sigma_3-U_w)}$

COMPACTION WATER CONTENT FOR BOTH TESTS: 7·3%

STRAIN IN UNCONFINED TEST ON PARTLY SATURATED SOIL. %

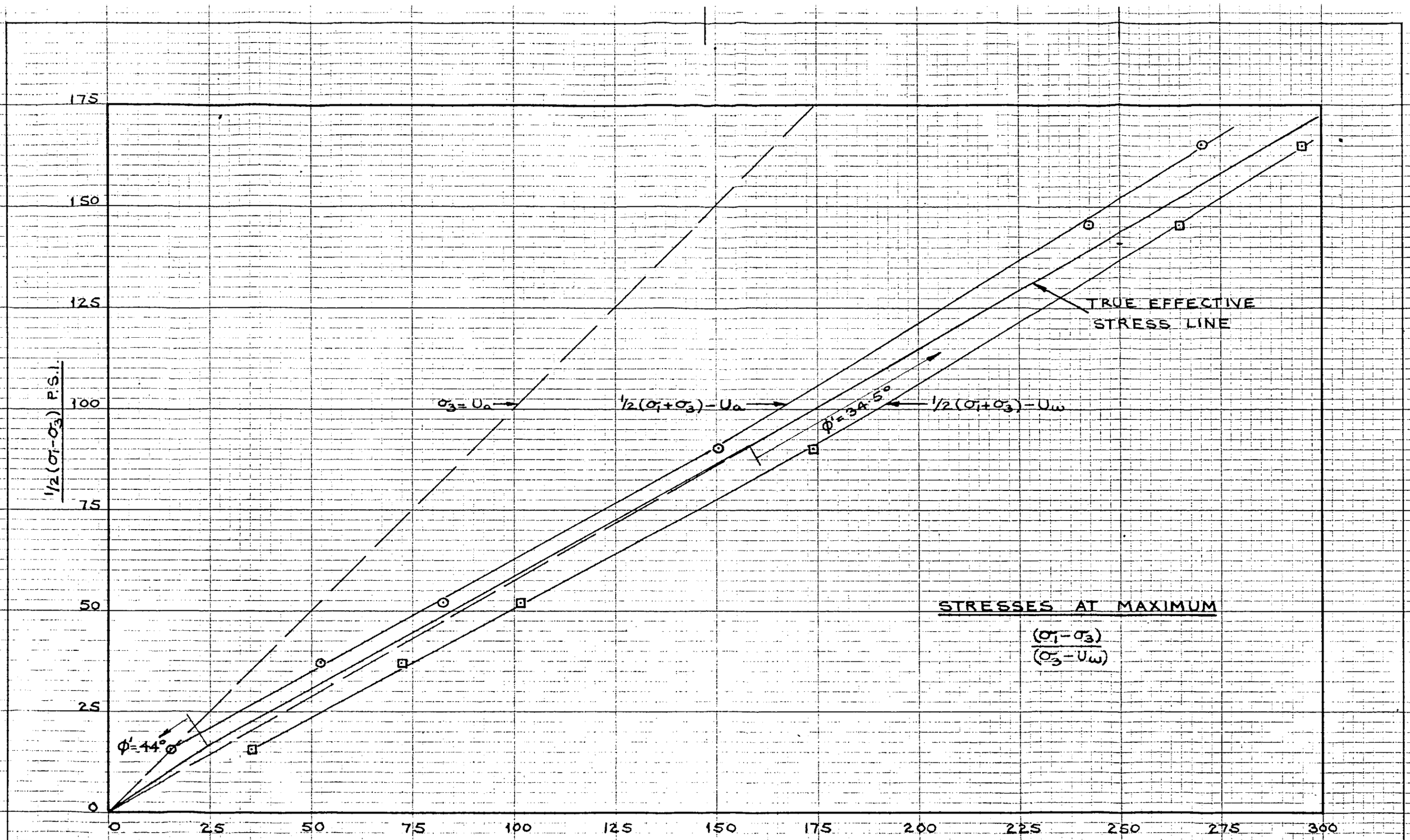
PARAMETER χ

χ IN UNCONFINED TEST ON PARTLY SATURATED SOIL.

PROPORTION OF STRAIN AT MAX. $\frac{(\sigma_1-\sigma_3)}{(\sigma_3-U_w)}$

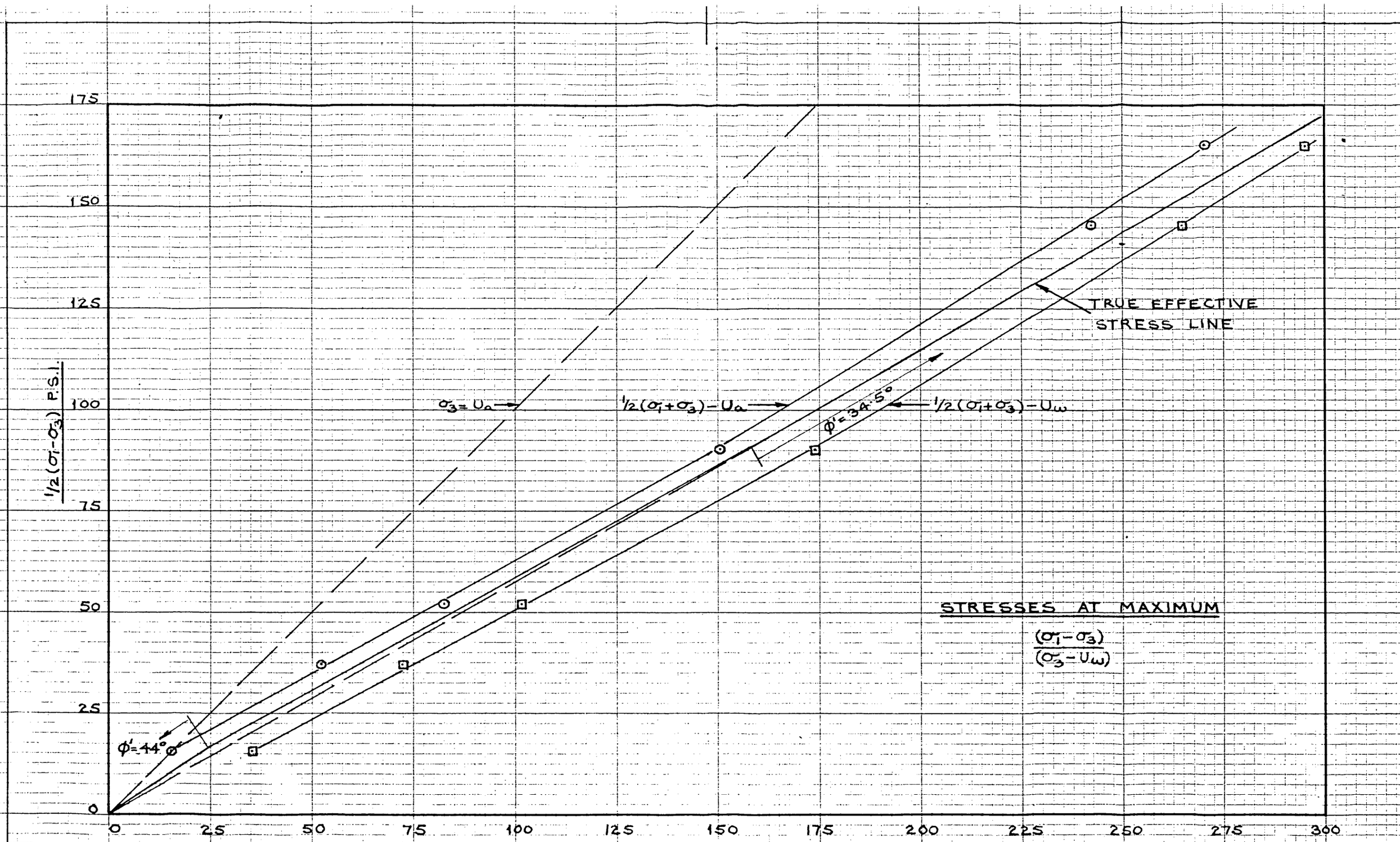
COMPARISON OF UNCONFINED TEST ON PARTLY SATURATED TALYBONT CLAY WITH SATURATED DRAINED TEST.

FIG. 7.5.



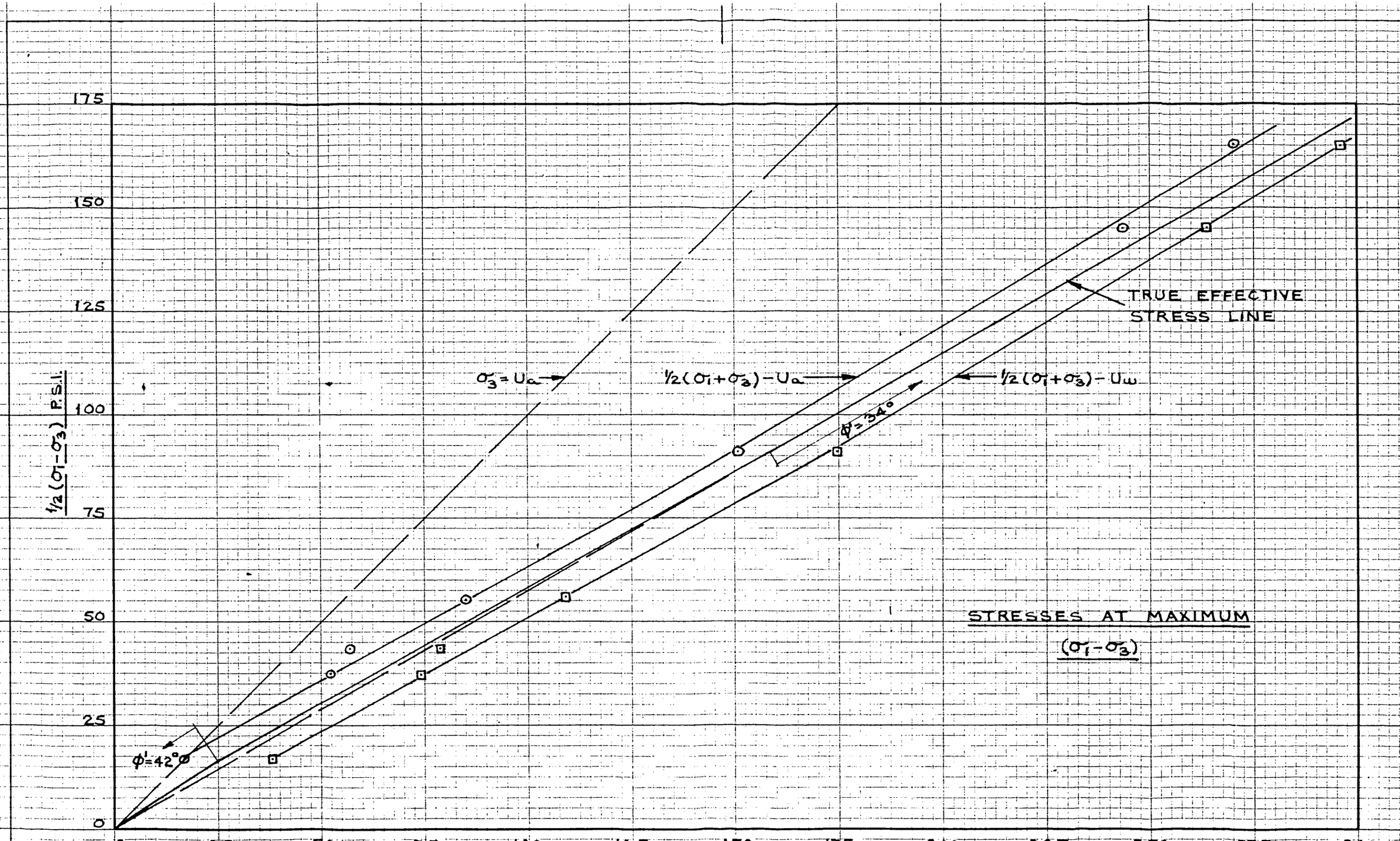
CONSTANT WATER CONTENT, CONSTANT (σ_3-U_a) TESTS ON TALYBONT CLAY SERIES 4.

FIG. 7.6.



CONSTANT WATER CONTENT, CONSTANT (σ_3-U_a) TESTS ON TALYBONT CLAY.
SERIES 4.

FIG. 7.6.



STRESSES AT MAXIMUM $(\sigma_1 - \sigma_3)$

CONSTANT WATER CONTENT, CONSTANT $(\sigma_3 - U_a)$ TESTS ON TALYBONT CLAY.

SERIES 4.

FIG. 7.7.

COMPACTION WATER CONTENT %

5 6 7 8 9 10 11

OPTIMUM W.C

RATE OF VOLUME CHANGE AT FAILURE $\frac{d(\Delta V/V_0)}{d\epsilon}$

0·8 0·6 0·4 0·2 0

VARIATION WITH $(\sigma_3 - U_a)$ AT $\omega = 6{\cdot}3\%$

VARIATION WITH ω AT $(\sigma_3 - U_a) = 30$ P.S.I.

0 20 40 60 80 100 120

$(\sigma_3 - U_a)$ P.S.I.

(a) VARIATION OF $\frac{d\Delta V/V_0}{d\epsilon}$ WITH $(\sigma_3 - U_a)$ AND WATER CONTENT.

$(U_a - U_w)$ P.S.I.

30 25 20 15 10

FAILURE CONDITIONS

INITIAL CONDITIONS

0 20 40 60 80 100 120

$(\sigma_3 - U_a)$ P.S.I.

(b) VARIATION OF $(U_a - U_w)$ WITH $(\sigma_3 - U_a)$

DEGREE OF SATURATION S %

60 55 50 45

FAILURE CONDITIONS

INITIAL CONDITIONS.

0 20 40 60 80 100 120

$(\sigma_3 - U_a)$ P.S.I.

(c) VARIATION OF DEGREE OF SATURATION WITH $(\sigma_3 - U_a)$

CONSTANT WATER CONTENT, CONSTANT $(\sigma_3 - U_a)$

TESTS ON TALYBONT CLAY. SERIES 4.

FIG. 7.8.

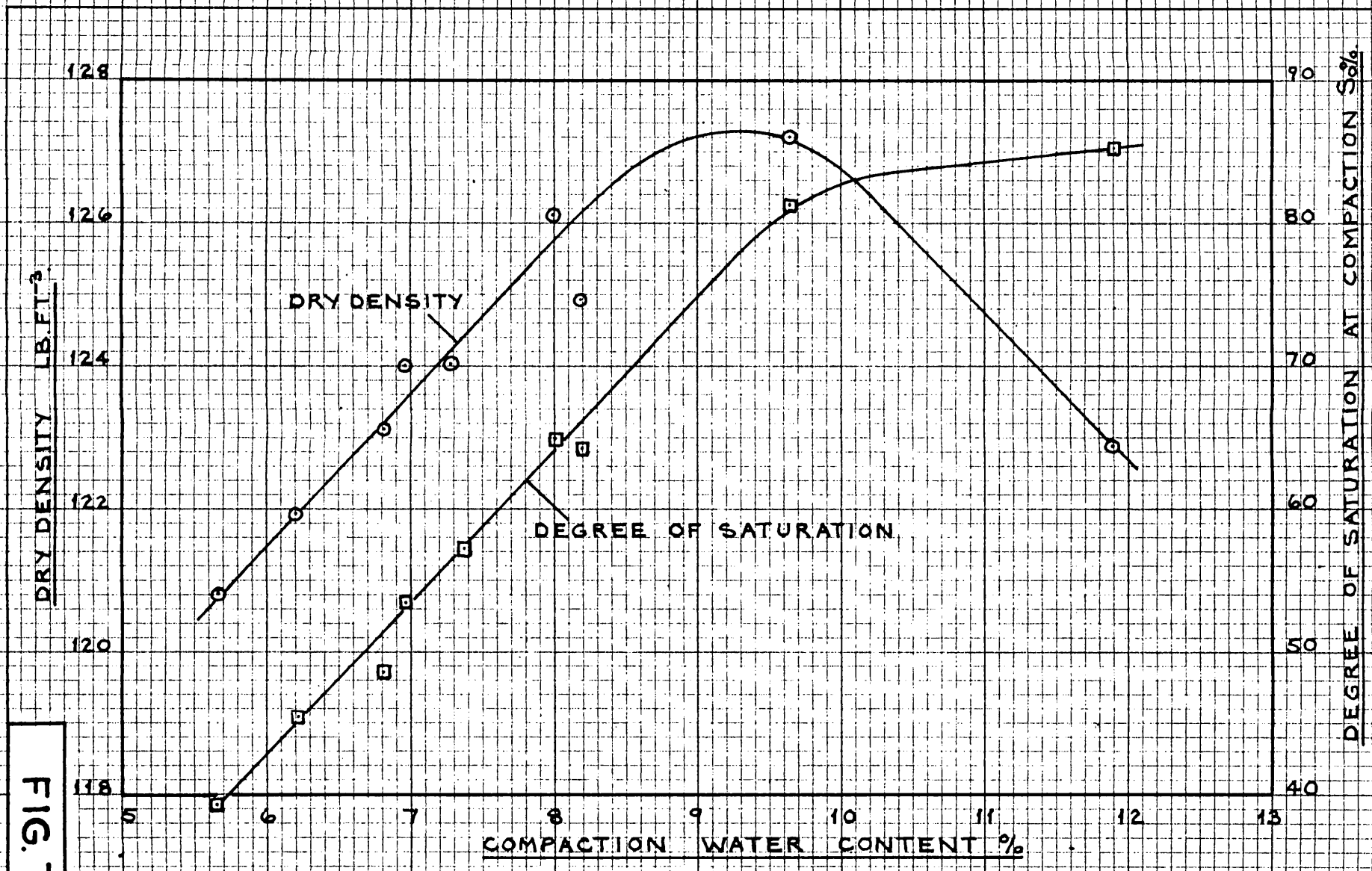
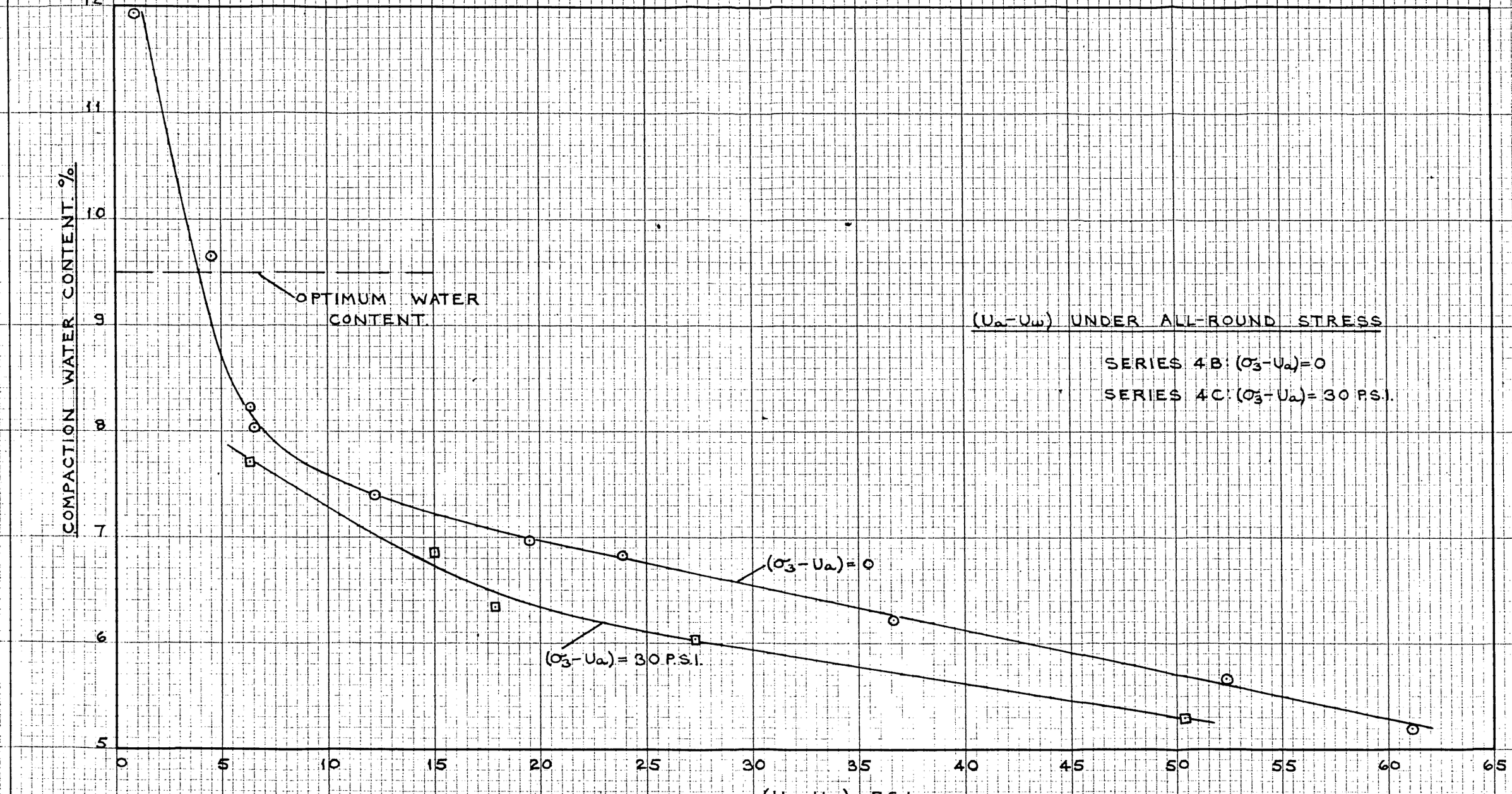


FIG. 7.9.

CONSTANT WATER CONTENT TESTS ON TALYBONT CLAY WITH $\sigma_3 = U_o$.

SERIES 4B.



(Ua-Uw) UNDER ALL-ROUND STRESS

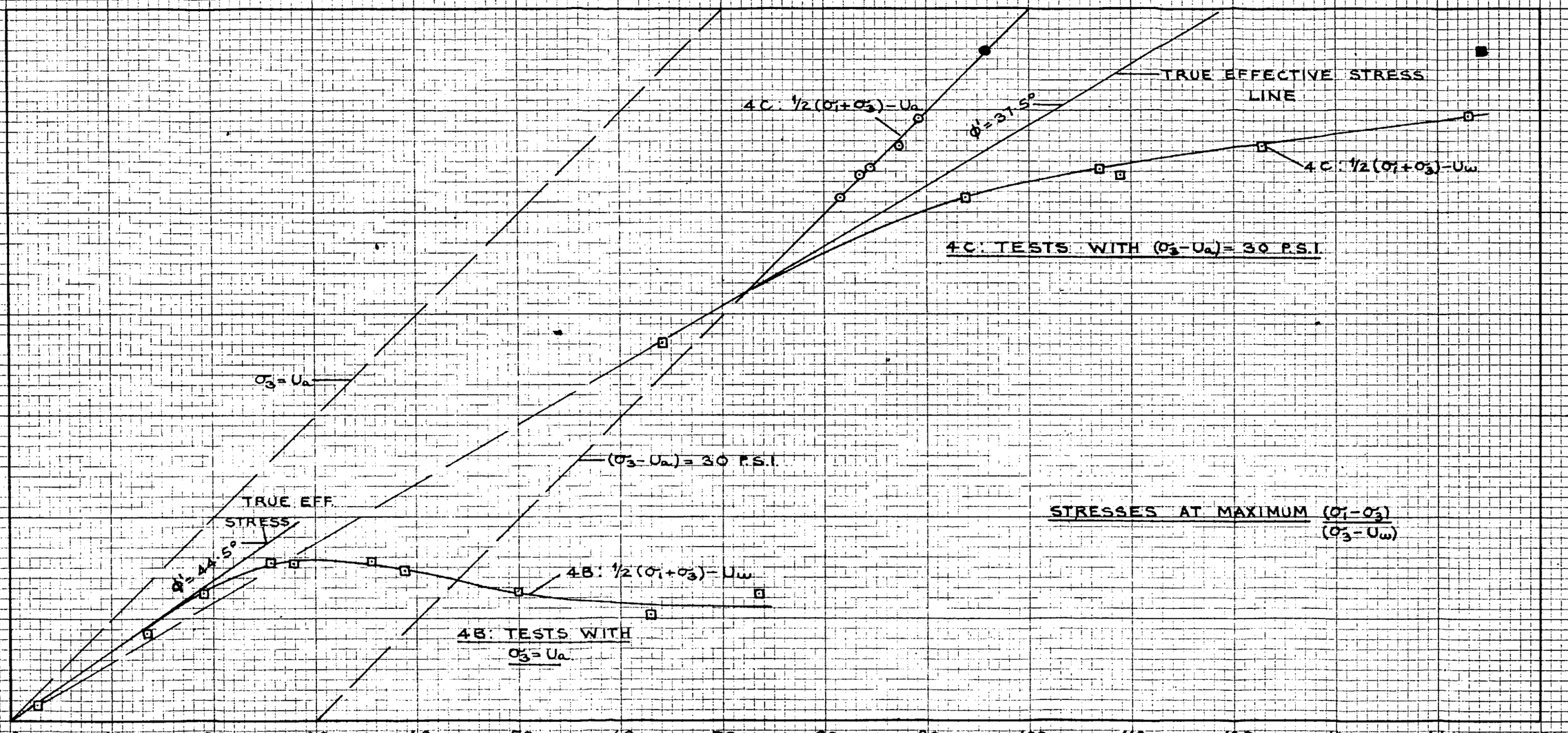
SERIES 4B: (σ3-Ua)=0

SERIES 4C: (σ3-Ua)= 30 P.S.I.

TESTS ON TALYBONT CLAY

VARIATION OF (Ua-Uw) WITH COMPACTION WATER CONTENT FOR TWO VALUES OF (σ3-Ua).

FIG. 7.10.

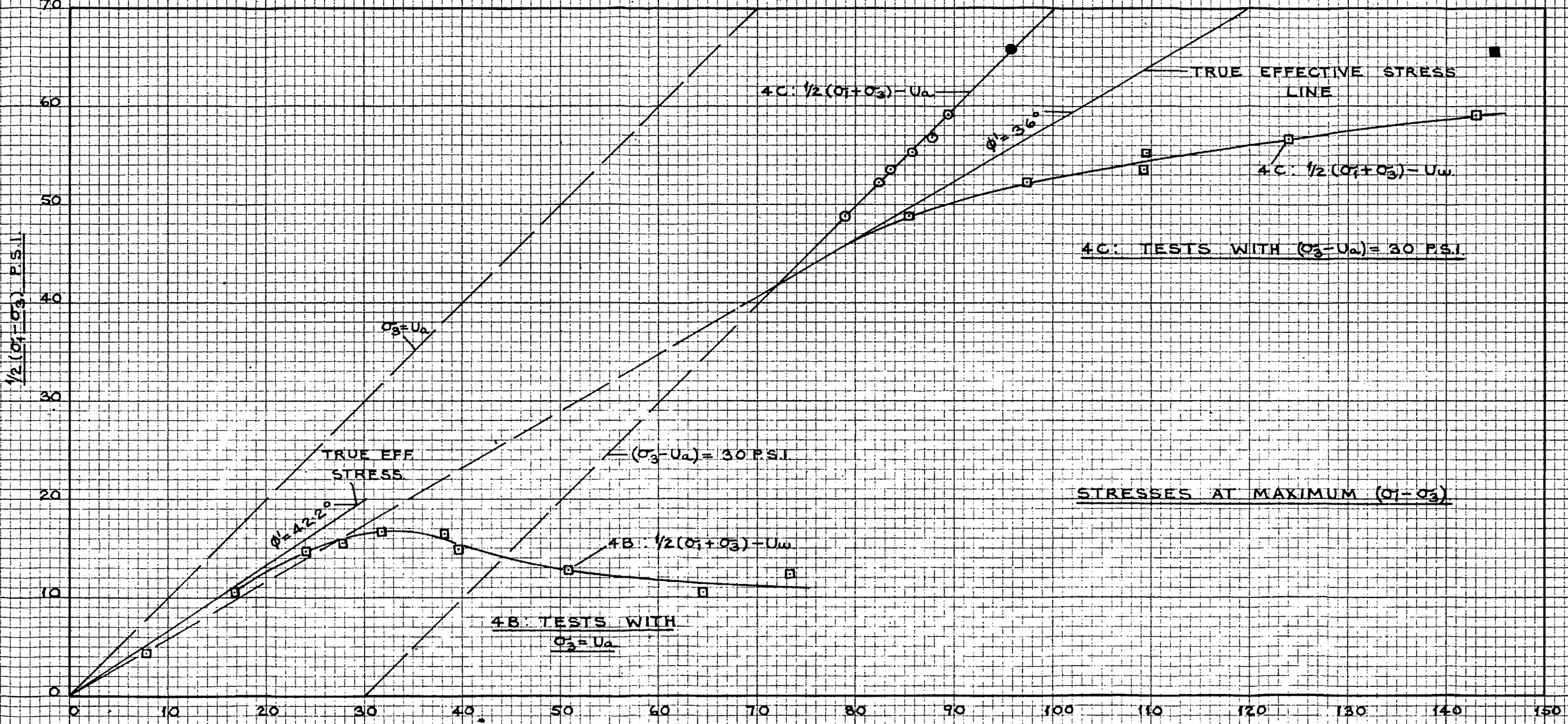


TESTS ON COMPACTED TALYBONT CLAY

SERIES 4B: TESTS AT VARIOUS WATER CONTENTS WITH $\sigma'_3 = U_a$

SERIES 4C: TESTS AT VARIOUS WATER CONTENTS WITH $(\sigma_3 - U_a) = 30$ P.S.I.

FIG. 7.11.

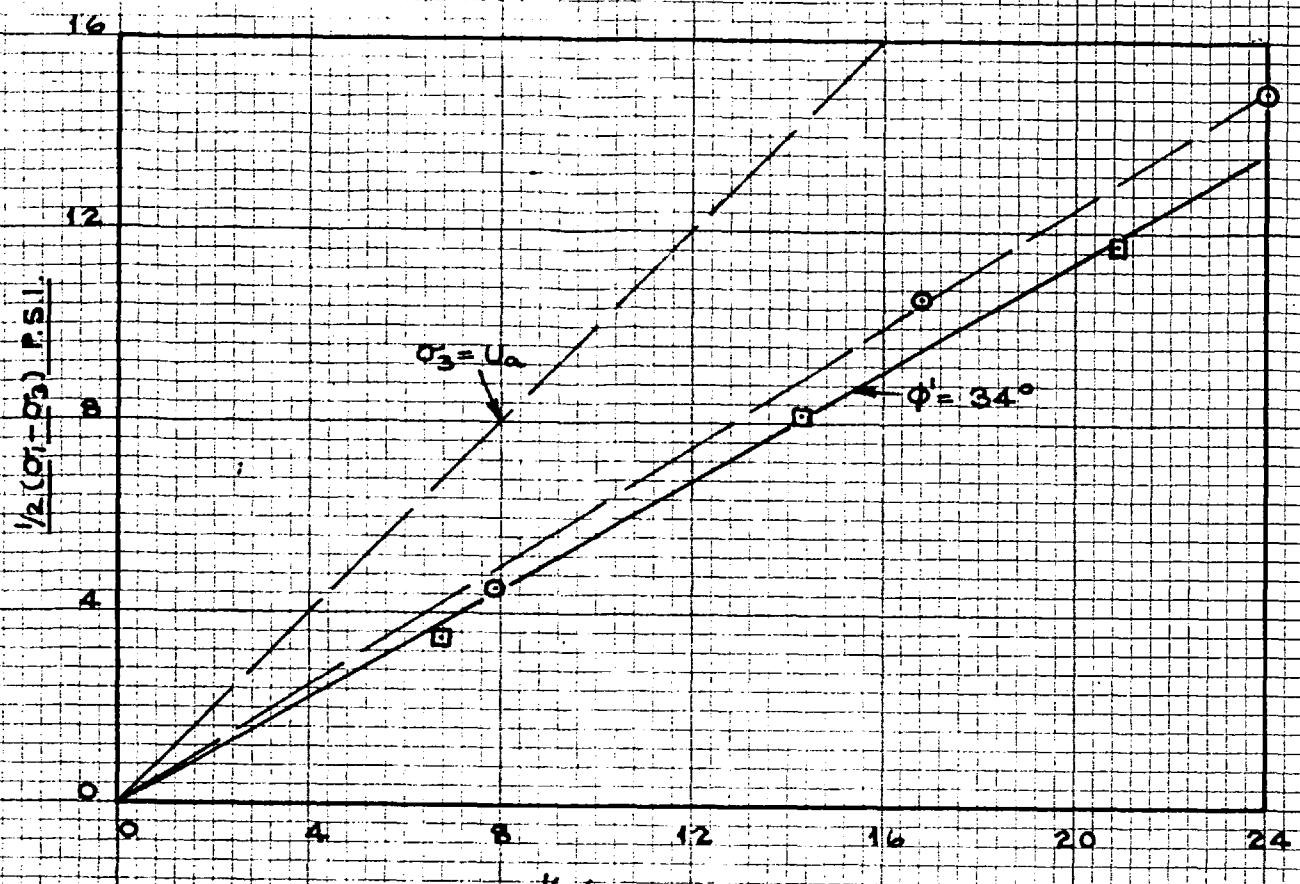


TESTS ON COMPACTED TALYBONT CLAY

SERIES 4B: TESTS AT VARIOUS WATER CONTENTS WITH $\sigma_3 = U_a$

SERIES 4C: TESTS AT VARIOUS WATER CONTENTS WITH $(\sigma_3 - U_a) = 30$ P.S.I.

FIG. 7.12.



TESTS ON UNCONFINED SAMPLES OF PARTLY SATURATED TALYBONT CLAY CORRECTED FOR RATE OF VOLUME CHANGE AT FAILURE.

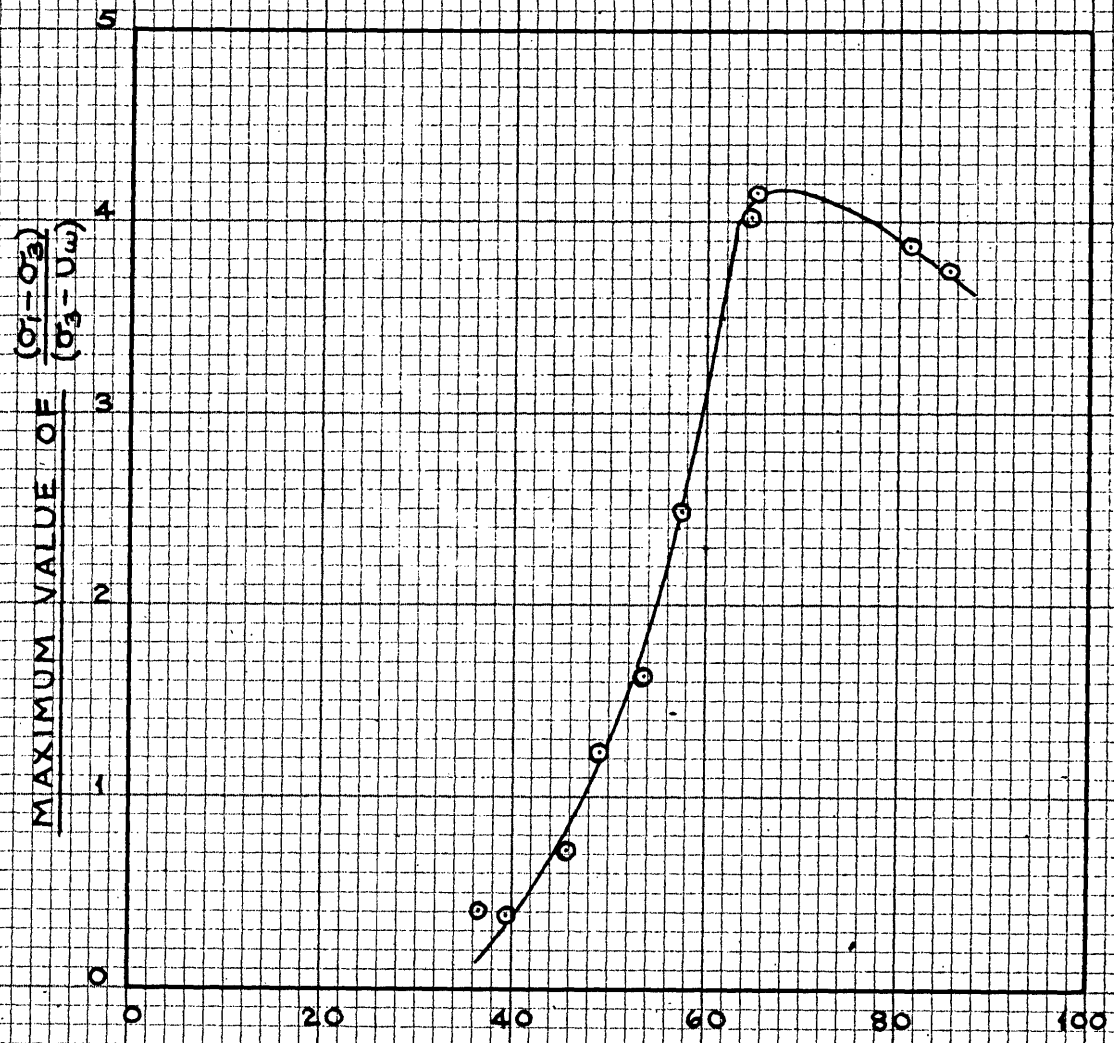
⊙ UNCORRECTED POINTS

⊡ POINTS CORRECTED BY

$$\chi(U_a - U_w) \cdot \left[\frac{d(\Delta V/V_o)}{d\epsilon}\right]$$

$\phi' = 34°$ CORRESPONDS TO CONSOLIDATED UNDRAINED TESTS ON SATURATED SOIL.

FIG. 7.13.

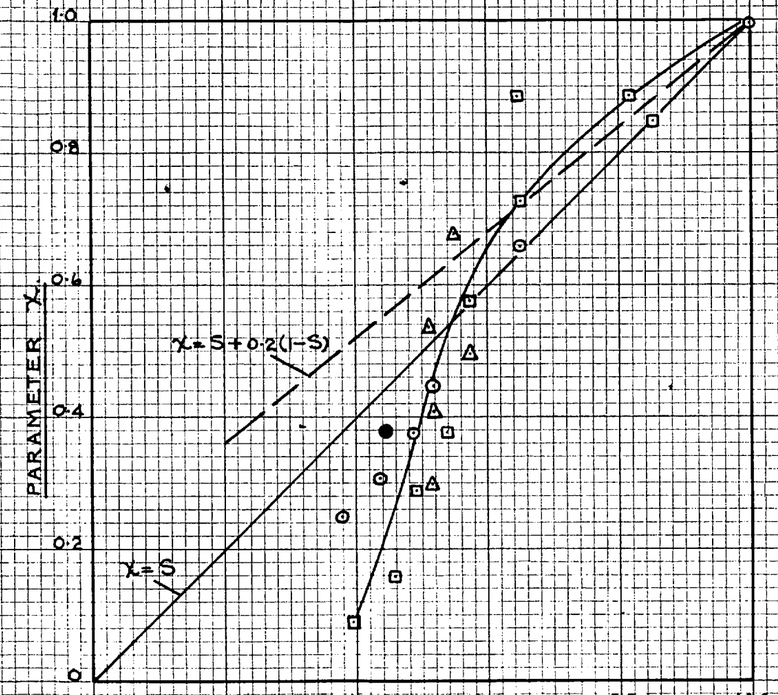


TESTS ON TALYBONT CLAY.

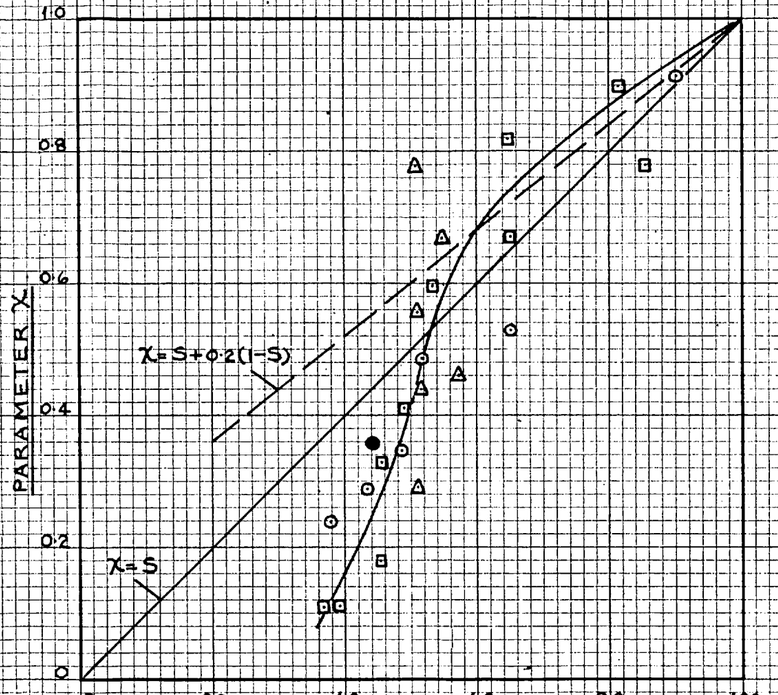
SERIES 4B.

VARIATION OF MAXIMUM $\frac{(\sigma_1-\sigma_3)}{(\sigma_3-U_w)}$ WITH DEGREE OF SATURATION

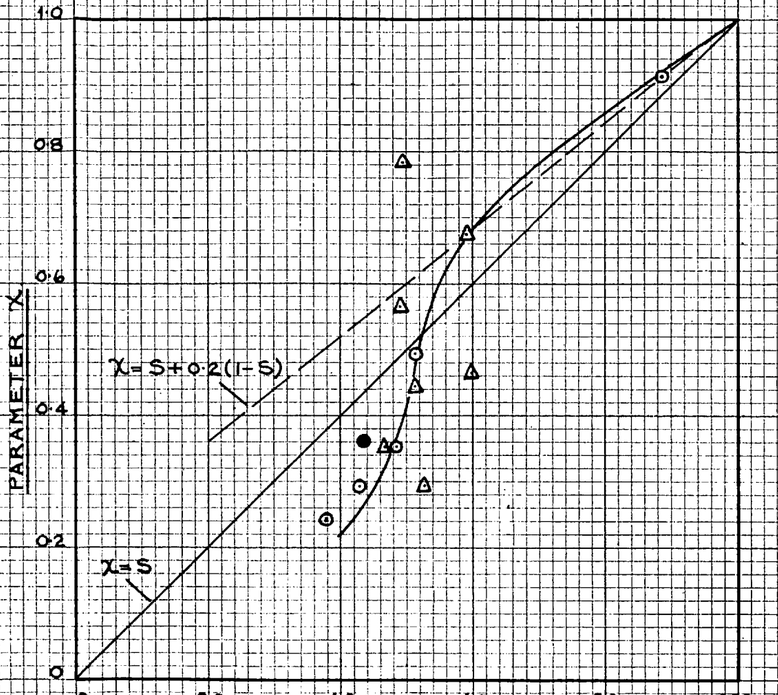
FIG. 7.14.



(a) CONDITIONS AT MAXIMUM $(\sigma_1-\sigma_3)$, $S_0-\chi$, (σ_3-U_w)



(b) CONDITIONS AT MAXIMUM $(\sigma_1-\sigma_3)$, $S_0-\chi$



(c) CONDITIONS AT MAXIMUM $(\sigma_1-\sigma_3)$, $S_f-\chi$

TESTS ON TALYBONT CLAY. SUMMARY OF DEGREE OF SATURATION — PARAMETER χ RESULTS

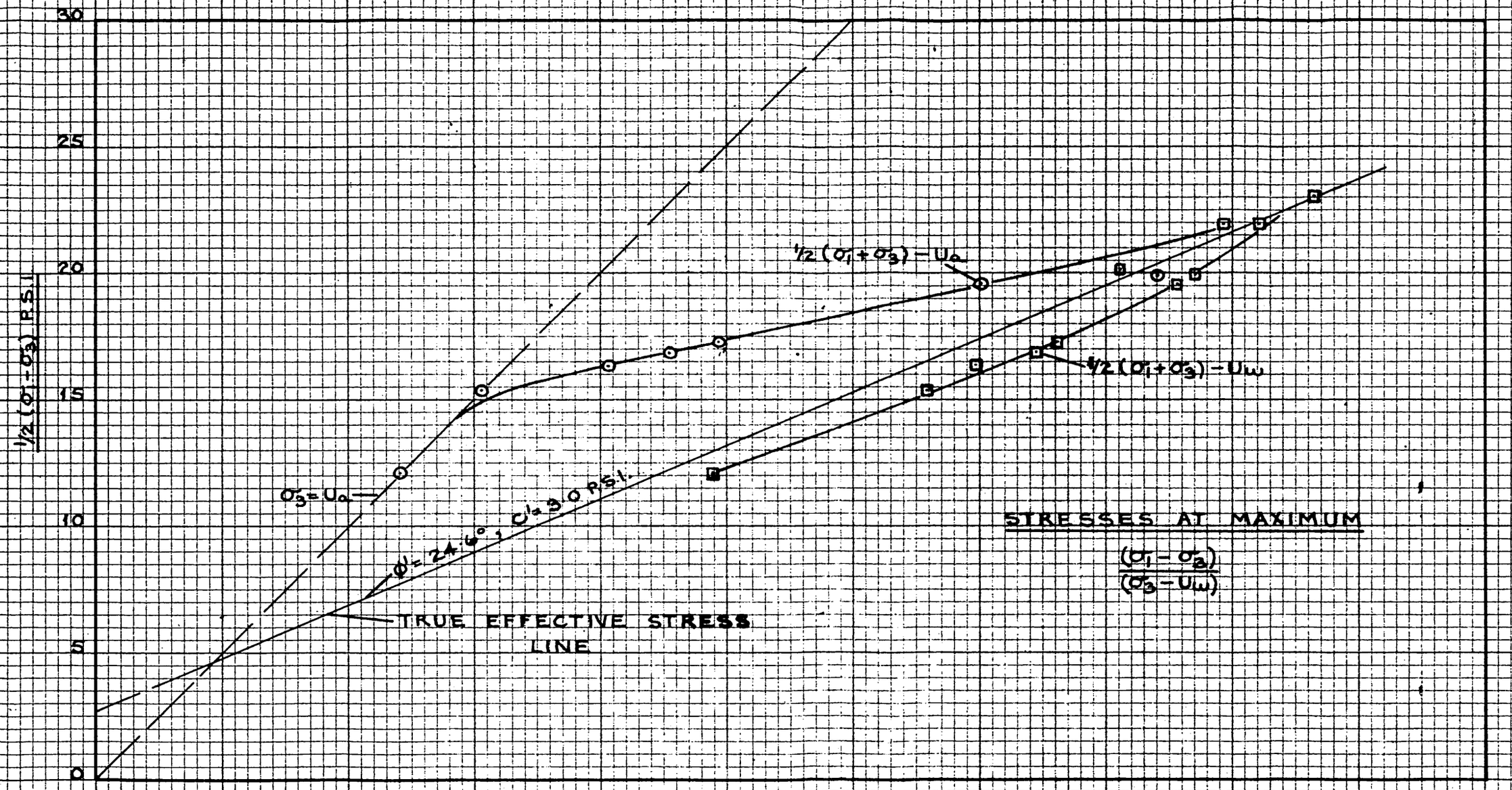
△ SERIES 4: COMPACTION W.C. CONSTANT VARIOUS INITIAL (σ_3-U_a)

⊡ SERIES 4B: COMPACTION W.C. VARYING, $(\sigma_3-U_a)=0$.

⊙ SERIES 4C: COMPACTION W.C. VARYING, $(\sigma_3-U_a)=30$ P.S.I.

● SERIES 4C: TEST T3A, 2ND STAGE.

FIG. 7.15.

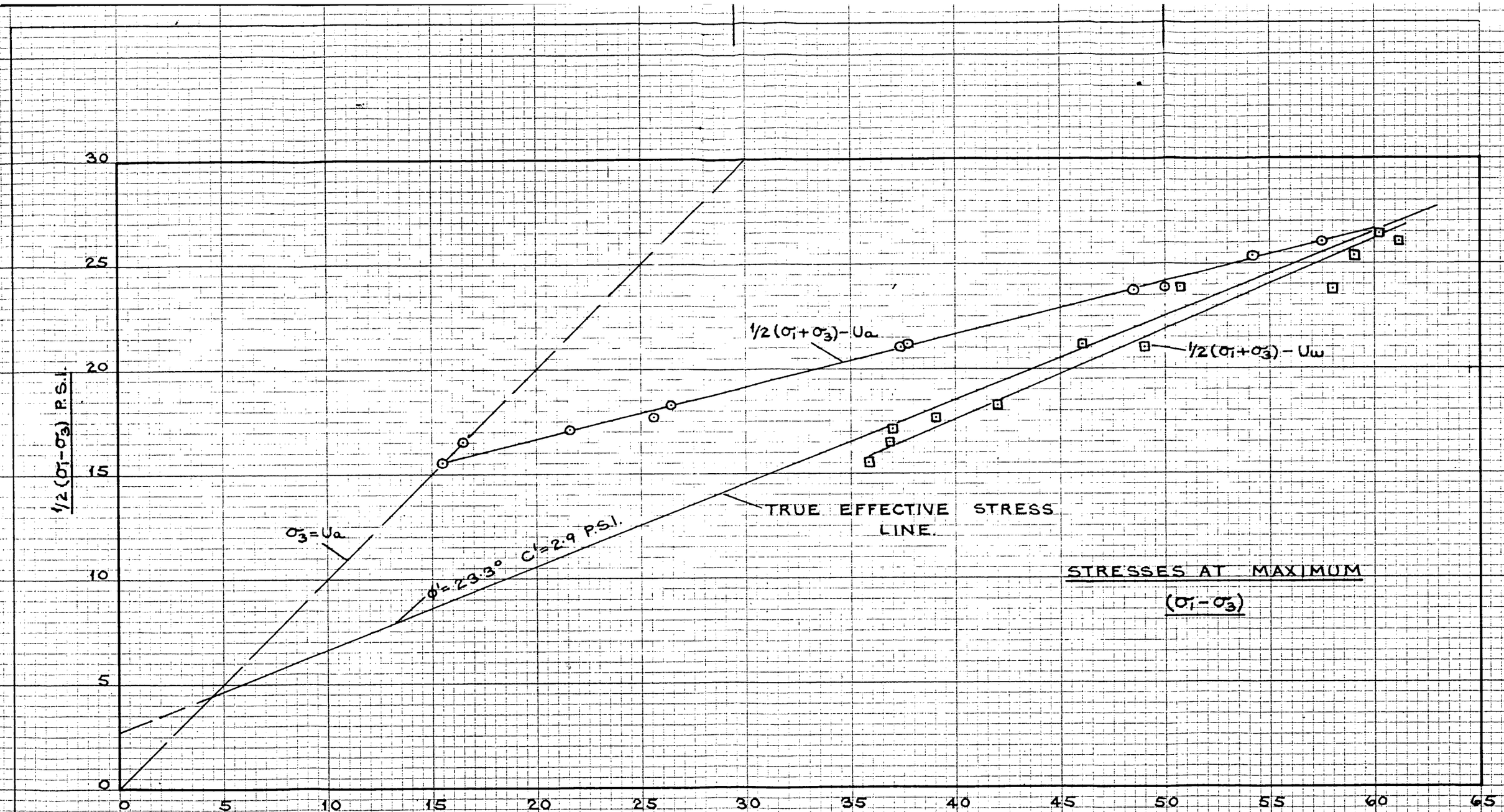


CONSTANT WATER CONTENT, VARYING $(\sigma_3 - U_a)$

TESTS ON MANGLA SHALE.

SERIES 1

FIG. 7.16.

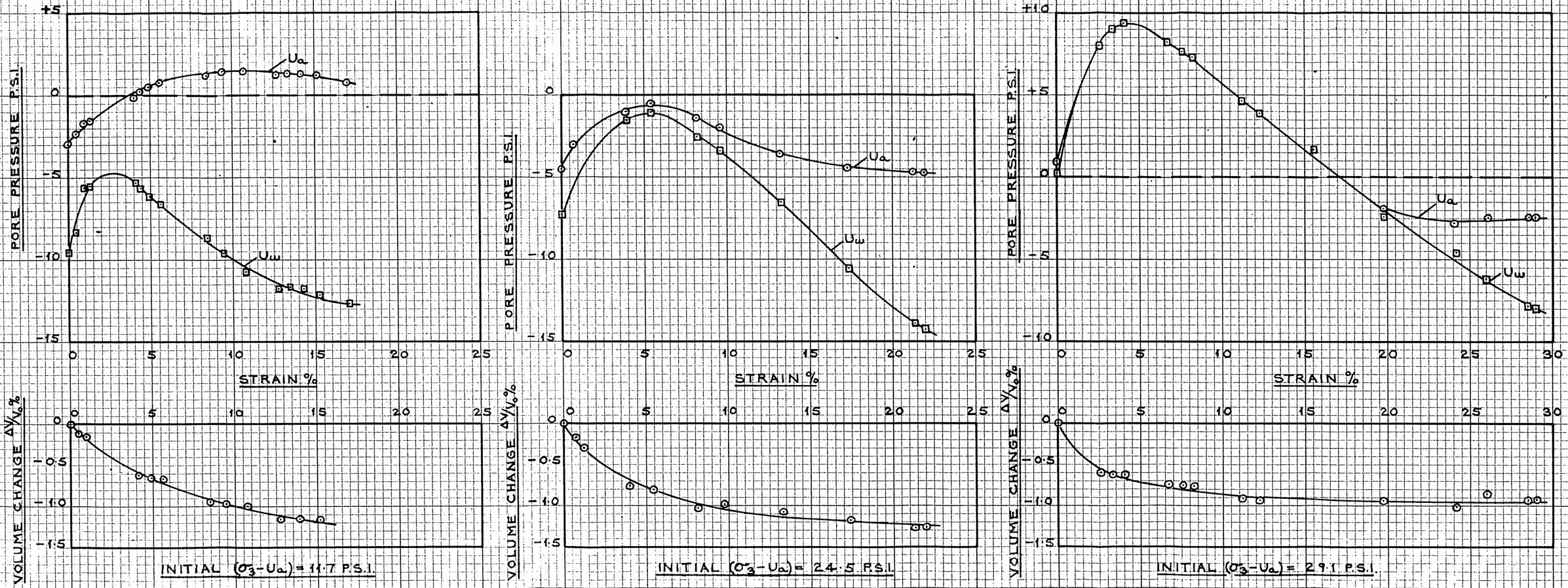


CONSTANT WATER CONTENT, VARYING $(\sigma_3 - U_a)$ TESTS

ON MANGLA SHALE

SERIES 1.

FIG. 7.17.



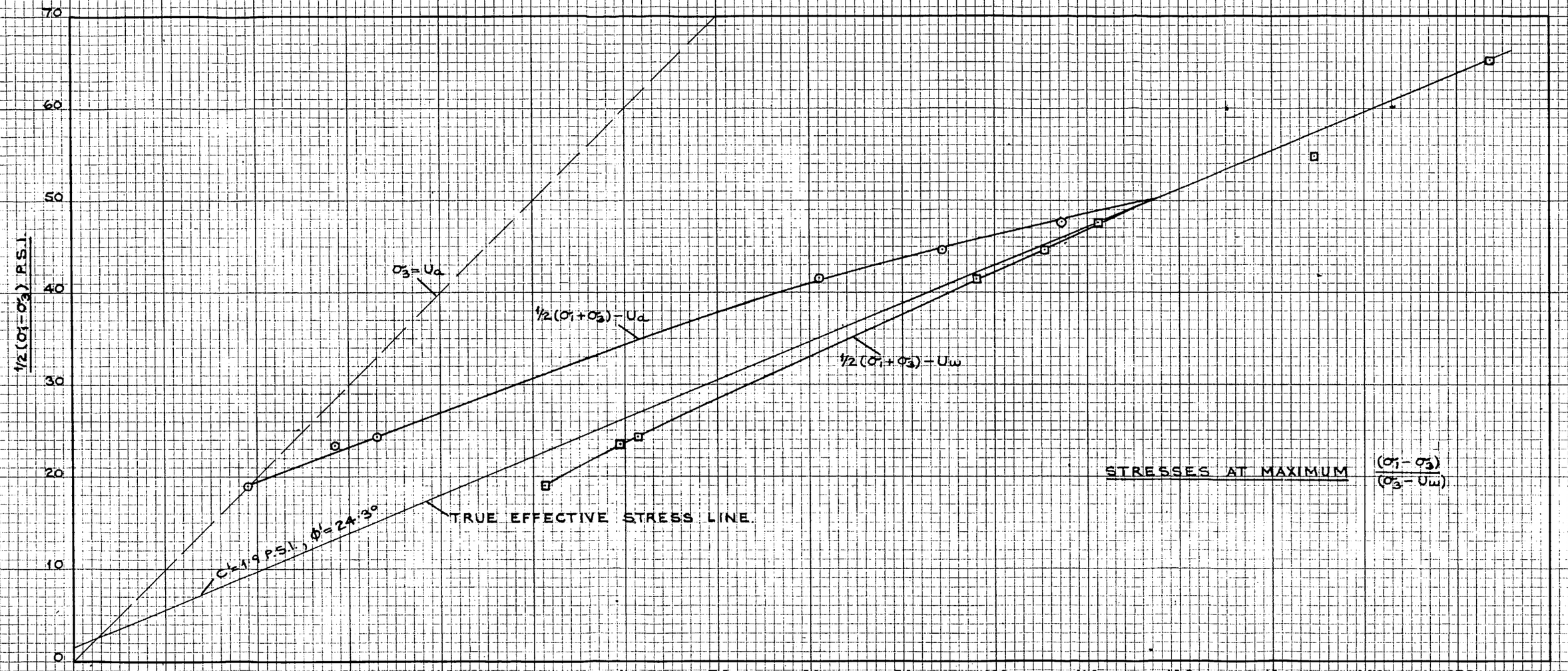
CONSTANT WATER CONTENT, VARYING $(\sigma_3 - U_a)$

TESTS ON COMPACTED MANGLA SHALE.

SERIES 1.

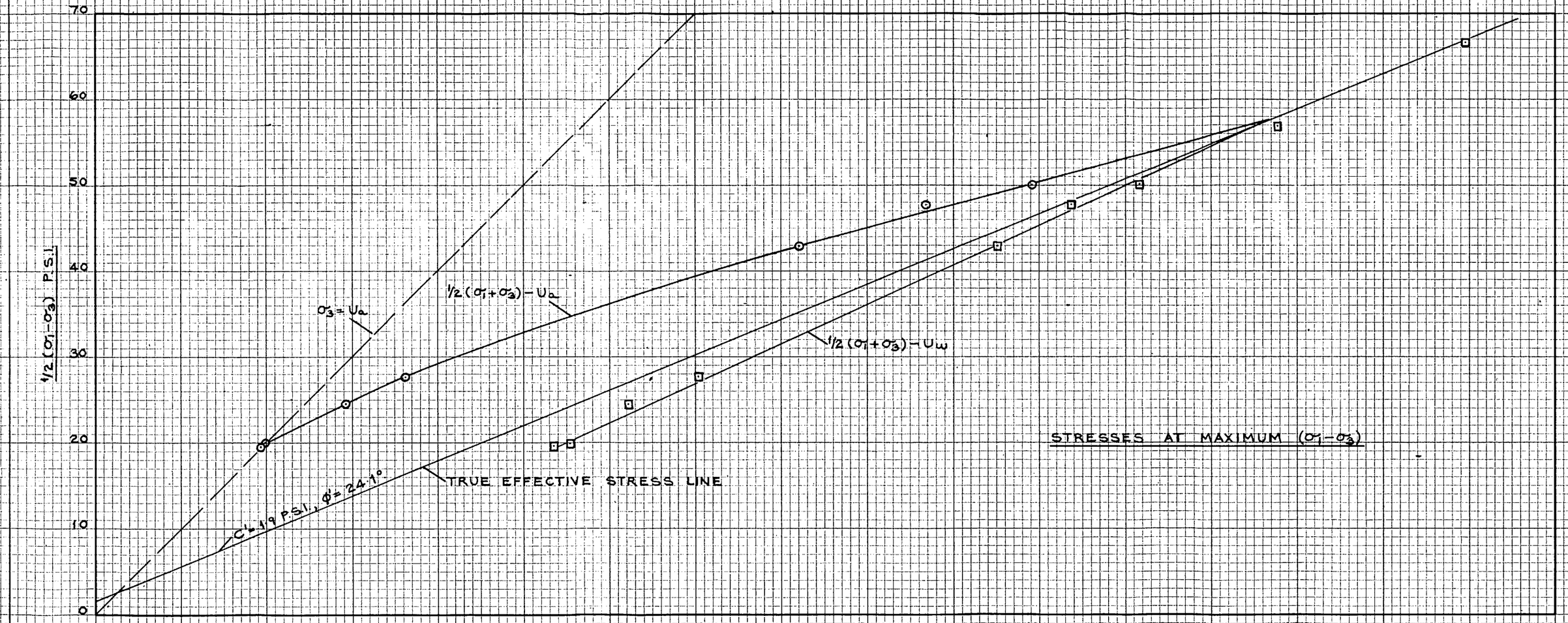
TYPICAL PORE PRESSURE CHANGES DURING SHEAR.

FIG. 7.18.



CONSTANT WATER CONTENT, CONSTANT $(\sigma_3 - U_a)$ TESTS ON MANGLA SHALE.
SERIES 3.

FIG. 7.19.

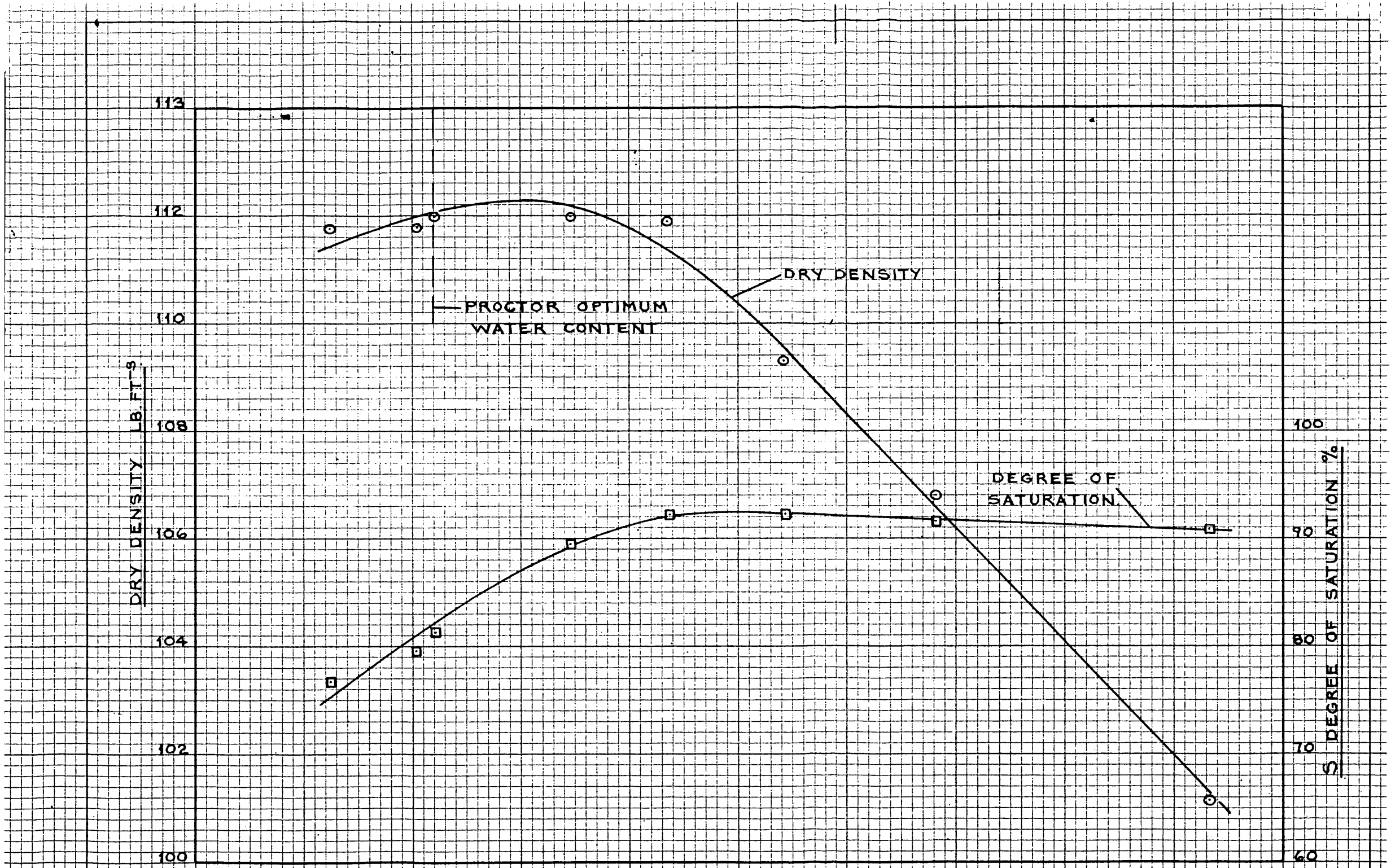


CONSTANT WATER CONTENT, CONSTANT $(\sigma_3 - U_a)$ TESTS

ON MANGLA SHALE

SERIES 3

FIG. 7.20.

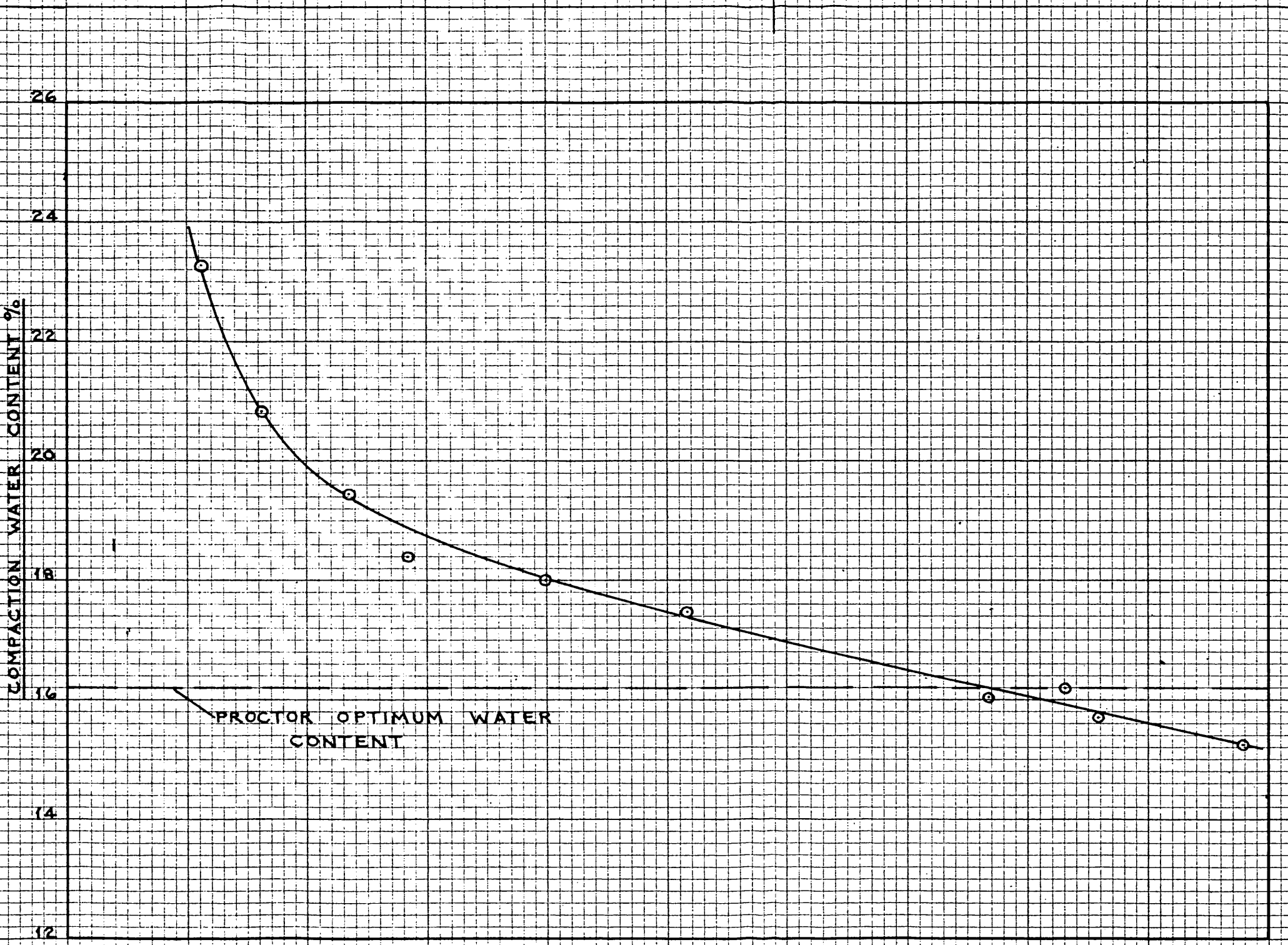


TESTS ON COMPACTED MANGLA SHALE WITH $\sigma_3 = U_a$

SERIES 1B

VARIATION OF DRY DENSITY AND SATURATION.

FIG. 7.21.

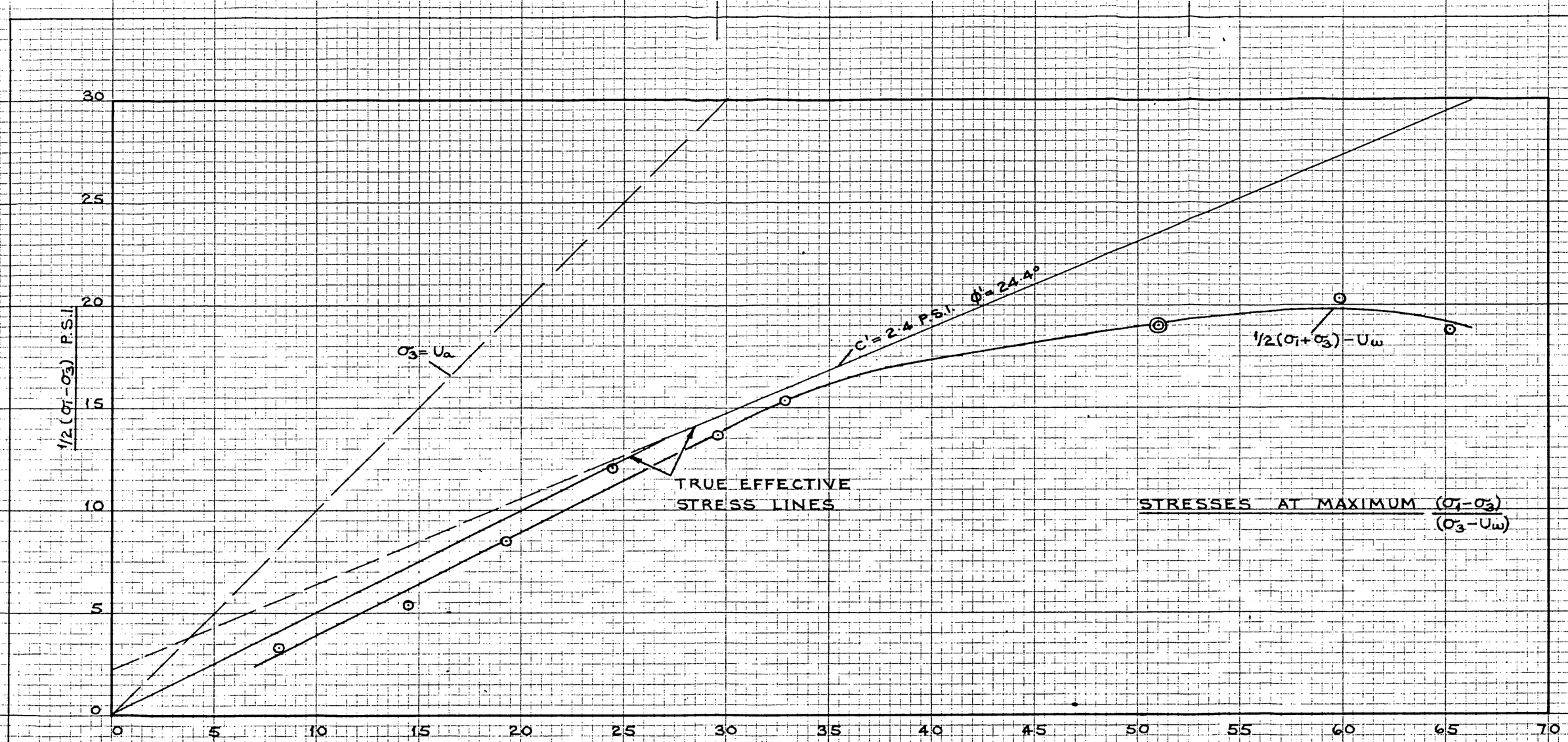


TESTS ON COMPACTED MANGLA SHALE WITH $\sigma_3 = U_a$

SERIES 1B

VARIATION OF INITIAL SUCTION WITH WATER CONTENT.

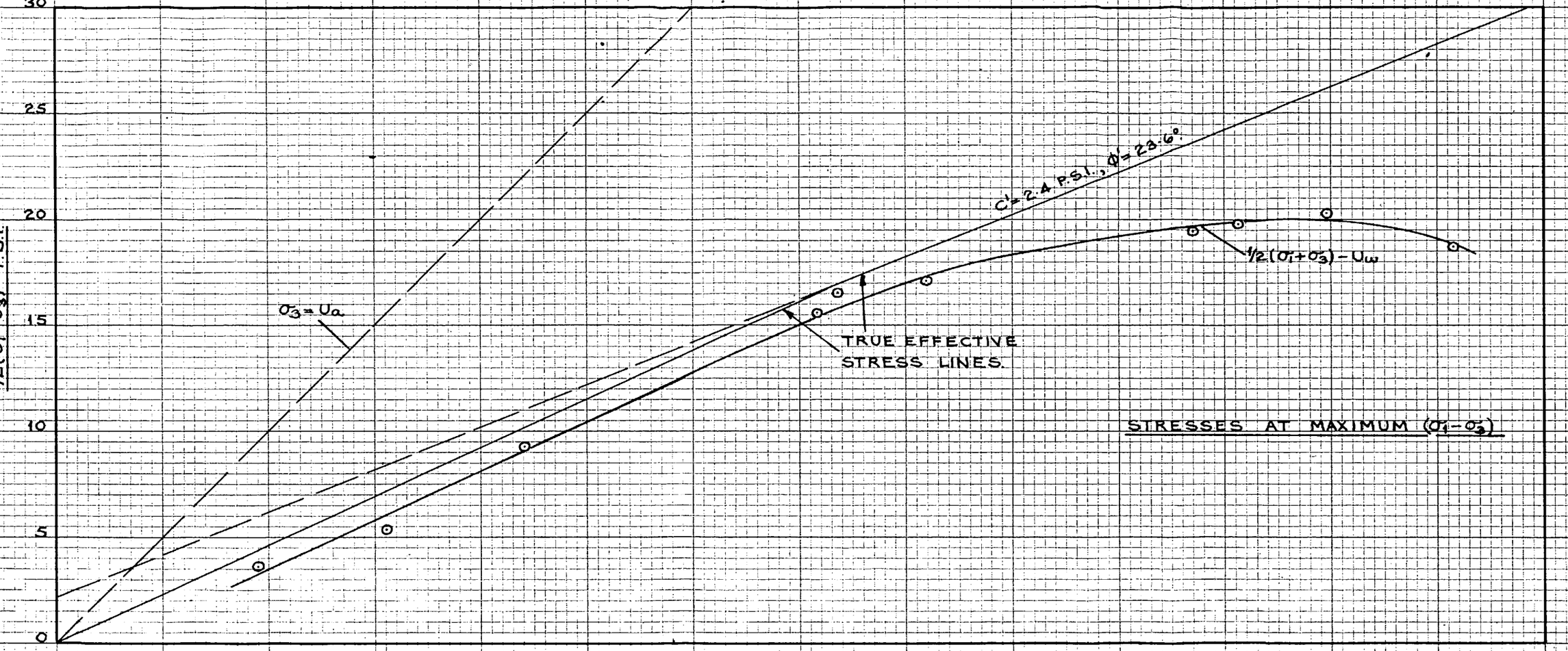
FIG. 7.22.



TESTS ON COMPACTED MANGLA SHALE WITH $\sigma_3 = U_a$ AT VARIOUS WATER CONTENTS

SERIES 1B

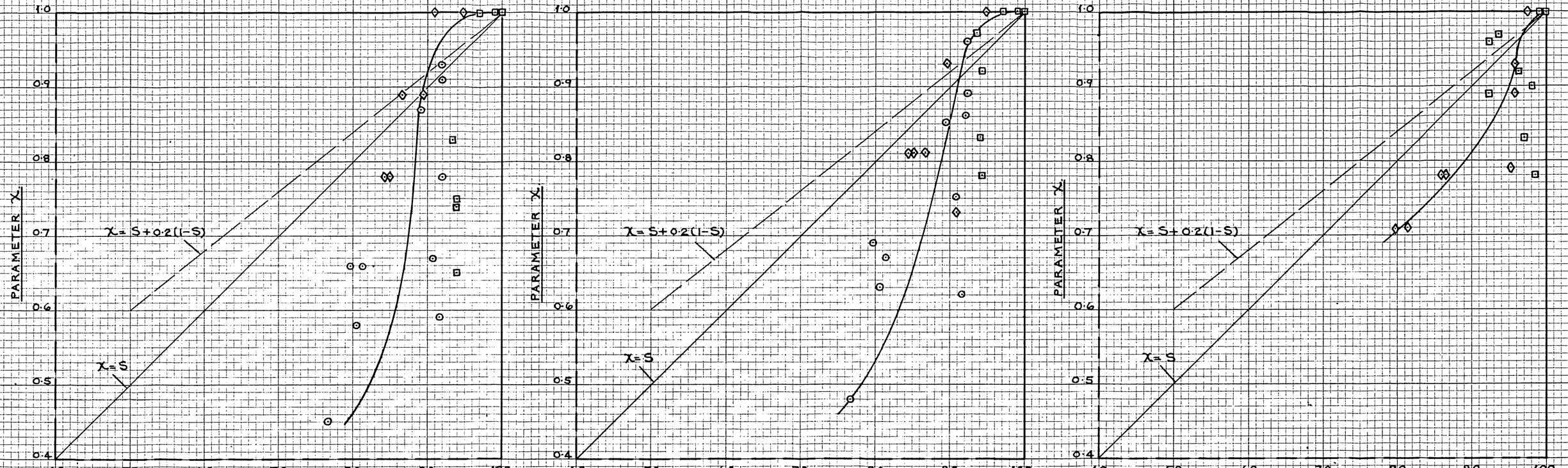
FIG. 7.23.



TESTS ON COMPACTED MANGLA SHALE WITH $\sigma_3 = U_a$, AT VARIOUS WATER CONTENTS.

SERIES 18.

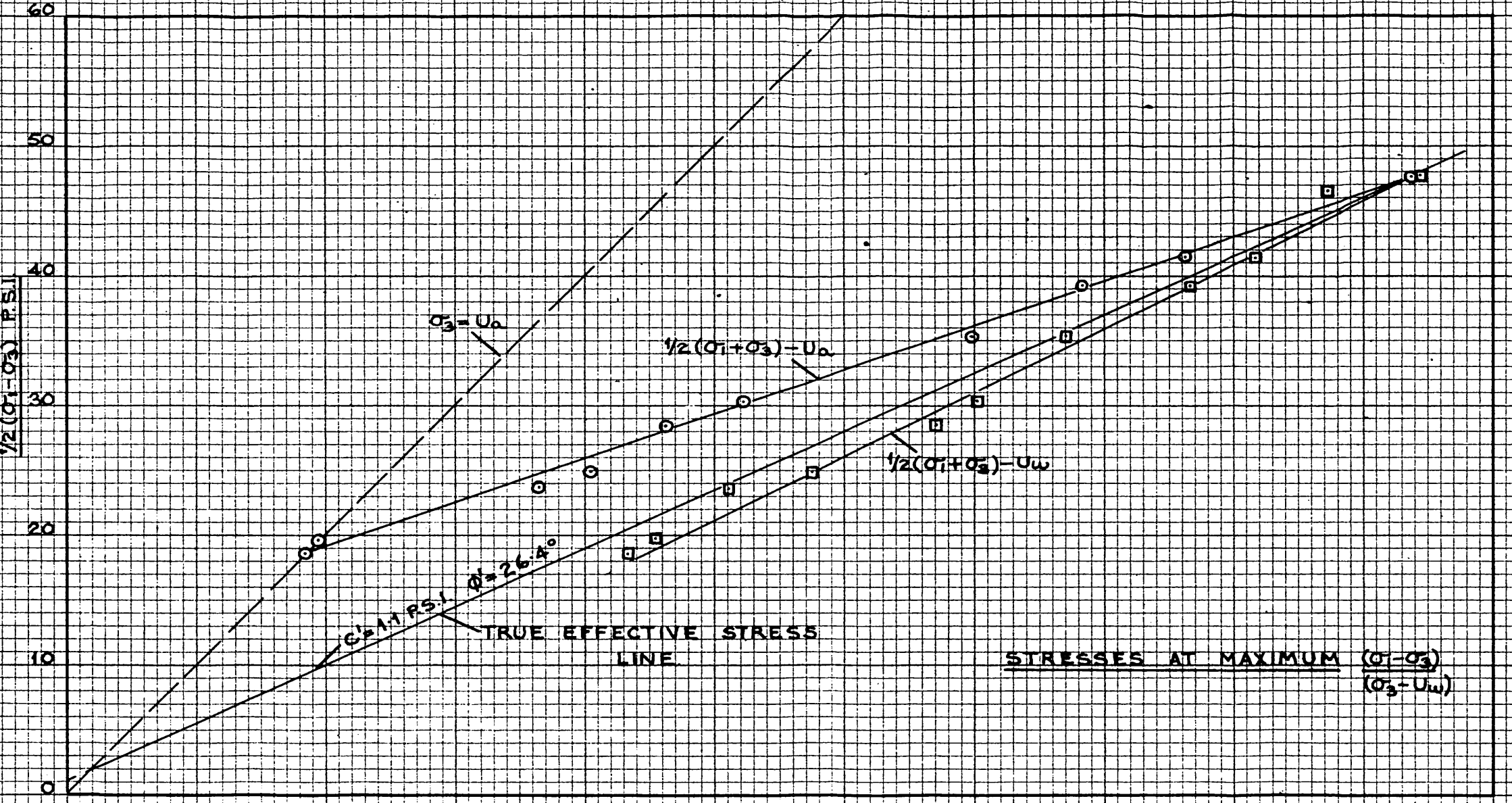
FIG. 7.24.



□ SERIES 1 COMPACTION W.C. CONSTANT, VARIOUS INITIAL $(\sigma_3 - U_a)$
⊙ SERIES 1B COMPACTION W.C. VARYING, $(\sigma_3 - U_a) = 0$.
◇ SERIES 3 COMPACTION W.C. CONSTANT, VARIOUS INITIAL $(\sigma_3 - U_a)$

TESTS ON MANGLA SHALE SUMMARY OF DEGREE OF SATURATION — PARAMETER χ RESULTS

FIG. 7.25.

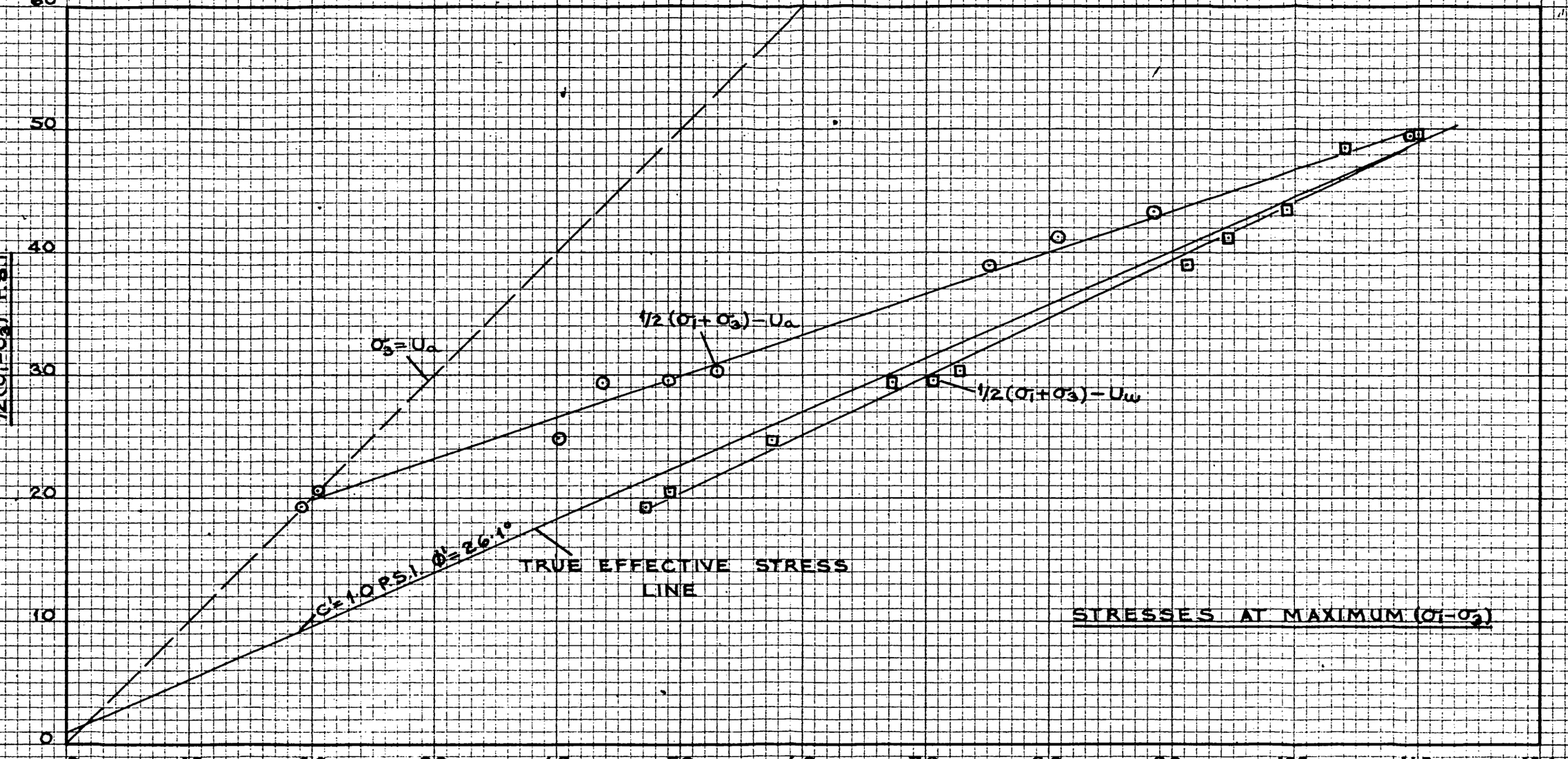


CONSTANT WATER CONTENT, VARYING $(\sigma_3 - U_o)$ TESTS ON

SELSET CLAY

SERIES 2

FIG. 7.26

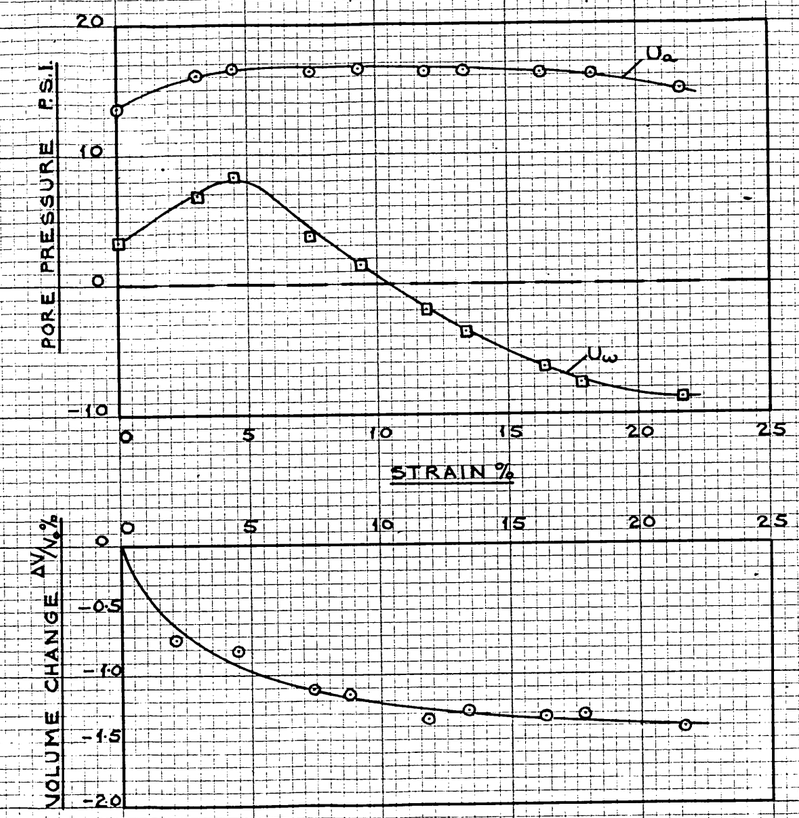


CONSTANT WATER CONTENT, VARYING $(\sigma_3 - U_a)$ TESTS ON

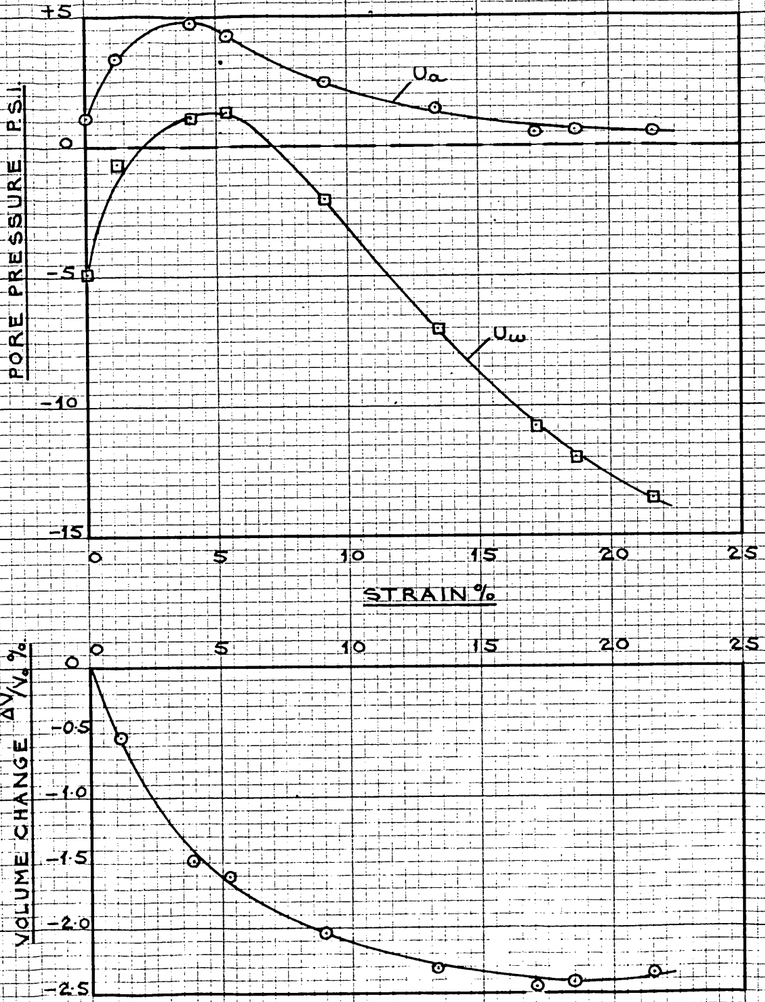
SELSET CLAY.

SERIES 2.

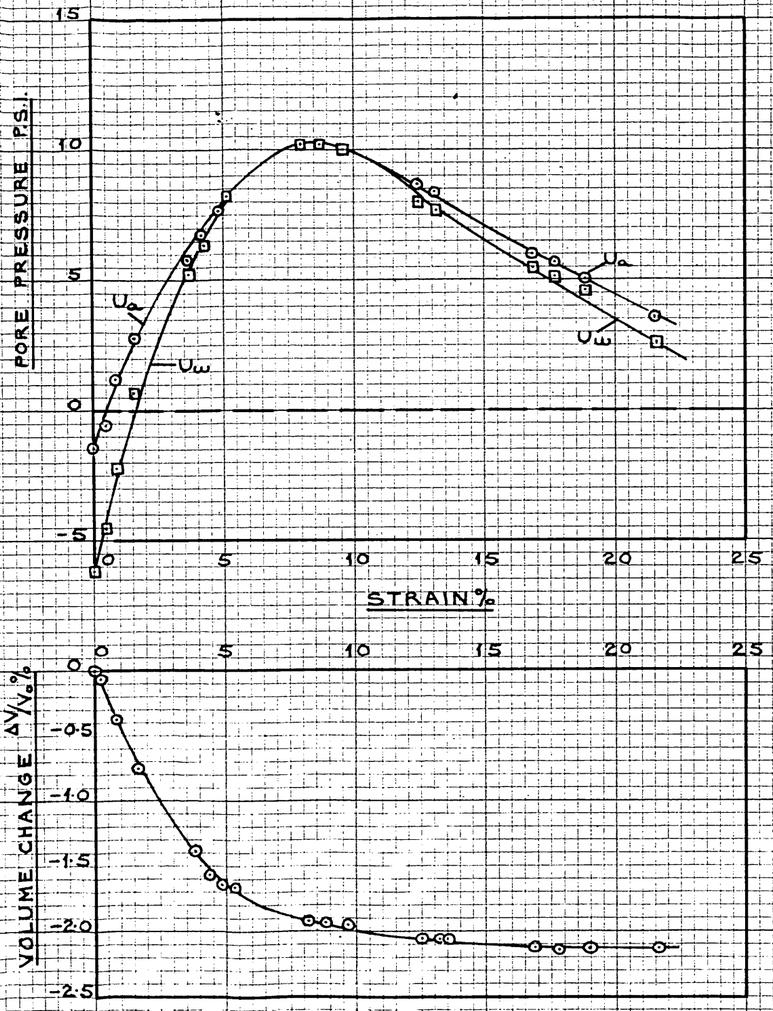
FIG. 7.27.



INITIAL $(\sigma_3 - U_a)$ = 13.1 P.S.I.



INITIAL $(\sigma_3 - U_a)$ = 38.8 P.S.I.



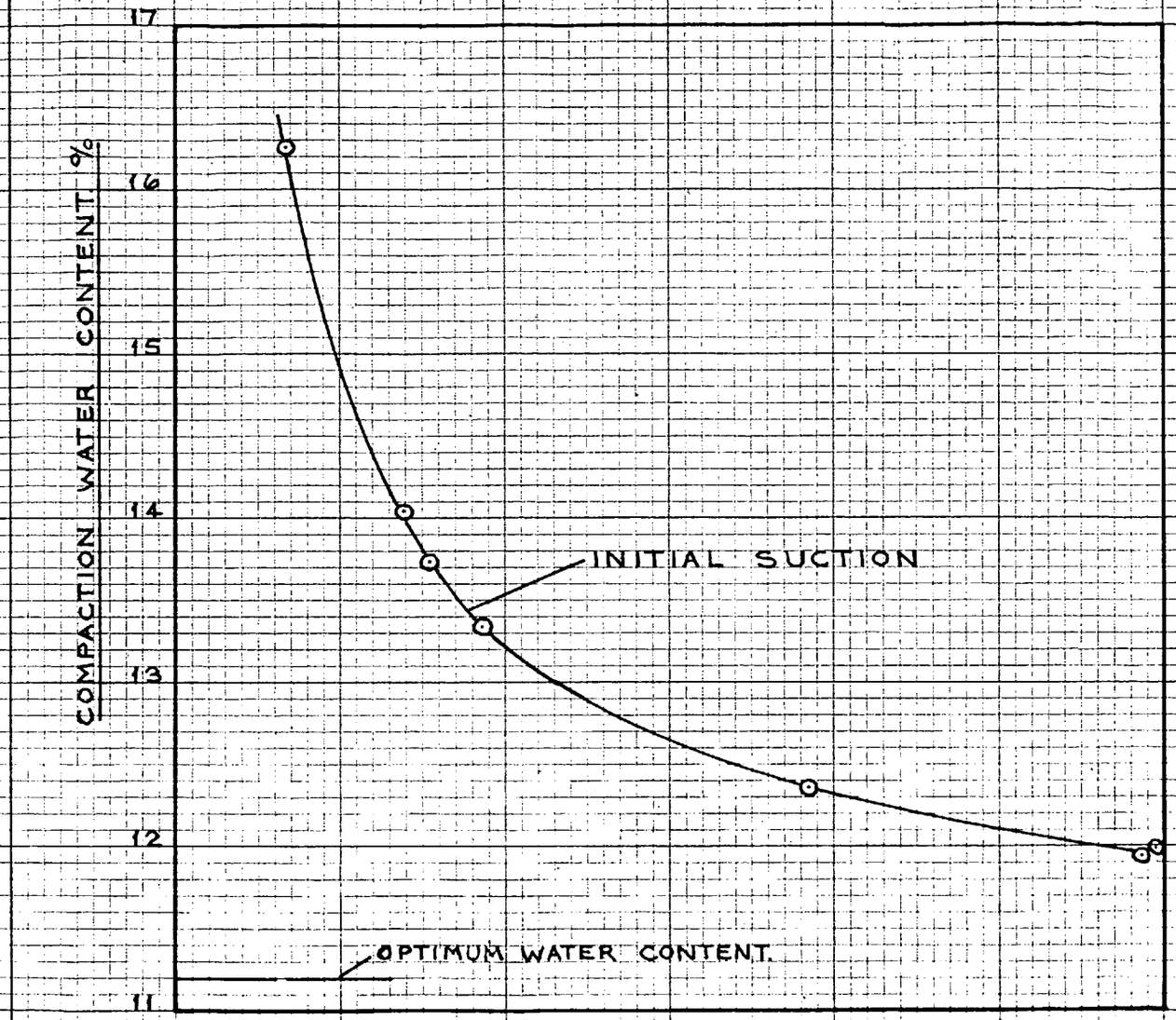
INITIAL $(\sigma_3 - U_a)$ = 66.6 P.S.I.

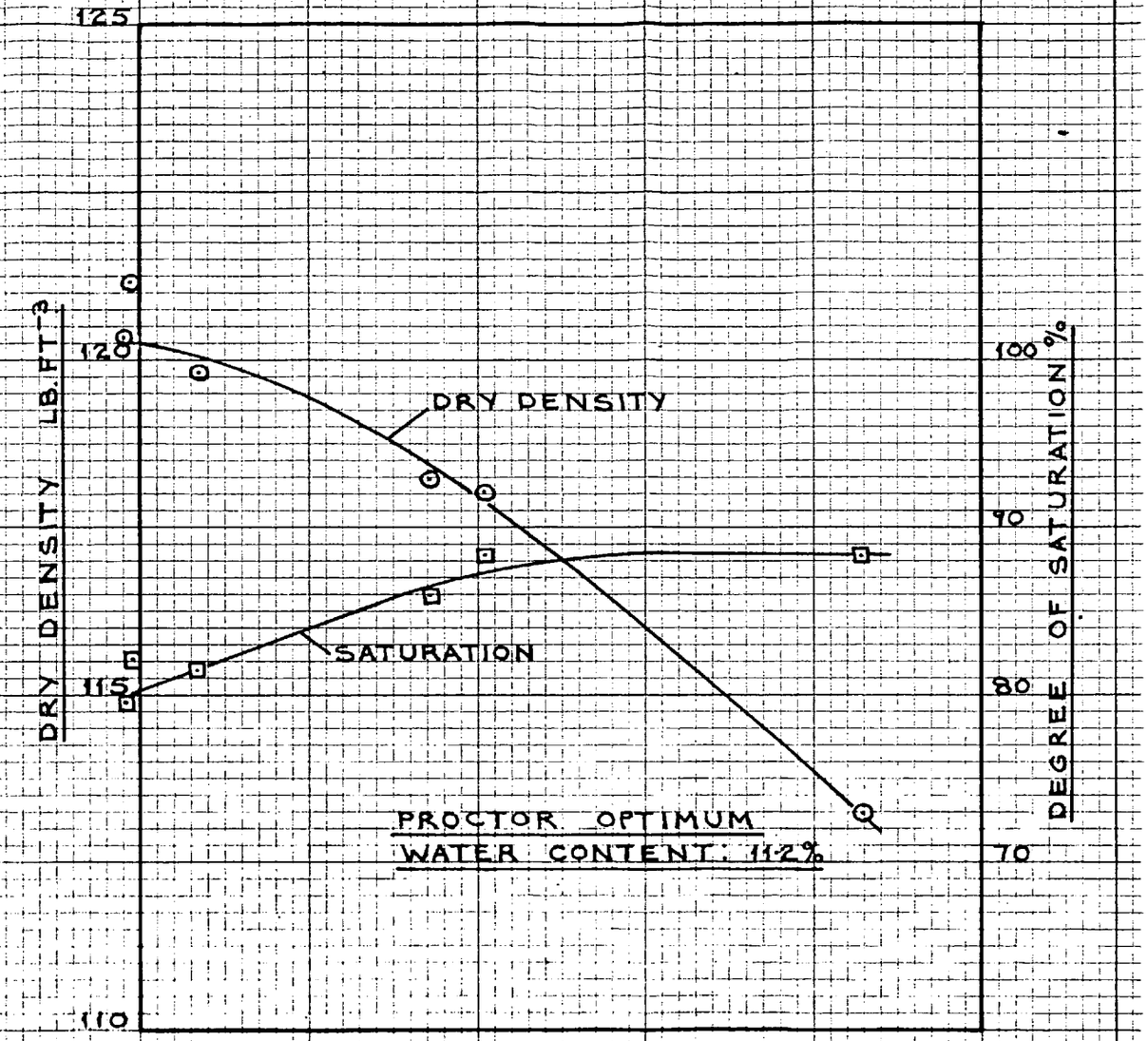
CONSTANT WATER CONTENT, VARYING $(\sigma_3 - U_a)$ TESTS ON SELSET CLAY

SERIES 2

TYPICAL PORE PRESSURE CHANGES DURING SHEAR.

FIG. 7.28.



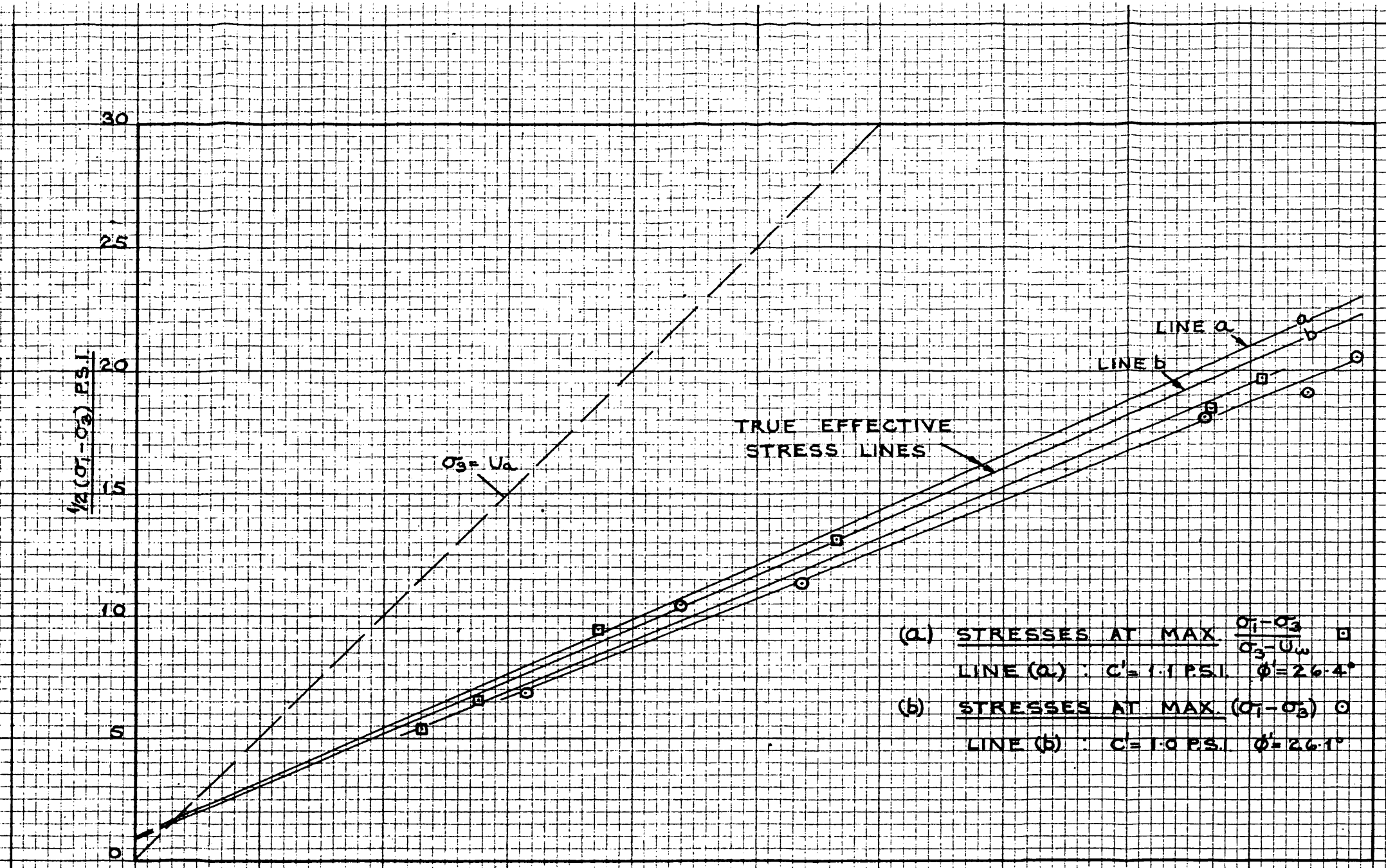


TESTS ON COMPACTED SELSET CLAY WITH $\sigma_3 = U_a$.

SERIES 2B.

VARIATION OF SUCTION, SATURATION AND DENSITY WITH WATER CONTENT.

FIG. 7.29.

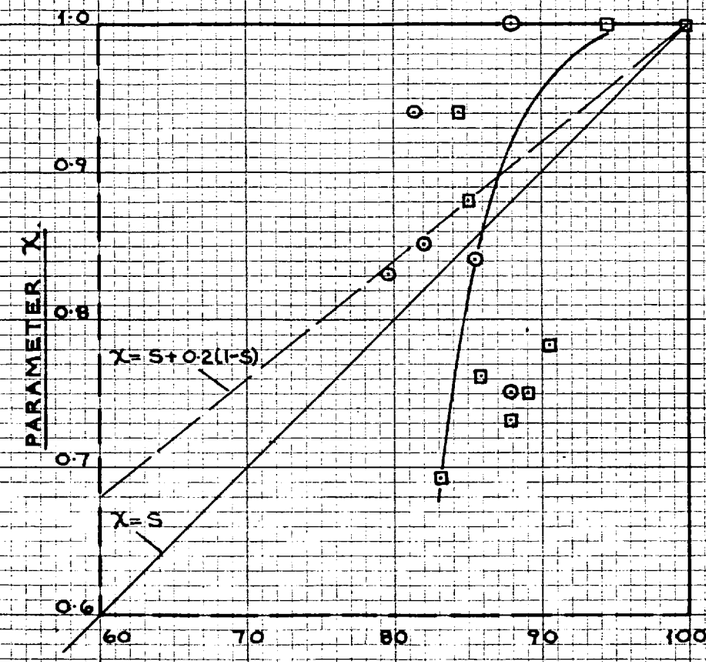


TESTS ON COMPACTED SELSET CLAY WITH $\sigma_3 = U_a$

AND AT VARIOUS WATER CONTENTS.

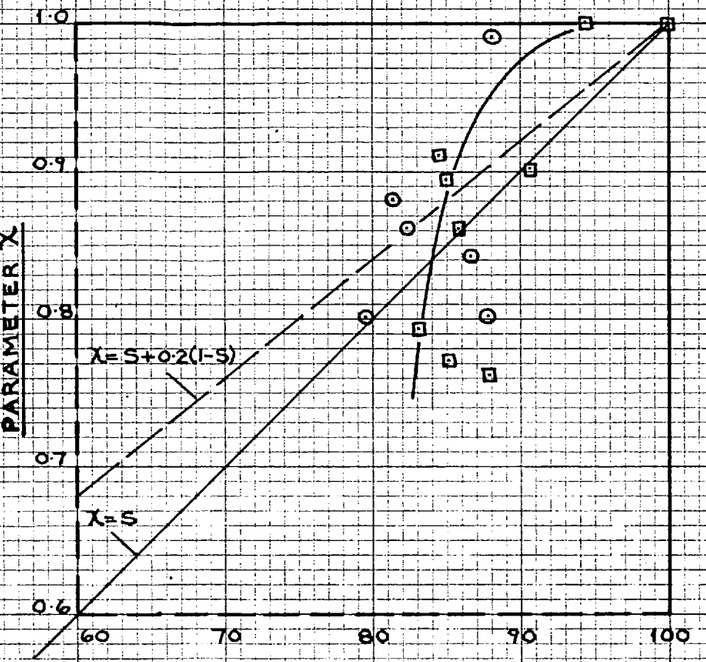
SERIES 2B.

FIG. 7.30.



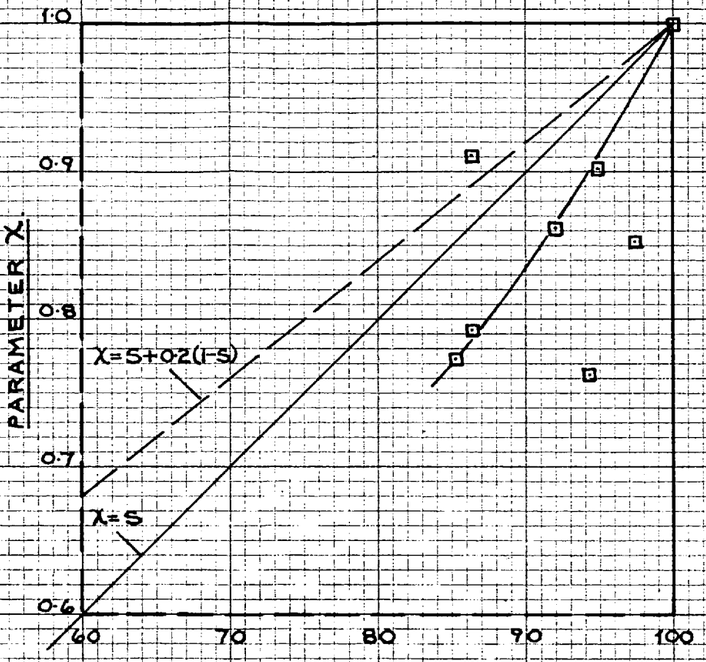
S_o DEGREE OF SATURATION BEFORE SHEAR %

(a) CONDITIONS AT MAXIMUM $\frac{(\sigma_1-\sigma_3)}{(\sigma_3-U_w)}$



S_o DEGREE OF SATURATION BEFORE SHEAR %

(b) CONDITIONS AT MAXIMUM $(\sigma_1-\sigma_3)$



S_f DEGREE OF SATURATION AT FAILURE %

(c) CONDITIONS AT MAXIMUM $(\sigma_1-\sigma_3)$

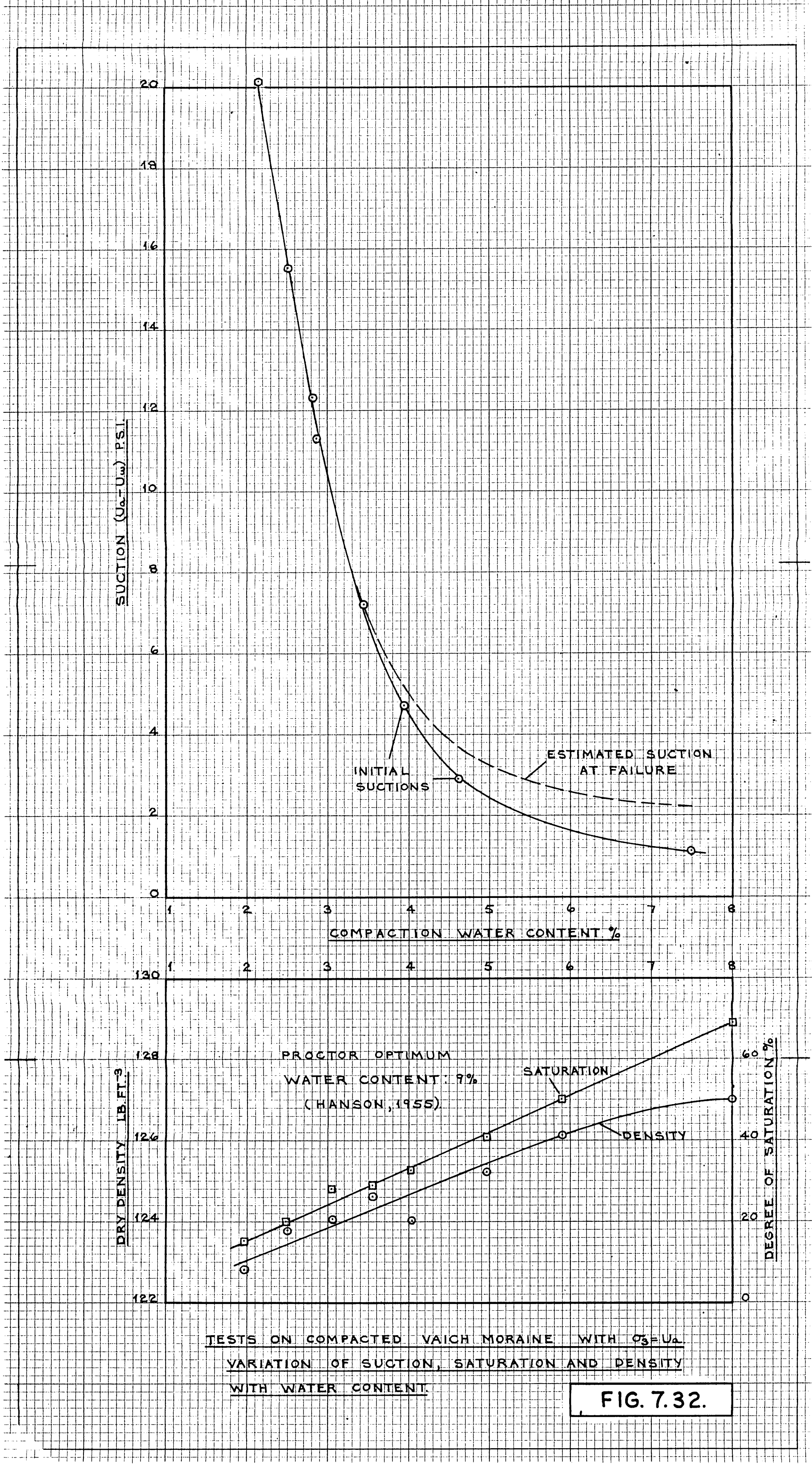
TESTS ON SELSET CLAY. SUMMARY OF DEGREE OF SATURATION — PARAMETER χ

RESULTS

□ SERIES 2

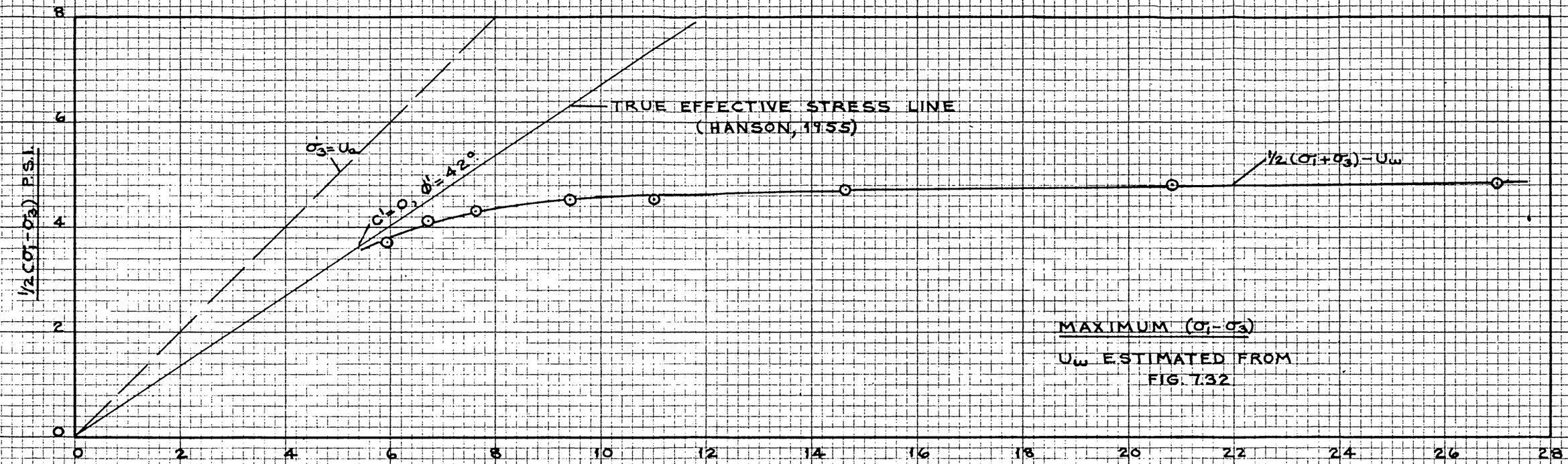
○ SERIES 2B.

FIG. 7.31.



TESTS ON COMPACTED VAICH MORAINE WITH $\sigma_3 = U_a$.
VARIATION OF SUCTION, SATURATION AND DENSITY WITH WATER CONTENT.

FIG. 7.32.



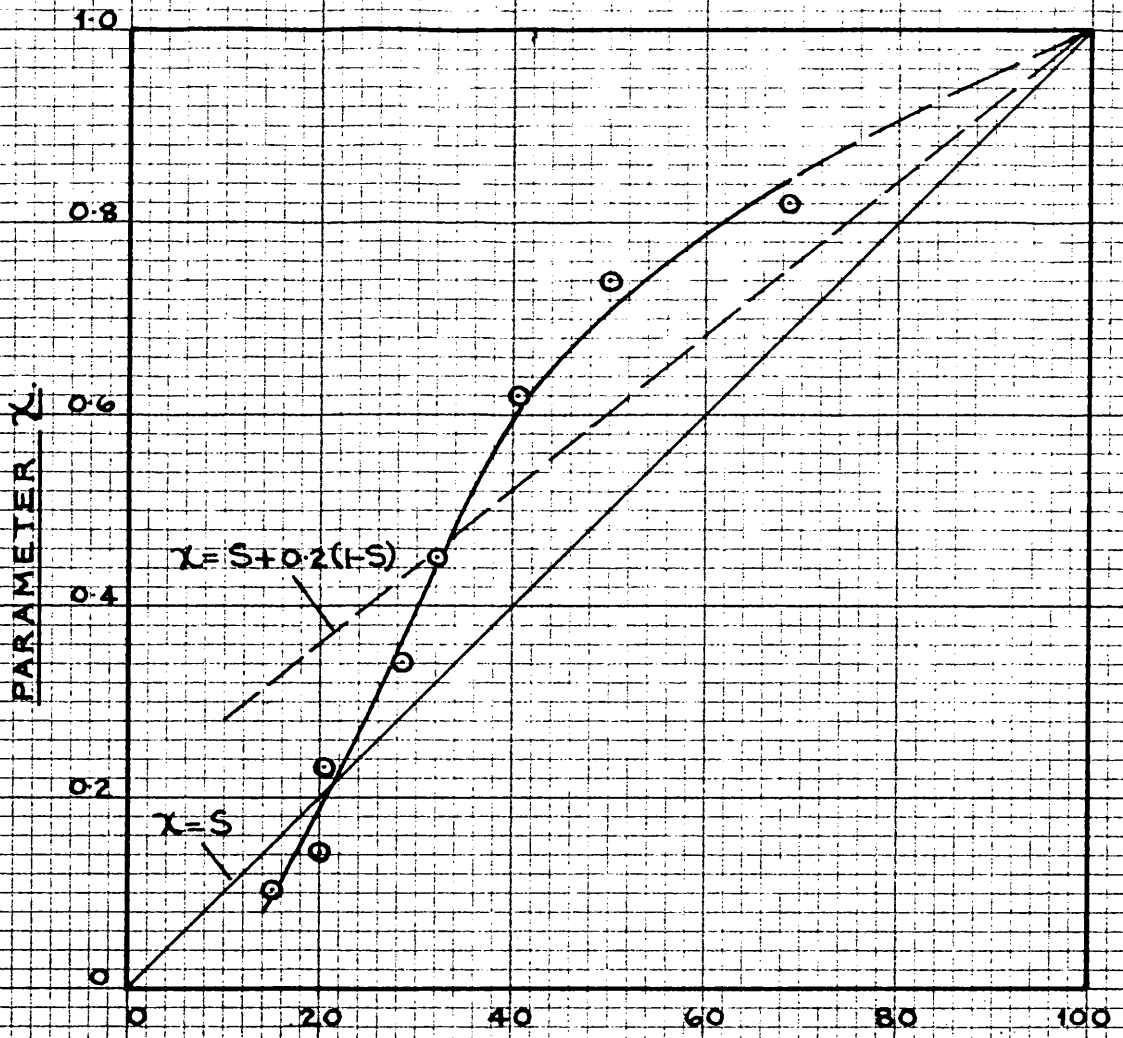
MAXIMUM $(\sigma_1 - \sigma_3)$

U_w ESTIMATED FROM FIG. 7.32

TESTS ON COMPACTED VAICH MORAINE WITH $\sigma'_3 = U_a$.

STRESSES AT FAILURE.

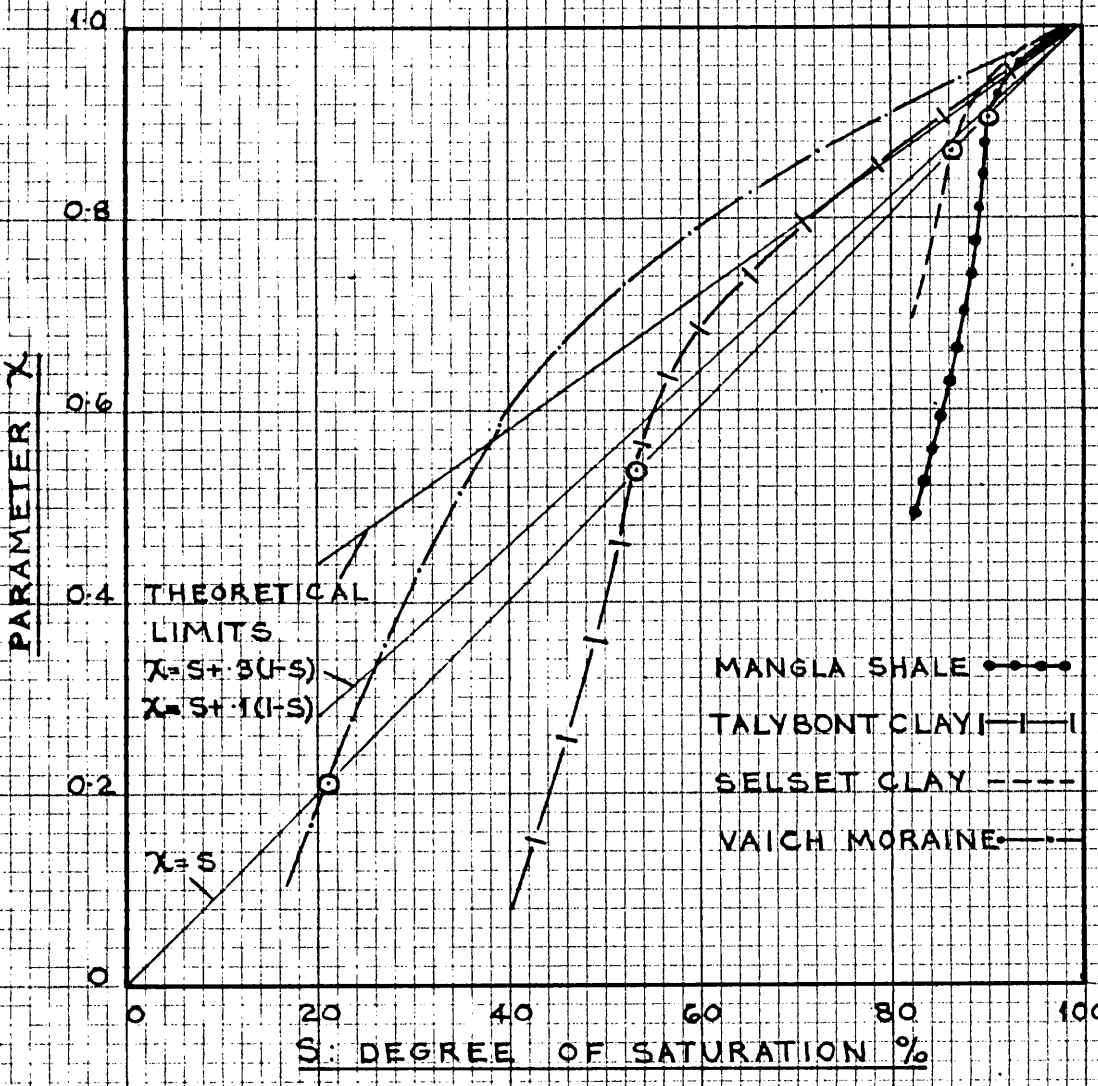
FIG. 7.33.

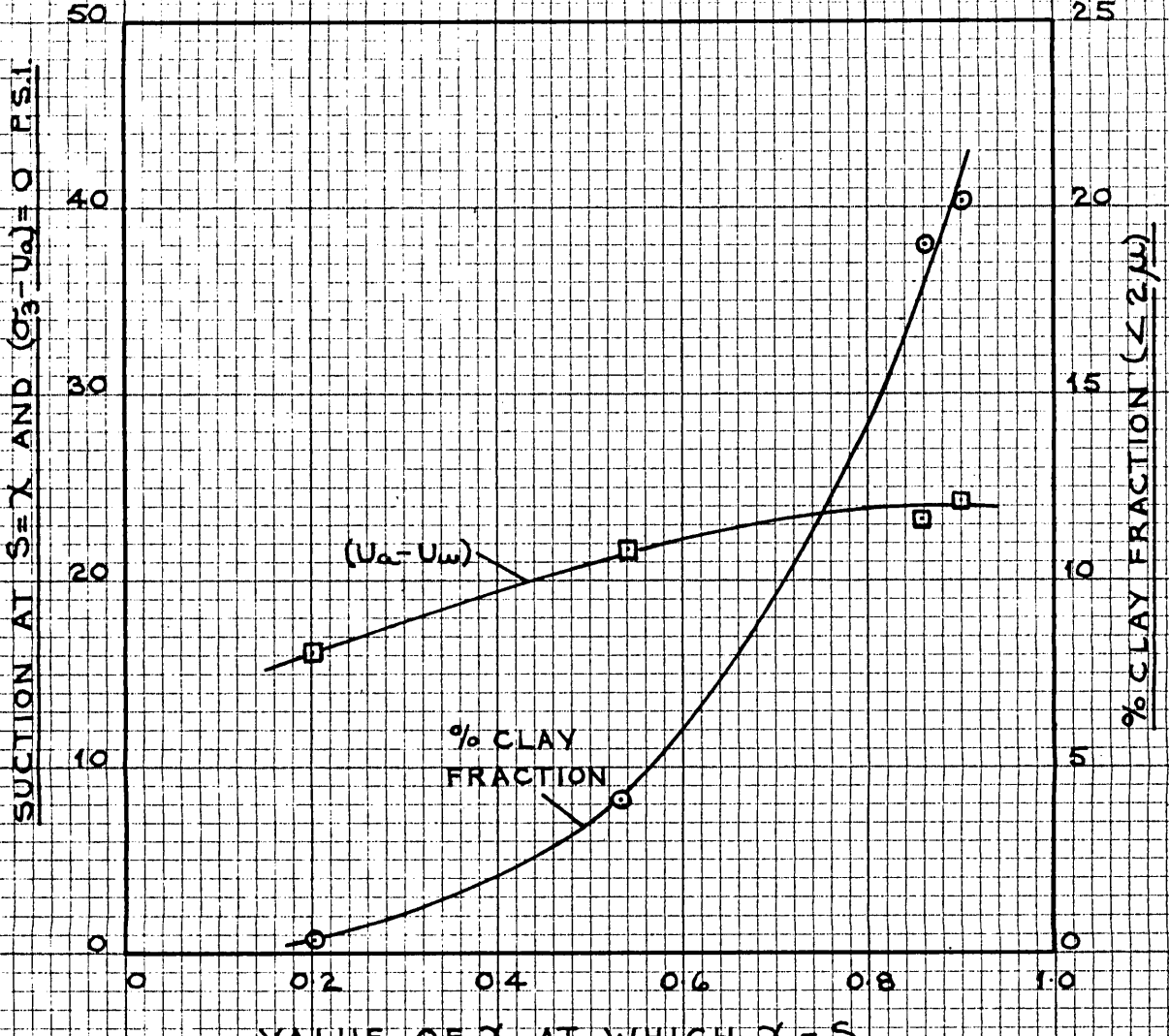


UNCONFINED ($\sigma_3 = U_a$) TESTS ON COMPACTED VAICH MORAINE

RELATION BETWEEN PARAMETER χ AND DEGREE OF SATURATION

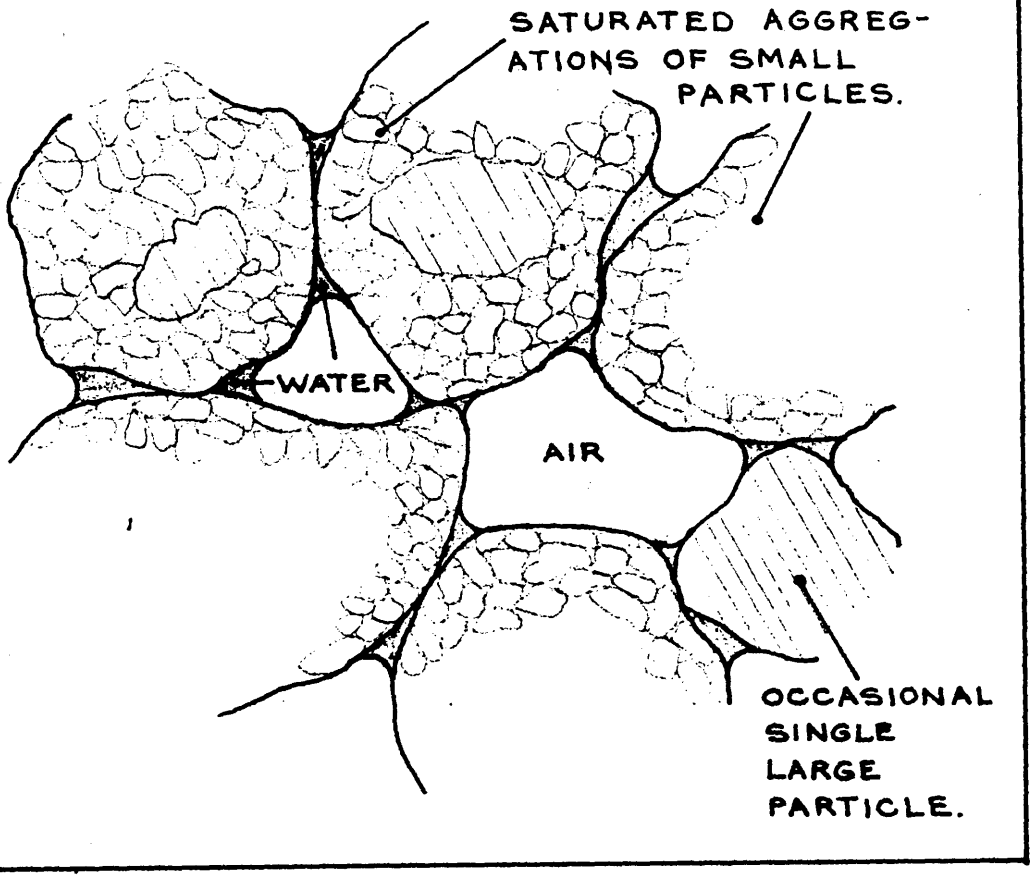
FIG. 7.34.





RELATION BETWEEN PARAMETER χ AND DEGREE OF SATURATION S FOR FOUR SOILS.

FIG. 7.35.



CONCEPT OF THE STRUCTURE OF A PARTLY SATURATED COMPACTED SOIL.

FIG. 7.36.

CHAPTER 8

NON-UNIFORMITY OF PORE PRESSURE DURING TRIAXIAL SHEAR

The pore pressure in a sample of soil undergoing triaxial compression will not in general be uniform. The normal procedure of interpreting test data in terms of pore pressures measured at a single point in a sample is dependent for its accuracy on the existence of a state of uniform pore pressure throughout the sample. Any significant departure from a state of uniformity can lead to serious errors in measured shear parameters. The simplest way to avoid errors due to non-uniformity of pore pressure is to run the test at a rate sufficiently slow to allow the pore pressures to equalise throughout the sample by transfer of moisture (and air in partly saturated samples). In saturated samples this transfer can be hastened by using paper circumferential drains.

(8.1) Causes of non-uniform pore pressures.

A major cause of pore pressure gradients during shear of samples which fail at large strains appears to be the non-uniform state of stress set up by friction on the end plates. This friction restrains the sample diameter to remain constant at the ends while that at the centre increases during shear. End restraint leads to non-uniform stresses at all stages of the test. At high axial strains the central bulge of the sample gives lower average vertical stresses than at the ends, because of its larger cross-section.

Another possible cause is the tendency towards narrow zone failure which is characteristic of many samples. A third cause might be due to allowing insufficient time for the sample to come

to full moisture and stress equilibrium before the commencement of loading. This aspect (which can be very important) will be discussed in Chapter 9. In what follows it will be assumed that all samples are in an equilibrium state before starting to shear. In soils having values of α appreciably less than unity, pore air pressures will usually equalise at least as rapidly as pore water pressures. In soils having α close to unity, pore air pressures are relatively unimportant. Thus it is the equalisation of the pore water pressure which is the critical factor in deciding on suitable rates of strain.

(8.2) Characteristics of pore pressure non-uniformity.

(a) Compacted soils.

Fig. (8.1) shows the results of a constant water content shear test on compacted Mangla shale (w = 18.5%) in which pore water pressures were measured simultaneously at the base and at a probe situated at mid-height of the sample. * Although the testing rate was slow by normal commercial standards (.038% per minute) there was a maximum pore pressure difference of 12 p.s.i. between the two points.

Fig. (8.2) shows Mohr stress circles for this test plotted in terms of pore pressures measured at base and mid-height. It is obvious that pore pressure differences of this magnitude can lead to very serious overestimation of cohesion intercepts.

Fig. (8.3) illustrates the effect of a twelve-fold decrease in rate of strain. The maximum pore pressure difference is reduced to a value of 2.6 p.s.i. which is a tolerable amount.

* For experimental procedure see section (8.4)a.
For appearance of probe see plate 4.

In fig. (8.4) the variation of the pore pressure difference $p = (u_E - u_c)$ is plotted against deviator stress for the test illustrated in fig. (8.1) and for a similar test on a drier sample of Mangla shale (w = 16%). It is seen that there is a linear relation between p and $(\sigma_1 - \sigma_3)$ over most of the stress range.

Note that in the tests shown in figs.(8.1) and (8.3) the pore pressure at the base is higher than that in the centre. This indicates a tendency for a migration of moisture from the ends of the sample towards the centre. This is borne out by fig. (8.5) which shows a pair of moisture content profiles with markedly higher moisture contents in the central failure zone. These profiles were measured on samples which were failed and then left under load until equilibrium pore pressure had been reached. The samples were then rapidly removed from their cells and moisture content specimens taken immediately. Each profile point represents the average moisture content of a thin layer over the whole diameter of the sample at the indicated distance from the central diameter. A similar trend was recorded in the tests described in Chapter 6.

The results of the two exploratory tests shown in figs. (8.1) and (8.3) showed that a more detailed investigation into the characteristics and effects of non-uniform conditions was necessary.

In order to learn more about the profile of pore pressure the test illustrated in fig. (8.6) was carried out. The sample was of Mangla shale (w = 18.5%) and the pore water pressure was measured simultaneously at the base, at a probe at mid-height of sample and at a probe 1" below the top of the sample. It will be noted that the pore pressure profiles are nearer linear than parabolic and

appear to remain geometrically similar when the rate of strain is altered.

(b) Saturated soils.

Tests on samples of Boston blue clay reported by Taylor (1951) and quoted by Whitman (1960) had showed the exact reverse of the above tests on compacted Mangla shale. Pore pressures had been found to be lower at the base than at the centre and moisture migration was away from the centre of the sample and towards the ends. The Boston clay was an undisturbed normally consolidated saturated clay and it was felt that the difference between the results might be due to differences of stress history. An attempt was made to duplicate Taylor's results by tests on samples prepared by remoulding Mangla shale at a sufficiently high water content to ensure an almost saturated sample, then consolidating enough to get the soil close to the virgin consolidation line for samples moulded near to the liquid limit and finally shearing undrained with base and mid-height measurement of pore pressures. To shorten the time required for consolidation, $1\frac{1}{2}$" diameter samples were used which were consolidated using filter paper side drains on a fine ceramic base. When consolidated, the samples were removed from the cell, the fine ceramic base minimising any gain in moisture by the sample on release of the cell pressure. The sample was then set up anew on a fine ceramic base without side drains and with a miniature ceramic probe at mid-height. * Plate 1 shows the appearance of the samples

* For method of setting up see section (8.4)a.

For appearance of miniature probe see plate 4.

before testing and illustrates the miniature perspex null indicator. After being allowed to come to equilibrium the samples were then sheared undrained in the usual way.

Two tests were done in all and the stress histories of the samples are shown in the appendix to this chapter (fig.A8.1). It was felt that the first test was not sufficiently close to the virgin line to qualify as normally consolidated and the second sample was therefore remoulded at a higher water content.

The results of the two tests are shown in fig. (8.7). In the early stages of loading there was a tendency in both cases for pore pressures to be higher in the centre than at the ends. This tendency was quickly reversed, however, and the final pore pressures and equilibrium moisture content profiles were similar to those of the compacted soil.

There is evidence that the moisture content also increases in the failure zones of samples of other consolidated clays moulded at water contents close to the liquid limit.

Henkel (1960) gives water content contours from drained and consolidated undrained tests on London and Weald clays. The contours are not equidistant, but converge towards failure thus indicating an increasing water content in the failure zones of the undrained tests.

(8.3) Special tests for detailed investigation of characteristics of pore pressure non-uniformity.

(a) Investigation of pore pressure profiles.

It was next decided to carry out a more detailed test on a 4" diameter x 8" high sample using five points of measurement. The object was to get detailed information on the nature of pore pressure

profiles under several loading conditions. The soil used was again Mangla shale. The four probes were arranged so as to give the equivalent of a measuring point at every inch of height up the side of the sample. The probes were arranged in a spiral up the height of the sample so that there were never two probes vertically above each other and so that all the probes were the maximum possible distance apart. This eliminated possible interference of one probe with another and minimised interference of all the probes with the behaviour of the sample as a whole.

The probes and membrane were set up on the triaxial base supported in position by a cylindrical cardboard former. The soil was then moulded directly into the supported membrane and around the probes. When formed, and with the membrane sealed to the top cap, the cardboard former was softened with water and peeled away. The appearance of the sample and the arrangement of the probes and null indicators before stripping off the cardboard former is shown in Plate 2 .

The sample was next put under a cell pressure of 50 p.s.i. and left for 36 hours to come to equilibrium. To check on the state of saturation of the sample, the cell pressure was then increased in stages to 140 p.s.i. The pore pressure was measured at the end of each stage and the sample was then allowed to consolidate. The progress of the consolidation was checked by measurements at the central probe. When all probes registered zero pore pressure, the drainage cocks were closed and the sample was loaded undrained.

Fig. (8.8) shows the variations with axial strain of the pore pressures registered at the various probes and also the variation

of deviator stress with strain. There was in this case a reversal of the pore pressure pattern at about 6% strain and the final pore pressure profile was similar to the previous profiles obtained for Mangla shale. The effect of a reduced rate of strain on the equalisation of the pore pressures is shown between 16.5% and 18.5% strain. The time of loading at the rapid rate was about 10 hours.

Once the pore pressures had reached equilibrium under the slowest rate of strain possible with the testing machine used, the sample was unloaded in approximately the same time as the duration of the rapid loading (10 hours). The resultant variation in deviator stress is shown in fig. (8.8). In fig. (8.9) are shown the variations of pore pressures with deviator stress. A complete reversal of the pore pressure profile was obtained. The equilibrium pore pressure after removal of the load was actually higher than that before removal of the load. This phenomenon of high residual pore pressures after unloading normally consolidated clays has been reported before by Bishop and Henkel (1953).

Once pore pressure equilibrium had been re-established the sample was reloaded. The deviator stress-strain curve is shown in fig. (8.8) and the variations of pore pressure with deviator stress are shown in fig. (8.9). The pore pressure profile on reloading was found to have reverted to the type found at the end of the first loading. The time taken to reach full load was closely equal to that of the initial loading.

The inset on fig. (8.8) shows the variation with strain of the pore pressure at the quarterpoints of the sample. O-a is the path of first loading, a-b is the path of unloading and b-c is the

path of reloading.

Fig. (8.10) gives a summary of the pore pressure profiles for the various stages of the test. The pore pressures have been expressed as a percentage deviation of the central pore pressure $\left(\frac{u - u_c}{u_c} \%\right)$ and have been plotted against the distance ratio z/H where z is the distance of any point from the centre of the sample and H is half the sample height.

The profiles on first loading were once again very close to linear. There was a tendency to approach a parabolic shape as the successive loading and unloading stages were performed. The loading stages appeared to give rise to greater non-uniformity in pore pressure than the unloading stage.

If the profiles are compared with the theoretical elastic stress distributions shown in fig. (8.28), it appears that as more and more work is done on the sample, the soil behaves more like an elastic material.

After finally unloading the soil and allowing equilibrium to be re-established, a large number of water content samples were taken. Layers at each probe height on both sides of the centre of the soil cylinder were sampled on three concentric circles. The results are shown in fig. (8.11). An important feature is the pronounced radial non-uniformity which is to be expected on the basis of elastic theory (see fig. (8.28)). The effect of the repeated reversals of the pore pressure profile is also reflected in the highly variable shape of the longitudinal water content profiles.

The probes penetrated the sample radially to a depth of $1\frac{1}{4}$" and thus reflect the average pore pressure in a cylindrical shell

of a probable thickness of $1\frac{3}{8}$". In a relatively rapid test of this nature they may not reflect pore pressures on the axis of the sample.

(b) The effect of reduced end restraint.

In order to determine to what extent non-uniformity of pore pressure is caused by frictional restraint on the ends of the sample, a special test was performed in which lubricated end plates were used. These end plates have been described in Chapter 2. A large reduction in friction was obtained by seating the ends of the sample against discs of thin latex rubber membrane which in turn rested against polished brass end plates. A layer of silicone grease was placed between the membrane and the brass. Tests by Wood (1958) have shown that the coefficient of friction of rubber on metal lubricated with silicone grease is very low ($\mu = 0.018$). The sample was centred on the end plates by drilling an accurately centred vertical hole ($\frac{1}{2}$" diameter x $\frac{3}{4}$" deep) in each end using a drill press. These holes fitted over matching central brass pegs in each end plate. The sample was of Mangla shale compacted at a water content of 17.9%. Pore pressures were measured using two probes - one at mid-height and one an inch below the top of the sample and a single perspex null indicator. The cell pressure of 100 p.s.i. was sufficient to saturate the sample.

In order to compare the results with those of the test described in fig. (8.1) the sample was strained at the same rate of .038% per minute.

A feature of the test was the partial elimination of the characteristic central bulge. The sample remained almost a right cylinder even when strained to 17%. A greater reduction in end

restraint seemed to have occurred at the base of the sample than at the top.

Fig. (8.12) shows the variation of the pore pressures with strain and also compares the deviator stress-strain curve for this test with that obtained in the equivalent test with normal end plates.

Fig. (8.13) compares the maximum pore pressure difference $p = u_E - u_c$ in the two tests. As the pore pressure in the test with reduced end friction was measured an inch away from the end of the sample, the measured difference was multiplied by $4/3$ to give the equivalent of an end measurement. The reduction in pore pressure difference achieved with the low friction end plates shows that end restraint is a major factor causing non-uniform pore pressures in triaxial tests on this type of soil.

The form of end plate used in this test was not completely satisfactory as the membrane discs covering the ends of the sample caused some restraint as they stretched with the increasing diameter of the sample. This is probably why the pore pressure difference increased after 10% strain.

The variation of pore pressures with deviator stress during the loading and unloading stages is shown in fig. (8.14). The unloading was completed in approximately the same time as the loading and the pore pressure difference was about the same in magnitude.

Also shown in fig. (8.13) is the variation of pore pressure difference with strain for the test illustrated in fig. (8.3). This brings out a significant result of the test: that even partial reduction of end restraint allows very much faster testing times without sacrificing any accuracy in pore pressure measurement.

A further comparison of this type of test with a test using normal end plates is made at the end of section (8.3)c.

When the test was dismantled, it was found that the sulphur in the two end discs of rubber membrane had reacted with the freshly machined brass of the end plates to produce a black sulphide. As the soil expanded radially during the test, it had left tracks in the sulphide deposit which recorded the radial movements. The appearance of these radial tracks is shown in plate 3.

(c) Radial pore pressure non-uniformity.

Radial water content profiles described in section (8.3)a showed that radial pore pressure differences might exist in rapid tests which were not recorded by the normal type of probe. The water content profiles showed that the biggest radial difference in pore pressures could be expected at the ends of a sample.

To measure this difference, a ceramic probe was sealed into the central hole of a 4" diameter triaxial base pedestal. The height of the probe was 1" and its diameter $\frac{3}{8}$". The radial grooves on the surface of the pedestal were filled with "twin-bond". A nylon lead was taken from the base pore pressure duct to a perspex null indicator through a T-piece. A second nylon lead was taken from the other branch of the T into the cell and communicated through the sample membrane with a band of saturated glass fibre ribbon 1" wide which was wrapped around the base of the sample. This ribbon acted as a collecting element for the measurement of pore pressure on the perimeter of the sample.

The sample was of Mangla shale compacted at a water content of 17.4%. The cell pressure of 100 p.s.i. was sufficient to saturate

the sample and thus enable the glass fibre ribbon to function as a saturated element.

A rate of strain of .038% per minute was used in loading.

The variation with deviator stress of the pore pressures at the perimeter and on the axis of the base are shown in fig. (8.15).

The maximum difference recorded was 1 p.s.i. which shows that radial pore pressure non-uniformity was in this test not a very important factor. That the difference is so small is probably because of the small drainage path involved and also because the volume of the central core towards or away from which most of the drainage must occur is only about 1/30 of the volume of the whole sample. Both these factors would greatly speed up equalisation.

The appearances of the samples described in (8.3)b and (8.3)c after testing to 17% strain are compared in Plate 4. The photograph also illustrates the arrangement of probes and null indicators used in these tests.

Fig. (8.16) compares the equilibrium moisture content profiles obtained in the two tests after loading and unloading, and also shows the differences in sample shape. The equilibrium water content distribution was very much more uniform in the test with lubricated end plates than in that using normal end plates. There was, however, a slightly larger radial non-uniformity in the test with lubricated end plates which was opposite in character to the pattern obtained from the test with normal end plates. The greater difference may be because the pore pressures did not reverse themselves so far on the unloading cycle in the test with lubricated end plates. Likely moisture content distributions at the end of loading are shown

sketched in on fig. (8.16). This pattern would fit in with the observed pore pressures (in the test with normal end plates) at the end of loading which were higher at the perimeter than at the centre.

(8.4) The theoretical relation between testing times and the degree of equalisation of pore pressure in the triaxial test.

The question of the speed at which triaxial tests can be run without setting up undesirable pore pressure gradients is of considerable importance in both commercial and research testing.

As the maximum pore pressure difference will generally be between the centre and ends of the sample, a measure of the uniformity of pore pressure will be $p = u_E - u_c$ where u_E = pore pressure at the ends (base and top) of the sample and u_c = pore pressure at the centre (mid-height) of the sample. Suppose that in a test carried out so rapidly that no equalisation can take place the value of p is p_o. Then the degree of equalisation of p is defined as:

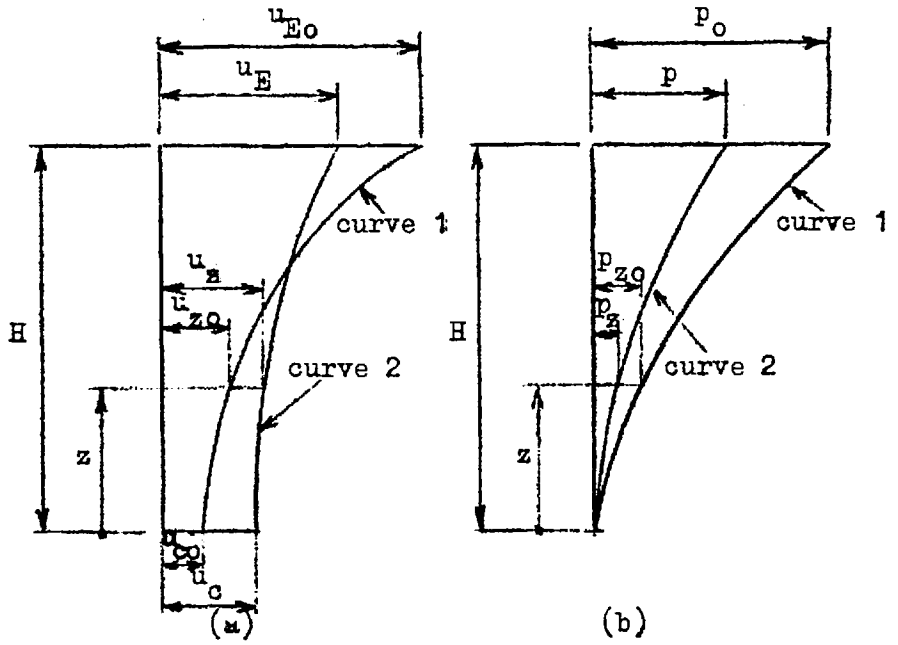
$$\Upsilon = 1 - \frac{p}{p_o} \qquad E(8.1)$$

For the purposes of this analysis it will be assumed that:

(a) The soil is saturated.

(b) The coefficients of consolidation and swelling are negligibly different, and that the relation between effective stress and volume change for the soil is reversible.

(c) That equalisation takes place by transfer of moisture in a purely axial direction. i.e. that the pore pressure and total stress are uniform across any plane normal to the axis of loading.



Curve 1 in diagram (a) shows the sort of pore pressure distribution which would be expected during shear in an "instantaneous" test with values of u_{co} at the centre and u_{Eo} at the ends. This distribution would partially equalise at a slower rate of testing (curve 2) to a value u_c at the centre and u_E at the ends.

By defining:

$$p_z = u_z - u_c \qquad p = u_E - u_c$$
$$p_{zo} = u_{zo} - u_{co} \qquad p_o = u_{Eo} - u_{co} \qquad \text{E(8.2)}$$

diagram (b) is obtained in which only pore pressure differences are shown.

If Δw_z is the volume change per unit volume of soil at point z due to migration of moisture then the relation between Δw_z and the change in principal effective stresses at z can be written as:

$$\Delta w_z = C_c\left[\Delta\sigma_3 - \Delta u_z + A_z\Delta(\sigma_1' - \sigma_3')\right] \qquad \text{E(8.3)}$$

Where

C_c is a compression index for the soil (with units of $\frac{\text{volume/unit volume}}{\text{stress}}$).

Similarly for the centre of the sample:

$$\Delta w_c = C_c\left[\Delta\sigma_3 - \Delta u_c + A_c\Delta(\sigma_1 - \sigma_3)\right] \qquad E(8.3)$$

(This assumes that C_c is the same throughout the sample).

Subtracting:

$$\Delta w_z - \Delta w_c = C_c\left[-(\Delta u_z - \Delta u_c) + (A_z - A_c)\Delta(\sigma_1 - \sigma_3)\right] \qquad E(8.4)$$

For convenience, write

$$\Delta w_z - \Delta w_c = \Delta w$$

also $$\Delta p_z = \Delta u_z - \Delta u_c$$

Fig. (8.4) shows that p can be related to $(\sigma_1 - \sigma_3)$ by the equation:

$$\Delta p = \alpha\Delta(\sigma_1 - \sigma_3) - \lambda \quad \text{where } \alpha \text{ and } \lambda \text{ are constants.}$$

Figs. (8.6) and (8.10) show that the geometry of the pore pressure profile does not alter very much as equalisation proceeds. Therefore, it is reasonable to assume for the "instantaneous" test that:

$$\Delta p_{zo} = \alpha_o\Delta(\sigma_1 - \sigma_3) - \lambda_o \qquad E(8.5)$$

or:
$$\Delta(\sigma_1 - \sigma_3) = \frac{\Delta p_{zo} + \lambda_o}{\alpha_o}$$

Substituting E(8.5) in E(8.4):

$$\Delta w = C_c\left[-\Delta p_z + \frac{(A_z - A_c)(\Delta p_{zo} + \lambda_o)}{\alpha_o}\right] \qquad E(8.6)$$

The basic one dimensional consolidation equation is:

$$\frac{k}{\gamma_w}\frac{\partial^2 p_z}{\partial z^2} + \frac{\partial\Delta w}{\partial t} = 0 \quad \text{(Gibson \& Henkel, 1954)} \qquad E(8.7)$$

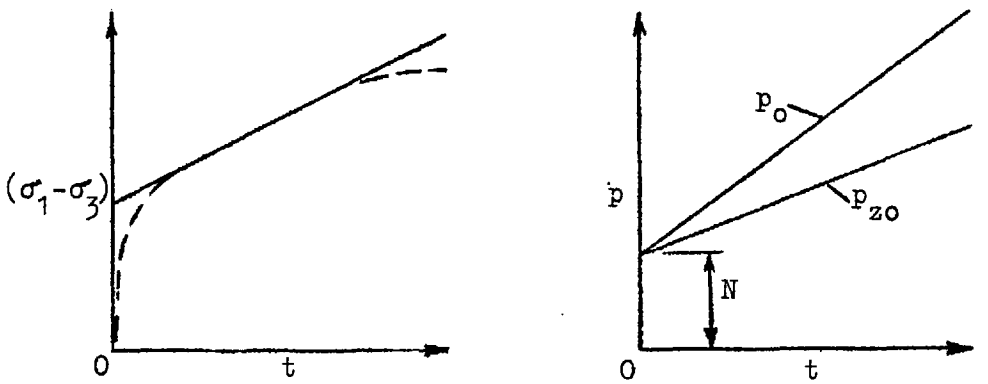
This can be written by E(8.6):

$$\frac{k}{\gamma_w}\frac{\partial^2 p_z}{\partial z^2} - C_c\left[\frac{\partial p_z}{\partial t} - \frac{(A_z - A_c)}{\alpha_o}\frac{\partial p_{zo}}{\partial t}\right] = 0$$

or:
$$c_t\frac{\partial^2 p_z}{\partial z^2} = \frac{\partial p_z}{\partial t} - \beta\frac{\partial p_{zo}}{\partial t} \qquad E(8.8)$$

where
$$\beta = \frac{A_z - A_c}{\alpha_o} \quad \text{and} \quad c_t = \frac{k}{\gamma_w C_c}$$

In order to proceed with equation E(8.8) it is necessary to assume the form of a function describing p_{zo}. p_{zo} will obviously be a function of z and it has been assumed by E(8.5) that p_{zo} is a linear function of the deviator stress. If a linear stress-strain curve is assumed as shown in the diagram,



then p_{zo} will be a linear function of time.

The simplest function of z which will reasonably approximate to the observed pore pressure profiles described in section (8.3)a is the parabola.

It is assumed therefore that p_{zo} can be described by:

$$p_{zo} = Mz^2(t + N) \quad \text{(where M \& N are constants)} \qquad E(8.9)$$

Referring to diagram b on page 125:

For a given value of $t > 0$

when $z = H, \quad p_{zo} = p_o$

i.e. $p_o = MH^2(t + N)$

But p_o must also be a linear function of time, say, $p_o = E(t + N)$

hence $MH^2(t + N) = E(t + N)$

or $M = \frac{E}{H^2}$

i.e. $p_{zo} = E.\frac{z^2}{H^2}(t + N)$

and $\frac{\partial p_{zo}}{\partial t} = E.\frac{z^2}{H^2}$

E(8.8) therefore becomes:

$$c_t \frac{\partial^2 p_z}{\partial z^2} = \frac{\partial p_z}{\partial t} - \beta' \frac{z^2}{H^2} \qquad \text{E(8.10)}$$

where $\beta' = E\beta$

The general solution to the equation

$$c_t \frac{\partial^2 p_z}{\partial z^2} = \frac{\partial p_z}{\partial t} - \beta \frac{\partial p_{zo}}{\partial t} \qquad \text{E(8.8)}$$

in which $p_{zo} = f_1(t) \cdot f_2(z)$

has been obtained by Dr. R.E. Gibson and is given here for the sake of completeness:

$$p = u_E - u_c = \frac{4}{h} \sum_{n=0}^{\infty} (-1)^n \left[\int_0^h f_2(\xi) \sin(2n + 1)\frac{\pi}{h}(\xi - \frac{h}{2}) \cdot d\xi \right] \cdot \left[\int_0^t f_1(\tau) \cdot \epsilon^{\frac{-\pi^2 c_t (2n + 1)^2 (t - \tau)}{h^2}} \cdot d\tau \right]$$

The solution to equation E(8.10) has also been obtained by Dr. R.E. Gibson and is:

$$\Upsilon = 1 - \frac{p}{p_o} = 1 - \frac{8}{\pi^4 T_v} \sum_{n=0}^{\infty} \frac{1}{(1+2n)^4} \left[1 - \epsilon^{-\pi^2(1+2n)^2 T_v}\right] \qquad E(8.11)$$

where $T_v = \frac{c_t t}{H^2}$

Corresponding values of time factor and degree of equalisation are given in the table below.

T_v	Υ	T_v	Υ	T_v	Υ	T_v	Υ
.001	.099	.04	.302	.4	.796	4	.979
.004	.120	.1	.474	.7	.881	10	.992
.01	.165	.2	.642	1	.917		

(8.5) Experimental confirmation of the theory.

Before describing the experimental results it is as well to review the limitations of the theory.

(a) If applied to the behaviour of partly saturated soils, deviations from ideal behaviour must be expected. The theory assumes an incompressible pore fluid (water) whereas the pore fluid in a partly saturated soil consists partly of an incompressible phase (water) and partly of a compressible phase (air).

(b) In normally consolidated soils, especially, consolidation behaviour is far from reversible. Even in compacted and heavily over-consolidated soils the coefficients of consolidation and swelling will be significantly different.

(c) Although greater non-uniformities have been observed

parallel to the axis of loading, significant radial non-uniformities have also been noted. The assumption of a one-dimensional moisture transfer is therefore not strictly correct.

(d) The shape of the pore pressure profile set up in an "instantaneous" test is unknown. It is only possible to infer that it lies somewhere between parabolic and linear in shape.

(a) Experimental procedure in rate of strain tests.

The procedure used in the rate of strain tests with pore pressure measurement at the base and at a single central probe was very similar to that used in tests with base measurement only (described in Chapter 7, section (7.6)). Air leads were usually not used. After connecting the ceramic probe to its null indicator using a small-bore nylon tube, the probe and base pore pressure measuring systems were de-aired by the technique described in Chapter 3 (section (3.3)).

The method of setting in the probe was as follows:

Using an ordinary twist drill, a hole was drilled in the side of the sample just large enough to accommodate the enlarged metal end of the probe. Choosing a drill slightly smaller than the diameter of the ceramic probe, the hole was deepened until it was a little shorter than the length of the probe. This ensured that when the probe was forced into its under-size hole by the cell pressure a good contact was made with the soil.

The membrane was next rolled up from the ends towards the middle with the rolled portions towards the outside. A hole was cut

in the centre of the length of the membrane to receive the probe. The two rolled portions were placed over two short split rings ($4\frac{1}{2}$" in diameter) and the probe, de-aired and joined to its null indicator, was connected through the membrane between the split rings. With the soil sample standing next to the triaxial base, the two split rings were placed over the sample and the probe was inserted into its hole. The split rings were now removed and the membrane was rolled down to cover the sample. The bottom O-rings were placed around the sample which was placed on the triaxial base. With the membrane overlapping the base, the O-rings were rolled down to seal the membrane to the base. The top O-rings were fitted in the usual way.

When two probes were used, the procedure was the same except that the second probe was connected through the membrane near the top of the sample before sealing the membrane to the top cap.

With the $1\frac{1}{2}$" diameter samples the procedure used was exactly the same except that the bottom O-rings were placed over a split ring at the bottom of the triaxial pedestal. When the membrane had been rolled down, and its end tucked under the split ring, the O-rings were rolled up onto it.

(b) Experimental results.

To test the theory three series of tests were carried out on the following soils:

(i) Mangla shale compacted at w = 18.5%.

(ii) Mangla shale compacted at w = 16%.

(iii) Selset clay compacted at w = 11.3%.

A number of tests were run at rates of strain varying from

the most rapid at which satisfactory pore pressure readings could be obtained to the lowest rate given by the testing machine gear box. This gave a ratio of fastest to slowest rates of 125.

In all tests pore water pressures were measured simultaneously at the base of the sample and at a probe situated at mid-height.

In tests on compacted soils cell pressures were chosen to give degrees of saturation of about 97% at the start of the test. The samples usually became saturated on shearing. This procedure avoided the difficulties of suction measurement and gave more rapid response at the probes.

Early on in the testing programme it was noticed that at a particular rate of strain, the pore pressure difference increases to a maximum and then remains almost constant as long as the deviator stress is increasing (see figs. (8.1) and (8.3)). Because of this it was decided to save time by running each test at two or three different rates. The tests were started at their most rapid rate. Once the maximum pore pressure difference had been developed, the rate of strain was stepped down to its next value. Readings were continued until the pore pressures had settled down to a steady difference once more. This process could also be used in reverse with increasing rates of strain provided the deviator stress was still increasing fairly rapidly.

The observed values of $p = u_E - u_c$ are plotted in figs.(8.17) and (8.18) against the time taken to reach 10% axial strain. In tests run at several different rates of strain, values of p for the first stage have been taken at 10% strain and are shown in figs. (8.17) and (8.18) by symbols in open outline. For subsequent stages

at different rates of strain, it has been assumed that the measured value of p would have occurred at 10% strain had the test been run at the same rate throughout. These values are shown in figs. (8.17) and (8.18) by shaded symbols. An important characteristic of these curves is the very rapid rise in the value of p as the rate of testing is increased.

The pore pressure-strain curves from which figs. (8.17) and (8.18) were constructed are included in Appendix 8A.

In order to calculate time factors an accurate measurement of the coefficient of consolidation c_t was required. 4" diameter x 4" high samples of each soil were compacted at the same moisture content as the samples used in the rate of strain tests. Each sample was set up on a fine ceramic base and compressed at constant water content until it became saturated. Drainage to a free water surface was then allowed from the top cap drainage lead while the dissipation of the pore pressures was followed at the base. From the resulting curve the coefficient of consolidation was calculated by the classical theory for saturated soils. The experimental dissipation curves are shown in Appendix 8A.

(c) Fitting experiment to theory.

Two difficulties arise in attempting to fit the experimental results to the theory:

(i) The choice of the time to be used in calculating the time factor.

(ii) The estimation of a value for p_o - a maximum pore pressure difference which would be obtained if no equalisation took place.

In the tests on compacted soils the maximum value of the pore pressure difference was usually reached at about 10% strain while the maximum value of $\frac{(\sigma_1 - \sigma_3)}{(\sigma_3 - u_w)}$ was reached between 10% and 15% strain. ▲ maximum value of the deviator stress was generally not reached until much later. (>20% strain). For the sake of uniformity of approach it was decided to adopt 10% strain as the general basis for the time factor in the tests on compacted Mangla shale and Selset clay. In tests run at several different rates of strain, the first stage was generally run at a constant rate and the time factor has been based on the strain at the end of the first stage (about 10%). Time factors for subsequent stages have been calculated assuming that the measured pore pressure difference occurred at 10% strain. Points for the first stage of any test are shown by symbols in open outline, while subsequent stages are shown by shaded symbols.

In order to estimate a value of p_o, the theoretical percentage equalisation at each value of the time factor was plotted against the observed pore pressure difference. If the experimental values are to agree with the theory, these points should lie on a straight line passing through the point ($p = 0$, $T = 100\%$). This line was next drawn through the experimental points and extrapolated. Its intercept with the $T = 0$ line was taken as the value of p_o. Using this value of p_o values of $T = 1 - p/p_o$ were calculated for each value of p.

The fitting diagrams are shown in figs. (8.19) and (8.20) while the experimental degree of equalisation-time factor points are compared with the theory in figs (8.21) and (8.22).

The agreement of experiment with theory is considered to be satisfactory. What deviations there are, are not much larger than the deviation of experiment from theory observed in the dissipation tests used to measure the coefficient of consolidation. (See fig. (8.23)).

Alpan (1959) carried out a series of tests on compacted Talybont clay which he sheared at different rates of strain with base measurement of pore water pressures. The effect of strain rate was then assessed in terms of the resultant variation in cohesion intercept with an assumed variation in ϕ'.

These results have been re-analysed as follows:

The strength envelope corresponding to the slow saturated tests on Talybont clay (vide Chapter 6) was chosen as datum and the pore pressure required to fit the deviator stress of the more rapid tests to this envelope was determined. This was compared with the pore pressure actually measured at the base to give a first estimate of the pore pressure difference at failure. (The theoretical degree of equalisation of the reference test was 95% and hence the pore pressure difference for the reference test also had to be estimated). These results are shown in fig. (8.24). Next a fitting curve was prepared (fig. (8.25)) plotting the reference test at its theoretical degree of equalisation and zero pore pressure difference. The time used in the calculation of time factors was that to reach $7\frac{1}{2}\%$ strain. This was the average strain at maximum $(\sigma_1 - \sigma_3)$. The fitting line was extrapolated to $\Upsilon = 100\%$ to estimate the pore pressure difference in the reference test. From this a corrected estimate was made of p_o and the values of p. The plot of Υ versus T_v for this set of

data is shown in fig. (8.26). There is once more general agreement between theory and experiment.

Finally, Taylor's tests on Boston clay have been re-investigated. The Boston clay was unlike the other soils so far investigated in that the maximum value of $(\sigma_1' - \sigma_3')$ occurred first at about 2% to 3% strain, followed by the maximum value of the pore pressure difference at about 4% strain and finally the maximum value of $\frac{(\sigma_1' - \sigma_3')}{\sigma_3'}$ at about 6% strain. As $(\sigma_1' - \sigma_3')$ was no longer increasing after 3% strain, times were calculated on a basis of the strain at maximum $(\sigma_1' - \sigma_3')$.

The writer's tests have all been on samples of the same initial height. Taylor's tests, however, incorporated tests on samples of different initial height which were tested at the same rate of strain.

The fitting diagram is shown in fig. (8.25) and the variation of T with T_v is shown in fig. (8.27) together with the results of the tests on $1\frac{1}{2}$" diameter samples of remoulded Mangla shale. Once again there is satisfactory agreement between theory and experiment.

(8.6) Estimation of the "instantaneous" pore pressure difference p_o from elastic stress theory.

The theory described in section (8.3) gives an estimate of the testing time required to give a desired degree of pore pressure equalisation. It does not give any idea of the magnitude of the pore pressure difference represented by the degree of equalisation. For instance 90% equalisation in a soil for which p_o = 6 p.s.i. represents a pore pressure difference of 0.6 p.s.i. which is a small error. The same degree of equalisation in a soil for which p_o = 60 p.s.i.

represents a pore pressure difference of 6 p.s.i. which may be considerable. The theory also gives no indication of the sign of the unequalised pore pressure difference $p = u_E - u_c$. Positive values of p give an overestimate of the cohesion intercept while negative values cause underestimation.

The magnitude of p_o will depend on the stress distribution within the triaxial sample and also on the values of the pore pressure parameter A at the centre and ends of the sample. The sign of p_o will depend on the relative values of A at the centre and ends of the sample.

Fig. (8.28) shows some elastic stress distributions in a circular cylinder under an axial compressive load applied through perfectly rough rigid end loading plates. The diagram was prepared from data given by Filon (1902). For convenience, Filon's nomenclature has been used in what follows. If the axial compressive stress on the loading plates is Q, and:

$\frac{\overline{ZZ}}{Q}$ is the average over the circular cross-section of the cylinder of the major principal stress.

$\frac{\overline{RR}}{Q}$ is the average over the circular cross-section of the cylinder of the intermediate principal stress.

$\frac{\overline{\phi\phi}}{Q}$ is the average over the circular cross-section of the cylinder of the minor principal stress.

Let $$\frac{\bar{\sigma}^*}{Q} = \frac{1}{2}\left(\frac{\overline{RR}}{Q} + \frac{\overline{\phi\phi}}{Q}\right) \qquad E(8.12)$$

Assume $$\frac{\Delta u}{Q} = \frac{\Delta \bar{\sigma}^*}{Q} + A\left[\frac{\Delta \overline{ZZ}}{Q} - \frac{\Delta \bar{\sigma}^*}{Q}\right]$$

$$\frac{p_o}{Q} = \frac{\Delta u_E}{Q} - \frac{\Delta u_c}{Q}$$

Let $A_E = \alpha A_c$

then $$\frac{p_o}{Q} = \left(\frac{\Delta\bar{\sigma}^*}{Q}\right)_E - \left(\frac{\Delta\sigma^*}{Q}\right)_c + A\left[\left(\frac{\Delta\overline{zz}}{Q}\right)_E - \left(\frac{\Delta\bar{\sigma}^*}{Q}\right)_E - \frac{1}{\alpha}\left[\left(\frac{\Delta\overline{zz}}{Q}\right)_c - \left(\frac{\Delta\bar{\sigma}^*}{Q}\right)_c\right]\right] \quad E(8.13)$$

Inserting numerical values for the stresses:

$$\frac{p_o}{Q} = 0.356 + A_E\left[0.921 - \frac{1.022}{\alpha}\right] \quad E(8.14)$$

This last equation has been plotted for all likely practical values of A_E and α in fig. (8.29).

From this diagram and an estimate of the values of A_E and α the value of p_o/Q can be read off in sign and magnitude.

The values of p_o/Q for the various test series analysed in section (8.4) have been estimated from the above theory. Using the most rapid test in each series, values of A_{end} and A_{centre} were estimated for the 'instantaneous' test as follows:

Let δu_{end} and δu_{centre} be the changes in pore pressure in the most rapid test and Δu_{end} and Δu_{centre} be those in the 'instantaneous' test.

If Δu_E exceeds Δu_c (i.e. p_o is positive), equalisation of pore pressure will cause Δu_E to diminish to δu_E while Δu_c increases to δu_c (and vice versa if p_o is negative).

The relative amounts by which Δu_E and Δu_c change are not known but since equalisation will change p_o to p, the sum of the changes in Δu_E and Δu_c will be $p_o - p$.

Hence: $$(\Delta u_E - \delta u_E) - (\Delta u_c - \delta u_c) = (p_o - p)$$

(- because changes at c and E are in opposite directions).

Two assumptions have been made in this case:

(i) That the change in Δu_E is numerically twice the change

in Δu_c.

(ii) That the changes in Δu_E and Δu_c are numerically equal.

Hence either: or:

$$\Delta u_E = \delta u_E \mp \frac{2(p_o - p)}{3} \qquad \Delta u_E = \delta u_E \mp \frac{(p_o - p)}{2}$$

$$\Delta u_c = \delta u_c \mp \frac{(p_o - p)}{3} \qquad \Delta u_c = \delta u_c \mp \frac{(p_o - p)}{2}$$

$\mp$ depending on the sign of p.

and

$$A_E = \frac{\Delta u_E}{\Delta(\sigma_1 - \sigma_3)} = \frac{\Delta u_E}{Q}$$

$$A_c = \frac{\Delta u_c}{\Delta(\sigma_1 - \sigma_3)} = \frac{\Delta u_c}{Q}$$

$$\alpha = \frac{A_E}{A_c}$$

Values of p_o/Q estimated by the two methods are compared in fig. (8.30).

There is an element of circularity in this comparison since the values of A_E and α used to estimate p_o by the elastic theory depend on the value of p_o estimated from consolidation theory. Nevertheless, the final stage is completely independent and estimates the sign of the pore pressure difference correctly.

(8.7) The effectiveness of paper drains.

Circumferential and end drains made of filter paper strips are commonly used to hasten consolidation and equalisation of pore pressures in saturated samples. Paper drains were used in all the consolidated undrained tests on $1\frac{1}{2}$" diameter samples described in Chapter 6.

These drains are of limited use for partly saturated samples since the air entry value of the most finely pored glass fibre filter paper is less than 1 p.s.i. Cellulose fibre papers such as Whatman's No. 54 have air entry values of about 0.6 p.s.i.

The permeability of filter papers is lower than is generally realised and decreases with the effective stress in the paper. This is shown by fig. (8.31). Whatman's No. 54 paper has a permeability of only 0.8 x 10^{-5} cm/sec. under an effective stress of 60 p.s.i.

It is sometimes assumed that paper drains give completely effective radial drainage. This has been questioned by Rowe (1959). That the drains are not fully effective is shown by fig. (8.31)b which compares values of c_t measured on 4" diameter x 4" high samples with single end drainage with values measured on $1\frac{1}{2}$" diameter x 3" high samples equipped with circumferential paper drains (which have been assumed fully effective). Values of c_t measured by the latter means are only .40 to .27 of the true values.

A theoretical study done some years ago by Dr. R.E. Gibson shows that paper drains with a permeability of 1 x 10^{-5} cm/sec. can only be considered fully effective when used with soils whose permeability is 1 x 10^{-9} cm/sec. or less. However, when calculating testing times for drained tests using paper drains, (Gibson and Henkel, 1957) the low apparent value of c_t due to the ineffectiveness of the drains compensates for the low effectiveness of the drains in equalising pore pressures. Testing times based on the apparent value of c_t will be near enough to correct.

(8.8) Summary.

Non-uniform stress conditions in the normal triaxial test can give rise to non-uniform pore pressures even at rates of strain which by commercial standards are considered slow. This non-uniformity can lead to serious errors in the measurement of shear strength parameters.

Uniform pore pressures can be obtained by using a suitably slow rate of strain. A rate of strain which will give a tolerable error in pore pressure readings at the base of a sample can be estimated theoretically from a knowledge of the consolidation characteristics of the soil. Alternatively, in soils which fail by bulging at high strains, if special precautions are taken to reduce end restraint higher rates of strain can be used without increasing the pore pressure non-uniformity.

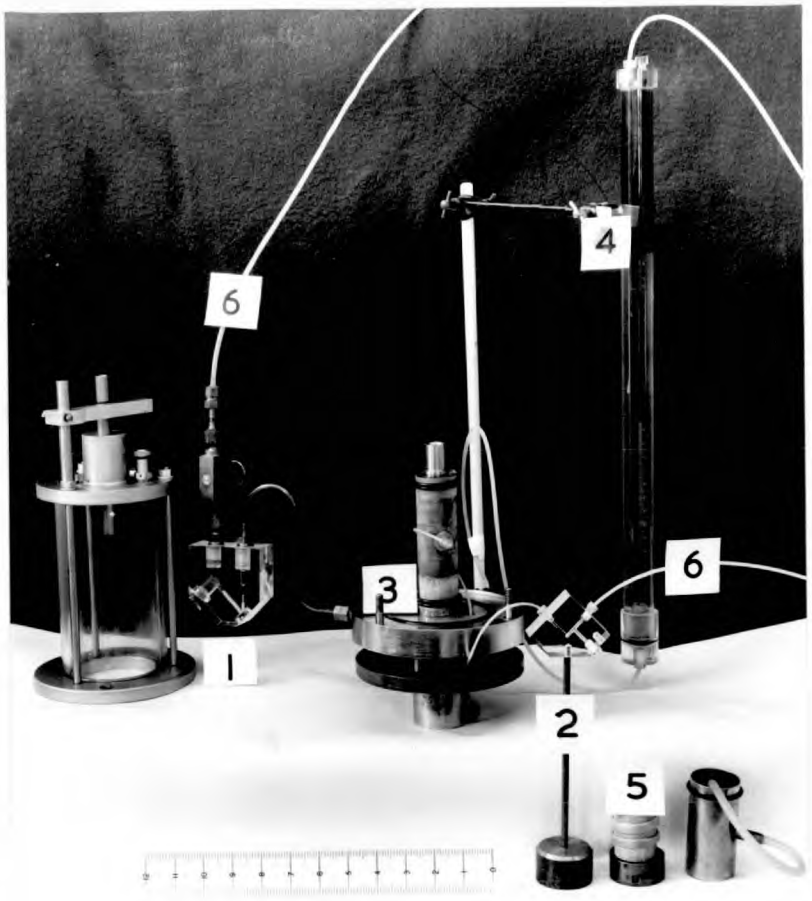


PLATE 1

Probe test on 1½" dia. x 3" high sample
(Photo by J. Gurr)

1. Null indicator, base pore pressure measurement.
2. Null indicator, mid-height pore pressure measurement.
3. Sample with probe in position.
4. Paraffin type volume gauge.
5. Membrane rolled prior to placing on sample.
6. Leads to pore pressure measuring system.

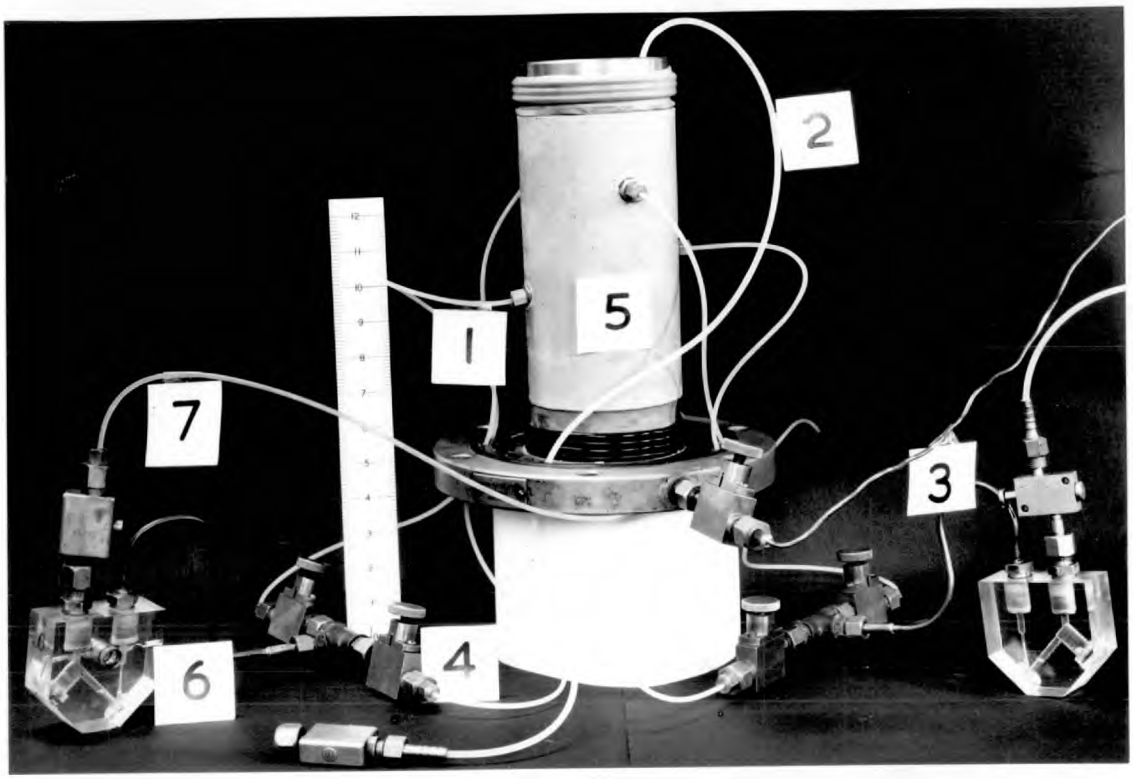


PLATE 2

Multi-probe test on 4" dia. x 8" high sample
(Photo by J. Gurr)

1. Probe and lead to null indicator.
2. Top cap drainage lead.
3. Base pore pressure measurement. Lead to null indicator.
4. Valves isolating probes from null indicator.
5. Cylindrical cardboard former.
6. Probe null indicator.
7. Lead to pore pressure measuring system.



PLATE 3

Appearance of lubricated end plates at end of test showing tracks caused by radial movement of soil
(Photo by J. Gurr)



PLATE 4

Comparison of tests using conventional
and lubricated end plates
(Photo by J. Gurr)

Left: Test using conventional end plates.
Right: Test using lubricated end plates.
Left foreground, left to right: probe for $1\frac{1}{2}$" dia. sample, connector for air lead (4" dia. sample), probe for 4" dia. sample, base porous disc for 4" dia. sample.

EFFECT OF RATE OF STRAIN ON NON-UNIFORMITY OF PORE PRESSURE IN TRIAXIAL TESTS

TEST ON 4" DIA. X 8" HIGH SAMPLE OF MANGLA SHALE COMPACTED AT W = 18·5%.

RATE OF STRAIN : 0·038 %/MIN.

FIG. 8.1.

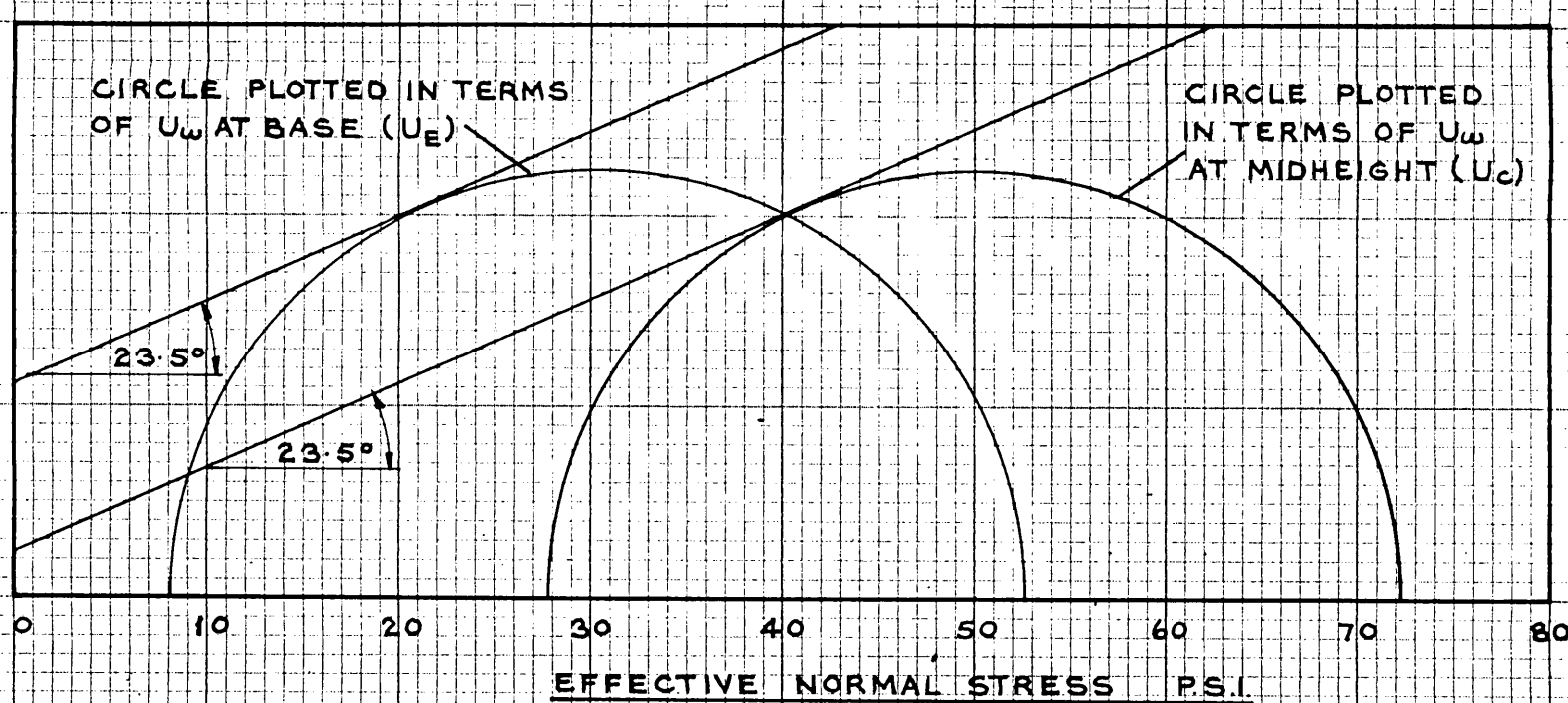
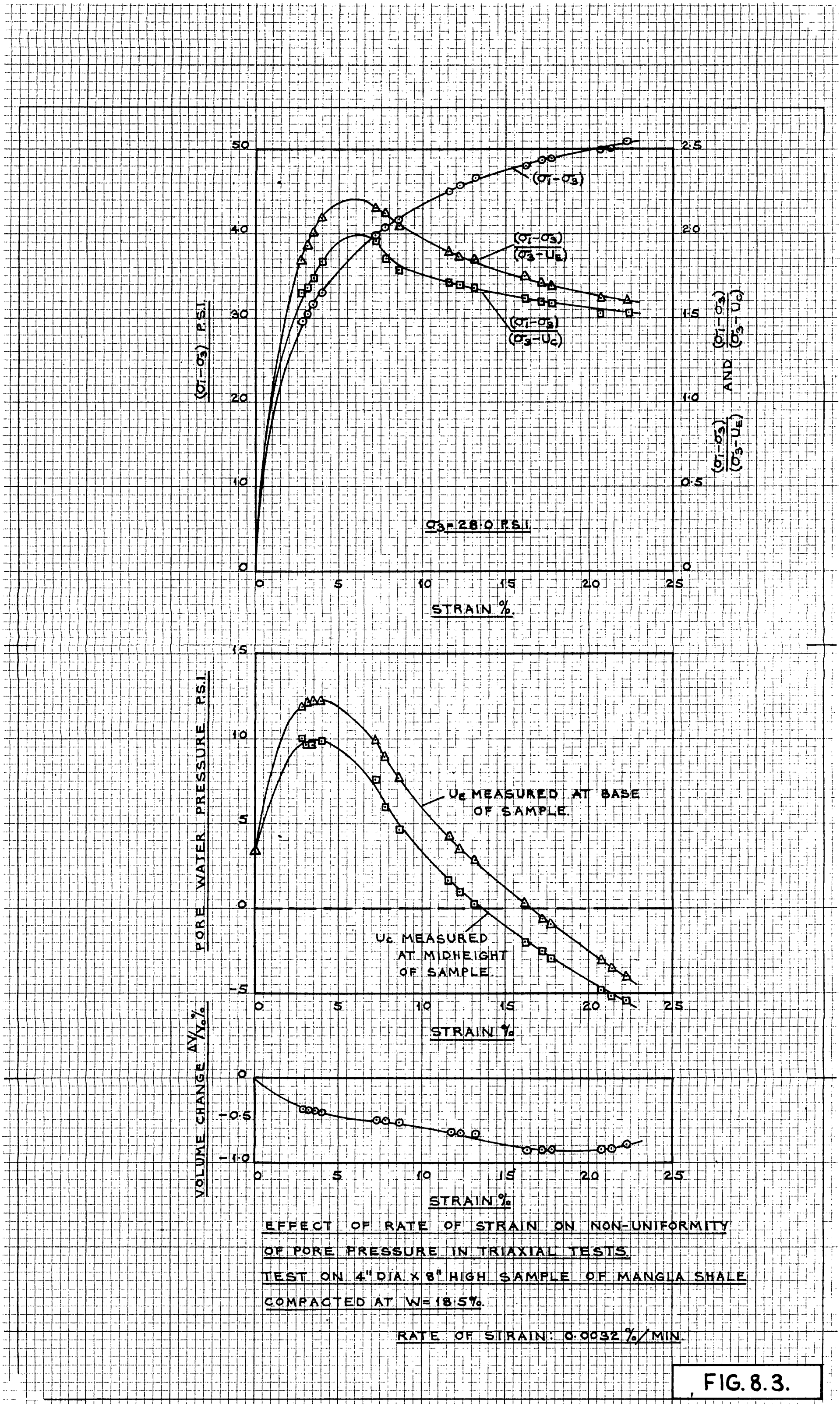


FIG. 8.2.

EFFECT OF UNEQUALIZED PORE PRESSURES ON APPARENT POSITION OF FAILURE ENVELOPE FOR COMPACTED MANGLA SHALE.

RATE OF STRAIN 0·038 %/MIN.

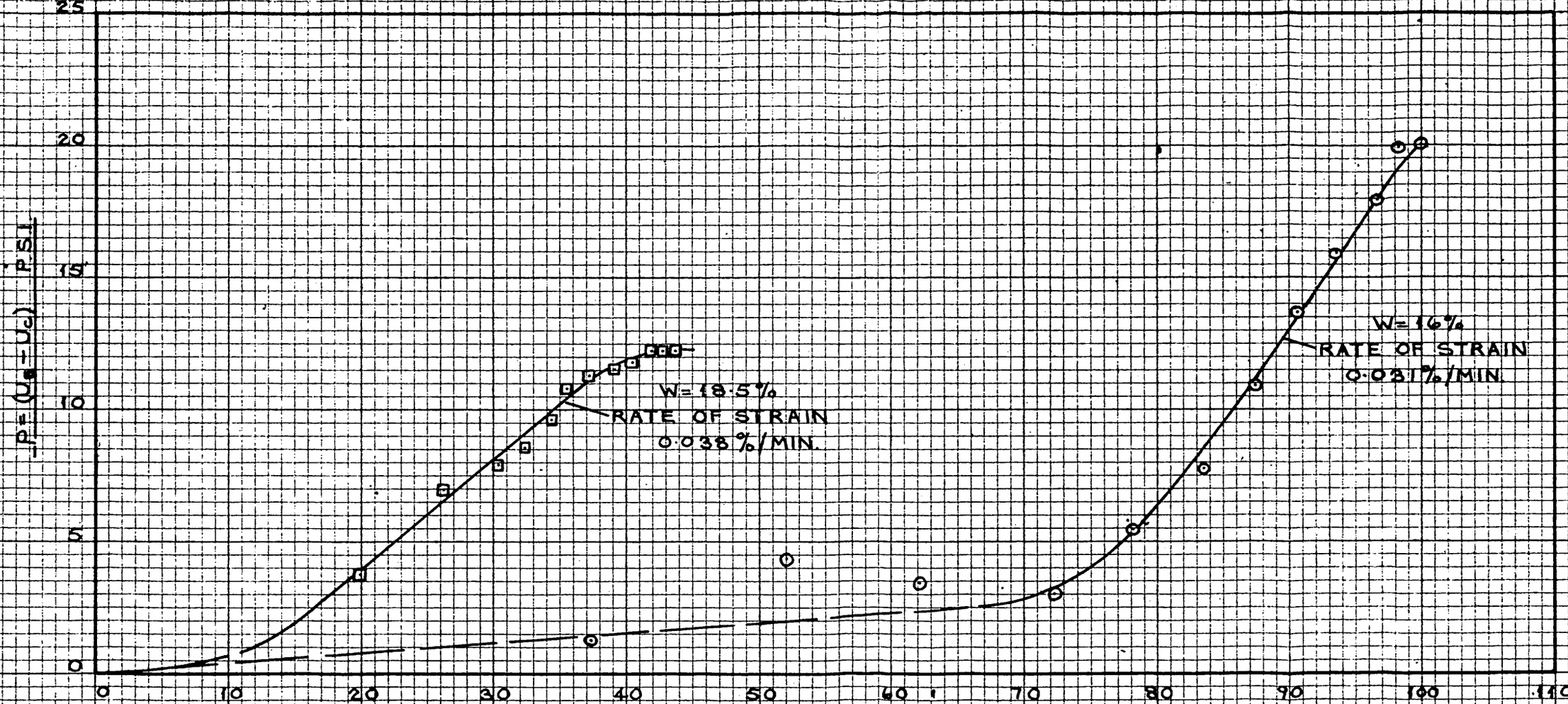


EFFECT OF RATE OF STRAIN ON NON-UNIFORMITY OF PORE PRESSURE IN TRIAXIAL TESTS.

TEST ON 4" DIA X 8" HIGH SAMPLE OF MANGLA SHALE COMPACTED AT W = 18.5%.

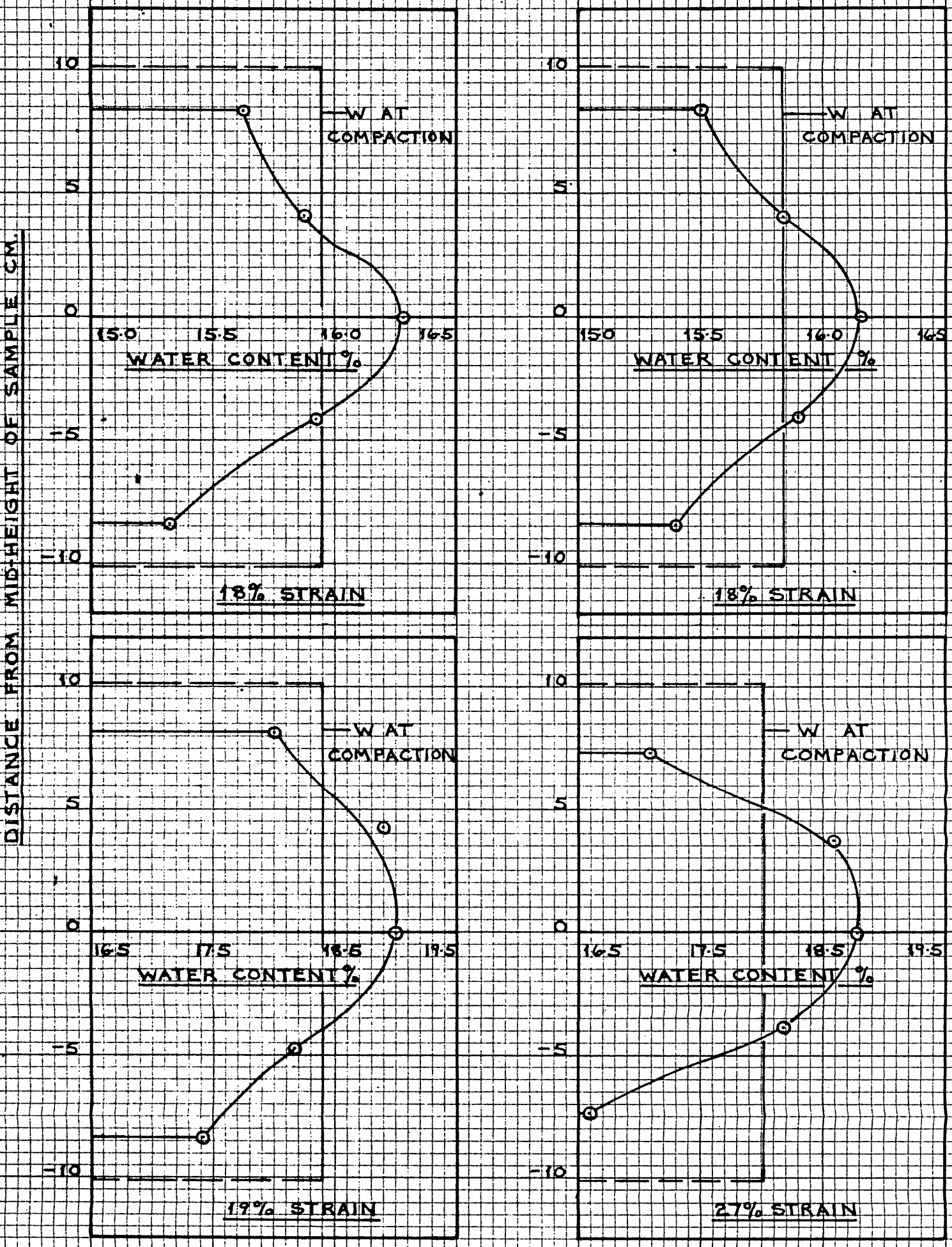
RATE OF STRAIN: 0.0032 %/MIN.

FIG. 8.3.



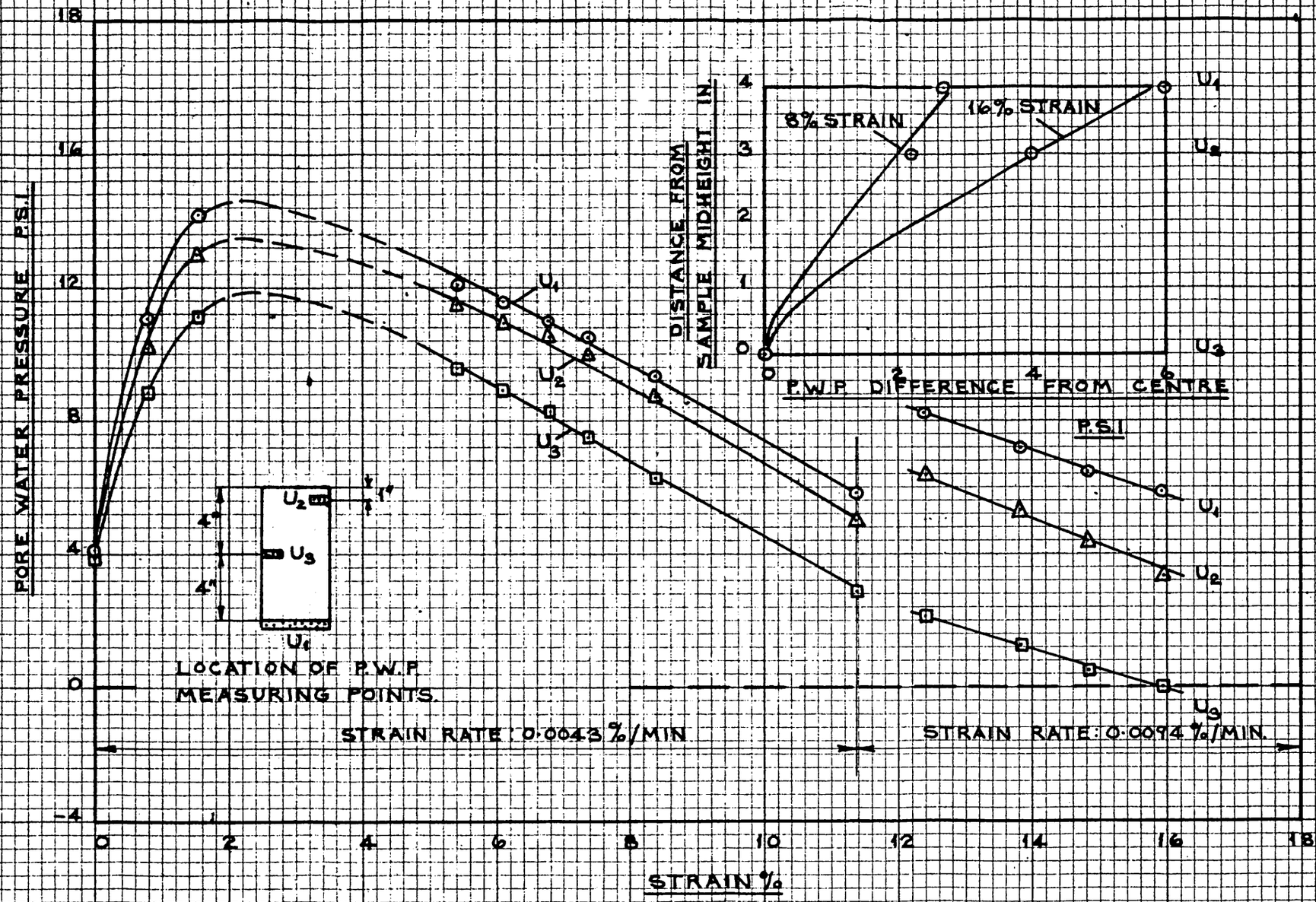
RELATION BETWEEN $p=(U_E-U_c)$ AND $(\sigma_1-\sigma_3)$ IN TWO TRIAXIAL TESTS ON COMPACTED MANGLA SHALE.

FIG. 8.4.



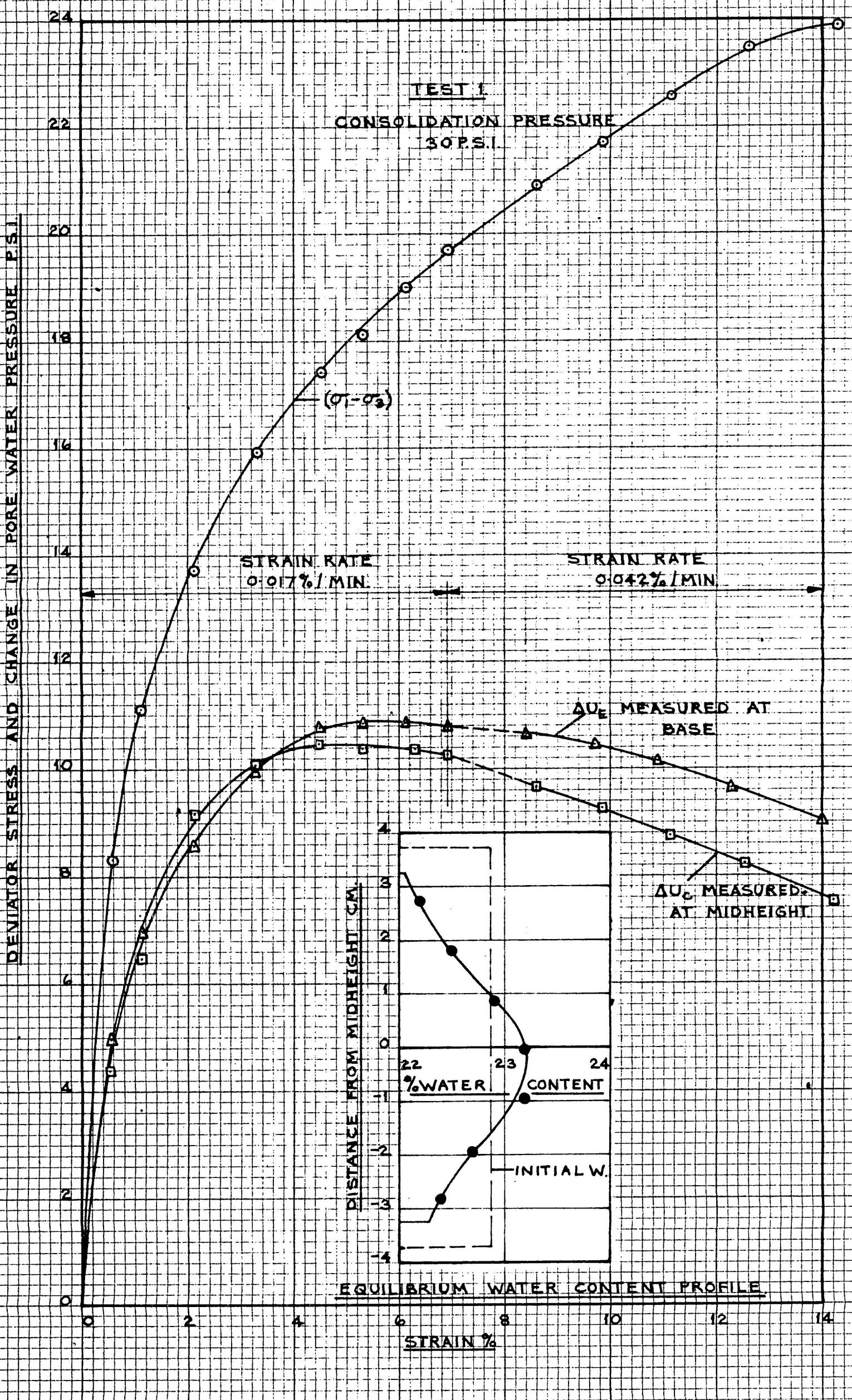
TYPICAL EQUILIBRIUM WATER CONTENT PROFILES IN SHEARED SAMPLES OF COMPACTED MANGLA SHALE

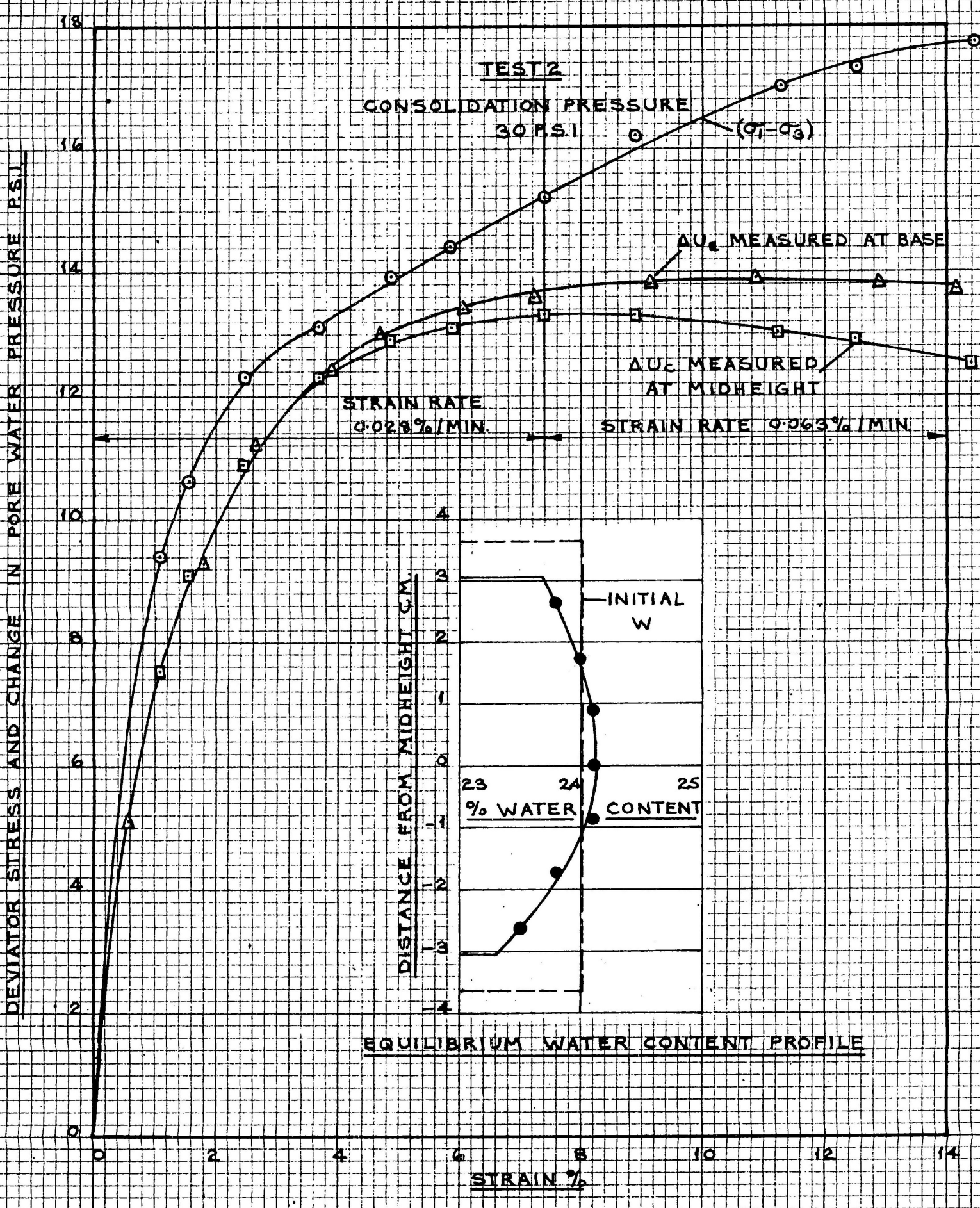
FIG. 8.5.



TRIAXIAL TEST ON 4" DIA X 8" HIGH SAMPLE OF MANGLA SHALE COMPACTED AT W=18·5% WITH PORE WATER PRESSURE MEASURED AT THREE POINTS.

FIG. 8.6.





TESTS ON MOULDED CONSOLIDATED SAMPLES (1½ DIA. X 3" HIGH) OF SATURATED MANGLA SHALE SHOWING EFFECT OF RATE OF STRAIN ON NON-UNIFORMITY OF PORE PRESSURE. (SEE FIG A8.1 FOR CONSOLIDATION HISTORY OF SAMPLES).

FIG. 8.7.

DEVIATOR STRESS AND PORE WATER PRESSURE (P.S.I.)

STRAIN RATE: 1·87%/HR.

DEVIATOR STRESS

·075% /HR. BASE

·018% /HR. PROFILE 5 (FIG 8.10)

PORE WATER PRESSURES

PROFILE 1 FIG 8.10

PROFILE 2 FIG 8.10

4

3

2

1

0

MIDHEIGHT

PORE PRESSURE AT Z/H = 0·5 (P.S.I.)

a

b

c

STRAIN %

4" DIA.

2H = 8"

Z & Z/H.

VALUES OF Z/H

0·75

0·50

0·25

1"

1"

1"

1"

Nº OF MEASURING POINT & SYMBOL

0

1

2

3

4

BASE

EQUIVALENT POSITIONS OF MEASURING POINTS.

PROFILE 4 (FIG 8.10).

PROFILE 3 (FIG 8.10)

RELOADING

UNLOADING

STRAIN %

TEST ON MOULDED CONSOLIDATED SAMPLE (4" DIA X 8" HIGH) OF SATURATED MANGLA SHALE WITH PORE WATER PRESSURES MEASURED AT FIVE POINTS. CONSOLIDATION PRESSURE 140 P.S.I.

FIG. 8.8.

PORE PRESSURE CHANGES IN SAMPLE BEFORE CONSOLIDATING.

CELL PRESSURE P.S.I.

150
125
100
75
50

1
1

25 50 75 100 125

PORE WATER PRESSURE P.S.I.

PROFILE Nº2 (FIG 8.10)

MEASUREMENT AT MIDHEIGHT

0 1 2 3 4

MEASUREMENT AT BASE

PROFILE Nº 1 (FIG 8.10)

SYMBOL Nº

⊙	0
●	1
△	2
■	3
⊡	4

LAYOUT OF MEASURING POINTS.

DEVIATOR STRESS P.S.I.

100 90 80 70 60 50 40 30 20 10 0

FIRST LOADING STAGE

0 10 20 30 40 50 60 70 80

PORE WATER PRESSURE P.S.I.

DEVIATOR STRESS P.S.I.

100 90 80 70 60 50 40 30 20 10 0

MEASUREMENT AT BASE

MEASUREMENT AT MIDHEIGHT.

PROFILE Nº 3 FIG(8.10)

4 3 2 0&1

UNLOADING STAGE.

50 60 70 80

PROFILE Nº 5 (FIG. 8.10)

0 1 2 3 4

MEASUREMENT AT MID-HEIGHT

MEASUREMENT AT BASE

PROFILE Nº 4 (FIG 8.10)

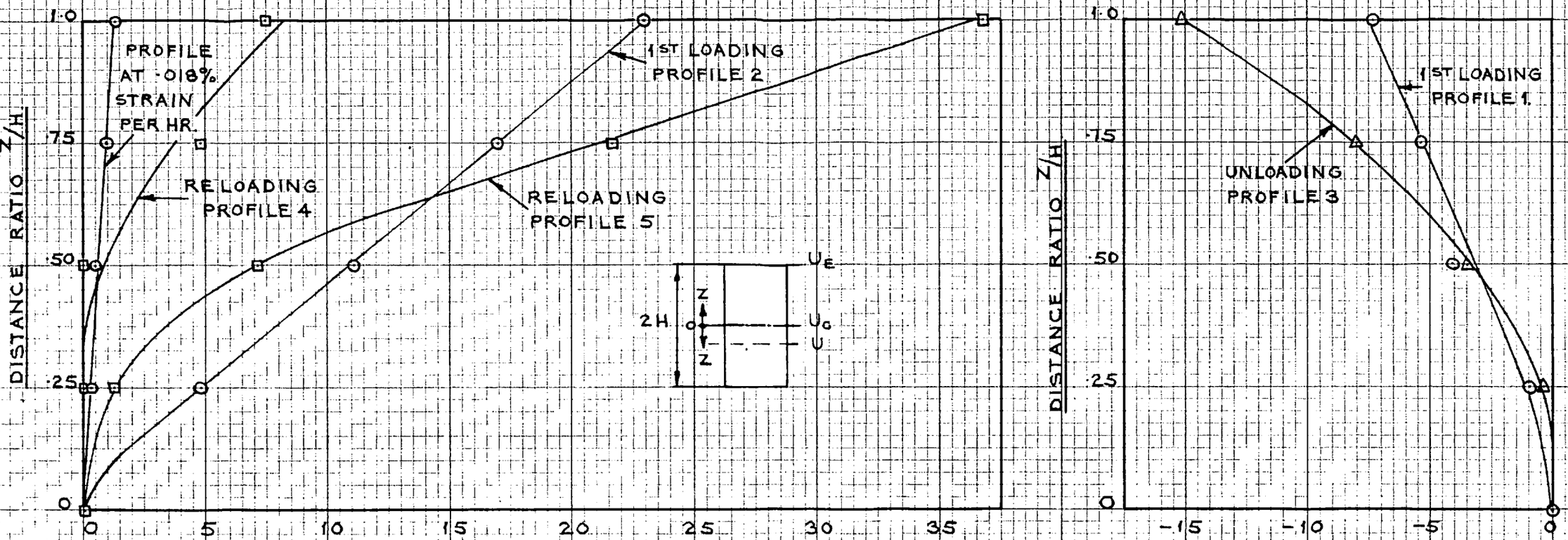
RELOADING STAGE

60 70 80 90 100

PORE WATER PRESSURE P.S.I.

TEST ON MOULDED CONSOLIDATED SAMPLE OF SATURATED MANGLA SHALE WITH MEASUREMENT OF PORE WATER PRESSURE AT FIVE POINTS. SEE ALSO FIGS. (8.8), (8.10) AND (8.11)

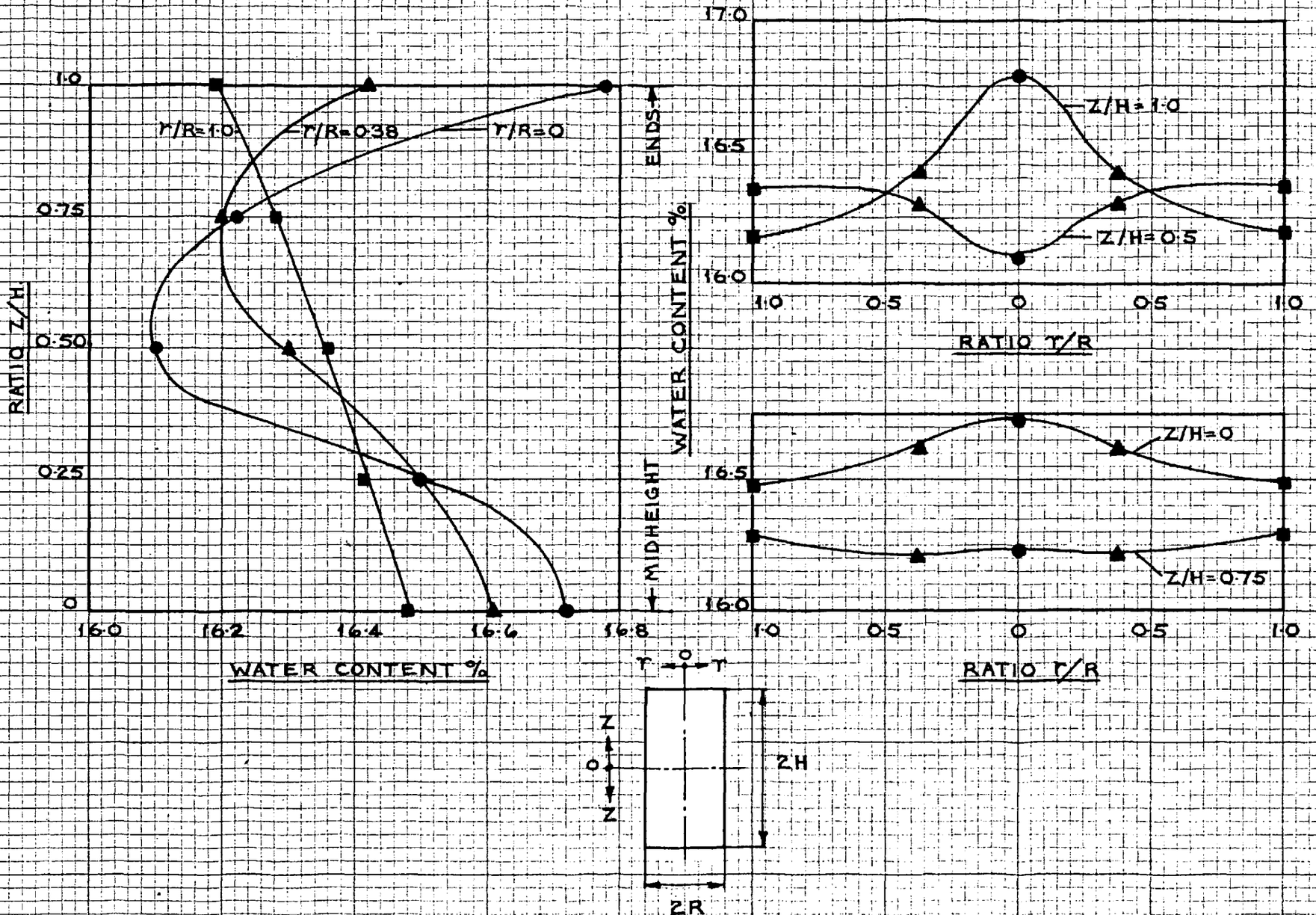
FIG. 8.9.



PROFILES OF PORE PRESSURE IN TEST ON MOULDED CONSOLIDATED SAMPLE OF SATURATED MANGLA SHALE.

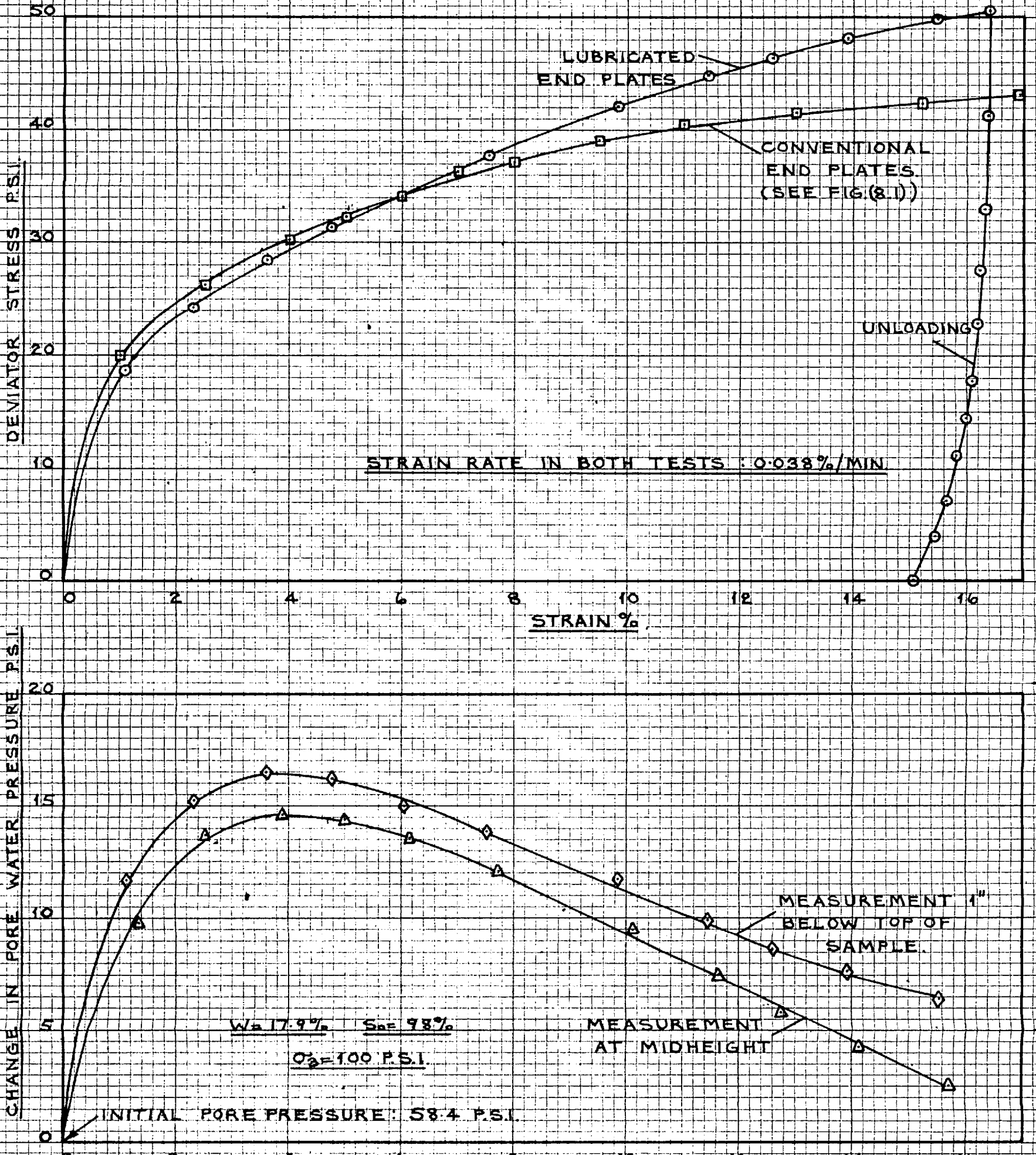
FOR LOCATION OF PROFILES SEE FIGS. 8.8 AND 8.9.

FIG. 8.10.



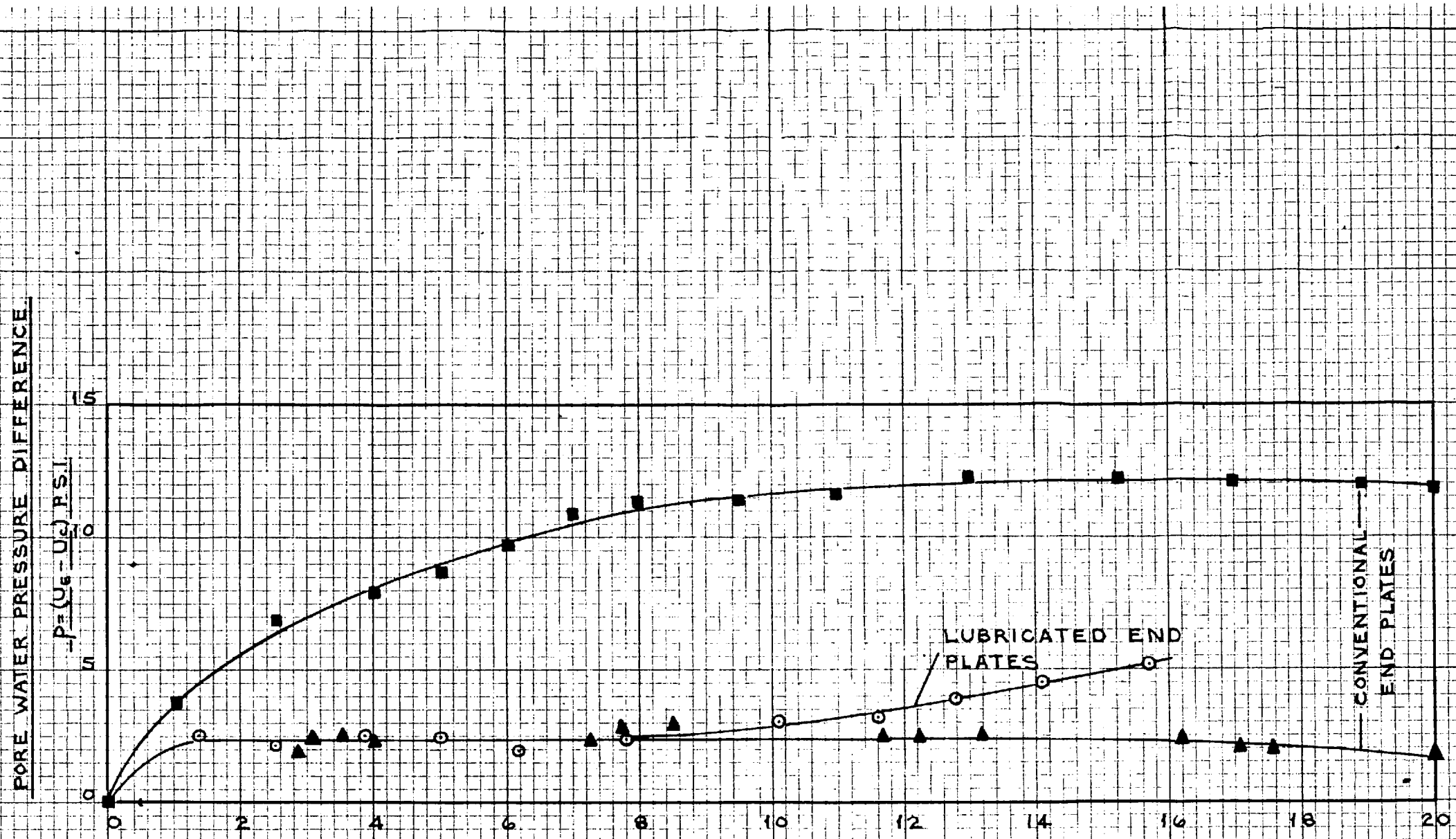
EQUILIBRIUM WATER CONTENT PROFILES IN TEST ON MOULDED CONSOLIDATED SAMPLE OF SATURATED MANGLA SHALE. SEE ALSO FIGS. 8.8, 8.9 AND 8.10.

FIG. 8.11.



TEST ON SAMPLE OF COMPACTED MANGLA SHALE COMPRESSED BETWEEN LUBRICATED END PLATES. (SEE ALSO FIGS. 8.13, 8.14)

FIG. 8.12.

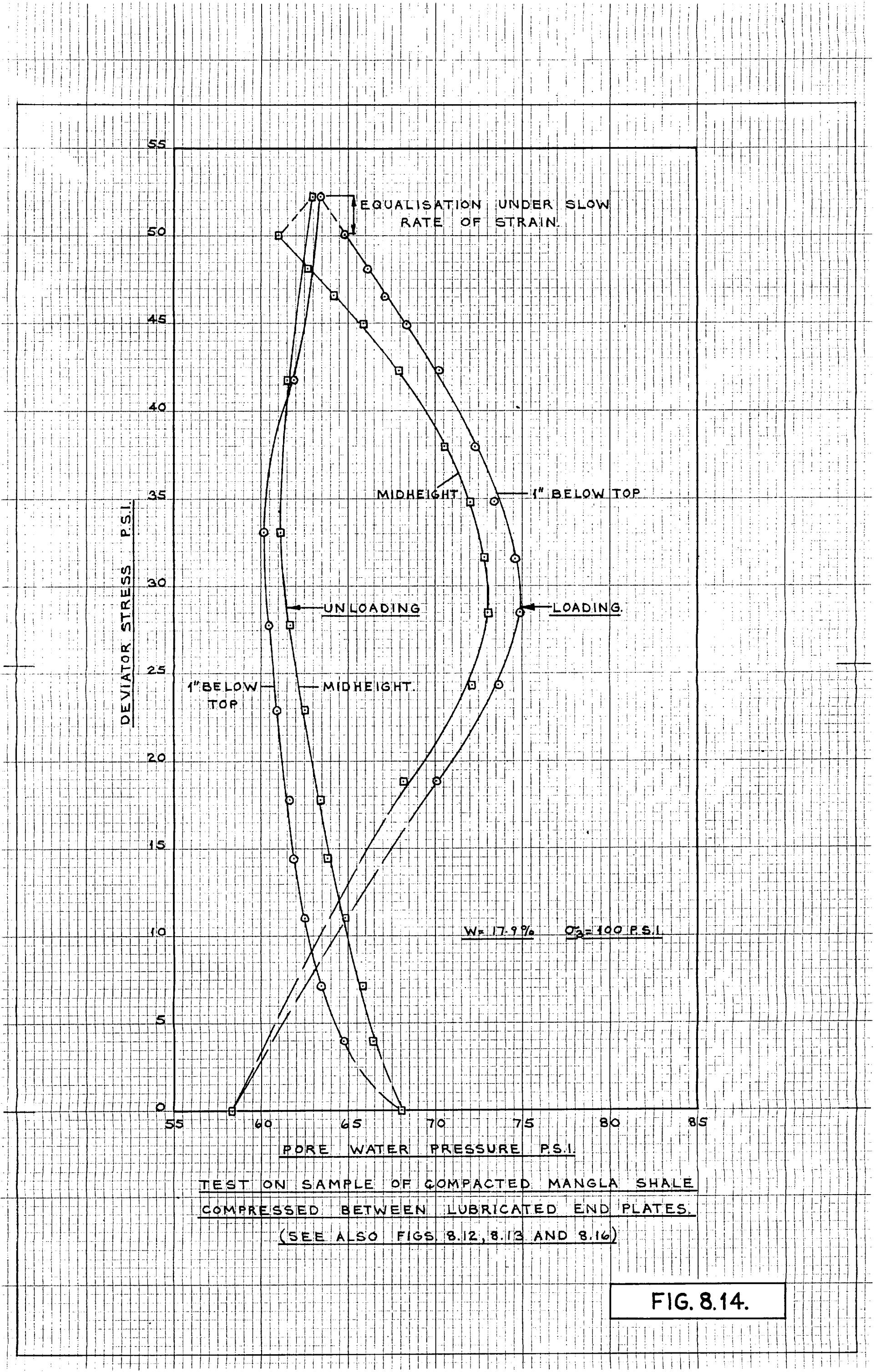


THE EFFECT OF LUBRICATED END PLATES ON NON-UNIFORMITY OF PORE WATER PRESSURE IN TESTS ON COMPACTED MANGLA SHALE

SYMBOL:
- ■ CONVENTIONAL END PLATES — STRAIN RATE: 0·038%/MIN.
- ▲ CONVENTIONAL END PLATES — 0·0031%/MIN.
- ⊙ LUBRICATED END PLATES — 0·038%/MIN.

SEE ALSO FIGS. 8.1, 8.3 AND 8.12

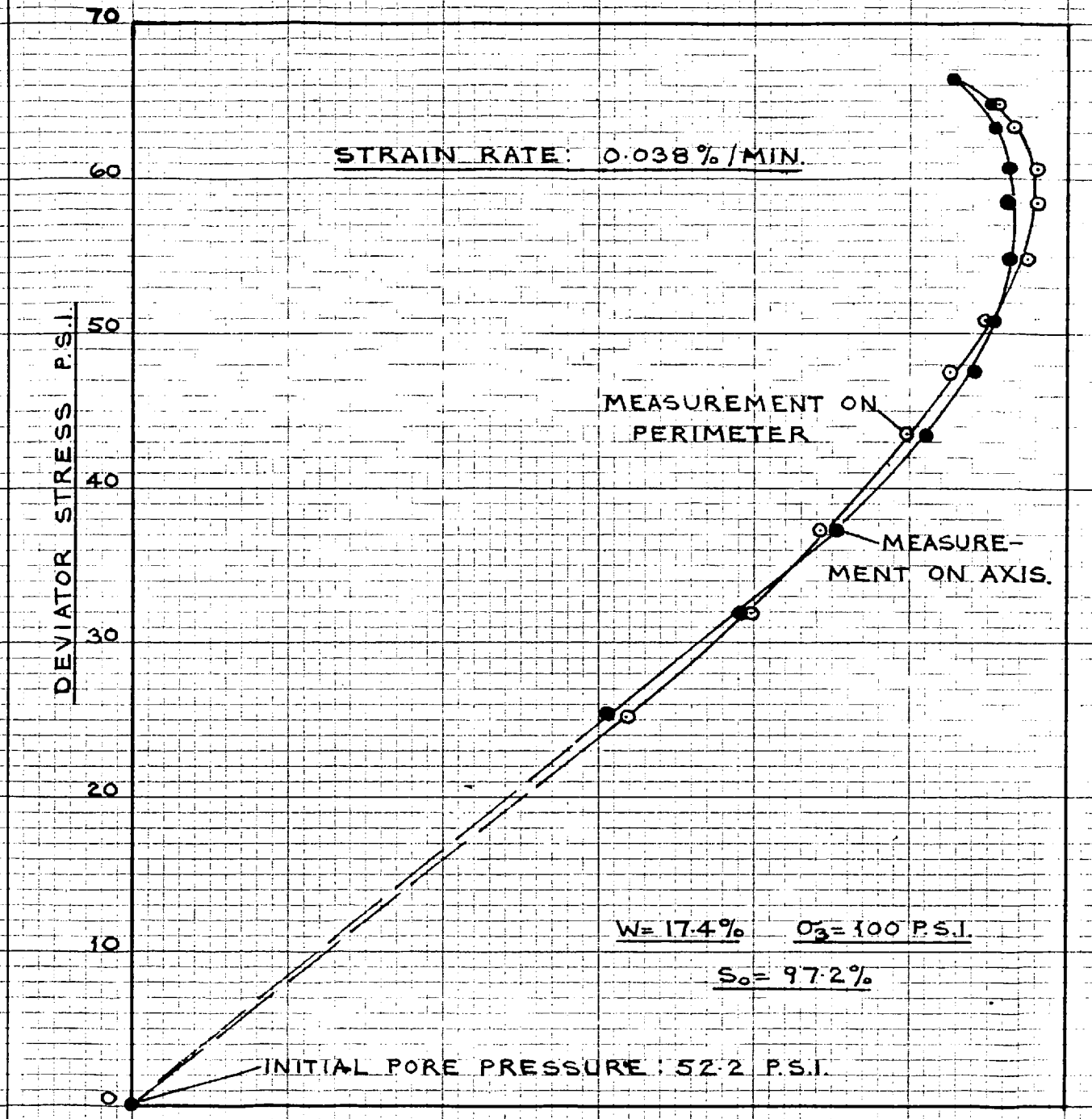
FIG. 8.13.



TEST ON SAMPLE OF COMPACTED MANGLA SHALE COMPRESSED BETWEEN LUBRICATED END PLATES.

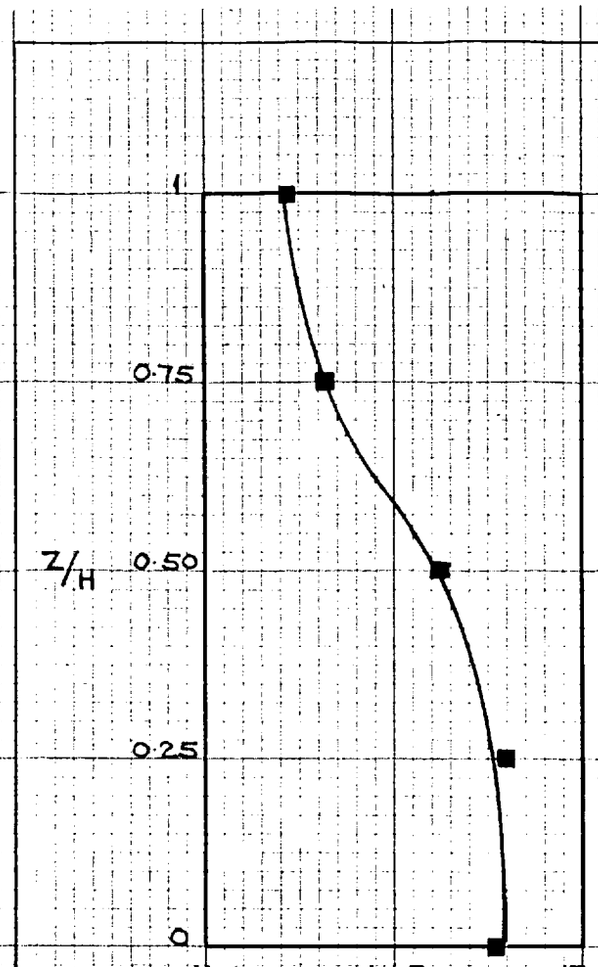
(SEE ALSO FIGS. 8.12, 8.13 AND 8.16)

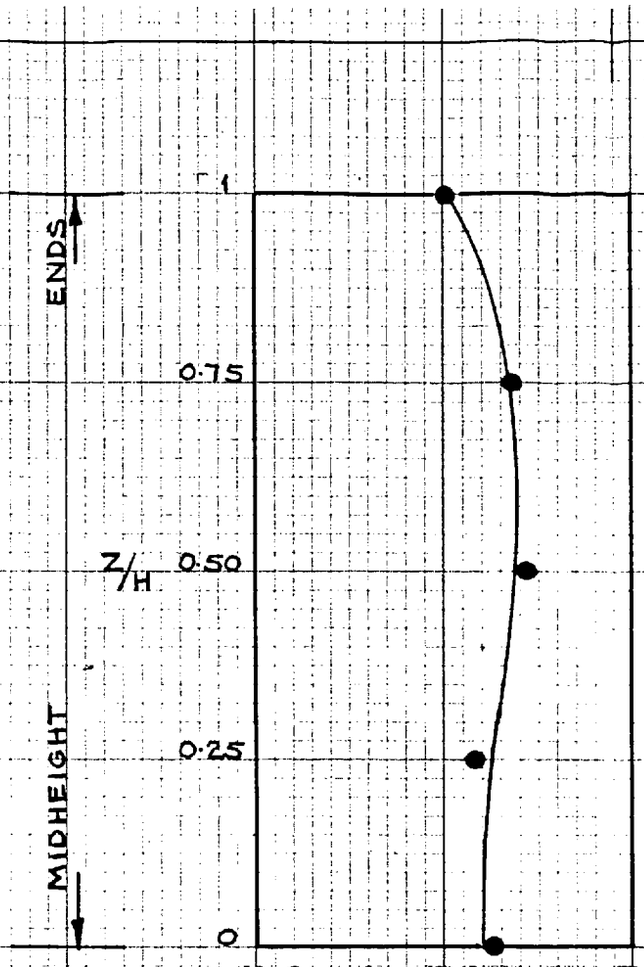
FIG. 8.14.

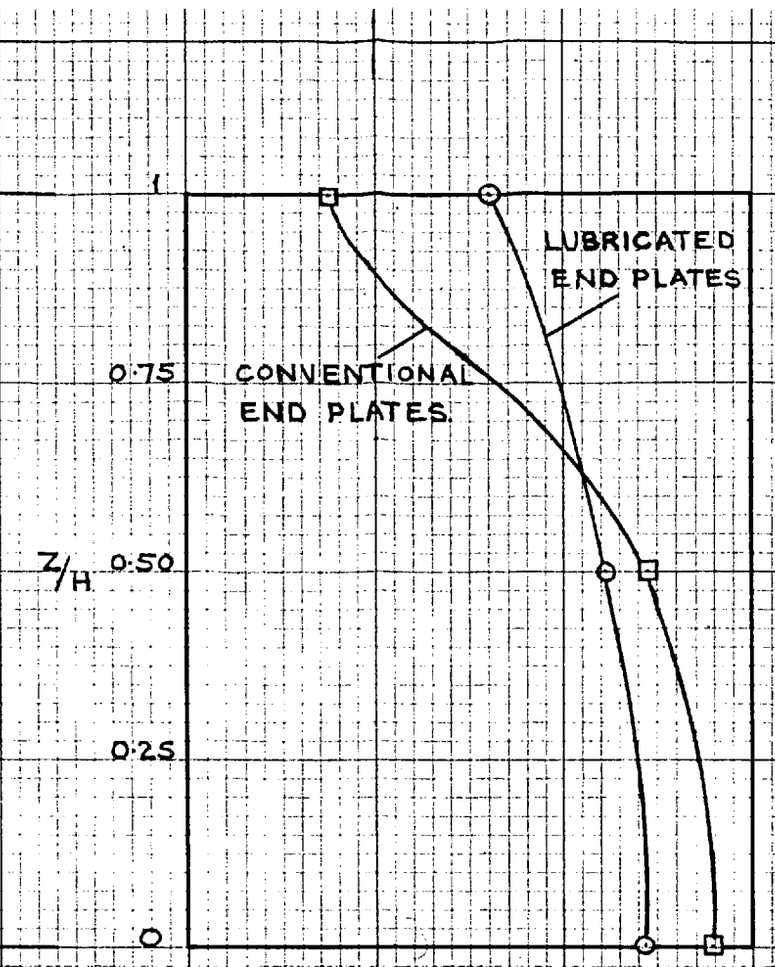


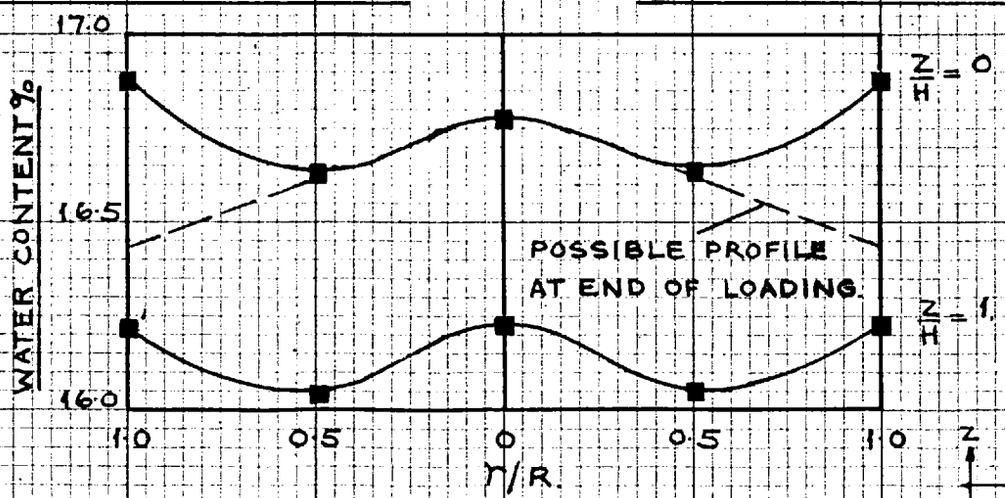
MEASUREMENT OF BASE PORE PRESSURE AT CENTRAL AXIS AND PERIMETER OF SAMPLE OF MANGLA SHALE (CONVENTIONAL END PLATES)

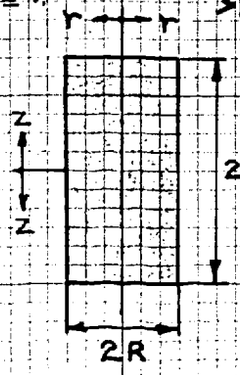
FIG. 8.15.

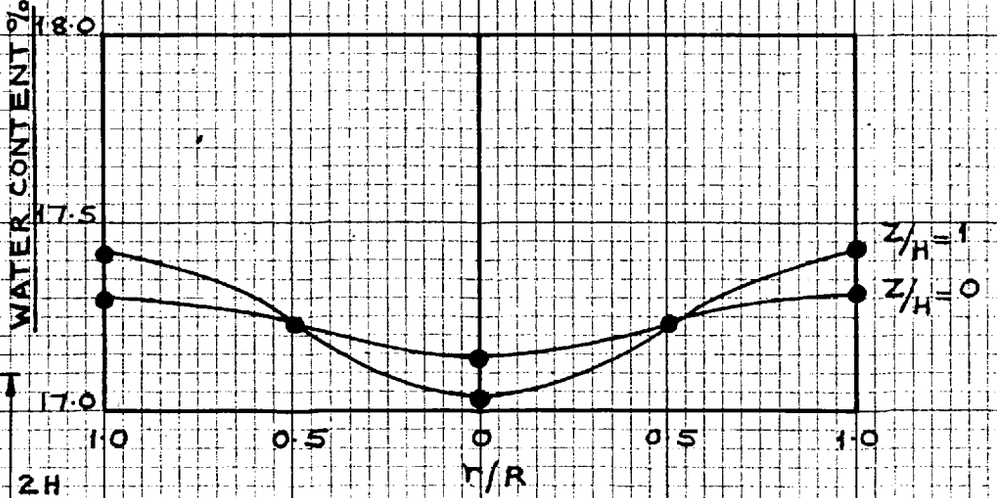






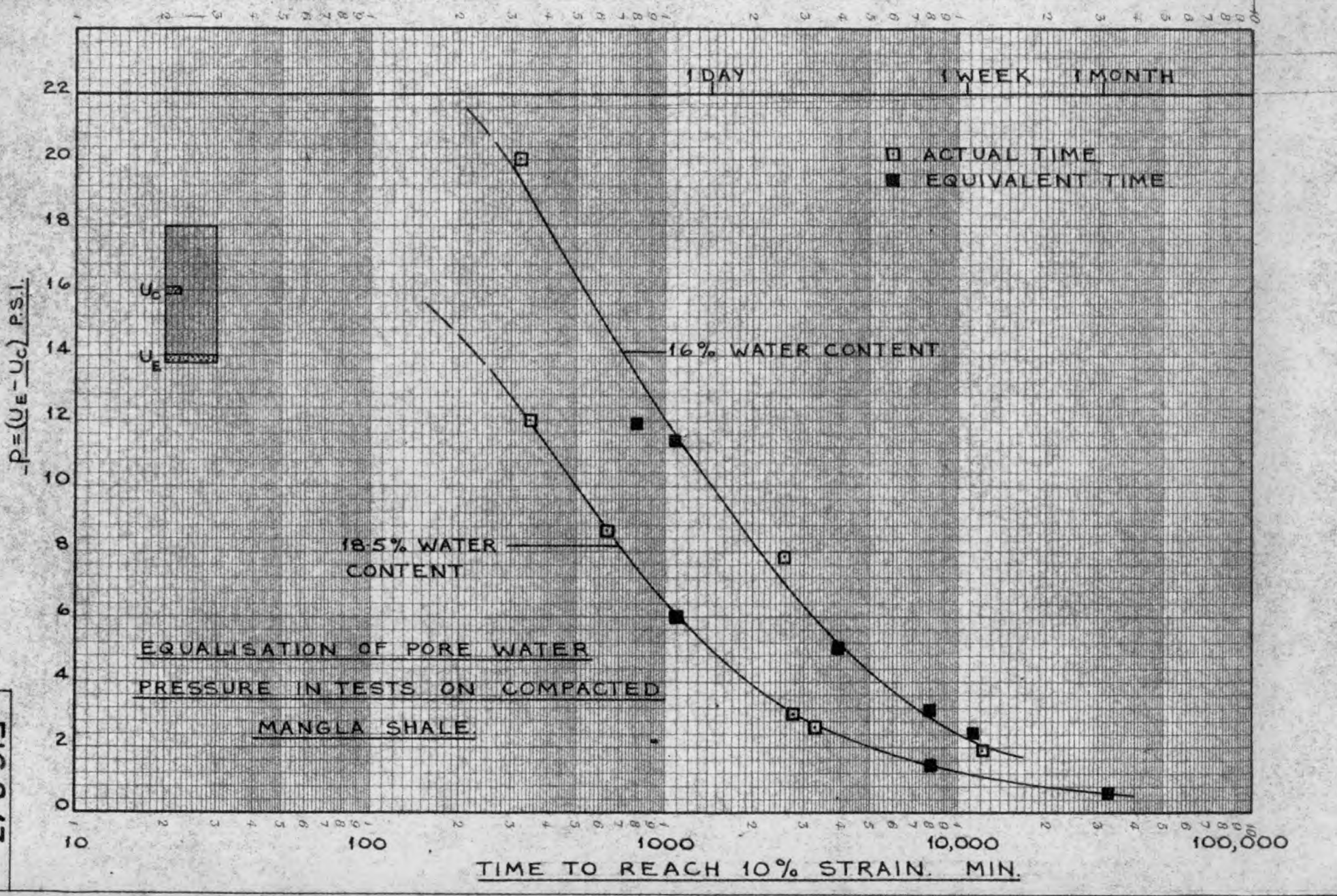






COMPARISON OF WATER CONTENT AND DIAMETER PROFILES IN TWO SAMPLES OF MANGLA SHALE LOADED BETWEEN CONVENTIONAL AND LUBRICATED END PLATES.

FIG. 8.16.



EQUALISATION OF PORE WATER PRESSURE IN TESTS ON COMPACTED MANGLA SHALE.

FIG. 8.17.

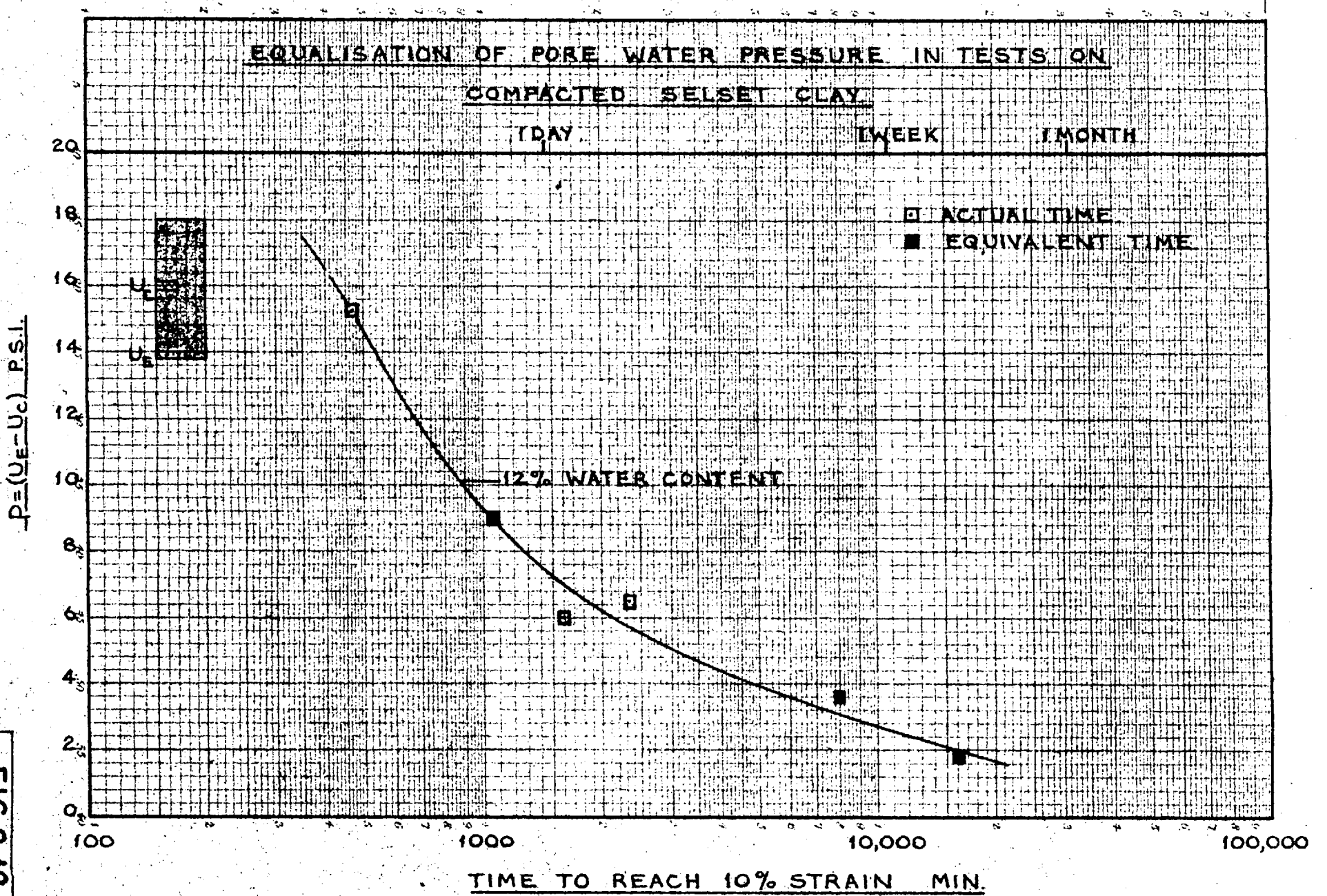
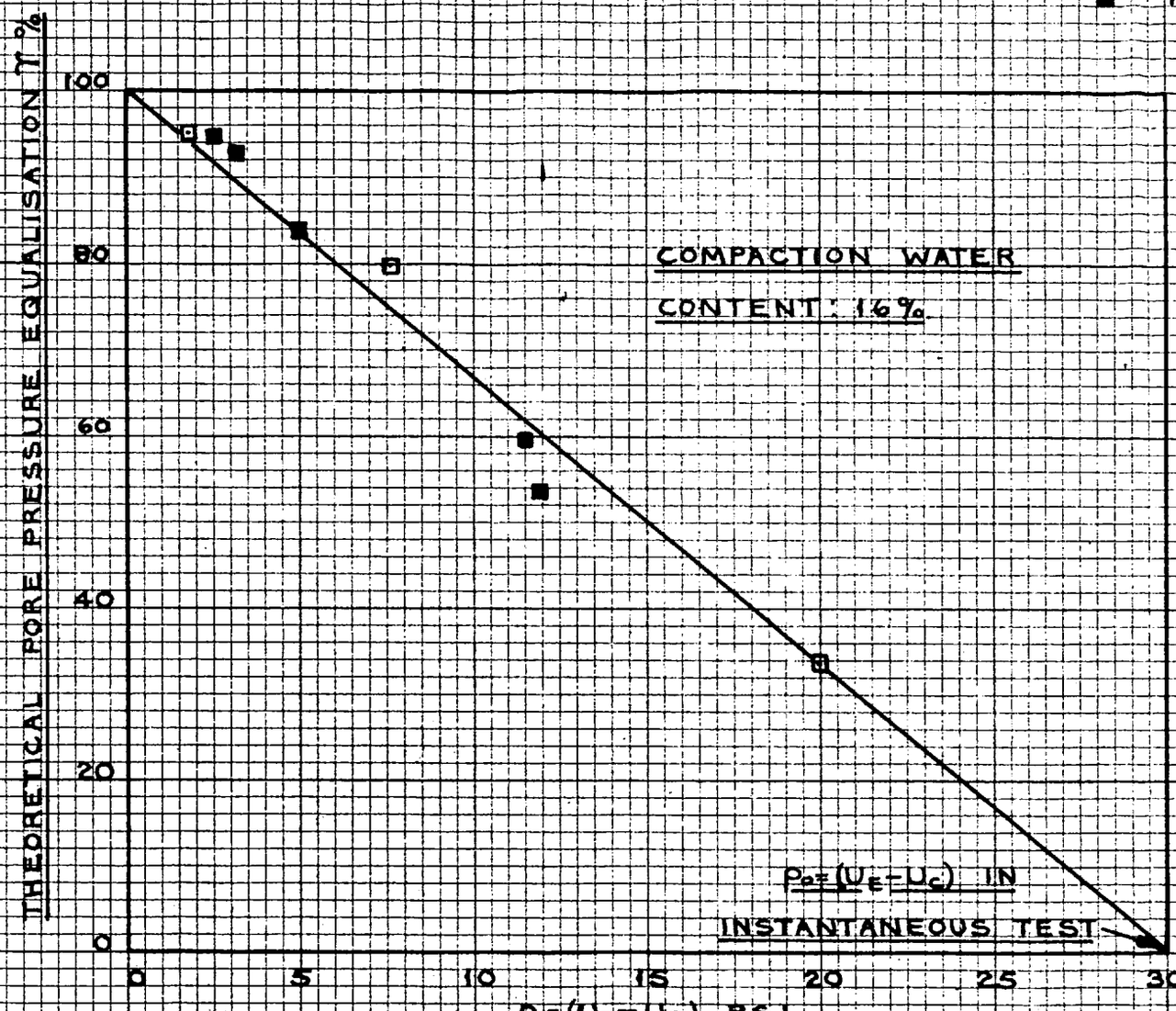
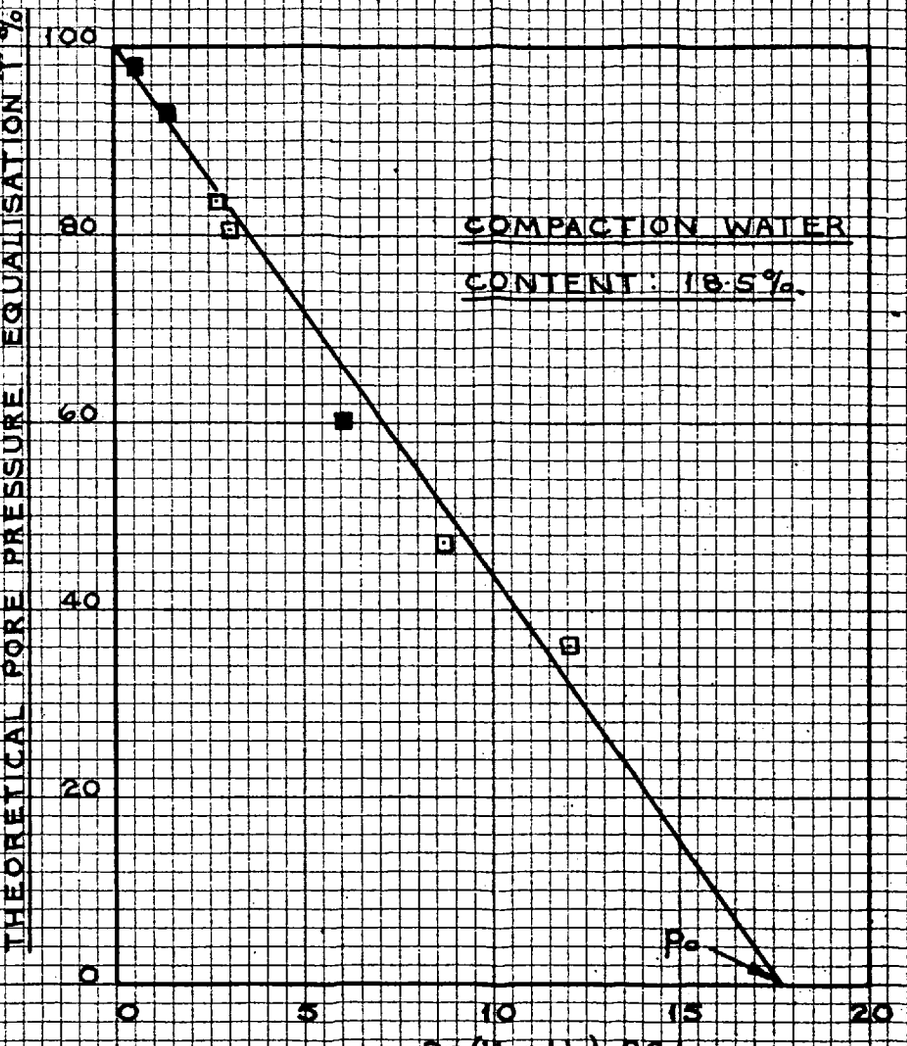

EQUALISATION OF PORE WATER PRESSURE IN TESTS ON
COMPACTED SELSET CLAY
1 DAY
1 WEEK
1 MONTH
ACTUAL TIME
EQUIVALENT TIME
12% WATER CONTENT
P=(UE-UC) P.S.I.
UC
UE
0
2
4
6
8
10
12
14
16
18
20
100
1000
10,000
100,000
TIME TO REACH 10% STRAIN MIN.

FIG. 8.18.

□ π FROM ACTUAL TIME.

■ π FROM EQUIVALENT TIME.



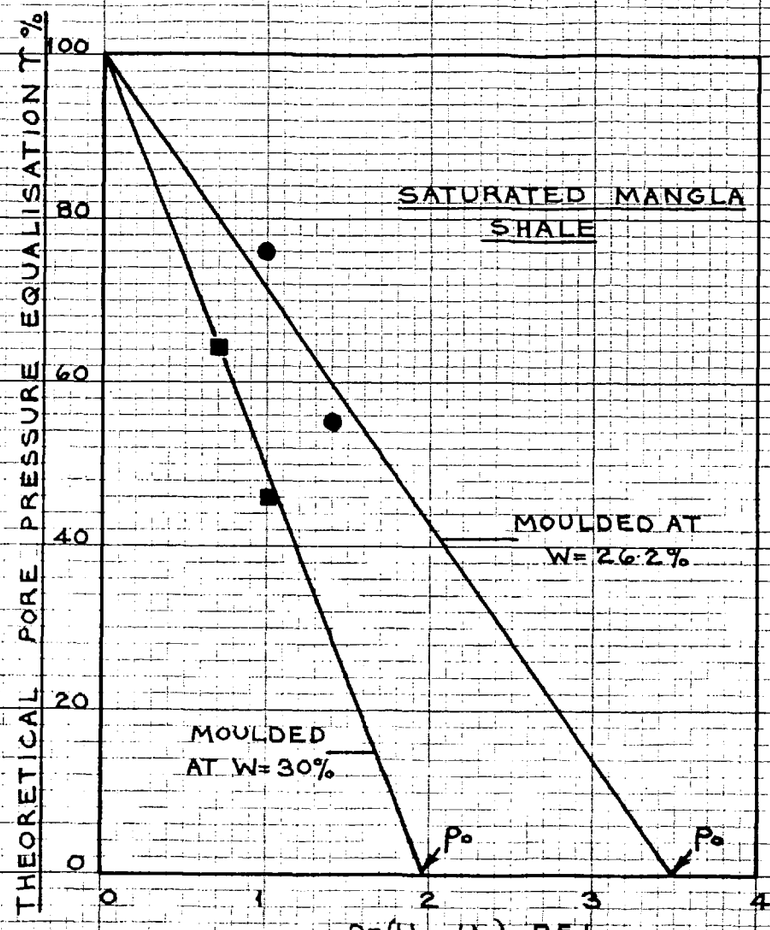


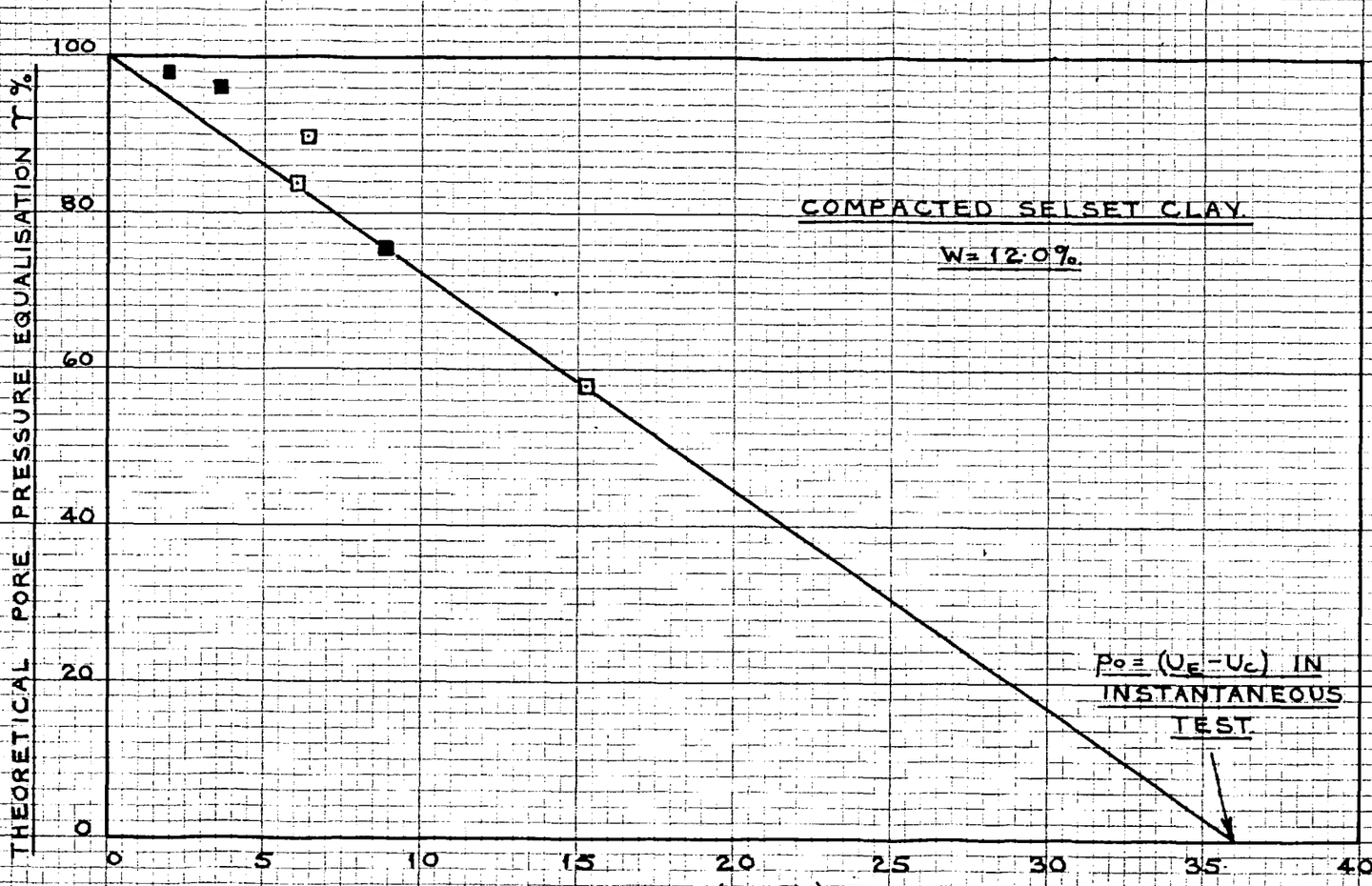
MEASURED PORE WATER PRESSURE DIFFERENCE.

EQUALISATION OF PORE WATER PRESSURE IN TESTS ON COMPACTED MANGLA SHALE. METHOD OF FITTING EXPERIMENTAL DATA TO THEORETICAL CURVE.

FIG. 8.19.

□ T FROM ACTUAL TIME.
● ■ T FROM EQUIVALENT TIME.





MEASURED PORE WATER PRESSURE DIFFERENCE.

EQUALISATION OF PORE WATER PRESSURE IN TRIAXIAL TESTS. METHOD OF FITTING EXPERIMENTAL DATA TO THEORETICAL CURVE.

FIG. 8.20.

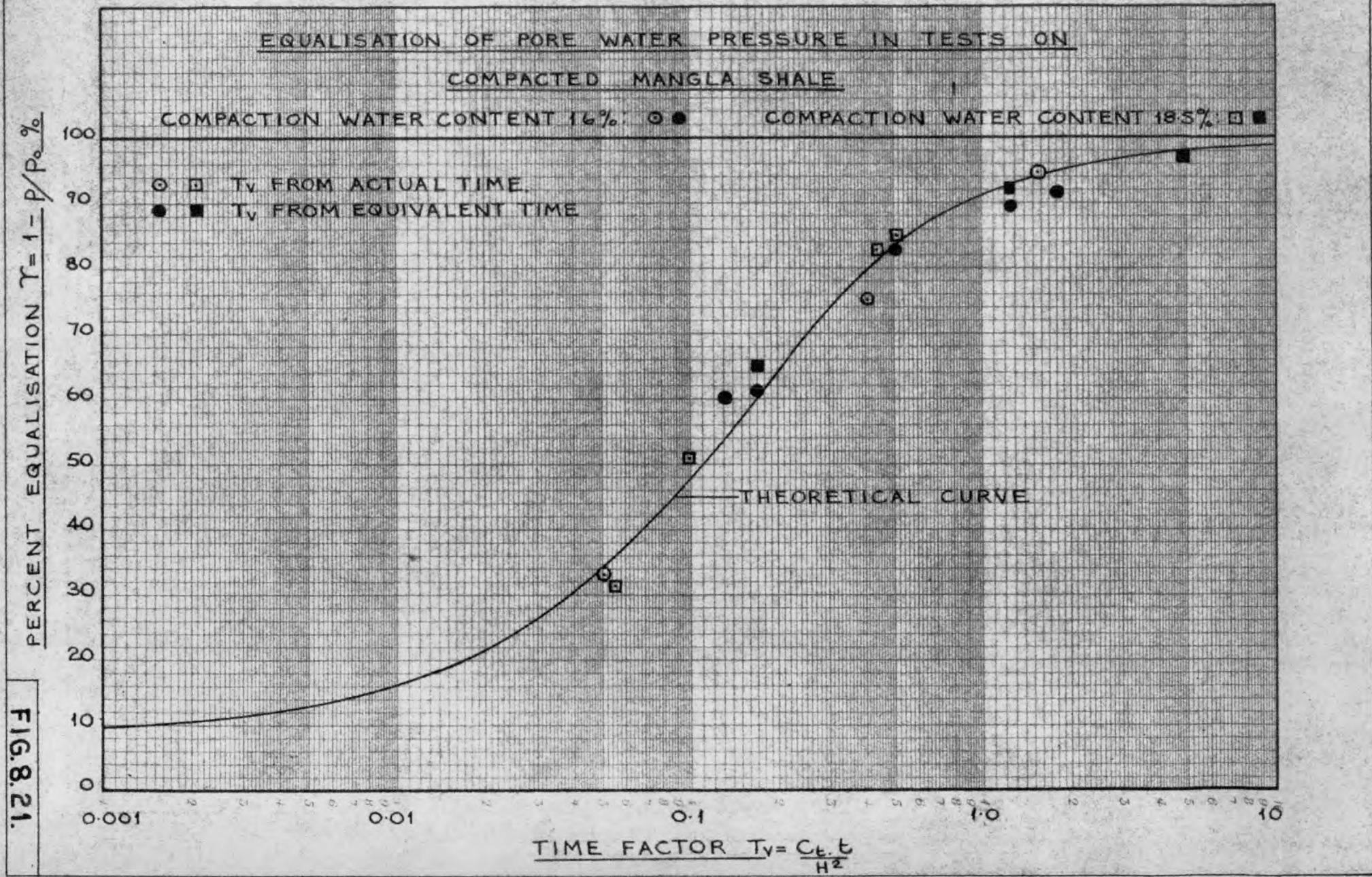

EQUALISATION OF PORE WATER PRESSURE IN TESTS ON
COMPACTED MANGLA SHALE
COMPACTION WATER CONTENT 16%.
COMPACTION WATER CONTENT 18·5%.
Tv FROM ACTUAL TIME.
Tv FROM EQUIVALENT TIME.
THEORETICAL CURVE
PERCENT EQUALISATION r = 1 − P/Po %
0
10
20
30
40
50
60
70
80
90
100
0·001
0·01
0·1
1·0
10
TIME FACTOR Tv = Cv.t / H²

FIG. 8.21.

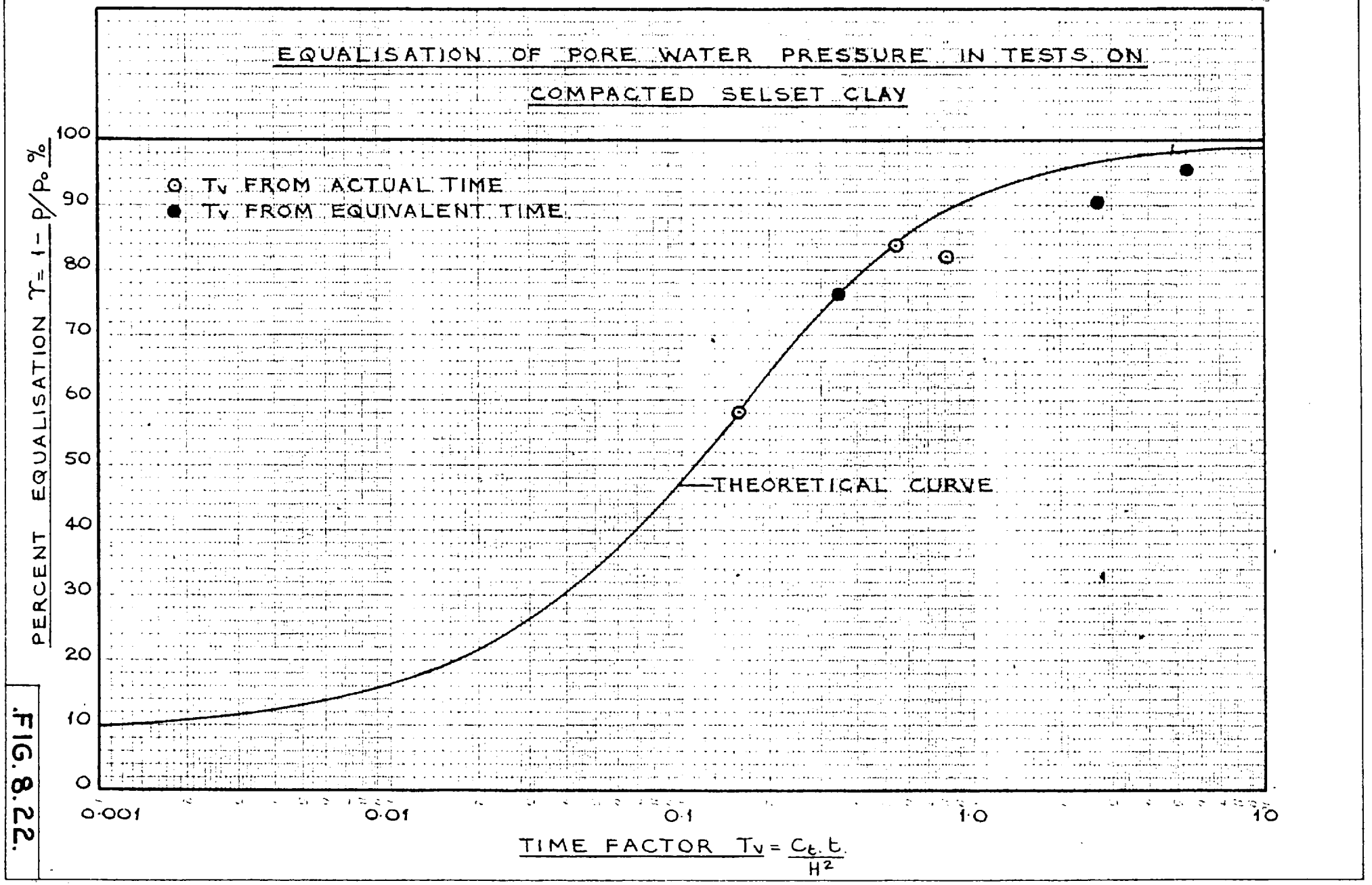
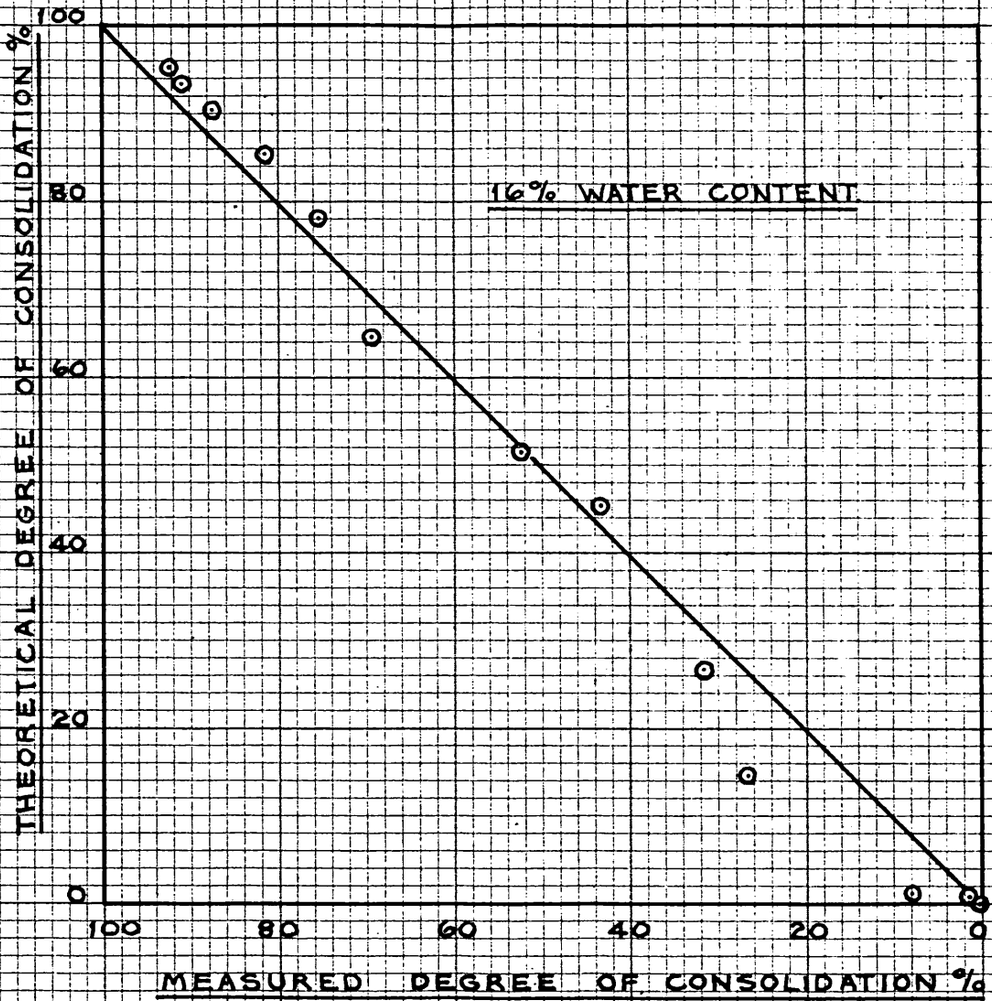
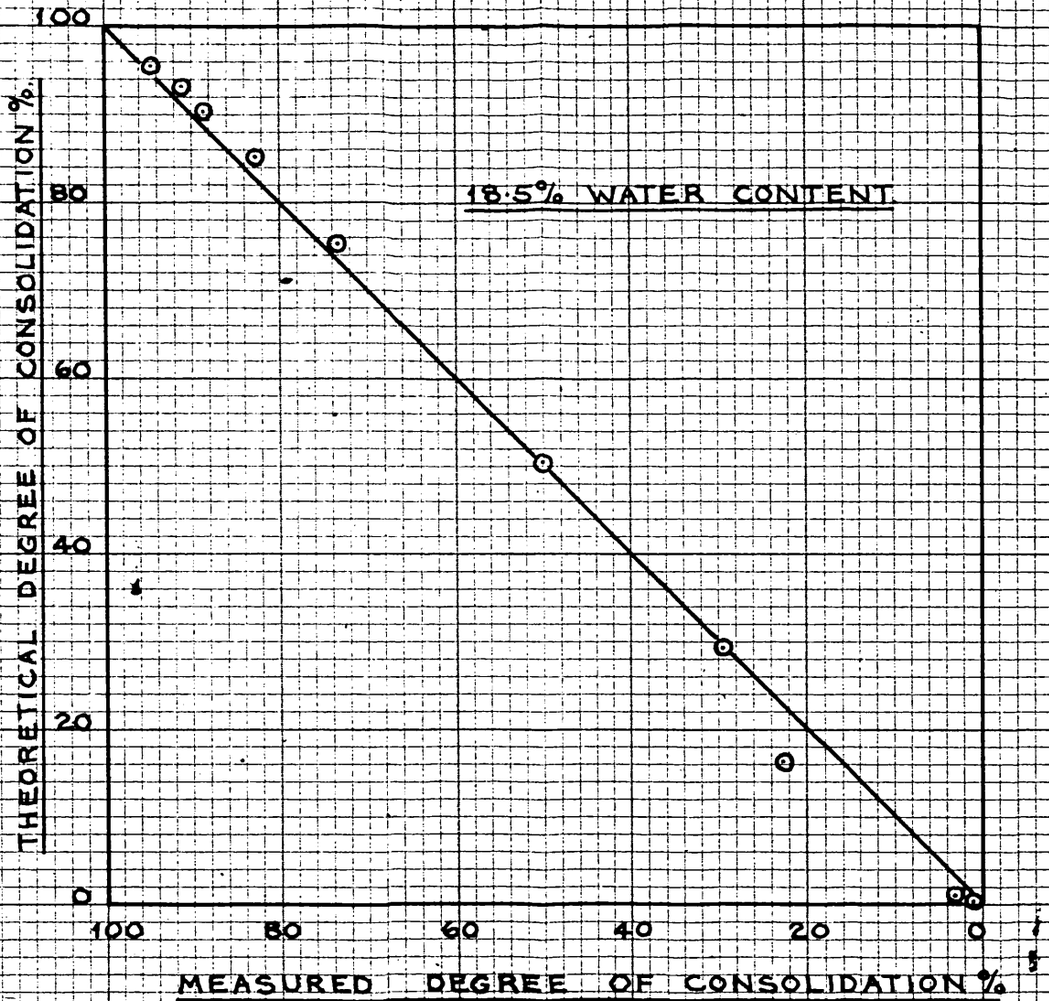

EQUALISATION OF PORE WATER PRESSURE IN TESTS ON
COMPACTED SELSET CLAY
PERCENT EQUALISATION U = 1 − P/P₀ %
100
90
80
70
60
50
40
30
20
10
0
⊙ Tv FROM ACTUAL TIME
● Tv FROM EQUIVALENT TIME.
THEORETICAL CURVE
0·001
0·01
0·1
1·0
10
TIME FACTOR Tv = Ct.t / H²

FIG. 8.22.





TRIAXIAL DISSIPATION TESTS ON COMPACTED MANGLA SHALE. DEVIATION OF EXPERIMENTAL DATA FROM THEORETICAL DISSIPATION CURVE

FIG. 8.23.

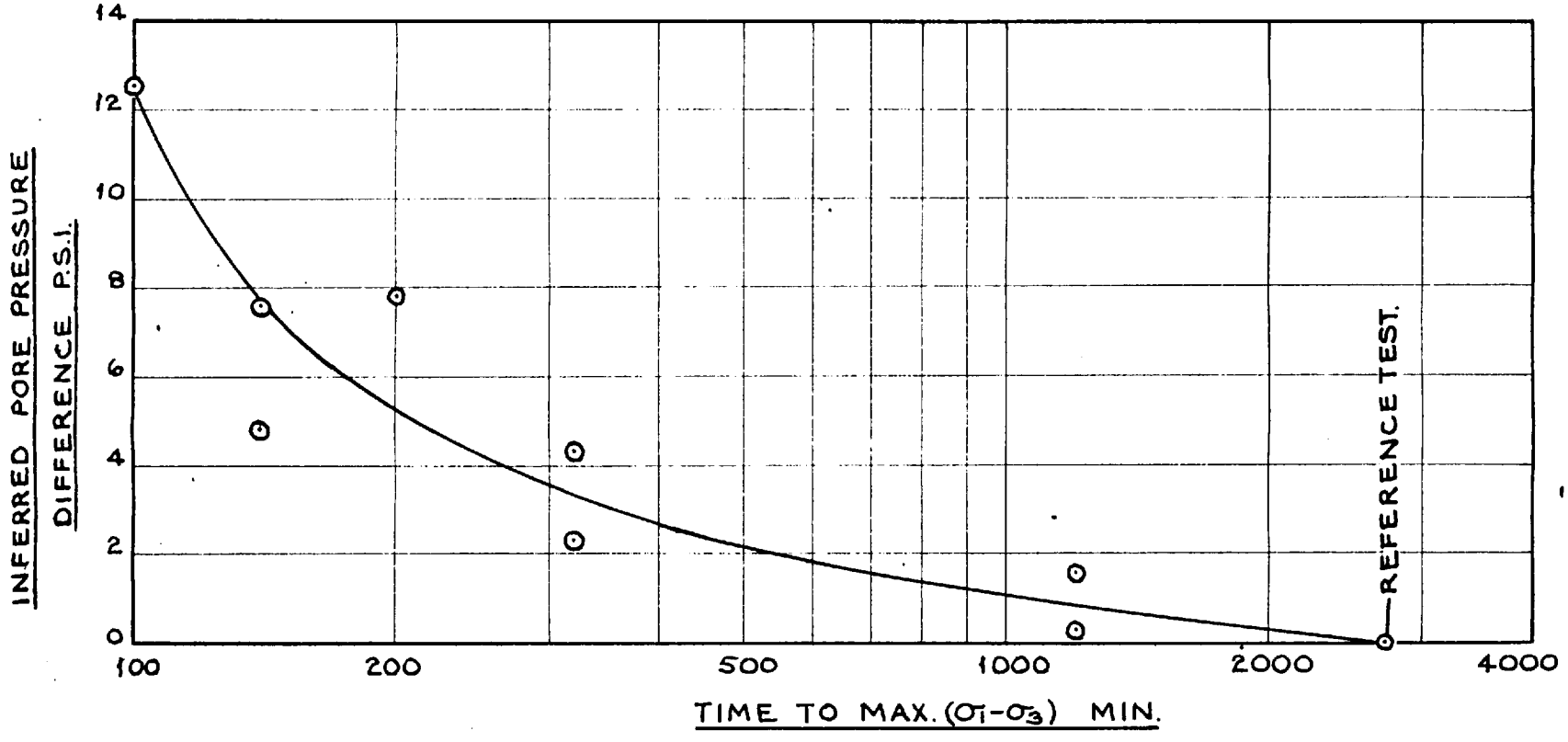
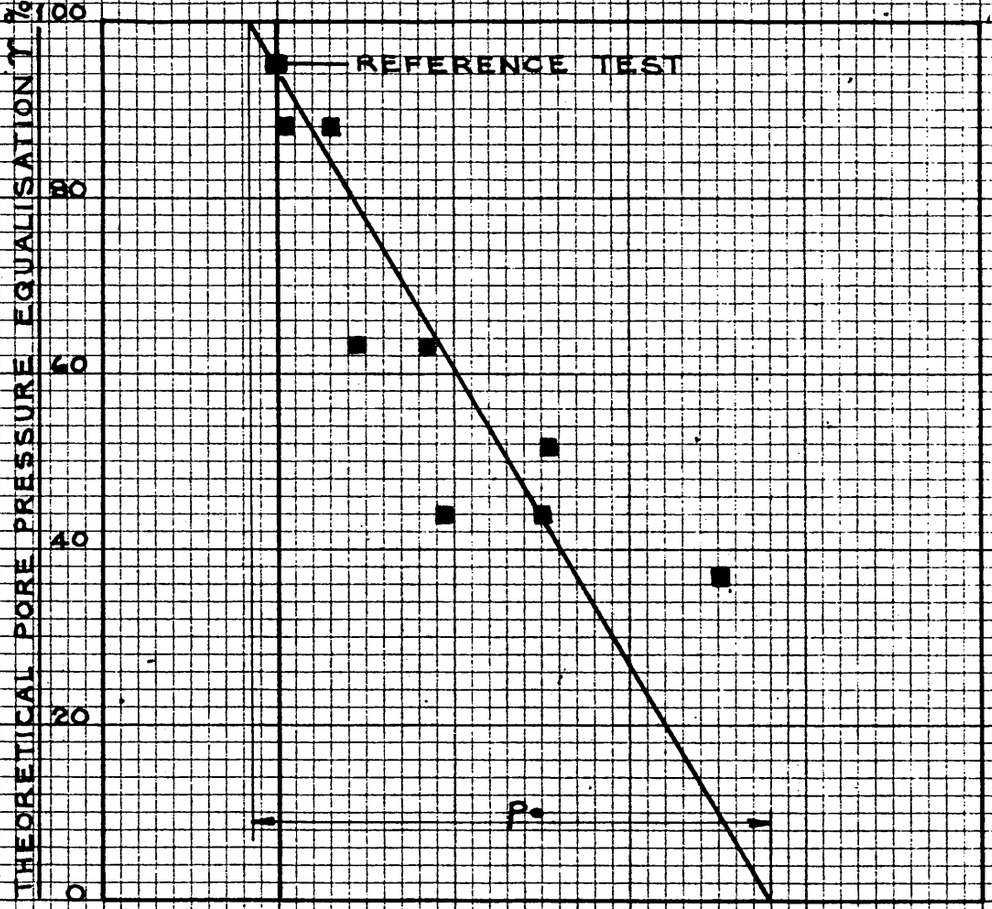


FIG. 8.24.

EQUALISATION OF PORE WATER PRESSURE IN TESTS ON COMPACTED TALYBONT CLAY. PORE PRESSURE DIFFERENCES INFERRED FROM TESTS BY ALPAN BY FITTING TO ENVELOPE: $C'=0$, $\phi'=36°$.

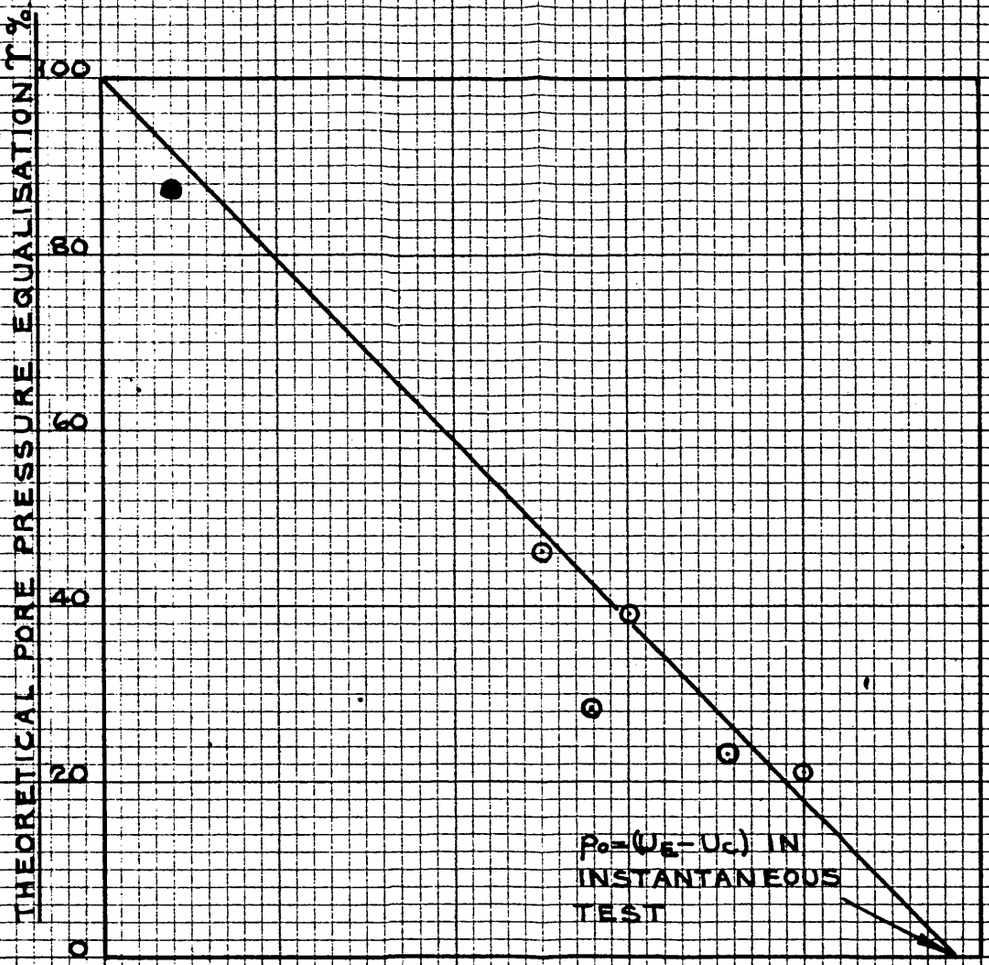


INFERRED PORE WATER PRESSURE DIFFERENCE

P.S.I.

TESTS BY ALPAN ON COMPACTED TALYBONT CLAY

WATER CONTENT: 9.2%



$p=(U_E-U_C)$ P.S.I.

MEASURED PORE WATER PRESSURE DIFFERENCE

TESTS BY TAYLOR ON BOSTON CLAY

EQUALISATION OF PORE WATER PRESSURE IN TRIAXIAL TESTS. FITTING OF EXPERIMENTAL DATA TO THEORETICAL CURVE

FIG. 8.25.

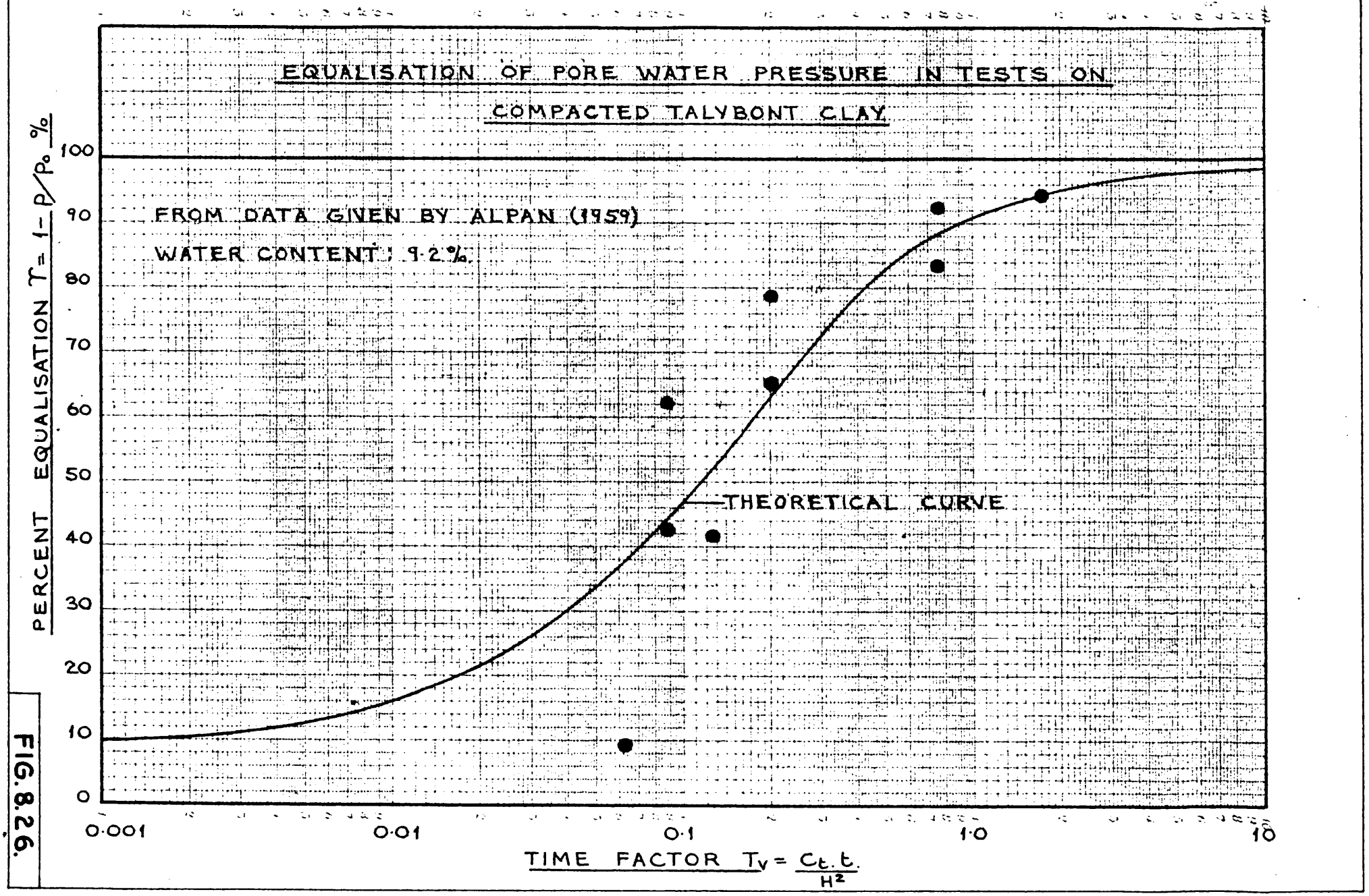

EQUALISATION OF PORE WATER PRESSURE IN TESTS ON
COMPACTED TALYBONT CLAY
FROM DATA GIVEN BY ALPAN (1959)
WATER CONTENT : 9·2 %
THEORETICAL CURVE
PERCENT EQUALISATION T = 1 - P/Po %
0
10
20
30
40
50
60
70
80
90
100
0·001
0·01
0·1
1·0
10
TIME FACTOR Tv = Cv.t / H²

FIG. 8.26.

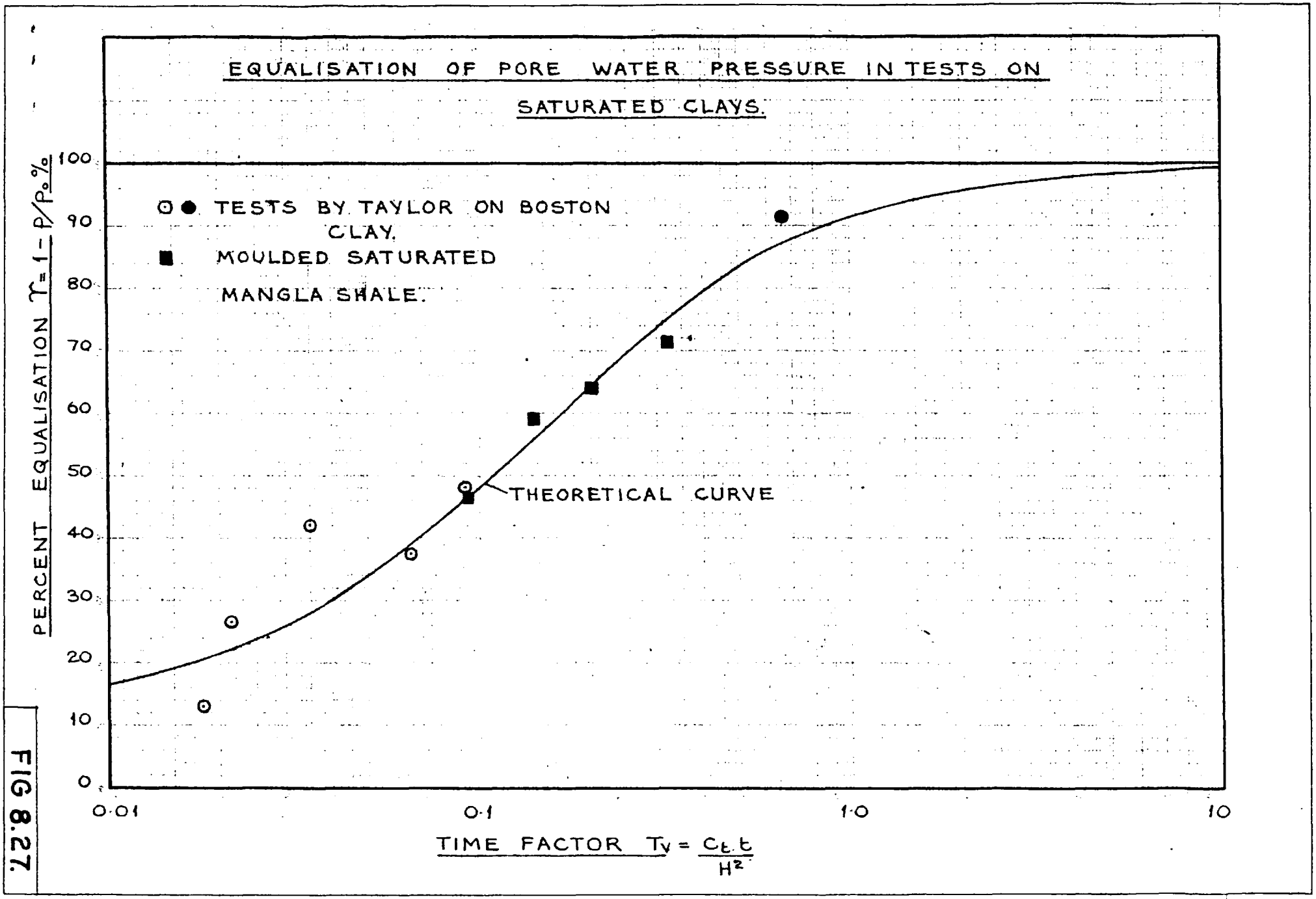
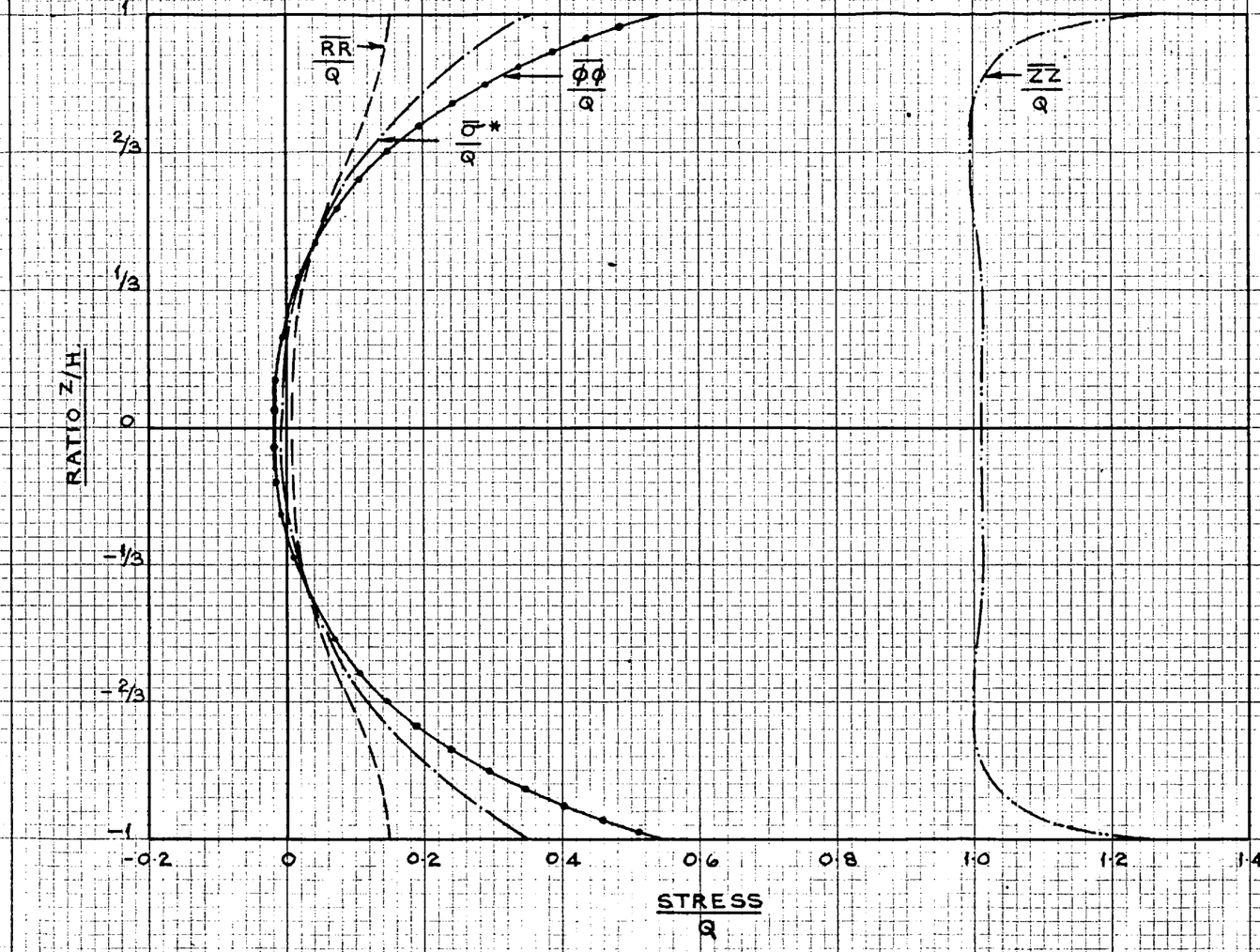
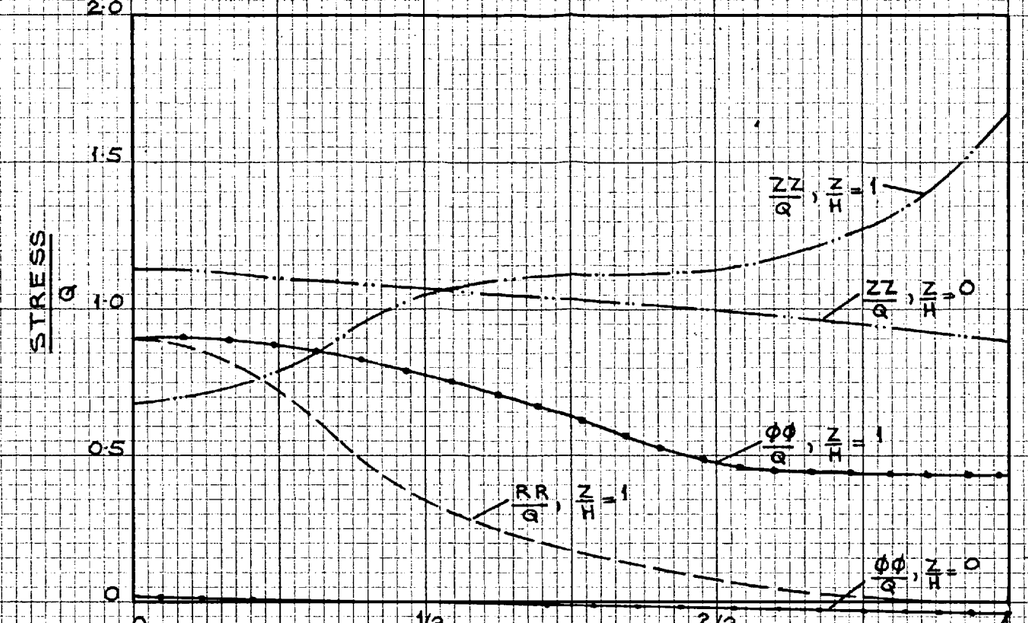
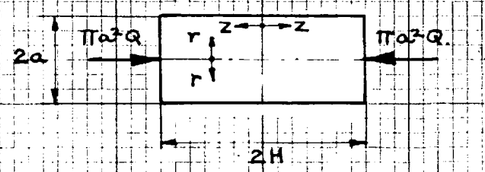
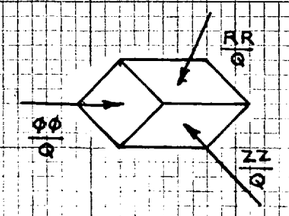

EQUALISATION OF PORE WATER PRESSURE IN TESTS ON SATURATED CLAYS.
PERCENT EQUALISATION U = 1 - P/Po %
100
90
80
70
60
50
40
30
20
10
0
TESTS BY TAYLOR ON BOSTON CLAY.
MOULDED SATURATED MANGLA SHALE.
THEORETICAL CURVE
0·01
0·1
1·0
10
TIME FACTOR Tv = Cv t / H²

FIG 8.27.









$$\frac{\overline{RR}}{Q} = \frac{1}{\pi a^2}\int_0^a\int_0^{2\pi}\frac{RR}{Q}\,dr\,d\theta$$

$$\frac{\overline{\phi\phi}}{Q} = \frac{1}{\pi a^2}\int_0^a\int_0^{2\pi}\frac{\phi\phi}{Q}\,dr\,d\theta$$

$$\frac{\overline{ZZ}}{Q} = \frac{1}{\pi a^2}\int_0^a\int_0^{2\pi}\frac{ZZ}{Q}\,dr\,d\theta$$

$$\frac{\sigma^*}{Q} = \frac{\frac{\overline{RR}}{Q} + \frac{\overline{\phi\phi}}{Q}}{2}$$

STRESSES IN A CIRCULAR CYLINDER OF ELASTIC MATERIAL UNDER AN AXIAL STRESS Q APPLIED THROUGH PERFECTLY ROUGH RIGID END PLATES.

DATA FROM FILON (1902).

FIG. 8.28.

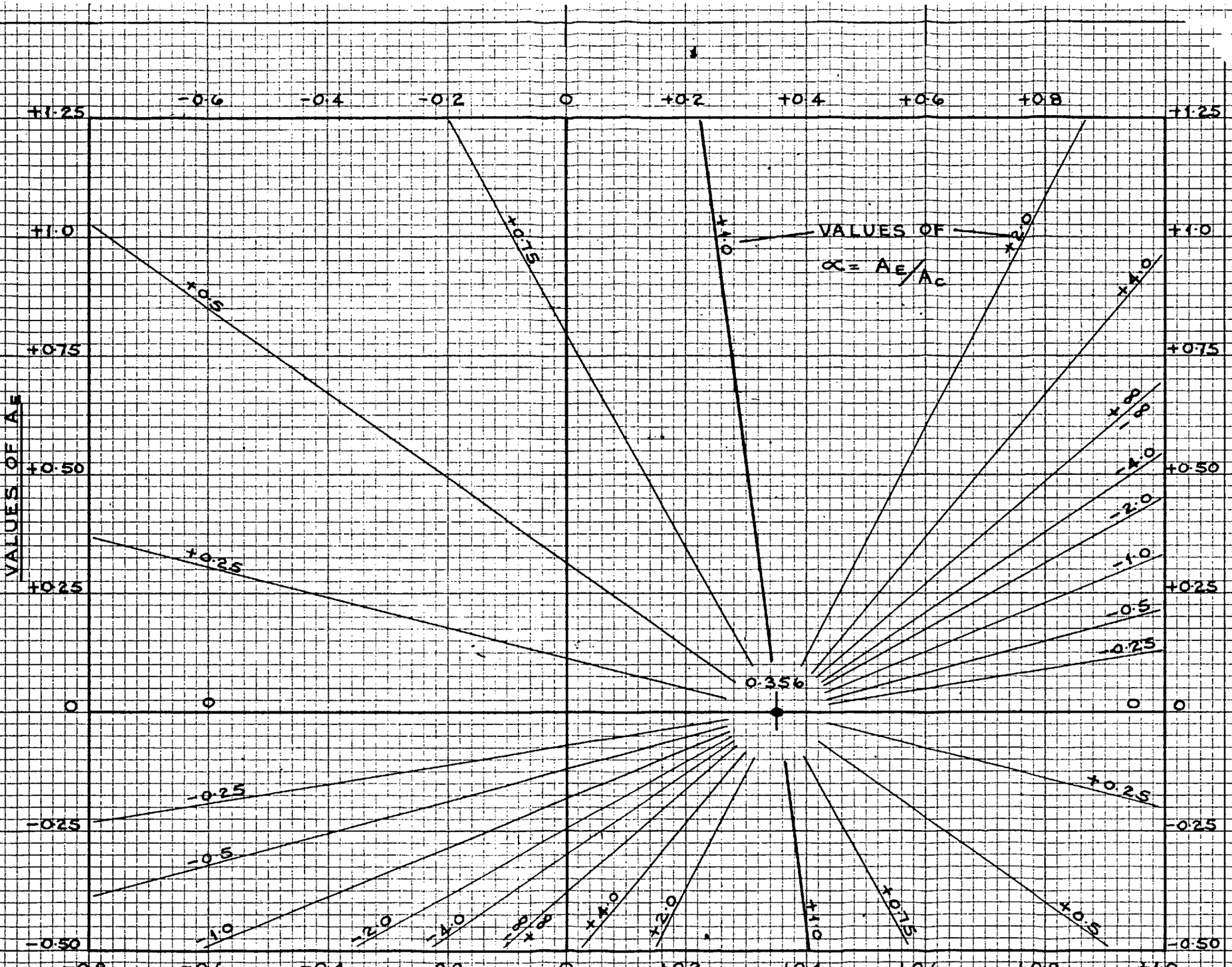


CHART FOR ESTIMATION OF $P_o = (U_E - U_c)$

CALCULATED FROM: $\frac{P_o}{Q} = 0.356 + A_E\left\{0.921 - \frac{1.022}{\alpha}\right\}$

FIG. 8.29.

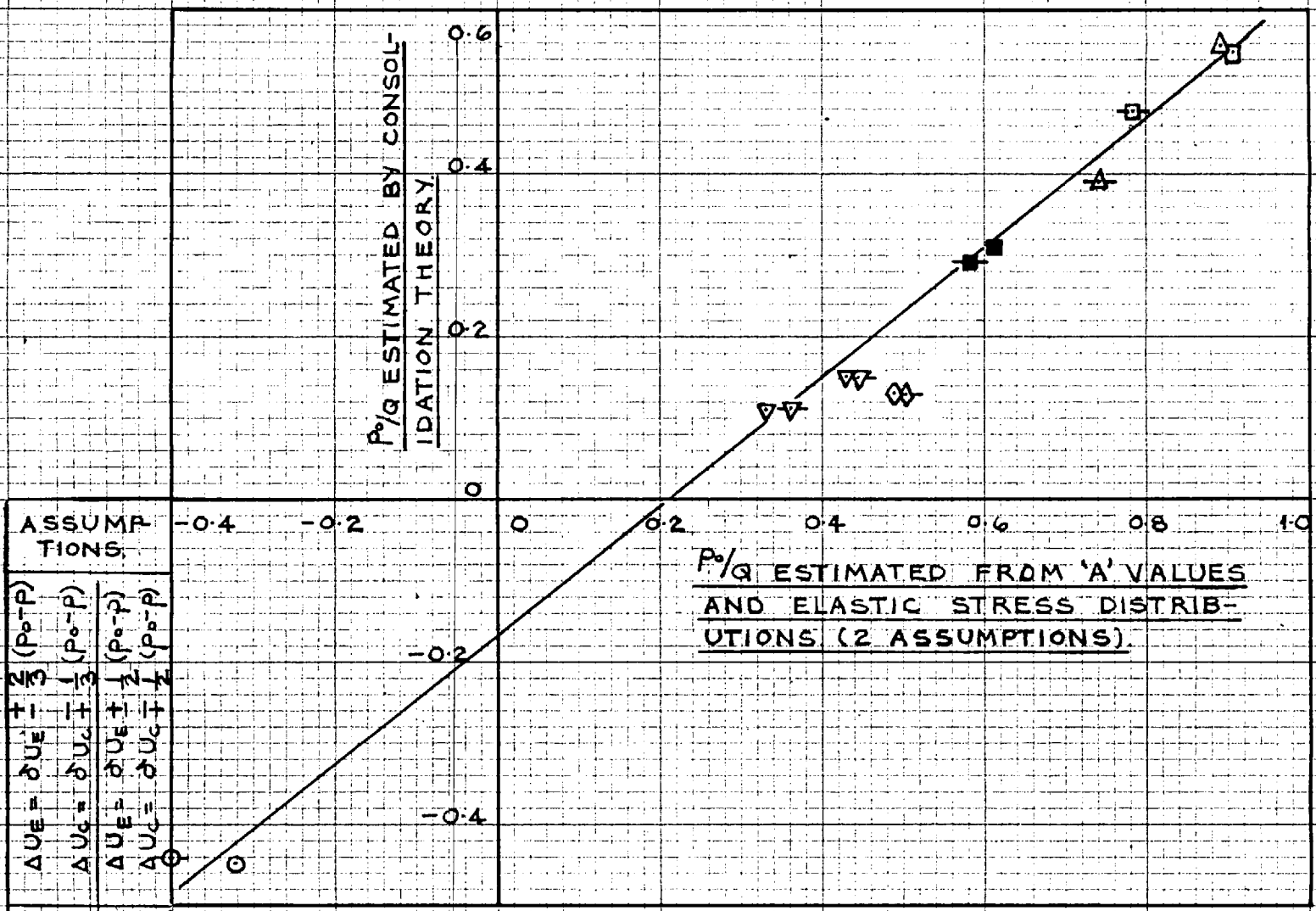


FIG. 8.30.

ESTIMATION OF P_o/Q BY TWO METHODS.

SEE TEXT FOR DETAILS.

CHAPTER 9

PROPERTIES OF PARTLY SATURATED COMPACTED SOILS AT CONSTANT WATER CONTENT UNDER ISOTROPIC STRESSES

This chapter will be used to discuss a number of miscellaneous properties of compacted partly saturated soils. Firstly, the soils' behaviour under equilibrium conditions will be considered and then the nature of some non-equilibrium states will be looked into.

(9.1) The principle of effective stress for volume change in partly saturated soils.

The relation between volume change and change in effective stress in a soil can be expressed by:

$$\Delta\sigma' = \frac{-1}{C_c}\left(\frac{\Delta V}{V_o}\right) \qquad E(9.1)$$

where

C_c is the compressibility of the soil skeleton.

$\Delta V/V_o$ is the percentage volume change due to a change in effective stress of $\Delta\sigma'$.

For a partly saturated soil, this equation becomes:

$$\Delta(\sigma - u_a) + \chi_v\Delta(u_a - u_w) = \frac{-1}{C_c}\left(\frac{\Delta V}{V_o}\right) \qquad E(9.2)$$

Values of the parameter χ_v in E(9.2) can be found by methods similar to those used to find χ from considerations of shear strength. The effective stress-volume change curve for the soil is first of all established from tests on the saturated soil. Values of χ_v are then found by comparing this curve with curves relating volume change to stress change for the partly saturated soil.

The difficulty in applying this simple procedure to compacted

soils is that while the partly saturated compacted soil changes volume at constant water content, the water content of the saturated soil changes continuously. This does not appear to have much effect on the shear strength of the soil, but does appear to alter the compressibility.

(9.2) Semi-graphical method of determining χ_v.

A semi-graphical method of determining χ_v which is similar to that described in Chapter 7 is illustrated in fig. (9.1).

For a partly saturated soil compressed at constant water content, curves of $(\sigma - u_a)$ and $(\sigma - u_w)$ are plotted against the percentage volume change. The only point which this pair of curves has in common with the true effective stress curve is the point at which the soil becomes saturated and $\chi_v = S = 1$. Through this point the true effective stress curve is fitted.

We have:

$$\sigma' = (\sigma - u_a) + \chi_v(u_a - u_w)$$

In the terms of the diagram: $a = (\sigma - u_a)$, $b = \sigma'$, $c = (\sigma - u_w)$ hence

$$b = a + \chi_v(c - a)$$

i.e. $$\chi_v = \frac{(b - a)}{(c - a)}$$

(9.3) Experimental values of χ_v.

Only two tests were carried out to determine experimental values of χ_v.

In the first experiment a sample of Mangla shale, compacted at a water content of 18.1% was compressed at constant water content with controlled pore air pressures. Fig. (9.2) shows the changes in

volume which took place as $(\sigma' - u_a)$ was varied. $(\sigma' - u_a)$ was increased and decreased in steps of 10 p.s.i. 48 hours was allowed for the initial equilibrium to be established and thereafter 24 hours was allowed to elapse between altering $(\sigma' - u_a)$ and reading u_w.

The true effective stress line for the first compression cycle was found from the consolidation results of test Series 1A. This line was fitted to the compression curve for the partly saturated soil at the point $\alpha_v = S = 1$ and appeared to agree fairly well with the trend of the results. The variation of α_v with S is shown to the left of the figure.

Fig. (9.3) shows the results of a similar test on Selset clay compacted at a water content of 11.7%. In this case an effective stress line obtained from the results of Series 2A was tried. However, the saturated soil was obviously much less compressible than the partly saturated soil. This may have been caused by the removal from the soil used for the saturated samples of all stones retained on an $\frac{1}{8}$" sieve, or may be due to a change in soil structure caused by saturation by back pressure.

The effective stress line which was finally used was obtained by plotting the results on a log. pressure scale and drawing a straight line parallel to the portion of the curve representing stresses in the saturated soil. The variation of α_v with S is also shown in fig.(9.3).

In both cases the variation of α_v with S was very similar to that found from shear strength tests. This seems to show that the structure of a compacted partly saturated soil has a similar effect on the effective stress relation for volume change to that which it has on the effective stress relation for shear strength.

(9.4) Theoretical relation between volume change and pore air pressure in undrained compression of a partly saturated soil.

Calculations based on the simultaneous application of Boyle's and Henry's laws to the compression of the pore fluid of a partly saturated soil have been fairly widely used to predict pore air pressures at the end of construction of rolled fill dams. (Bruggeman, Zanger and Brahtz, 1939, Hilf, 1948, Bishop, 1957).

The relation between pore air pressure and volume change has usually been expressed as:

$$\Delta u_a = u_{a_o} \cdot \frac{-\Delta V/V_o}{\Delta V/V_o + n_o(1 - S_o + S_o H)} \qquad E(9.3)$$

where

u_{a_o} = initial pore air pressure.

n_o = initial porosity.

S_o = initial degree of saturation.

H = Henry's coefficient of solubility in terms of volume/volume.

This equation is based on a consideration of volumes of air compressed and dissolved in corresponding volumes of water. It is rather cumbersome to use but can be put in a graphical form by considering the equivalent mass relations.

Suppose a volume $V_v = (V_a + V_w)$ of voids in a partly saturated soil contains a mass m_w of water and m_a of air. Suppose that of the mass of air, proportion h_a is dissolved in the water and proportion $(1 - h_a)$ is in the gaseous form. Then Henry's law of solubility can be stated as:

$$u_a = H \cdot \frac{h_a m_a}{w_a} \Big/ \frac{m_w}{w_w} \qquad \text{(Adam, 1956)} \qquad E(9.4)$$

where

u_a is the absolute pressure of the air in atmospheres.

H is Henry's coefficient of solubility in atmospheres per mole of air per mole of water.

w_a & w_w are the molecular weights of air and water respectively.

Applying the universal gas law to the gaseous air:

$$u_a . V_a = (1 - h_a) \frac{m_a}{w_a} . R\Theta \qquad E(9.5)$$

where

R is the universal gas constant.

Θ is the absolute temperature.

Substituting for h_a from E(9.4) in E(9.5):

$$u_a = \frac{R\Theta \cdot \frac{m_a}{w_a}}{\left[V_a + \frac{R\Theta}{H} \cdot \frac{m_w}{w_w}\right]} \qquad E(9.6)$$

The degree of saturation is given by:

$$S = \frac{V_w}{V_w + V_a}$$

i.e. $$V_a = \frac{1 - S}{S} \cdot V_w = \frac{1 - S}{S} \cdot \frac{m_w}{\rho_w}$$

where

ρ_w is the specific gravity of water.

Substituting in E(9.6) and dividing the denominator by $\frac{m_w}{w_w}$

$$u_a = \frac{R\Theta \cdot \frac{m_a}{w_a} \cdot \frac{w_w}{m_w}}{\left[\frac{1-S}{S} \cdot \frac{w_w}{\rho_w} + \frac{R\Theta}{H}\right]}$$

Finally, writing $\frac{m_a}{w_a} \Big/ \frac{m_w}{w_w} = N \qquad E(9.8)$

we have:

$$u_a = \frac{NR\theta}{\left[\frac{1-S}{S} \cdot \frac{w_w}{\rho_w} + \frac{R\theta}{H}\right]} \qquad E(9.9)$$

The pore air pressure at which the soil becomes saturated is given by putting $S = 1$ in E(9.9).

$$u_{a(S=1)} = \frac{NR\theta}{\frac{R\theta}{H}} = NH \qquad E(9.10)$$

i.e. The pressure required to cause saturation is directly proportional to the ratio of the masses of air and water contained by the soil.

E(9.9) represents a family of curves relating S to u_a for different values of N. Fig.(9.4) shows the family of curves calculated for the range of values of S most common in compacted soils. A single pair of values of u_a and S will enable the correct value of N to be estimated and hence the correct curve to be chosen.

It must be emphasised that equation E(9.9) applies only to equilibrium conditions. Henry's law does not operate instantaneously and an appreciable time must elapse before solution of the compressed air in the pore water can be completed.

Dorsey (1940) states that the relation between the mass of air dissolved and time is:

$$\frac{m_t - m_o}{m_\infty - m_o} = 1 - e^{-\beta \frac{A}{V} t}$$

where

m is a mass of air dissolved in a volume V of water through a surface area A.

t is the time.

β is a constant.

He quotes a value for β at 20°C of 0.53 cm/min.

The following numerical values of the various constants appearing in E(9.9) are useful in calculations of this sort. (Hilf, 1956, Dorsey, 1940).

w_w = molecular weight of water = 18.015

w_a = molecular weight of air = 28.960

R = universal gas constant = 82.06 $\frac{cc.atm.}{°K.mol.}$

Absolute temperature θ°K	Henry's Constant H atm./mole of air/mole of water
273	43,200
278	48,800
283	54,900
288	60,700
293	66,400
298	72,000

In calculating the curves shown in fig. (9.4) the following values were assumed:

θ = 20°C = 293°K

1 atmosphere = 14.7 p.s.i.

(9.5) Initial pore air pressures in compacted soils.

In calculations of pore air pressures according to equation E(9.3) it has been commonly assumed in the past that the initial pore air pressure after compaction is atmospheric. There is no reason why this should be so especially under laboratory conditions.

Pore air pressures set up by compaction.

The pore air pressure set up in a soil by compaction was measured in the following way.

A special compaction mould was used which had an air tight O-ring seal between the cylinder and the base of the mould. A series of circular grooves, machined in the base plate, connected with an outlet channel which was closed by an air tight valve. The machined grooves were filled by a wick of glass fibre ribbon.

The soil was compacted into the mould in the usual way, the final level of the soil being about 1" below the top of the mould. A layer of molten wax was poured over the surface of the soil and while this was still soft, a perspex disc was placed over it and the space around the disc was filled with plasticine. A rubber membrane was stretched over the top of this and held down by an O-ring. The valve at the base was connected to a null indicator and the pore air pressure set up by compaction was measured.

Fig. (9.5)a shows a record of these measurements. The initial pore air pressure was + 6.9 p.s.i. This gradually declined over a period of 3 days to a pressure of + 1.9 p.s.i.

Equilibrium pore pressure under completely undrained conditions.

Fig. (9.5)b shows the changes in pore air pressure with time in an unstressed freshly compacted sample of Talybont clay. The sample was enclosed in a rubber membrane sealed to perspex end plates. The whole was completely immersed in mercury to preserve a fully undrained condition.

In this case the equilibrium pore air pressure was - 2.4 p.s.i.

(9.6) Changes in pore water pressure after compression of freshly compacted soils.

This investigation is of a very limited nature as it was abandoned when it was realised that latex rubber membranes were permeable to air. However, it is felt that the following data will be of interest.

Fig. (9.6) shows measured pore pressure changes in three separate samples of Mangla shale compacted at a water content of 18½%. In each case, as soon as the sample was set up, an initial reading of pore water pressure was taken and the final cell pressure was immediately applied in one increment.

In two of the tests, ($\Delta\sigma$ = 22.2 p.s.i. and $\Delta\sigma$ = 45 p.s.i.), the pore water pressure was found to increase to a peak and then decline again. Part of this decline in pore pressure is undoubtedly due to loss of air from the sample by diffusion through the rubber membrane. The peak pore pressure had in both cases been passed by the time 20 minutes had elapsed. Comparison with fig.(3.5) shows that very little of the pressure decline between 0 and 200 minutes could have been caused by loss of air through the membrane.

In fig. (9.6) calculated pore pressure changes have been shown for two of the samples assuming that $(u_a - u_w)$ remains constant and that u_a changes according to Boyle's law. The variation in u_w measured in the sample for which σ_3' = 2.3 p.s.i. has been superimposed on the calculated curves. The solid lines represent the summation of these two curves and agree in shape with the experimental points.

This suggests that the mechanism which causes the humped shape of the pore water pressure curves is due to the superimposition

of two effects:

(i) Increasing pore air pressures due to compression by Boyle's law.

(ii) Decreasing pore air pressures due to solution of air in the pore water by Henry's law and loss of air through the membrane.

It is clear from the curves shown in fig. (9.6) that 48 hours is a reasonable time to allow for equilibrium to be reached.

(9.7) Changes in pore water pressure in unconfined samples of freshly compacted soils.

Fig. (9.7) shows measured variations in u_w with time for a selection of freshly compacted soil samples. The samples were set up unconfined and were surrounded by a loose rubber membrane to prevent evaporation.

The change in u_w cannot in this case be attributed to loss of air through the membrane. It can only be put down to a rearrangement of the water films and air-water menisci in the soil or to changes due to the clay minerals.

When the soil is first compacted, the air-water menisci are bound to be more or less haphazardly arranged. Radii of curvature will be non-uniform, interconnected air voids will be interspersed with closed bubbles of various sizes, etc. Before equilibrium can be established, all air-water menisci have to equalise to a common average curvature. This equalisation will probably occur by the disappearance of the small bubbles and the growth of the larger bubbles to form interconnected voids. It will be shown in section (9.8) how this redistribution could cause an overall decrease in

volume and also a decrease in u_w.

(9.8) Simulation of the non-equilibrium behaviour of partly saturated soils by a simple model.

One aspect of the behaviour of a freshly compacted partly saturated soil which is puzzling at first sight is shown in fig.(9.6). Here, a decrease in pore water pressure is accompanied by a decrease in volume. This phenomenon can be simulated by means of a simple model consisting of a bubble of air contained in a sealed compressible container. The sealed container represents the compressible soil skeleton, while the water and air it contains represent the gaseous and liquid components of the pore fluid. The curved air-water interfaces of the pore water menisci are represented by the spherical surface of the bubble.

The first stage of the present investigation was to find whether the effects of surface tension in combination with Henry's law could cause changes in volume in a system consisting of an air bubble in air-saturated water at atmospheric pressure. This represented the limiting case of the pore fluid in a partly saturated soil of infinite compressibility.

It is a common misconception that it requires an infinite pressure to dissolve a bubble in water. The argument is as follows:

The pressure in a bubble of radius r contained in water at pressure u_w is:

$$u_a = u_w + 2T/r$$

therefore as r tends to zero, u_a tends to infinity. This is untrue.

A small bubble should in fact spontaneously dissolve in air saturated water maintained at atmospheric pressure. Since the pressure

of the air in the bubble exceeds that in the water by $2T/r$, the air should dissolve according to Henry's law and the solution rate should accelerate as the radius decreases.

To observe this expected phenomenon the following experiment was performed.

A small quantity of distilled water was placed in a watch glass and left in a dust free cupboard for some days to ensure that it was air-saturated. Using a hypodermic syringe, a drop of this water was suspended from the underside of a slip of glass. A large bubble was blown in the drop using the hypodermic syringe and when this burst, it left several minute bubbles behind. One of these bubbles was then observed through a microscope, the diameter being measured using a graticule. To prevent the drop of water from evaporating, the slip of glass was placed across a conical depression in a polished piece of perspex, the depression containing a second drop of water.

In every case, the bubble radius decreased slowly at first and then at accelerating rate and the bubble finally vanished.

The variations in radius with time for five bubbles of various initial radii are shown in fig. (9.8). This established that the effects of surface tension alone were capable of producing volume changes and also showed that solution by Henry's law takes place in a finite time and not almost instantaneously. The next step was to introduce the effect of a soil skeleton of finite compressibility.

The compressible container consisted of a small perspex block with a conical depression in it. An O-ring was set into a groove in the perspex around the depression. The depression was covered and

sealed by a plate of perspex which was fastened down to the block by four screws. The pressure in the container could be varied by tightening or loosening the screws.

The perspex block with its cover in position, but with the screws slack, was immersed in air-saturated distilled water and a small bubble was introduced into the cavity. The screws were then just tightened enough to take up slack but not enough to compress the container. The container was now removed from the water and the initial diameter of the bubble at atmospheric water pressure was measured. The screws were rapidly tightened and the new initial radius of the bubble was measured. Then the changes of radius of the bubble with time were recorded.

Fig. (9.9) shows a set of four radius-time curves for bubbles of various initial sizes dissolving in the elastic container. The curves are very similar to those obtained for the free bubbles. Once the bubbles had completely disappeared, they could be made to re-appear by slackening the screws.

The relation between changes in volume of the dissolving bubble and the pressure in the water in the sealed container can be found as follows:

Let the bubble dissolve until its volume changes by dV_a.

The corresponding change in volume of the container will be:

$$dV = C_c V d\sigma'$$

where

V is the volume of the container.

$d\sigma'$ is the change in stress in the container caused by dV.

C_c is the compressibility of the container.

For compatibility of strains $dV_a = dV$.

Hence

$$\frac{dV}{V} = C_c d\sigma' \qquad \text{or} \qquad \log_e V = C_c \sigma' + K$$

If r is the radius of the bubble and V_w the volume of water in the container

$$V = V_w + 4/3\pi r^3.$$

Suppose that at $r = r_o$, $\sigma' = \sigma'_o$

then $$K = \log_e(V_w + 4/3\pi r_o^3) - C_c\sigma'_o$$

i.e. $$C_c(\sigma' - \sigma'_o) = \log_e\left[\frac{V_w + 4/3\pi r^3}{V_w + 4/3\pi r_o^3}\right] = \log_e\left[\frac{V_w}{V_w + V_{a_o}} + \frac{V_a/V_{a_o}}{1 + \frac{V_w}{V_{a_o}}}\right]$$

Note that $\frac{V_w}{V_w + V_{a_o}} = S_o$ and $1 + \frac{V_w}{V_{a_o}} = \frac{1}{1 - S_o}$

hence $$C_c(\sigma' - \sigma'_o) = \log_e\left[S_o + (1 - S_o)\left(\frac{r}{r_o}\right)^3\right] \qquad \text{E(9.11)}$$

Since the interior of the container is everywhere in contact with water:

$$d\sigma' = du_w$$

or $$(\sigma' - \sigma'_o) = (u_w - u_{w_o})$$

and $$u_w = u_{w_o} + \frac{1}{C_c}\log_e\left[S_o + (1 - S_o)\left(\frac{r}{r_o}\right)^3\right] \qquad \text{E(9.12)}$$

In this expression provided $r/r_o < 1$, the 'log' term is negative, and decreasing values of the bubble radius lead to a decreasing pressure in the water.

u_{w_o} and C_c for the system could be calculated by applying Boyle's law to the sudden initial change in volume on tightening the screws. Boyle's law gave an estimate of the initial pressure in the bubble: u_{a_o} and $u_{w_o} = u_{a_o} - \frac{2T}{r_o}$. The change in volume of the container was calculated from the change in radius of the bubble.

Fig. (9.10) shows three pressure-time curves calculated from the data of fig. (9.9) using equation E(9.12). These curves are very similar in shape to the suction-time curves found with freshly compacted soil.

Unless the degree of saturation of the model soil was very high ($>99\%$) the compressibility of the container was too low to allow the bubbles to dissolve completely. Fig. (9.11) shows a set of curves for four bubbles which did not dissolve completely. The initial and final degrees of saturation are given. Here again the likeness of these curves to suction-time curves for a soil is striking.

The next step in the investigation was to observe the air-water menisci in a partly saturated soil after a sudden stress change. To do this a quantity of very fine uniform moist sand was placed in the depression of the compressible container and the cover was screwed down. At first the air-water menisci were arranged haphazardly, were of different radii and several complete bubbles were visible. Soon the complete bubbles had disappeared and after a time the air was arranged in an interconnected network similar to that illustrated in Chapter 5 (fig. (5.1)). Incidentally, the structure illustrated in fig. (5.1) is the only one which explains how $(u_a - u_w)$ can decrease as S increases. Compression of the soil skeleton to increase S will cause the menisci to flatten and advance into the voids. Hence the radii of curvature will increase and $(u_a - u_w)$ will decrease. In any structure containing completely closed bubbles, an increase in S will cause an increase in $(u_a - u_w)$.

It thus appears unlikely that a partly saturated soil <u>in</u>

equilibrium will contain any completely enclosed bubbles.

The pressure on the soil was increased and the radius of curvature of one of the menisci in contact with the perspex cover plate was observed. The radius-time curve is shown in fig. (9.11). This showed by direct observation that the behaviour of the bubble model was very similar to that of a partly saturated soil.

(9.9) Calculated variation of pore water and pore air pressure in a compacted soil.

Equation E(9.12) can be used to calculate the variation in pore air and water pressure with decreasing radii of curvature of the air-water menisci under completely undrained conditions.

This calculation was carried out as an example for two samples of Mangla shale. The compressibility of the soil was estimated by oedometer tests. For the purpose of the calculation, the soil was assumed to be divided into a number of small elements, each consisting of a single bubble in a compressible container. Starting off with an initial measured suction and assuming that the pressure in the pore air was initially atmospheric, values of u_a and u_w were calculated for decreasing values of the radius of curvature r.

The calculated curves for the two samples of Mangla shale are shown in fig. (9.12). While the decrease in radius of the air bubbles has a relatively small effect on $(u_a - u_w) = 2T/r$, the compressibility of the soil skeleton causes a much larger decrease in the value of u_w. Thus one would expect the variation of u_w and u_a with time in a freshly compacted soil under completely undrained conditions to be represented by a pair of lines for decreasing u_a and u_w with $(u_a - u_w)$ almost constant. The true variation of u_a for

small times in a freshly compacted soil is difficult to measure, but for large times measurements by Donald (1961) using a sample surrounded by mercury have confirmed this idea.

The reverse of this effect is shown by fig. (9.13) which represents changes in air and water pore pressures in a sample of Mangla shale which had been saturated by compression at constant water content. The sample was allowed to come to equilibrium and the cell pressure was suddenly decreased. After the initial rapid expansion of the sample, $(u_a - u_w)$ remained fairly constant, but u_a increased slowly as air came out of solution in the pore water.

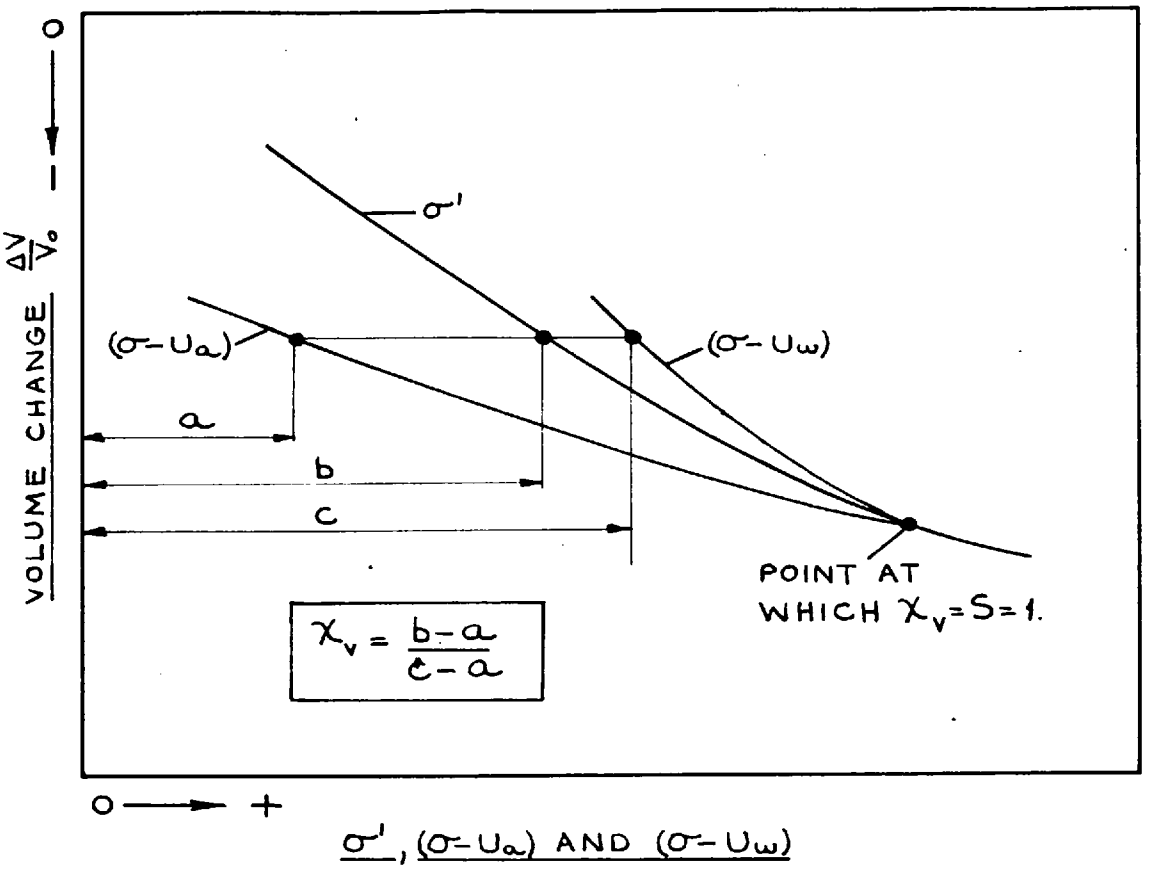
(9.10) Summary.

(a) The evidence of two tests seems to show that in compacted soils, the variation between α and S for volume change is similar to that for shear.

(b) A chart has been constructed for predicting pore air pressures from volume changes of a soil under undrained conditions.

(c) Some of the features of non-equilibrium pore pressures in compacted soils have been pointed out and possible mechanisms for the pore pressure changes have been suggested.

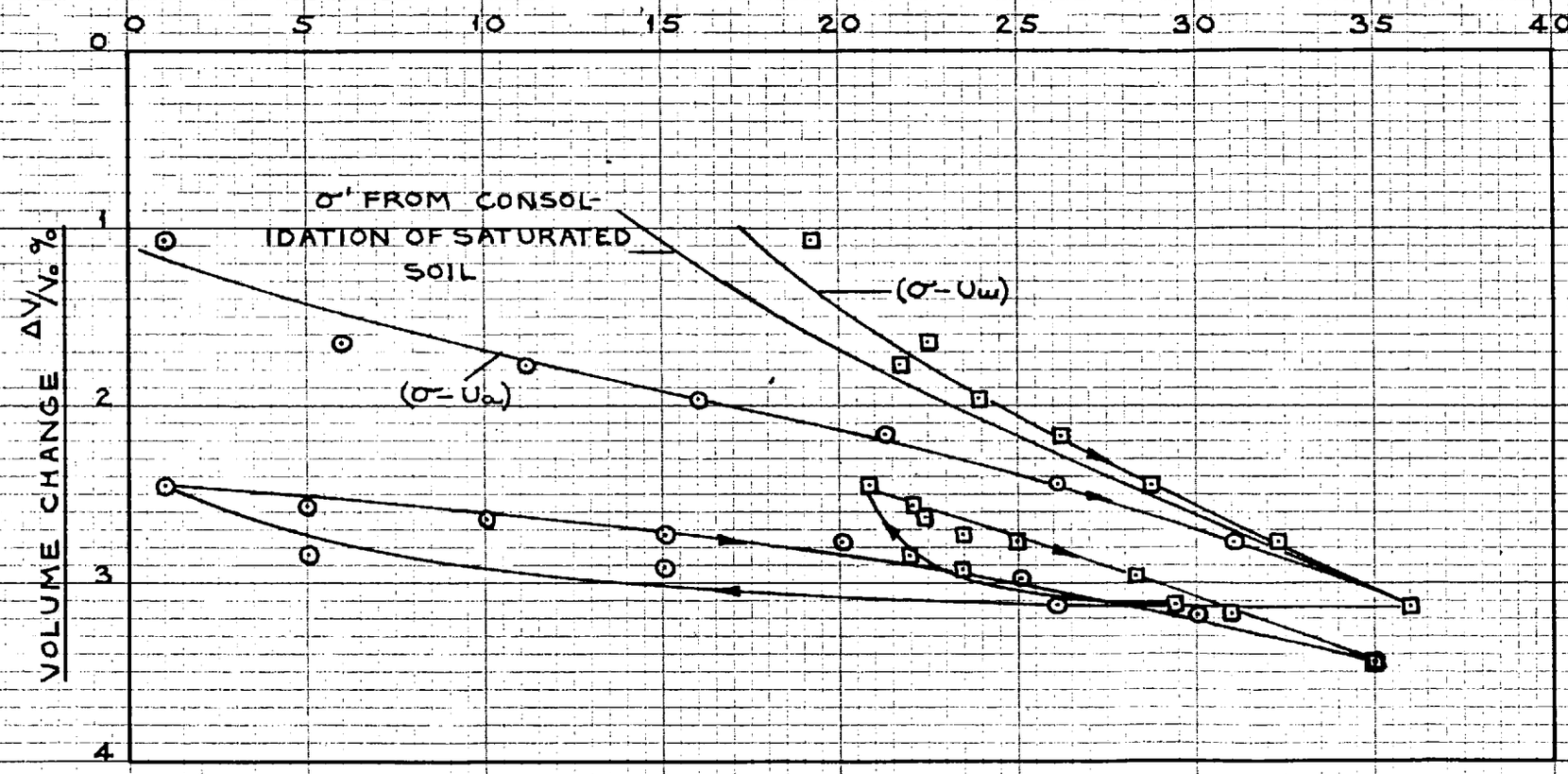
(d) The effect of solution of the pore air in the pore water according to Henry's law has been illustrated by the behaviour of a bubble model.

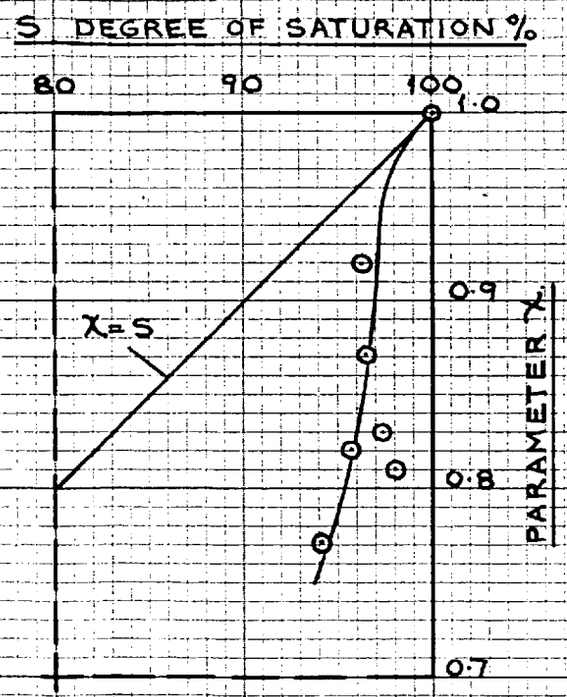


σ', $(\sigma - U_a)$ AND $(\sigma - U_w)$

SEMI-GRAPHICAL METHOD OF DETERMINING χ_v IN THE EQUATION: $\Delta(\sigma - U_a) + \chi_v \Delta(U_a - U_w) = -\frac{1}{C_c} \cdot \frac{\Delta V}{V_0}$

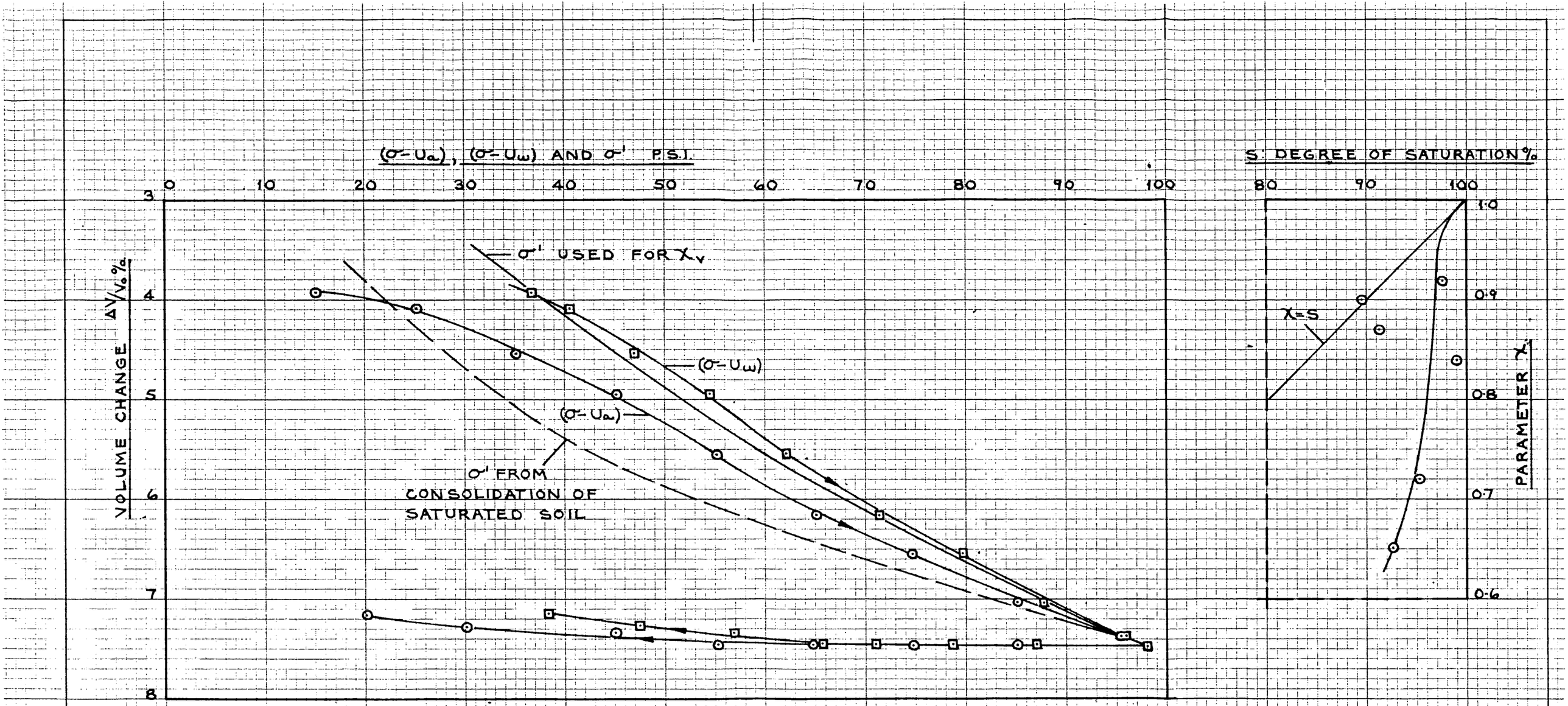
FIG. 9.1.





VALUES OF χ_v FROM TEST ON SAMPLE OF MANGLA SHALE COMPACTED AT 18.1% WATER CONTENT AND COMPRESSED WITH CONTROLLED PORE AIR PRESSURE AT CONSTANT WATER CONTENT.

FIG. 9.2.



VALUES OF X_v FROM TEST ON SAMPLE OF SELSET CLAY COMPACTED AT 11·7 % WATER CONTENT AND COMPRESSED WITH CONTROLLED PORE AIR PRESSURE AT CONSTANT WATER CONTENT.

FIG. 9.3.

$\theta = 20°C$

$R = 82.06 \ \frac{CC.\ ATM.}{°K.\ MOLE.}$

$H = 66,400$ ATM./MOLE/MOLE.

PORE AIR PRESSURE P.S.I.

VALUES OF N

80x10⁻⁵
60x10⁻⁵
50x10⁻⁵
40x10⁻⁵
35x10⁻⁵
30x10⁻⁵
25x10⁻⁵
20x10⁻⁵
16x10⁻⁵
12x10⁻⁵
8x10⁻⁵
4x10⁻⁵
2x10⁻⁵
1x10⁻⁵

40 35 30 25 20 15 10 5 0 -5 -10 -15

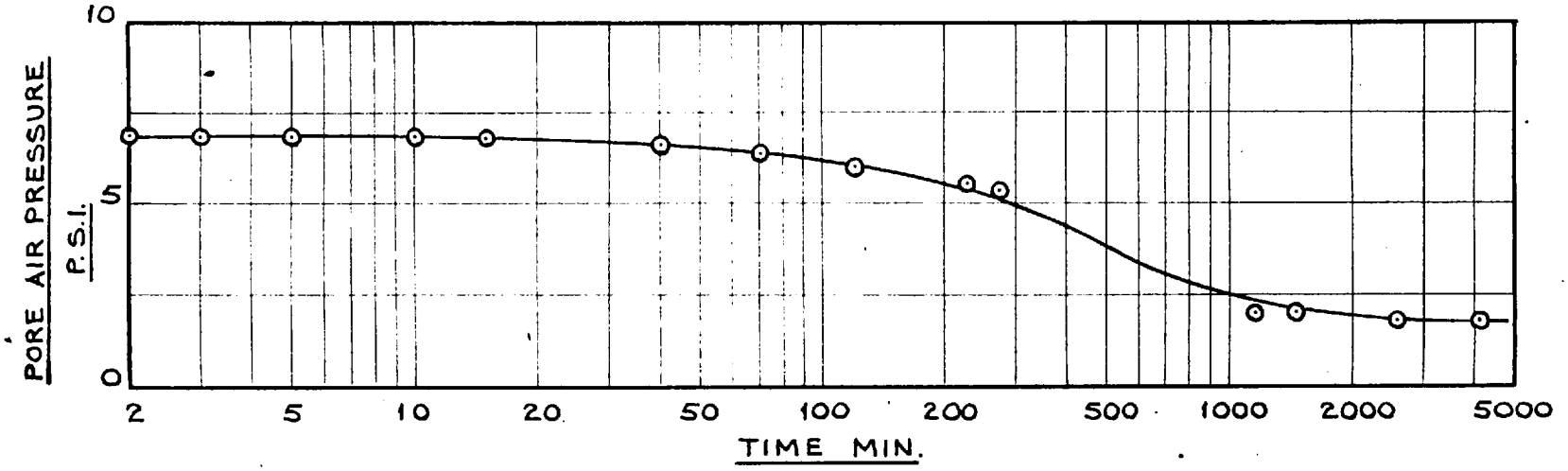
65 70 75 80 85 90 95 100

DEGREE OF SATURATION S %.

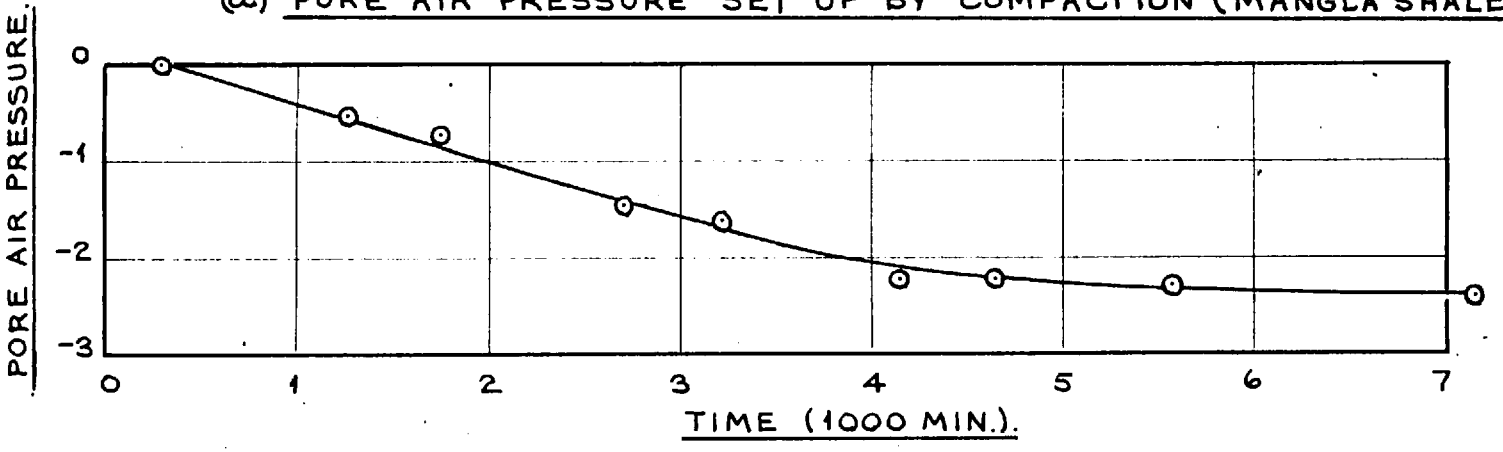
CALCULATED VARIATION OF PORE AIR PRESSURE WITH DEGREE OF SATURATION IN UNDRAINED COMPRESSION OF PARTLY SATURATED SOIL.

FROM: $U_a = \frac{NR\theta}{\left[\frac{1-S}{S}\frac{\omega_w}{\rho_w} + \frac{R\theta}{H}\right]}$, $N = \frac{m_a/\omega_a}{m_w/\omega_w}$

FIG. 9.4.



(a) PORE AIR PRESSURE SET UP BY COMPACTION (MANGLA SHALE).



(b) CHANGE IN PORE AIR PRESSURE IN A SAMPLE OF COMPACTED TALYBONT CLAY UNDER TRUE UNDRAINED CONDITIONS (SAMPLE UNCONFINED).

FIG. 9.5.

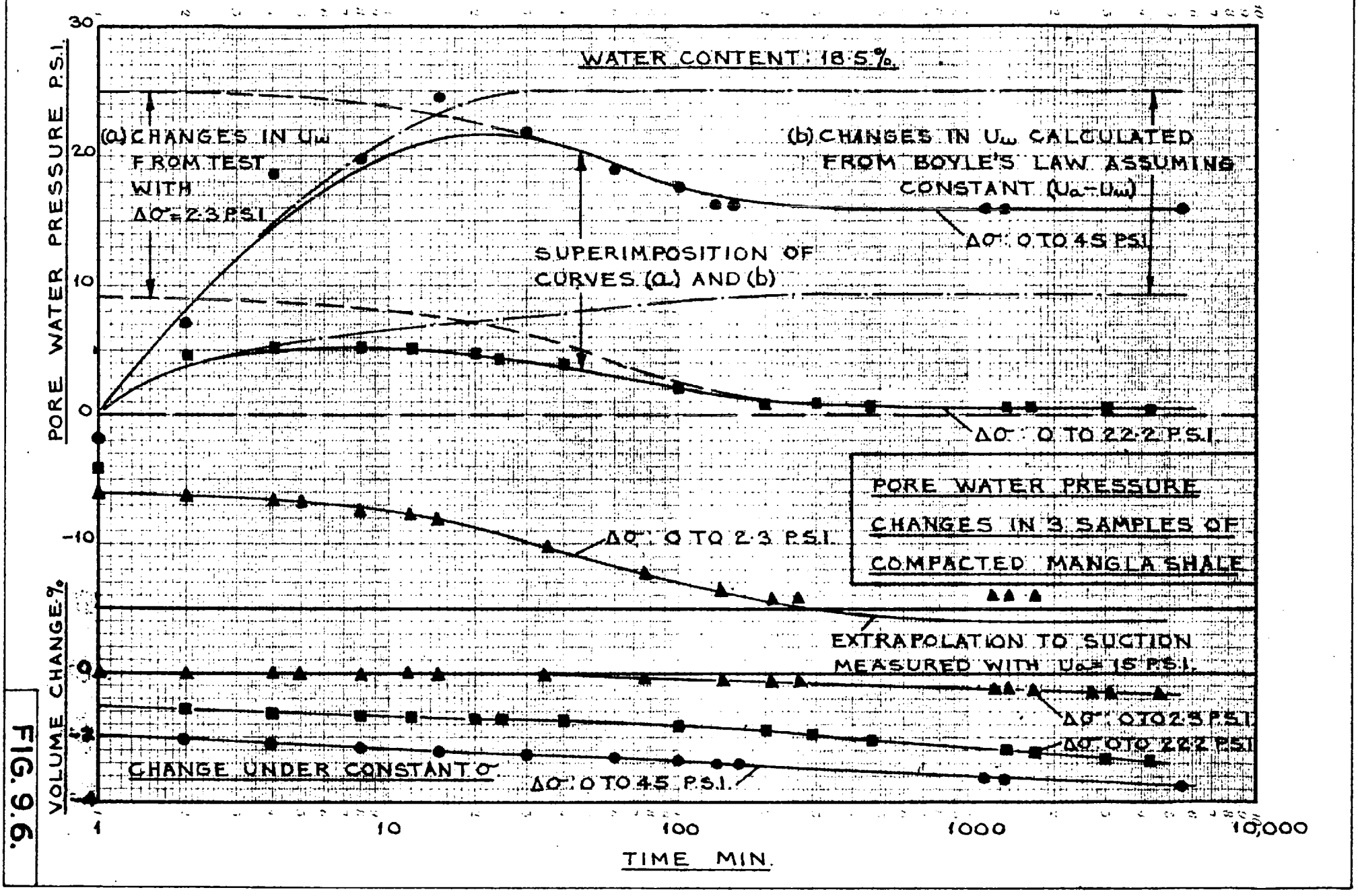

WATER CONTENT: 18.5%
(a) CHANGES IN U_w FROM TEST WITH $\Delta\sigma$=2.3 P.S.I.
(b) CHANGES IN U_w CALCULATED FROM BOYLE'S LAW ASSUMING CONSTANT $(U_a - U_w)$
SUPERIMPOSITION OF CURVES (a) AND (b)
$\Delta\sigma$: 0 TO 45 P.S.I.
$\Delta\sigma$: 0 TO 22.2 P.S.I.
$\Delta\sigma$: 0 TO 2.3 P.S.I.
PORE WATER PRESSURE CHANGES IN 3 SAMPLES OF COMPACTED MANGLA SHALE
EXTRAPOLATION TO SUCTION MEASURED WITH U_a= 15 P.S.I.
$\Delta\sigma$: 0 TO 2.3 P.S.I.
$\Delta\sigma$: 0 TO 22.2 P.S.I.
CHANGE UNDER CONSTANT σ
$\Delta\sigma$: 0 TO 45 P.S.I.
PORE WATER PRESSURE P.S.I.
VOLUME CHANGE %
30
20
10
0
-10
-9
-8
1
10
100
1000
10,000
TIME MIN.

FIG. 9.6.

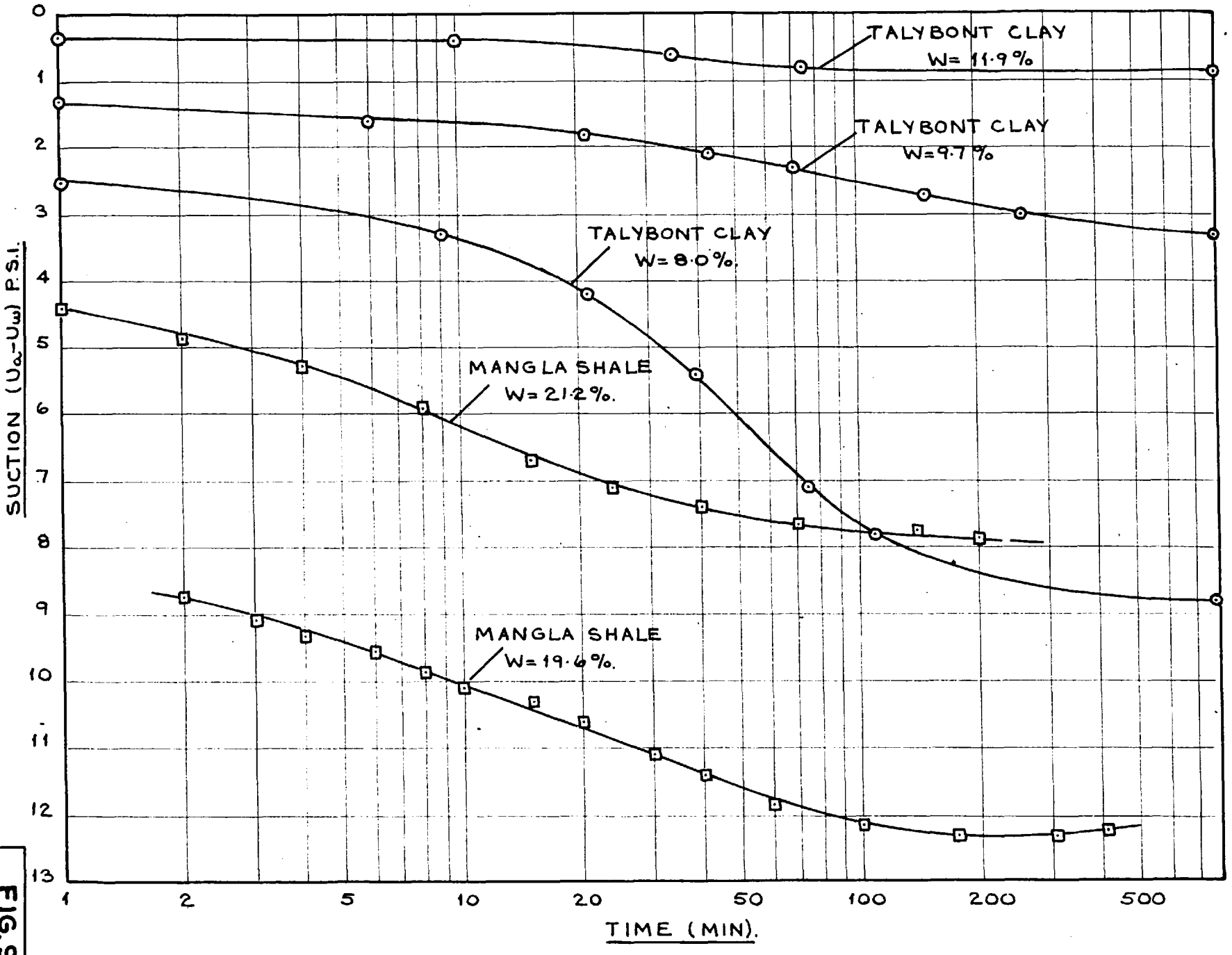


FIG. 9.7.

SUCTION CHANGES IN FIVE FRESHLY COMPACTED UNCONFINED SOIL SAMPLES.

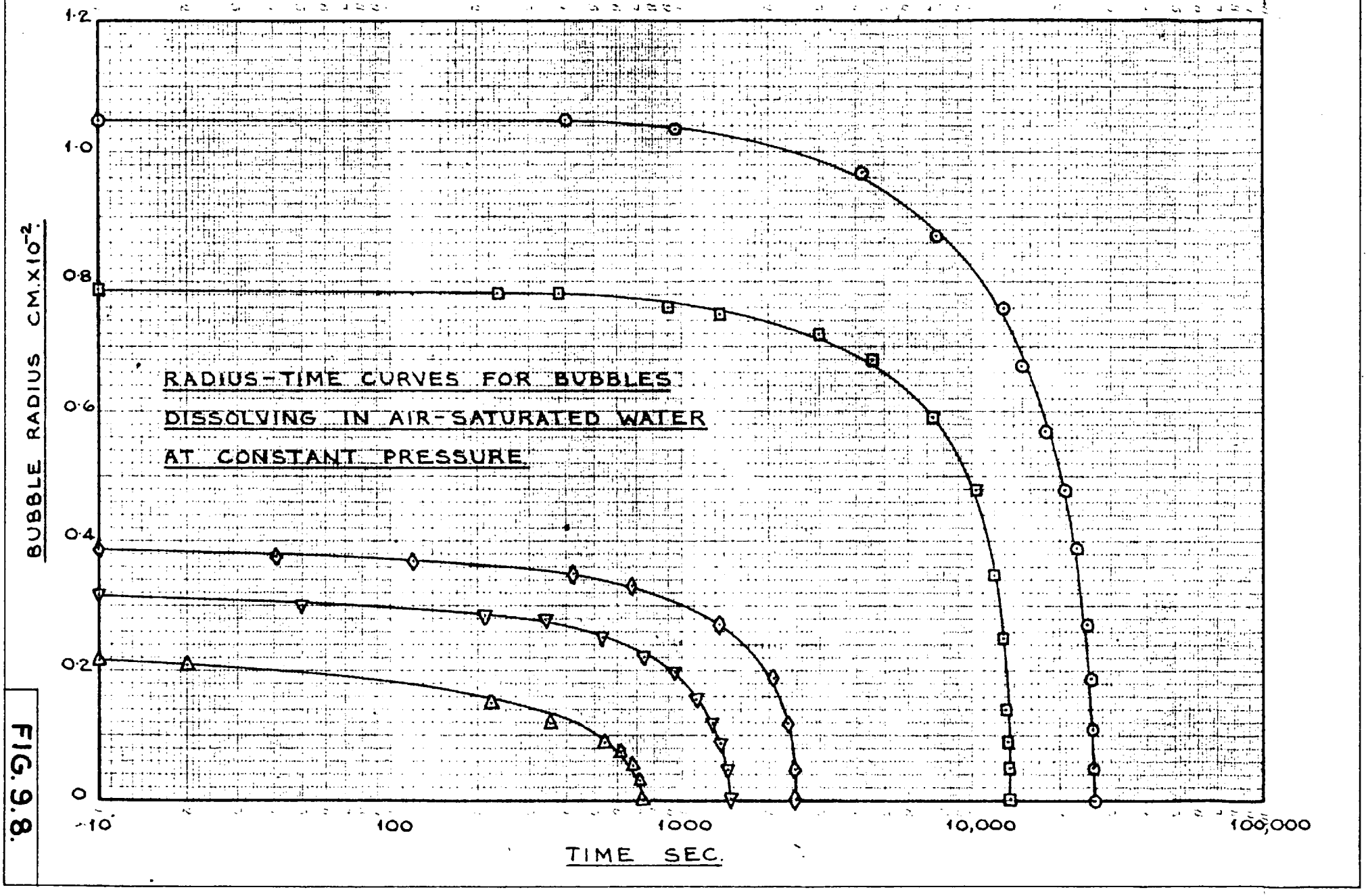

1·2
1·0
0·8
0·6
0·4
0·2
0
BUBBLE RADIUS CM.X10⁻².
RADIUS-TIME CURVES FOR BUBBLES
DISSOLVING IN AIR-SATURATED WATER
AT CONSTANT PRESSURE.
10
100
1000
10,000
100,000
TIME SEC.

FIG. 9.8.

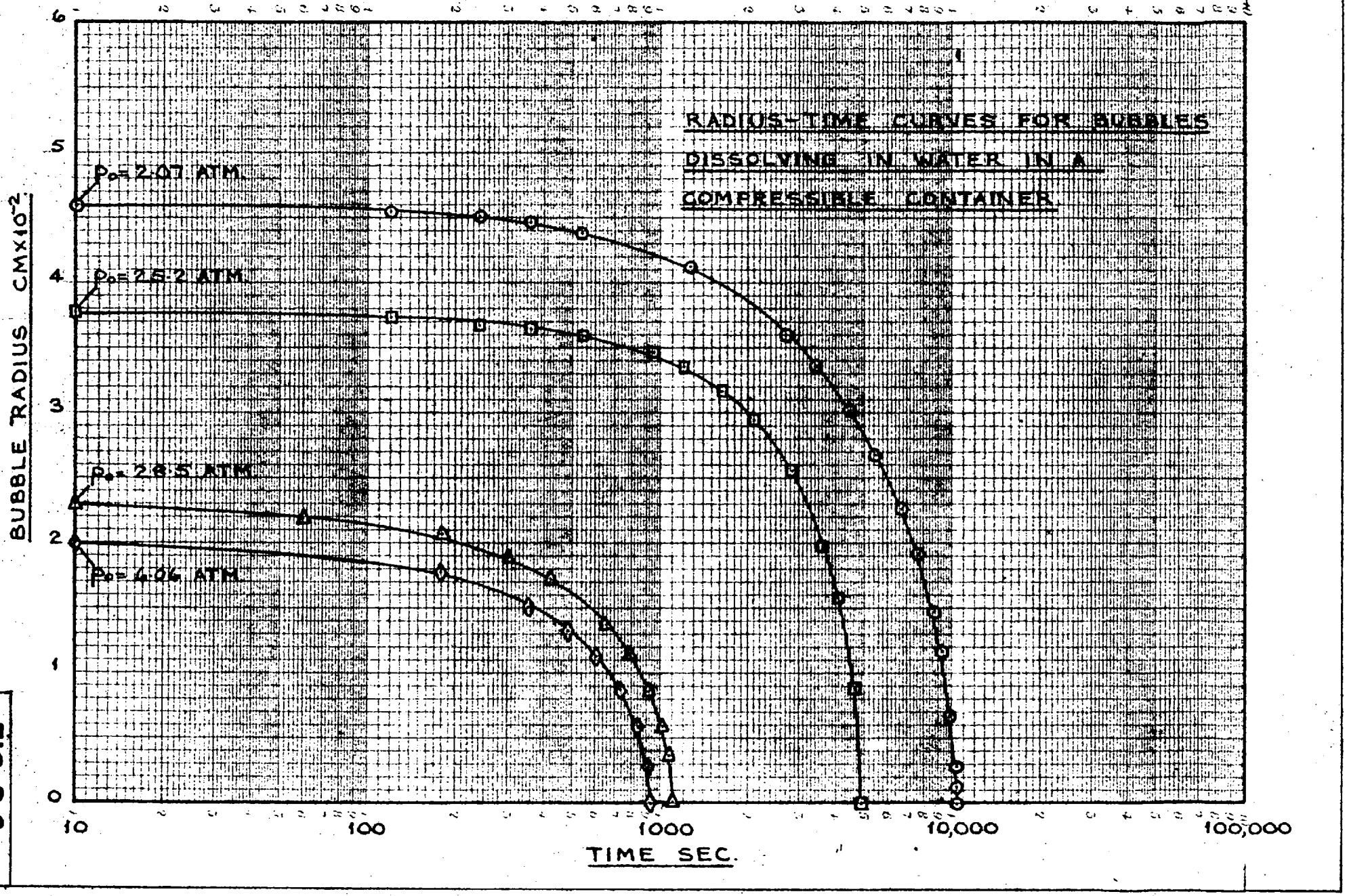

RADIUS-TIME CURVES FOR BUBBLES DISSOLVING IN WATER IN A COMPRESSIBLE CONTAINER
P_o= 2.07 ATM.
P_o= 2.52 ATM.
P_o= 2.85 ATM.
P_o= 4.04 ATM.
BUBBLE RADIUS CM X 10^{-2}
TIME SEC.
0
1
2
3
4
5
6
10
100
1000
10,000
100,000

FIG. 9.9.

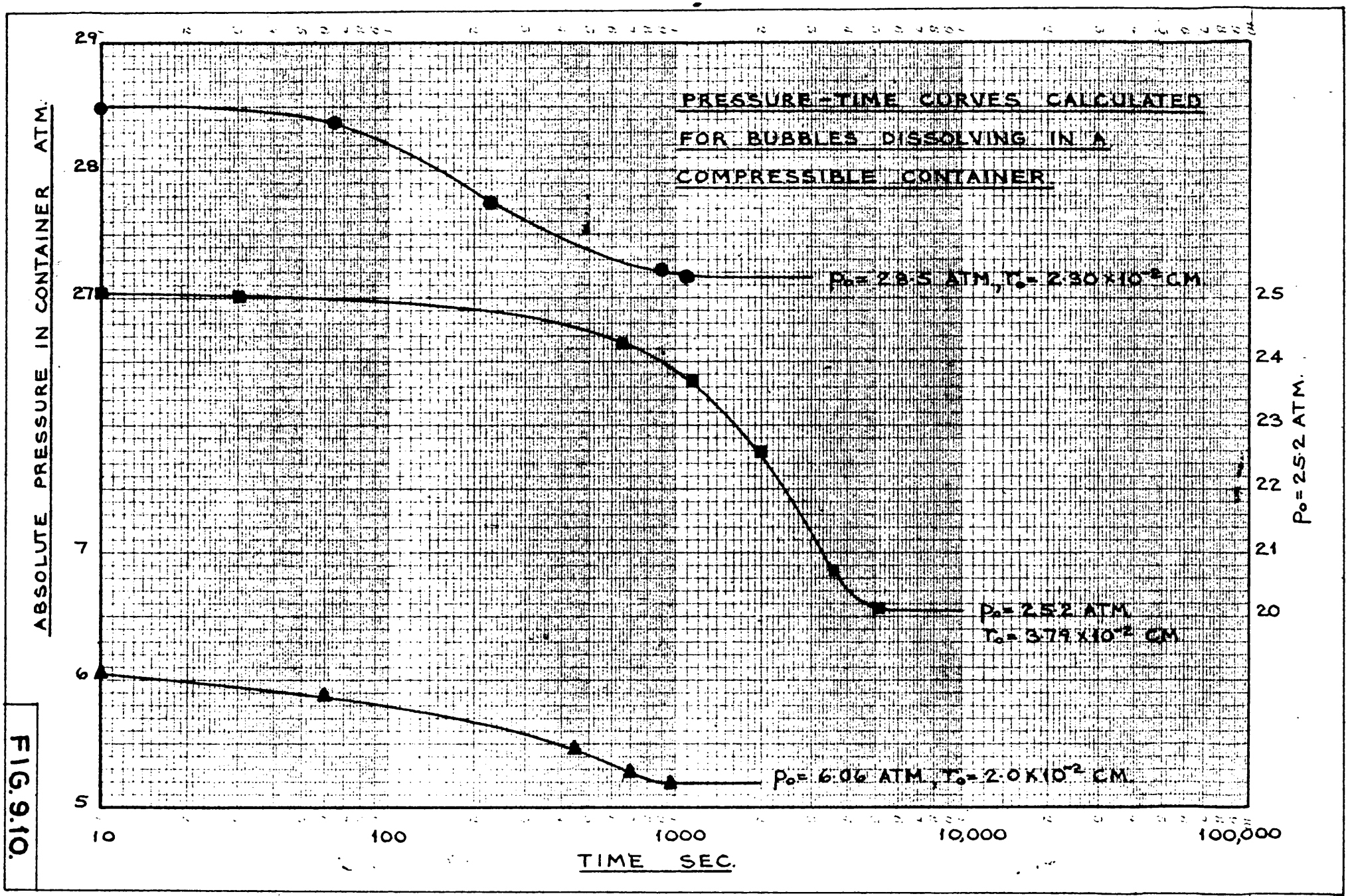

PRESSURE-TIME CURVES CALCULATED FOR BUBBLES DISSOLVING IN A COMPRESSIBLE CONTAINER.
ABSOLUTE PRESSURE IN CONTAINER ATM.
TIME SEC.
29
28
27
7
6
5
25
24
23
22
21
20
10
100
1000
10,000
100,000
P_o= 28·5 ATM, T_o= 2·30 x 10^{-2} CM.
P_o= 25·2 ATM. T_o= 3·79 x 10^{-2} CM.
P_o= 6·06 ATM, T_o= 2·0 x 10^{-2} CM.
P_o= 25·2 ATM.

FIG. 9.10.

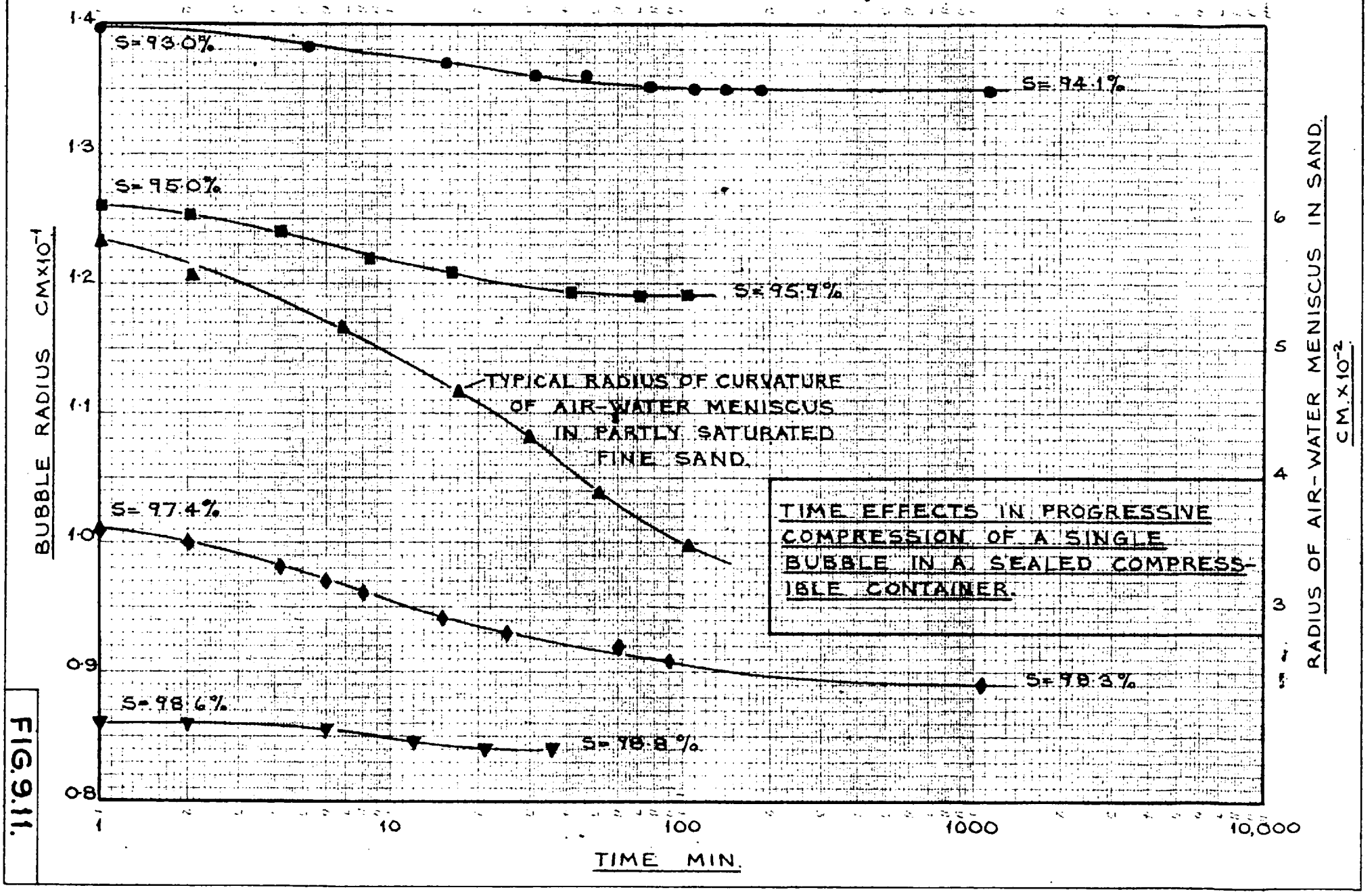
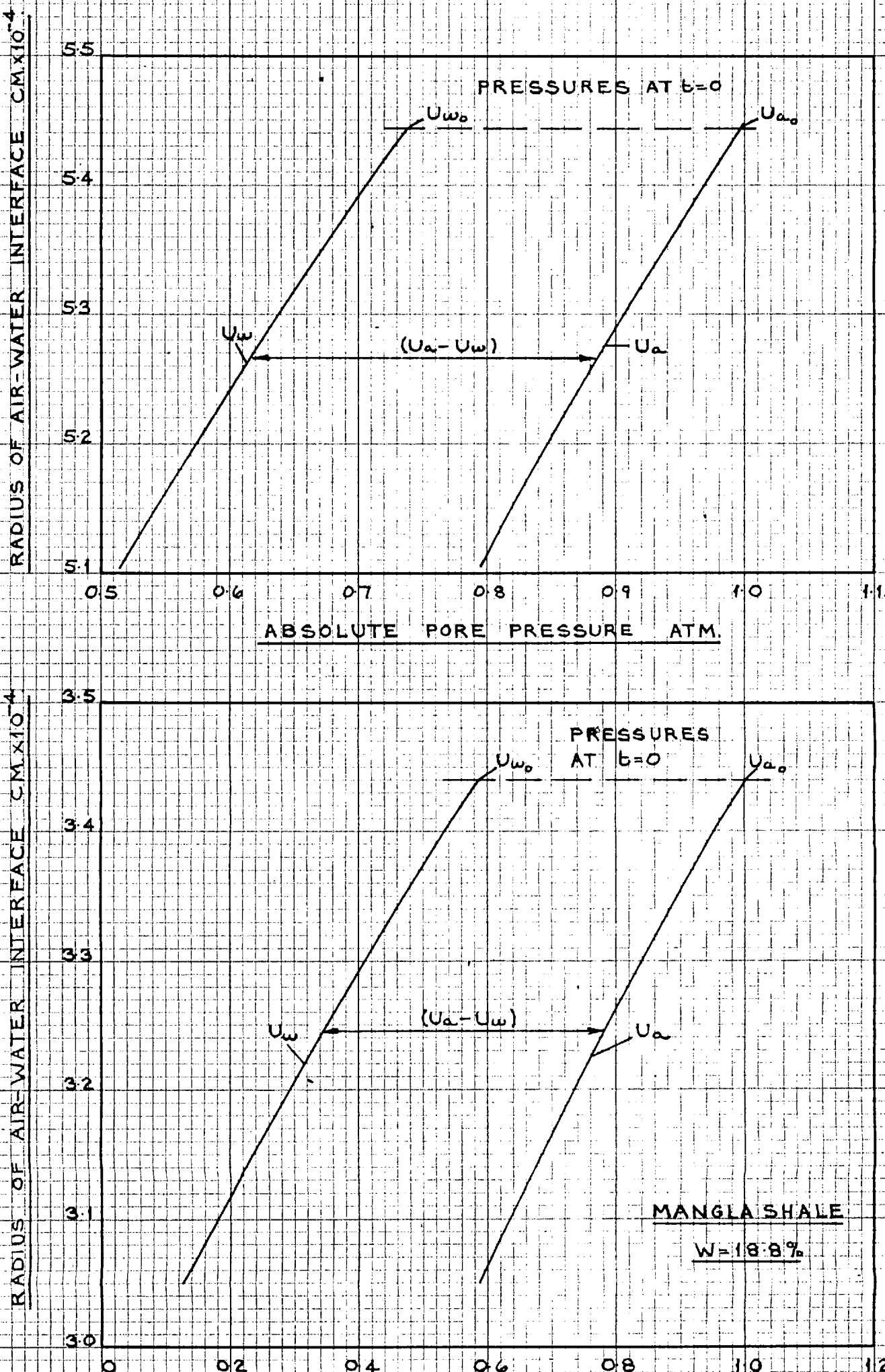

BUBBLE RADIUS CM X 10⁻¹
RADIUS OF AIR-WATER MENISCUS IN SAND CM. X 10⁻²
TIME MIN.
1·4
1·3
1·2
1·1
1·0
0·9
0·8
1
10
100
1000
10,000
6
5
4
3
2
1
S=93·0%
S=94·1%
S=95·0%
S=95·9%
S=97·4%
S=98·3%
S=98·6%
S=98·8%
TYPICAL RADIUS OF CURVATURE OF AIR-WATER MENISCUS IN PARTLY SATURATED FINE SAND.
TIME EFFECTS IN PROGRESSIVE COMPRESSION OF A SINGLE BUBBLE IN A SEALED COMPRESSIBLE CONTAINER.

FIG. 9.11.



CALCULATED VARIATION OF PORE PRESSURE WITH RADIUS OF AIR-WATER INTERFACE FOR TWO FRESHLY COMPACTED SAMPLES OF MANGLA SHALE.

FIG. 9.12.

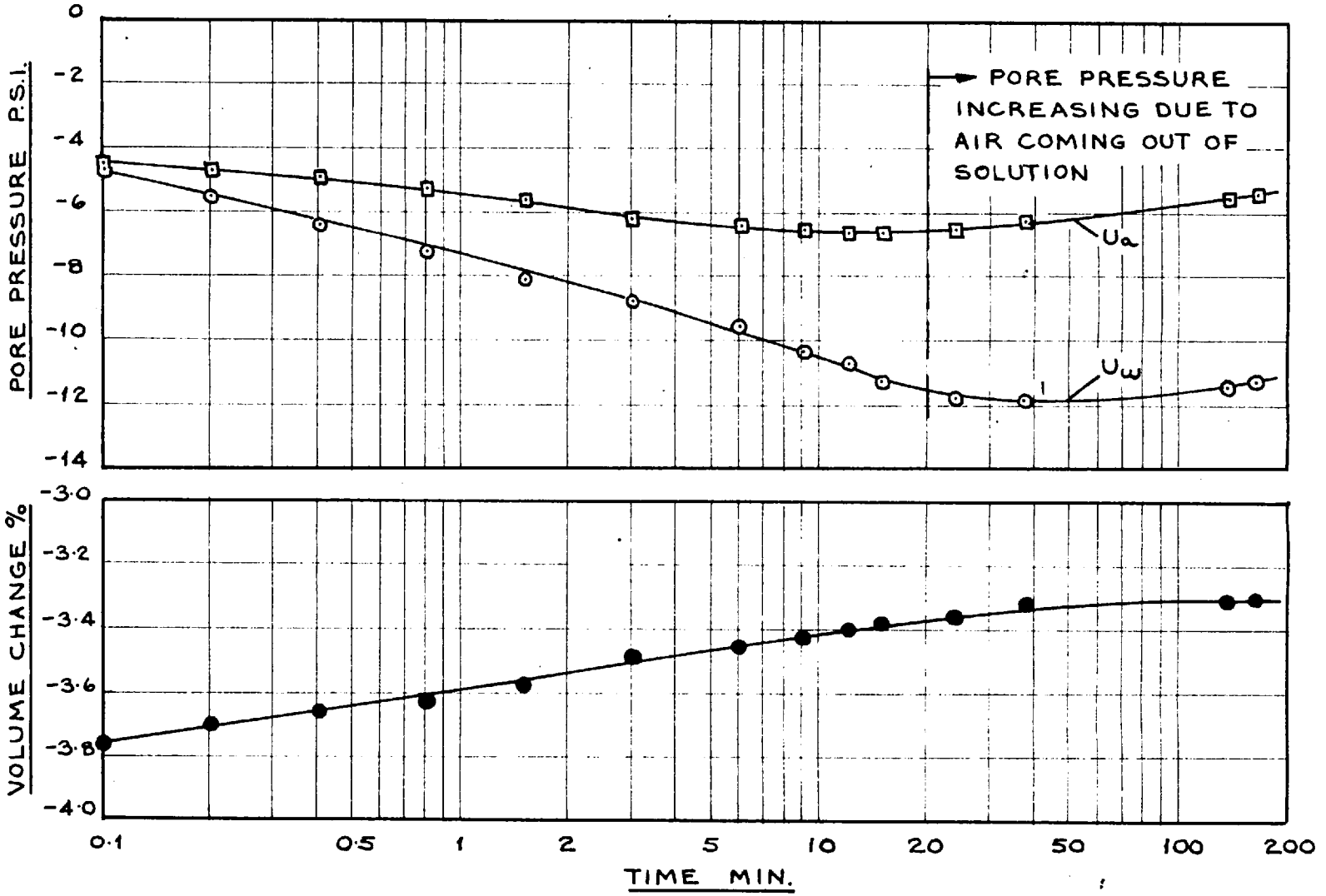


FIG. 9.13.

PORE PRESSURE CHANGES IN A SAMPLE OF COMPACTED MANGLA SHALE AFTER SUDDEN REDUCTION OF CELL PRESSURE.

CHAPTER 10

THE FLOW OF AIR THROUGH DRY SOILS

The work described in this chapter is part of a preliminary investigation into the more general problem of the consolidation of partly saturated soils. The process of consolidation in a partly saturated soil is extremely complex and appears to depend on a number of factors concerning which very little experimental information has been published. Without further information on these subjects, little progress can be made on the problem as a whole.

(10.1) Summary of factors affecting consolidation in partly saturated soils.

Consolidation in a partly saturated soil, as in a fully saturated soil is basically a process of mass transfer or flow of the pore fluid from one region of the soil to another. This flow is due to a pressure gradient set up in the pore fluid due to the application of external loads or due to other causes and results in a gradual transfer of load from the pore fluid to the soil skeleton.

The consolidation process in a partly saturated soil differs from that in a fully saturated soil in the following respects:

(a) In a saturated soil the pore fluid is water only which is relatively incompressible. In a partly saturated soil the pore fluid is a two-component, two-phase fluid of air and water which is compressible.

(b) In a saturated soil from which drainage is prevented, any increase in total load on the soil is supported entirely

by an increase in pore pressure, the effective stresses remaining unchanged. In a partly saturated soil, an increase in total load on the soil will be supported partly by an increase in pore pressure and partly by an increase in effective stress.

(c) The two components of the pore fluid are mutually soluble. The air component exists in the gaseous phase as gaseous air and in the liquid phase in solution in the pore water. The water component exists in the liquid phase and also in the gaseous phase as water vapour. Because of this state of affairs, any change in pressure, volume or temperature will lead to a certain interchange of mass between the two phases.

(d) Because of the two phase character of the pore fluid the soil contains innumerable gas liquid interfaces which call into play the forces of surface tension. The result of the surface tension forces is that the two phases will generally be in equilibrium under differing pressures.

(e) The principle of effective stress which governs the distribution of the total stress in a soil between the soil skeleton and the pore fluid is straight-forward in saturated soils. In partly saturated soils it is complicated by certain factors:

(i) The differing pressures in the two phases of the pore fluid.

(ii) The differing compressibilities of the two phases.

(iii) The differing areas of the soil skeleton over

which the pore fluid pressures act.

(iv) The action of capillary tensions between the grains of the soil skeleton.

(f) In formulating the equations for flow of the composite pore fluid, other difficulties are met with, viz:

(i) The known laws for the flow of liquids and gases through porous media are of basically the same type, but differ somewhat in formulation and in the variables employed.

(ii) Both laws have been established for flow through channels of constant cross-section whereas in a consolidating soil the cross-sections of the flow channels are continually varying both due to compression of the soil skeleton and due to the varying proportions of space occupied by the liquid and gas phases.

(iii) Both laws relate to flow past boundaries fixed in space. In actual fact, in a soil of low permeability, the rate of movement of the soil skeleton as it compresses during consolidation might be of the same order of magnitude as the velocity of the escaping pore fluid.

(g) Nothing has been said as yet of the interaction between the pore fluid and the clay minerals composing the soil skeleton. This interaction is known to occur in practically every soil and is known to have a very important influence on flow through partly saturated soils. As this interaction is as

yet imperfectly understood and is of an extremely complicated nature, it will be ignored for the present. The soil skeleton will be assumed to be a completely inert assemblage of solid particles, the physico-chemical properties of which play no part in the consolidation process.

The main questions which must be settled before any progress can be made with the problem of consolidation in a partly saturated soil are those posed by (e) and (f).

The principle of effective stress for partly saturated soils has been considered earlier in this thesis from the point of view of shear strength, and to a lesser extent, volume change. We will now consider the laws of fluid flow in partly saturated soils.

(10.2) Nomenclature of this chapter.

The nomenclature of this chapter is slightly different to that used in the rest of the thesis. The following is a list of symbols and their meanings:

Suffices:

a denotes a property of the air phase.

w " " " " " water phase.

s " " " " " soil skeleton.

f " " " " a fluid.

p = pore pressure in absolute units.

v = velocity = volume of flow per unit area of pore space per unit time.

m = mass.

z = linear dimension along axis in direction of flow.

t = time.

μ = viscosity.

ρ = fluid density.

A = cross-sectional area normal to direction of flow.

R = universal gas constant.

w = molecular weight.

θ = absolute temperature.

V = volume.

n = porosity.

S = degree of saturation.

F = a mass per unit volume per unit area.

g = acceleration due to gravity.

k, D, B = transmission constants or measureable parameters.

Z = a force component in direction z.

σ = a total stress.

σ' = an effective stress.

T = surface tension of water.

r = average radius of curvature of the air-water interfaces in the pore fluid.

(10.3) The laws of fluid flow through partly saturated soils.

Opinions differ as to which is the most general form of the law governing the flow of fluids through porous media. There are two clear cut schools of thought one of which supports D'Arcy's law and the other Fick's law.

For flow through porous media, it does not appear to be possible to derive either of these laws from first principles. The form of the equations can, however, be obtained by analogy with flow through various model systems such as bundles of straight

capillary tubes of various diameters, etc.

D'Arcy's Law:

Scheidegger (1957) states that there is no unique way of expressing this law in a general form which is applicable to the flow of both gases and liquids. He quotes two forms:

(a) That due to Hubbert:

If $$F = \int_{p_o}^{p} \frac{dp}{\rho(p)} + gz; \quad v = -\frac{k\rho}{\mu} \cdot \frac{\partial F}{\partial z} \qquad E(10.1)a$$

(b) That due to Gardner, Collier & Farr:

$$\psi = \frac{kp}{\mu} + \int_{z_o}^{z} \frac{k\rho g}{\mu} dz; \quad v = -\frac{\partial \psi}{\partial z} \qquad E(10.1)b$$

Neglecting for simplicity the gravitational terms and taking as the equation of state for air: $pV = \frac{m}{w} R\theta$, both equations reduce for both air and water flow to:

$$v = -\frac{k}{\mu} \cdot \frac{\partial p}{\partial z} \qquad E(10.1)c$$

Fick's Law:

This can be stated in its simplest form as:

$$\frac{\partial m}{\partial t} = -D\frac{\partial p}{\partial z} \qquad \text{(Adam, 1941)} \qquad E(10.2)$$

The minus sign indicates that the direction of flow is opposite to the direction of increasing p.

Justification for the use of Fick's Law.

(a) Various forms of this equation have been found to apply to almost every form of mass transport process. Amongst many others, Adam (1941) and Denbigh (1951) mention forms of it as being valid for: thermal, pressure and osmotic, migration of liquids through a permeable barrier. Crank (1957),

Philip (1957) and others apply it to the molecular diffusion of gases and liquids, adsorbtion problems, etc. For problems of partly saturated soils it has been found to apply to the movement of water vapour in soils under both temperature and electrical gradients (see Winterkorn (1947), Rollins & Spangler (1954), Low (1959)).

(b) It can be proved using thermodynamic reasoning that if equation E(10.2) holds for, say, mass flow under an osmotic gradient, it also holds for flow under pressure, concentration, electrical and thermal gradients in a gas-liquid system.

(c) Equation E(10.1)c is a particular form of equation E(10.2) for incompressible fluids, thus:

$$\frac{\partial m}{\partial t} = -D \frac{\partial p}{\partial z} \qquad \text{E(10.2)}$$

Dividing both sides by a constant fluid density and flow area:

$$v = \frac{-D}{A\rho} \frac{\partial p}{\partial z} = \frac{-k}{\mu} \frac{\partial p}{\partial z} \qquad \text{E(10.1)c}$$

For a perfect gas E(10.2) becomes:

$$v = \frac{-D}{A} \cdot \frac{R\theta}{wp} \cdot \frac{\partial p}{\partial z} = -k' \cdot \frac{R\theta}{w} \cdot \frac{1}{p} \cdot \frac{\partial p}{\partial z} \qquad \text{E(10.3)}$$

Justification for the use of D'Arcy's Law:

Many theories have been advanced in attempts to justify D'Arcy's law on theoretical grounds. These theories have mainly been based on the theoretical behaviour of various model porous media, and can be summarised as follows:

(i) Capillaric models (Scheidegger's terminology) in which a porous medium is represented by a bundle of straight

capillaries of various diameters and in various arrangements.

(ii) Hydraulic radius theories in which the porous medium is represented by a series of tortuous channels (e.g. the Kozeny theory).

(iii) Drag theories in which the walls of the pores of the porous medium are treated as obstacles to the otherwise straight flow of the viscous fluid.

None of these theories are very satisfactory since all depend for their accuracy on experimental "fitting factors". It is interesting to note that all are based on the application to porous media of pipe and channel flow theories for viscous fluids.

It is most significant that the greatest deviations from equation E(10.1)c have been observed for the flow of gases. This usually appears to have been put down to the effects of molecular phenomena and various semi-empirical, semi-theoretical formulae based on analogy with 'Knudsen' or 'slip' flow of gases through capillaries have been advanced.

These typically take the form:

$$v = \frac{-1}{\mu}\left(b + \frac{m}{p}\right) \cdot \frac{\partial p}{\partial z}$$ where b and m are constants (due to Klinkenberg).

or $$v = A\frac{\partial p}{\partial z} + B\sqrt{\frac{R\theta}{w}} \cdot \frac{1}{p} \cdot \frac{\partial p}{\partial z}$$ where A and B are complicated constants (due to Adzumi).

Note how closely these expressions approach to

$$v = -k' \cdot \frac{R\theta}{w} \cdot \frac{1}{p} \cdot \frac{\partial p}{\partial z} \qquad E(10.3)$$

Summary.

There are thus two possible forms of expression describing the flow of fluids through porous media. These expressions are typified by equations E(10.1)c and E(10.2).

For the flow of incompressible fluids, E(10.1)c reduces to E(10.2). It is therefore only for the flow of gases that differences between the two need be studied.

(10.4) Experiments on the steady state flow of air through dry soils.

(a) Experimental apparatus and procedure.

The samples used in these experiments usually consisted of cylinders of soil which had been compacted in a moist condition and were then allowed to become air-dry. One sample was a cylinder cut from a block of weakly cemented sandstone while in another case the permeability of a disc of porous ceramic material was measured.

The samples were set up in a triaxial cell in the normal way, with a top cap drainage lead. Sintered bronze porous discs were placed at either end of the sample to distribute or collect air flow. The base of the triaxial cell was equipped with a single central drainage hole. The layout of the apparatus is shown in fig. (10.1). A cell pressure was used which was greater than the largest air pressure which was subsequently to be applied to the interior of the sample.

The air pressure was supplied by a "constant leak" pressure control valve connected to a manometer which was used to measure the air pressure to $\pm$ 0.1 p.s.i.

The air lead from the "down-stream" end of the sample was connected to a T-piece from which one tube lead to a null-indicator which was used to measure the loss in head across the sample. The second tube from the T-piece was connected to a two-way valve. This valve could either pass air flow straight through or else out to atmosphere. This was achieved by removing one O-ring from a standard

piston type valve and reversing the piston.

In the "straight-through" position the flow of air passed into the pot of an ordinary self-compensating mercury volume gauge. The graduated tube of this gauge was open to atmosphere and the quantity of air flowing in a given time was measured by the volume of mercury which flowed from the pot into the tube.

If the pressure gradient down the length of the sample was to be measured, a number of tapping points were provided which were connected through holes in the membrane in the same way as the pore water pressure probes described in Chapter 8. One of these connectors is shown in Plate 4 of Chapter 8. Small bore nylon tubes connected the tapping points to a valve manifold which in turn was connected to a null indicator. The pressure could thus be measured at one point at a time by opening the appropriate valves.

In measuring the permeability of the sample, the procedure was as follows:

With the piston of the two way valve removed, the mercury level in the volume gauge was lowered to the bottom of the graduated tube. The piston was then replaced in the "through to atmosphere" position and a constant air pressure was applied to the "upstream" end of the sample.

After sufficient time had elapsed to allow the flow of air through the soil to become steady, the difference in mercury levels in the volume gauge was measured, the pressure at the "downstream" end of the sample was noted and the two-way valve was put into the "straight through" position. Simultaneously a stop watch was started.

Due to the flow resistance of the volume gauge, the pressure loss across the sample decreased slightly during the test and periodic readings were taken to allow for this. When sufficient air had been collected in the volume gauge, the gauge was sealed by the two-way valve and readings of the graduated tube of the gauge and the difference in mercury levels were made.

The whole procedure was then repeated using a different applied air pressure.

In measuring the pressure gradients through a sample, the piston of the two way valve was removed and air was passed through the sample under a constant supply pressure. When a steady state was reached, the air pressure was measured at each tapping point down the length of the sample.

The porous ceramic disc was sealed into the ordinary metal holder and mounted on the base of the triaxial cell. Air pressures were applied directly into the cell.

(b) Calculation of results.

The mass of air collected in the volume gauge during each test was calculated as follows:

Suppose the volume gauge contains initially:
mass m of air occupying volume V at pressure p. Then

$$p.V = \frac{R\theta}{w} . m$$

If the changes in pressure, volume and mass in the gauge during the test are

$$\delta p, \delta V \text{ and } \delta m$$

respectively, then at the end of the test:

$$(p + \delta p).(V + \delta V) = \frac{R\theta}{w}(m + \delta m)$$

Hence the mass of air collected during the test is:

$$\delta m = \frac{w}{R\theta}\left[p\delta V + V\delta p + \delta p.\delta V\right]$$

If the cross-sectional area of the sample is A and the porosity n, then the mass of air per unit area of pore space which has flowed through the sample is:

$$\frac{\delta m}{An} = \frac{w}{AnR\theta}\left[p\delta V + V\delta p + \delta p.\delta V\right] \qquad E(10.4)a$$

The corresponding volume of air per unit area of pore space at the average pressure (u_a) in the pore space of the soil is:

$$\frac{\delta m}{An} \cdot \frac{R\theta}{u_a w} = \frac{1}{Anu_a}\left[p\delta V + V\delta p + \delta p.\delta V\right] \qquad E(10.4)b$$

(c) Experimental results.

In comparing the experimental results the following terms have been used:

Linear velocity = $\frac{1}{An}\frac{dV}{dt}$ = rate of flow of volume per unit area of voids through soil.

= flow rate corresponding to equation E(10.1)c.

Mass velocity = $\frac{1}{An}\frac{dm}{dt}$ = rate of flow of mass per unit area of voids through soil.

= flow rate corresponding to equation E(10.2).

In fig. (10.2) are shown the results of two tests on a porous ceramic disc. One test measured the air permeability of the dry disc while the second measured the water permeability of the saturated disc. In fig. (10.2)a the results have been plotted in terms of mass velocity

while in fig. (10.2)b the corresponding linear velocities are shown. The mass velocity for air flow is seen to be more closely proportional to the pressure gradient than the linear velocity. D'Arcy's law was only approximately true even for the flow of water through the saturated disc. This may have been due to a transition at a gradient of about 8 $atm.cm^{-1}$ from laminar to turbulent flow. Experimental points were obtained for increasing and decreasing values of the pressure gradient.

The coefficient of permeability for the flow of water through the porous disc was 0.9×10^{-6} cm/sec. while that for the flow of air through the disc was 6×10^{-4} cm/sec.

Figs. (10.3) and (10.4) summarise the results of permeability tests on five different samples.

In fig. (10.3), the mass velocity has been plotted against the pressure gradient. None of the curves are perfectly linear but all are approximately linear over much of their length.

In the tests on Mangla sandstone, the head losses through the sample were so small that they were really beyond the accuracy of calibration of the manometers. Calibration errors are probably the reason why the experimental curve does not pass through the origin.

In all tests, measurements were made with both increasing and decreasing values of the pressure gradient.

In fig. (10.4) the linear velocity has been plotted against the pressure gradient. Here again the relation is approximately linear but is much less linear than that of fig. (10.3).

Some examples of measured pore pressure gradients are shown in figs. (10.5) and (10.6). The gradients were measured for both

possible directions of flow through the samples. The pressure gradients are obviously almost exactly linear.

In fig. (10.5) the gradients did not converge to zero pressure at the "downstream" end of the sample. This was probably caused by an exit head loss. Similarly in fig. (10.6) the gradients converged too soon. This appeared to be caused by a shrinkage crack in the sample.

(d) Discussion of results.

The equation $\frac{\partial m}{\partial t} = -D\frac{\partial p}{\partial z}$ agrees more closely with the experimental results than does the alternative form of flow law. The classical experiments of Graham (quoted by Starling, 1946) showed that the rate of diffusion of a gas varies inversely as the square root of the density of the gas. This implies that the equation for the flow of a gas is:

$$\frac{\partial m}{\partial t} = -D'\sqrt{\frac{R\theta}{wp}} \cdot \frac{\partial p}{\partial z}$$

This may account for the departure from linearity of the curves in fig. (10.3).

(i) Since $pV = m \cdot \frac{R\theta}{w}$

$$\frac{V\partial p}{\partial t} + p\frac{\partial V}{\partial t} = \frac{R\theta}{w} \cdot \frac{\partial m}{\partial t}$$

But, under steady state conditions, the pressure at every point in the sample is independent of time, therefore

$$p\frac{\partial V}{\partial t} = \frac{R\theta}{w}\frac{\partial m}{\partial t} \qquad E(10.5)$$

Hence if Fick's law is correct

$$p\frac{\partial V}{\partial t} = -D\frac{R\theta}{w} \cdot \frac{\partial p}{\partial z}$$

i.e. $\frac{1}{A}\frac{\partial V}{\partial t} = -\frac{DR\theta}{Aw} \cdot \frac{1}{p}\frac{\partial p}{\partial z}$ or $\frac{\partial V/\partial t}{\partial p/\partial z} = -\frac{DR\theta}{w} \cdot \frac{1}{p}$

From this equation one would expect the slope of the linear velocity-pressure gradient curves to drop off as p and hence $\frac{\partial p}{\partial z}$ increase. Fig. (10.4) shows that this does in fact happen.

(ii) On the assumption that D'Arcy's law is valid, E(10.5) becomes

$$-ADp \frac{\partial p}{\partial z} = \frac{R\theta}{w} \cdot \frac{\partial m}{\partial t}$$

but we have seen that the pressure gradients in the steady state flow of air are linear. Hence $\frac{\partial p}{\partial z}$ is constant. Thus, following on the assumption of D'Arcy's law, we have:

$$\frac{\partial m}{\partial t} \propto - p$$

This does not seem to be true since the rate of flow of air does not appear to depend on the absolute value of the air pressure. This point is illustrated by fig. (10.8) for the unsteady flow of air through a dry soil. (See section (10.7)). It can thus be concluded that equation E(10.2) represents more correctly the form of the equation describing the flow of both air and water through a soil.

(10.5) Simplified equations for the consolidation of partly saturated soils.

On the basis of a number of simplifying assumptions, a set of equations will now be set up which describe the process of consolidation in a partly saturated soil.

(a) Assumptions.

(1) The first assumption is that the consolidation is a result of pressure gradients only. This limits the applicability of the equations to conditions in which gradients due to

Temperature)
)
Osmotic effects) are absent.
)
Electrical effects)

(2) The flow of the pore fluid is assumed to obey the equation

$$\frac{\partial m}{\partial t} = -D\frac{\partial p}{\partial z}$$

For any fluid the quantity flowing is assumed to be directly proportional to the cross-sectional area of pore space occupied by the fluid. Fig (10.7), after Wyckoff & Botset, (1936) shows the limitations of this assumption. Both phases of the pore fluid are assumed to be continuous and interconnected throughout the soil.

(3) The principle of effective stress is assumed to be valid throughout the soil so that the deformation of the soil skeleton is a function of effective stress only.

(4) The consolidation is assumed to take place slowly enough to enable the liquid and gaseous phases of the pore fluid to remain in equilibrium throughout.

(5) The pressure difference between the two phases can be expressed by a simple relationship involving the surface tension of the liquid phase.

(6) In order to work in terms of absolute pressure, the effects of gravity will be assumed to be included in the pore pressure gradients.

(b) General equations.

(1) Equations of flow.

Consider an elemental region in a mass of consolidating partly

saturated soil in which consolidation is able to take place in one direction only. Let the elemental region be of fixed size dx.dy.dz and be fixed in space and let consolidation be taking place in the z-direction only. The soil in the element is assumed to have porosity n and degree of saturation S. Applying equation E(10.2) in turn to the gas and liquid phases:

(a) For flow in the gas phase, if

F_a = mass of air entering the elemental region in the z-direction in unit time.

$$F_a = -A_a D_a \frac{\partial p_a}{\partial z}$$

$$F_a = -(1 - S)n\, D_a \frac{\partial p_a}{\partial z} \cdot dx.dy \qquad E(10.6)$$

(b) Similarly, for flow in the liquid phase:

$$F_w = -Sn\, D_w \cdot \frac{\partial p_w}{\partial z} \cdot dx.dy \qquad E(10.7)$$

(2) Equations of continuity of mass.

(a) For mass continuity in the gas phase:

rate of change of mass of air in element = rate of mass entry into element - rate of mass exit from element.

If m_a = mass of air contained in the element

$$\frac{\partial m_a}{\partial t} = F_a - \left[F_a + \frac{\partial F_a}{\partial z} \cdot dz\right] = -\frac{\partial F_a}{\partial z} \cdot dz \qquad E(10.8)$$

Applying the universal gas law to the air in the element:

$$p_a(1 - S)n\, dx.dy.dz = \frac{m_a}{w_a} \cdot R\theta \qquad E(10.9)$$

i.e. $$m_a = \frac{w_a}{R\theta} \cdot p_a(1 - S)n\, dx.dy.dz$$

Hence from E(10.8)

$$\frac{w_a}{R\theta}\frac{\partial}{\partial t}\left[p_a(1-S)n\right] = \frac{\partial}{\partial z}\left[(1-S)n\, D_a \frac{\partial p_a}{\partial z}\right]$$

$$\frac{\partial}{\partial t}\left[p_a(1-S)n\right] = \frac{D_a R\theta}{w_a}\cdot\frac{\partial}{\partial z}\left[(1-S)n\cdot\frac{\partial p_a}{\partial z}\right] \qquad E(10.10)$$

(b) For mass continuity in the liquid phase.

As before:

$$\frac{\partial m_w}{\partial t} = -\frac{\partial F_w}{\partial z}\cdot dz \qquad E(10.11)$$

In this case $m_w = \rho_w . Sn\, dx.dy.dz$ E(10.12)

and from E(10.11)

$$\rho_w \frac{\partial}{\partial t}(Sn) = D_w \frac{\partial}{\partial z}\left[Sn\frac{\partial p_w}{\partial z}\right]$$

$$\frac{\partial}{\partial t}(Sn) = \frac{D_w}{\rho_w}\frac{\partial}{\partial z}\left[Sn\cdot\frac{\partial p_w}{\partial z}\right] \qquad E(10.13)$$

(3) Deformation of the soil skeleton.

If m_s is the mass of soil grains per unit volume of soil, assume by the principle of effective stress, that

$$dm_s = k_s d\sigma'_z \qquad E(10.14)$$

where k_s is a constant.

Since $m_s = (1-n)\rho_s$ E(10.15)

$$dm_s = -\rho_s dn$$

i.e. $$dn = -\frac{k_s}{\rho_s} d\sigma'_z$$

or
$$\left.\begin{aligned} dn &= -D_s\, d\sigma'_z \\ n &= n_o - D_s\sigma'_z \end{aligned}\right\} \qquad E(10.16)$$

Where n_o is the porosity of the soil when $\sigma'_z = 0$.

Equations E(10.10), E(10.13) and E(10.16) are the general equations for the consolidation of a partly saturated soil. Together

with the equation of effective stress:

$$\sigma'_z = (\sigma_z - p_a) + \chi(p_a - p_w)$$

and the equation linking p_a to p_w:

$$p_a = p_w + 2T/r$$

They form a set of five simultaneous equations in which the variables are:

$$p_a,\ p_w,\ S,\ n \text{ and } \sigma'_z.$$

(c) Application of general equations to particular cases.

(1) Consolidation in a saturated soil.

With $S = 1$ and $p_w = p_a = p$ the consolidation equations become:

$$\frac{\partial n}{\partial t} = \frac{D_w}{\rho_w}\frac{\partial}{\partial z}\left[n\frac{\partial p}{\partial z}\right] = \frac{D_w}{\rho_w}\left[n\frac{\partial^2 p}{\partial z^2} + \frac{\partial n}{\partial z}\cdot\frac{\partial p}{\partial z}\right] \qquad E(10.17)$$

$$n = n_o - D_s(\sigma_z - p) \qquad E(10.18)$$

Hence if σ_z is constant

$$dn = D_s d_p$$

and from E(10.17)

$$D_s\frac{\partial p}{\partial t} = \frac{D_w}{\rho_w}\left[\left[n_o - D_s(\sigma_z - p)\right]\frac{\partial^2 p}{\partial z^2} + D_s\left[\frac{\partial p}{\partial z}\right]^2\right]$$

or approximately:

$$\frac{\partial p}{\partial t} = C_v n\cdot\frac{\partial^2 p}{\partial z^2} \qquad E(10.19)$$

Alternatively:

$$p = \frac{n - n_o + D_s\sigma_z}{D_s}$$

and if σ_z is constant

$$\frac{\partial p}{\partial z} = \frac{1}{D_s}\frac{\partial n}{\partial z};\quad \frac{\partial^2 p}{\partial z^2} = \frac{1}{D_s}\frac{\partial^2 n}{\partial z^2}$$

i.e. $$\frac{\partial n}{\partial t} = C_n . n \frac{\partial^2 n}{\partial z^2} \qquad E(10.20)$$

where C_V and C_n are constants.

(2) Consolidation in a dry soil.

With S = 0 and $p_a = p$ the consolidation equations become:

$$\frac{\partial}{\partial t}\left[np\right] = \frac{D_a R\theta}{w_a} \cdot \frac{\partial}{\partial z}\left[n \frac{\partial p}{\partial z}\right] \qquad E(10.21)$$

$$n = n_o - D_s(\sigma_z - p)$$

$$\frac{\partial}{\partial t}(np) = n \frac{\partial p}{\partial t} + p \frac{\partial n}{\partial t} = (n + D_s p) \frac{\partial p}{\partial t}$$

and from E(10.19)

$$\left[1 + \frac{D_s p}{n}\right] \frac{\partial p}{\partial t} = C_V \frac{\partial^2 p}{\partial z^2} \qquad E(10.22)$$

(3) Unsteady flow of a gas through a dry rigid soil.

For this case with S = 0, n a constant and $p_a = p$, E(10.10) becomes:

$$\frac{\partial p}{\partial t} = C_V' \frac{\partial^2 p}{\partial z^2} \qquad E(10.23)$$

(4) Application to general case of partly saturated soil.

Equations E(10.10) and E(10.13) reduce to equations in the limiting cases of completely dry and completely saturated soils which are in reasonable accord with the experimental results. In the intermediate cases of partly saturated soils the equations cannot be solved because:

(a) Although pressures in the liquid and gaseous phases can be expressed by $p_a = p_w + 2T/r$, experiments show that r is not approximately a constant for a given soil compacted at a given water content but varies a great deal with:

(i) The magnitude of the effective stress.

(ii) The degree of saturation.

r will also vary during the course of the consolidation process.

(b) The variation of S during the consolidation process is unknown, but will be affected by the compression of the soil skeleton and the drainage of the liquid phase of the pore fluid.

(c) The effective stress law for the partly saturated soil contains the unknown parameter χ which requires evaluation in each case and which varies with S.

(d) As the equations are, the assumption is that the liquid and gaseous phases of the pore fluid are each continuous and that consolidation or swelling takes place as a pair of parallel processes. As will be shown in a later section, this is only one of a number of possible ways in which consolidation can take place in partly saturated soils.

(e) Fig. (10.7) shows that the assumption that for a given fluid the quantity of flow is directly proportional to the cross-sectional area of pore space occupied by the fluid is an approximation similar in nature to the approximation $\chi = S$ for the effective stress expression.

(10.6) <u>The sub-division of consolidation and swelling processes in partly saturated soils</u>.

The process of consolidation or swelling in partly saturated soils can take on several possible forms, each form being a distinct process and requiring separate consideration. Five basic types of process are set out below.

Type No.	Type of Process	Description of Process	* Pore Pressure State	Occurrence
1 a	Simultaneous drainage of both fluid phases.	Both fluid phases continuous and moving.	Pore pressures both positive.	Moderately wet soils.
1 b		Gas phase in form of minute bubbles. Pore fluid behaving & moving as homogeneous compressible fluid.	Pore pressure positive.	Very wet soils.
2 a	Drainage of either liquid or gas phase only.	Gas phase in form of trapped bubbles or voids. Liquid phase only moving.	Pore pressure positive.	Very wet soils.
2 b		Liquid phase in form of capillary films covering particle surfaces. Gas phase only moving.	Pore pressure positive in gas phase, negative in liquid phase.	Very dry soils. Drainage to gaseous atmosphere.
3	Absorption of both liquid and gas phases.	Both fluid phases continuous and moving.	Both pore pressures positive or negative.	Fluid migration from a wetter to a dryer soil.
4	Absorption of either liquid or gas phase only.	(a) Gas only supplied for absorption. (b) Liquid only supplied for absorption.	Both pore pressures negative.	Swelling of any soil.
5	Drainage of one phase, simultaneous absorption of the other.	As 2b but drainage to liquid atmosphere.	As 2b.	Very dry soils.

* 'Positive' or 'negative' refers to the datum pressure of the atmosphere (gas or liquid) to which drainage is taking place.

Consideration of the main types of consolidation in partly saturated soils will show that equations E(10.10) and E(10.13) can

be used in slightly modified form to describe most of the processes tabled above.

The processes can be broken down basically into two main sub-divisions:

A: flow of a compressible fluid through a compressible grain skeleton - described by:

$$\frac{\partial}{\partial t}\left[p(1 - S)n\right] = D.\frac{\partial}{\partial z}\left[(1 - S)n \frac{\partial p}{\partial z}\right] \qquad E(10.24)$$

B: flow of an incompressible fluid through a compressible grain skeleton - described by:

$$\frac{\partial}{\partial t}\left[Sn\right] = D \frac{\partial}{\partial z}\left[Sn \frac{\partial p}{\partial z}\right] \qquad E(10.25)$$

Type A:

Sub-divisions 1b, 2b and 4a can be regarded as examples of a type A process in which the soil is effectively saturated by a homogeneous compressible fluid. Equation E(10.24) will be applicable in the form:

$$\frac{\partial}{\partial t}(np) = D \frac{\partial}{\partial z}\left[n \frac{\partial p}{\partial z}\right] \qquad E(10.26)$$

also $\quad n = n_o - D_s(\sigma'_z - p) \qquad np = (n_o - D_s\sigma'_z)p + D_s p^2$

If σ'_z is constant during the consolidation process:

$$dn = D_s dp \qquad d(np) = (n_o - D_s\sigma'_z + 2D_s p)dp$$

and putting $(n_o - D_s\sigma'_z) = B$ (which is constant).

$$(B + 2D_s p)\frac{\partial p}{\partial t} = D\left[D_s\left(\frac{\partial p}{\partial z}\right)^2 + (B + D_s p)\frac{\partial^2 p}{\partial z^2}\right]$$

Neglecting the term $\left(\frac{\partial p}{\partial z}\right)^2$

$$(B + 2D_s p)\frac{\partial p}{\partial t} = D(B + D_s p)\frac{\partial^2 p}{\partial z^2} \qquad E(10.27)$$

Type B:

Sub-divisions 2a and 4b can be regarded as examples of a type B process in which trapped air will act together with the grain skeleton to produce effectively a skeleton composed of very compressible grains.

For grain skeleton:

$dn = D_s dp$

p increases, n increases.

For trapped air:

$pV_a = N_a R\theta$ (neglecting the effect of solution of air).

p increases, V_a decreases.

$\therefore Sn = \dfrac{V_w}{V_a + V_w + V_s}$ increases.

and vice-versa

$$\therefore \quad d(Sn) = D_s' \, dp, \quad (Sn) = (Sn)_o - D_s'(\sigma_z - p) \qquad E(10.28)$$

Equation E(10.25) can now be written:

$$\frac{\partial (Sn)}{\partial t} = D' \frac{\partial}{\partial z}\left[Sn \frac{\partial p}{\partial z}\right] \qquad E(10.29)$$

If σ_z is constant and $B' = (Sn)_o - D_s \sigma_z$

$$D'_s \frac{\partial p}{\partial t} = D' \left[D'_s \left(\frac{\partial p}{\partial z}\right)^2 + (B' + D'_s p) \frac{\partial^2 p}{\partial z^2}\right]$$

or, approximately:

$$D'_s \frac{\partial p}{\partial t} = D' \left[B' + D'_s p\right] \frac{\partial^2 p}{\partial z^2} \qquad E(10.30)$$

Equations E(10.27) and E(10.30) are non-linear and hence cannot be solved exactly. The simplest and most realistic method of approximate solution appears to be the following.

If the shape of the isochrones is found experimentally and is fitted by a fairly simple algebraic equation, we then have a relation between p and z at any time t. This relation can be substituted into the partial differential equation which is then

reduced to an ordinary differential equation which can be integrated fairly simply.

(10.7) Experimental data on unsteady flow of air through dry rigid soils.

According to E(10.23) the equation governing the unsteady flow of air through a dry rigid soil is:

$$\frac{\partial p}{\partial t} = C'_v \frac{\partial^2 p}{\partial z^2} \qquad E(10.23)$$

This is the simplest case of unsteady flow which can be investigated experimentally, and is the only case in which the flow equation is linear.

(a) Experimental confirmation of the form of the equation.

E(10.23) is identical to the classical consolidation equation for a saturated soil. The correctness of the equation was confirmed in the following way.

Exactly the same set up and sample was used as in the case of the air permeability tests, except that the lead to the volume gauge was sealed off. The air pressure in the sample was allowed to dissipate to zero and the valve leading to the air pressure control valve was closed. A pressure was set on the control valve and the valve leading to the sample was suddenly opened. The changes in air pressure at the base were recorded as the pressure throughout the sample built up to the supply pressure. Once 100% build-up had been reached, the supply valve was closed and the controlled pressure was reduced to zero. The supply valve was then opened and the dissipation of the air pressure at the base with time was recorded.

Fig. (10.8) shows a set of build-up and dissipation curves

for different pressure ranges measured at the base of a dry rigid sample of compacted Mangla shale. The curves representing E(10.23) were fitted at the time taken to reach 50% dissipation or build-up. The agreement of the experimental points with theory is satisfactory. The experimental curves were unaffected by the magnitude of the total pressure change or the initial value of the air pressure. This shows that the rate of flow of air depends only on the pressure gradient and not on the magnitude of the pressure in the air. The duration of the unsteady flow was very short (10 minutes) and readings had to be taken extremely rapidly. Most of the deviation of experiment from theory was probably caused by instrument lag. The value of the constant C_V' (E.10.23) for the curves shown in fig. (10.8) is $C_V' = 1.4$ $cm^2.sec^{-1}$. The corresponding value of the coefficient of consolidation for the compacted saturated soil is $C_t = 2.7 \times 10^{-4}$ $cm^2 sec^{-1}$. (See Chapter 8).

(b) Experimental determination of isochrones.

The experimental set up which was used to determine the shape of isochrones experimentally was the same as that used to measure pressure gradients under steady state flow conditions. The lead from the base of the sample was connected into the valve manifold along with the leads from the various tapping points.

Because of the short duration of the unsteady flow, build-up and dissipation curves were measured at each of the tapping points in turn. This resulted in a set of curves representing pore pressure changes at different positions in the sample.

Fig. (10.9) shows a typical set of curves for a dry compacted sample of Selset clay while in fig. (10.10) a second set of curves is

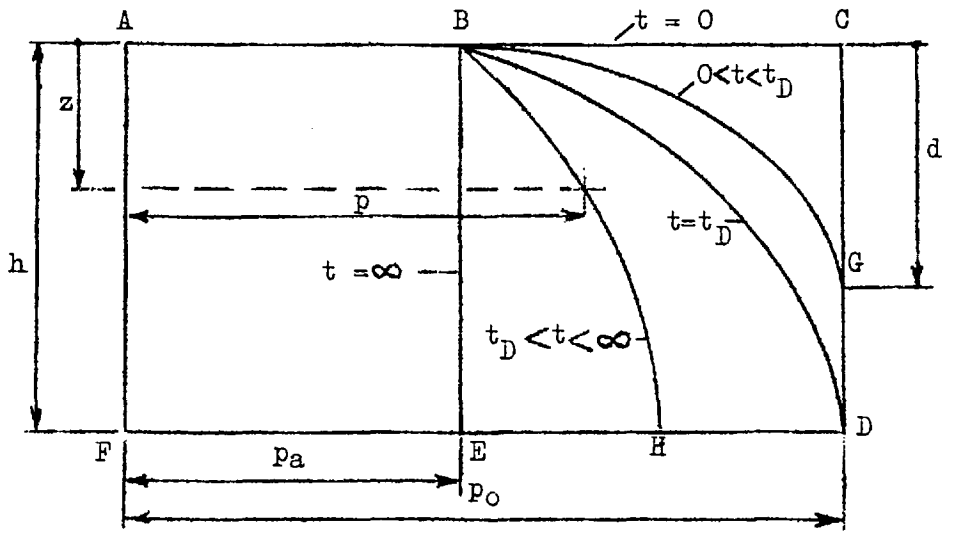
shown for flow through a dry compacted sample of Mangla shale. Additional sets of pressure-time curves are included in the appendix to this chapter.

Isochrones could be constructed from each set of curves by reading off values of the percentage dissipation or build up at various points in a sample at a given time. Examples of these experimental isochrones are shown in figs. (10.11) and (10.12). Additional sets of isochrones are included in the appendix to this chapter.

The main experimental difficulty again proved to be the short duration of the unsteady flow. This made accurate pressure readings extremely difficult to make and probably accounts for much of the scatter in the experimental results.

(10.8) Approximate solution of consolidation equations from known shape of isochrones.

The process of build-up or dissipation in the type of test described in (10.7) can be divided into two stages as shown in the diagram:



Stage 1: $0 < t \leq t_D$: During this stage the isochrones have not yet reached the impermeable base of the sample and point G is moving down from C to D.

Stage 2: $t_D < t < \infty$: The isochrones have now reached the base of the sample and point H is moving across from D to E.

The method of solution is as follows:

Stage 1.

(i) Having assumed a suitable shape for the isochrone, an expression is obtained relating p to p_o, p_a, d and z. Hence expressions for $\frac{\partial p}{\partial z}$ and $\frac{\partial^2 p}{\partial z^2}$ are found.

(ii) These expressions are substituted into the differential equation which is then integrated partially with respect to z over the range 0 to d.

(iii) This results in a simple differential equation involving t and d (which is a function of t). This equation is then integrated to get the full solution for stage 1.

Stage 2:

The procedure for stage 2 is very similar to that used for stage 1.

The function which appeared to fit the experimental isochrones of stage 1 best was one of the form

$$p = a\sqrt{z} + bz + c$$

The isochrones of stage 2 for Selset clay were fitted best by a function of the form $p = a \sin bz + c$, while those for Mangla shale agreed best with $p = a\sqrt{x} + bx^3 + c$. These lines have been shown in figs. (10.11) and (10.12). A parabola is a fair approximation to all these curves (see fig. (10.13)). To investigate the feasibility

of this method of solution it was decided to solve equations E(10.27) and E(10.30) assuming that the shape of the isochrones was parabolic. The solutions are given below.

(a) Equation E(10.27).

$$(B + 2D_s p)\frac{\partial p}{\partial t} = D\left[D_s\left(\frac{\partial p}{\partial z}\right)^2 + (B + D_s p)\frac{\partial^2 p}{\partial z^2}\right]$$

For stage 1: $0 \leq t \leq t_D$. The solution in terms of the parabolic approximation is:

$$1 - U_z = \frac{p - p_a}{p_o - p_a} = 2\frac{z}{d} - \left(\frac{z}{d}\right)^2$$

where

U_z = degree of equalisation at point z.

$$d = \sqrt{\frac{60D(B + D_s p_a)}{5B + D_s(3p_a + 7p_o)} \cdot t}$$

For stage 2: $t_D \leq t \leq \infty$:

Writing $T = \frac{Dt}{h^2}$ = time factor.

$$\frac{z}{h} = r, \quad (1 - U_z) = \frac{p - p_a}{p_o - p_a}$$

$$T = \frac{5B + D_s(3p_a + 7p_o)}{60(B + D_s p_a)} - \frac{2}{5}\log_e\left[\frac{(1 - U_z)}{(2r - r^2)}\right] + \frac{(4D_s p_a - B)}{(D_s p_a + B)}\log_e\left[\frac{(1-U_z)\left[3B + D_s(4p_o - p_a)\right]}{3(B+D_s p_a)(2r-r^2) + 4D_s(p_o-p_a)(1-U_z)}\right]$$

(b) Equation E (10.30).

$$\frac{\partial p}{\partial t} = D\left[(B + D_s p)\frac{\partial^2 p}{\partial z^2} + D_s\left(\frac{\partial p}{\partial z}\right)^2\right]$$

For stage 1: $0 \leq t \leq t_D$.

$$1 - U_z = \frac{p - p_a}{p_o - p_a} = 2.\frac{z}{d} - \left(\frac{z}{d}\right)^2$$

$$d = \sqrt{12D(B + D_s p_a)t}$$

or:

$$(1 - U_z) = \frac{z}{\sqrt{12D(B + D_s p_a)t}}\left[2 - \frac{z}{\sqrt{12D(B + D_s p_a)t}}\right]$$

For stage 2: $t_D \leq t \leq \infty$:

With $T = \frac{Dt}{h^2}$ = time factor, $\frac{z}{h} = r$

$$T = \frac{1}{12(B+D_s p_a)} + \frac{1}{(B+D_s p_a)} \log_e\left[\frac{3(B+D_s p_a)(2r-r^2)+4D_s(p_o-p_a)(1-U_z)}{(1-U_z)\left[3A + D_s(4p_o-p_a)\right]}\right]$$

(c) Both equations E(10.27) and E(10.30) reduce to equation E(10.23) if $B = 1$ and $D_s = 0$. In this case both the above solutions reduce to:

For stage 1:

$$d = \sqrt{12Dt}$$

or $$(1 - U_z) = \frac{z}{\sqrt{12Dt}}\left[2 - \frac{z}{\sqrt{12Dt}}\right]$$

For stage 2:

$$T = \frac{1}{12} - \log_e\left[\frac{(1 - U_z)}{(2r - r^2)}\right]$$

for $z = h$, $r = 1$ and $T = \frac{1}{12} - \log_e(1 - U_z)$

Results calculated from this equation are compared with values from an exact solution for E(10.23) in the table below.

U_z	T	
	Exact Theory	Parabolic Approximation
0.003	0.05	.08
.051	0.10	.11
.228	0.20	.19
.393	0.30	.30
.524	0.40	.40
.822	0.80	.83
.934	1.20	1.26
.991	2.00	2.13

Although these solutions are based on a shape of isochrone which does not really agree with the experimental data, the table of values shows that the resulting solution is quite close to the truth. The assumption of a more realistic shape for the isochrones would improve the accuracy of the solution.

The approximate solutions for E(10.27) and E(10.30) illustrate some of the factors on which theoretical consolidation curves for partly saturated soils will depend. There is only one theoretical curve for a saturated soil or a dry rigid soil. For partly saturated soils, a different curve will correspond to each combination of values of p_o, p_a, B and D_s. The calculation and tabulation of these theoretical curves will be an extremely arduous task.

(10.9) Experimental data on consolidation of dry compressible soils.

Experimental data on this subject was extremely difficult to get because of the high permeability of pulverised soils. Several

tests were attempted, but the total duration of the consolidation was usually too short to enable an experimental curve to be obtained.

Fig. (10.14) shows a set of curves for the consolidation of a dry powdered kaolin. Unfortunately, in order to reduce the permeability enough to enable a curve to be measured, large effective stresses had to be used and consequently there was little volume change during consolidation. For this reason, the consolidation curves differ little from the theoretical curve for the unsteady flow of air through a rigid soil. The curves are, however, steeper than the theoretical curve and "tail off" more gradually.

Alpan (1959) measured similar curves for the build-up of air pressure in samples of partly saturated soil. A constant air pressure was applied at the top of the sample and resultant changes in pore water pressure were measured at the base.

(10.10) Summary and conclusions.

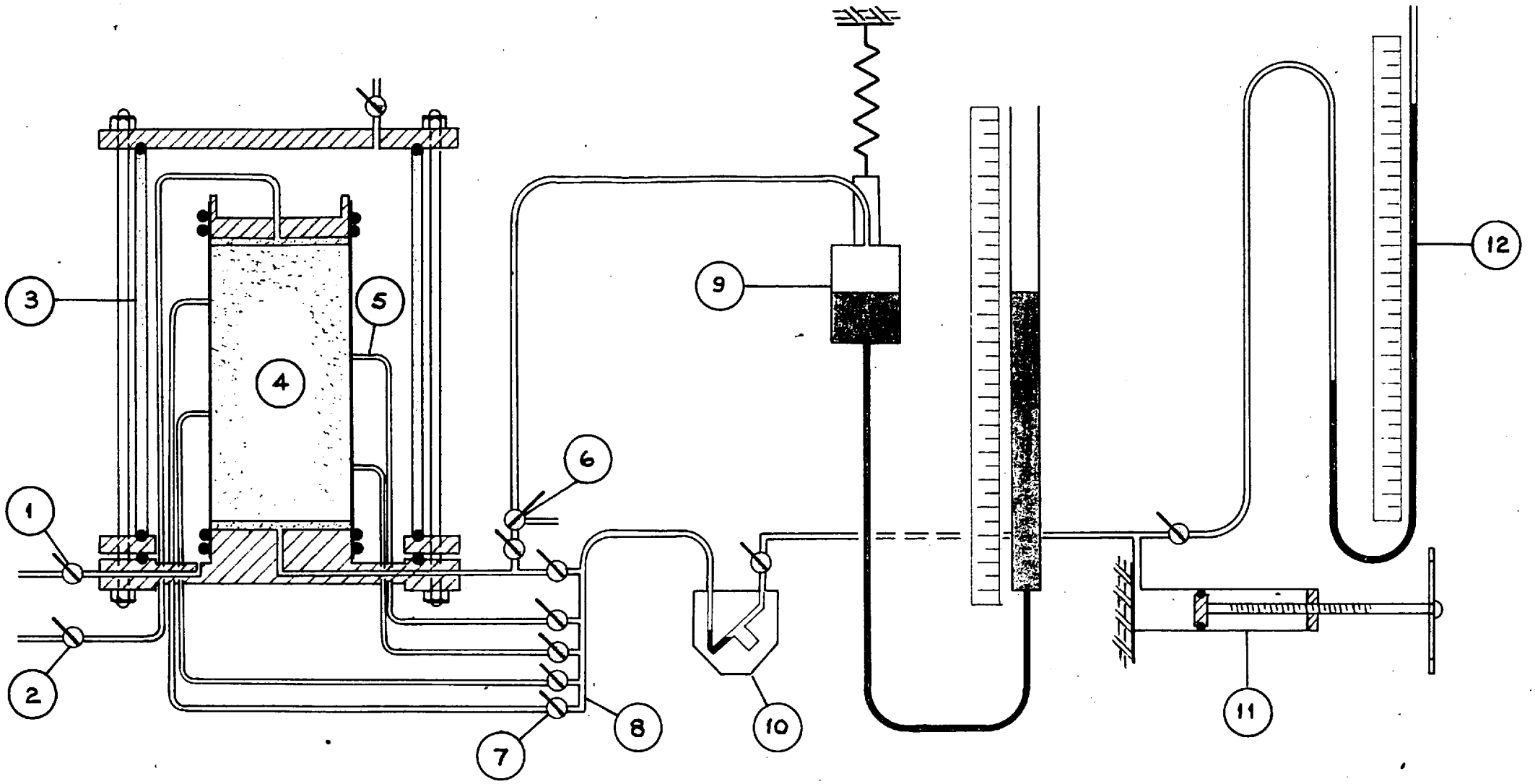
This chapter has described a preliminary investigation into some of the factors controlling consolidation in partly saturated soils. A very great deal of work remains to be done on this subject. The following conclusions can be made.

(a) The correct expression for the description of the flow of both compressible and incompressible fluids through porous media is:

$$\frac{\partial m}{\partial t} = -D\frac{\partial p}{\partial z}$$

(b) Using a set of simplifying assumptions, equations have been formulated which describe the consolidation process in partly saturated soils.

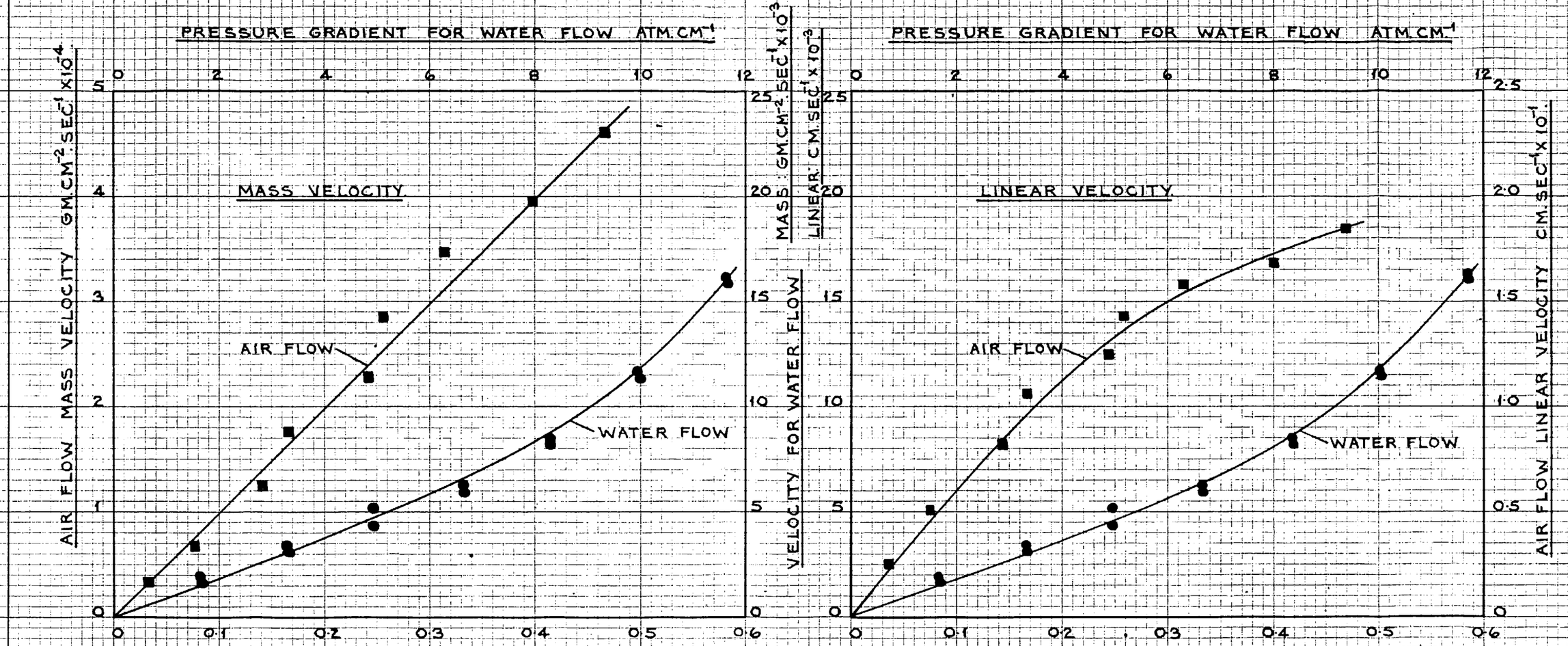
(c) In certain limiting cases these equations can be solved approximately from a knowledge of the shape of the isochrones. The shape of the isochrones can be determined experimentally.



1	VALVE FROM CELL PRESSURE CONTROL.	7	ON-OFF VALVES.
2	VALVE FROM AIR PRESSURE CONTROL.	8	VALVE MANIFOLD.
3	FLAT TOPPED CELL.	9	SELF COMPENSATING VOLUME GAUGE.
4	SAMPLE.	10	NULL INDICATOR.
5	PORE AIR PRESSURE TAPPING POINT.	11	SCREW RAM.
6	TWO-WAY VALVE	12	MERCURY MANOMETER.

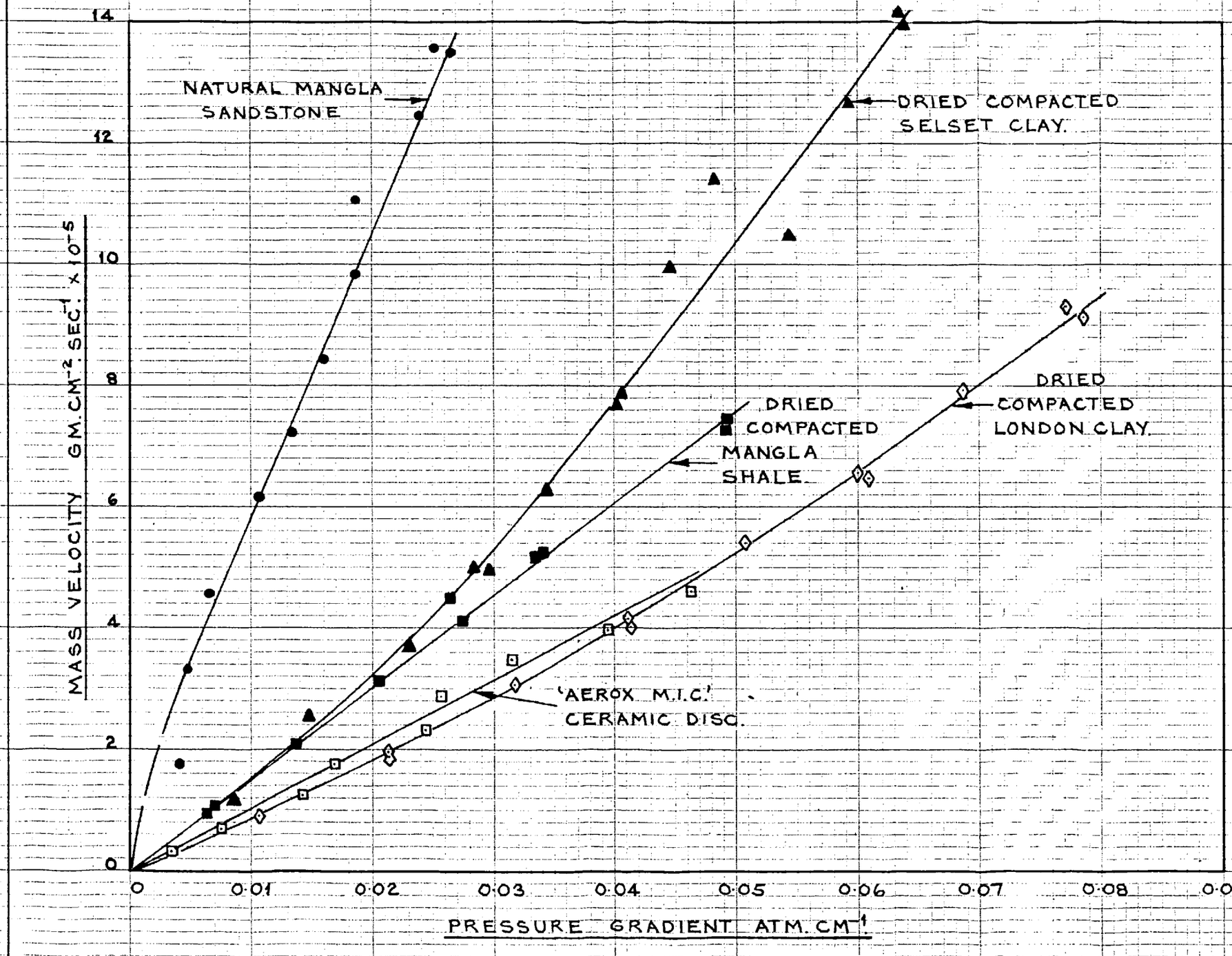
FLOW OF AIR THROUGH DRY SOILS — LAYOUT OF APPARATUS.

FIG. 10.1.



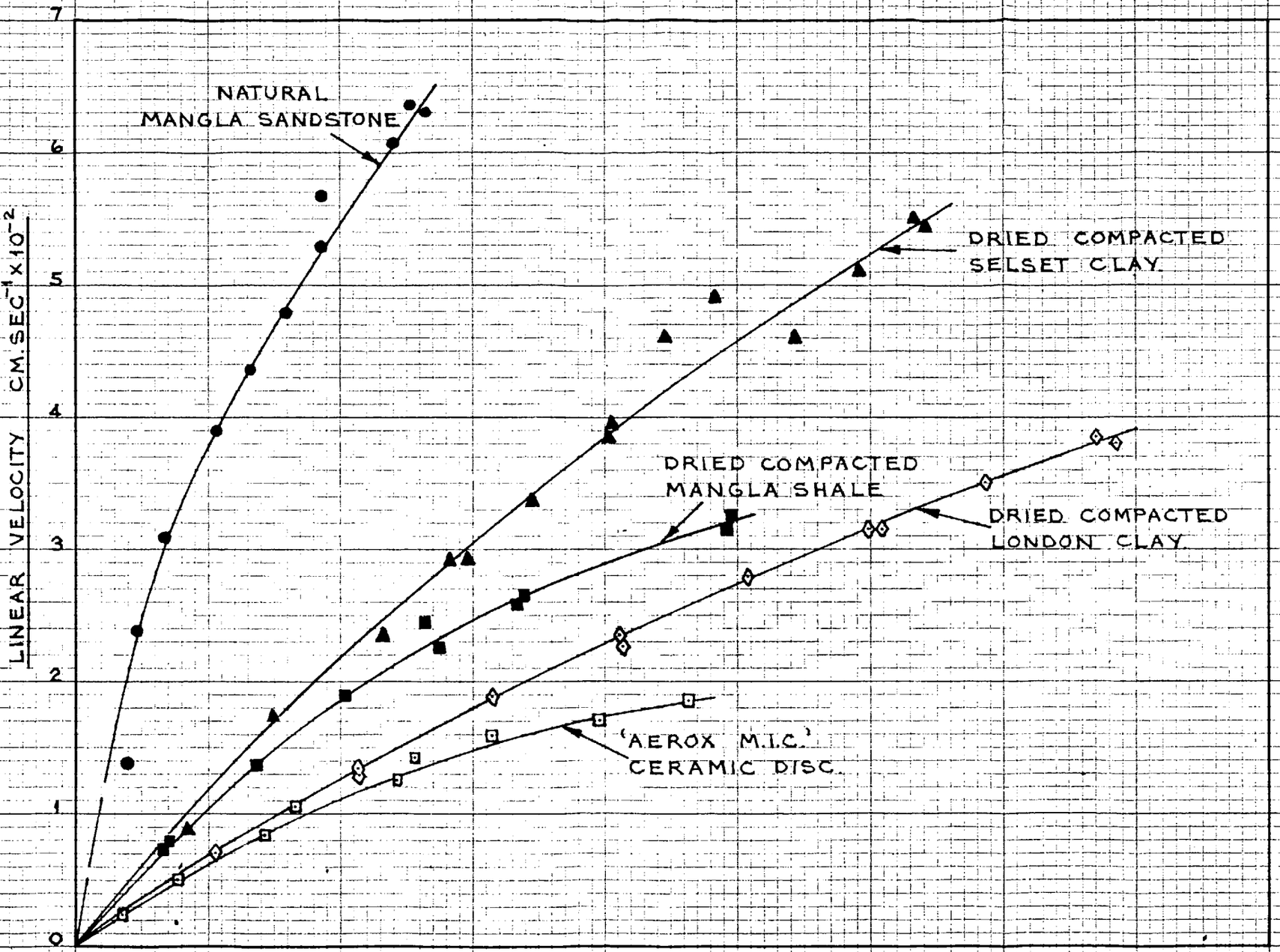
FLOW OF AIR (AT S=0) AND WATER (AT $\bar{S}$=100%) THROUGH THE SAME POROUS CERAMIC DISC RESULTS IN TERMS OF MASS AND LINEAR VELOCITIES

FIG. 10.2.



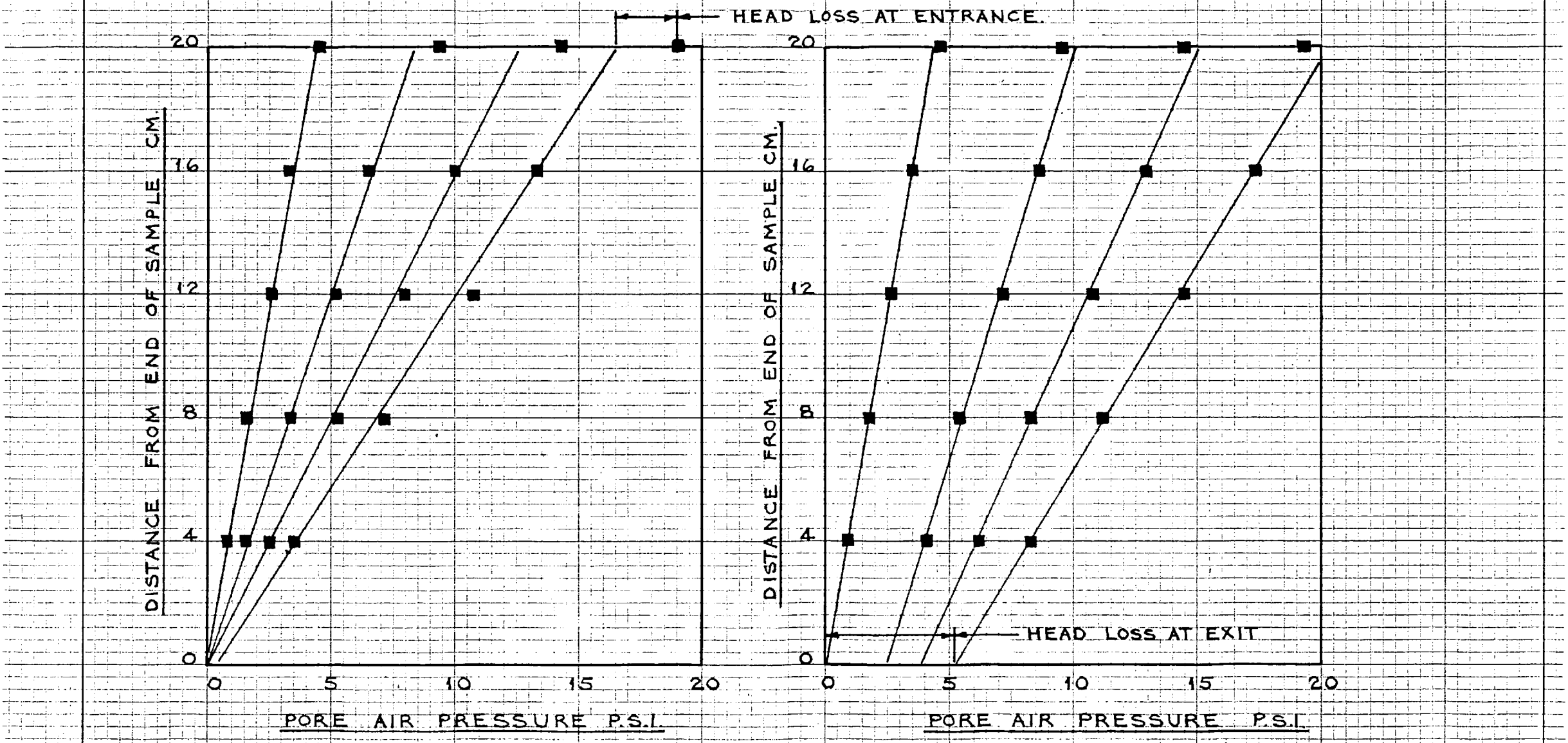
STEADY STATE FLOW OF AIR THROUGH SEVERAL POROUS MEDIA. RELATION BETWEEN MASS VELOCITY AND PRESSURE GRADIENT.

FIG. 10.3.



STEADY STATE FLOW OF AIR THROUGH SEVERAL POROUS MEDIA. RELATION BETWEEN LINEAR VELOCITY AND PRESSURE GRADIENT.

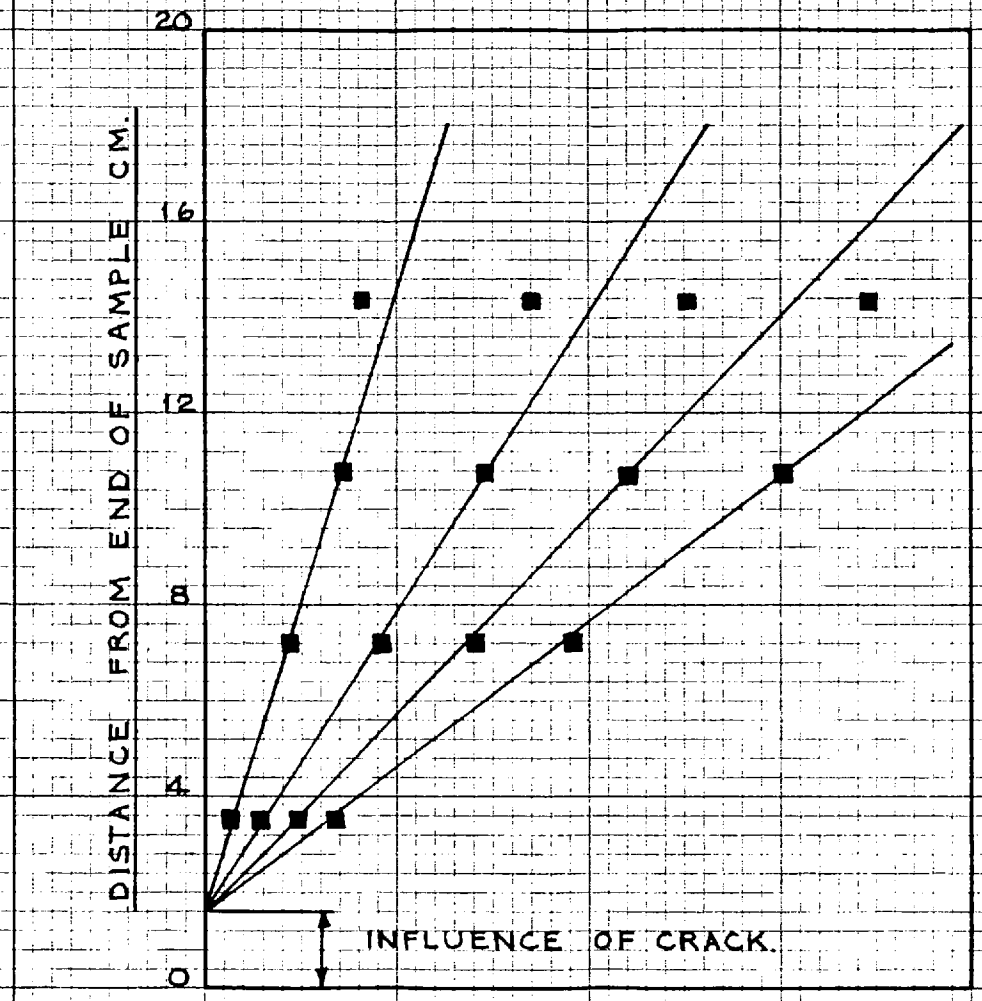
FIG. 10.4.

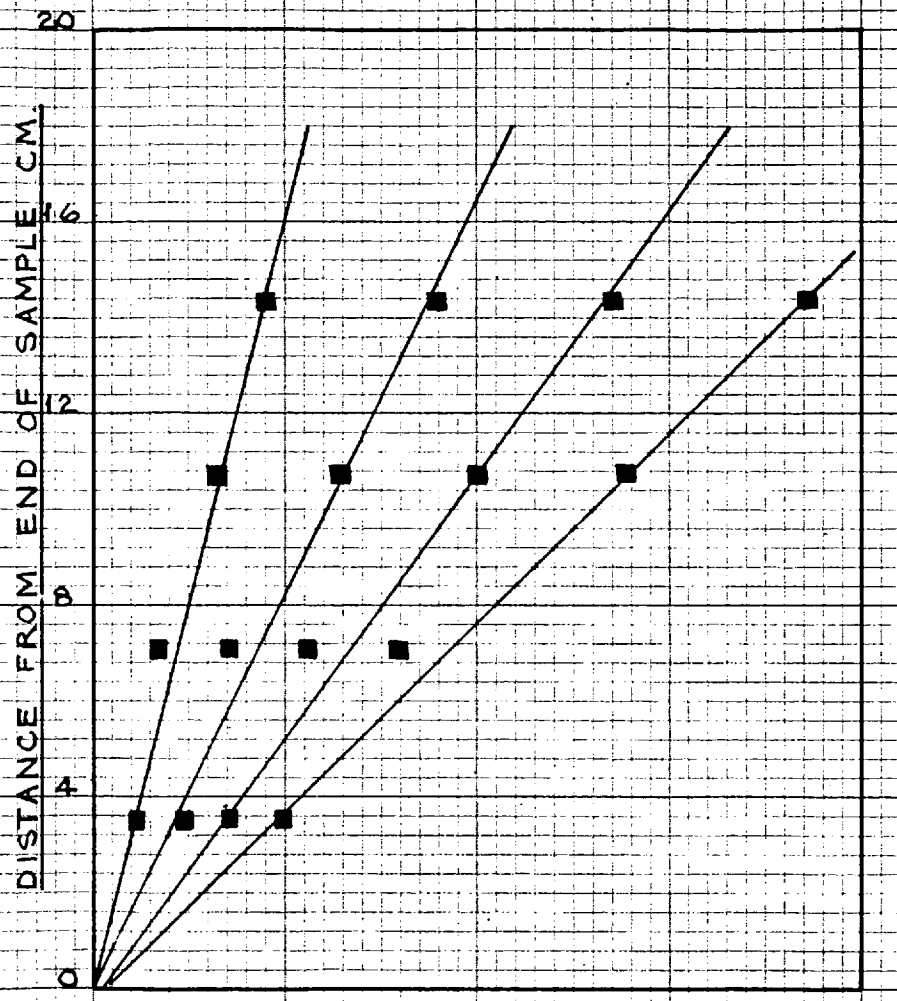


PROFILES OF PORE AIR PRESSURE DURING STEADY STATE FLOW OF AIR THROUGH A SAMPLE OF DRY COMPACTED MANGLA SHALE.

FLOW IN 2 DIRECTIONS.

FIG. 10.5.

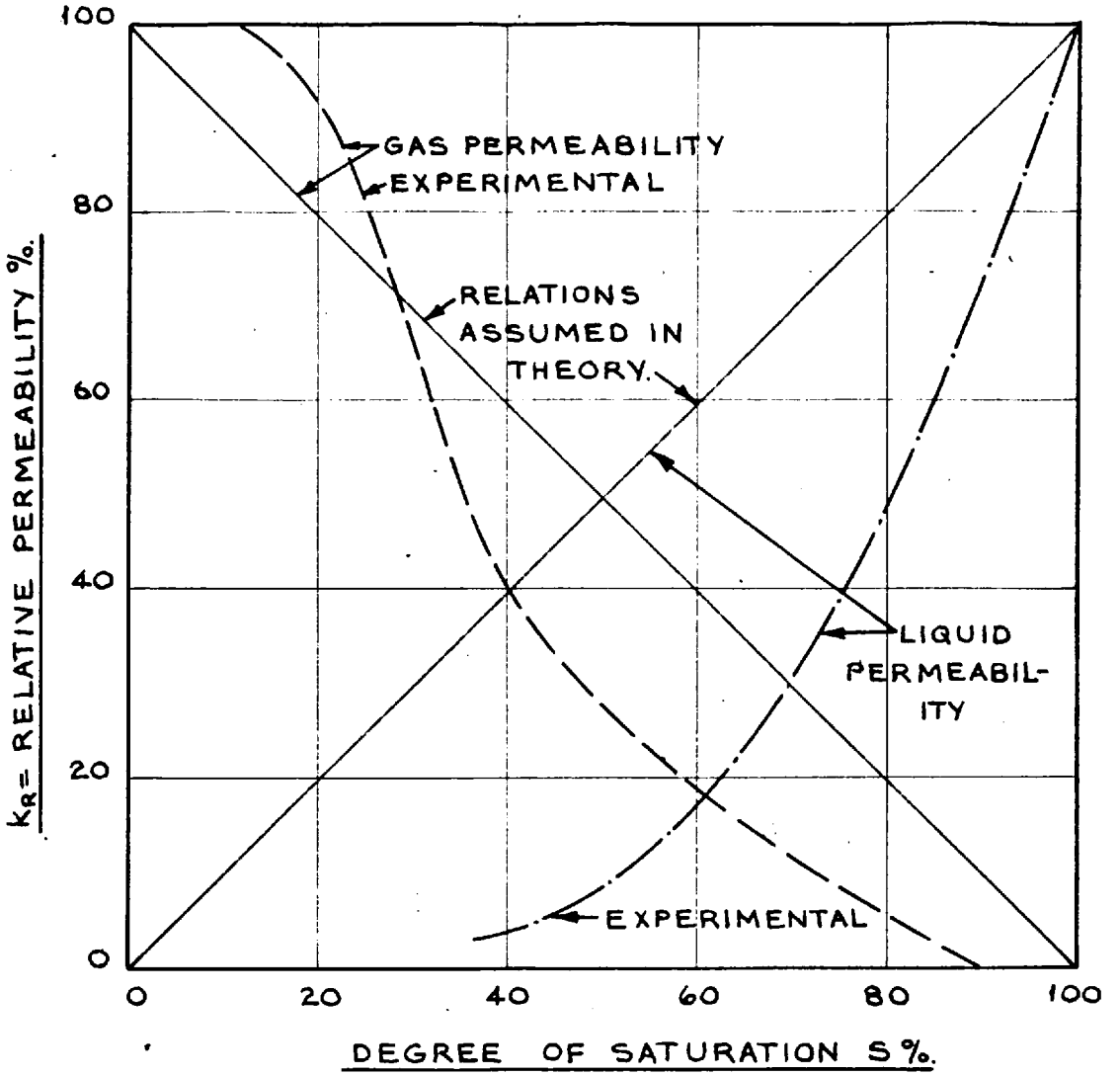




PROFILES OF PORE AIR PRESSURE DURING STEADY STATE FLOW OF AIR THROUGH A SAMPLE OF DRY COMPACTED SELSET CLAY

FLOW IN 2 DIRECTIONS.

FIG. 10.6



EXPERIMENTAL PERMEABILITY CURVES FOR TWO-PHASE FLOW OF A LIQUID AND A GAS THROUGH A POROUS MATERIAL.

(AFTER WYCKOFF & BOTSET, 1936, QUOTED BY SCHEIDEGGER, 1957.).

LIQUID FLOW : k_R = K AT S = S% / K AT S = 100%

GAS FLOW: k_R = K AT S = S% / K AT S = 0.

FIG.10.7.

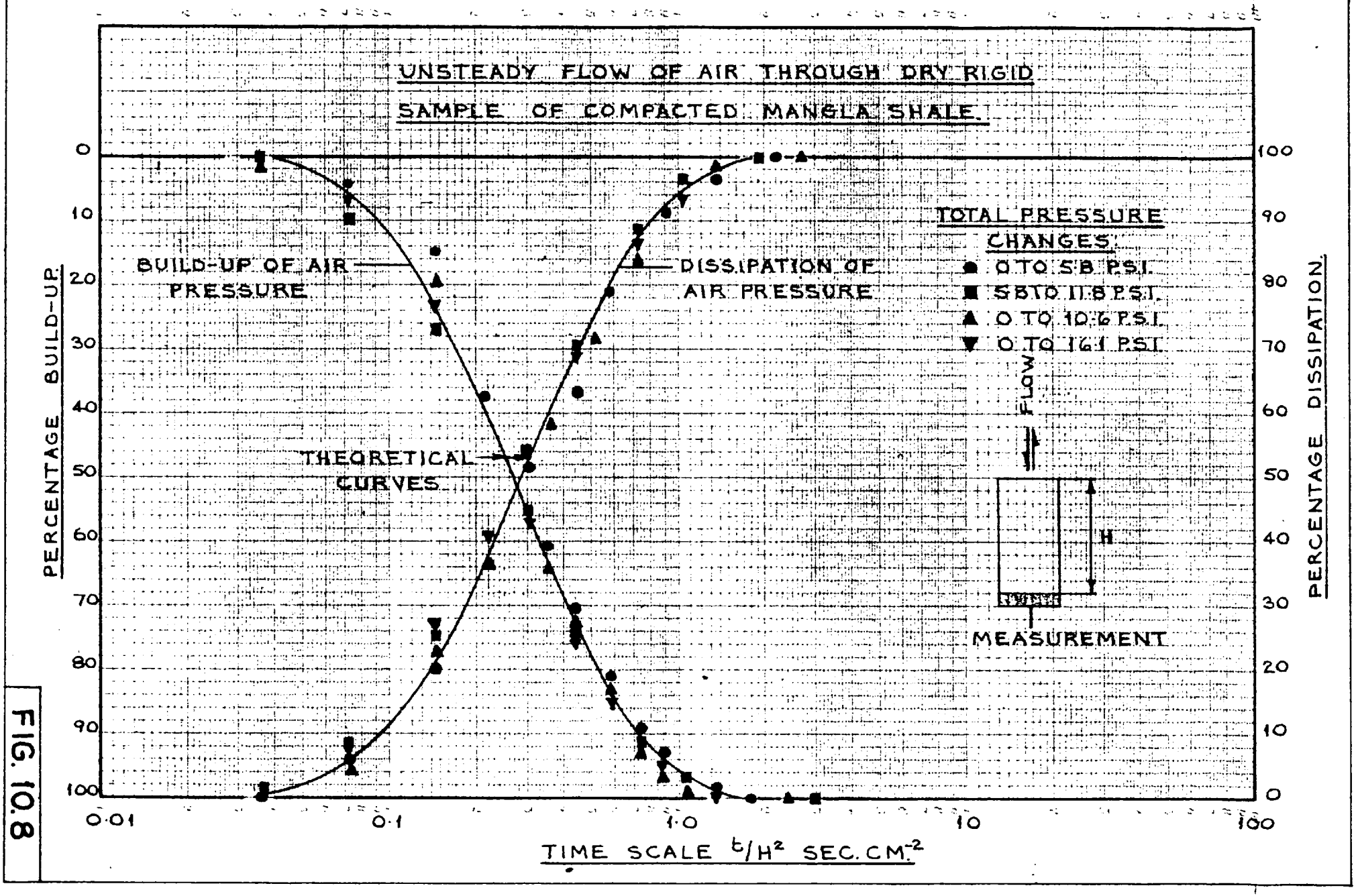

UNSTEADY FLOW OF AIR THROUGH DRY RIGID
SAMPLE OF COMPACTED MANGLA SHALE.
BUILD-UP OF AIR PRESSURE
DISSIPATION OF AIR PRESSURE
THEORETICAL CURVES
TOTAL PRESSURE CHANGES:
0 TO 5·8 P.S.I.
5·8 TO 11·8 P.S.I.
0 TO 10·6 P.S.I.
0 TO 16·1 P.S.I.
FLOW
H
MEASUREMENT
PERCENTAGE BUILD-UP
PERCENTAGE DISSIPATION
0
10
20
30
40
50
60
70
80
90
100
0·01
0·1
1·0
10
100
TIME SCALE t/H² SEC. CM.⁻²

FIG. 10.8

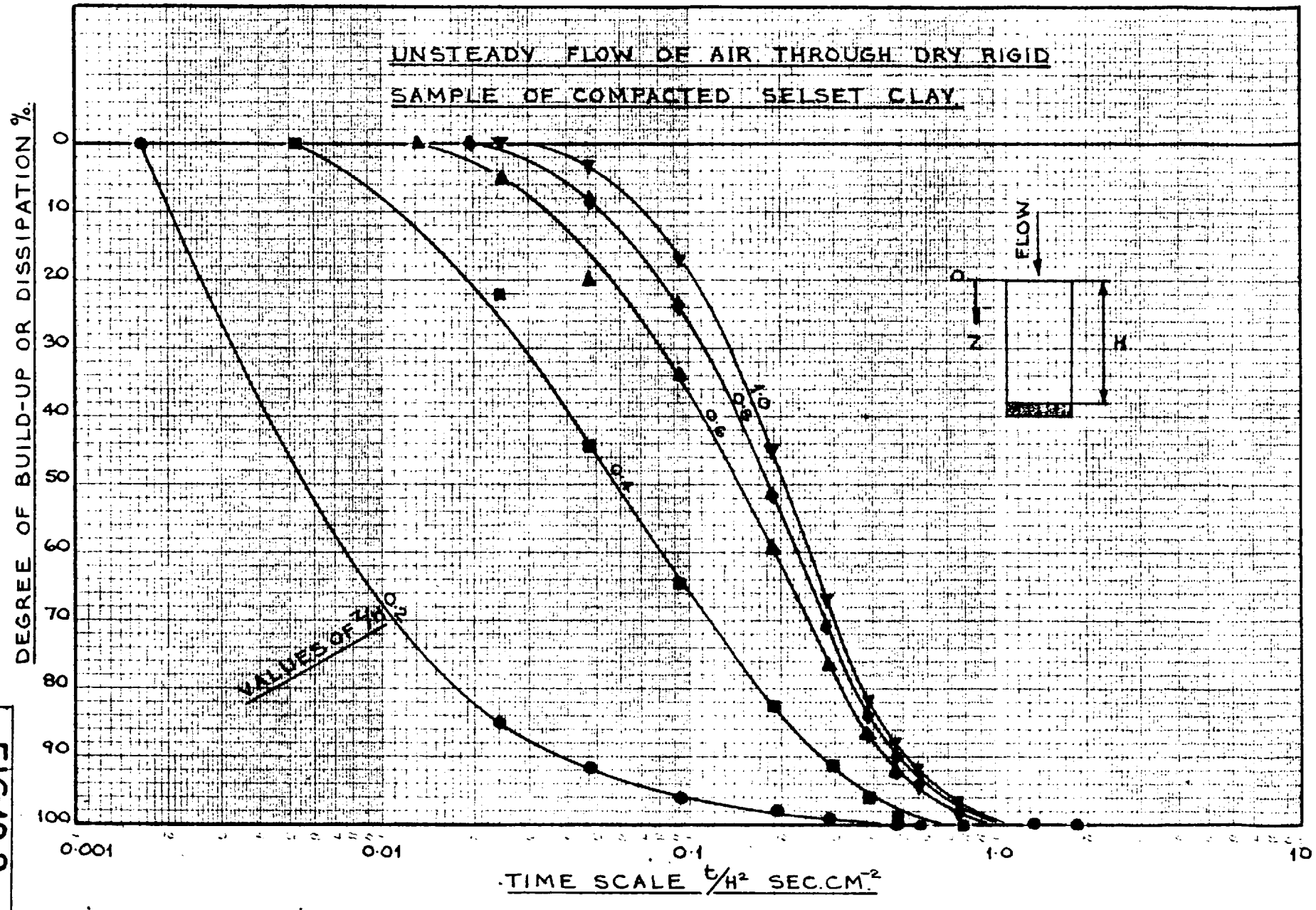

UNSTEADY FLOW OF AIR THROUGH DRY RIGID
SAMPLE OF COMPACTED SELSET CLAY
DEGREE OF BUILD-UP OR DISSIPATION %.
0
10
20
30
40
50
60
70
80
90
100
0·001
0·01
0·1
1·0
10
TIME SCALE t/H² SEC.CM⁻²
VALUES OF z/H
0·2
0·4
0·6
0·8
1·0
FLOW
z
H

FIG.10.9.

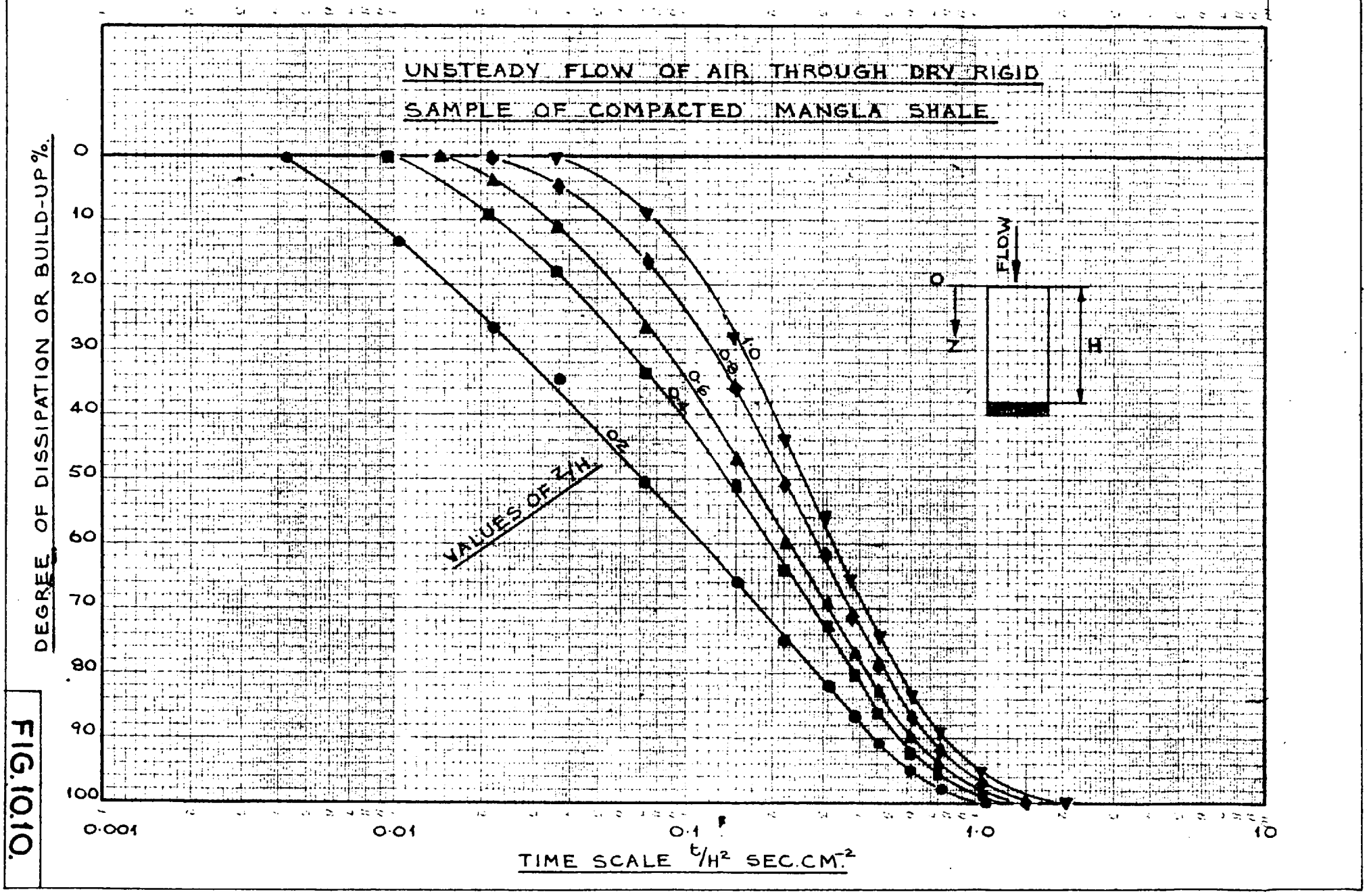
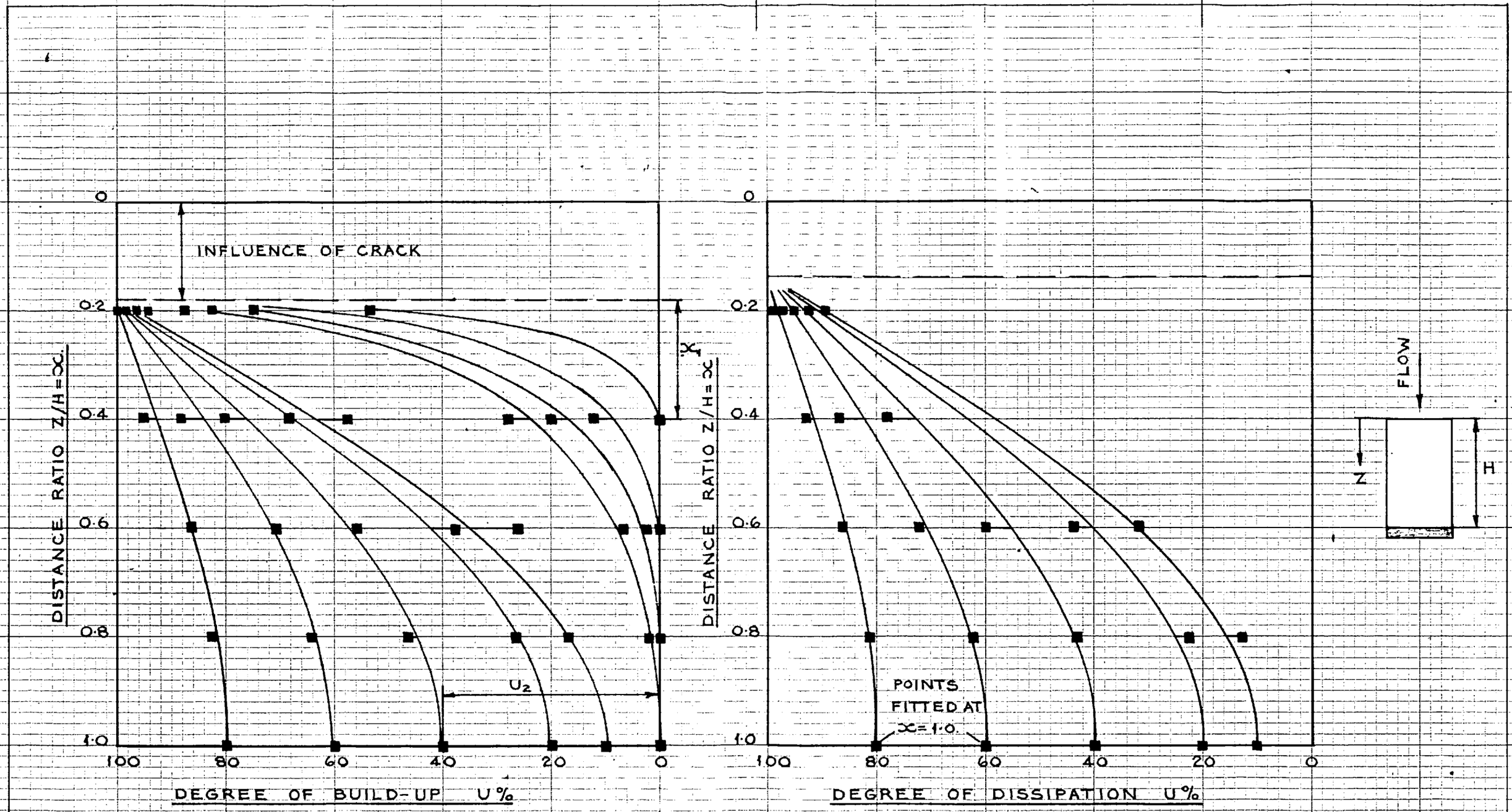

UNSTEADY FLOW OF AIR THROUGH DRY RIGID
SAMPLE OF COMPACTED MANGLA SHALE
DEGREE OF DISSIPATION OR BUILD-UP %.
0
10
20
30
40
50
60
70
80
90
100
0·001
0·01
0·1
1·0
10
TIME SCALE t/H² SEC.CM.⁻²
VALUES OF Z/H.
0·2
0·4
0·6
0·8
1·0
FLOW
O
Z
H

FIG.10.10.

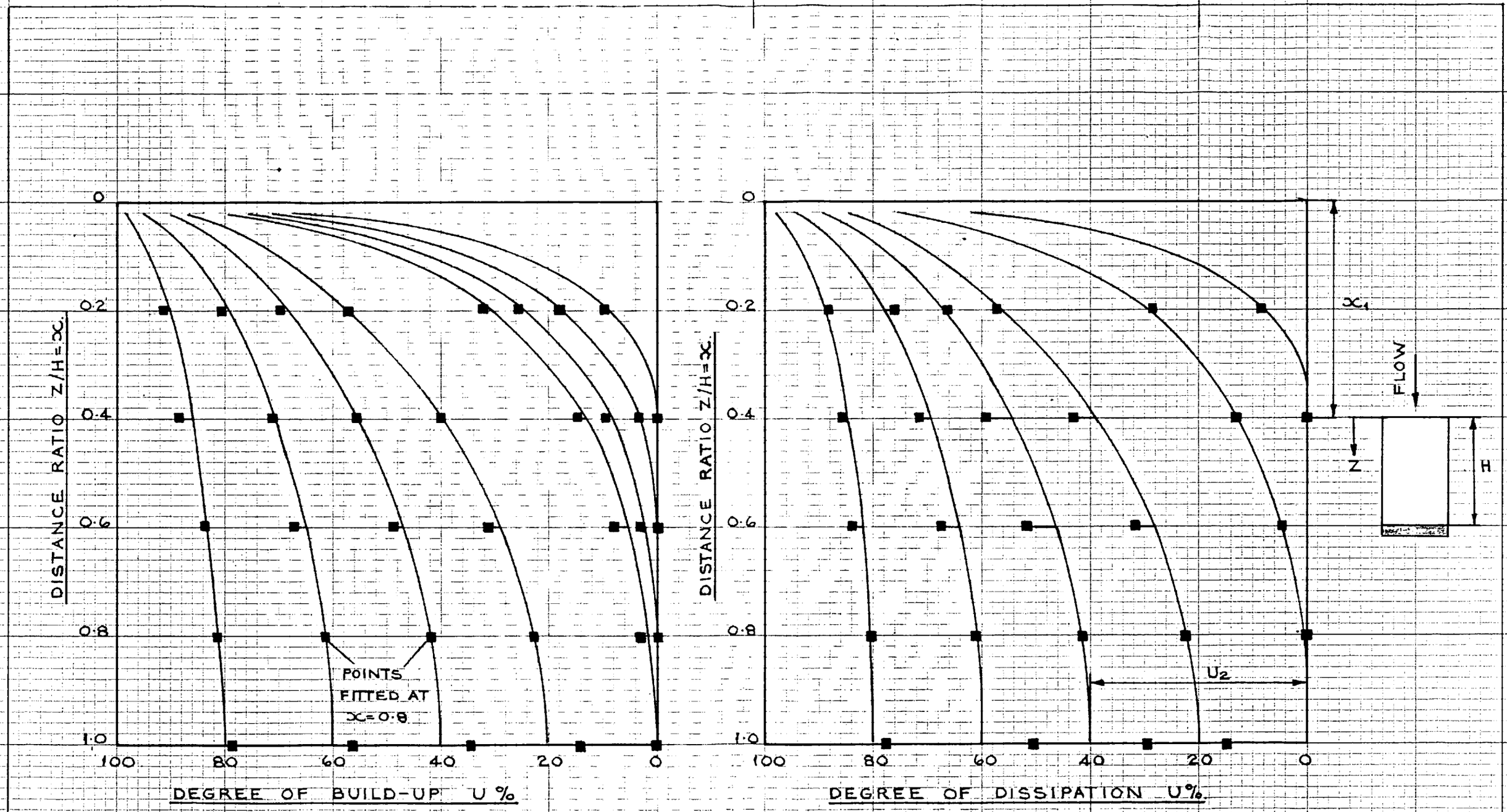


EXPERIMENTAL ISOCHRONES FOR UNSTEADY FLOW OF AIR THROUGH A SAMPLE OF DRY COMPACTED SELSET CLAY.

LINES ARE: STAGE 1: $(1-U)=2\sqrt{\frac{x}{x_1}}-\frac{x}{x_1}$

STAGE 2: $(1-U)=(1-U_2)\sin\frac{\pi x}{2}$

FIG. 10.11.

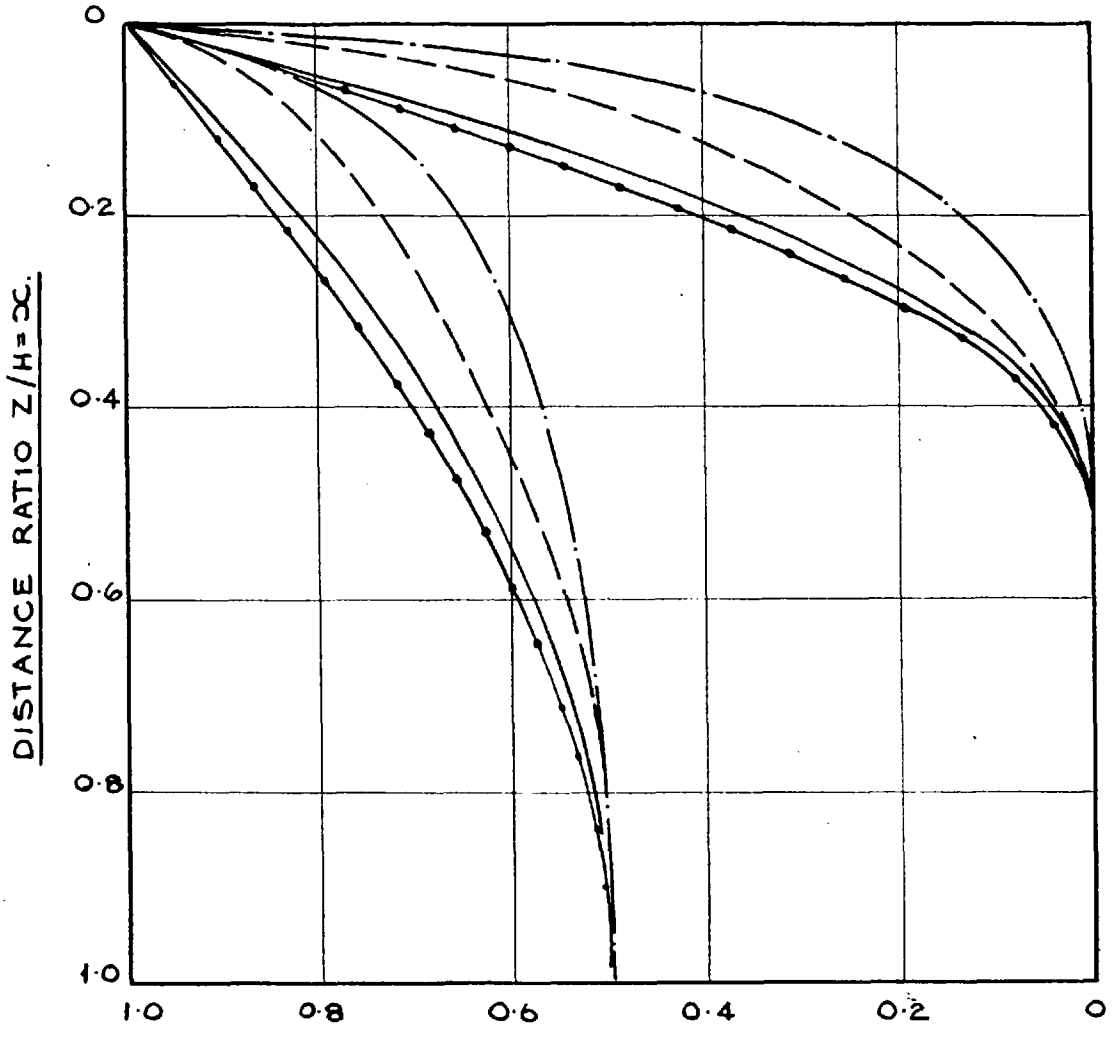


EXPERIMENTAL ISOCHRONES FOR UNSTEADY FLOW OF AIR THROUGH A SAMPLE OF DRY COMPACTED MANGLA SHALE.

LINES ARE: STAGE 1: $(1-U)=2\sqrt{\frac{x}{x_1}-\frac{x}{x_1}}$

STAGE 2: $(1-U)=(1-U_2)\left[6/5\sqrt{x}-1/5\,x^3\right]$

FIG. 10.12.



FLOW OF AIR THROUGH DRY RIGID SOILS.

CHOICE OF APPROXIMATE THEORETICAL SHAPE FOR ISOCHRONES.

FIG. 10.13.

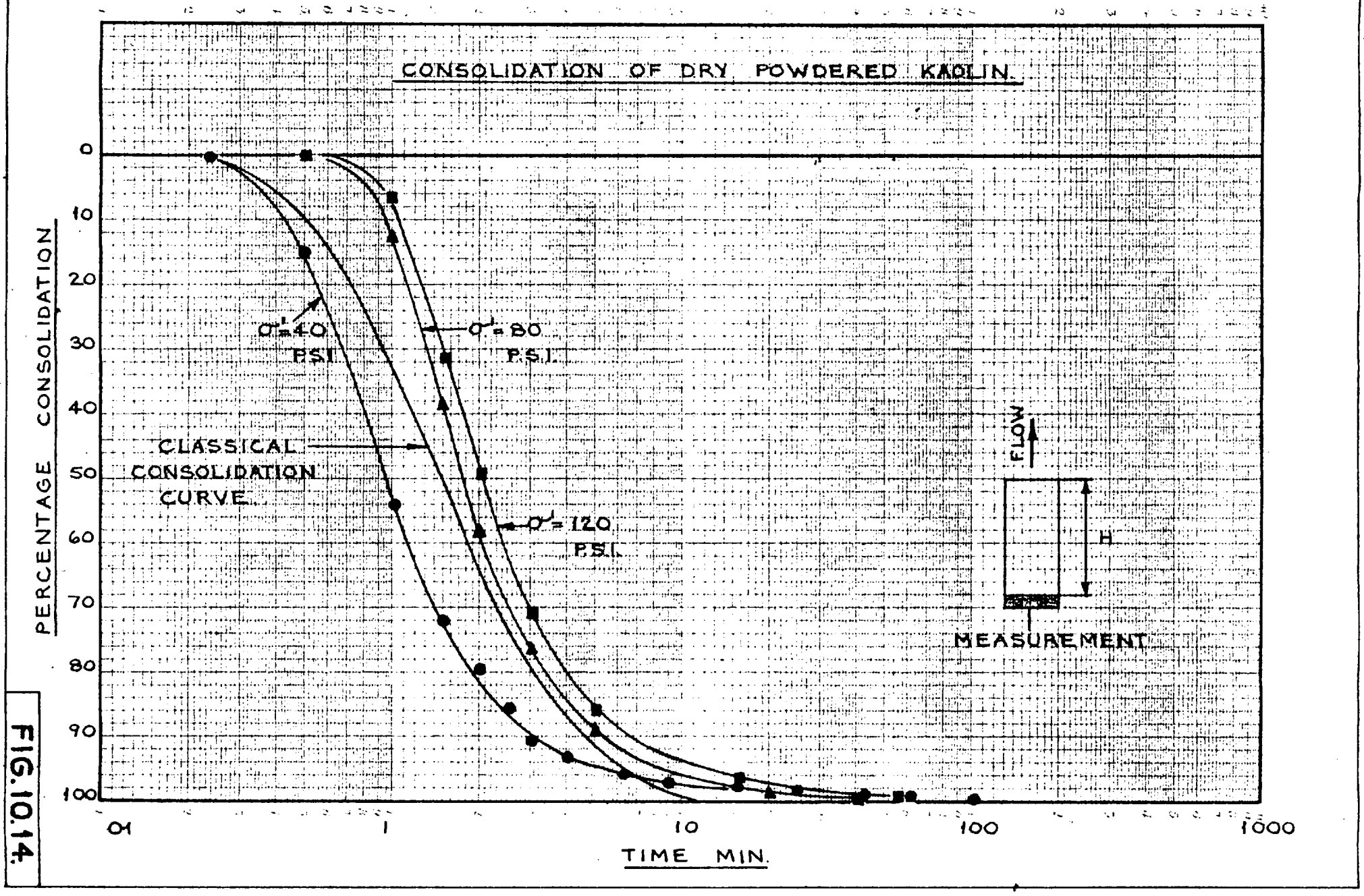

CONSOLIDATION OF DRY POWDERED KAOLIN.
PERCENTAGE CONSOLIDATION
0
10
20
30
40
50
60
70
80
90
100
0.1
1
10
100
1000
TIME MIN.
σ'=40 P.S.I.
σ'=80 P.S.I.
σ'=120 P.S.I.
CLASSICAL CONSOLIDATION CURVE.
FLOW
H
MEASUREMENT

FIG. 10.14.

CHAPTER 11

REVIEW AND CONCLUDING REMARKS

(11.1) Measurement of pore pressures.

In Chapter 3 a discussion was given of the techniques which have been used to measure pore pressures in the work of this thesis. It is hoped that this will be a useful guide to future workers in this field. The reader's attention is drawn to the difference of the technique used to measure pore water pressures to that usually advocated. It is felt that when used in long term tests with intermittent readings, the "rate of creep method" which was described in section (3.1)b is superior to the commonly used method of maintaining a constant level in the null indicator.

The brief study of the properties of porous ceramic materials should be useful in choosing a suitable porous element for use in the range of values of $(u_a - u_w)$ from 0 to 75 p.s.i.

(11.2) The principle of effective stress in partly saturated soils.

The experiments described in Chapter 5 illustrate that the fundamental form of the effective stress equation which has been adopted in this thesis is correct. The effective stress in a partly saturated soil for both shear stress and volume change has been shown (in Chapters 5, 7 and 9) to depend on the sum of two pressure differences and to be independent of the absolute magnitude of total stress and pore pressure (within the range of pressures investigated).

The relationships between the parameter χ and the degree of saturation S for shear tests on compacted soils were summarised in fig. (7.35). Two tests relating volume change to effective stress

(Chapter 9) gave very similar χ-S curves. For comparison, fig.(11.1) shows a set of χ-S curves obtained for remoulded partly saturated soils by Donald (1961). These curves have many features in common with those for compacted soils, viz: Soils containing little or no clay behave almost like assemblages of ideal spheres, but the behaviour of clay soils is far from ideal.

It can thus be concluded that values of χ measured by comparing the behaviour of partly saturated soils with that of saturated soils leads to 'apparent' values of χ which depend a good deal on the structure and composition of the soil. The relation between χ and S for volume change appears to be similar to that for shear strength, but there is insufficient data to show whether or not the two relations are identical.

Several experimental difficulties are encountered in relating χ to S. The true effective stress relations for partly saturated soils can only be inferred from the behaviour of saturated soils. There is evidence, however, (Chapters 7 and 9) that the shear strength parameters and compressibility of a soil in terms of effective stress may be modified by unsaturation. The extent of the modification is difficult to assess.

Not only do measured values of the degree of saturation appear unrepresentative of the soil structure, but non-uniform stress conditions in triaxial testing make the measurement of representative volume changes difficult. Hence changes of saturation of the failure zone during testing cannot be estimated reliably, nor can accurate corrections be made to the shear strength for the rate of volume change of the failure zone.

False "cohesion intercepts" which arise from ignoring the true nature of effective stress in partly saturated soils were illustrated in Chapter 5 and can be seen in the results of Chapter 7.

(11.3) Non-uniform pore pressures in triaxial testing.

It was shown in Chapter 8 that a good deal of attention must be paid to choosing a suitable rate of strain if representative pore pressure measurements and accurate shear strength parameters are to be determined. It is also difficult to obtain a representative pore pressure value from a fairly rapid test even with measurements taken at several points. This would require integration of the pore pressure over the volume of the failure zone. The simplest method of obtaining representative pore pressures is to use base measurement in conjunction with a suitably slow rate of strain. The rate of strain required to give a desired degree of pore pressure equalisation can be estimated from the consolidation characteristics of the soil.

It was shown that the elimination of frictional restraint from the loading plates in a triaxial test leads to more uniform stress conditions and pore pressures. It should prove worth while to extend this work. Not only will it allow greater rates of strain to be used, but overall volume changes will become more representative of the failure zone (which extends throughout the sample in a test of this type on a soil which does not fail in a narrow zone).

Data presented in Chapter 9 shows that the time taken by the soil to reach initial equilibrium under its confining pressure must also be kept in mind in triaxial testing.

(11.4) Consolidation of partly saturated soils.

Chapter 10 described a preliminary investigation of some of

the factors controlling the consolidation of partly saturated soils.

A great deal of work remains to be done on this subject, especially with regard to steady and unsteady state flow of two phase fluids through porous media (i.e. with $0 < S < 1$). It is hoped that Chapter 10 will provide a useful introduction to future work.

(11.5) Concluding remarks.

The study of shear strength, volume change and consolidation in partly saturated soils is very complex and a great deal of experimental work is required before useful progress can be made in the understanding of the subject.

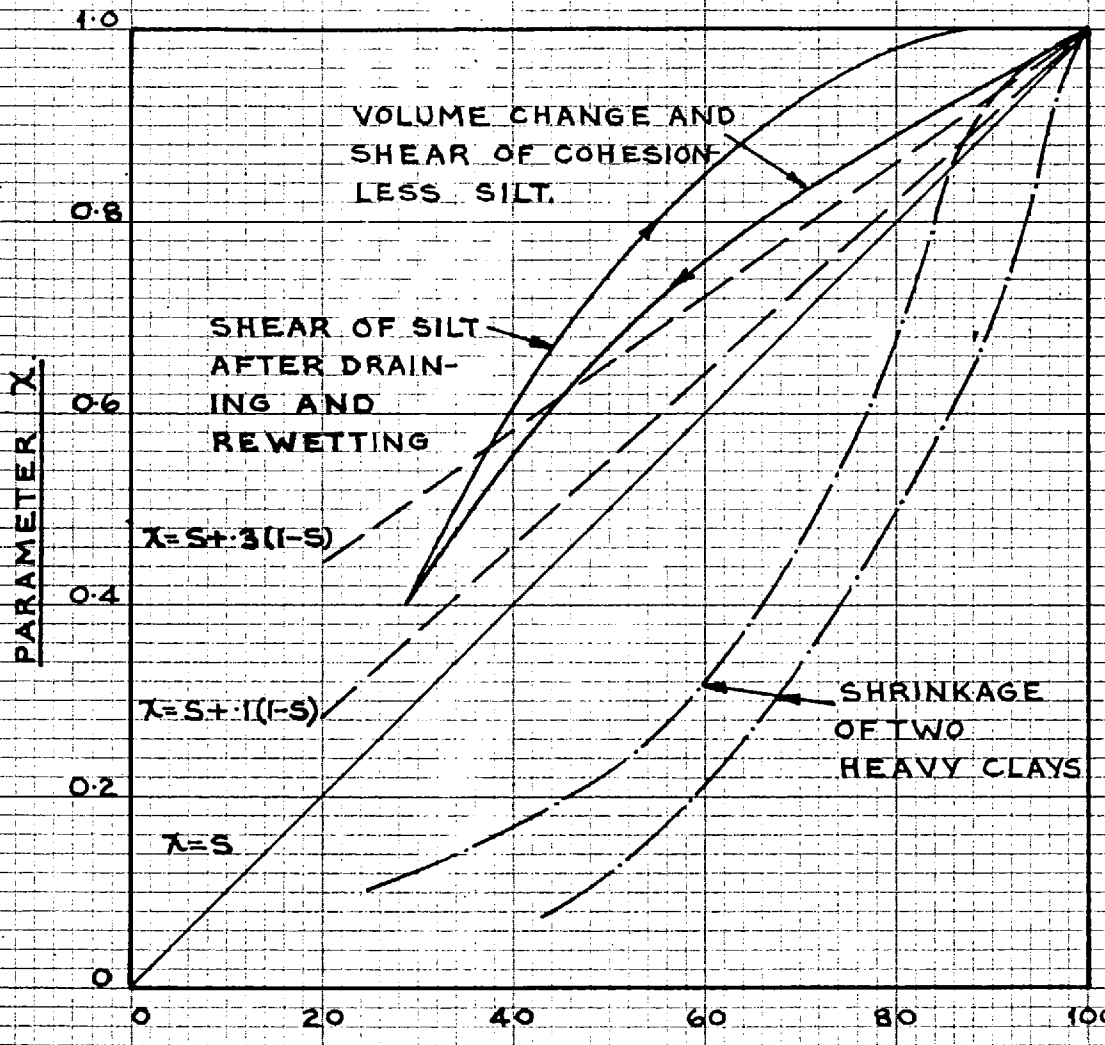
As far as compacted soils are concerned, it is clear that more work will have to be done on the investigation of the behaviour of compacted soils at constant water content. It is suggested that the use of techniques which ensure uniform stresses in the triaxial test will be useful in future work.

It will also be interesting to investigate effective stresses in partly saturated soils which are compacted at a given water content and then conditioned by drying or wetting up under confined conditions. This would simulate conditions in partly saturated zones of an earth dam or embankment which are not subject to saturation by seepage. (e.g. in a sloping core dam where large portions of the embankment are protected from seepage by filters).

The effect of differing stress ratios on the effective stress parameter χ in partly saturated compacted soils will also be of great interest.

It will be very useful if the range of suction measurement

in triaxial testing which was achieved in this thesis can be extended to cover the full range of suctions which can be expected in compacted soil structures.



DONALD'S RESULTS FOR VOLUME CHANGE AND SHEAR OF PARTLY SATURATED SOILS.

FIG. 11.1.

ACKNOWLEDGEMENTS

The work described in this thesis was carried out in the Soil Mechanics Laboratory of the Imperial College of Science and Technology and was financed by a scholarship awarded by the Council of the University of the Witwatersrand and a grant from the South African Council for Scientific and Industrial Research.

With gratitude, I wish to acknowledge the help of the following persons:

(i) Dr. A.W. Bishop who supervised the thesis and was always ready to discuss the various problems which arose and make helpful suggestions for their solution.

(ii) The staff of the Soil Mechanics Department of Imperial College under the leadership of Professor A.W. Skempton.

(iii) Dr. R.E. Gibson who spent a considerable time in the solution of the various mathematical problems which arose.

(iv) The writer's fellow research students (and in particular Mr. I.B. Donald) for their cheerful discussions and helpful criticisms.

(v) Mr. David Evans who, often under great pressure of work, never failed to complete urgently needed items of apparatus in time.

Finally, I wish to thank my wife who has helped and encouraged me all along and who also typed this thesis.

G.E. BLIGHT.

LIST OF REFERENCES

ADAM, N.K. (1941) "The physics and chemistry of surfaces". Oxford. U.P.

ADAM, N.K. (1956) "Physical Chemistry". Oxford. U.P.

AITCHISON, G.D. (1956) "The circumstances of unsaturation in soils". Proc. 2nd Aust. - N.Z. Conf. Soil Mech. & Found. Eng.

AITCHISON, G.D. & DONALD, I.B. (1956) "Effective stresses in unsaturated soils". Proc. 2nd Aust. - N.Z. Conf. Soil Mech. & Found. Eng.

AITCHISON, G.D. (1957) "The strength of quasi-saturated and unsaturated soils in relation to the pressure deficiency in the pore water". Proc. 4th Int. Conf. Soil Mech. & Found. Eng.

AITCHISON, G.D. (1960) "Relationships of moisture stress and effective stress functions in unsaturated soils". Proceedings of conference on pore pressure and suction in soils. Butterworth, London.

ALPAN, I. (1959) "A study of the principle of effective stress in partly saturated soils". Ph.D. Thesis, University of London.

A.S.T.M. "Recommended firing rate for ceramic whitewear materials". Standards, Part 3 (1955).

ARONOFSKY, J.S. (1954) "Effect of gas slip on unsteady flow of gas through porous media". Jour. App. Phys. V.25, N.1.

ARONOFSKY, J.S. & FERRIS, O.D. (1954) "Transient flow of non-ideal gases in porous solids". Jour. App. Phys. V.25, N.10.

BISHOP, A.W. (1950) Correspondence. Geotechnique 2, 113-116.

BISHOP, A.W. & ELDIN, G. (1950) "Undrained triaxial tests on saturated sands and their significance in the general theory of shear strength". Geotechnique V.2.

BISHOP, A.W. (1955) "The principle of effective stress". Excerpt from lecture to Norwegian Geotechnical Society in 1955. Teknisk Ukeblad, V.39, 1959.

BISHOP, A.W. & HENKEL, D.J. (1957) "The measurement of soil properties in the triaxial test". Edward Arnold.

BISHOP, A.W. (1957) "Some factors controlling the pore pressures set up during the construction of earth dams". Proc. 4th Int. Conf. Soil Mech. & Found. Eng. Butterworth, London.

BISHOP, A.W. (1959) "Concepts of uplift in soil and concrete". Unpublished note.

BISHOP, A.W. (1960) "The measurement of pore pressure in the triaxial test". Proceedings of conference on pore pressure and suction in soils. Butterworth, London.

BISHOP, A.W. (1960) Discussion of conference on pore pressure and suction in soil. Butterworth, London.

BISHOP, A.W., ALPAN, I., BLIGHT, G.E. & DONALD, I.B. (1960) "Factors controlling the strength of partly saturated cohesive soils". Proceedings and discussion of A.S.C.E.research conference on shear strength of cohesive soils.

BLACK, W.P.M., CRONEY, D. & JACOBS, J.C. (1958) "Field studies of the movement of soil moisture" Road research technical paper No. 41. London (H.M.S.O.).

BROWN, J.D. (1961) "Stability of clay slopes". M.Sc. Thesis, University of London.

BRUGGEMAN, J.R., ZANGER, C.N. & BRAHTZ, J.H.A.(1939) "Notes on analytical soil mechanics". Tech. Mem. No. 592 U.S. Bur. Recl.

CARMAN, P.C. (1956) "Flow of gases through porous media". Butterworth, London.

CASAGRANDE, A. & HIRSCHFELD, R.C.(1960) "Investigation of stress-deformation and strength characteristics of compacted clays". Proc. of A.S.C.E. Research Conf. on shear strength of cohesive soils.

COX, A.D., EASON, G. & HOPKINS, H.G. (1958) "Axially symmetric plastic deformations in soils". A.R.D.E. Report (B) 14/58 War Office internal report.

CRANK, J. (1956) "The mathematics of diffusion". Oxford. U.P.

CRANK, J. (1957) "Diffusion coefficients in solids, their measurement and significance". Faraday Soc. Disc. No. 23.

CRONEY, D., COLEMAN, J.D. & BRIDGE, P.M. (1952) "The suction of moisture held in soil and other porous materials". Road Research Technical Paper No. 24. London, (H.M.S.O.).

CRONEY, D., COLEMAN, J.D. & BLACK, W.P.M. (1958) "The movement & distribution of water in soil in relation to highway design & performance". Highway Research Board, Sp. Report No. 40.

CRONEY, D. & COLEMAN, J.D. (1960) "Pore pressure and suction in soil". Proceedings of conference on pore pressure and suction in soils. Butterworth, London.

CRONEY, D. & COLEMAN, J.D. (1960) Discussions of conference on pore pressure and suction in soils. Butterworth, London.

DENBIGH, K.G. (1951) "The thermodynamics of the steady state". Methuen.

DONALD, I.B. (1956) "Shear strength measurements in unsaturated non-cohesive soils with negative pore pressures". Proc. 2nd Aust. N.Z. Conf. Soil. Mech. & Found. Eng.

DONALD, I.B. (1960) Discussion of conference on pore pressure and suction in soil. Butterworth, London.

DONALD, I.B. (1961) "The mechanical properties of saturated and partly saturated soils with particular reference to the effects of negative pore water pressures". Ph.D. Thesis, University of London.

DORSEY, E.N. (1940) "Properties of ordinary water substance". Rheinhold, New York.

DUPUIT, A.J.E.J.(1863) "Etudes theoretiques et pratiques sur le mouvement des eaux".

EPSTEIN, P.S. & PLESSET, M.S. (1950) "On the stability of gas bubbles in liquid-gas solutions". Jour. Chem. Phys. V.18, N.11.

FILON, L.N.G. (1902) "On the elastic equilibrium of circular cylinders under certain practical systems of load". Phil. Trans. Roy. Soc. V.198(A) 147-223.

FRAZER, A.M. (1957) "The influence of stress ratio on compressibility and pore pressure coefficients in compacted soils". Ph.D. Thesis, University of London.

GARDNER, W.R. (1959) "Mathematics of isothermal water conduction in unsaturated soil". International symposium on water and its movement in soils. Highway Research Board. Bulletin 40.

GARDNER, W.R. (1960) "Soil suction and water movement". Proceedings of conference on pore pressure and suction in soils. Butterworth, London.

GIBSON, R.E. & HENKEL, D.J. (1954) "Influence of duration of tests at constant rate of strain on measured 'drained' strength". Geotechnique 4: 6-15.

HANSON, B. (1955) "Shear strength and pore pressure characteristics of compacted soils". M.Sc. Thesis, University of London.

HENKEL, D.J. (1958) "The correlation between deformation, pore water pressure, and strength characteristics of saturated clays". Ph.D. Thesis, University of London.

HILF, J.W. (1948) "Estimating construction pore pressures in rolled earth dams". Proc. 2nd Int. Conf. Soil Mech. & Found. Eng. V.3. 234-240.

HILF, J.W. (1956) "An investigation of pore water pressure in compacted cohesive soils". Tech. Mem. No. 654, Bureau of Reclamation.

HVORSLEV, M.J. (1937) "Über die Festigkeitseigenschaften gestörter bindiger Böden". Ingeniørvidenskabelige Skifter, A No. 45, Copenhagen.

JENNINGS, J.E. (1960) "A revised effective stress law for use in the prediction of the behaviour of unsaturated soils". Proc. Conference on pore pressure and suction in soils. Butterworth, London.

LAUGHTON, A.S. (1955) "The compaction of ocean sediments". Ph.D. Thesis, University of Cambridge.

LEWIS, W.A. & ROSS, N.F. (1955) "An investigation of the relationship between the shear strength of remoulded cohesive soil and the soil moisture suction". R.R.L. Research Note RN/2389/WAL.NFR.

LOW, P.F. (1959) "The condition of water in soil systems and its response to applied force fields". International symposium on water and its movement in soils. Highway Res. Bd. Bul. 40.

MARSHALL, T.J. (1959) "Relations between water and soil". Commonwealth Bureau Soils Tech. Comm. No.50, C.A.B. Harpenden.

PHILIP, J.R. (1957) "The theory of infiltration 1 to 7". Soil Science V.83 to V.85.

RENDULIC, L. (1937) "Ein Grundgesetz der Tonmechanik und sein experimentaler beweis". Bauingenieur, 18.

ROLLINS, R.L., SPANGLER, M.G. & KIRKHAM, D. (1954) "Movement of soil moisture under a thermal gradient". Proc. Highways Res. Bd. V.33.

ROWE, P.W. (1959) "Measurement of the coefficient of consolidation of lacustrine clay". Geotechnique 9, 107-118.

SCHEIDEGGER, A.E. (1957) "The physics of flow through porous media". University of Toronto.

SCHMERTMAN, J.H. & OSTERBERG, J.O. (1960) "An experimental study of the development of cohesion & friction with axial strain in saturated cohesive soils". A.S.C.E. Research Conf. on shear strength of cohesive soils.

SCHOFIELD, R.K. (1935) "The pF of the water in soil". Trans. 3rd International Congr. Soil Sci. V.2.

SCHOFIELD, R.K. (1958) Discussion of Proceedings 10th Symposium Colston Research Society.

SCHOFIELD, R.K. (1960) "Suction in swollen clays". Proceedings of conference on pore pressure and suction in soils. Butterworth, London.

SHOCKLEY, G.W. & AHLVIN, R.G. (1960) "Non-uniform conditions in triaxial test specimens". A.S.C.E. Research conf. on shear strength of cohesive soils.

SKEMPTON, A.W. & BISHOP, A.W. (1954) "Soils" Chapter X of "Building materials. Their elasticity and inelasticity". North Holland Pub. Co.

SKEMPTON, A.W. (1960) "Effective stress in soils, concrete & rocks". Proc. conf. on pore pressure and suction in soils. Butterworth, London.

STARLING, S.G. (1946) "Mechanical properties of matter". Macmillan, London.

TAYLOR, D.W. (1944) Tenth progress report on shear research to U.S. Engineers. M.I.T. Publication.

TAYLOR, D.W. (1951) "Report on research on shearing characteristics of clay". M.I.T. Publication.

TERZAGHI, K. (1923) "Die berechnung der durchlässigkeitsziffer des tones aus dern verlauf der hydrodynamischen spannungserscheinungen". Sitz. Akad. Wissen. wien Math. Naturw. Kl. Abt. 11a, 132.

TERZAGHI, K. (1932) "Tragfahigkeit der flachgrundungen". Int. Assoc. Bridge struct. eng. Prelim. Publ.

TERZAGHI, K. (1934) "Der spannungszustand im porenwasser trochnender betonkörper". Der Bauingenieur, V.15, 303.

TERZAGHI, K. (1948) "Theoretical soil mechanics". Wiley, New York.

TOWNER, G.D. (1958) "Some moisture-dependent properties of porous materials". Ph.D. Thesis, University of Cambridge.

WHITMAN, R.V. (1960) "Some considerations and data regarding the shear strength of clays". Proc. A.S.C.E. Research conf. on shear strength of cohesive soils.

WINTERKORN, H.F.(1947) "Fundamental similarities between electro-osmotic and thermo-osmotic phenomena". Highway Res. Bd., Proc. 27.

WINTERKORN, H.F.(1959) "Mass transport phenomena in moist porous systems as viewed from the thermodynamics of irreversible processes". International symposium on water and its movement in soils. Highway Res. Bd. Bul. 40.

WOOD, C.C. (1958) "Shear strength and volume change characteristics of compacted soil under conditions of plane strain".
Ph.D. Thesis, University of London.

APPENDIX TO CHAPTER 6

SUMMARY OF TEST RESULTS

(A.6.1) Stresses at failure.

Soil	Series Test No.	At Max. $(\sigma_1-\sigma_3)/\sigma_3'$			At 20% Strain		
		σ_3' p.s.i.	$\frac{1}{2}(\sigma_1-\sigma_3)$ p.s.i.	$\frac{1}{2}(\sigma_1'+\sigma_3')$ p.s.i.	σ_3' p.s.i.	$\frac{1}{2}(\sigma_1-\sigma_3)$ p.s.i.	$\frac{1}{2}(\sigma_1'+\sigma_3')$ p.s.i.
Mangla Shale	Series 1A						
	N.C.*						
	S1A T1	80.4	57.4	137.8	79.0	57.4	136.4
	T3	7.0	8.5	15.5	21.3	17.5	38.8
	T4	49.9	36.3	86.2	59.4	41.8	101.2
	T7	30.2	24.5	54.7	41.9	31.2	73.1
	T8	17.1	14.1	31.2	27.1	19.8	46.9
	T9	77.0	55.1	132.1	83.3	58.6	141.9
	O.C.*						
	S1A T2	8.3	9.9	18.2	24.1	19.6	43.7
	T5	61.2	44.9	106.1	71.1	50.5	121.6
	T6	53.0	38.7	91.7	58.3	42.7	101.0
	T10	24.9	20.0	44.9	42.1	30.3	72.4
	Series 3A						
	S3A T1	68.0	47.9	115.9	80.0	55.2	135.2
	T2	10.6	9.4	20.0	21.1	15.2	36.3
	T3	20.4	16.1	36.5	33.0	22.9	55.9
	T4	30.9	23.6	54.5	44.9	31.5	76.4
	T5	48.6	36.4	85.0	59.4	42.0	101.4
Selset Clay	Series 2A						
	S2A T1	68.2	54.3	122.5	80.2	62.5	142.7
	T2	51.8	41.7	93.5	64.1	48.7	112.8
	T3	8.9	7.6	16.5	17.2	13.6	30.8
	T4	20.0	17.0	37.0	29.7	23.4	53.1
	T5	34.4	28.3	62.7	45.7	35.8	81.5
Talybont Clay Alpan's Tests	155	10.0	13.2	23.2	11.8	13.9	25.7
	156	19.2	24.1	43.3	21.2	26.5	47.7
	157	31.6	41.3	72.9	34.8	43.6	78.4
	150	15.6	22.2	37.8	22.2	26.3	48.5
	151	34.4	47.1	81.5	45.3	54.3	99.6
	152	38.8	55.2	94.0	61.8	73.8	135.6

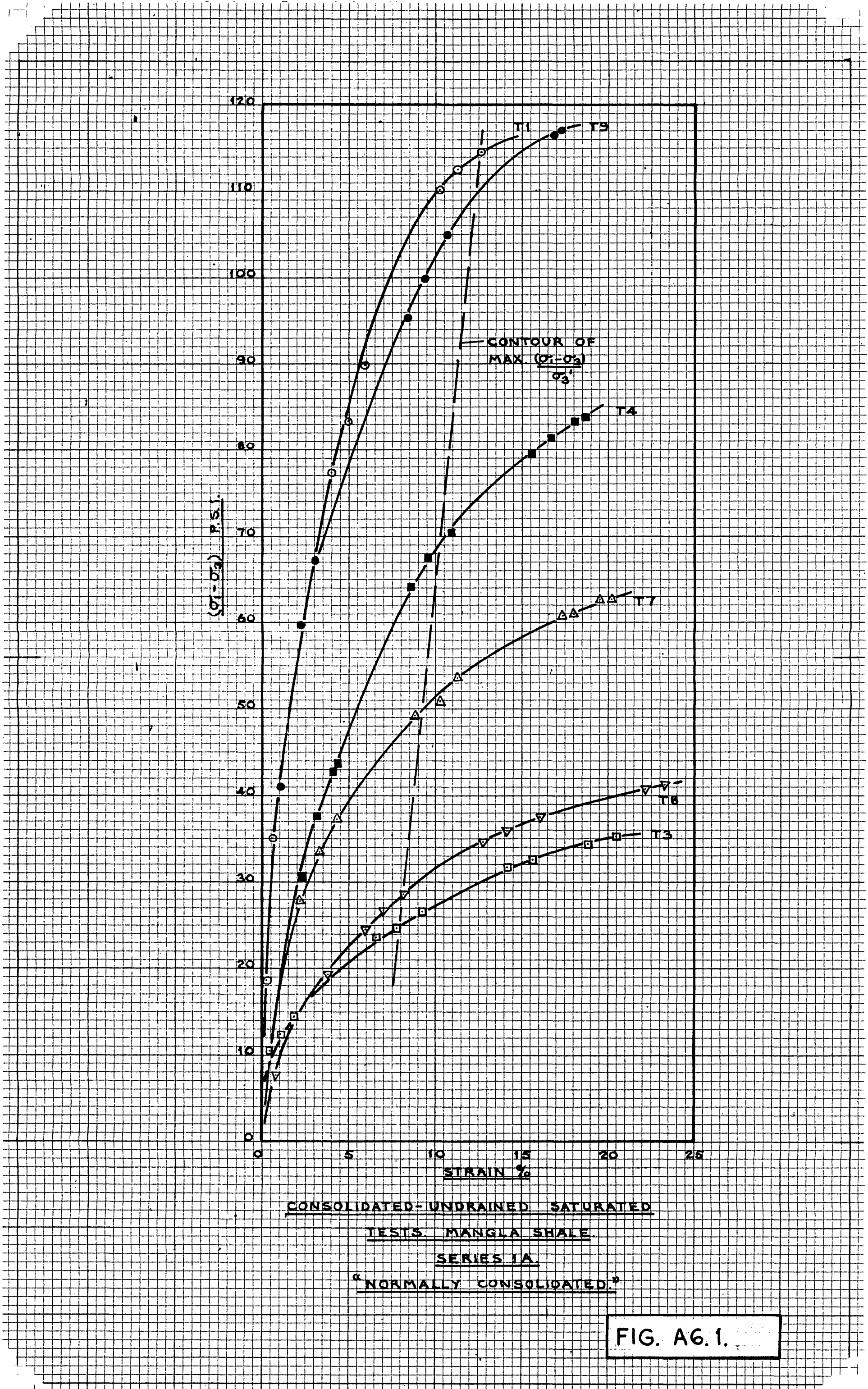
* N.C. = "normally consolidated".
O.C. = "over consolidated".

Soil	Series, Test No.	σ_3' p.s.i.	At Max. $(\sigma_1 - \sigma_3)$				
			$(\sigma_1-\sigma_3)$ p.s.i.	$d\frac{\Delta V}{V_o}/d\epsilon$	$\sigma_3' d\frac{\Delta V}{V_o}/d\epsilon$	Corrected $\frac{1}{2}(\sigma_1-\sigma_3)$ p.s.i.	$\frac{1}{2}(\sigma_1'+\sigma_3')$ p.s.i.
Talybont Clay	Series 4A						
	S4A T1	20	56.0	.040	0.8	27.6	47.6
	T2	35	92.0	.072	2.5	44.8	79.8
	T3	42	111.6	.088	3.7	53.9	95.9
	T4	10	28.5	.020	0.2	14.2	24.2
	T5	45	142.3	.25	11.2	65.6	110.6
	T6	10	34.0	.06	0.6	16.7	26.7
	T7	30	104.2	.16	4.8	49.7	79.7
	T8	61.3	194.0	.33	20.2	86.9	148.2

(A.6.2) Water contents, consolidation stresses, etc.

Soil	Series, Test No.	Water Contents %			Initial σ_3' p.s.i.	Max. Value of $\frac{(\sigma_1-\sigma_3)}{\sigma_3'}$
		Compaction	Overall at Failure	Failure Zone		
Mangla Shale	Series 1A					
	S1A T1	18.00	15.4	15.80	109.3	1.66
	T3	18.20	20.5	21.00	6.2	2.55
	T4	18.71	17.0	17.40	65.0	1.47
	T7	18.52	18.2	18.72	42.0	1.64
	T8	19.17	19.8	19.91	17.8	1.64
	T9	18.92	15.6	15.90	100.8	1.44
	T2	18.00	19.2	19.80	4.1	2.52
	T5	18.30	16.6	16.70	65.0	1.47
	T6	19.19	17.6	17.07	38.9	1.47
	T10	18.92	18.2	18.72	15.7	1.65
	Series 3A					
	S3A T1	15.85	15.9	16.2	105.6	1.42
	T2	16.00	19.1	20.2	7.0	1.83
	T3	16.00	18.3	19.1	16.6	1.62
	T4	16.78	17.1	17.8	31.2	1.57
	T5	16.78	16.4	17.0	63.2	1.50

Soil	Series, Test No.	Water Contents %			Initial σ_3' p.s.i.	Max. Value of $\frac{(\sigma_1-\sigma_3)}{\sigma_3'}$
		Compaction	Overall at Failure	Failure Zone		
Selset Clay	Series 2A					
	S2A T1	11.30	12.1	12.3	108.6	1.60
	T2	11.68	12.7	13.0	61.8	1.59
	T3	11.95	14.7	15.6	6.2	1.77
	T4	11.55	14.0	14.6	17.3	1.75
	T5	11.73	13.1	13.5	31.2	1.66
Talybont Clay Alpan's Tests	155	7.07	12.5	13.1	7.5	2.6
	156	6.52	11.8	12.4	40	2.7
	157	7.15	11.5	12.1	80	2.7
	150	9.04	11.9	12.5	5	2.9
	151	8.83	11.1	11.6	30	2.7
	152	9.17	10.7	11.2	50	2.9
Talybont Clay	Series 4A					
	S4A T1	7.52		12.4	20	2.76
	T2	7.37		11.5	35	2.56
	T3	6.86		11.4	42	2.56
	T4	7.67		13.0	10	2.83
	T5	9.22		10.6	45	2.92
	T6	8.84		12.0	10	3.34
	T7	9.16		11.3	30	3.31
	T8	9.16		10.7	61.3	2.84

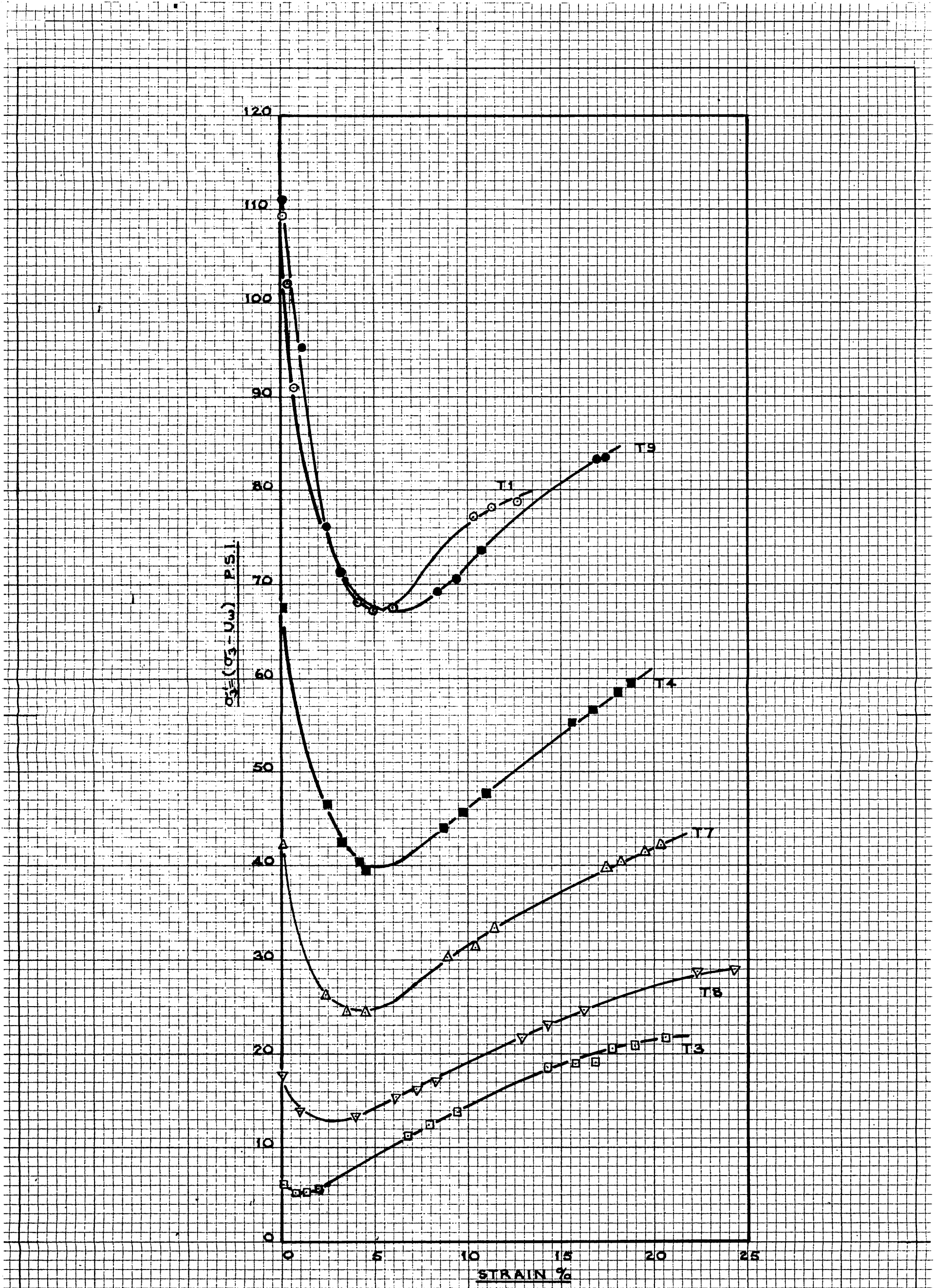


CONSOLIDATED-UNDRAINED SATURATED TESTS. MANGLA SHALE.

SERIES 1A.

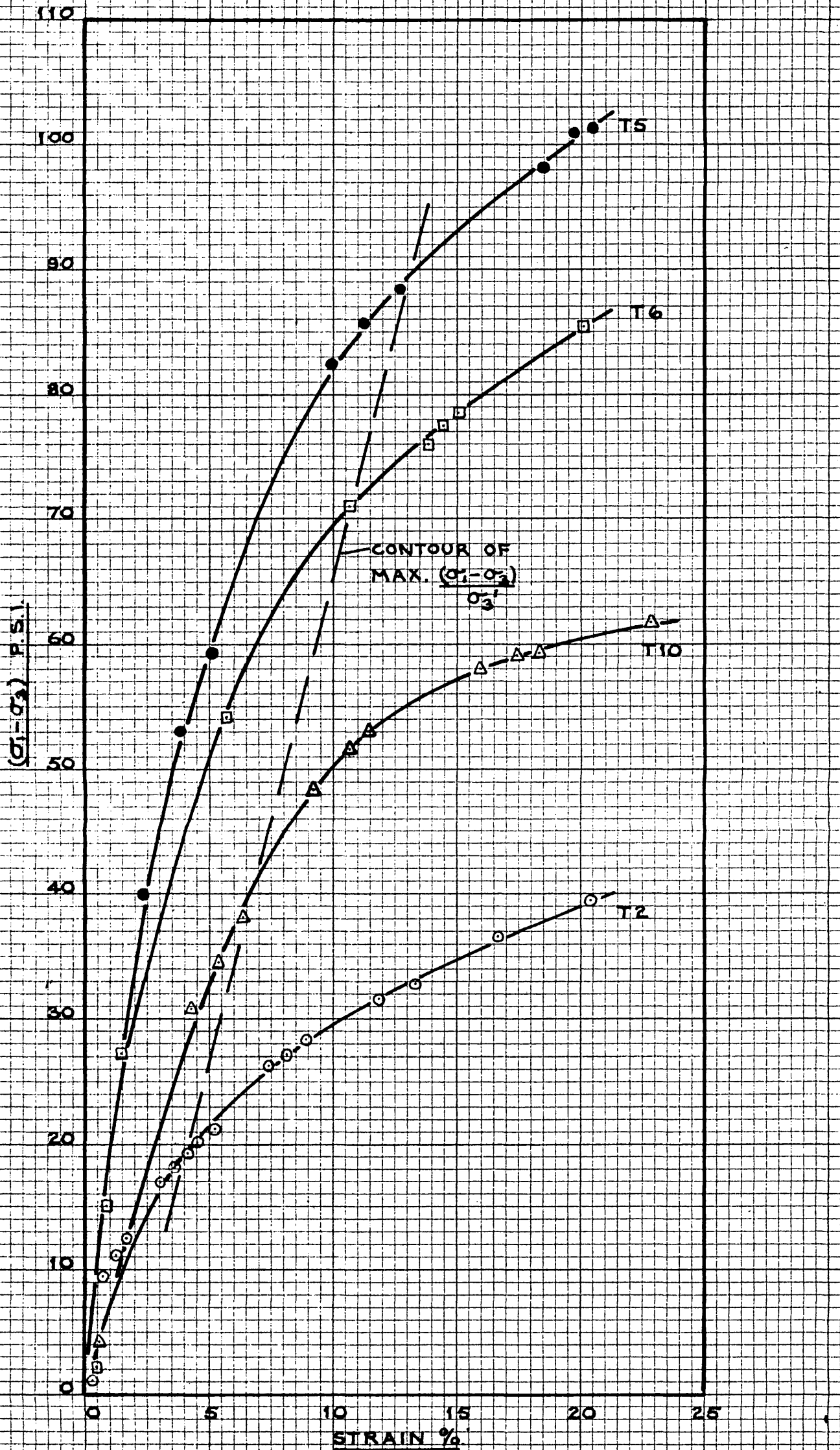
"NORMALLY CONSOLIDATED."

FIG. A6.1.



CONSOLIDATED - UNDRAINED SATURATED TESTS. MANGLA SHALE SERIES IA "NORMALLY CONSOLIDATED"

FIG. A6.2.

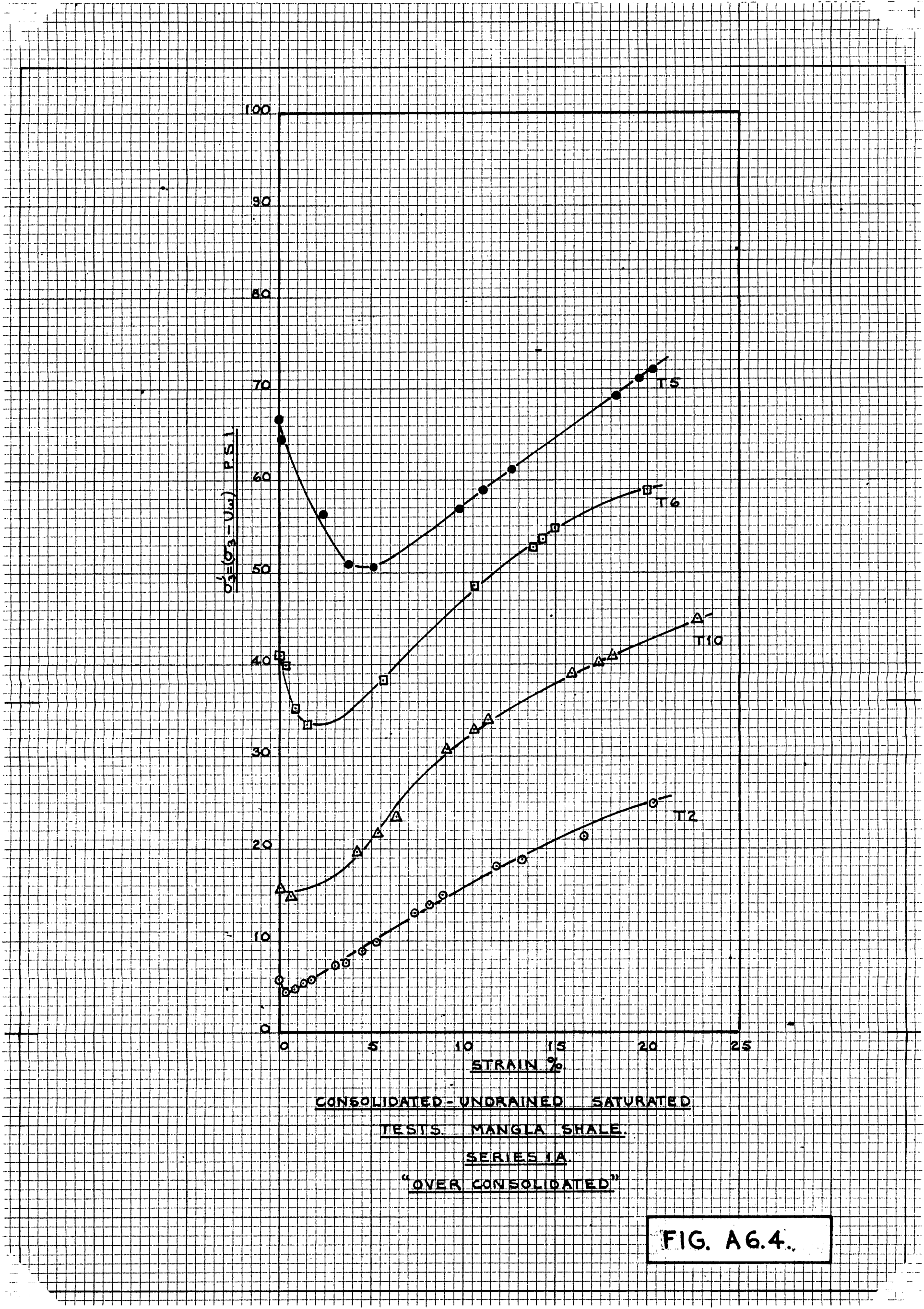


CONSOLIDATED - UNDRAINED SATURATED TESTS. MANGLA SHALE.

SERIES 1A

"OVER CONSOLIDATED"

FIG. A6.3.



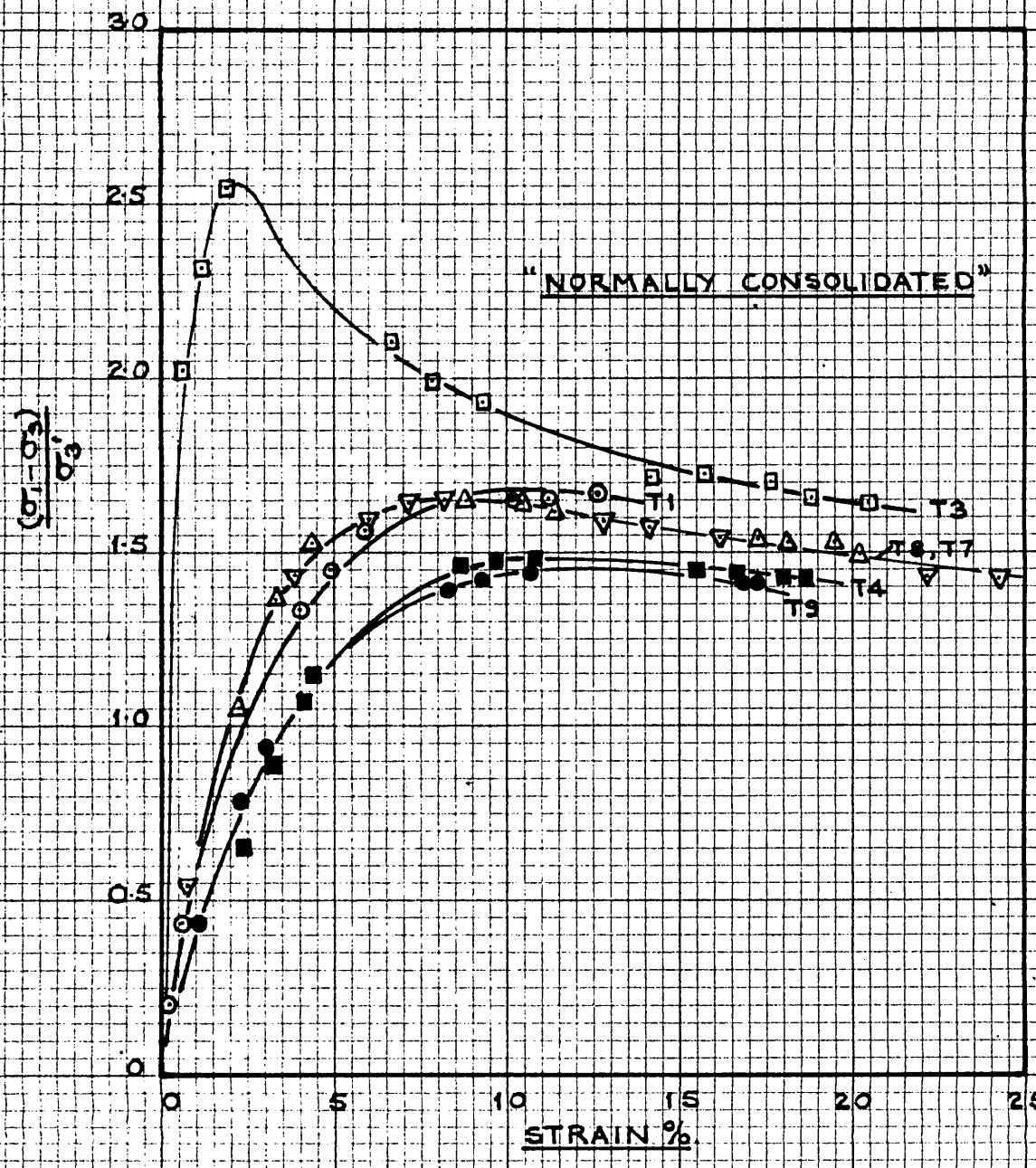
CONSOLIDATED - UNDRAINED SATURATED

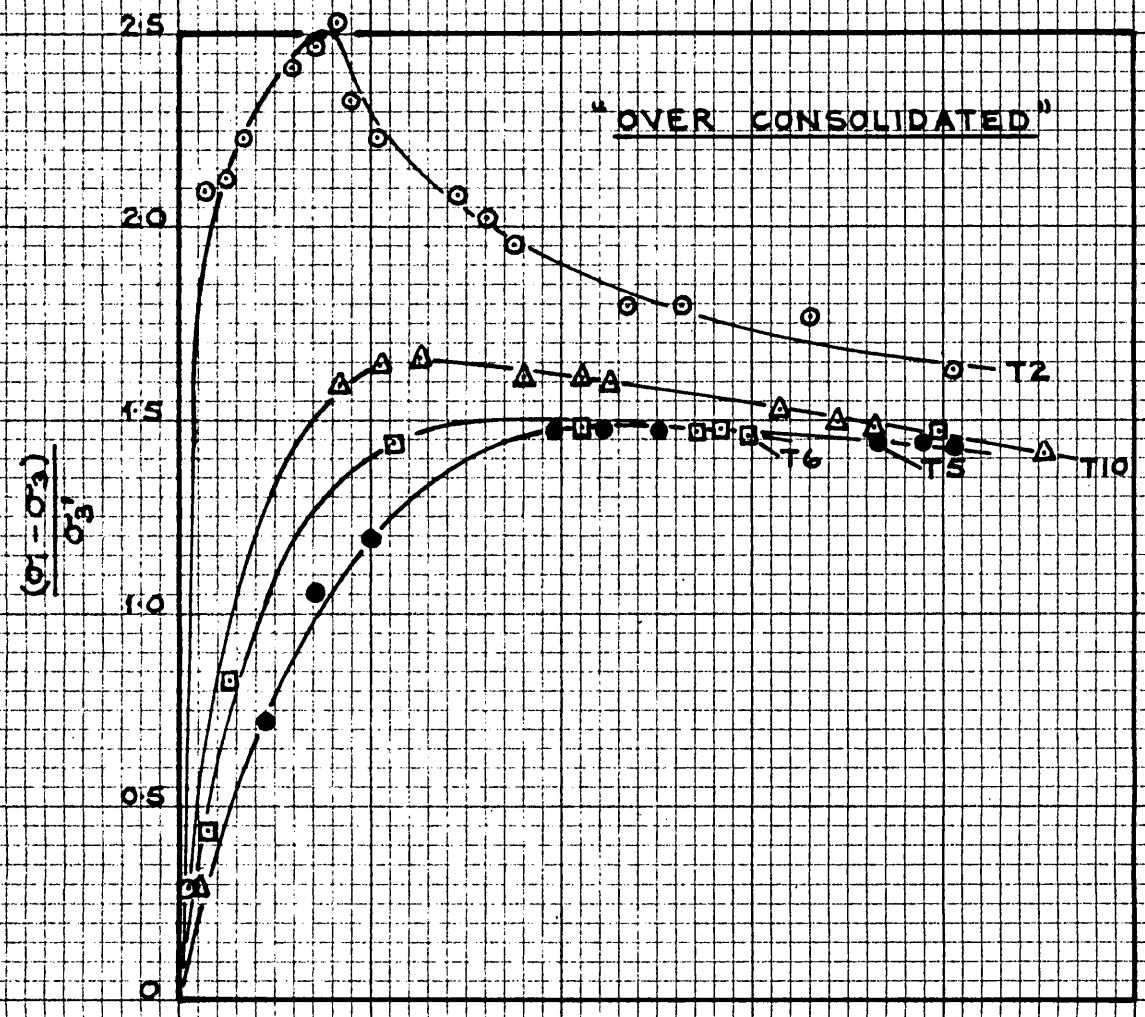
TESTS. MANGLA SHALE.

SERIES 1A.

"OVER CONSOLIDATED"

FIG. A6.4.

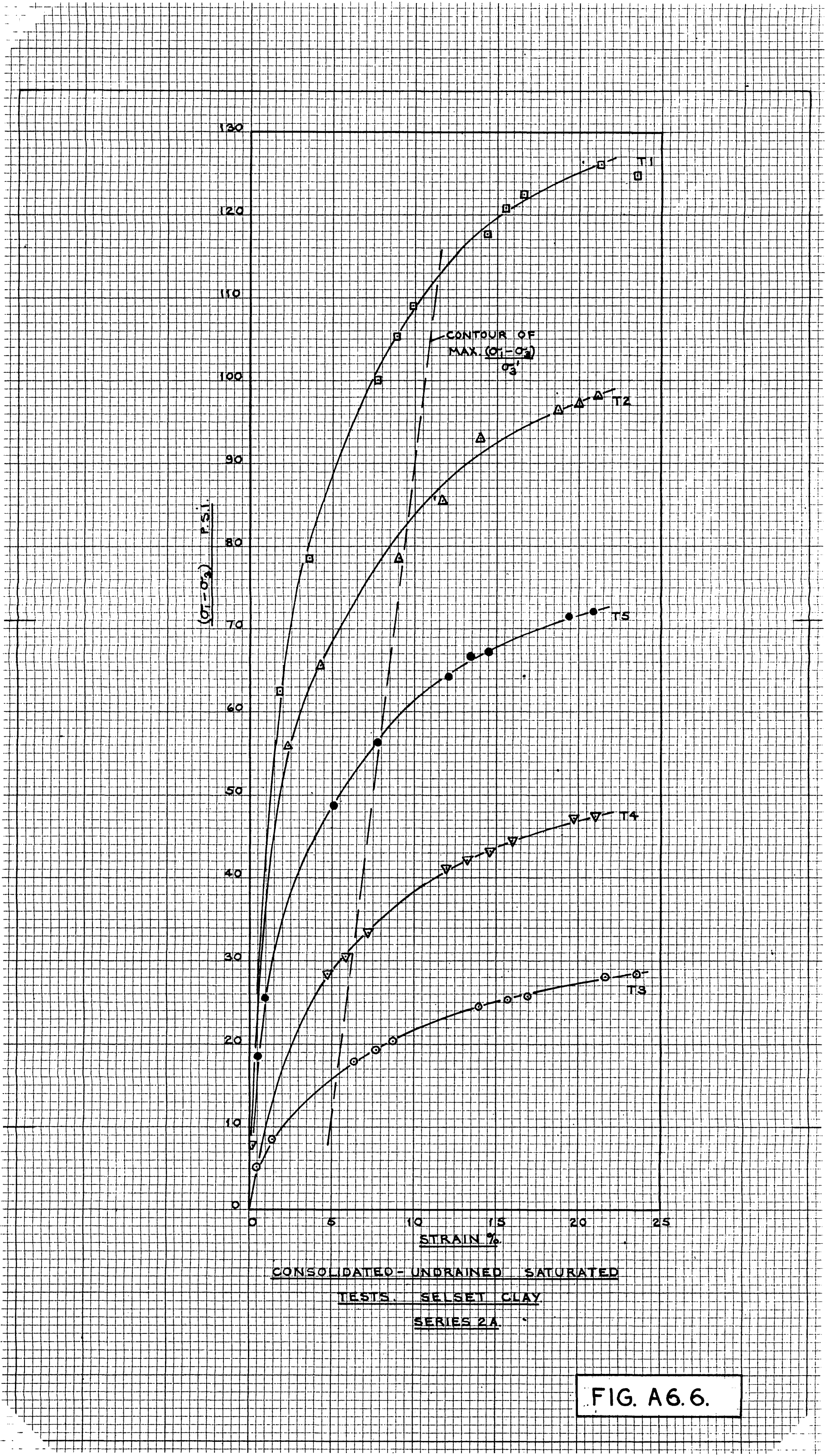




CONSOLIDATED - UNDRAINED SATURATED TESTS. MANGLA SHALE.

SERIES IA.

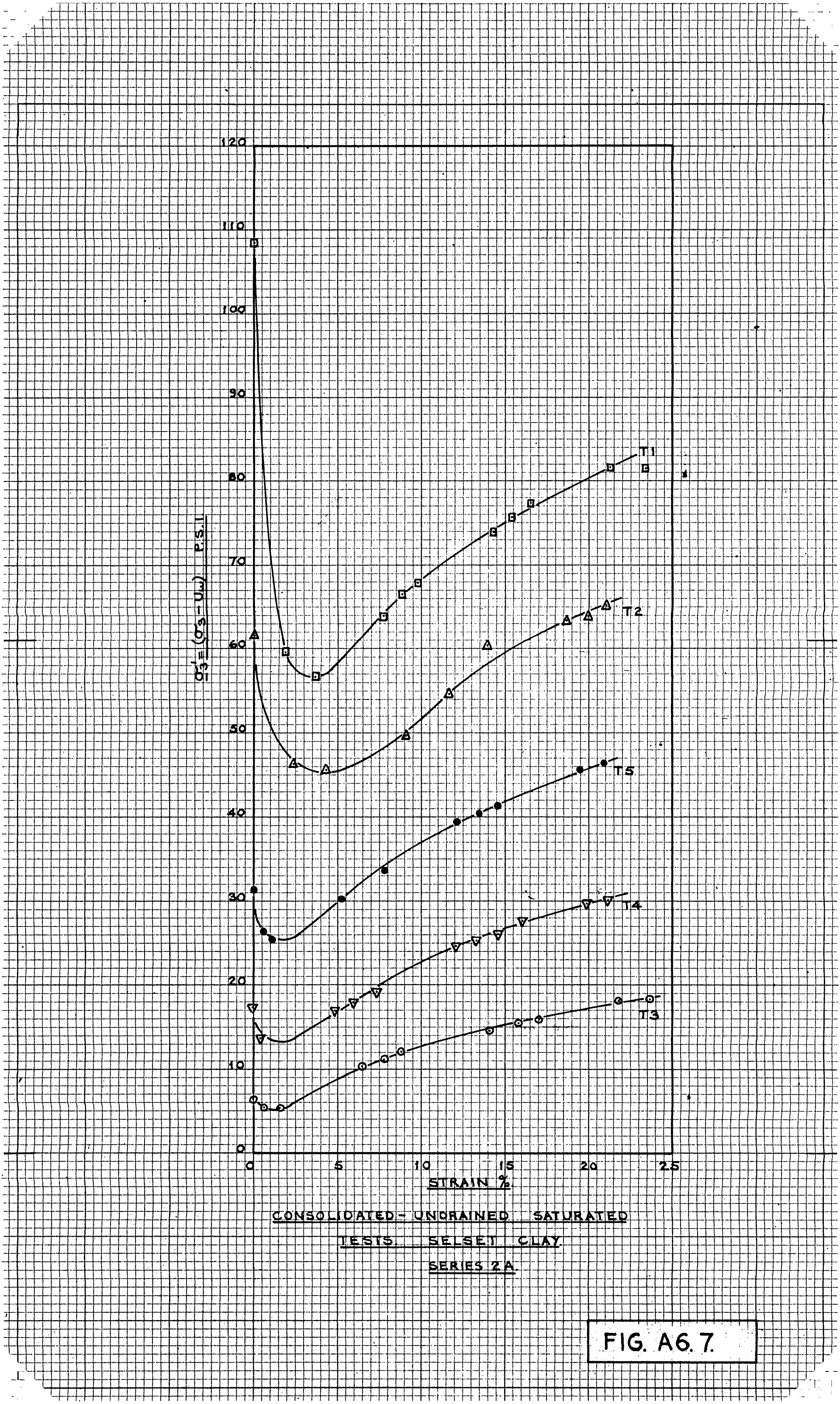
FIG. A6.5.



CONSOLIDATED - UNDRAINED SATURATED TESTS. SELSET CLAY.

SERIES 2A.

FIG. A6.6.



CONSOLIDATED - UNDRAINED SATURATED TESTS. SELSET CLAY.

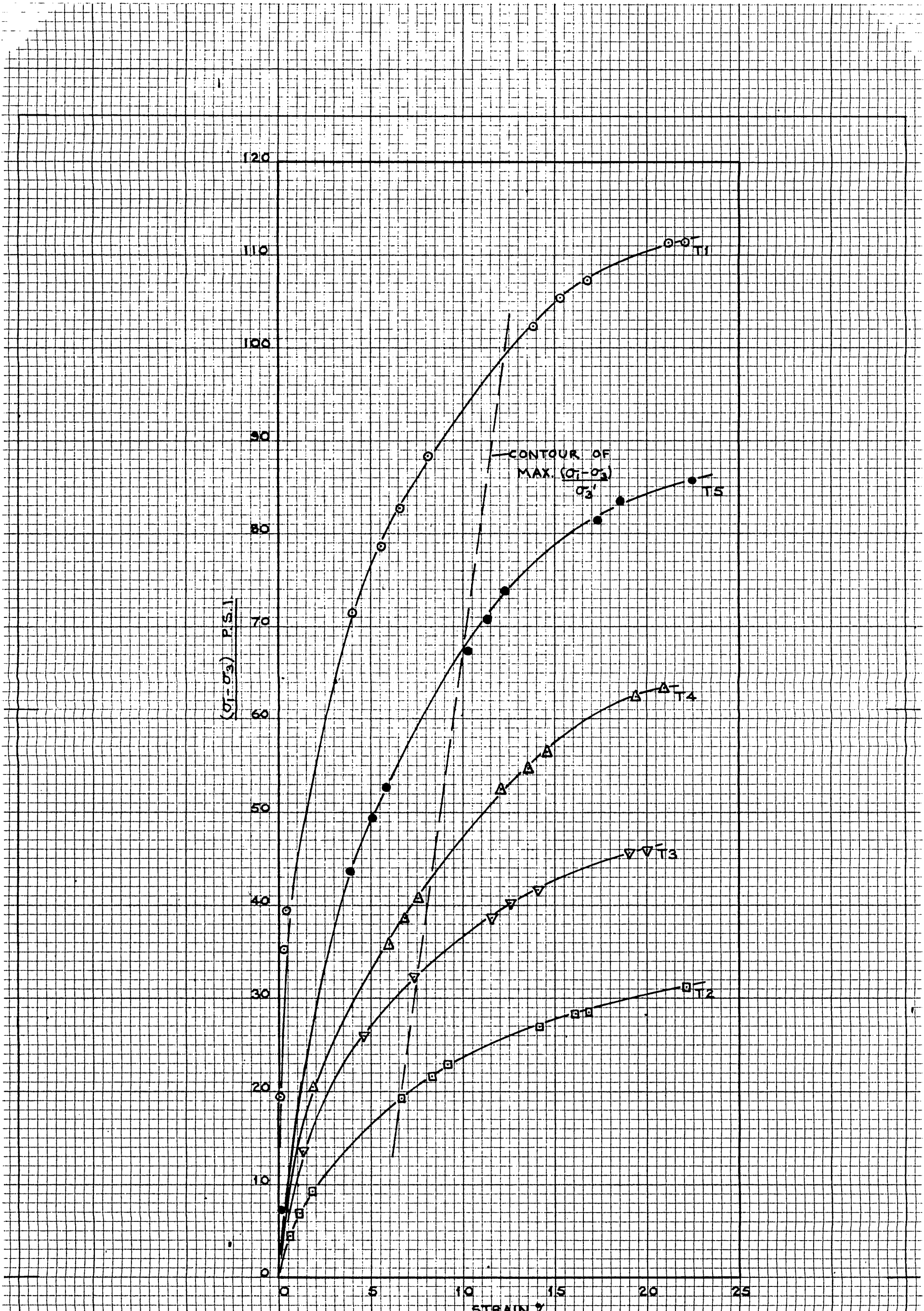
SERIES 2A.

FIG. A6.7.

CONSOLIDATED – UNDRAINED SATURATED TESTS. SELSET CLAY.

SERIES 2A.

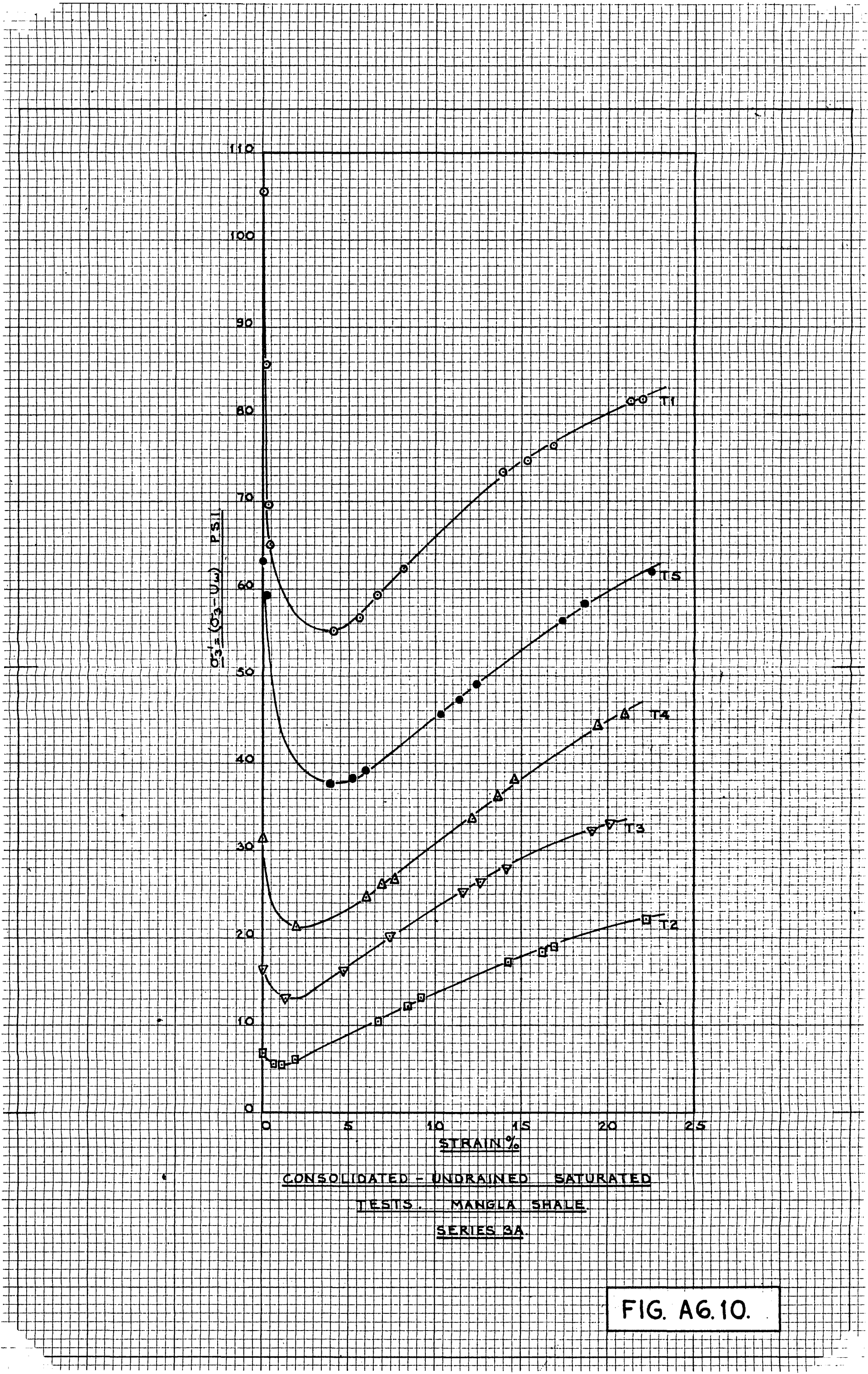
FIG. A6.8.



CONSOLIDATED - UNDRAINED SATURATED TESTS. MANGLA SHALE.

SERIES 3A.

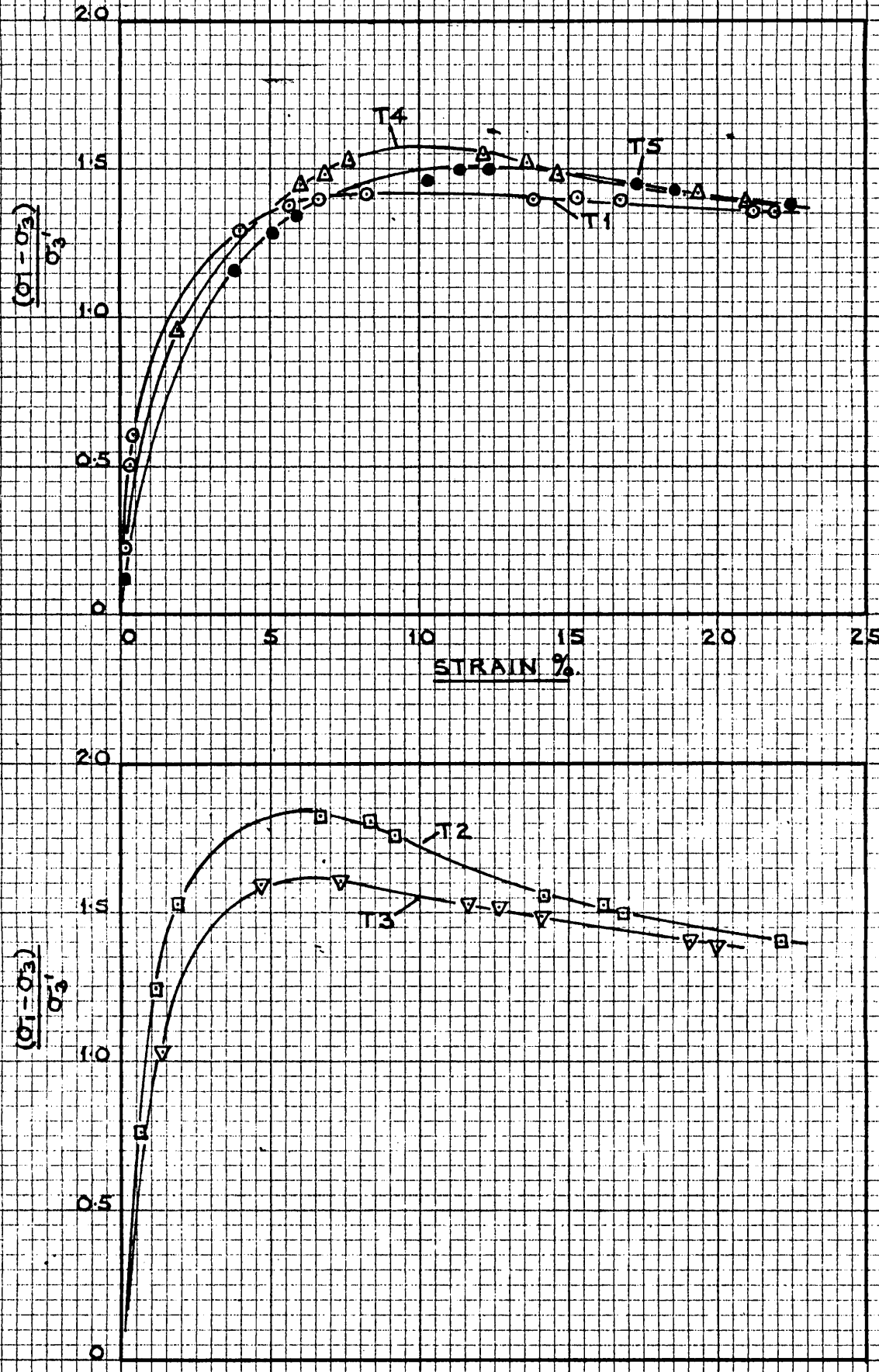
FIG. A6.9.



CONSOLIDATED - UNDRAINED SATURATED TESTS. MANGLA SHALE.

SERIES 3A.

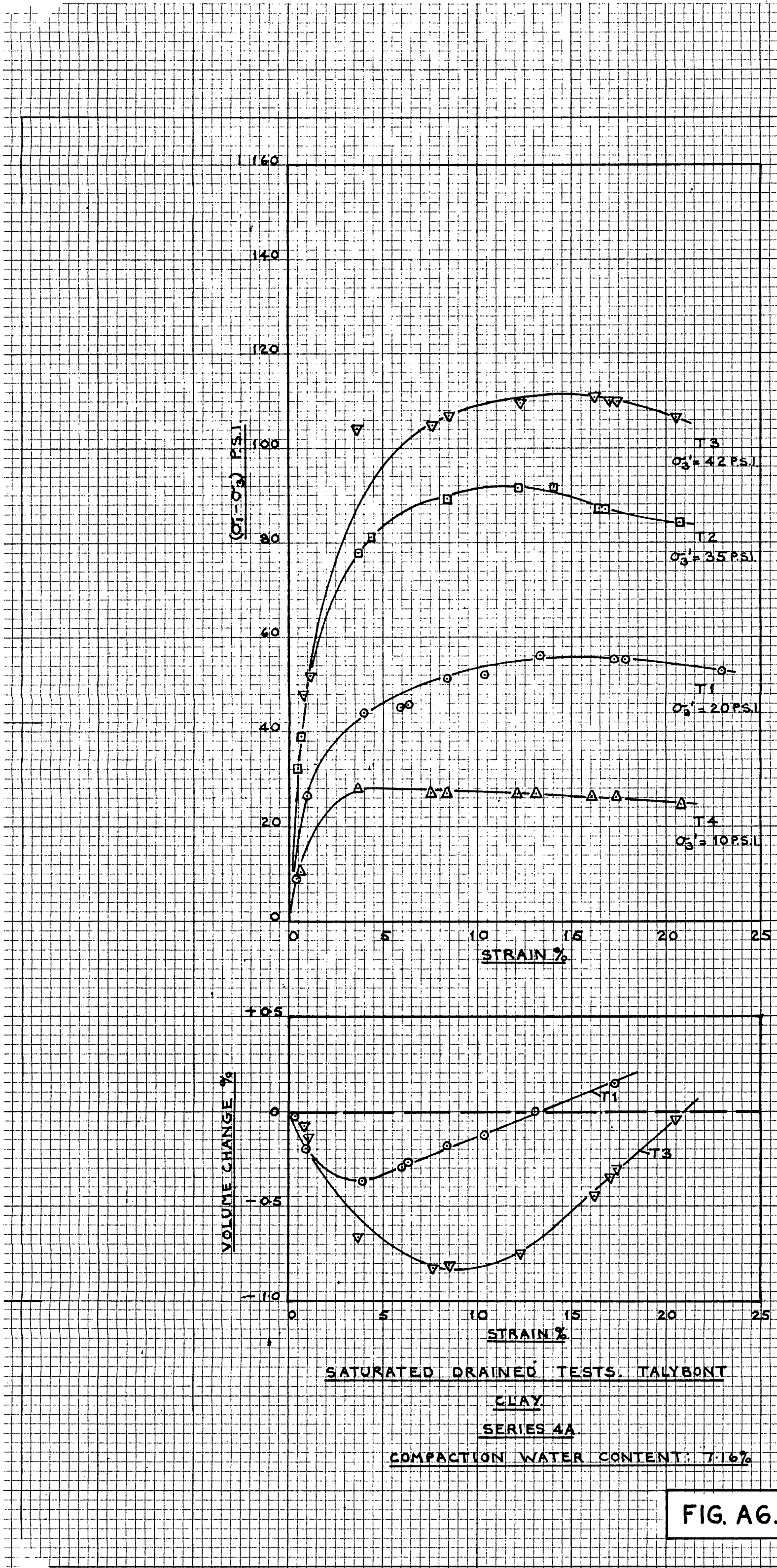
FIG. A6.10.



CONSOLIDATED - SATURATED UNDRAINED TESTS. MANGLA SHALE.

SERIES 3A.

FIG. A6.11.

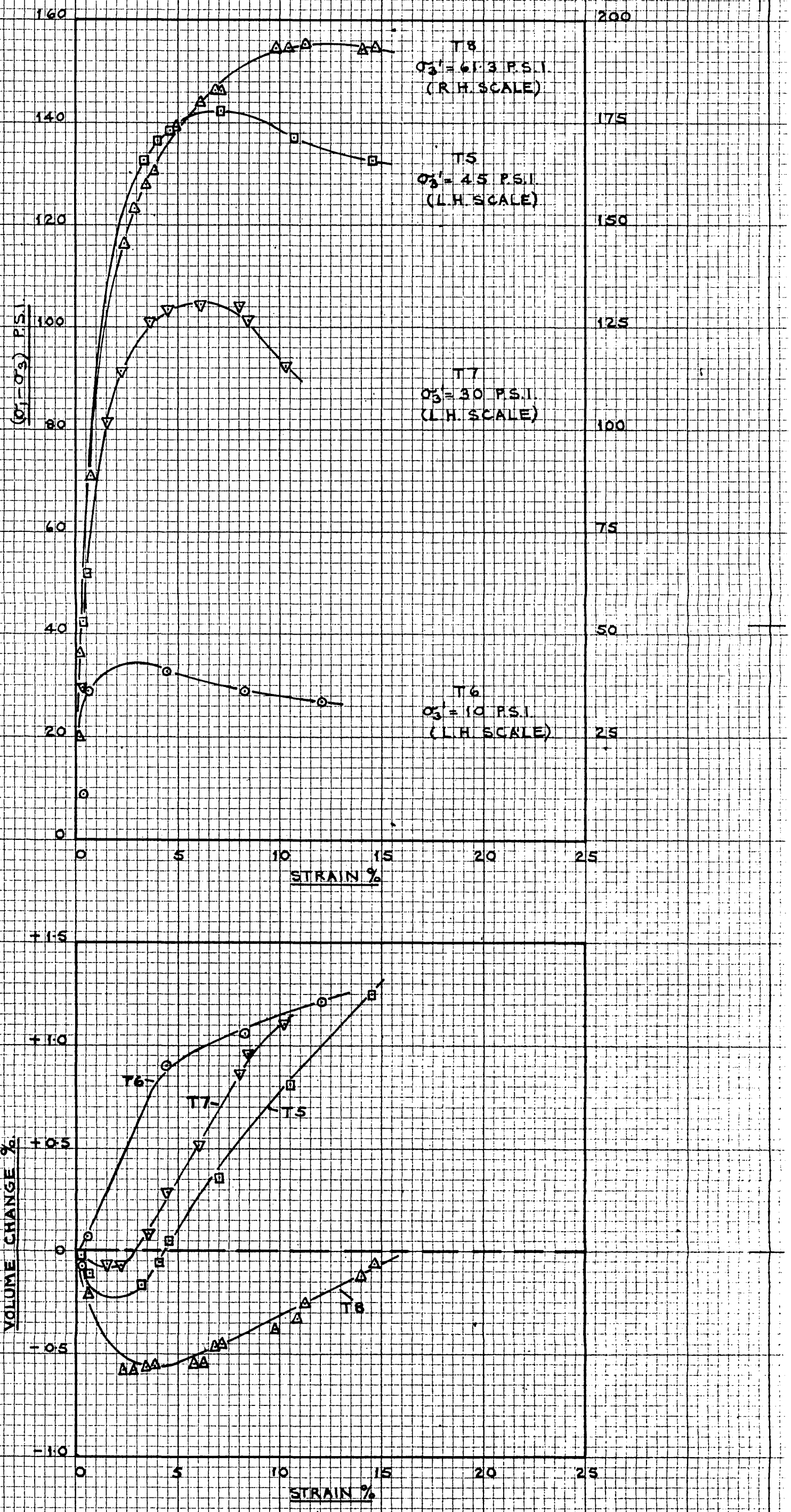


SATURATED DRAINED TESTS. TALYBONT CLAY.

SERIES 4A.

COMPACTION WATER CONTENT: 7·16%

FIG. A6.12.



SATURATED DRAINED TESTS. TALYBONT CLAY.

SERIES 4A.

COMPACTION WATER CONTENT : 9·06%

FIG. A6.13.

APPENDIX TO CHAPTER 7

SUMMARY OF TEST RESULTS

(A.7.1) Stresses at failure.

Soil	Series, Test No.	Failure Criterion	(σ_3-u_w) p.s.i.	(σ_3-u_a) p.s.i.	$\frac{1}{2}(\sigma_1-\sigma_3)$ p.s.i.	$\frac{1}{2}(\sigma_1+\sigma_3)-u_w$ p.s.i.	$\frac{1}{2}(\sigma_1+\sigma_3)-u_a$ p.s.i.
Talybont Clay	Series 4	Max. $\frac{(\sigma_1-\sigma_3)}{(\sigma_3-u_w)}$					
	S4 T1		130.5	105.2	165.1	295.6	270.3
	T2		119.0	99.9	146.0	265.0	245.9
	T3		83.4	60.0	90.6	174.0	150.6
	T5		35.3	15.2	37.3	72.6	52.5
	T6		53.8	30.2	55.5	109.3	85.7
	T7		19.5	0	15.8	35.3	15.8
	T1	Max. $(\sigma_1-\sigma_3)$	130.5	105.2	165.1	295.6	270.3
	T2		118.0	98.9	145.3	263.3	243.2
	T3		84.0	60.0	90.6	174.6	150.6
	T5		36.7	15.2	37.3	74.0	52.5
	T6		53.8	30.0	55.5	109.3	85.5
	T7		21.4	0	16.7	38.1	16.7
	Series 4B	Max. $\frac{(\sigma_1-\sigma_3)}{(\sigma_3-u_w)}$					
	S4B T1		6.5	0	13.5	20.0	$=\frac{1}{2}(\sigma_1-\sigma_3)$
	T2		0.9	all	1.7	2.6	
	T3		4.5	tests	8.7	13.2	
	T4		6.3		12.5	18.8	
	T5		52.5		10.3	62.8	
	T6		36.7		12.9	49.6	
	T7		23.9		14.9	38.8	
	T8		19.5		15.8	35.3	
	T9		12.2		15.4	27.6	
	T10		60.7		12.5	73.2	
	T1	Max. $(\sigma_1-\sigma_3)$	11.9	0	15.7	27.6	$=\frac{1}{2}(\sigma_1-\sigma_3)$
	T2		3.4	all	4.5	7.9	
	T3		6.1	tests	10.6	16.7	
	T4		9.1		14.9	24.0	
	T5		53.9		10.6	64.5	
	T6		37.8		13.0	50.8	
	T7		24.6		15.0	39.6	
	T8		21.4		16.7	38.1	
	T9		14.8		16.9	31.7	
	T10		60.7		12.5	73.2	

Soil	Series, Test No.	Failure Criterion	(σ_3-u_w) p.s.i.	(σ_3-u_a) p.s.i.	$\frac{1}{2}(\sigma_1-\sigma_3)$ p.s.i.	$\frac{1}{2}(\sigma_1+\sigma_3)-u_w$ p.s.i.	$\frac{1}{2}(\sigma_1+\sigma_3)-u_a$ p.s.i.
Talybont Clay	Series 4C	Max. $\frac{(\sigma_1-\sigma_3)}{(\sigma_3-u_w)}$					
	S4C T1		55.0	30	53.9	108.9	83.5
	T2		65.7	all	56.6	122.3	87.4
	T3		83.2	tests	59.4	142.6	89.2
	T3A		78.4		66.0	144.4	95.7
	T4		26.8		37.1	63.9	63.9
	T5		42.4		51.5	93.9	81.5
	T6		52.6		54.3	106.9	84.5
	T1	Max. $(\sigma_1-\sigma_3)$	55.1	30	53.9	109.0	83.5
	T2		66.6	all	57.0	123.6	87.9
	T3		83.2	tests	59.4	142.6	89.2
	T3A		78.4		66.0	144.4	95.7
	T4		36.3		49.0	85.3	79.0
	T5		44.8		52.4	97.2	82.4
	T6		53.8		55.5	109.3	85.7
Mangla Shale	Series 1	Max. $\frac{(\sigma_1-\sigma_3)}{(\sigma_3-u_w)}$					
	S1 T1		18.6	4.0	16.4	35.0	20.4
	T2		20.9	7.5	17.3	38.2	24.8
	T3		17.0	16.7	19.3	36.3	36.0
	T4		22.8	22.8	22.0	44.8	44.8
	T4'		24.2	24.2	22.0	46.2	46.2
	T5		25.3	25.3	23.1	48.4	48.4
	T6		20.5	20.5	20.2	40.7	40.7
	T7		23.4	15.6	19.6	43.0	35.2
	T8		20.5	6.0	16.9	37.4	22.9
	T9		23.7	22.2	20.0	43.7	42.2
	T1	Max. $(\sigma_1-\sigma_3)$	19.9	4.5	17.2	37.1	21.7
	T2		21.4	7.9	17.8	39.2	25.7
	T3		24.9	16.6	21.3	46.2	37.9
	T4		33.7	28.9	25.5	59.2	54.4
	T4'		35.0	31.5	26.2	61.2	57.7
	T5		33.7	33.7	26.6	60.3	60.3
	T6		26.9	26.1	24.0	50.9	50.1
	T7		28.1	16.5	21.1	49.2	37.6
	T8		23.7	8.1	18.4	42.1	26.5
	T9		34.3	24.7	23.9	58.2	48.6

Soil	Series, Test No.	Failure Criterion	(σ_3-u_w) p.s.i.	(σ_3-u_a) p.s.i.	$\frac{1}{2}(\sigma_1-\sigma_3)$ p.s.i.	$\frac{1}{2}(\sigma_1+\sigma_3)-u_w$ p.s.i.	$\frac{1}{2}(\sigma_1+\sigma_3)-u_a$ p.s.i.
Mangla Shale	Series 3	Max. $\frac{(\sigma_1-\sigma_3)}{(\sigma_3-u_w)}$					
	S3 T1		89.0	89.0	65.0	154.0	154.0
	T2		32.1	0	19.0	51.1	19.0
	T3		32.1	0	19.0	51.1	19.0
	T4		61.0	50.0	44.5	105.5	94.5
	T5		63.6	60.0	47.5	111.4	107.5
	T6		37.1	8.8	24.2	61.3	33.0
	T7		56.8	40.0	41.3	98.1	81.3
	T8		80.3	80.3	54.6	134.9	134.9
	T9		35.9	5.0	23.4	59.3	28.4
	T1	Max. $(\sigma_1-\sigma_3)$	94.2	94.2	66.1	160.3	160.3
	T2		34.2	0	19.5	53.7	19.5
	T3		36.0	0	19.8	55.8	19.8
	T4		66.9	50.0	47.5	114.4	97.5
	T5		72.2	60.0	49.9	122.1	109.9
	T6		43.2	8.9	27.5	70.7	36.4
	T7		63.0	40.0	42.7	105.7	82.7
	T8		80.0	82.0	56.5	138.5	136.5
	T9		38.2	5.0	24.3	62.5	29.3
	Series 1B	Max. $\frac{(\sigma_1-\sigma_3)}{(\sigma_3-u_w)}$					
	S1B T1		9.1	0	5.4	14.5	$=\frac{1}{2}(\sigma_1-\sigma_3)$
	T2		4.9	all	3.3	8.2	
	T3		10.9	tests	8.5	19.4	
	T4		16.0		13.7	29.7	
	T5		46.4		18.8	65.2	
	T6		39.7		20.3	60.0	
	S1 T10		17.6		15.4	33.0	
	T11		12.4		12.1	24.5	
	S1B T1	Max. $(\sigma_1-\sigma_3)$	10.2	0	5.4	15.6	$=\frac{1}{2}(\sigma_1-\sigma_3)$
	T2		6.0	all	3.6	9.6	
	T3		12.8	tests	9.3	22.1	
	T4		24.0		17.1	41.1	
	T5		47.0		18.8	65.8	
	T6		39.7		20.3	60.0	
	S1 T10		20.4		16.6	37.0	
	T11		20.4		15.6	36.0	

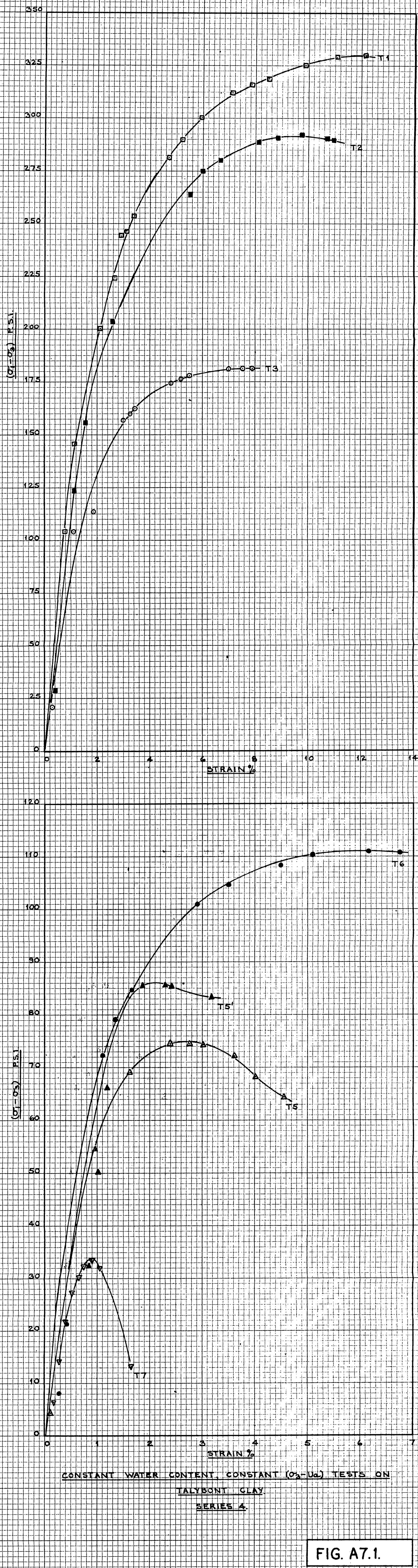
Soil	Series Test No.	Failure Criterion	(σ_3-u_w) p.s.i.	(σ_3-u_a) p.s.i.	$\frac{1}{2}(\sigma_1-\sigma_3)$ p.s.i.	$\frac{1}{2}(\sigma_1+\sigma_3)-u_w$ p.s.i.	$\frac{1}{2}(\sigma_1+\sigma_3)-u_a$ p.s.i.
Selset Clay	Series 2	Max. $\frac{(\sigma_1-\sigma_3)}{(\sigma_3-u_w)}$					
	S2 T1		51.2	51.2	46.6	97.8	97.8
	T2		42.0	34.9	35.2	77.2	70.1
	T3		27.3	13.0	23.8	51.1	36.6
	T4		50.8	45.2	41.4	92.2	86.6
	T5		57.2	57.0	47.7	104.9	104.7
	T6		39.0	18.2	28.3	67.3	46.5
	T7		40.2	22.1	30.2	70.4	52.3
	T8'		32.9	15.6	24.9	57.8	40.5
	T8		25.7	0	19.8	45.5	19.8
	T9		48.1	39.7	39.1	87.1	78.8
	T10		24.9	0	18.5	43.4	18.5
	T1	Max. $(\sigma_1-\sigma_3)$	55.9	55.9	48.8	104.7	104.7
	T2		52.9	36.7	39.0	91.9	75.7
	T3		38.4	14.6	29.4	67.8	44.0
	T4		56.6	45.7	43.4	100.0	89.1
	T5		61.3	60.8	49.6	110.9	110.4
	T6		41.4	19.8	29.6	71.0	49.4
	T7		42.9	23.1	30.2	73.1	53.3
	T8'		32.9	15.6	24.9	57.8	40.5
	T8		28.7	0	20.6	49.3	20.6
	T9		54.0	40.2	41.1	95.1	81.3
	T10		28.1	0	19.2	47.3	19.2
	Series 2B	Max. $\frac{(\sigma_1-\sigma_3)}{(\sigma_3-u_w)}$					
	S2B T1		9.1	0	9.5	18.6	$=\frac{1}{2}(\sigma_1-\sigma_3)$
	T2		6.2	all	5.4	11.6	
	T3		15.0	tests	13.2	28.2	
	T4		7.1		6.7	13.8	
	T1	Max. $(\sigma_1-\sigma_3)$	11.5		10.5	22.0	
	T2		9.1		6.8	15.9	
	T3		25.0		18.2	43.2	
	T4		15.4		11.4	26.8	
Vaich Moraine	T1		22.2	0	4.8	27.0	$=\frac{1}{2}(\sigma_1-\sigma_3)$
	T2		16.0	all	4.8	20.8	
	T3		9.9	tests	4.7	14.6	
	T4		6.5		4.5	11.0	
	T5		4.9		4.6	9.5	
	T6		3.3		4.3	7.6	
	T7		2.7		4.1	6.8	
	T8		2.3		3.6	5.9	

(A.7.2) Compaction water contents, degrees of saturation, α factors, etc.

Soil	Series, Test No.	Water Content %	Degree of Saturation		α Factor		Initial (σ_3-u_w)
			Before Shear %	At Failure %	Max. $\frac{(\sigma_1-\sigma_3)}{(\sigma_3-u_w)}$	Max. $(\sigma_1-\sigma_3)$	
Talybont Clay	Series 4						
	S4 T1	6.85	54.8	59.3	.68	.67	118.3
	T2	6.85	57.1	60.1	.50	.46	109.8
	T3	6.70	51.4	52.9	.30	.29	73.8
	T5	6.76	50.7	48.9	.43	.78	31.7
	T6	6.87	51.8	51.6	.41	.56	45.0
	T7	6.87	48.9	47.0	.35	.44	23.3
	Series 4B						
	S4B T1	8.02	65.1		.73	.67	7.7
	T2	11.93	85.4		.85	.78	0.9
	T3	9.66	81.6		.89	.90	3.4
	T4	8.21	64.4		.89	.82	8.2
	T5	5.66	39.4		.09	.11	52.4
	T6	6.21	45.7		.16	.18	41.8
	T7	6.81	48.9		.29	.33	30.4
	T8	6.98	53.8		.38	.41	23.3
	T9	7.40	57.4		.58	.60	15.3
	T10	5.2	36.2		.11	.11	61.6
	Series 4C						
	S4C T1	6.33	48.3	48.6	.38	.35	47.8
	T2	6.04	43.4	43.3	.31	.29	57.3
	T3	5.30	37.8	38.0	.25	.24	80.5
	T3A		44.1	43.6	.38	.36	76.7
	T4	9.69	90.1	88.6	1.00	.91	24.6
	T5	8.04	65.0	69.1	.66	.53	36.3
	T6	6.87	51.8	51.6	.45	.49	45.0
Mangla Shale	Series 1						
	S1 T1	18.06	93.4	93.5	.83	.97	
	T2	18.43	94.1	96.1	.75	.92	
	T3	18.78	97.0	99.1	-	1.00	
	T4	18.15	-	100	1.00	-	
	T4'	18.11	99.6	100	1.00	-	
	T5	18.42	-	100	1.00	1.00	
	T6	18.31	99.2	100	1.00	-	
	T7	18.39	94.4	98.6	.65	.78	
	T8	18.11	94.0	97.0	.74	.83	
	T9	18.68	97.4	98.0	-	.80	

Soil	Series, Test No.	Water Content %	Degree of Saturation		α Factor		Initial (σ_3-u_w)
			Before Shear %	At Failure %	Max. $\frac{(\sigma_1-\sigma_3)}{(\sigma_3-u_w)}$	Max. $(\sigma_1-\sigma_3)$	
Mangla Shale	Series 3						
	S3 T1	16.16	94.9	99.9	1.00	1.00	122.5
	T2	16.04	79.6	-	.72	.71	41.5
	T3	16.21	81.2	-	.72	.71	38.5
	T4	16.26	89.5	95.9	.89	.93	59.3
	T5	16.30	90.9	97.4	1.00	.73	68.6
	T6	16.36	85.0	86.4	.78	.81	34.8
	T7	16.36	86.6	95.2	.89	.81	50.2
	T8	16.16	100	100	1.00	1.00	85.4
	T9	16.41	84.5	86.2	.78	.81	37.2
	Series 1B						
	S1B T1	20.82	91.6		.59	.62	8.9
	T2	23.33	90.8		.67	.75	5.7
	T3	19.44	92.1		.78	.86	11.0
	T4	17.48	89.2		.87	.85	25.9
	T5	15.25	76.9		.45	.48	49.0
	T6	15.69	80.5		.58	.63	43.0
	S1 T10	18.00	92.1		.91	.96	20.0
	T11	18.39	92.5		.93	.89	14.3
Selset Clay	Series 2						
	S2 T1	11.23	100.0	100.0	1.00	1.00	89.5
	T2	10.92	85.1	86.6	.88	.77	44.7
	T3	11.62	84.6	86.1	.94	.91	26.8
	T4	11.90	89.1	97.4	.75	.85	49.0
	T5	11.77	94.4	100.0	1.00	1.00	71.2
	T6	11.37	83.1	86.2	.69	.79	22.9
	T7	11.55	88.0	94.1	.73	.76	36.9
	T8'	11.90	86.0	92.0	.76	.86	22.0
	T8	11.98	82.2	-	.85	.86	29.7
	T9	12.02	90.6	95.0	.78	.90	50.0
	T10	11.92	79.8	-	.83	.80	29.2
	Series 2B						
	S2B T1	14.04	88.1		1.00	.99	6.9
	T2	16.26	88.0		.75	.80	3.3
	T3	12.34	81.4		.94	.88	19.1
	T4	13.73	85.9		.86	.84	7.7

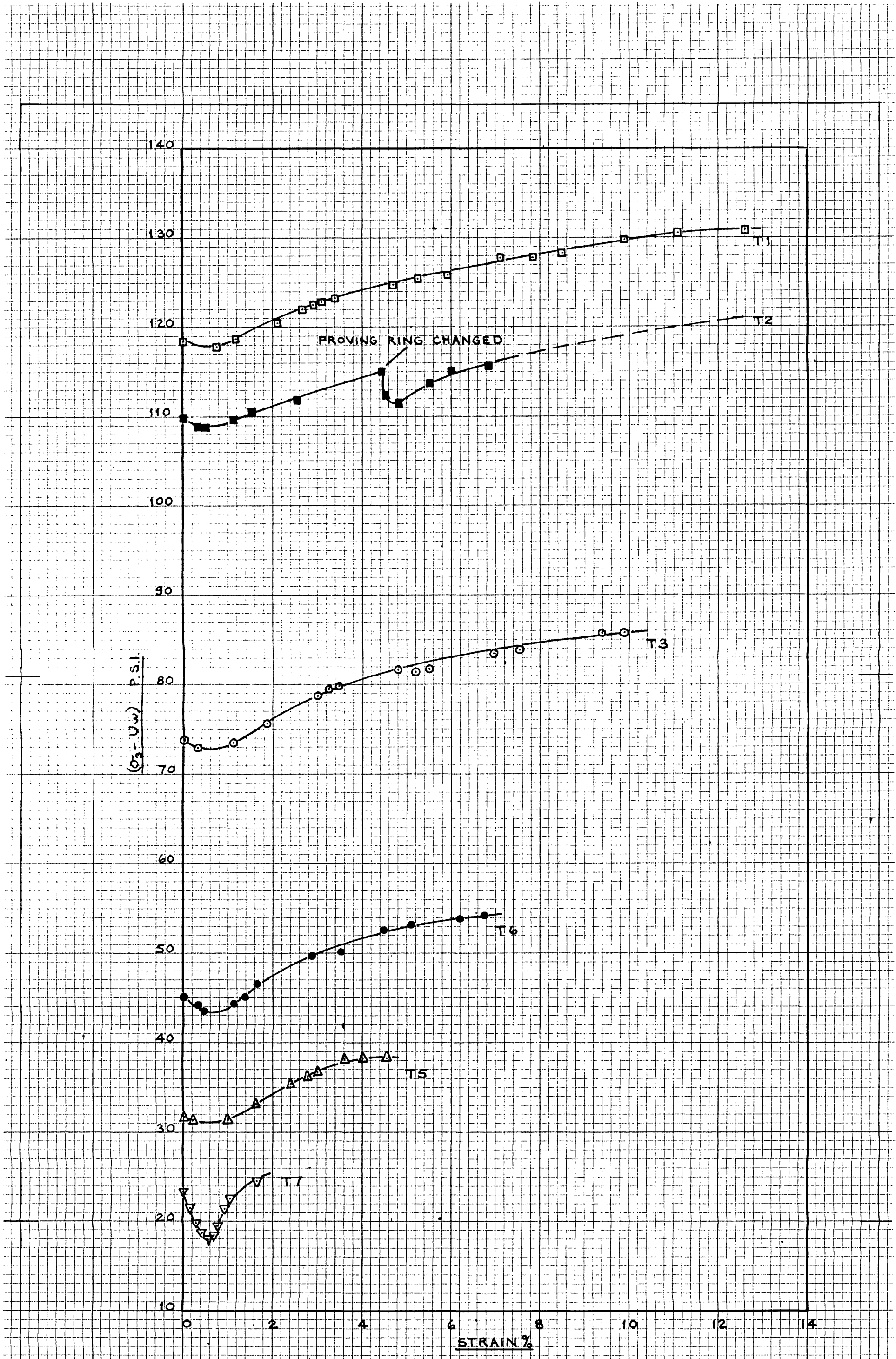
Soil	Series, Test No.	Water Content %	Degree of Saturation		χ Factor		Initial (σ_3-u_w)
			Before Shear %	At Failure %	Max. $\frac{(\sigma_1-\sigma_3)}{(\sigma_3-u_w)}$	Max. $(\sigma_1-\sigma_3)$	
Vaich Moraine	T1	1.98	15.3			.10	
	T2	2.49	20.0			.14	
	T3	3.06	20.2			.23	
	T4	3.54	28.4			.34	
	T5	4.03	32.1			.45	
	T6	4.97	40.2			.62	
	T7	5.90	50.0			.78	
	T8	8.00	68.6			.82	



CONSTANT WATER CONTENT, CONSTANT (σ_3-U_a) TESTS ON TALYBONT CLAY.

SERIES 4.

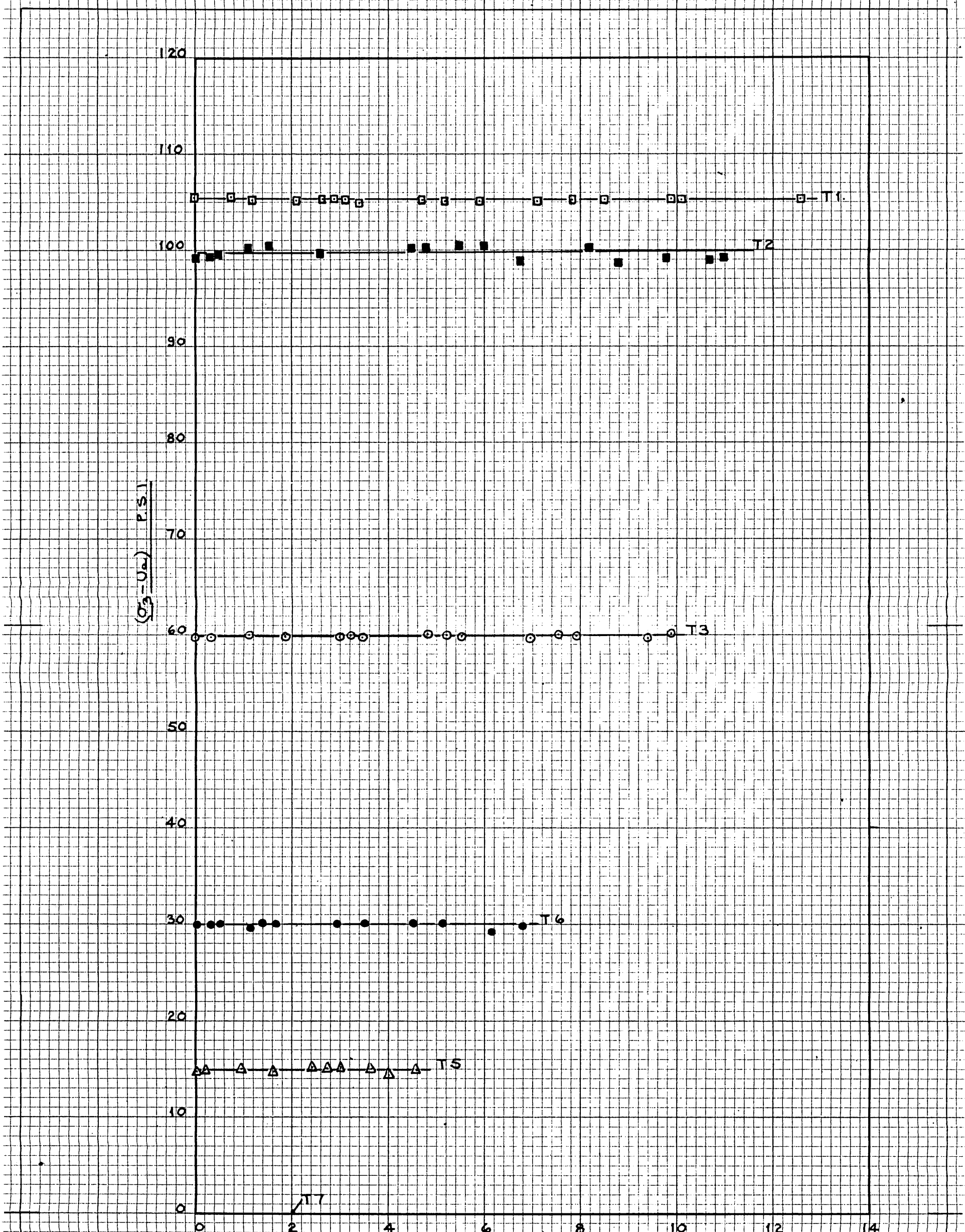
FIG. A7.1.



CONSTANT WATER CONTENT, CONSTANT $(\sigma_3 - U_a)$ TESTS ON TALYBONT CLAY.

SERIES 4.

FIG. A7.2.

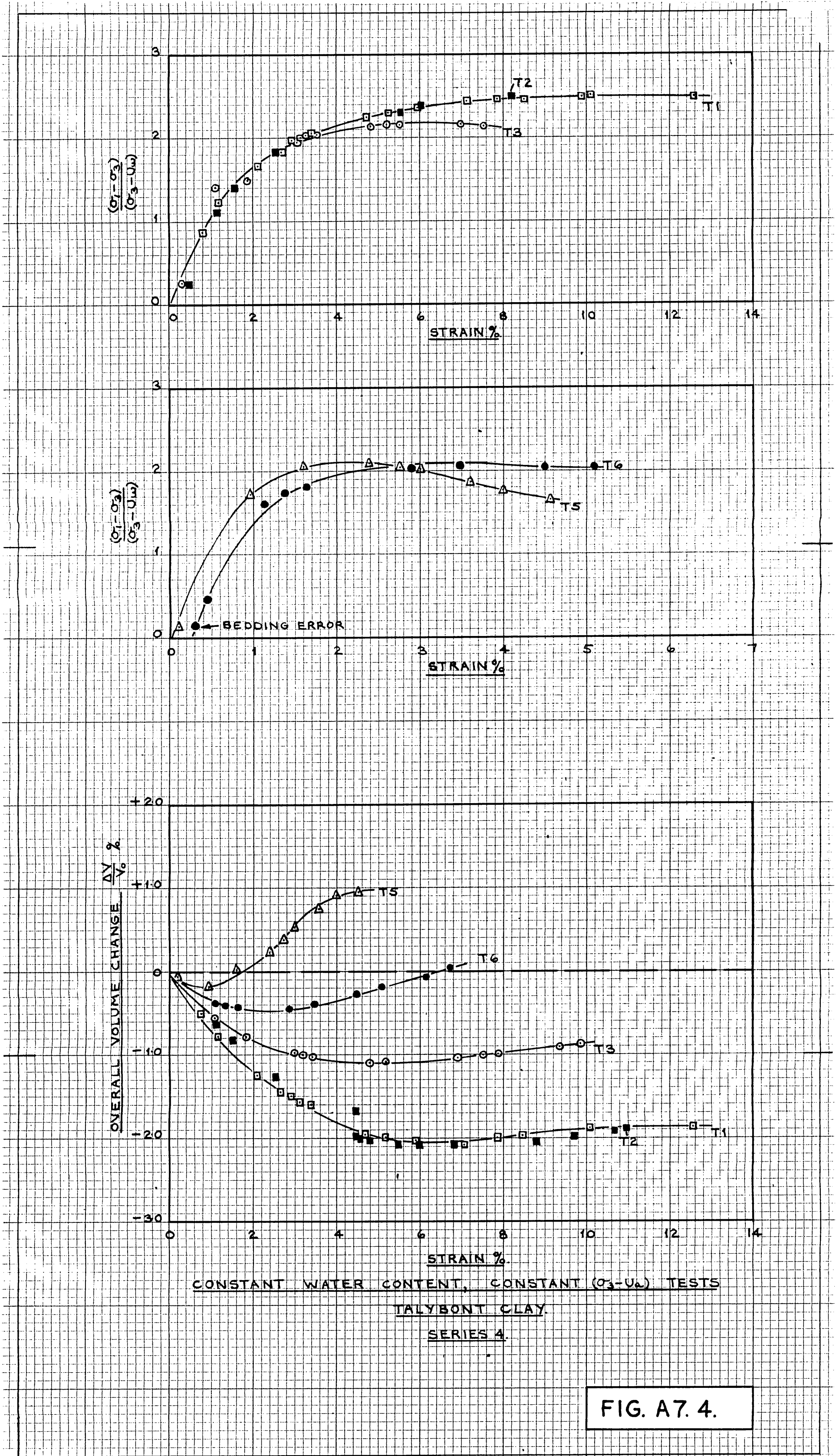


CONSTANT WATER CONTENT, CONSTANT $(\sigma_3 - u_a)$ TESTS

TALYBONT CLAY

SERIES 4.

FIG. A7.3.

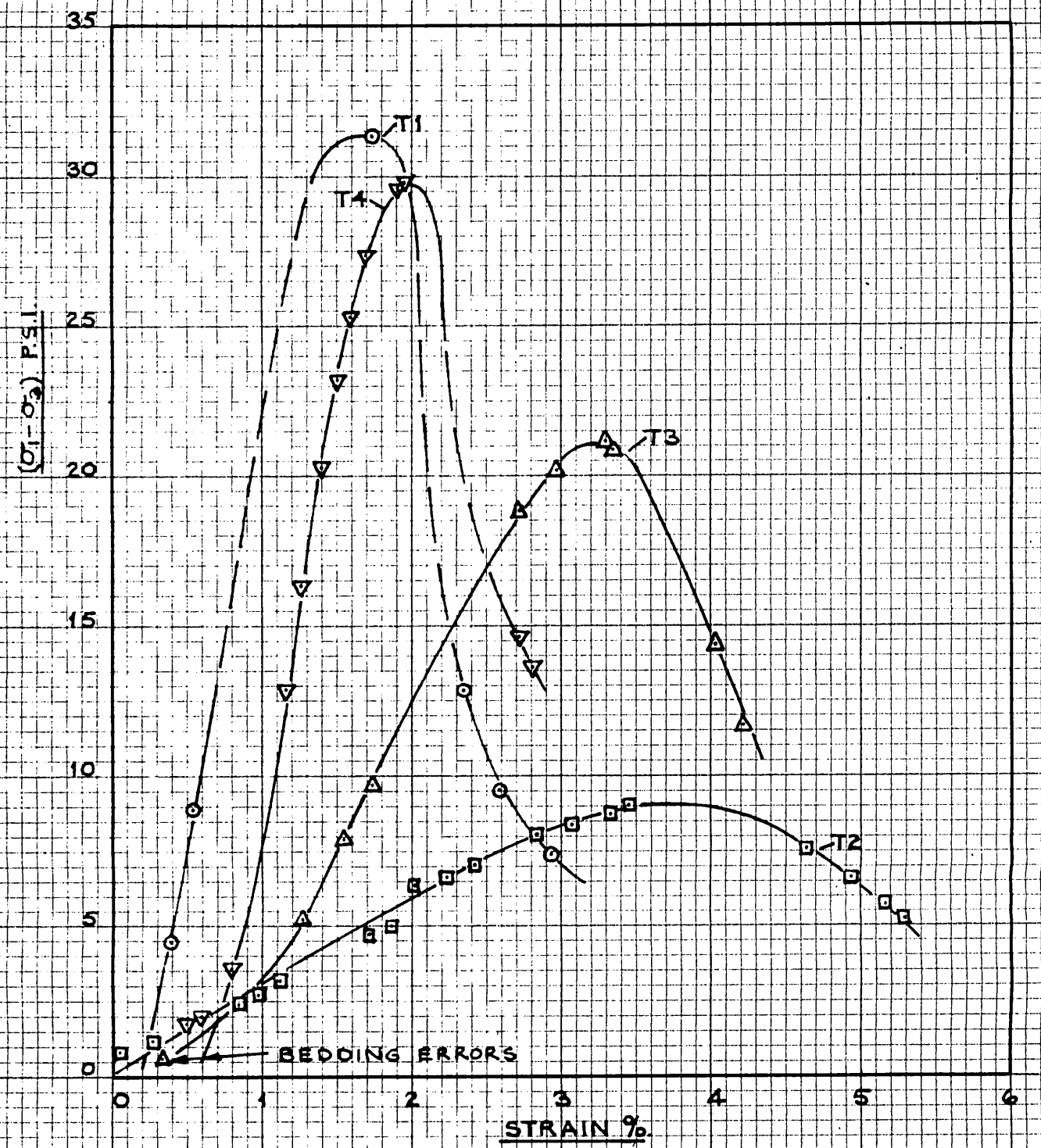


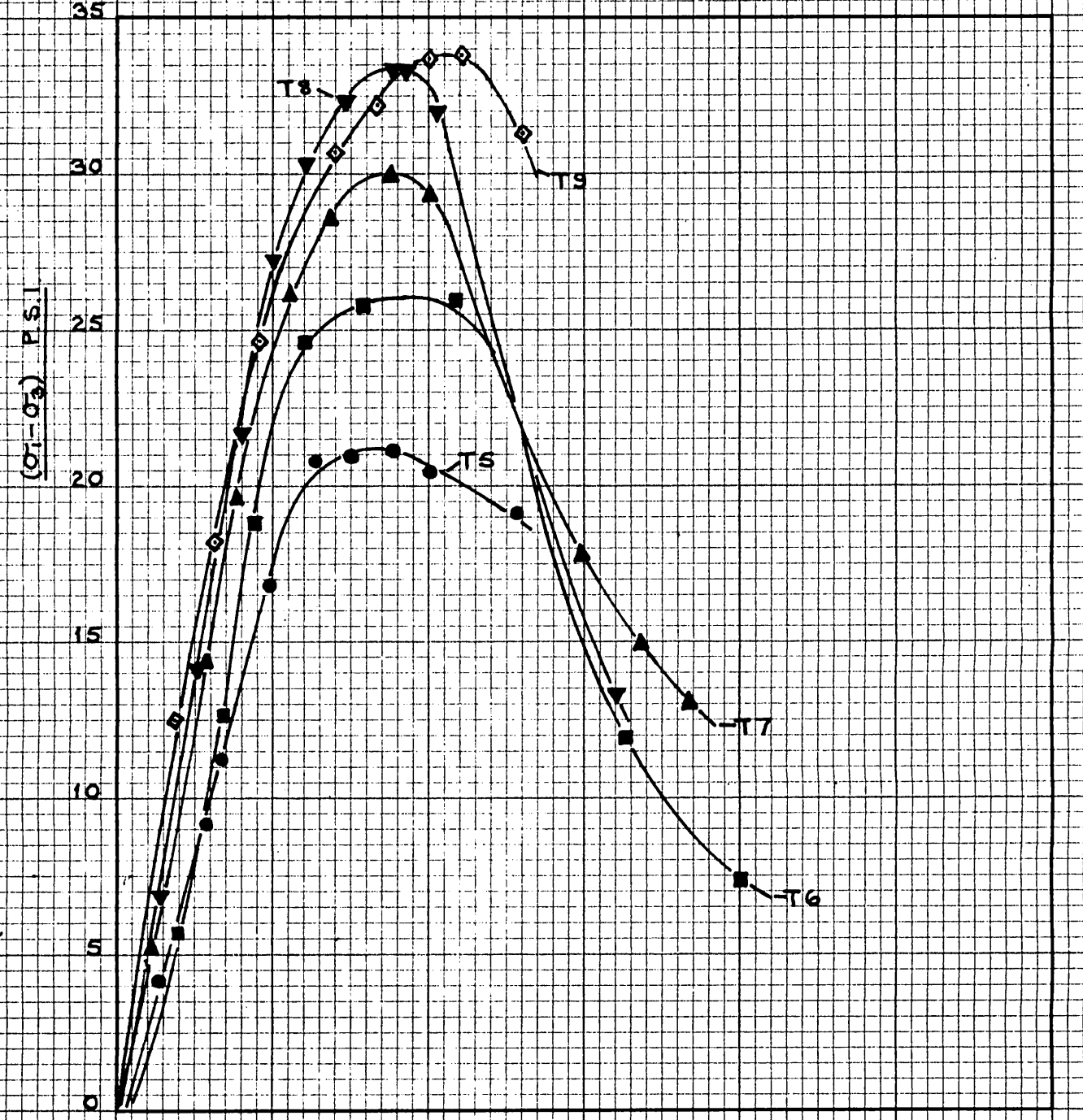
CONSTANT WATER CONTENT, CONSTANT (σ_3-U_a) TESTS

TALYBONT CLAY

SERIES 4.

FIG. A7. 4.

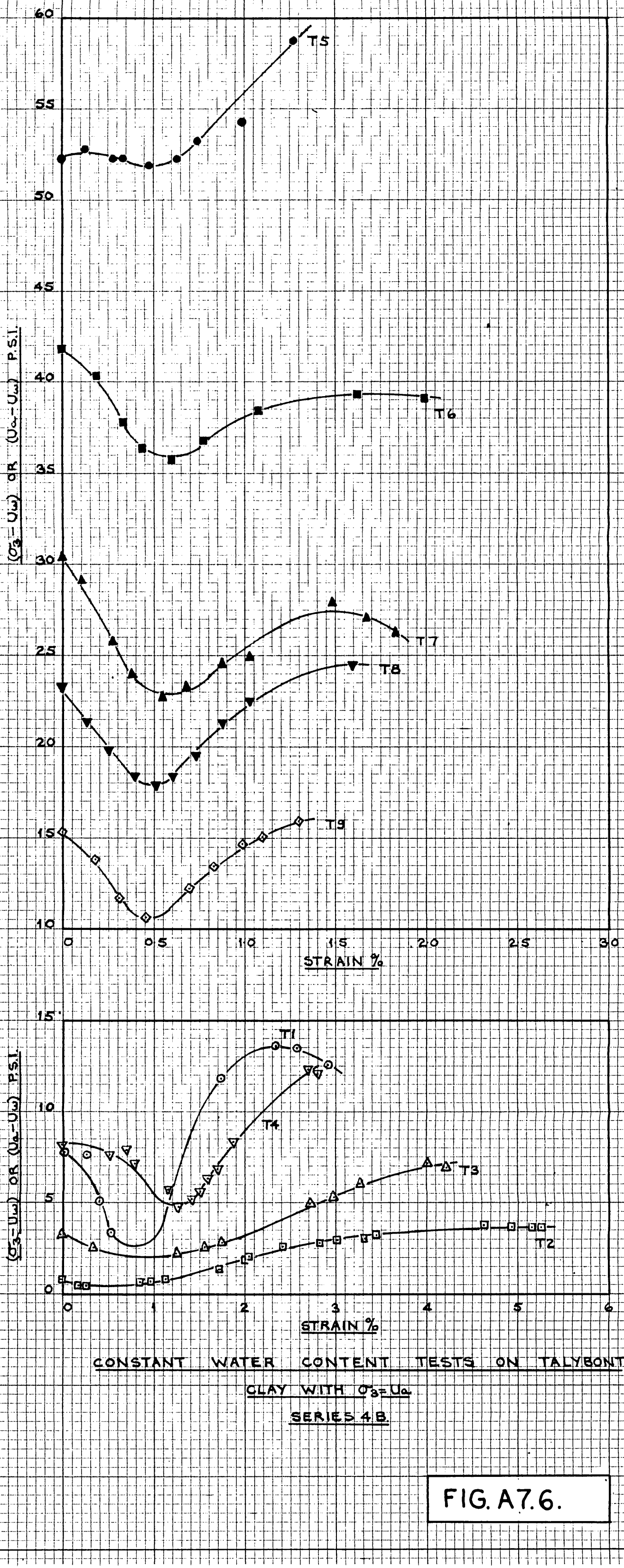




CONSTANT WATER CONTENT TESTS ON TALYBONT CLAY WITH $\sigma_3 = U_a$.

SERIES 4B.

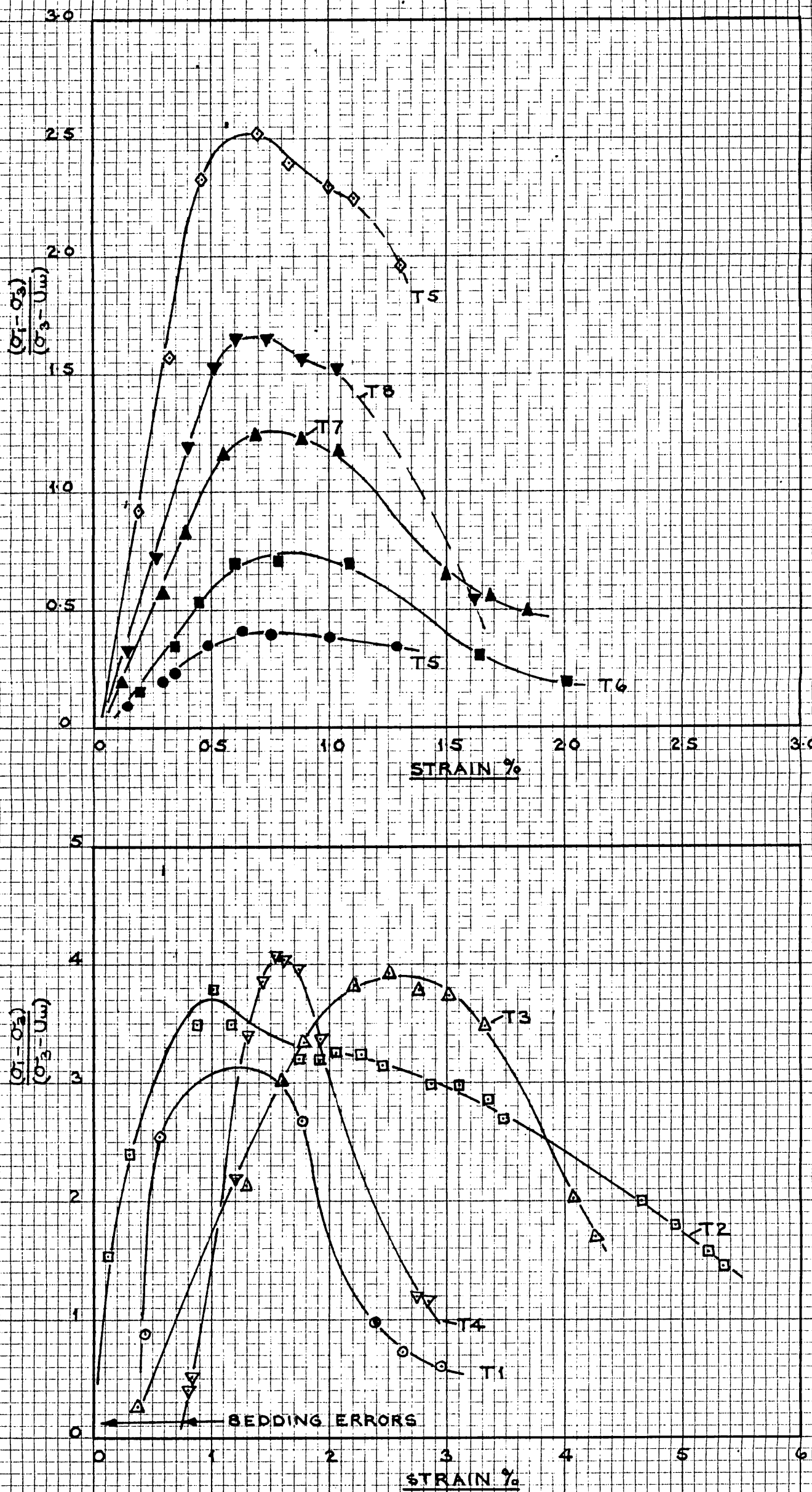
FIG. A7.5.



CONSTANT WATER CONTENT TESTS ON TALYBONT CLAY WITH $\sigma_3 = U_a$

SERIES 4B.

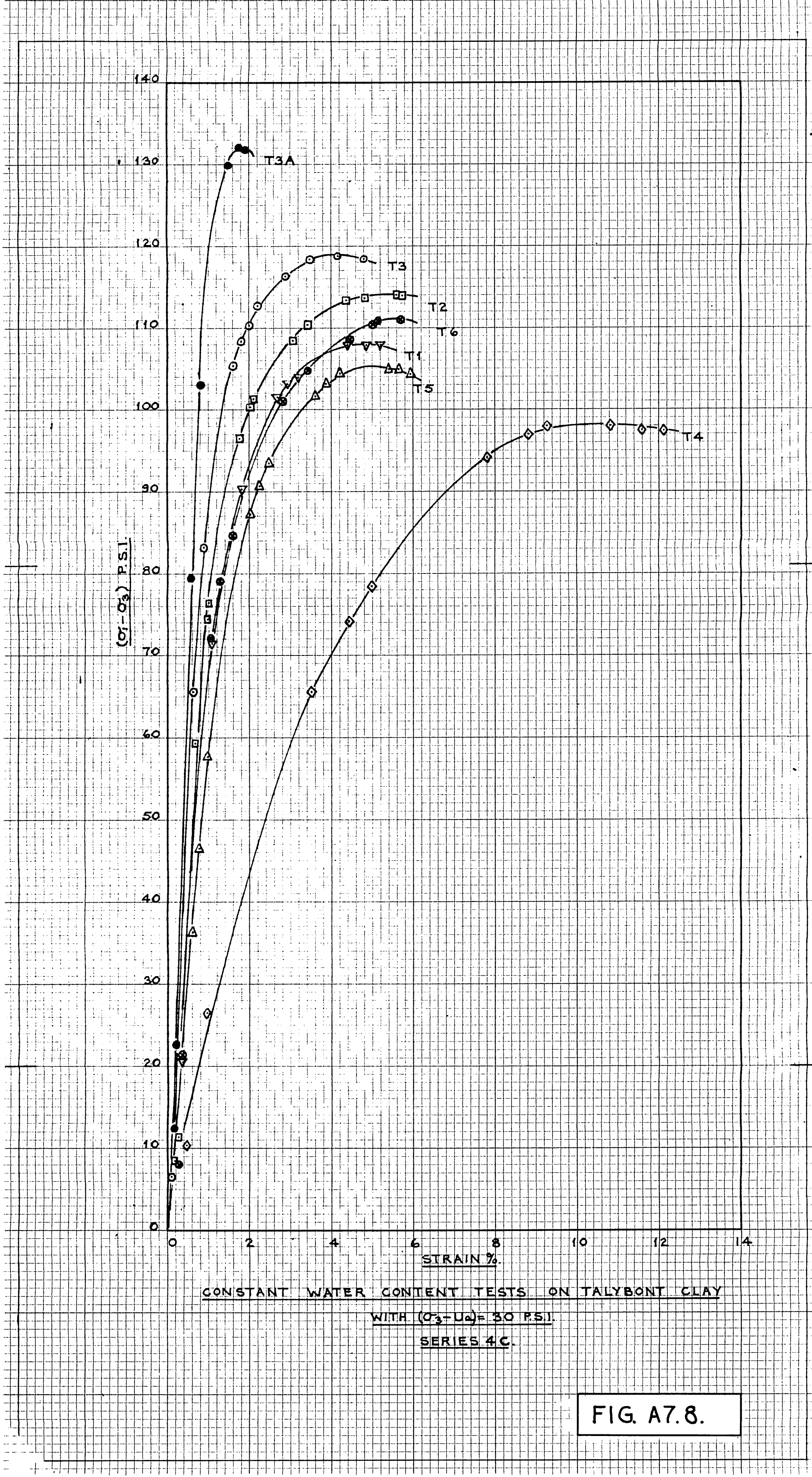
FIG. A7.6.



CONSTANT WATER CONTENT TESTS ON TALYBONT CLAY WITH $\sigma_3 = U_a$.

SERIES 4B.

FIG. A7.7.

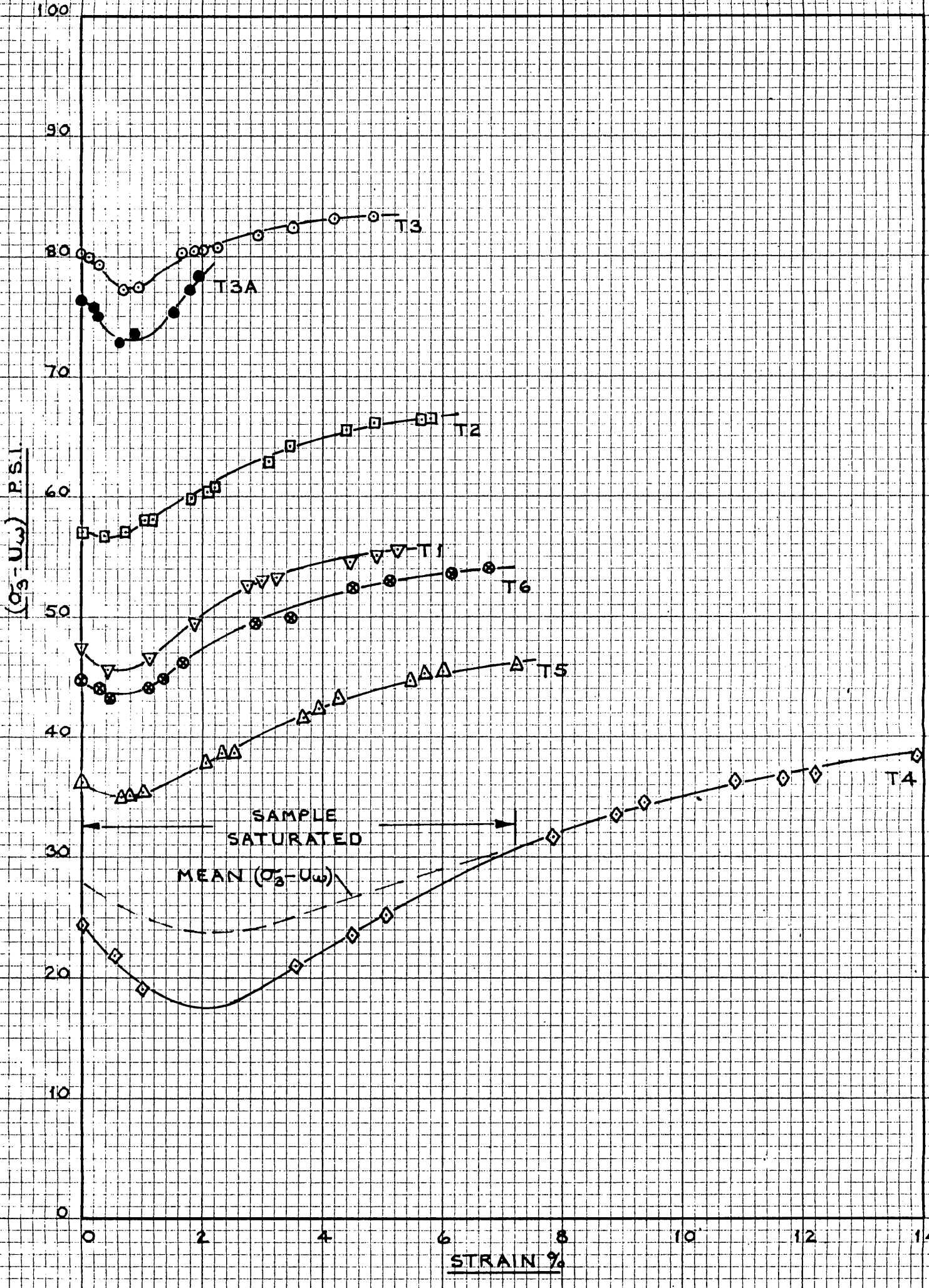


CONSTANT WATER CONTENT TESTS ON TALYBONT CLAY

WITH $(\sigma_3 - U_a) = 30$ P.S.I.

SERIES 4C.

FIG. A7.8.

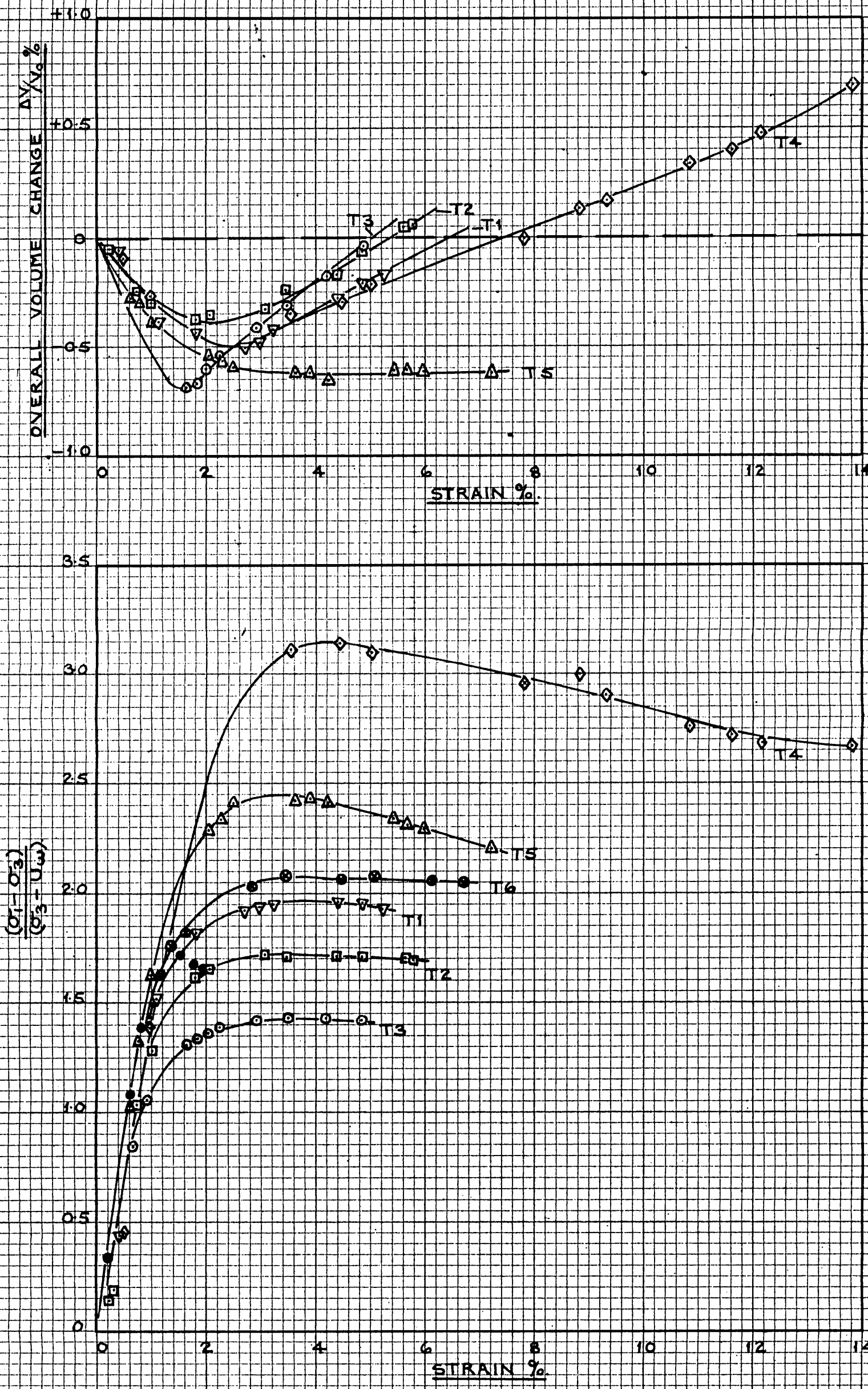


CONSTANT WATER CONTENT TESTS ON TALYBONT CLAY

WITH $(\sigma_3 - U_a) = 30$ P.S.I.

SERIES 4 C.

FIG. A7.9.

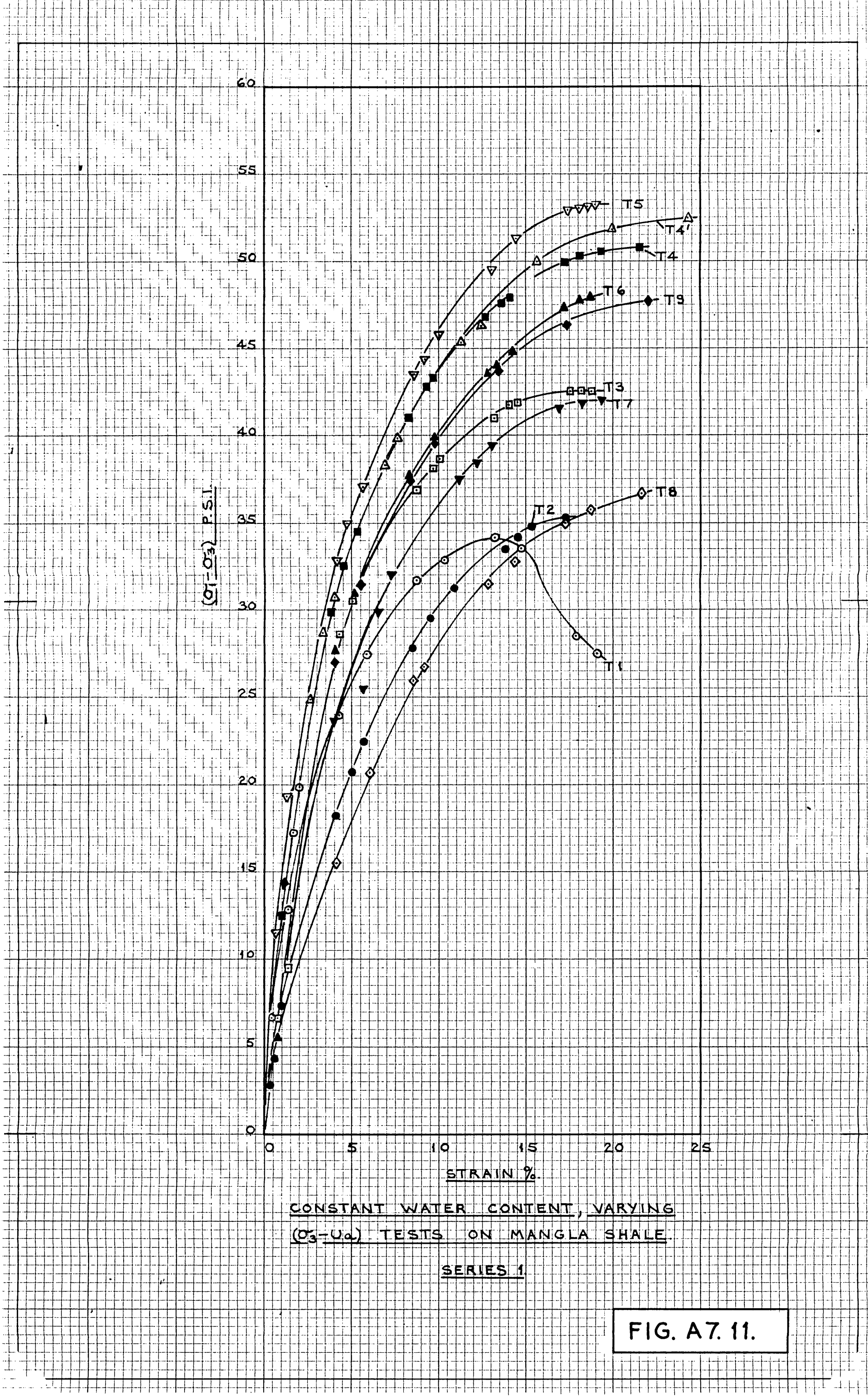


CONSTANT WATER CONTENT TESTS ON TALYBONT CLAY

WITH $(\sigma_3 - U_w) = 30$ P.S.I

SERIES 4C.

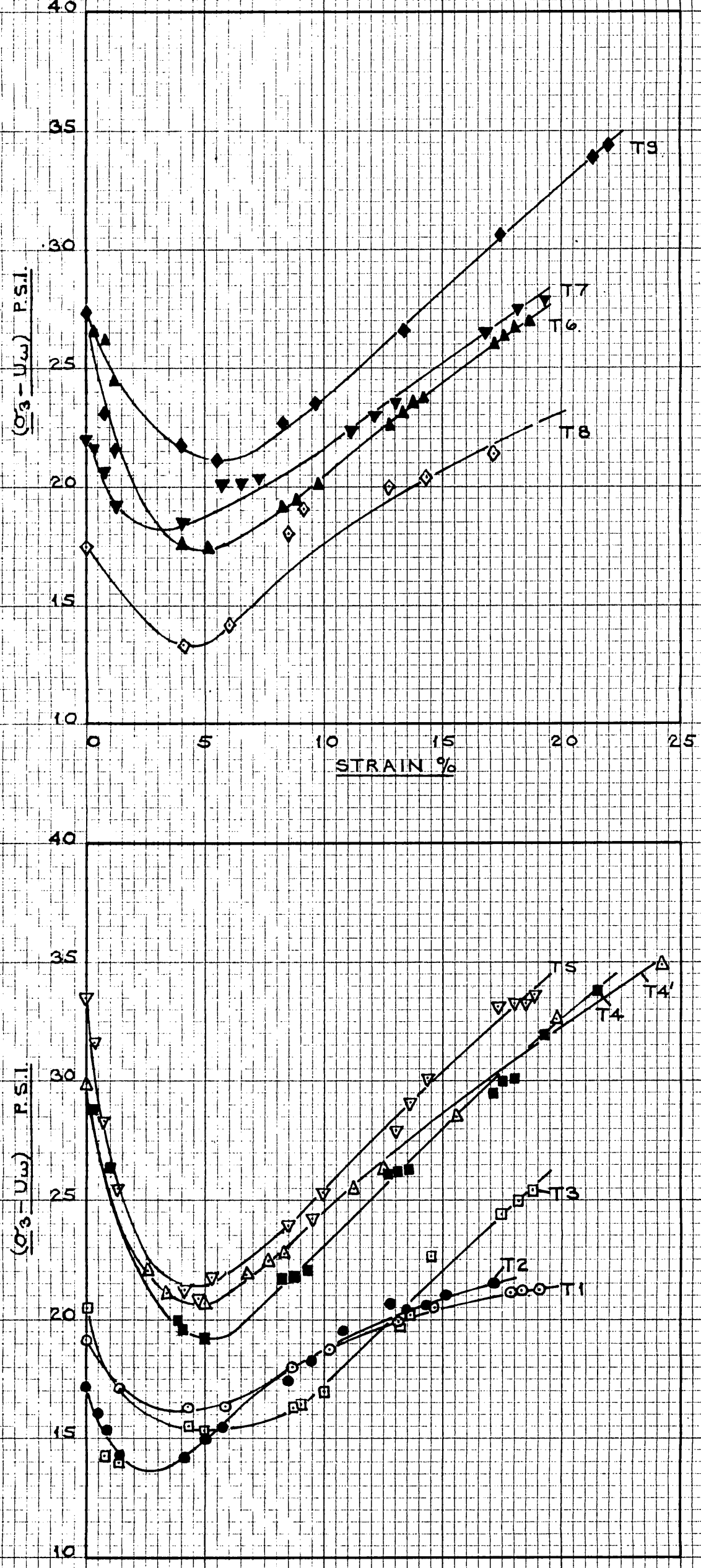
FIG. A7.10.



CONSTANT WATER CONTENT, VARYING (σ_3-U_a) TESTS ON MANGLA SHALE.

SERIES 1.

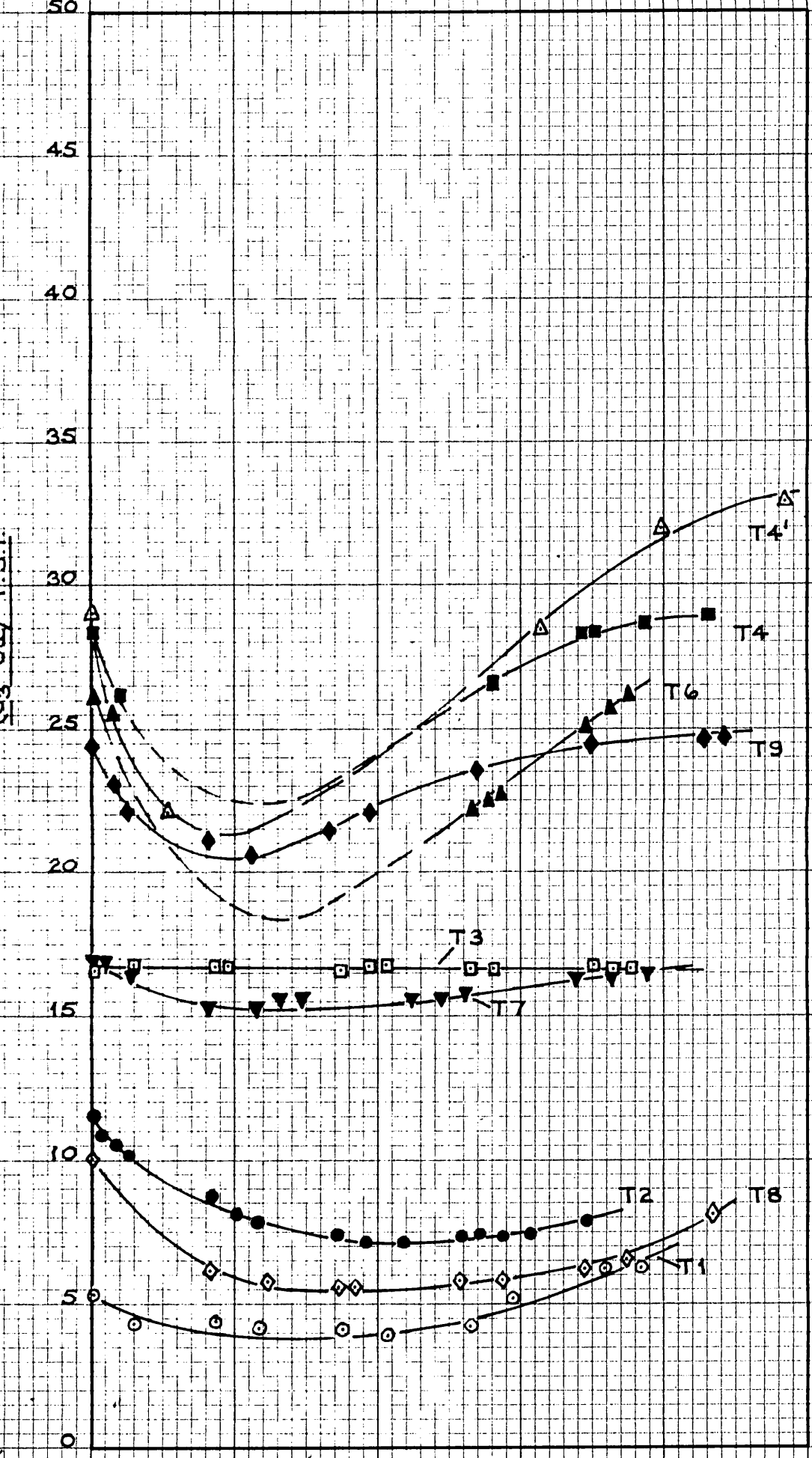
FIG. A7. 11.



CONSTANT WATER CONTENT, VARYING $(\sigma_3 - U_a)$ TESTS ON MANGLA SHALE.

SERIES I.

FIG. A7.12.

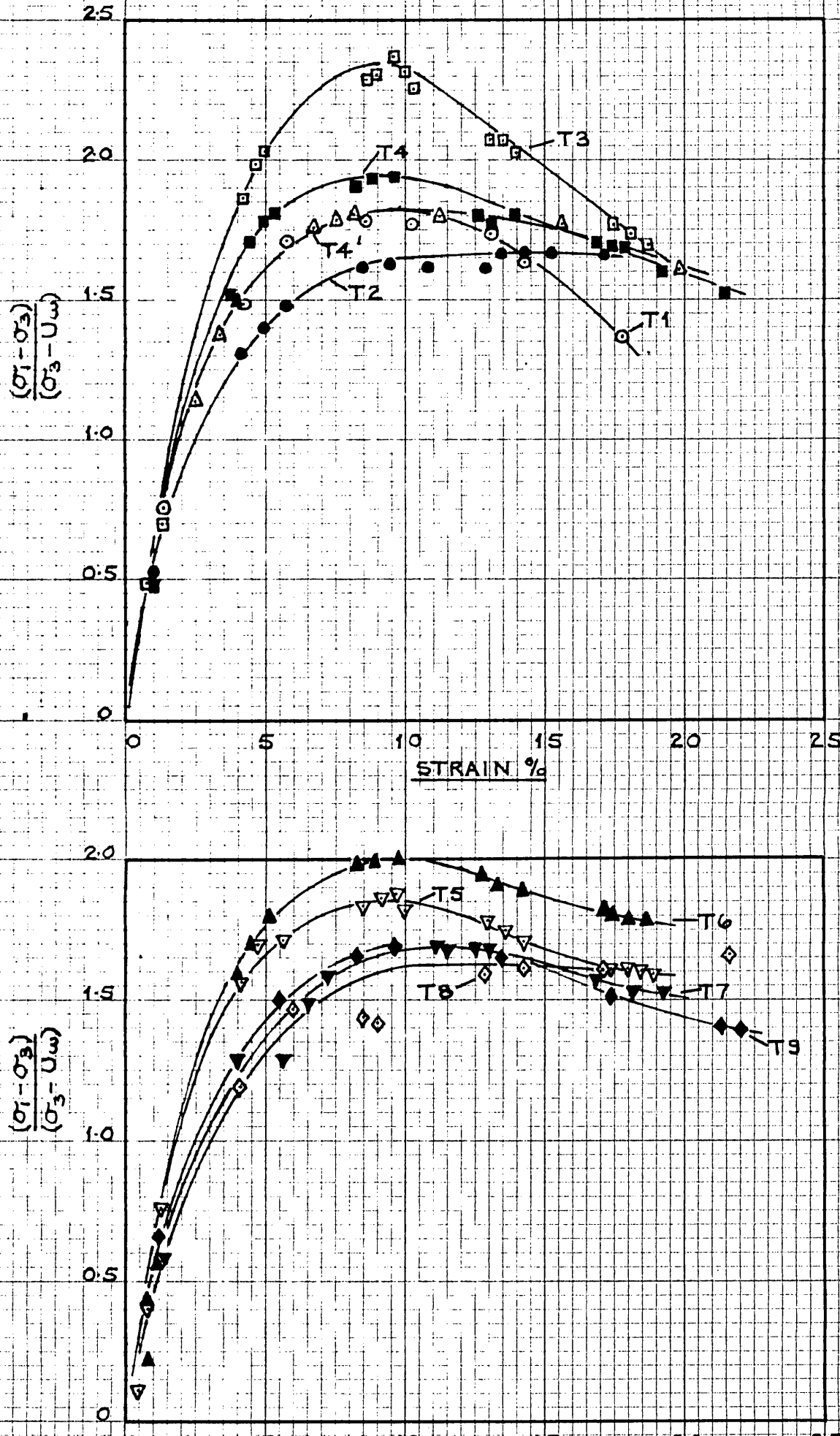


CONSTANT WATER CONTENT, VARYING $(\sigma_3 - U_a)$

TESTS ON MANGLA SHALE.

SERIES I.

FIG. A7.13.

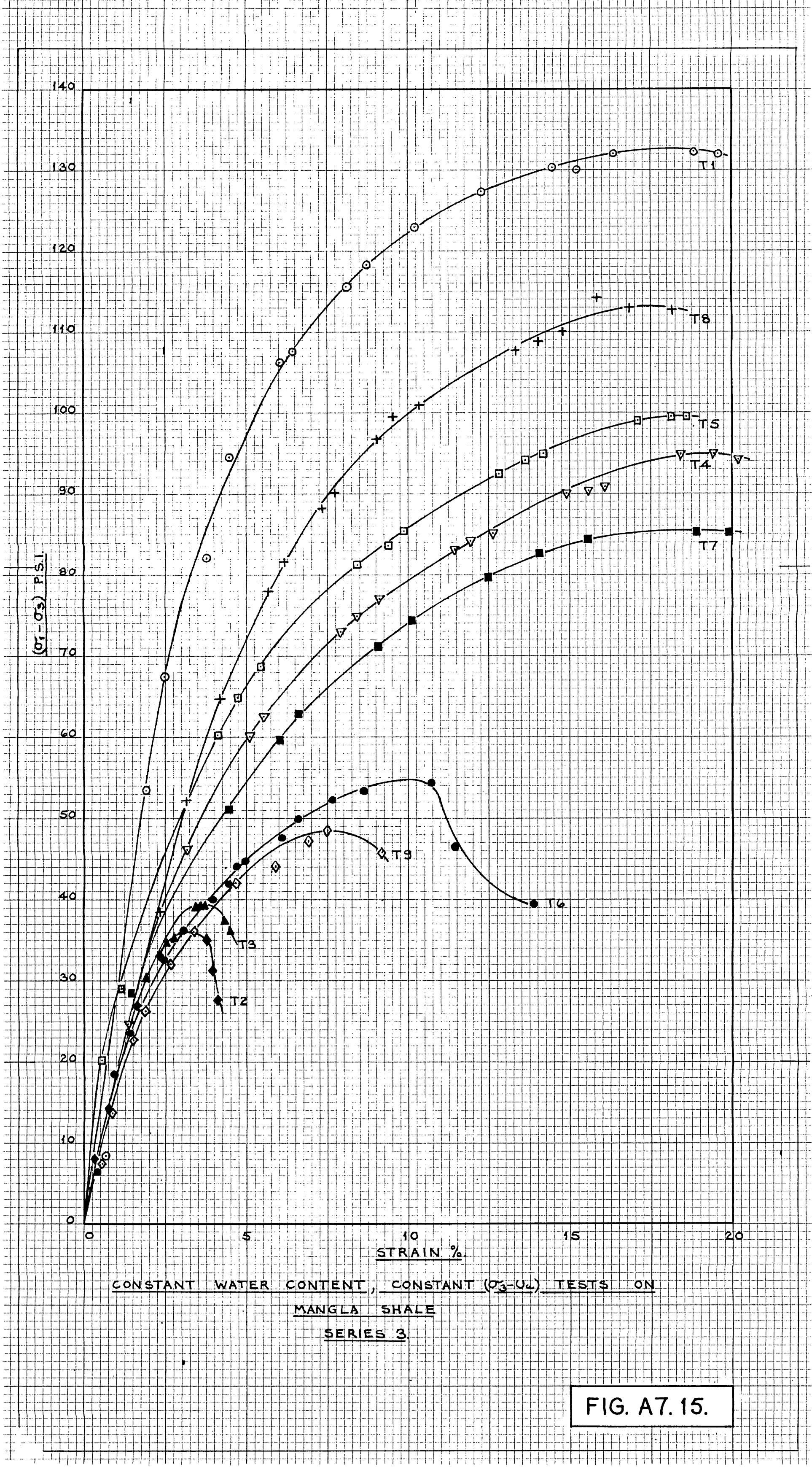


CONSTANT WATER CONTENT, VARYING (σ_3-U_a)

TESTS ON MANGLA SHALE

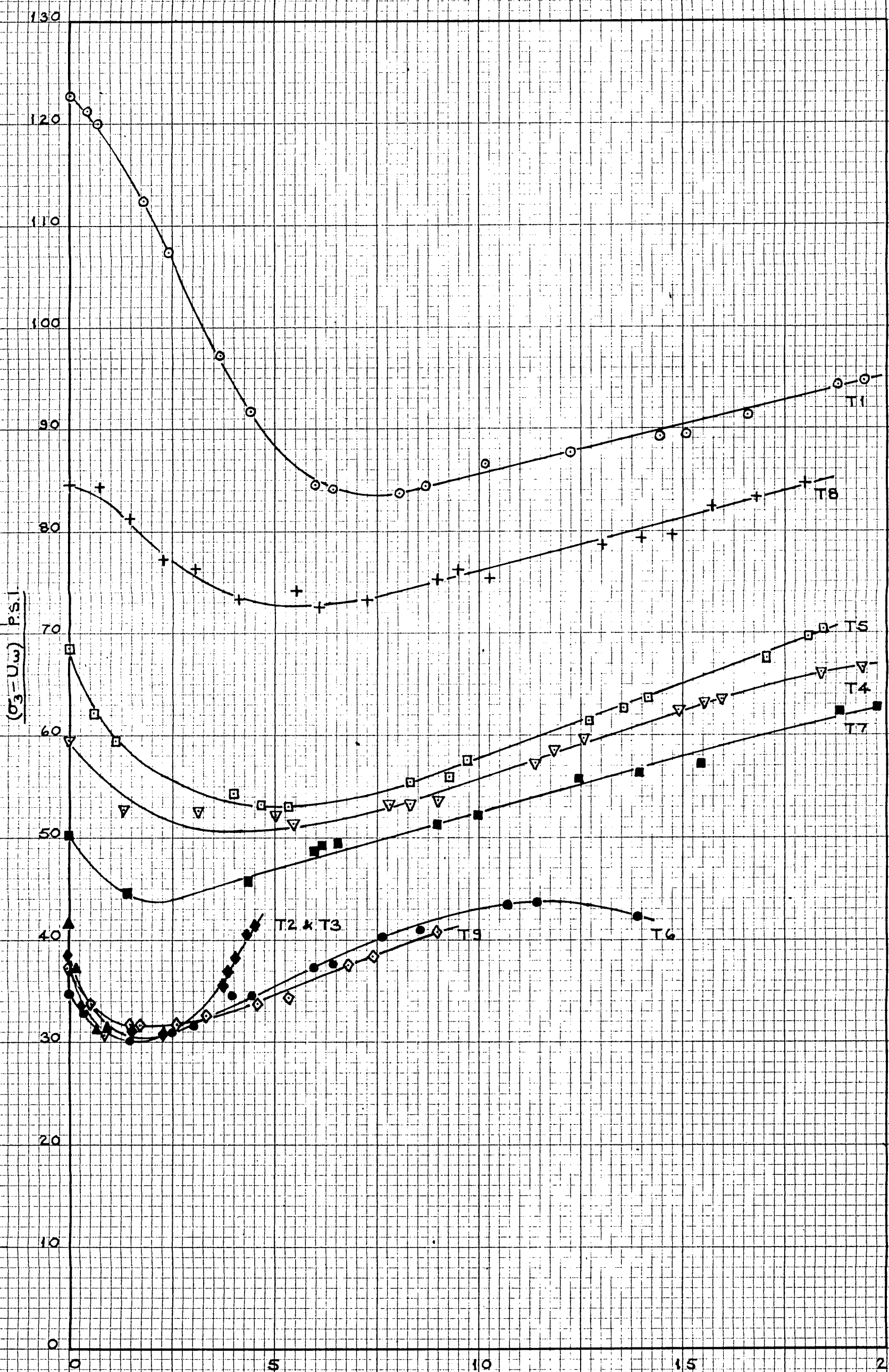
SERIES 1.

FIG. A7.14.



CONSTANT WATER CONTENT, CONSTANT ($\sigma_3 - U_a$) TESTS ON MANGLA SHALE SERIES 3.

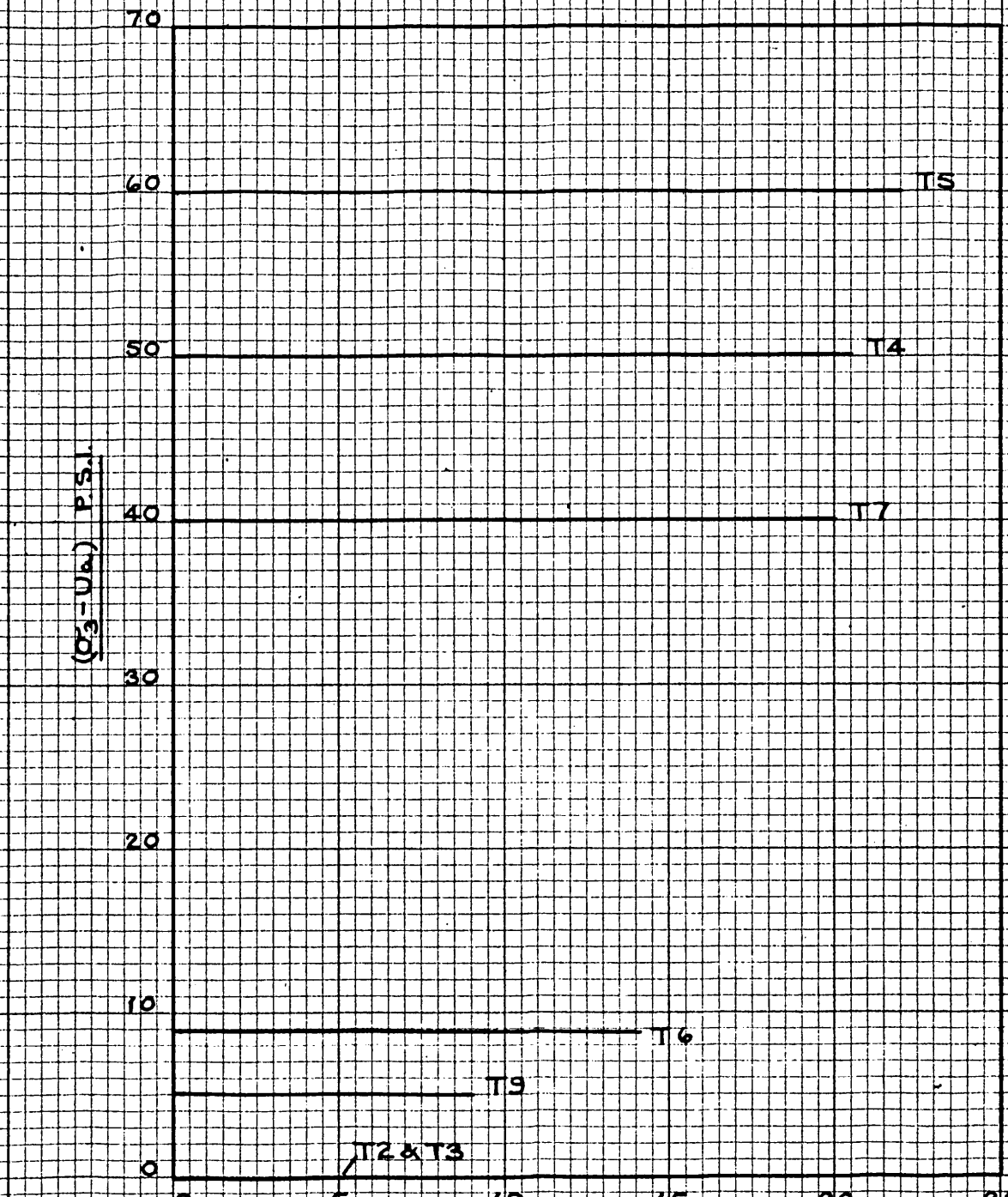
FIG. A7.15.



CONSTANT WATER CONTENT, CONSTANT $(\sigma_3 - U_a)$ TESTS ON MANGLA SHALE.

SERIES B.

FIG. A7.16.

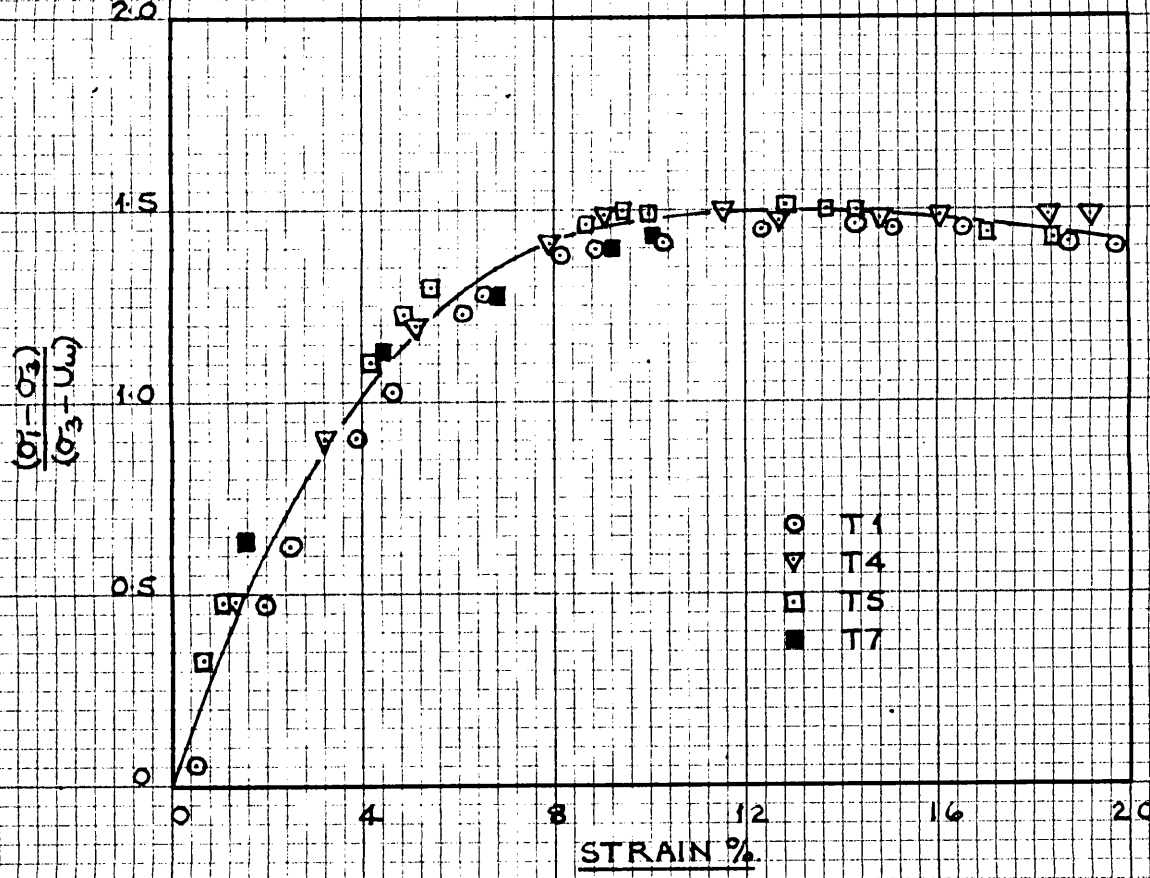


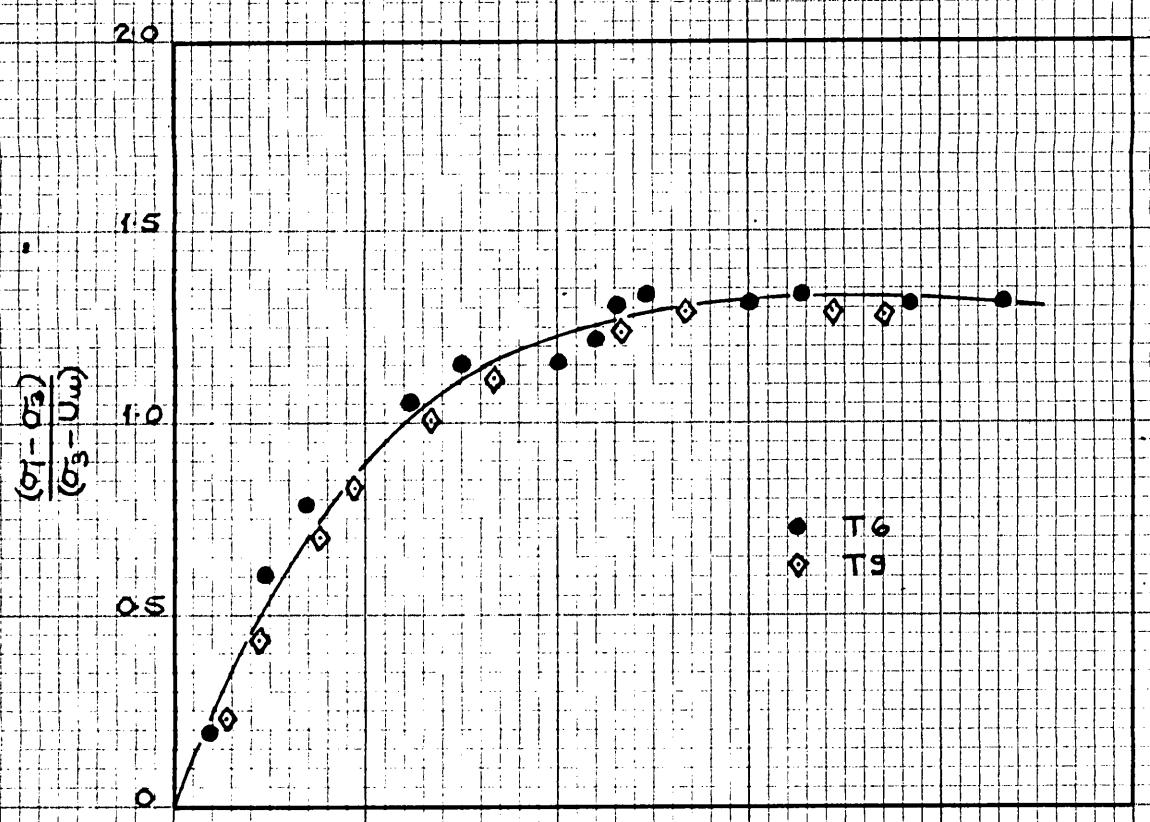
CONSTANT WATER CONTENT, CONSTANT $(\sigma_3 - U_a)$

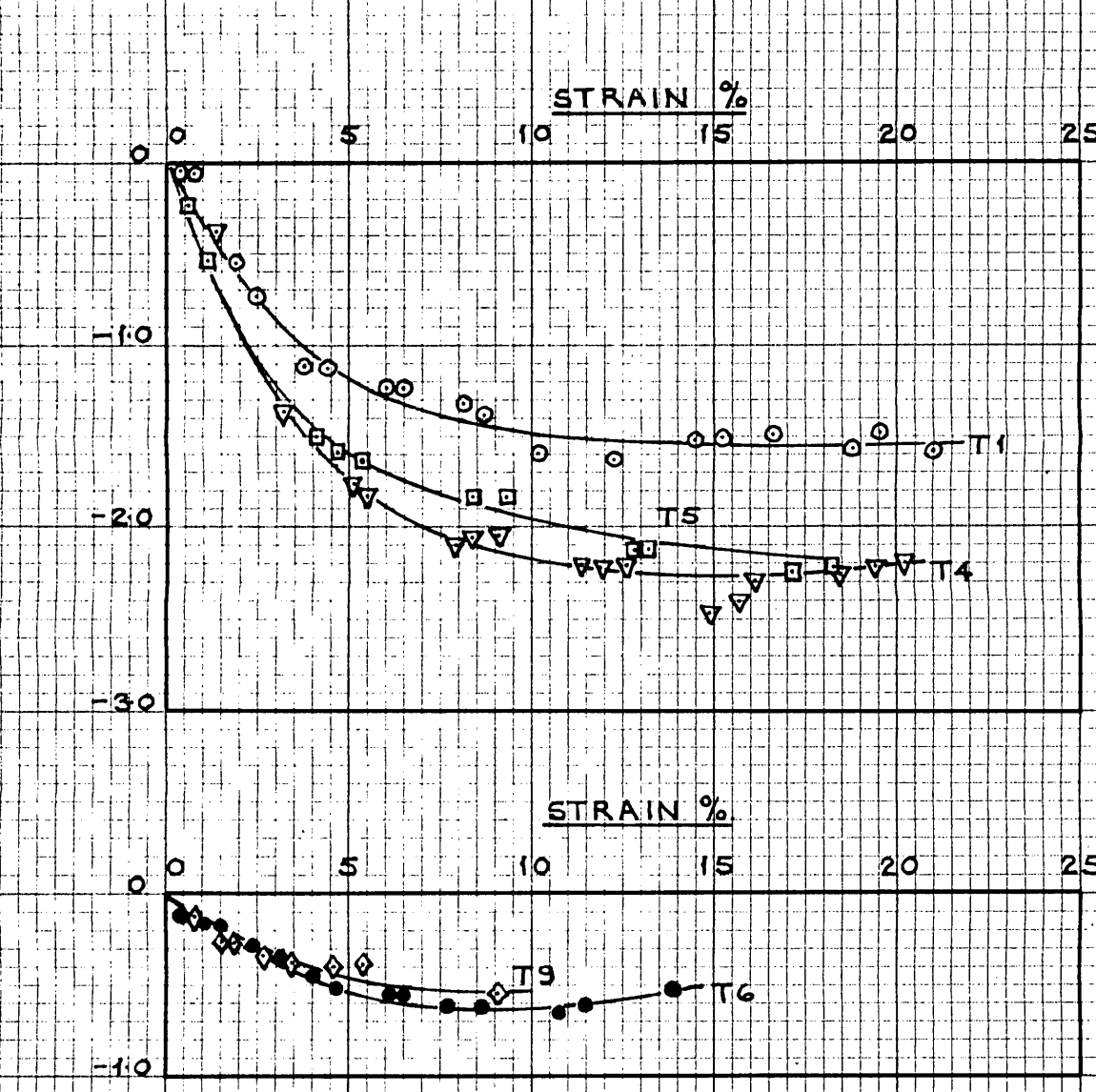
TESTS ON MANGLA SHALE.

SERIES 3.

FIG. A7.17.





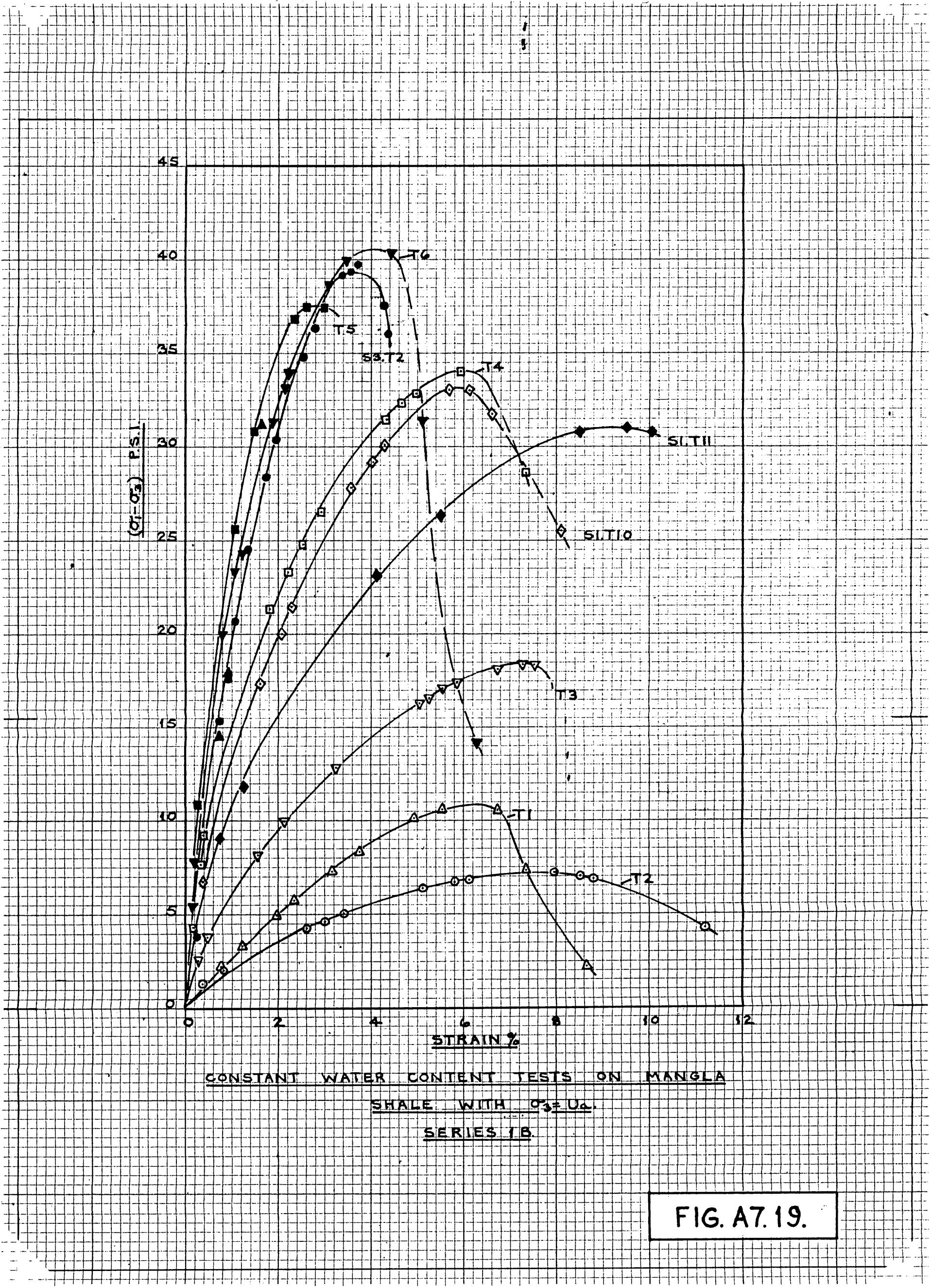


CONSTANT WATER CONTENT, CONSTANT (σ_3-U_a)

TESTS ON MANGLA SHALE.

SERIES 3.

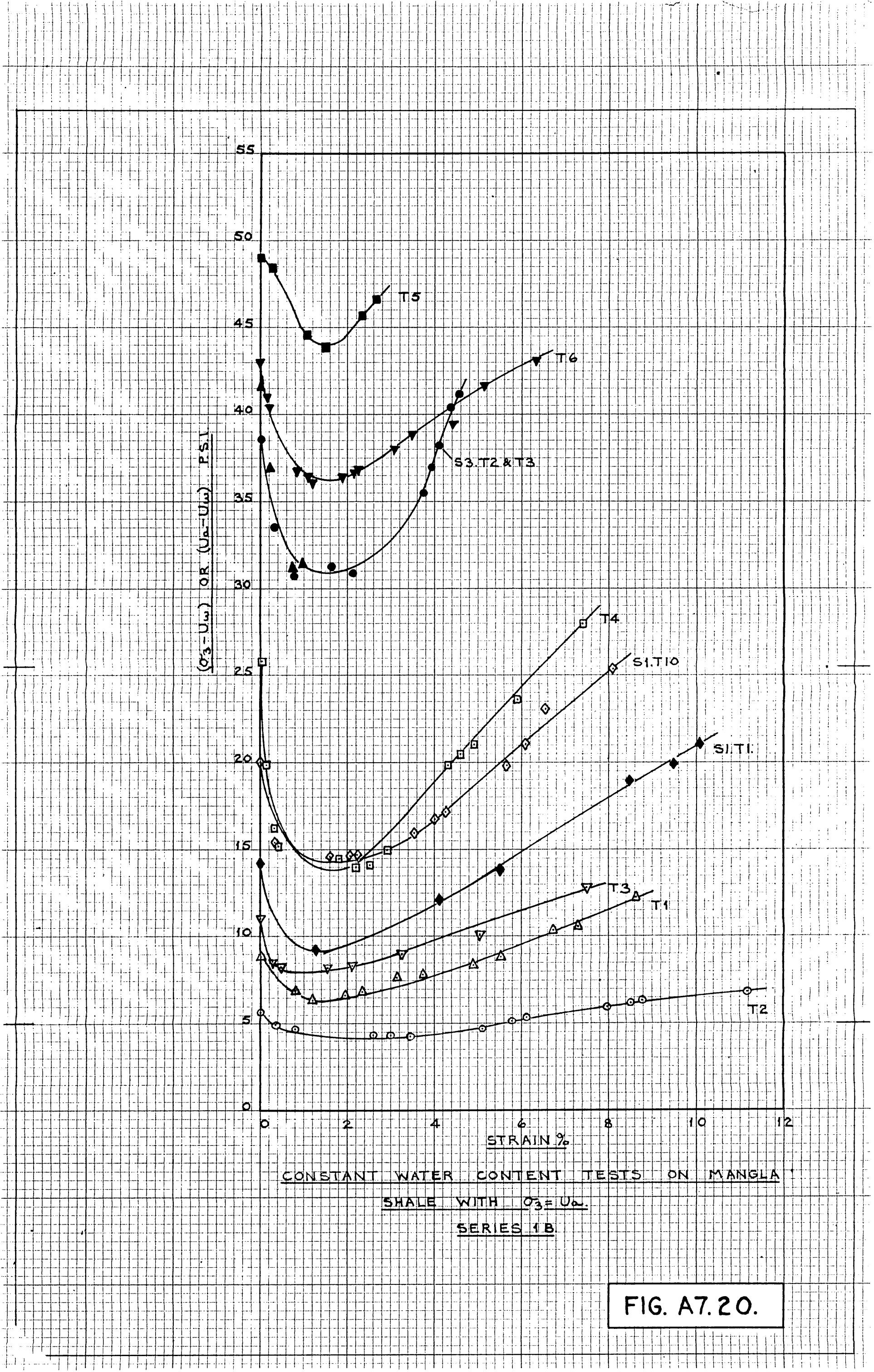
FIG. A7.18.



CONSTANT WATER CONTENT TESTS ON MANGLA SHALE WITH $\sigma_3 = U_a$.

SERIES 1B.

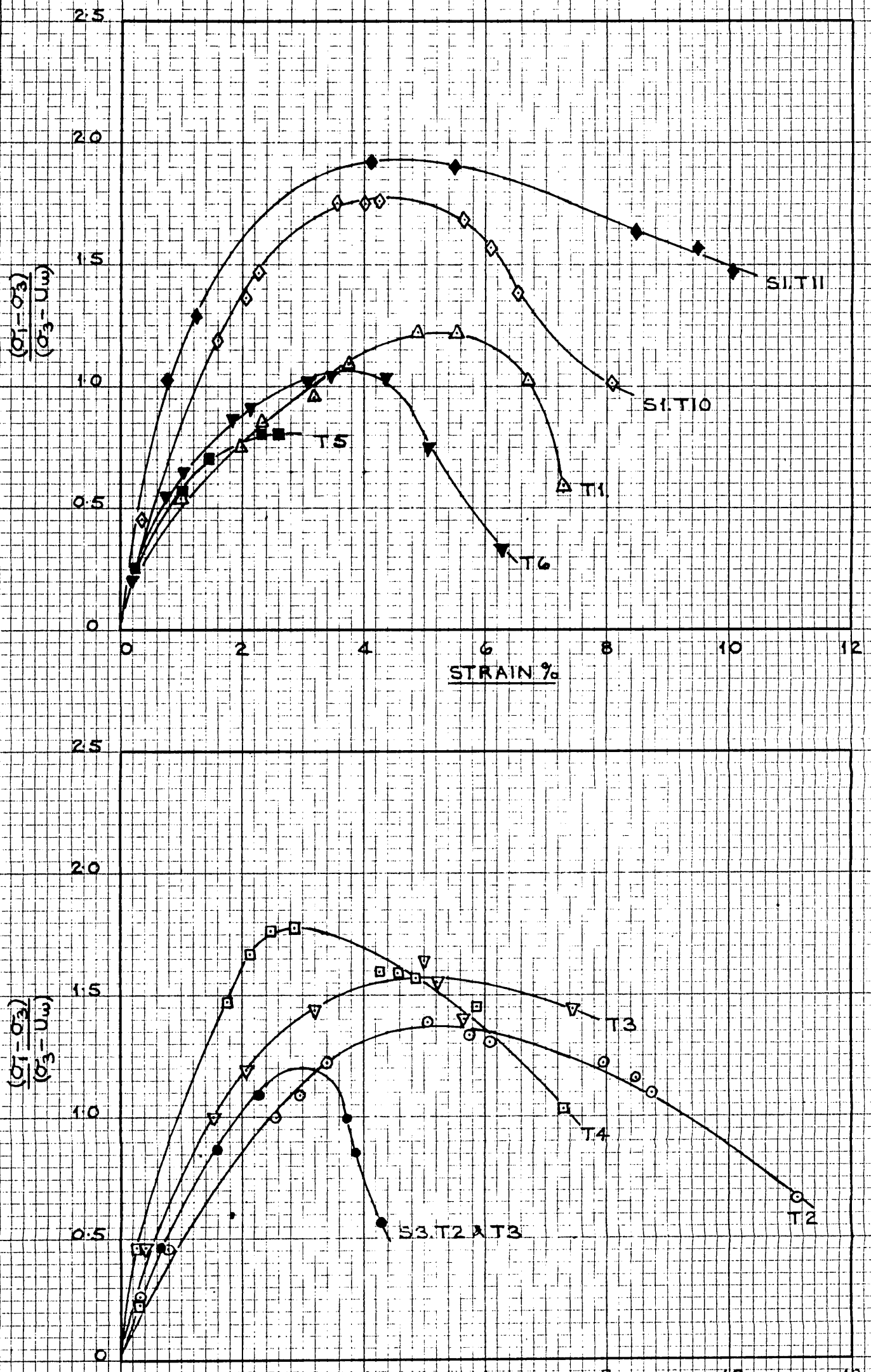
FIG. A7.19.



CONSTANT WATER CONTENT TESTS ON MANGLA SHALE WITH $\sigma_3 = U_a$.

SERIES 1B.

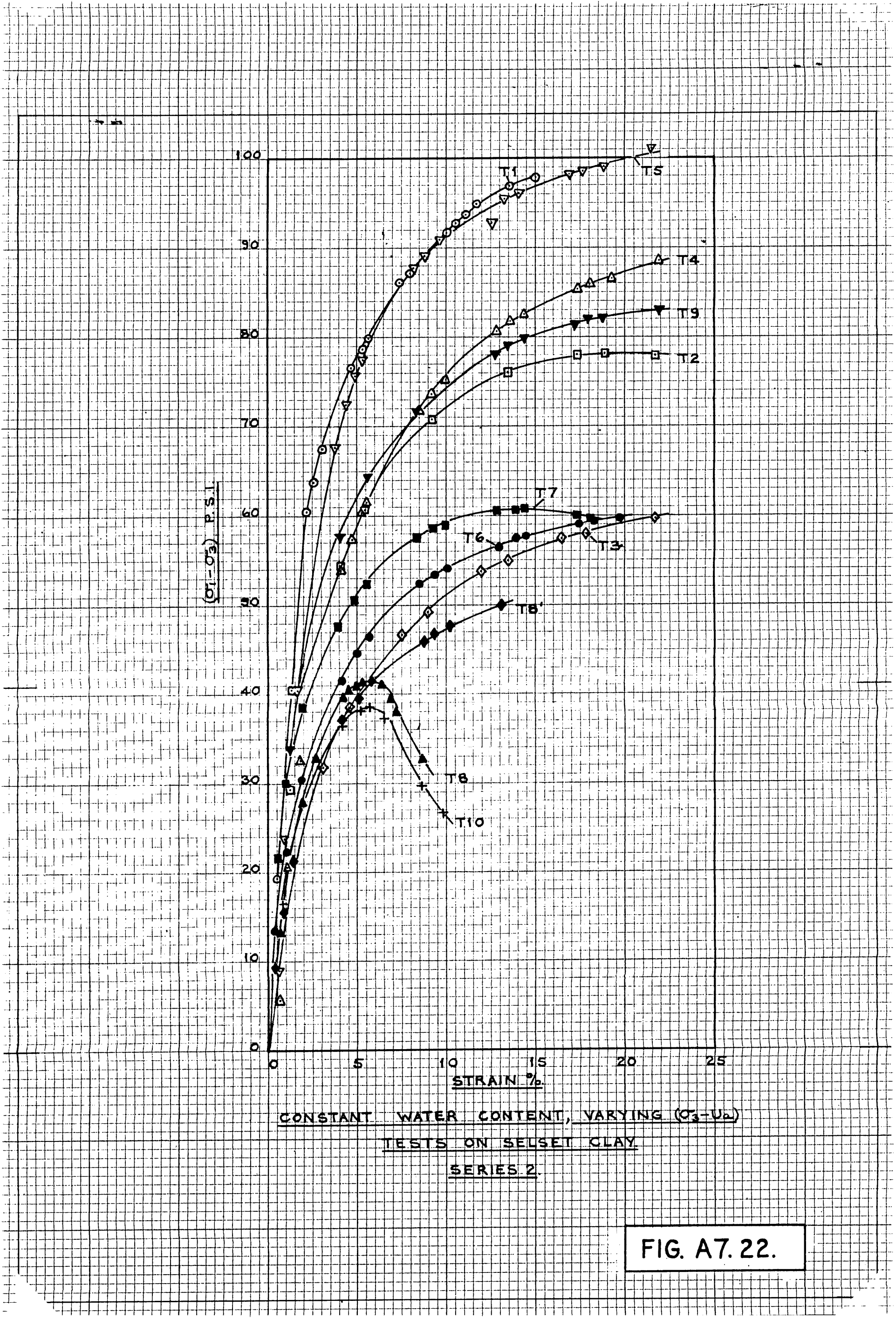
FIG. A7.20.



CONSTANT WATER CONTENT TESTS ON MANGLA SHALE WITH $\sigma_3 = U_a$

SERIES 1B.

FIG. A7.21.

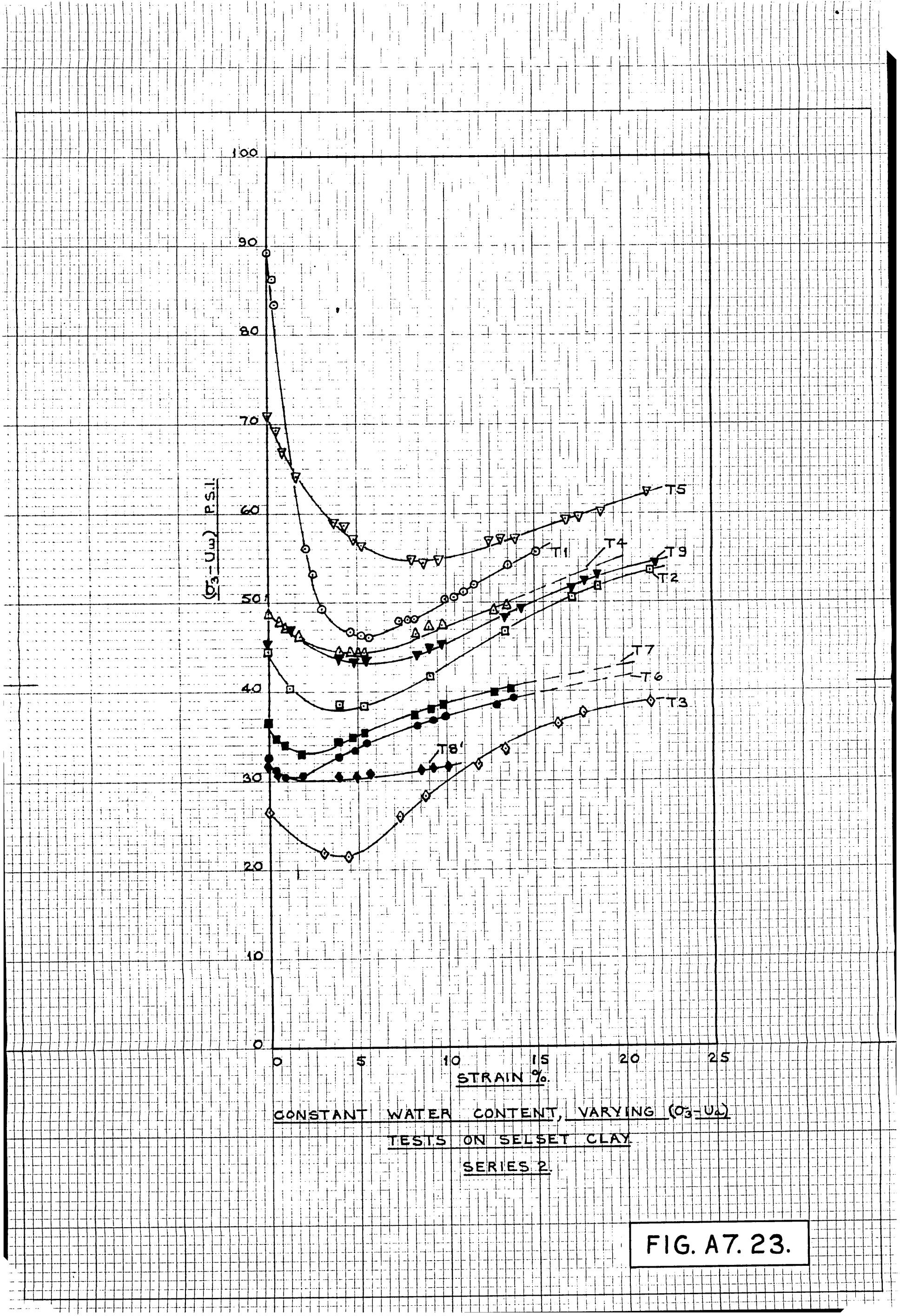


CONSTANT WATER CONTENT, VARYING (σ_3-U_b)

TESTS ON SELSET CLAY.

SERIES 2.

FIG. A7.22.

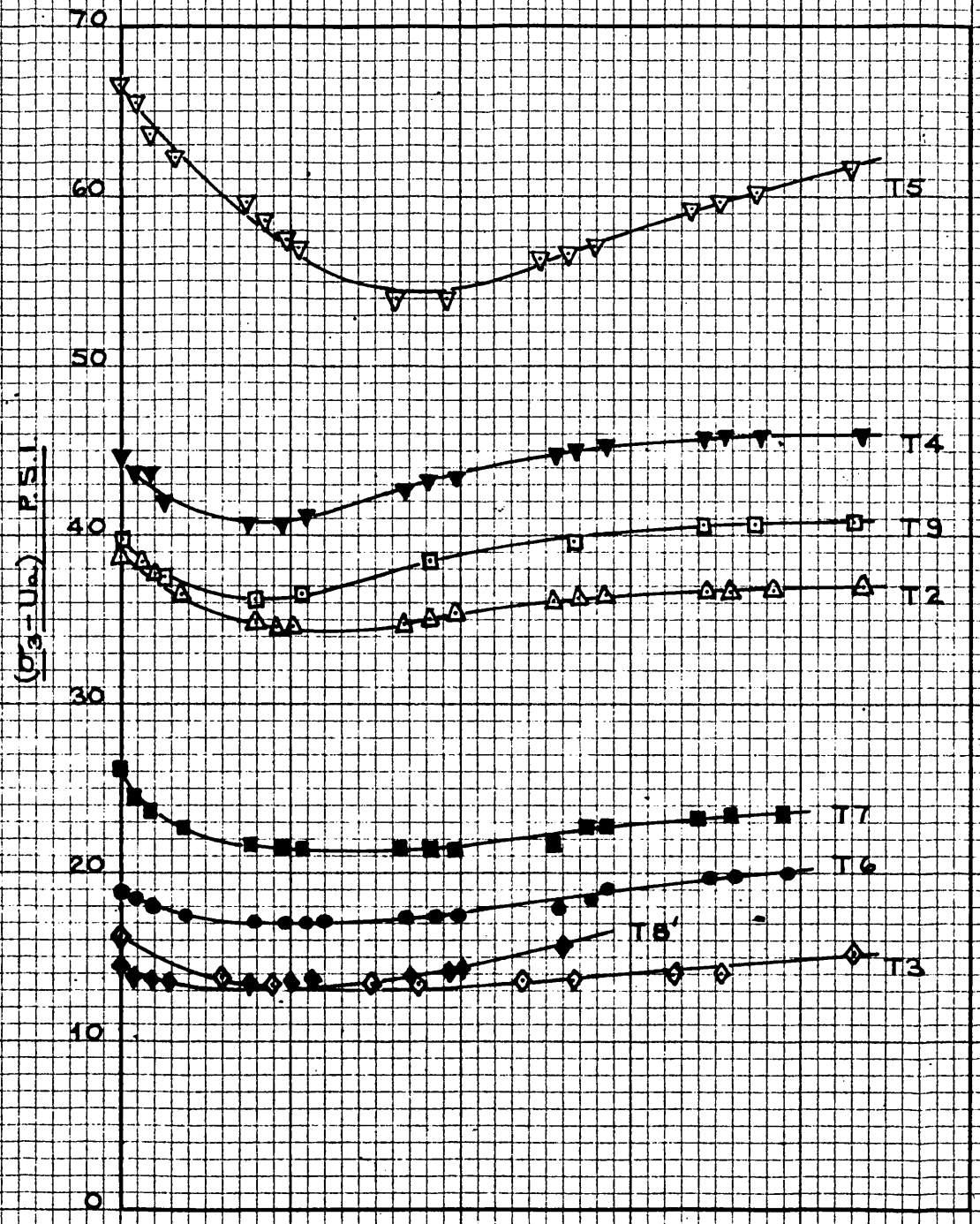


CONSTANT WATER CONTENT, VARYING $(\sigma_3 - U_a)$

TESTS ON SELSET CLAY.

SERIES 2.

FIG. A7.23.

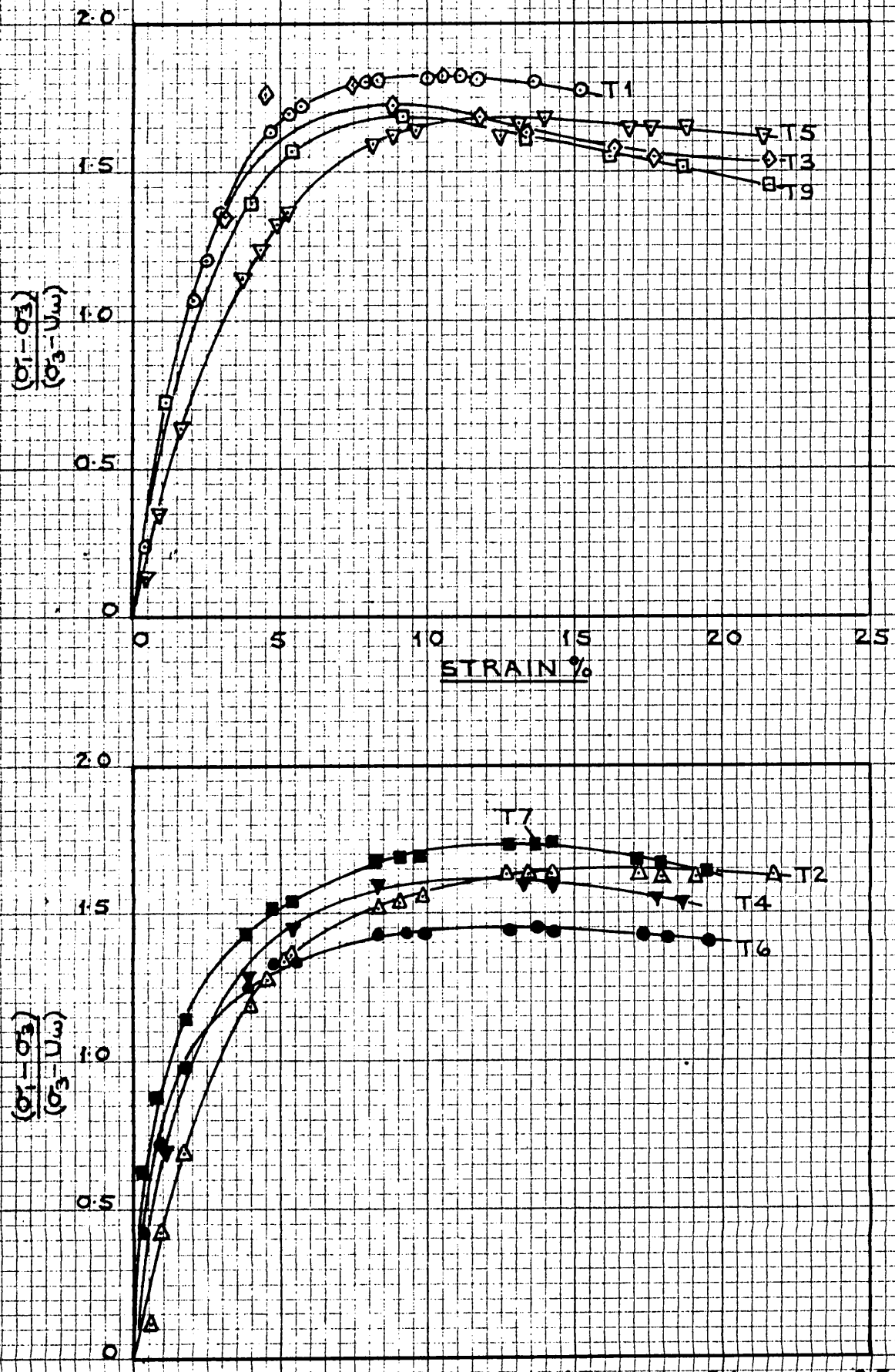


CONSTANT WATER CONTENT, VARYING $(\sigma_3 - U_a)$

TESTS ON SELSET CLAY.

SERIES 2

FIG. A7.24.



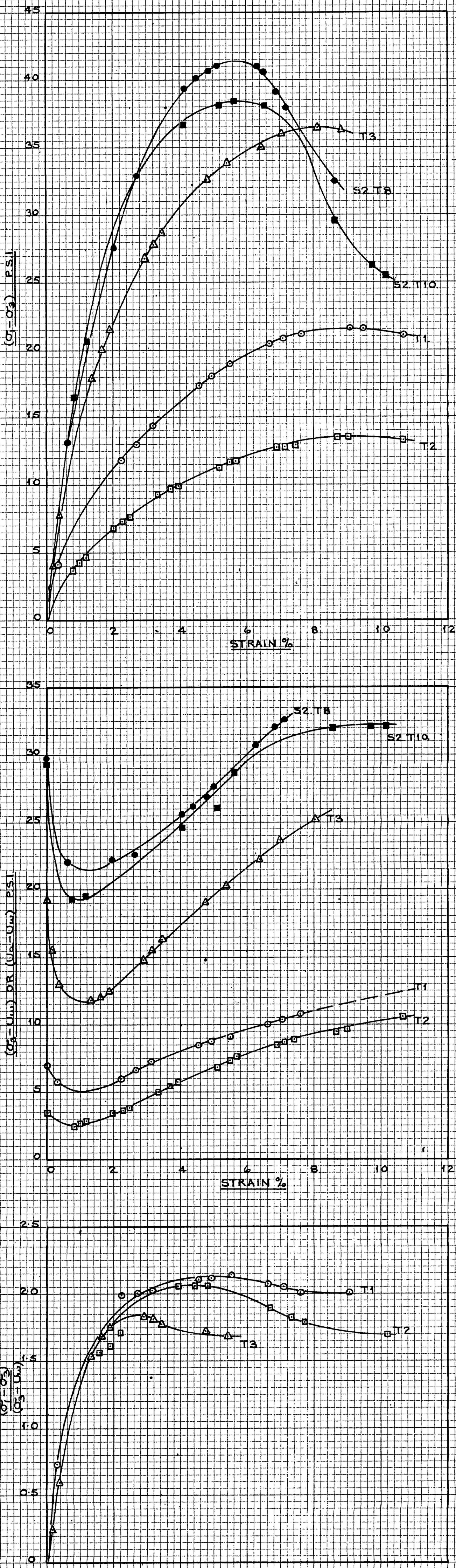
STRAIN %.

CONSTANT WATER CONTENT, VARYING $(\sigma_3 - U_0)$

TESTS ON SELSET CLAY

SERIES 2.

FIG. A7.25.



CONSTANT WATER CONTENT TESTS ON SELSET CLAY

WITH $\sigma_3 = U_a$

SERIES 26.

FIG. A7.26.

APPENDIX TO CHAPTER 8

(A.8.1) Data on equalisation of pore pressures during shear.

COMPACTED SOILS							
Soil	Strain Rate "/min.	Strain as basis for t %	t min.	C_t $cm^2/sec.$	T_v	$p = u_E - u_c$ p.s.i.	$\Upsilon = (1-p/p_o)$
Mangla Shale w=16%	.00005	6	9,600	2.76 x 10^{-4}	1.58	1.7	.944
	.00007	10	11,400		1.84	2.5	.917
	.0001	10	8,000		1.28	3.2	.894
	.00025	10	3,850		0.51	5.0	.833
	.00034	11	2,600		0.41	7.7	.744
	.00075	10	1,070		0.17	11.6	.614
	.001	10	800		0.13	11.9	.604
	.003	12	320		0.051	20.0	.333
						p_o:	30.0
Mangla Shale w=18.5%	.000025	10	32,000	2.66 x 10^{-4}	4.94	0.5	.971
	.0001	10	8,000		1.23	1.4	.920
	.00025	10	3,200		0.51	2.6	.851
	.00034	11.5	2,700		0.43	3.0	.829
	.00075	10	1,070		0.17	6.0	.657
	.00125	10	640		0.10	8.6	.509
	.003	13	350		0.056	12.0	.314
						p_o:	17.5
Selset Clay	.00005	10	16,000	5.76 x 10^{-4}	5.36	1.8	.950
	.0001	10	8,000		2.68	3.6	.900
	.00025	5	1,600		0.54	6.0	.833
	.00034	10	2,350		0.81	6.4	.821
	.00075	10	1,070		0.35	8.9	.752
	.0017	10	474		0.16	15.2	.578
						p_o:	36.0
Talybont Clay (from tests by Alpan)	.0019	9	320	17.1 x 10^{-4}	0.195	3.1	.790
	.0030	7	200		0.122	8.6	.419
	.0042	7	140		0.085	5.6	.622
	.0019	7	320		0.195	5.1	.656
	.0042	6	140		0.085	8.4	.433
	.0005	8	1,200		0.730	1.1	.926
	.0005	9	1,200		0.730	2.4	.838
	.006	8	100		0.061	13.4	.095
	.0005	17			1.66	0.8	.946
		Av. $7\frac{1}{2}$				p_o:	14.8

SATURATED SOILS								
Soil	Strain Rate %/min.	Strain as Basis for t %	t min.	C_t cm^2/sec	2H in.	T_v	$p=u_E-u_c$ p.s.i.	$\Upsilon=(1-p/p_o)$
Mangla Shale remoulded at								
26.2%	.017	13	760	1.07×10^{-4}	3	0.34	1.0	.711
	.042	13	310			0.14	1.4	.596
							p_o:	3.47
30.0%	.028	13	460			0.20	0.7	.640
	.063	13	210			0.092	1.0	.485
							p_o:	1.94
Boston Clay (Tests by Taylor)	0.16	3	18.8	4×10^{-3}	6.5	.066	15.0	.375
	.016	3	18.8		6.5	.66	-2	.918
	0.16	3	18.8		11.0	.015	17.7	.262
	0.16	3	18.8		9.0	.023	13.9	.421
	0.16	3	18.8		5.5	.092	12.5	.479
	0.67	3	4.5		6.5	.013	20.8	.133
							p_o:	24

(A.8.2) Elastic stresses in a cylinder compressed between rough rigid end loading plates.

Data from Filon,(1902.) Refer also to fig. (8.28)

(i) Principal stresses:

ØØ/Q

r	z=0	z=h/6	z=2h/6	z=3h/6	z=4h/6	z=5h/6	z=h
0	.00274	.01414	.05134	.12416	.25325	.48151	.89668
a/3	-.00299	.00737	.04126	.10748	.22288	.42120	.77728
2a/3	-.01744	-.01017	.01461	.06480	.15199	.28607	.48160
a	-.03265	-.03013	-.02030	.00516	.06344	.18728	.43801

RR/Q

r	z=0	z=h/6	z=2h/6	z=3h/6	z=4h/6	z=5h/6	z=h
0	.00274	.01414	.05134	.12416	.25325	.48151	.89668
a/3	.00181	.01113	.04199	.10178	.20063	.33690	.34800
2a/3	.00110	.00457	.01758	.04405	.08433	.09804	.09139
a	0	0	0	0	0	0	0

ZZ/Q

r	z=0	z=h/6	z=2h/6	z=3h/6	z=4h/6	z=5h/6	z=h
0	1.13382	1.13436	1.13322	1.12146	1.08000	1.03372	0.68576
a/3	1.09971	1.10057	1.10018	1.09039	1.05849	0.99907	1.06087
2a/3	1.00724	1.00898	1.01314	1.01628	1.01467	1.01602	1.11961
a	0.89430	0.88809	0.87216	0.85845	0.88177	1.04077	1.68635

+ve stress: Compression
-ve stress: Tension

(ii) Average principal stresses.

z/h	$\overline{\phi\phi}/Q$	$\overline{RR}/Q$	$\overline{ZZ}/Q$	$\overline{\sigma^*}/Q$
1	0.545	0.151	1.269	0.348
5/6	0.293	0.132	1.010	0.212
4/6	0.144	0.091	1.000	0.118
3/6	0.059	0.048	1.002	0.054
2/6	0.010	0.019	1.013	0.014
1/6	-0.013	0.008	1.013	- .002
0	-0.019	0.004	1.014	- .008

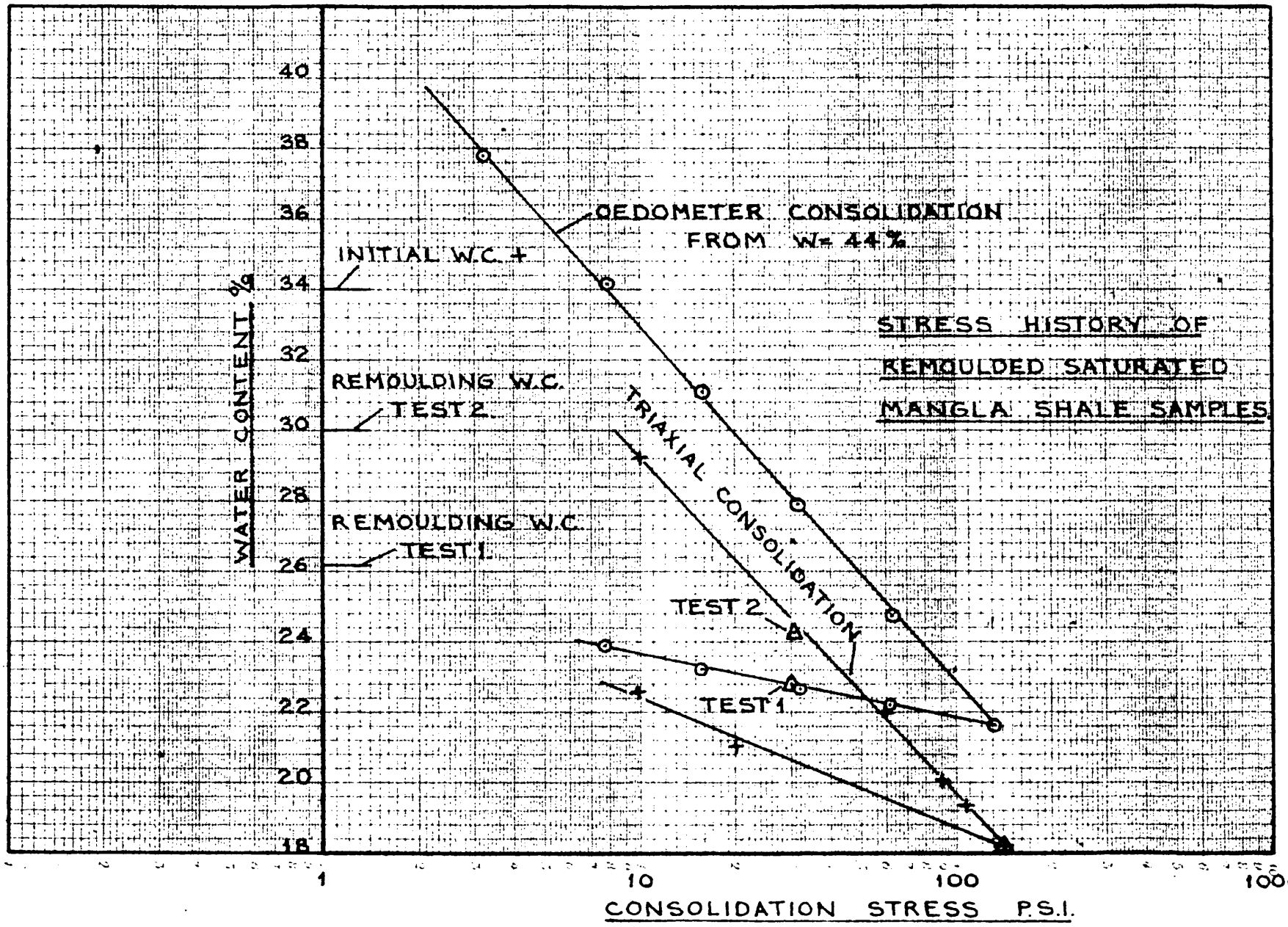
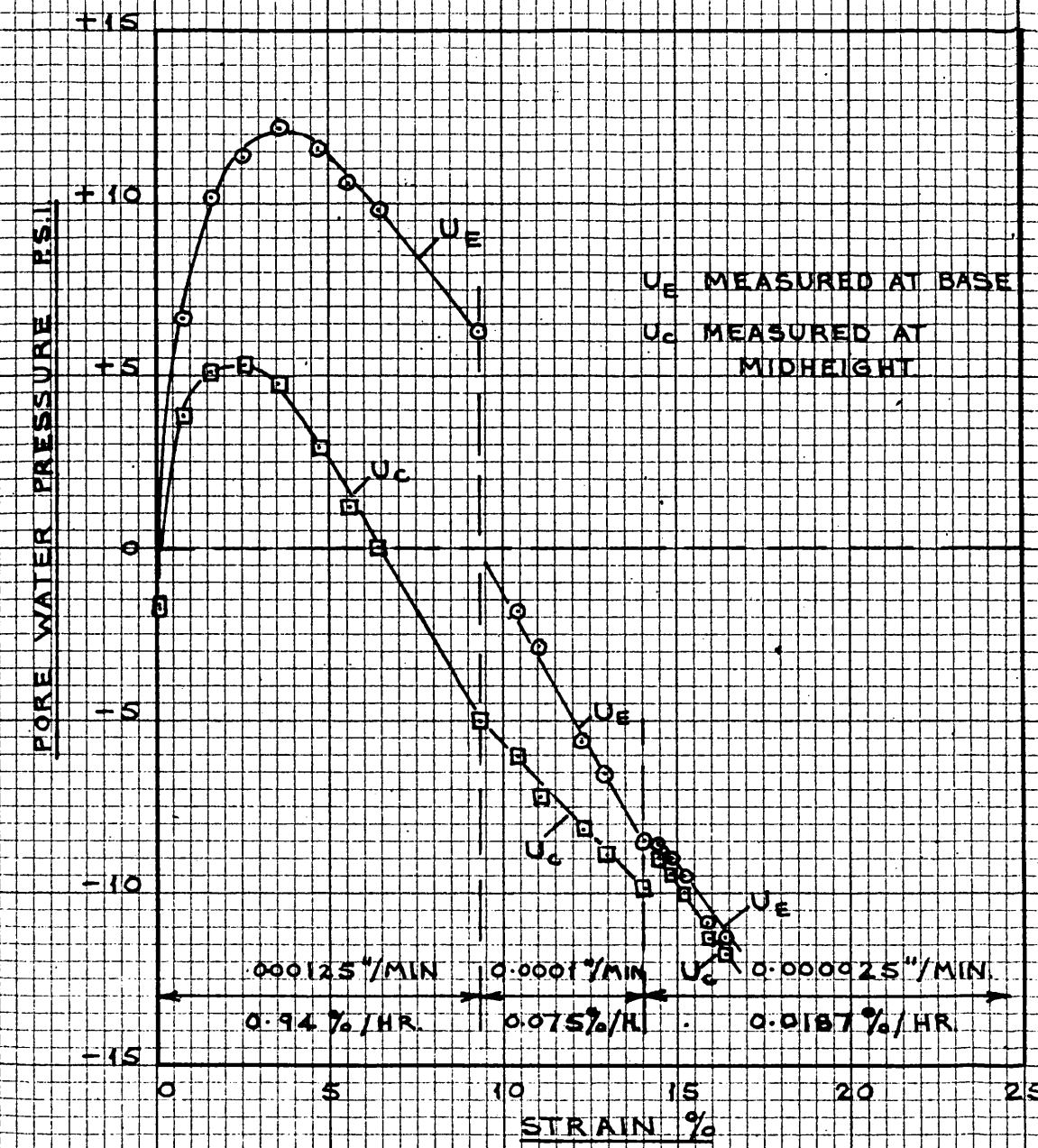

40
38
36
34
32
30
28
26
24
22
20
18
WATER CONTENT %
OEDOMETER CONSOLIDATION
FROM w= 44%
INITIAL W.C.
REMOULDING W.C.
TEST 2.
REMOULDING W.C.
TEST 1.
TRIAXIAL CONSOLIDATION
TEST 2
TEST 1
STRESS HISTORY OF
REMOULDED SATURATED
MANGLA SHALE SAMPLES.
1
10
100
1000
CONSOLIDATION STRESS P.S.I.

FIG. A8.1.

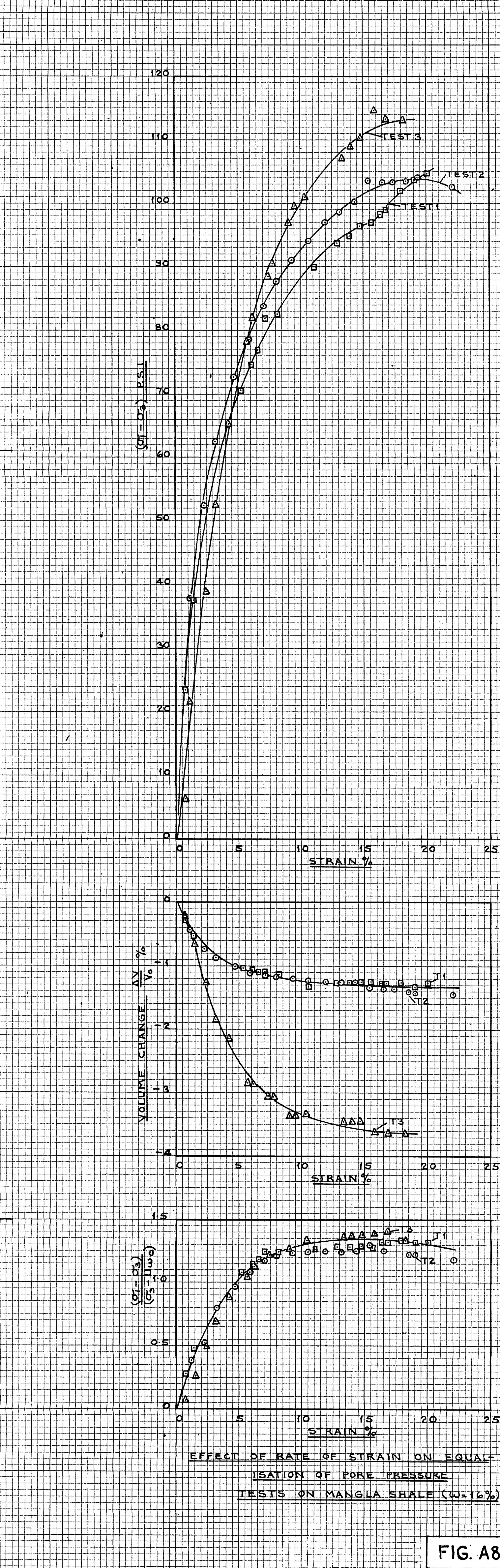


EFFECT OF RATE OF STRAIN ON EQUALISATION OF PORE PRESSURE.

MANGLA SHALE

$w = 18\frac{1}{2}\%$

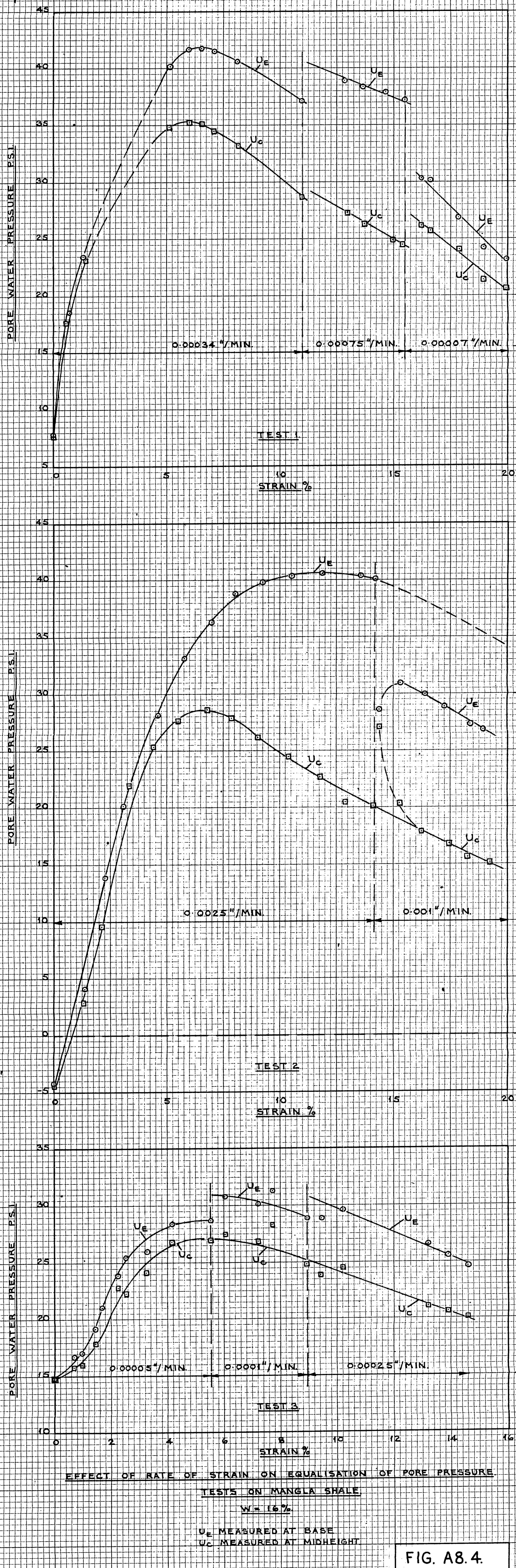
FIG. A8.2.



EFFECT OF RATE OF STRAIN ON EQUALISATION OF PORE PRESSURE.

TESTS ON MANGLA SHALE (ω = 16%).

FIG. A8.3.



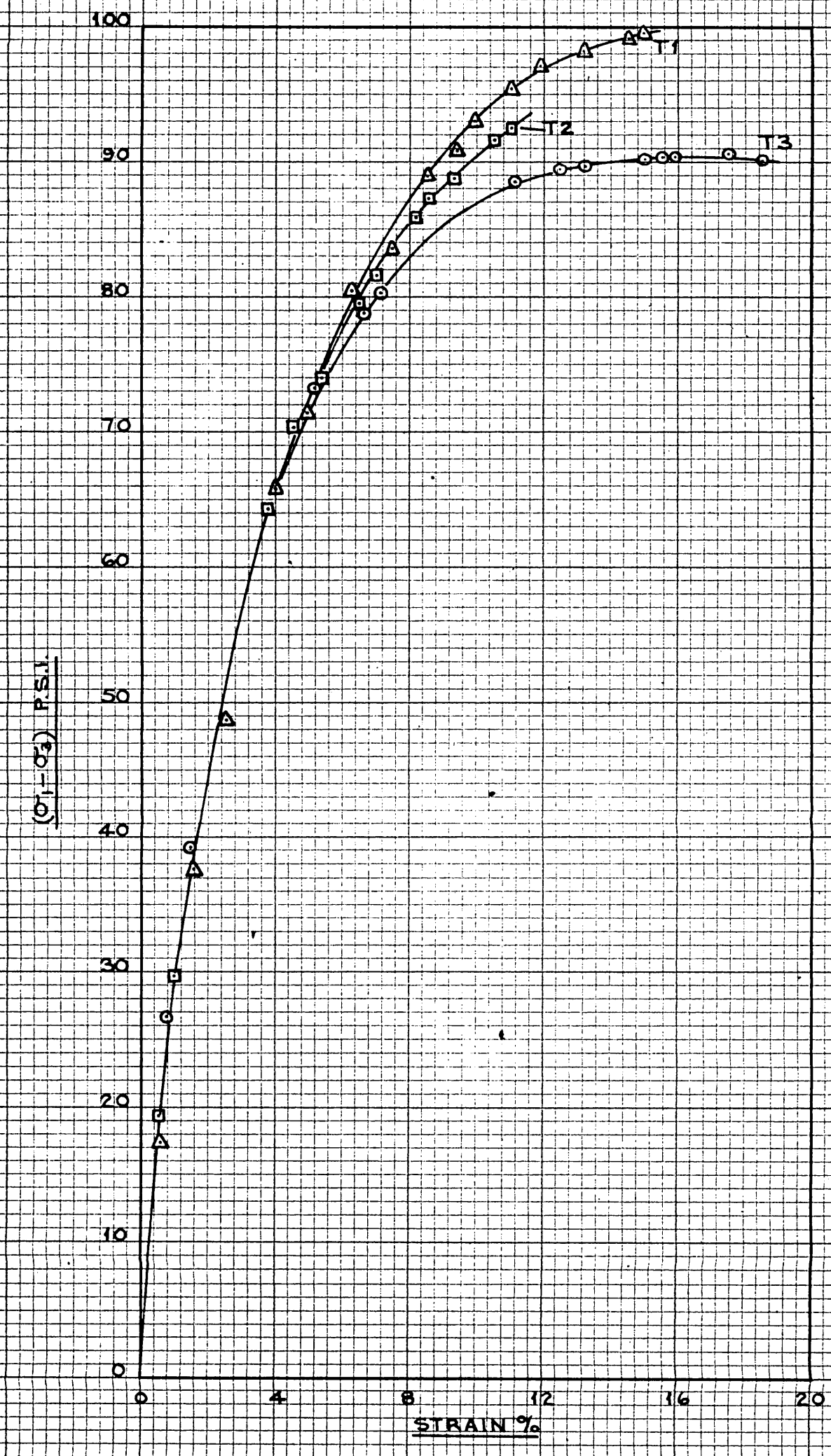
EFFECT OF RATE OF STRAIN ON EQUALISATION OF PORE PRESSURE.

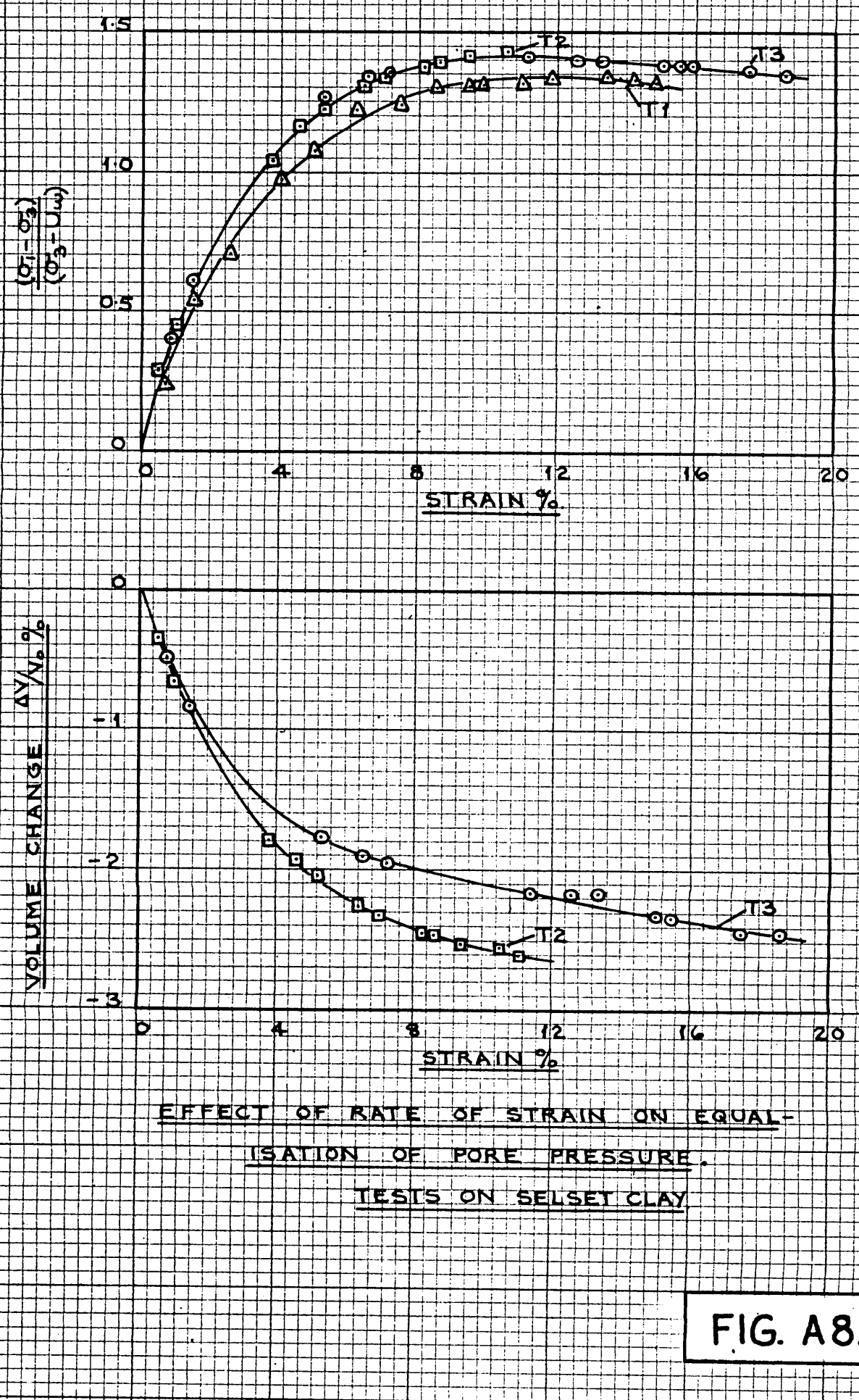
TESTS ON MANGLA SHALE.

W = 16 %.

U_E MEASURED AT BASE
U_C MEASURED AT MIDHEIGHT

FIG. A8.4.

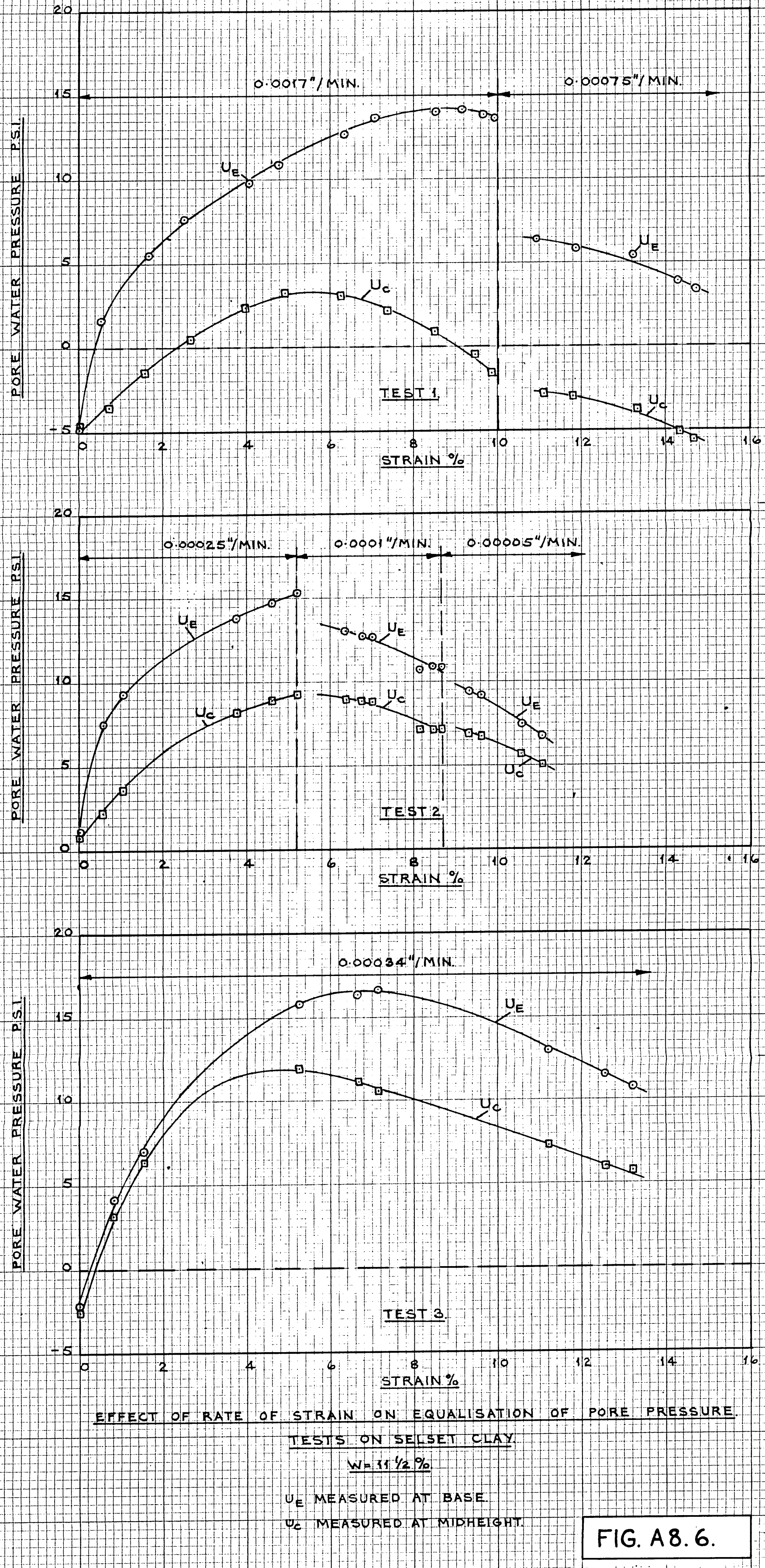




EFFECT OF RATE OF STRAIN ON EQUALISATION OF PORE PRESSURE.

TESTS ON SELSET CLAY

FIG. A8.5.



EFFECT OF RATE OF STRAIN ON EQUALISATION OF PORE PRESSURE.

TESTS ON SELSET CLAY.

W = 11 1/2 %.

U_E MEASURED AT BASE.

U_C MEASURED AT MIDHEIGHT.

FIG. A8.6.

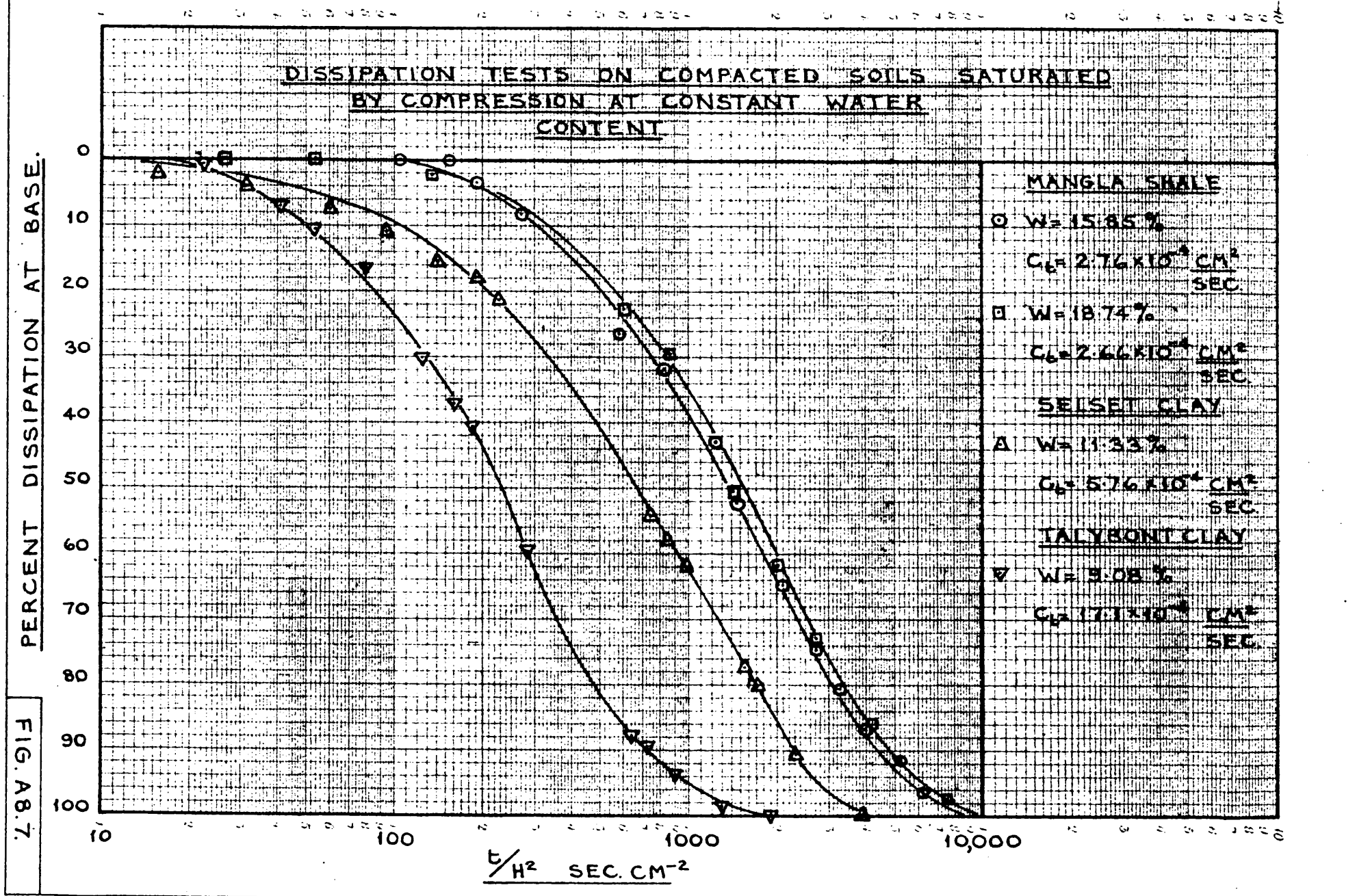
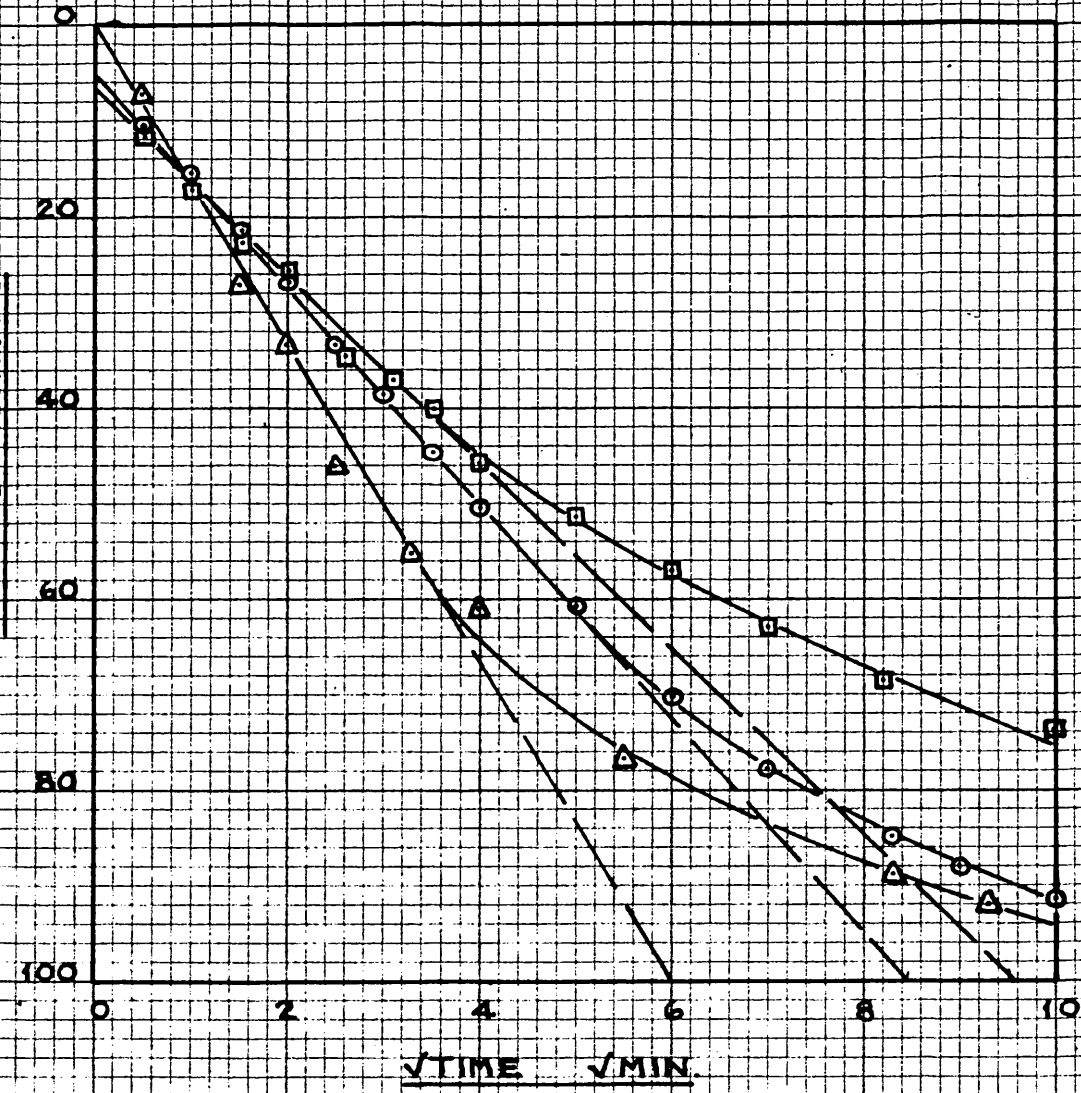

DISSIPATION TESTS ON COMPACTED SOILS SATURATED BY COMPRESSION AT CONSTANT WATER CONTENT
PERCENT DISSIPATION AT BASE.
0
10
20
30
40
50
60
70
80
90
100
10
100
1000
10,000
t/H² SEC. CM⁻²
MANGLA SHALE
W= 15.85 %
Cv= 2.76 x 10⁻⁴ CM²/SEC
W= 18.74 %
Cv= 2.66 x 10⁻⁴ CM²/SEC
SELSET CLAY
W= 11.33 %
Cv= 5.76 x 10⁻⁴ CM²/SEC
TALYBONT CLAY
W= 9.08 %
Cv= 17.1 x 10⁻⁴ CM²/SEC

FIG. A8.7.



CONSOLIDATION CURVES USING PAPER DRAINS TO GIVE ALL-ROUND DRAINAGE

VALUES OF C_v ASSUMING DRAINS ARE 100% EFFECTIVE

○	MANGLA SHALE REMOULDED AT	W=26·2% :	$1{\cdot}07\times10^{-4}$
□	MANGLA SHALE COMPACTED AT	W=16 % :	$0{\cdot}84\times10^{-4}$
△	SELSET CLAY COMPACTED AT	W=11·7% :	$2{\cdot}29\times10^{-4}$

FIG. A8.8.

APPENDIX TO CHAPTER 10

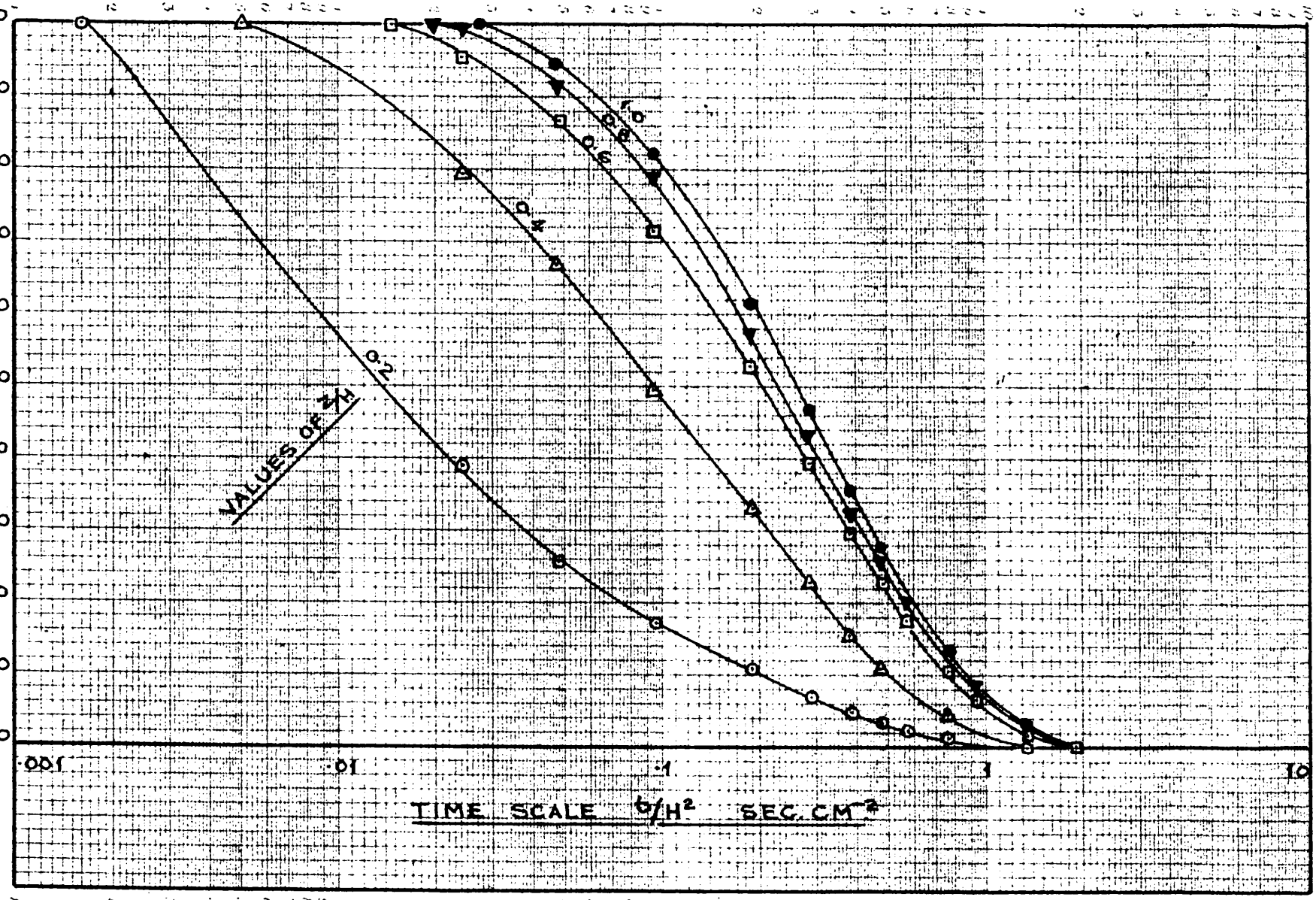
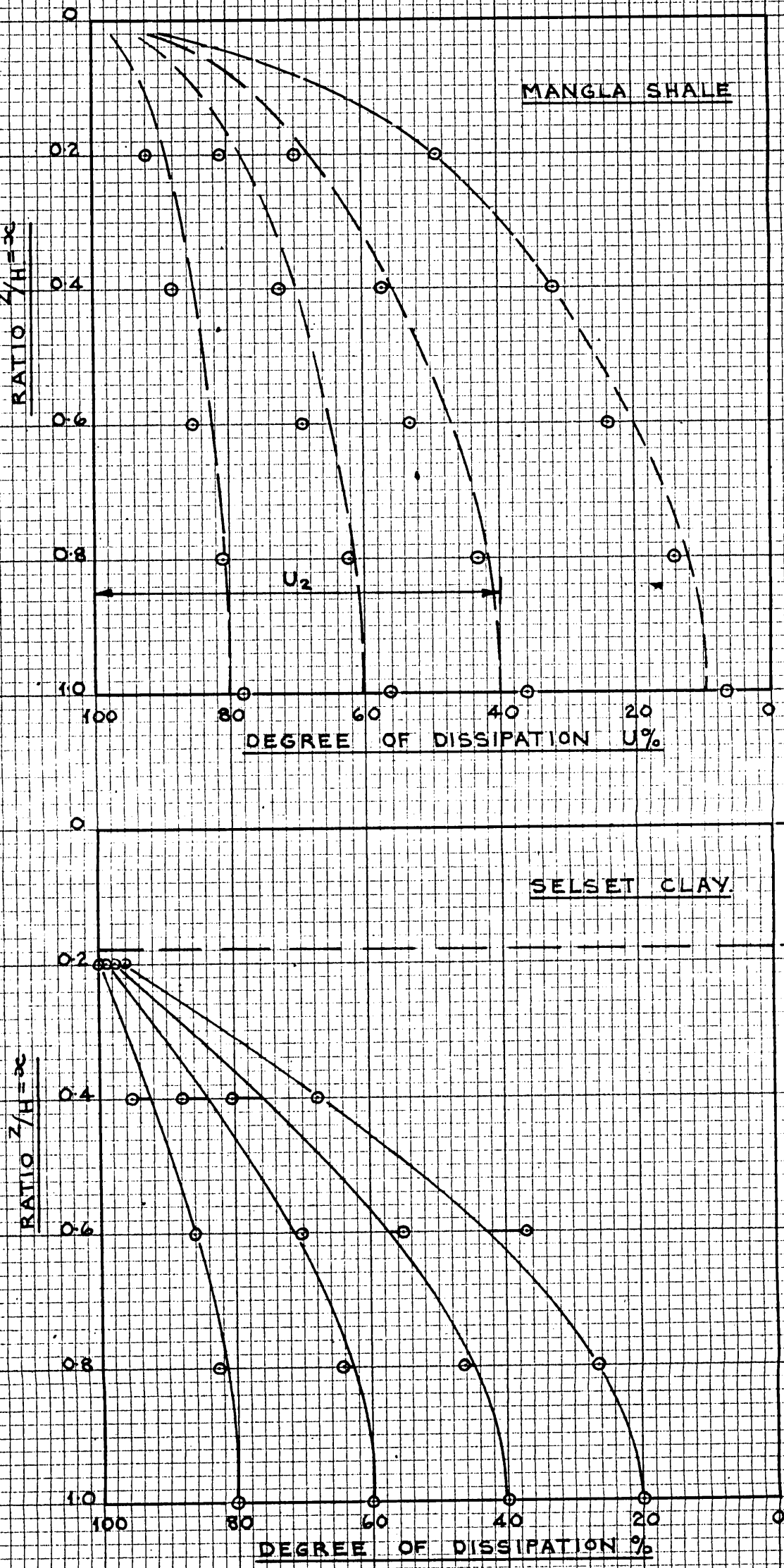


FIG. A10.1.

UNSTEADY FLOW OF AIR THROUGH DRY COMPACTED SELSET CLAY. FLOW DIRECTION 1.



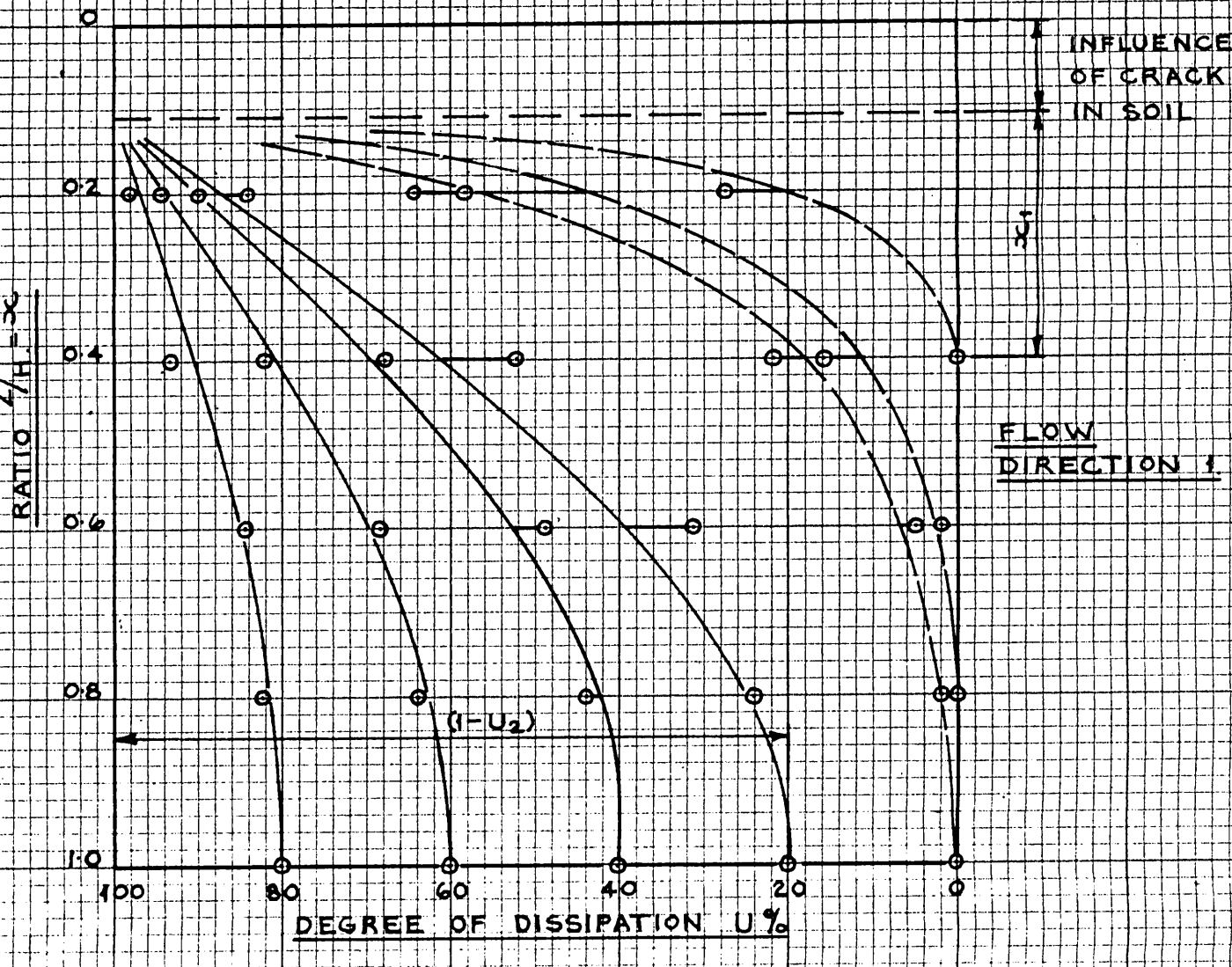
EXPERIMENTAL ISOCHRONES FOR UNSTEADY FLOW OF AIR THROUGH DRY COMPACTED SOIL.

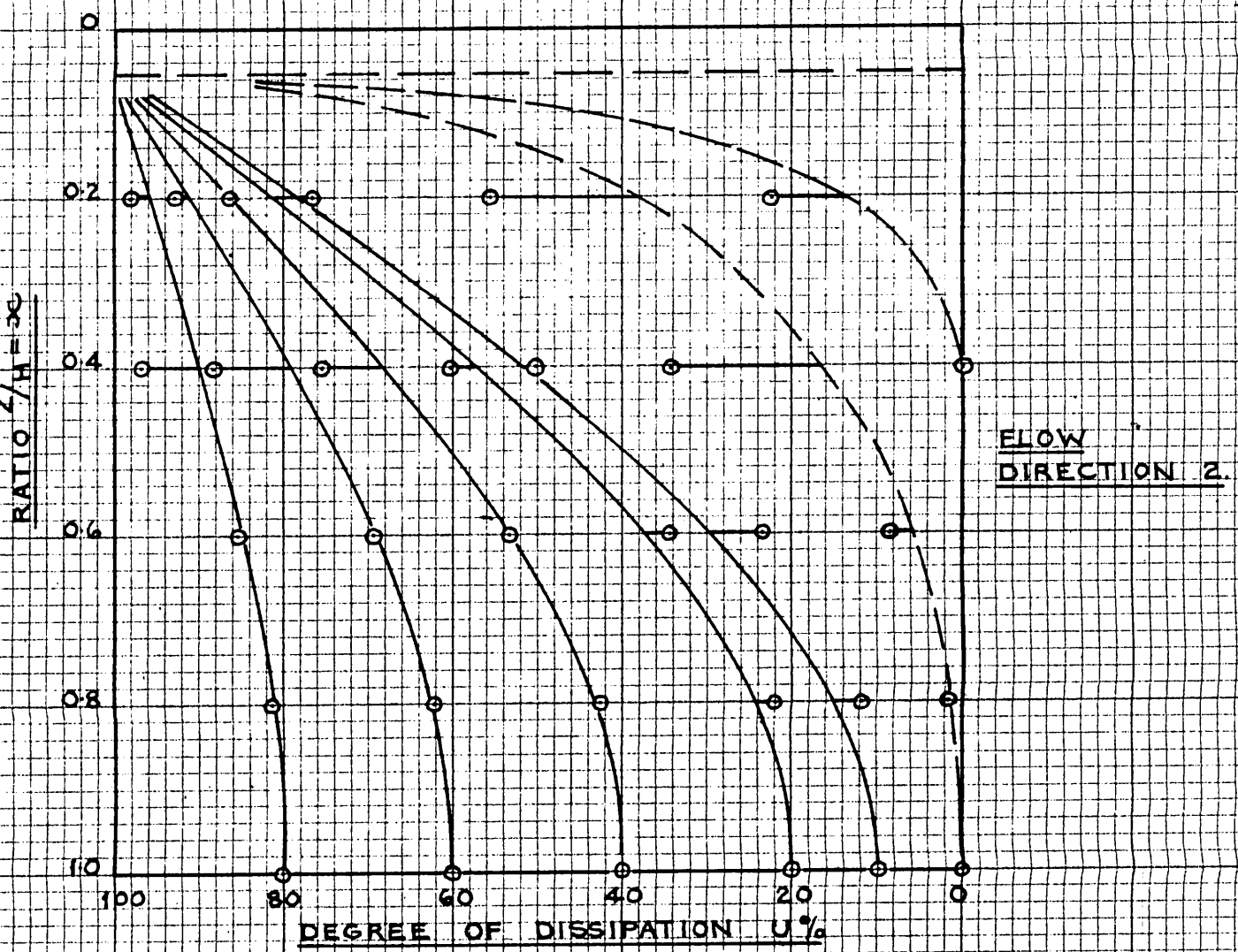
VALUES OF x WERE CORRECTED FOR INFLUENCE OF CRACK.

—— —— ← $(1-U) = \frac{1}{5}[6\sqrt{x} - x^3](1-U_2)$

———— $(1-U) = (1-U_2)\sin\frac{\pi}{2}x.$

FIG. A10. 2





EXPERIMENTAL ISOCHRONES FOR UNSTEADY FLOW OF AIR THROUGH DRY COMPACTED SELSET CLAY.

VALUES OF x WERE CORRECTED FOR INFLUENCE OF CRACK.

— — — STAGE 1: $(1-U) = 2\sqrt{\frac{x}{x_1} - \frac{x}{x_1}}$

——— STAGE 2: $(1-U) = (1-U_2)\sin\frac{\pi}{2}x$

FIG. A10:3.